United States
Environmental Protection
Agency

Industrial Environmental Research
Laboratory
Research Triangle Park NC 27711

EPA-600/7-79-181
August 1979

EPA

Design Criteria for Stationary Source Catalytic Combustion Systems

Interagency Energy/Environment R&D Program Report

RESEARCH REPORTING SERIES

Research reports of the Office of Research and Development, U.S. Environmental Protection Agency, have been grouped into nine series. These nine broad categories were established to facilitate further development and application of environmental technology. Elimination of traditional grouping was consciously planned to foster technology transfer and a maximum interface in related fields. The nine series are:

1. Environmental Health Effects Research
2. Environmental Protection Technology
3. Ecological Research
4. Environmental Monitoring
5. Socioeconomic Environmental Studies
6. Scientific and Technical Assessment Reports (STAR)
7. Interagency Energy-Environment Research and Development
8. "Special" Reports
9. Miscellaneous Reports

This report has been assigned to the INTERAGENCY ENERGY-ENVIRONMENT RESEARCH AND DEVELOPMENT series. Reports in this series result from the effort funded under the 17-agency Federal Energy/Environment Research and Development Program. These studies relate to EPA's mission to protect the public health and welfare from adverse effects of pollutants associated with energy systems. The goal of the Program is to assure the rapid development of domestic energy supplies in an environmentally-compatible manner by providing the necessary environmental data and control technology. Investigations include analyses of the transport of energy-related pollutants and their health and ecological effects; assessments of, and development of, control technologies for energy systems; and integrated assessments of a wide range of energy-related environmental issues.

EPA REVIEW NOTICE

This report has been reviewed by the participating Federal Agencies, and approved for publication. Approval does not signify that the contents necessarily reflect the views and policies of the Government, nor does mention of trade names or commercial products constitute endorsement or recommendation for use.

This document is available to the public through the National Technical Information Service, Springfield, Virginia 22161.

EPA-600/7-79-181

August 1979

Design Criteria for Stationary Source Catalytic Combustion Systems

by

J.P. Kesselring, W.V. Krill, H.L. Atkins,
R.M. Kendall, and J.T. Kelly

Acurex/Energy and Environmental Division
485 Clyde Avenue
Mountain View, California 94042

Contract No. 68-02-2116
Program Element No. EHE624A

EPA Project Officer: G. Blair Martin

Industrial Environmental Research Laboratory
Office of Energy, Minerals, and Industry
Research Triangle Park, NC 27711

Prepared for

U.S. ENVIRONMENTAL PROTECTION AGENCY
Office of Research and Development
Washington, DC 20460

TABLE OF CONTENTS

TABLE OF CONTENTS (Continued)

TABLE OF CONTENTS (Continued)

TABLE OF CONTENTS (Concluded)

LIST OF ILLUSTRATIONS

LIST OF ILLUSTRATIONS (Continued)

LIST OF ILLUSTRATIONS (Continued)

LIST OF ILLUSTRATIONS (Continued)

LIST OF ILLUSTRATIONS (Continued)

LIST OF ILLUSTRATIONS (Continued)

LIST OF ILLUSTRATIONS (Continued)

LIST OF TABLES

LIST OF TABLES (Continued)

LIST OF TABLES (Continued)

LIST OF TABLES (Concluded)

ACKNOWLEDGEMENTS

This document presents the results of a research and development program to determine catalyst and combustion system design criteria for stationary source catalytic combustors. During the course of the program, valuable contributions were made by many individuals. In particular, Acurex extends its appreciation to W. A. Boyer and R. I. Frost of Corning Glass Works, Dr. J. M. Maselli of W. R. Grace & Co., Dr. W. B. Retallick of Oxy-Catalyst, Dr. A. S. D'Alessandro of Matthey Bishop, Inc., Dr. G.J.K. Acres and Dr. B. E. Enga of Johnson Matthey Corp., and Dr. G. R. Lester of Universal Oil Products for their support in providing test materials. Special thanks are extended to Dr. G. Voecks of the Jet Propulsion Laboratory for his work in the catalyst screening program. Additional thanks go to Dr. R. M. Pierce, B. Hinton, and C. Smith of Pratt & Whitney Aircraft for their support of the gas turbine model combustor test program. The significant contributions of Dr. W. C. Pfefferle, private consultant, and Dr. R. Levy, Dr. J. A. Cusumano, and Dr. R. Dalla Betta of Catalytica Associates, Inc. in catalyst selection are gratefully acknowledged.

This program was conducted for the Combustion Research Branch of the Industrial Environmental Research Laboratory, U.S. Environmental Protection Agency. G. B. Martin was the Project Officer. The Acurex Program Manager was Dr. J. P. Kesselring. Valuable contributions to the final report were made by R. J. Schreiber, A. J. Murphy, and R. E. Maurer. Additional key Acurex contributors include D. Knirck, M. Angwin, M. Greer, W. Nurick, Dr. J. T. Pogson, and C. D. Hartman.

SECTION 1

SUMMARY

The use of catalytic combustors in place of conventional burners has been shown to reduce CO, HC, and NO_x emissions in laboratory scale tests with both clean and ammonia-doped fuels. The operating conditions for these catalytic combustors are limited by the catalyst bed temperature capability. Since the adiabatic, one-stage, low excess air operation that is necessary for high system efficiency produces temperatures that are outside the current temperature capability of catalyst materials, concepts to operate the catalysts at permissible temperatures are required. Successful system concepts tested include direct heat removal from the catalyst through radiant heat transfer, simulated exhaust gas recirculation, two stage catalytic combustion, and high excess air (gas turbine) combustion. A summary of results from the program and the program conclusions follow. For simplicity, the program has been divided into two parts: (1) catalyst screening tests and (2) system configuration tests.

1.1 CATALYST SCREENING TEST RESULTS

The results for catalyst screening tests include information obtained from the catalyst materials review, catalyst preparation and characterization, catalytic combustor analysis, and both single cell catalyst and graded cell catalyst screening tests. These results are summarized below.

1.1.1 Catalyst Materials Review

A review of mid-temperature catalyst application literature has shown that the monolithic honeycomb support is the most technologically advanced configuration among catalyst carriers. The configuration minimizes pressure drop by having a straight through flow channel and large void area and also

minimizes required catalyst volume by providing a large total surface area per unit of volume. Monolithic supports are currently available in a variety of ceramic and metallic materials.

To obtain maximum combustion catalyst performance at high temperature (in excess of 1367K), it is desirable to have a high temperature support material capable of maintaining a uniformly dispersed catalyst. The catalyst should exhibit a low lightoff temperature and sustained high activity. To obtain these properties, some tradeoffs in performance at varying combustion conditions may be necessary.

Previous catalysis applications had shown that the noble metal (platinum and palladium) catalysts are the most promising for high activity and low lightoff temperature. Simple oxides of the transition metals should have good catalytic activity but will have higher lightoff temperatures than the noble metals. For very high temperature (>1778K) applications, mixed oxides containing either free nickel oxides or cobalt oxide are the most promising candidates.

1.1.2 Catalytic Combustor Analysis

A catalytic combustor code (PROF-HET) has been used to predict the performance of various catalyst combinations and configurations. It has shown that the overall success of the catalyst in reducing HC and CO emissions to low levels in a short bed length is dependent on both surface and gas phase reactions. Surface reactions alone are insufficient to achieve the desired low levels.

Predictions from the PROF-HET code show the maximum mass throughput for a catalytic combustor is determined by blowout of the surface and gas phase reactions. Blowout is predicted to increase nearly linearly with increasing cell diameter, thermal conductivity, and catalyst/support surface activity. The maximum mass throughput is also predicted to increase exponentially with increasing preheat temperature and fuel/air ratio for lean operation.

Small monolith cells allow fuel conversion to occur in a shorter channel length than for large cells. An increase in preheat temperature

also should result in a more rapid conversion of the fuel as it passes through the channel.

A catalytic combustor capable of high mass throughput and low emissions can be constructed by joining two or more bed segments in series. The first segment would have large diameter cells to prevent blowout. The final segment would have small diameter cells to initiate gas phase reactions and achieve low emissions of CO, NO_x, and HC.

1.1.3 Catalyst Screening Tests

Thirty-six catalyst material combinations were screened under combustion conditions to investigate the effects of support, washcoat, and catalyst properties and their interactions on combustion performance. Mullite and cordierite substrates performed adequately with platinum catalysts at 1367K temperatures. Tests conducted at higher temperatures show that platinum catalysts on alumina substrates perform well up to 1783K but experience mild thermal cracking. Cobalt and nickel oxide catalysts on zirconia spinel substrates have high use temperatures (up to 1978K) but have severe thermal shock problems.

The washcoat provides a great increase in surface area of the support materials, but exposure of the washcoat to high temperature results in significant loss of pore area. Typical changes in γ-alumina surface area for catalysts operated at 1367K were from 8 m^2/g pre-test to 0.6 m^2/g post-test. Presintering tests of washcoats confirmed the loss of surface area but did not have a negative effect on combustion properties. This presintering may reduce burying of subsequently applied active catalyst below the surface during combustion. Sintering of both washcoat and catalyst, however, results in a reduction of the active platinum available to the reactants and thus, reduced activity. Therefore, higher catalyst loadings are required on unsintered supports to provide activity equal to that of a catalyzed presintered support.

Precious metal catalysts undergo degradation by oxidation and vaporization as they operate at combustor temperatures. Large decreases in surface area (from as much as 20 m^2/g to zero m^2/g for catalysts operated above 1600K)

and dispersion (from 100 percent to zero percent) are indicators of this degradation. The impact of degradation on combustor performance can be minimized by using increased catalyst loading and hydrogen sulfide fixation of platinum to the support.

A series of tests were conducted with platinum catalysts on varying cell size supports. Large cell monoliths exhibited very high mass throughputs without blowout, but CO and HC emissions were high. Small cell monoliths exhibited very low emissions but were easily blown out. This result is a direct confirmation of performance predictions from the catalytic combustor analysis.

A catalyst with graded cell segments (6.35×10^{-3}m, 4.76×10^{-3}m, and 3.18×10^{-3}m) was tested to verify the concept. The mass throughput capabilities were markedly increased over those of small cell catalysts, such that the graded cell catalyst could not be blown out at the maximum flow capacity of the test facility (0.85 Kg/hr of methane). Comparable small cell monolithic catalysts were easily blown out at approximately 0.20 Kg/hr of methane. No carbon monoxide emissions were measurable, and only trace hydrocarbons (<0.02 Kg/hr) were present in the exhaust.

The graded cell model was further tested with a variety of fuels. It was found that heavier gaseous hydrocarbon fuels promote lightoff at lower ignition temperature. The lightoff temperature is fairly consistent for a given fuel and catalyst type. Lightoff between 672K and 788K temperatures is typical for methane on platinum catalysts.

1.1.4 Graded Cell Catalyst Tests

Additional testing of various catalysts on graded cell supports provided further verification of the high throughput, low emissions capability of these systems. Sixteen additional graded cell combustors were fabricated or procured for these tests.

Precious metal catalysts degrade rapidly at temperatures above 1589K (2400^{o}F) due to oxidation and vaporization of the metals, resulting in greatly reduced throughput ability as well as reduced catalyst lifetime. Operation of precious metal catalysts below 1587K temperature appears feasible.

Simple metal oxide catalysts of NiO and Co_2O_3 were tested and found to operate successfully at temperatures to 1978K without noticeably altering catalyst activity under lean combustion conditions. Sooting of oxide catalysts under rich conditions does affect catalyst activity, however.

Regardless of pretest BET surface area on both precious metal and metal oxide catalysts, post-test BET areas are always less than 0.50 m^2/g. While this change in surface area does alter lightoff conditions, very high steady state maximum throughputs have been achieved with catalysts having almost no BET surface area. For precious metal catalysts operating at 1589K (2400°F), volumetric heat release rates of 2.76×10^6 J/hr-Pa-m^3 (7.5×10^6 Btu/hr-atm-ft^3) are typical. For oxide catalysts operating at 1700K (2600°F), volumetric heat release rates in excess of 7.0×10^6 J/hr-Pa-m^3 were achieved.

Catalytic combustors appear to be effective in the control of thermal NO_x emissions by minimizing the gas phase reactions that occur. Emissions of less than 5 ppm at zero percent excess oxygen and 1587K temperature are typical. Catalysts are also effective in controlling the conversion of a simple fuel nitrogen compound (NH_3) to NH_3, HCN, and NO_x species at some fuel/air ratios, always under fuel-rich conditions. Conversions of less than 20 percent of the fuel-nitrogen to NO_x under rich conditions were measured for the metal oxide catalysts. Control of fuel NO_x under lean conditions appears to be difficult for single stage combustion for either low or high pressure systems.

Parametric combustion tests indicate that the maximum throughput that can be obtained with the graded cell catalyst is a linear function of pressure and an exponential function of preheat temperature. This implies that, for a given fuel and preheat, the catalyst is limited by the velocity of incoming reactants.

1.2 SYSTEM CONFIGURATION TEST RESULTS

The results for system configuration testing include information obtained from the stationary combustion system characterization study, combustion system configuration testing, and conceptual design of prototype systems. These results are summarized here.

1.2.1 Characterization of Stationary Combustion Systems

The gas turbine combustor appears well suited to catalytic combustor redesign/retrofit because it operates with considerable excess air and uses clean gaseous or light distillate fuels.

Warm air gas- or oil-fired furnaces are also candidates for catalytic combustor redesign/retrofit because of their use of clean fuels. However, since they are not maintained closely, early application of catalytic combustors to these systems may be difficult.

Scotch firetube boilers appear to offer advantages for a catalytic combustor retrofit due to the unique internal, first pass furnace volume. Watertube boilers, however, appear to require a system redesign incorporating the catalytic combustor with a compact heat exchanger. Package boiler applications also require demonstration with the more common heavy oil fuels.

1.2.2 Combustion System Configuration Tests

Three combustion system concepts were tested to evaluate heat removal techniques for catalytic combustors. The radiative catalyst/watertube concept showed that direct heat removal from a catalyst surface by radiation to a watertube heat exchanger is a viable concept for system temperature control. It is possible that different catalysts (precious metals and metal oxides) can be used in the system by varying the amount of heat removal from the catalyst surface and hence the operating temperature. Stable operation of the system over a wide range of flowrates and preheat temperatures was possible with less than 2 ppm of thermal NO_x emissions. Tests with ammonia-doped natural gas indicated a potential for fuel NO_x control under rich conditions.

A two-stage catalytic combustor, incorporating a fuel-rich first-stage, interstage heat exchanger, secondary air injector, and second-stage catalyst was also tested. The first-stage catalyst runs at a predetermined stoichiometry (50 to 80 percent theoretical air) to minimize NO_x precursor species. The second stage completes the combustion with minimum emissions. Overall control of fuel-nitrogen species shows conversion rates below 30 percent. The staged combustor appears applicable to both boiler and gas turbine systems.

The third system concept, a model single stage gas turbine combustor, showed less than 5 ppm thermal NO_x emissions with clean gaseous and distillate oil fuels. The combustor exhaust temperature is adequately controlled by excess air levels. Premixed, lean burning fuel injection systems are a major development area for the catalytic gas turbine combustor. Single step lean combustion of ammonia- and pyridine-doped fuels showed conversions of fuel-nitrogen to NO_x of approximately 80 percent.

1.2.3 Prototype System Design Concepts

Based on the performance of the three system concepts, firetube boiler and stationary gas turbine applications appear promising for first generation catalytic combustor retrofit. Considerable system redesign will probably be required for applications involving watertube boilers, residential heaters, and mobile gas turbines.

The two stage combustor appears promising for all applications involving nitrogen-containing fuels due to the ability of this combustor to control the conversion of fuel-bound nitrogen to nitrogen oxides. Since fuel-nitrogen is most prominent in residual and solvent refined oils and coal, staged combustor demonstration must be extended beyond clean fuels. Additional development of fuel and air injection systems, premixing systems, and prevaporizing systems is required for catalytic applications with these fuels. Ignition system development is also required.

1.3 CONCLUSIONS

The results of this program have brought catalytic combustion closer to concept demonstration. Before this step can be taken, however, further work on the integration of the catalytic combustor into the total system must be undertaken. At the same time, the search for additional catalyst materials capable of high temperature operation must be continued. Therefore, the following program is recommended:

- Screening tests of various oxide and mixed oxide catalyst/support combinations at temperatures above 1644K ($2500^{o}F$) to determine combustion performance over a range of fuel/air ratios.

- Further evaluation of high-performance oxide systems with nitrogen-doped fuels and at pressure, and determination of the operating limits and fuel-nitrogen performance of the catalysts.
- Extended life testing of selected catalysts to demonstrate high activity over long periods of time.
- Additional testing of the radiative catalyst/watertube system and the two stage combustor over a wider range of throughputs, pressures, and fuels.
- Testing of subsystems important to the ultimate success of the catalytic combustor, including lightoff systems, fuel/air mixing systems, fuel vaporization systems, catalyst bed temperature control systems, and heat exchange systems.
- Testing of potential staged combustors which require no interstage cooling, with both clean and nitrogen-containing fuels.
- Exploratory combustion testing of heavy fuel oils.
- Design and development of suitable boiler/furnace systems utilizing catalytic combustors to demonstrate low NO_x performance in actual field tests.

SECTION 2

INTRODUCTION

Interest in materials capable of promoting heterogeneous combustion reactions has continued in varying degrees ever since Sir Humphrey Davy discovered over 150 years ago that platinum wires could promote combustion reactions in flammable mixtures. An identification of some of the early work in surface combustion is given in References 2-1 and 2-2. Since catalytic combustors have excellent potential for low NO_x emissions, a number of research programs investigating their use in gas turbine, domestic appliance, and home furnace applications are currently underway. This section describes these ongoing research programs in catalytic combustion, and outlines the program purpose and goals of EPA Contract 68-02-2116.

2.1 RELATED RESEARCH PROGRAMS IN CATALYTIC COMBUSTION

The main focus in current catalytic combustion research is the application to gas turbine engines. Additional work is being conducted for application to residential furnaces, domestic appliances, and life-support systems. There is also active research in the areas of analytical modeling and fundamental experimentation. Each of these research areas is described below.

2.1.1 Gas Turbine Applications

Research in catalytic combustion for gas turbines includes application to automotive, aircraft, and stationary power generation systems as well as laboratory scale tests.

2.1.1.1 NASA Lewis Research Center Program

NASA has two active programs in catalytic combustion; the Air Breathing Engines Division of the Emission Technology Branch is pursuing the application

of catalytic combustors to aircraft gas turbines, while the Power Generation and Storage Division of the Combustion Power Section is interested in catalytic combustors for automotive gas turbines.

Automotive Gas Turbine Program

There are three major research areas in the automotive gas turbine program: 1) fuel preparation system studies, 2) catalyst evaluation tests, 3) catalyst life tests. The proposed gas turbine operating conditions are:

- Pressure: 1.5 to 4.5 atm
- Inlet temperature: 1210 to 970K
- Exit temperature: 1310K
- Primary zone temperature: 1350 to 1425K
- Reference velocity: 11.4 to 12.9 m/sec
- Airflow: 0.1 to 0.5 kg/sec

The goals of this program are to limit emissions from the combustor to half of those required by the most stringent emission standards, and to keep the total combustor system (fuel preparation plus combustion chamber) pressure drop under 3 percent.

For the fuel preparation system, the program goals are:

- Spatial fuel distribution within 10 percent of mean
- 90 percent of fuel vaporized at 800K
- Velocity distribution within 10 percent of mean
- No autoignition
- Less than 1 percent pressure drop

Four different fuel injectors were tested; (1) air assist sonicore injector, (2) splash-groove injector, (3) multiple-jet injector, and (4) multiple conical tube injector. Air swirlers were used with the sonicore and splash-groove injectors to improve spatial fuel/air distributions. The multiple conical tube fuel injector was generally able to meet the program

goals if sufficient mixing length was allowed. This system is shown in Figure 2-1; Reference 2-3 describes the fuel injection concepts in more detail.

In the catalyst evaluation program, the objectives are the identification of a catalytic combustor capable of:

- Emissions
  - -- 1.6 g NO_2/kg fuel
  - -- 13.6 g CO/kg fuel
  - -- 1.64 g HC/kg fuel
- Pressure drop
  - -- Less than 2 percent

The catalyst evaluation program has two elements; furnace screening tests of monoliths and pellets of small size by passing 500 ppm of propane in air over the catalyst, and combustion tests of monoliths (0.12 m in diameter) with 800K inlet temperature and premixed propane, diesel, and Jet A fuels in air at equivalence ratios between 0.1 and 0.3. Results from the furnace screening tests are presented as oxidized fuel fraction versus catalyst temperature and serve to identify the most suitable catalysts for further testing. The furnace tests have indicated that the most effective catalysts for gas turbine combustor applications will probably be noble metals on monoliths. Results of the furnace screening tests are described in Reference 2-4.

The combustion test rig has a long mixing section, and the reactor can hold from one to six individual catalyst elements in series. Each element is located between thermocouple arrays. All tests were performed at an inlet temperature of 800K, pressure of 3×10^5 Pa (3 atm), and a range of velocities from 10 to 25 m/sec. Adiabatic reaction temperatures from 1100 to 1600 K were obtained by varying fuel/air ratio.

Catalyst elements obtained from Engelhard Industries, W. R. Grace and Co., Johnson Matthey Corporation, and Oxy-Catalyst, Inc., have been tested. All elements were 0.12 m in diameter. The Johnson Matthey elements

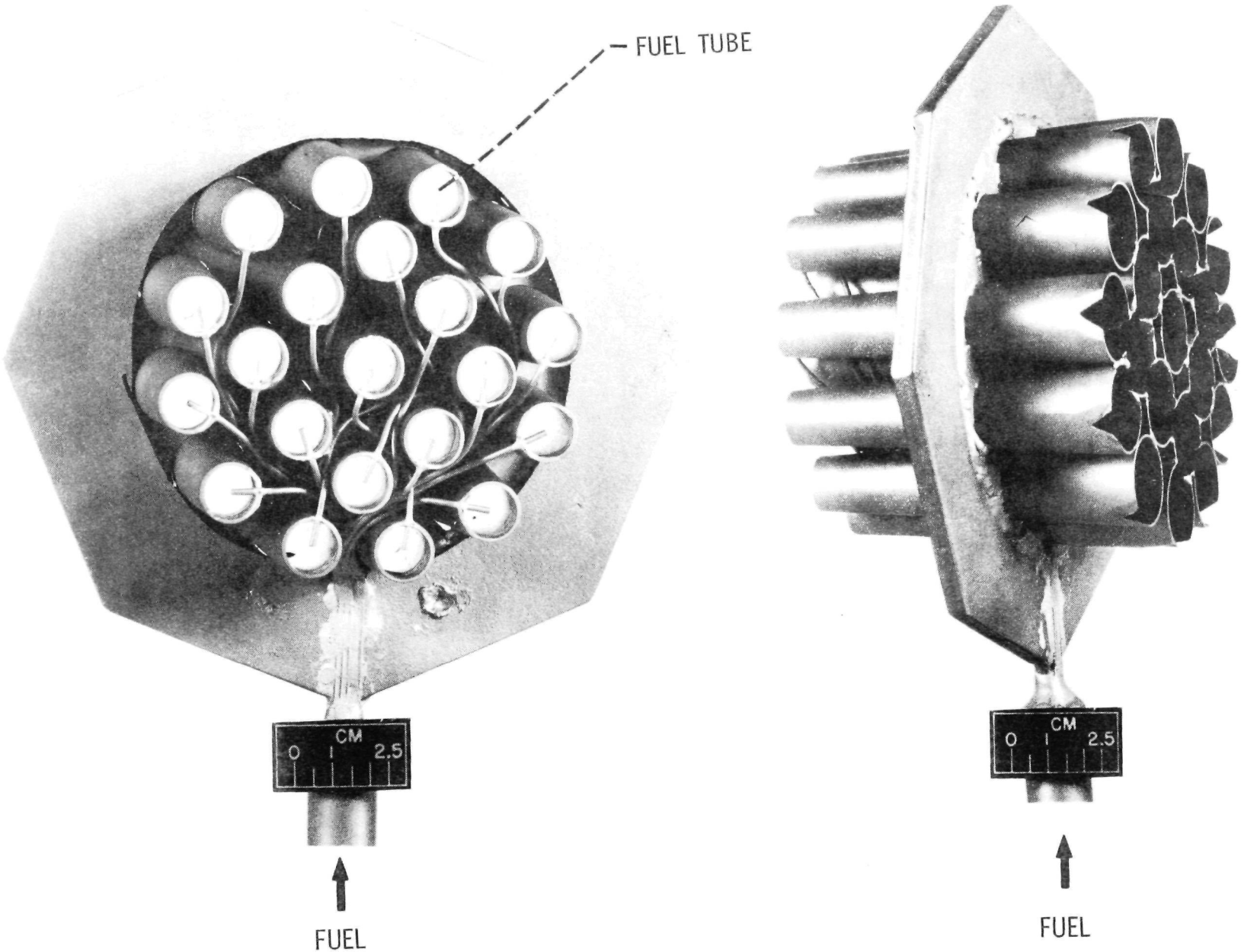

Figure 2-1. NASA multiple conical tube fuel injector.

used a metal substrate; all other elements used a ceramic substrate. Emissions measurements were made in combustion tests to determine the minimum exit temperature at which the reactors should be operated to obtain the steady-state emission objectives. Effects of reactor length, cell density, and gas phase reactions were considered.

The feasibility of using a catalytic reactor in an automotive gas turbine engine and meeting both emissions and pressure drop goals was demonstrated in this program. Potential problems for such a system include the loss of catalytic activity with time and transient operation characteristics. This work is described in further detail in References 2-5 through 2-7.

Concurrent with the fuel preparation and catalyst evaluation studies, Engelhard Industries has conducted durability tests of two proprietary Engelhard catalysts at one atmosphere pressure. The test sequence for the two catalysts included a 24-hour break-in period, a CO activity test, a test with propane to determine the performance range, another CO activity test, a 1000-hour life test with No. 2 diesel fuel (with CO activity tests every 250 hours), and a final propane test to determine performance range changes.

A summary of the test results showed emissions to be the same for both catalysts during the 1000-hour test with No. 2 diesel fuel. One catalyst required a higher inlet temperature to maintain low emissions after 600 hours of testing. The propane parametric studies showed this catalyst had deactivated completely for high efficiency combustion, and the CO activity test showed significant deactivation of both catalysts between 24 and 250 hours of aging.

Emissions with No. 2 diesel fuel after the 1000-hour test were 4 ppm HC, 50 ppm CO, and 4 ppm NO_x. These emissions are well below the 1977 and 1978 automotive standards. Details of the durability testing are given in Reference 2-8. Further work to perform the testing at 5-atmosphere pressure is now underway.

Aircraft Gas Turbine Program

In addition to the automotive work, NASA is pursuing aircraft gas turbine engine emission reduction programs using catalytic combustors. Two programs are currently active; the aircraft gas turbine engine Low-Power Emission Reduction (LOPER) technology program, and the Advanced Low Emissions catalytic combustor program.

The LOPER experimental program, being conducted by General Electric Co., is to evolve jet aircraft engine combustion technology and reduce low-power CO and HC emissions to extremely low levels. Three design concepts will be screened over a limited range of operating conditions. The three designs include a hot wall combustor, a recuperative combustor, and a catalytic combustor. The catalyst system was prepared for GE by Engelhard Industries.

The Advanced Low Emissions catalytic combustor program is being conducted by General Electric Co., and Pratt and Whitney Aircraft. The purpose of this program is to evaluate the feasibility of employing catalytic combustion technology in aircraft gas turbine engines to achieve the control of NO_x emissions for subsonic, stratospheric cruise operation while retaining or improving system performance. This program is jointly sponsored by NASA and the U.S. Air Force.

2.1.1.2 Air Force Aero Propulsion Laboratory Program

The AFAPL has been involved in both in-house and contractual programs in the application of catalytic combustors to aircraft systems. The in-house program addresses the use of catalysts in both mainburner and afterburner applications. For the afterburner test program, a honeycomb flameholder consisting of silicon nitride monolith segments coated with Pt/Pd catalyst has been fabricated. Test plans are for an inlet temperature of 975K, with the surface temperature between 1640 and 1920K.

Contractual work has focused on the development of a hybrid catalytic combustor and on a fuel preparation system. Exxon Research and Engineering Company performed the work on the hybrid system for aircraft turbine applications, as described in Reference 2-9. The hybrid catalytic combustor minimizes pollution problems associated with unburned hydrocarbons and

carbon monoxide in the idle mode, and NO_x and smoke production in the power mode of aircraft gas turbine operation. This combustor consists of a fuel rich thermal precombustor, secondary air quenching zone, and monolithic catalyst stage which rapidly oxidizes CO and UHC produced in the precombustor.

Noble metal catalysts on various monolithic support materials and geometries were found to be the most active materials for CO and UHC oxidation in the temperature range of 700 to 1200K. The hybrid catalytic combustor combustion efficiency for JP-4 fuel containing 535 ppm sulfur was found to be 99.8 percent under realistic conditions. Combustor pressure drop was less than 6 percent. For a Johnson Matthey metal-supported Pt catalyst, average emission indices of CO, UHC, and NO_x were 0.95, 0.43, and 1.8 g/kg of fuel, respectively. This catalyst was effective in reducing CO by 86 percent and UHC by 94 percent, while increasing NO_x by 68 percent relative to catalyst inlet values. It was estimated that the hybrid catalytic combustor can meet the 1979 new aircraft emission standards, but must be modified slightly to reduce UHC emissions to meet the 1981 new aircraft emission standards.

General Applied Science Laboratories, Inc. conducted the development work on a fuel preparation system for the catalytic combustor, as described in Reference 2-10. Objectives for the fuel system were to provide uniform velocity and fuel distribution profiles, complete vaporization of the fuel, and reasonable pressure drop. Operating conditions for the system include flow velocities of 15.2 to 38.1 m/sec (50 to 125 ft/sec), pressures of 6.8 to 13.6 atm, temperatures of 645 to 810K, and fuel/air ratios of 0.018 to 0.028. The approach taken in developing the fuel preparation system was to design for a limited residence time to prevent autoignition, to provide for adequate exit blockage to prevent flashback, to produce small droplets to get good evaporation, to use a high flow velocity to preclude flame stabilization prior to entering the combustor, and to obtain the best possible initial dispersion of the fuel to enhance mixing. Three candidate designs were tested, consisting of pressure atomization, air blast atomization, and air assist atomization systems. Following testing of these systems and some modifications, an air assist atomization system with an upstream swirl generator was selected as the final design.

2.1.1.3 Westinghouse Electric Company-Engelhard Industries Joint Program

Beginning in 1973, Westinghouse and Engelhard have conducted a joint program to assess the applicability of catalytic combustors to gas turbines. As described in Reference 2-11, experimental test results were obtained for No. 2 distillate oil and low Btu gas. Pressure, temperature, and mass flowrate were varied during the tests. The catalyst bed exit temperature profile was very uniform for low Btu gas, but not as uniform for No. 2 oil. Exceptionally low emissions (2-3 ppm NO_x, 20-30 ppm CO) were achieved for both fuels, and unburned hydrocarbons were less than 1 ppm.

2.1.1.4 Johnson Matthey Research Centre Program

The Johnson Matthey Research Centre in Reading, England, has begun laboratory scale testing of metal monolith catalyst systems for gas turbine application. Results of this testing are not yet available.

2.1.2 Residential Furnace Applications

A prototype surface combustion residential furnace has been developed by R. S. Bratko of Slyman Manufacturing Corporation in Parma, Ohio. The furnace has been evaluated by the Combustion Research Branch of the Industrial Environmental Research Laboratory of the U.S. Environmental Protection Agency as reported in Reference 2-12. The furnace passes premixed fuel and air through a refractory matrix, and the premixed gases then burn on the refractory surface. Heat is transferred from the surface to the air-cooled firebox wall by radiation. Furnace emissions were evaluated over a range of excess air from 5 to 45 percent with both propane and natural gas fuels. For a nominal operating point on natural gas at 10 percent excess air, NO_x emissions were less than 15 ppm as measured, with correspondingly low CO and HC emissions. The low NO_x emissions are a result of the low surface temperature (1255K maximum) of the refractory, and the low excess air capability gives potential for high system efficiency.

2.1.3 Domestic Appliance Applications

The Institute of Gas Technology has been conducting research and development on catalytic combustors for domestic appliance applications for several years. These programs include:

- Contractor to Southern California Gas Company on conceptual burners and model ventless appliances for catalytic combustion of hydrogen and steam-reformed natural gas (1972-1976),
- Contractor on a joint U.S. Environmental Protection Agency/Southern California Gas Company contract to develop a catalytic range-top burner (1975),
- Contractor since 1974 on a catalytic ignition system for gas appliances using hydrogen as an ignition fuel ignited in air on a platinum catalyst.

The instantaneous ignition system stores hydrogen in the form of a metal hydride. When ignition is required, small quantities of hydrogen are released by valving. This catalytic ignition system could become an alternate to standing pilot or electric systems.

The model catalytic appliances operate at low combustion temperatures and produce very low emissions of nitrogen oxides. Because of the low emission levels, outside venting of the products of combustion is not required.

2.1.4 Life Support Systems

Energy Systems Corporation in Nashua, New Hampshire has developed various thermal protection equipment using catalytic combustors. Existing products include belt-mounted Arctic ambulatory heater systems, SCUBA diver heaters, hypothermia prevention and treatment systems, casualty evacuation bag heaters, and downed airman power sources.

The downed airman power source system supplies warmth to airmen in life rafts by circulating heated water through turbulated undergarments or blankets. These systems use either propane or propylene fuel combusted on 1-percent Pt on alumina pellets manufactured by Matthey Bishop. Catalyst bed temperatures are between 922 to 1033K. Heat extraction pins or fins conduct heat to a hot plate and finally to the fluid heat exchanger.

ESC is also currently developing a catalytic/thermoelectric SCUBA diver heater for the U.S. Navy. This system will be capable of delivering 500 thermal watts to a diver in 275K seawater.

2.1.5 Fundamental Programs

Several ongoing research programs are currently developing information which would have application to a broad class of catalytic combustion systems. These programs include both analytical and experimental projects.

2.1.5.1 Analytical Programs

Analytical models for application to high temperature catalytic combustors are in development at Exxon Research and Engineering Company and at Stanford Research Institute. Each of these programs is described below.

Exxon Research and Engineering Company Model

Under joint National Science Foundation/U.S. Environmental Protection Agency/Exxon sponsorship, Exxon has developed a practical model of catalytic combustor operating characteristics for analysis of advanced power systems and test data. The model is described in detail in Reference 2-13. The major physical assumptions of the steady-state model are:

- Uniform gas phase properties at a cross section
- Uniform catalyst/substrate temperature and fuel concentration at a cross section
- Conversion of reactants to products both at the catalyst surface and in the gas phase
- Axial variations in velocity are allowed
- Axial heat conduction in the substrate is included, but radiation and gas phase conduction are neglected

The model consists of a variable-order finite-difference method to solve the two-point boundary value problem. Comparisons of catalytic combustor data and model predictions show excellent agreement. When the model is used to examine conversion as a function of gas inlet temperature for typical lean operating conditions with a noble metal catalyst, a sharp catalytic lightoff temperature is predicted, as is a lightoff/extinction hysteresis At higher temperatures the onset of gas phase combustion occurs, resulting in complete conversion.

Further work on expanding the model to include internal heat removal, CO kinetics, multiple fuel species, and NO_x kinetics is planned.

Stanford Research Institute Model

Under Air Force Office of Scientific Research funding, Stanford Research Institute has initiated an analytical study to determine the contribution of catalytic wall reactions to combustion initiation. The temperature distribution on the duct wall is found, taking into account wall heat conduction, convective heat transfer, and heat generation and fuel consumption. For Lewis numbers greater than one, the temperature increases with distance down the duct, while for smaller Lewis numbers the temperature passes through a maximum whose value depends on flow speed. Ultimately, this work will be used to predict the distribution of catalyst on a substrate required for startup and shutdown in a practical system. Work to date is described in Reference 2-14; experimental evaluations will also be conducted in this program.

2.1.5.2 Experimental Programs

Laboratory scale experimental programs are currently in progress at United Technologies Research Center, Princeton University, Lawrence Berkeley Laboratory, and the University of California. These programs are discussed below.

United Technologies Research Center Program

The UTRC program in catalytic combustion seeks to determine the feasibility of utilizing catalyzed surface reactors in the combustion of multicomponent fuels. As described in Reference 2-15, the program is currently involved in simple burner experiments using propane fuel and in an analytical study which combines heat and mass transfer and homogeneous reactions in the analysis.

The experimental program uses a catalytic burner apparatus to determine ignition temperature, steady-state operating conditions, and species concentrations by varying mixture ratio, temperature, bed length, flow velocity, bed material, and diluent. The combustible mixture is usually

oxygen-propane with argon diluent, but helium and nitrogen diluent have also been used. Isothermal experiments are then run to determine ignition temperature.

The modeling program takes into account both heterogeneous and homogeneous reactions, and seeks to fit experimental data over a range of temperatures with single heterogeneous and homogeneous rate constants. Matching of temperature rise and concentration data has been done for propane combustion with argon diluent.

Princeton University Program

The Department of Aerospace and Mechanical Sciences at Princeton University has undertaken a program to clarify the relative influences of chemical kinetics and transport processes in a catalytic combustion system. This work is sponsored by the Air Force Office of Scientific Research. A steady combustion system has been constructed and some preliminary data obtained. Measurements to be taken include velocity, temperature, pressure, and gas composition within a honeycomb catalyst system and its boundary layer using both physical and optical techniques.

University of California/Berkeley Program

The Department of Mechanical Engineering at the University of California/Berkeley recently completed a study on fuel-nitrogen conversion with catalytic combustors for the Department of Energy (References 2-16, 2-17). A platinum catalyst was operated with propane/oxygen/argon mixtures at equivalence ratios between 0.7 and 1.6. Trace amounts of either nitric oxide or ammonia were added to the gases, and the conversion of these fuel-nitrogen compounds to nitric oxide was measured as a function of equivalence ratio, adiabatic flame temperature, and fuel-nitrogen concentration. It was concluded that surface reactions dominate the fuel-nitrogen conversion mechanism, with the conversion found to be strongly dependent on equivalence ratio, weakly dependent on calculated adiabatic flame temperature, and moderately dependent on fuel-nitrogen concentration.

Lawrence Berkeley Laboratory Program

Under Department of Energy support, the Lawrence Berkeley Laboratory has been investigating the effect of a heated catalytic surface on combustion in lean hydrogen-air mixtures (References 2-18, 2-19). The velocity and density profiles of the boundary layer have been measured with laser Doppler velocimetry and Rayleigh scattering, respectively. Measurements on a platinum catalytic surface indicate that, at a surface temperature of 1000K, not only is there significant surface combustion but that homogeneous combustion in the boundary layer is induced by active species generated at the catalytic surface. An analytical model has also been developed to aid the investigation. This work will help improve the understanding of high temperature heterogeneous catalysis of combustion reactions and the coupling with homogeneous reactions and fluid mechanics.

2.2 PROGRAM PURPOSE AND GOALS

The objective of the research and development program described in detail in the remainder of this report is to establish design criteria for the application of catalytic combustion to low emission, high efficiency stationary combustion systems. This objective was met by conducting a two phase program which included the following tasks:

- Phase I -- Small Scale Catalyst and Combustion Concept Screening
  - -- Review the available information on stationary combustion system design and operating characteristics, including residential heating systems, commercial and industrial boilers, stationary gas turbines, and supercharged boilers. Consider system impacts as to the applicability of catalytic combustor retrofit or redesign.
  - -- Review available catalyst materials, including substrates, washcoats, and catalysts, and select materials for testing at temperatures between 1360 and 1980K.

-- Determine catalyst preparation and characterization techniques. Catalysts prepared include both precious and base metal catalysts. Catalyst characterization parameters include total surface area, selected surface area (dispersion) of precious metal catalysts, visual surface appearance by scanning electron microscopy, and surface composition by energy-dispersive x-ray analysis.

-- Develop the basic understanding of the catalytic combustor, including the effects of preheat temperature, catalyst system material, and catalyst system geometry. Use this information to develop a computer code capable of giving quantitative information on catalyst performance as a function of operating parameters.

-- Perform catalyst screening tests of at least 30 catalyst systems with up to four different fuels (natural gas, propane, methanol, distillate oil). Obtain radial and axial temperature profiles within the catalyst bed. Test these catalysts at temperatures to 1980K and pressures to 1.01 MPa (10 atmospheres).

-- Perform a more extensive evaluation of those catalysts exhibiting good combustion characteristics. Use ammonia dopant to simulate fuel-nitrogen compounds and measure the ammonia conversion to nitrogen oxide.

-- Build and test two small scale (1.05×10^8 joules/hr) combustion systems which would have application to practical combustors. These systems are to include FGR, two-stage combustion, or direct bed heat removal for temperature control.

- Phase II -- Scale-up of Catalyst and System Concepts

  -- Perform catalyst scale-up tests at a nominal heat release rate of 1.05×10^9 joules/hr. Test results were compared to the small scale tests to determine scaling parameters

-- Perform scale-up testing of one combustion system and compare to small-scale system tests.

-- Develop conceptual designs for the application of catalytic combustors to practical combustion systems.

Sections 3-11 of this report describe the tasks outlined above in detail.

REFERENCES

2-1. Kesselring, J. P., et al., "Catalytic Oxidation of Fuels for NO_x Control from Area Sources," Environmental Protection Technology Series Report EPA-600/2-76-037, February 1976.

2-2. Pfefferle, W. C., "The Catalytic Combustor -- A Look Back, A Look Forward," Paper 77-31, presented at the Western States Section/The Combustion Institute Meeting, October 17-18, 1977, Stanford, California.

2-3 Tacina, R., "Experimental Evaluation of Two Premixing-Prevaporizing Fuel Injection Concepts for a Gas Turbine Combustor," NASA TM X-73422, May 1976.

2-4 Anderson, D. N., "Preliminary Results from Screening Tests of Commercial Catalysts with Potential Use in Gas Turbine Combustors, Part I. Furnace Studies of Catalyst Activity," NASA TM X-73410, May 1976.

2-5 Anderson, D. N., "Preliminary Results from Screening Tests of Commercial Catalysts with Potential Use in Gas Turbine Combustors, Part II. Combustion Test Rig Evaluation," NASA TM X-73412, May 1976.

2-6 Anderson, D. N., et al., "Catalytic Combustion for the Automotive Gas Turbine Engine," NASA TM X-73589, April 1977.

2-7. Anderson, D. N., "Performance and Emissions of a Catalytic Reactor with Propane, Diesel, and Jet A Fuels," NASA TM-73786, October 1977.

2-8. Heck, R. M., et al., "Durability Testing at One Atmosphere of Advanced Catalysts and Catalyst Supports for Automotive Gas Turbine Engine Combustors," NASA CR-135132, June 1977.

2-9. Siminski, V. J., and Shaw, H., "Development of a Catalytic Combustor for Aircraft Gas Turbine Engines," Technical Report AFAPL-TR-76-80, September 1976.

2-10. Roffe, G., "Development of a Catalytic Combustor Fuel/Air Carburetion System," Technical Report AFAPL-TR-77-19, March 1977.

2-11. De Corso, S. M., et al., "Catalysts for Gas Turbine Combustors-Experimental Test Results," ASME Paper 76-GT-4, March 1976.

2-12. Martin, G. B., "Evaluation of a Prototype Surface Combustion Furnace," published in "Proceedings of the Second Stationary Source Combustion Symposium, Volume III," EPA-600/7-77-073c, July 1977.

2-13. Cerkanowicz, A. E., et al., "Catalytic Combustion Modeling: Comparisons with Experimental Data," ASME Paper 77-GT-85, March 1977.

2-14. Ablow, C. M. and Wise, H., "Contribution of Catalytic Wall Reaction to Combustion Initiation," Paper 77-39 presented at the Western States Section/The Combustion Institute Meeting, Stanford, California, October 17-18, 1977.

2-15. Marteney, P. J., and Kesten, A. S., "Studies of the Rate of Oxidation of Propane on a Catalytic Surface," Paper 77-36 presented at the Western States Section/The Combustion Institute Meeting, Stanford, California, October 17-18, 1977.

2-16. Matthews, R. D., "The Nature and Formation of Nitrogenous Air Pollutant Emissions from Combustion Systems," University of California/Berkeley, Energy and Environment Division Report LBL-6850, October 1977.

2-17. Matthews, R. D., and Sawyer, R. F., "Fuel Nitrogen Conversion and Catalytic Combustion," University of California/Berkeley, Energy and Environment Division Report LBL-6396, October, 1977.

2-18. Robben, F., et al., "Catalyzed Combustion in a Flat Plate Boundary Layer. I. Experimental Measurements and Comparison with Numerical Calculations," Lawrence Berkeley Laboratory, Energy and Environment Division Report LBL-6841, September 1977.

2-19. Schefer, R. and Robben, F., "Catalyzed Combustion in a Flat Plate Boundary Layer. II. Numerical Calculations," Lawrence Berkeley Laboratory, Energy and Environment Division Report LBL-6842, September 1977.

SECTION 3

CHARACTERIZATION OF STATIONARY COMBUSTION SYSTEMS

Background information on stationary combustion systems which is required for future catalytic combustor retrofit or redesign is presented in this section. Discussion includes:

- General considerations in which the nature of area source sectors is described
- A description of the design and operating characteristics of gas turbines and supercharged boilers
- Air pollutant emission characteristics
- Conclusions

3.1 GENERAL CONSIDERATIONS

Emissions of nitrogen oxides from stationary source combustion account for 94 percent of the nation's stationary source total of 1.14×10^{13} g/year (12.6 million tons/yr.). Developing technology to ultimately produce a reduction in these NO_x emissions is the objective of the present program.

The options available for controlling these NO_x emissions include fuel modification, flue gas treatment, modification of combustor operating conditions, or use of alternate processes. The first three methods have, in the recent past, been vigorously investigated, and one of these control techniques, combustion modification, has proven successful for the more prolific NO_x emitters. In order to have the technology available to further reduce NO_x emissions from sources as well as to bring those sources which do not respond to the simpler reduction options into compliance with future emission regulations, alternate processes must be explored. One of these, catalytic combustion, is the focus of this report.

Catalytic combustion offers significant NO_x, CO, and unburned hydrocarbon emission reduction potential due to a low operating temperature and a concurrent promotion of oxidation reactions. An early assessment of the applicability of catalytic concepts to gas turbines and utility boilers was performed by the Aerospace Corporation in 1973 (Reference 3-1). This report concluded that catalytic oxidation might be applicable to gas turbines, but that application to a utility boiler would require a new system design. The report also indicated that only gaseous fuels and light, sulfur-free hydrocarbons could be used in catalytic systems due to system requirements and catalyst poisoning difficulties.

Acurex extended the applicability assessment of catalytic combustors to gas- and oil-fired home heaters and commercial and industrial boilers in 1976 (Reference 3-2). These area-source combusters use gaseous or light distillate oil fuels, and may be amenable to redesign. It was concluded that there are no theoretical barriers to the application of catalytic combustors in any of these area sources on either a retrofit or redesign basis.

3.2 EQUIPMENT AND OPERATING CHARACTERISTICS

A detailed discussion of residential heating equipment and commercial and industrial boilers is given in Reference 3-2. This section will describe equipment and operating characteristics for gas turbines and supercharged boilers.

3.2.1 Stationary Gas Turbines

3.2.1.1 Introduction

The gas turbine is a rotary internal combustion engine based on the Brayton cycle. All gas turbines use these same equipment components:

- Compressor -- pressurizes and forces primary air into the combustion chamber,
- Combustor -- combusts the injected fuel and primary air and allows for injection of secondary air to complete the combustion reaction,

- Turbine -- transforms the enthalpy of the gas into mechanical energy by expanding the gas through the turbine blades to drive the compressor and do useful shaft work.

Table 3-1 provides a breakdown of the many types of stationary gas turbine equipment. The first column shows the initial design either as a derivative of an existing aircraft unit or exclusively for stationary use. The remaining columns break down the major equipment components as listed previously. Each of these equipment subcategories is described below.

TABLE 3-1. TYPES OF STATIONARY GAS TURBINE EQUIPMENT

Design	Compressor	Combustor	Turbine
Stationary design	Axial flow	Annular	Axial flow
Aircraft derivative	Axial and Centrifugal flow	Can	Radial inflow
	Centrifugal flow	Canannular	

In addition to the available component combinations, several cycle options exist. The most important are:

- Simple cycle -- Air and fuel are burned in the combustor, and the hot combustion products are expanded through the power turbine and exhausted to the atmosphere. Figure 3-1 is a schematic of this cycle.
- Regenerative cycle -- The combustion products are directed through a heat exchanger to preheat the primary combustion air.
- Combined cycle -- The hot exhaust gases of the simple cycle turbine pass through a waste heat boiler to increase the thermal efficiency of the unit.

Several subclassifications of these cycles exist. Intercooling is a modification of the simple cycle which uses two compressors separated by a

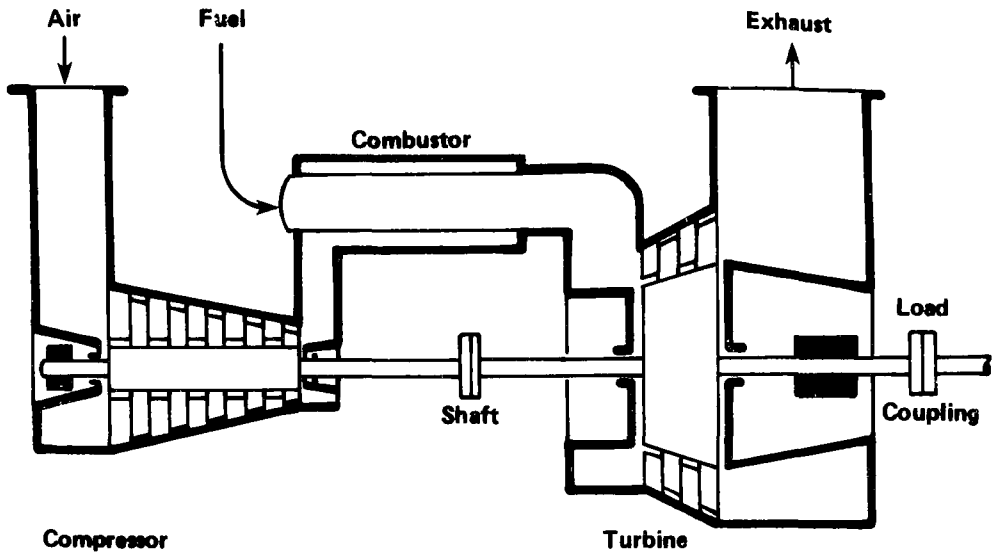

Figure 3-1. Simple cycle gas turbine system.

heat exchanger which lowers the second stage compressor inlet temperature, decreasing its energy requirements and thus increasing thermal efficiency. Reheating is another modification of the simple cycle wherein two combustors and turbines are used to raise the average temperature of heat addition, also increasing thermal efficiency.

The stationary gas turbine serves in a variety of applications, the most common of which are electricity generation and pumping. Table 3-2 gives the principal applications of turbines in the United States. Also shown are the typical locations of these installations, which is an important factor when emission regulations are being considered. Table 3-3 shows the relative installed horsepower and associated fuel consumption for the three primary users. Although the electric power generation community appears to be the largest user of gas turbines, the use factor for these installations is far lower than for the other sectors. The majority of electric generating units are used for peaking power only.

A major disadvantage of the gas turbine is its requirement for clean fuels such as natural gas and distillate oil. Newer units, however, are being designed to use low sulfur residual oil, and the number of units firing residual oil is expected to increase.

TABLE 3-2. PRINCIPAL APPLICATIONS OF STATIONARY GAS TURBINES IN THE UNITED STATES

Industry	Applications	Typical Locations
Electric utility	Base load Intermediate load Peak load Standby power Total energy	Near populated areas
Natural gas utility	Compressor drives	Remote
Petroleum	Pumping Compressor drives Electric power	Remote
Chemical	Compressor drives Electric power	Near populated areas
General industrial	Electric power Mechanical drive	Near populated areas
Commercial & municipal	Electric power Total energy Pumping	Near populated areas

TABLE 3-3. STATIONARY GAS TURBINE POWER GENERATION (1973 data)

Industry	Rated Capacity	Power Generation	Fuel Consumption	
	Mw (10^3 Bhp)	M joule (10^6 Bhp-hr)	10^{15} J (10^{12} Btu)	
			Natural gas	No. 2 oil
Electric power	22.83 (30,440)	89,750 (33,240)	134 (127)	295 (280)
Oil & gas pipelines	2.64 (3,520)	57,402 (21,260)	846 (802)	43 (41)
Natural gas processing	1.15 (1,530)	40,527 (15,010)	457 (433)	-- --

3.2.1.2 Equipment Characteristics

The wide variation in gas turbine equipment design is determined by the various combinations of compressor, combustor, and turbine. The first stationary units were modifications of existing aircraft designs. At present, units specifically designed for stationary use are common. Stationary designers need not conform to the aircraft engine's geometry and weight constraints, although in many instances uniform compressor and turbine designs are used in both applications. The remainder of this subsection will describe the various types of compressors, combustors, and turbines.

Compressor Types

The compressor is one of the most important gas turbine components since the energy released in the combustor is directly proportional to the mass of air consumed. Basically, the compressor provides high pressure air to the combustion chamber. The most efficient compressor operation provides maximum compression with minimum temperature rise. Two basic compressor designs exist:

- Centrifugal flow
- Axial flow

A centrifugal compressor consists of an air impeller, a diffuser manifold, and a compressor manifold to direct the compressed air to the combustor. The primary advantages of the centrifugal compressor are its simplicity, ruggedness, and low manufacturing cost. They are capable of compression ratios of about 4 or 5 to 1, with an efficiency of about 80 percent. Because compression ratios above 5 to 1 reduce specific fuel consumption, these compressors are generally ruled out for use in very large units. However, 5 to 1 compression ratio regenerative turbines are competitive in thermal efficiency with high compression ratio simple cycle turbines.

The axial flow compressor consists of a series of rotating airfoils (rotor blades) and a stationary set of airfoils (stator vanes). Though capable of producing very high compression ratios, the design has its disadvantages. Manufacturing is very costly, and it is very susceptible to particulate damage. Axial flow designs find greatest use where requirements for high efficiency and output predominate considerations of cost and flexibility.

Combustor Types

The combustor converts chemical energy to thermal energy through combustion of a fuel/air mixture. Of all gas turbine components, the combustor presents the most difficult design problems since it must withstand the high temperatures of combustion in addition to diluting and cooling the combustion products prior to their entry into the turbine.

The following are important goals in the design of a combustor:

- High combustion efficiency.
- Stable operation, free from blowout over large operating ranges.
- Low pressure loss, ensuring that pressure drop will be taken across turbine.
- Uniform temperature distribution.
- Low carbon deposition.
- Long material lifetimes.

Only about one-fourth of the compressor's air is used in the primary combustion process. The remainder is used as a film coolant for the combustor and as secondary dilution air.

Three basic combustor designs have evolved throughout the developmental stages of the aircraft gas turbine:

- can
- annular
- canannular

In an aircraft engine utilizing the can design, several combustors are mounted around the engine axis. Each consists of a cylindrical shroud with an inner liner, a fuel nozzle, and an igniter. The ease of maintenance, due to the modular design, is this engine's major advantage. Its main disadvantage, the poor use of available space, is generally not important in stationary applications.

The annular type combustor is a single combustor composed of two large concentric cylinders. Structural problems are usually a concern due to the

large diameter, thin wall construction that is typical of this design. Such problems are magnified with increasing engine size and diameter. Other inherent difficulties include maintenance and parts replacement. The major advantage of this type of combustor, especially in aircraft applications, is its effective use of available space.

The canannular type of combustor is a combination of the can and the annular. It consists of inner and outer combustion casings mounted coaxially about the engine axis, in addition to several cylindrical combustion cans mounted within the annular housing. This design reduces the structural problems found in the annular design and in general experiences a lower pressure drop than the can design.

The stationary application has spurred several new designs in combustors, primarily because of the absence of the geometry constraints in aircraft turbines. Chief among these developments has been the vertical combustor. These are typically very large, modified versions of the can design which are mounted vertically.

In the vertical combustor, fuel is introduced by a fuel nozzle which creates a highly atomized, accurately shaped pattern to facilitate rapid mixing and high combustion efficiency. The two basic nozzle designs are known as the simplex and duplex. The simplex nozzle is generally unable to provide satisfactory spray patterns under varying conditions but is entirely adequate for continuous loads, while the duplex nozzle is capable of optimizing spray patterns to suit the operating conditions and is preferred for varying load conditions.

Burner performance is determined by the interaction of several operating variables and various design factors. The operating variables are:

- pressure
- inlet air temperature
- fuel/air ratio
- flow velocity

Important design factors are:

- methods of air distribution
- physical dimensions of the combustor
- fuel/air operating ranges
- fuel nozzle design

The interrelationships between these operating and design variables must be exploited in order to optimize the performance of the combustor.

Turbine Types

Following their formation in the combustor, the exhaust products enter and expand through the turbine. The extracted energy is used to drive the compressor and other turbine accessories, including generators and pumps.

Two turbine designs exist:

- axial flow
- radial inflow

The axial flow turbine is the most widely used of the two designs and consists of one or more turbine rotors and an accompanying set of stationary vanes. These vanes, sometimes called the turbine nozzle, are configured so that the gas is discharged directly onto the turbine blades.

The radial inflow turbine is less common than the previous type, but smaller units are gaining in popularity. In this design, the gas flows through peripheral nozzles and enters the wheel passages in an inward, radial direction. The primary advantages of this type of turbine are its ruggedness and ease of manufacture relative to the axial flow design.

3.2.1.3 Operating Characteristics

In simple-cycle gas turbines, the optimum pressure ratio increases substantially with increasing turbine inlet temperature. For instance, for a turbine inlet temperature of 1256K, which is close to current practice, the optimum pressure ratio is about 18:1 and the cycle efficiency is approximately 30 percent. At 1922K, the optimum simple cycle pressure ratio

increases to over 30:1. The corresponding cycle efficiency is of the order of 40 percent, which is comparable to the efficiency of current steam power plants.

Substantially higher thermal efficiencies can be achieved at much lower cycle pressure ratios by means of regeneration. The thermal efficiency of current steam power plants can be matched with regenerative gas turbines operating at a turbine inlet temperature of about 1367K and a regenerator effectiveness of 90 percent. Under these conditions, the optimum pressure ratio is only about 4:1.

Predicted combustor inlet temperatures for simple-cycle gas turbines are presented in Figure 3-2 as a function of compressor pressure ratio. The data are based on a compressor efficiency of 86 percent, a turbine efficiency of 88 percent, and an ambient temperature of 289K. For the region of interest, the combustor inlet temperature of simple-cycle gas turbines varies between about 672K and 811K.

The combustor inlet temperatures of regenerative-cycle gas turbines are depicted in Figures 3-3 and 3-4 for regenerator effectiveness values of 90 percent and 70 percent, respectively. Because of the high degree of regeneration, the temperatures are substantially higher than those of the simple-cycle gas turbines. The curves of Figures 3-3 and 3-4 are based on the same turbomachinery efficiencies used in the simple-cycle calculations and a combined regenerator and combustor pressure loss of 4 percent of the compressor discharge pressure.

Predicted air/fuel ratios for natural gas are presented in Figure 3-5 for both simple-cycle and regenerative cycle gas turbines. As expected, the required air/fuel ratio decreases with increasing turbine inlet temperature and decreasing degree of regeneration.

3.2.2 Supercharged Boilers

A supercharged boiler cycle refers to a system where a steam boiler is operated in conjunction with a gas turbine in such a manner that combustion air for the boiler comes from a compressor driven by a gas turbine which, in turn, is driven by the expansion of the combustion gases leaving the boiler.

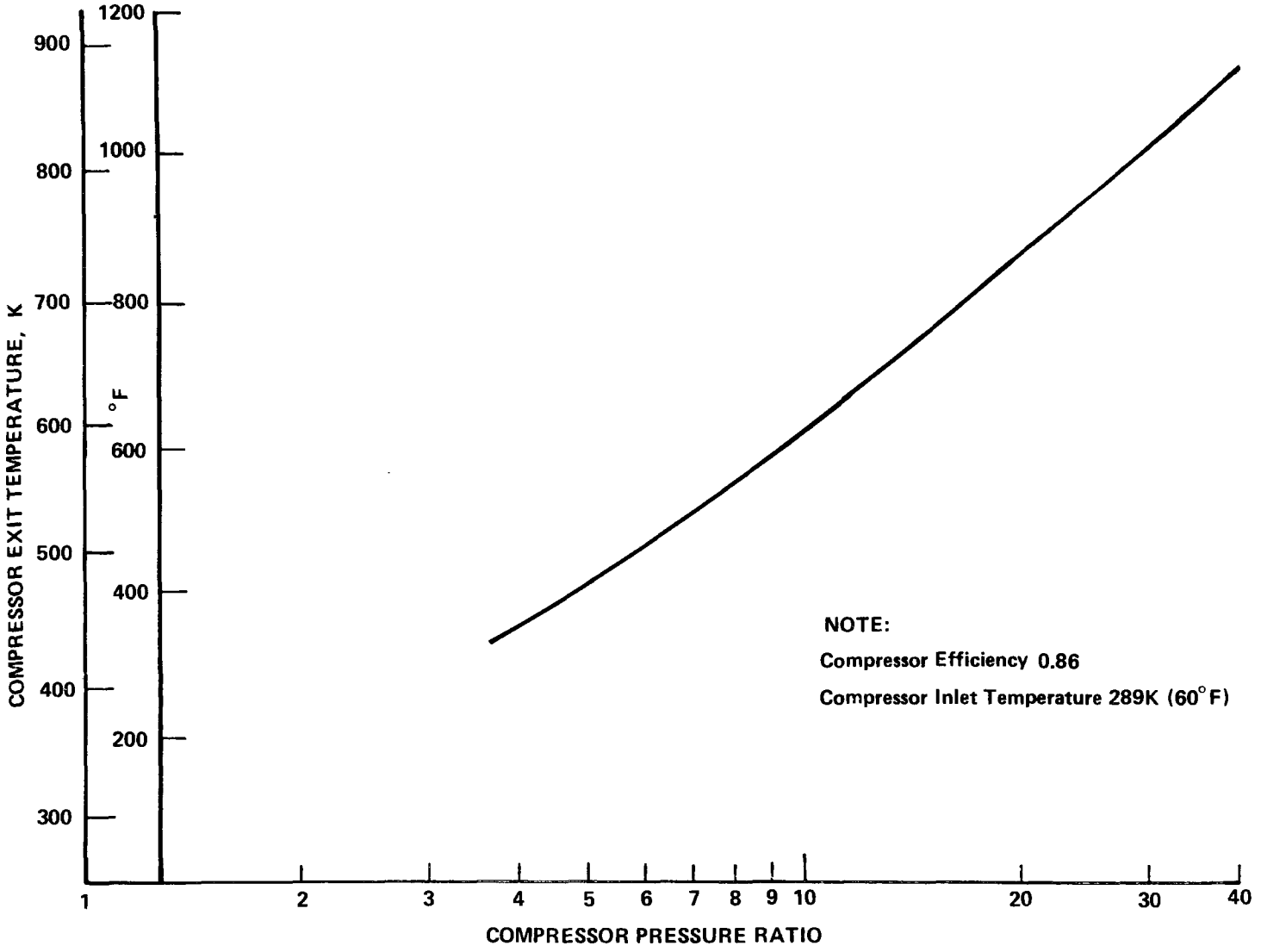

Figure 3-2. Simple cycle gas turbine combustor inlet temperature vs compressor pressure ratio.

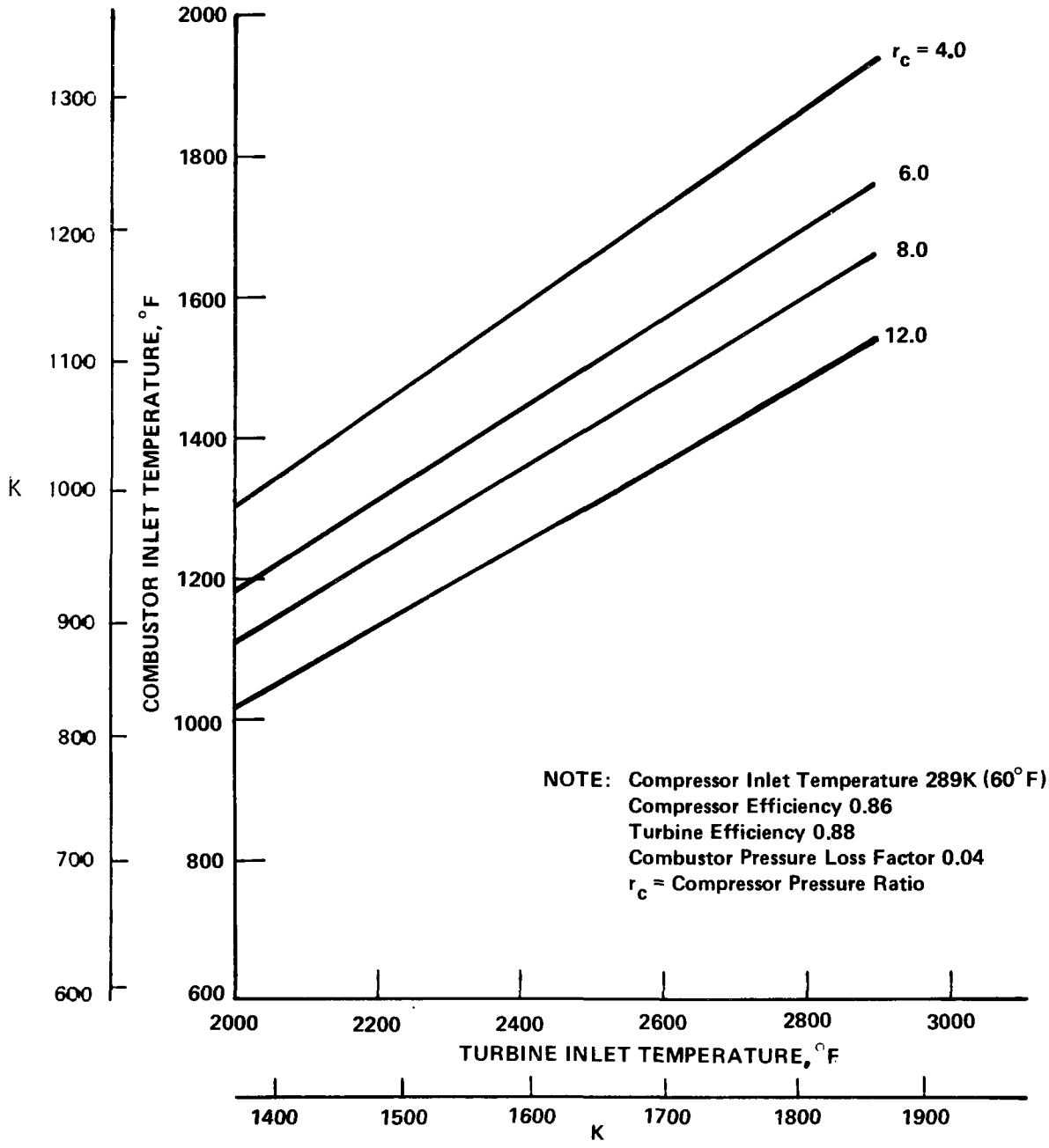

Figure 3-3. Regenerative-cycle gas turbine combustor inlet temperature vs turbine inlet temperature-regenerator effectiveness 0.90.

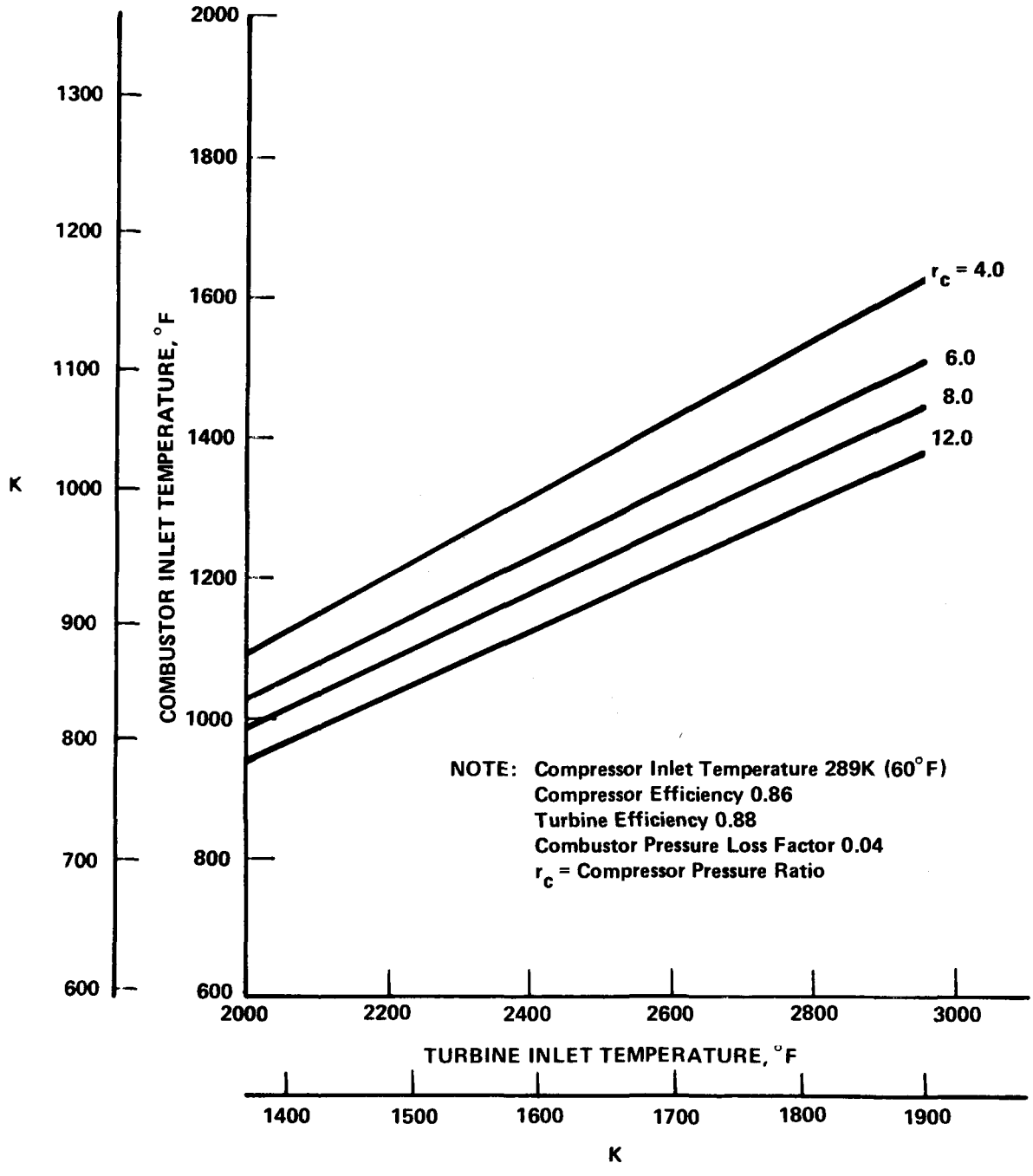

Figure 3-4. Regenerative-cycle gas turbine combustor inlet temperature vs turbine inlet temperature-regenerator effectiveness 0.70.

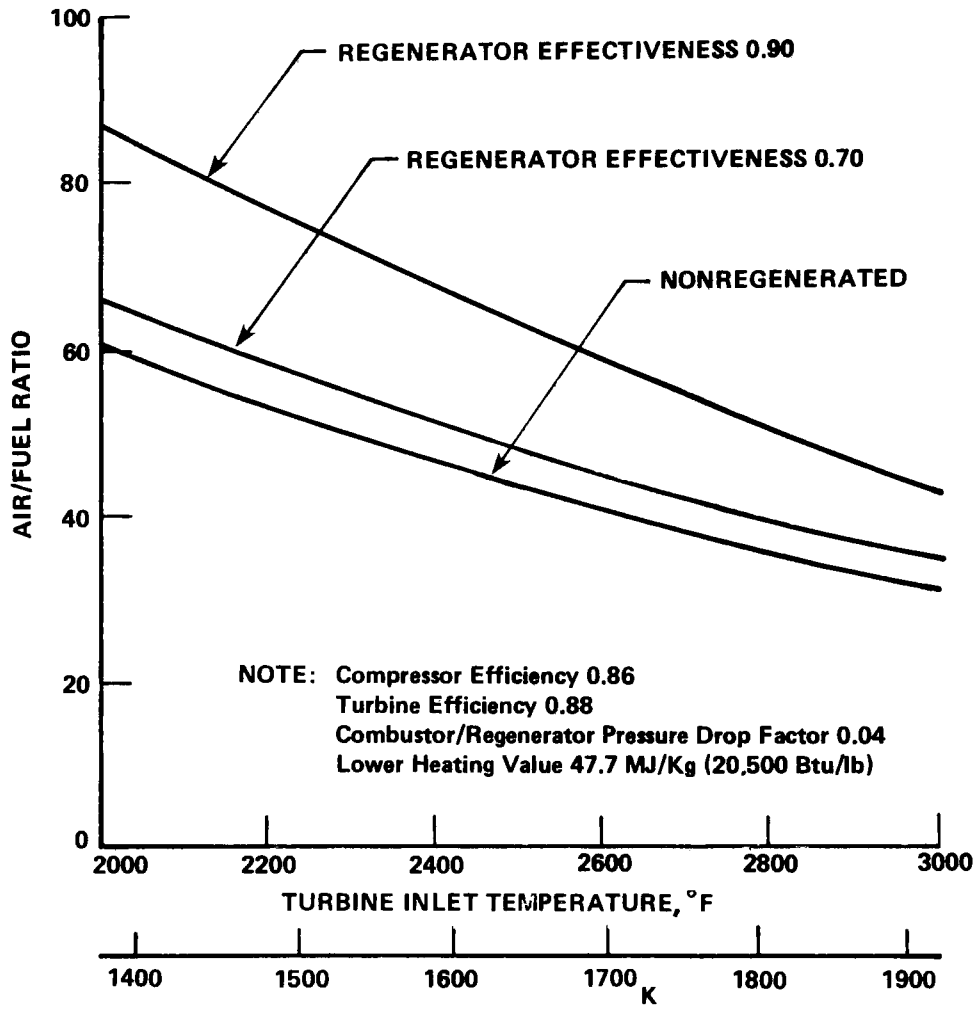

Figure 3-5. Predicted air/fuel ratio vs turbine inlet temperature (natural gas).

There are two types of supercharged cycles, differing by the operation of the gas turbine. The first is termed the self-sustaining cycle and is similar to the Velox system where the gas turbine drives only the compressor. In the second type, called the power cycle, the gas turbine generates electrical power as well as driving the compressor.

The self-sustaining cycle is of special interest to the marine industry due to its compact size. Because of its improved cycle efficiency, the power cycle is of particular interest in large operating stations.

In general, the supercharged power cycle has several advantages over conventional steam boilers. Primary among them are:

- A 5- to 9-percent improvement in plant heat rate over that of a conventional cycle of equivalent rating and steam conditions
- Greatly reduced boiler size and weight
- Improved load response and reduced starting time
- Savings in piping due to closer equipment grouping (Reference 3-3)

The Foster Wheeler Corporation has been the leading figure in the development and manufacture of the supercharged boiler. Both Foster Wheeler and the Sulzer Company in Europe have seriously investigated the adaptation of the supercharged cycle to electrical power generation, with the latter company having built several European pilot plants (Reference 3-4).

As discussed previously, marine applications have been of primary interest for the self-sustaining cycle. Figure 3-6 shows the Foster Wheeler unit as presently installed in several destroyer escort (DE) class naval vessels, and Figure 3-7 shows the cycle schematically.

A schematic of the power cycle for supercharged boilers is given in Figure 3-8. The plant utilizes a gas turbine which drives an electrical generator in addition to the combustion air compressor, while the steam turbine drives a 400 Mw generator. Fuels for both cycles are limited to natural gas, fuel oil, and other clean fuels.

The design of the supercharged boiler differs from the conventional boiler in that it must contain the relatively high pressure combustion gases.

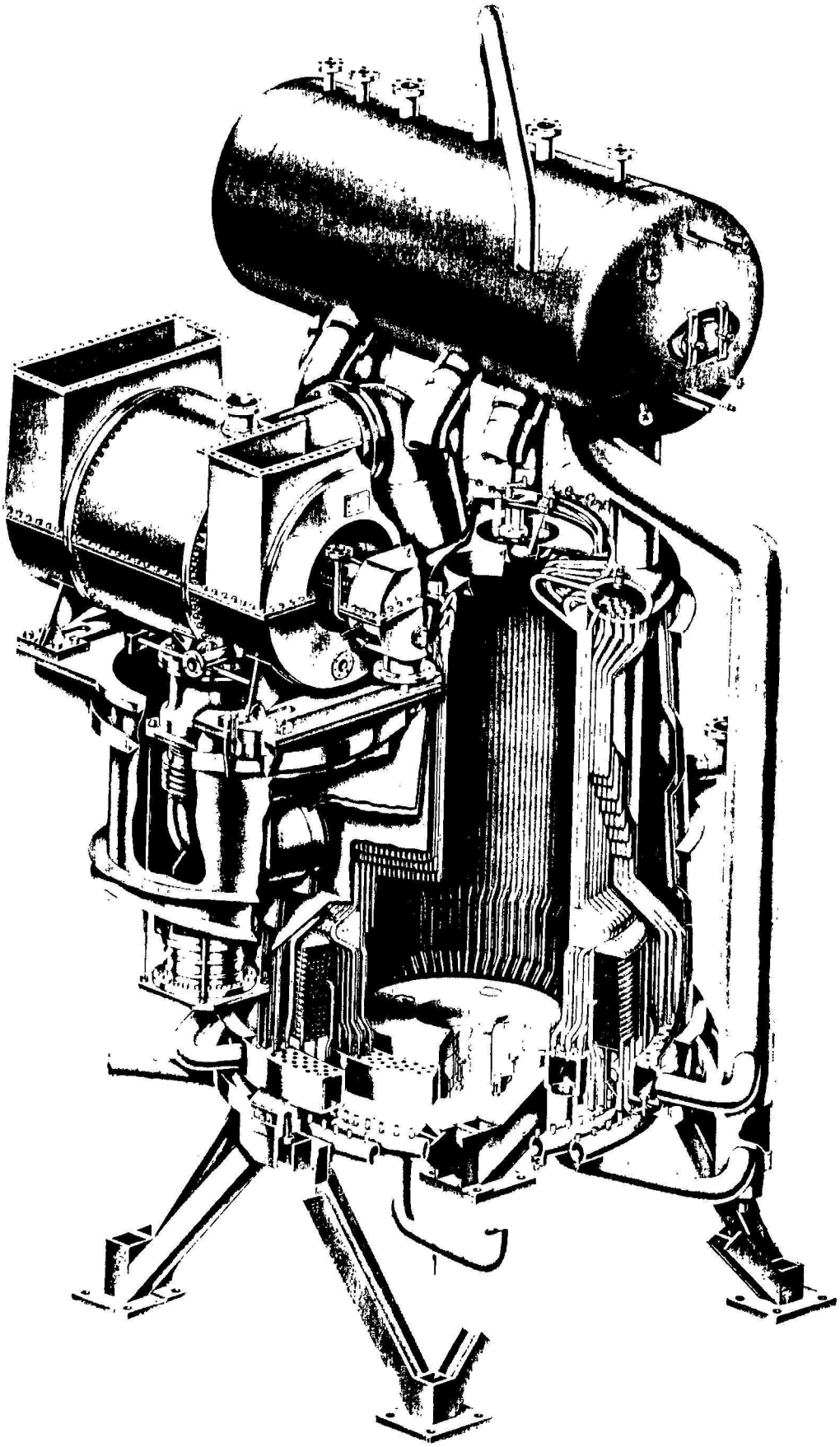

Figure 3-6. Marine supercharged boiler.

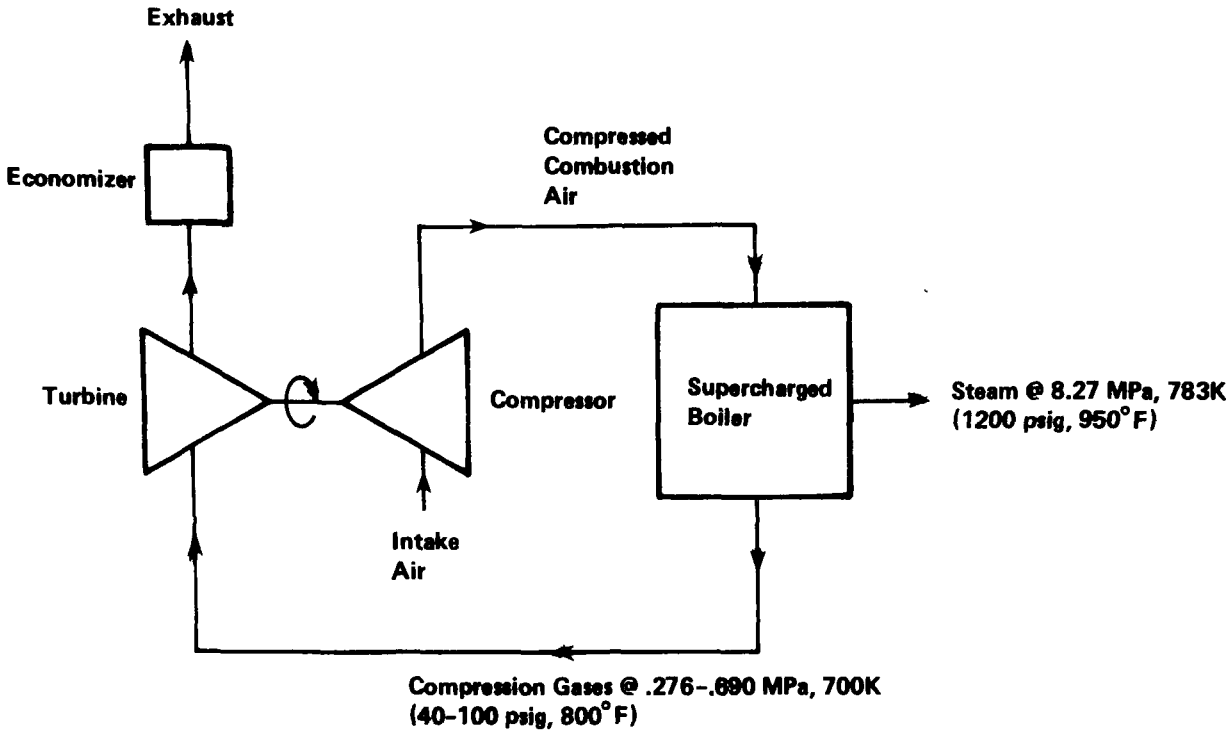

Figure 3-7. The self-sustaining supercharged cycle.

This constraint generally results in a multi-walled, cylindrical shell design. Also, supercharged boilers are smaller and lighter than conventional ones, due mainly to the higher heat transfer rates. An increased average furnace temperature as well as the increased emissivity of the combustion products due to higher pressure cause the higher transfer rate. Heat transfer surface areas are reduced to about one-third of conventional boilers.

While little general data exist on the operating characteristics of supercharged boilers, some data on specific units is available. Full load performance figures for a gas-fired self-sustaining supercharged cycle, in addition to selected physical data, is presented in Table 3-4.

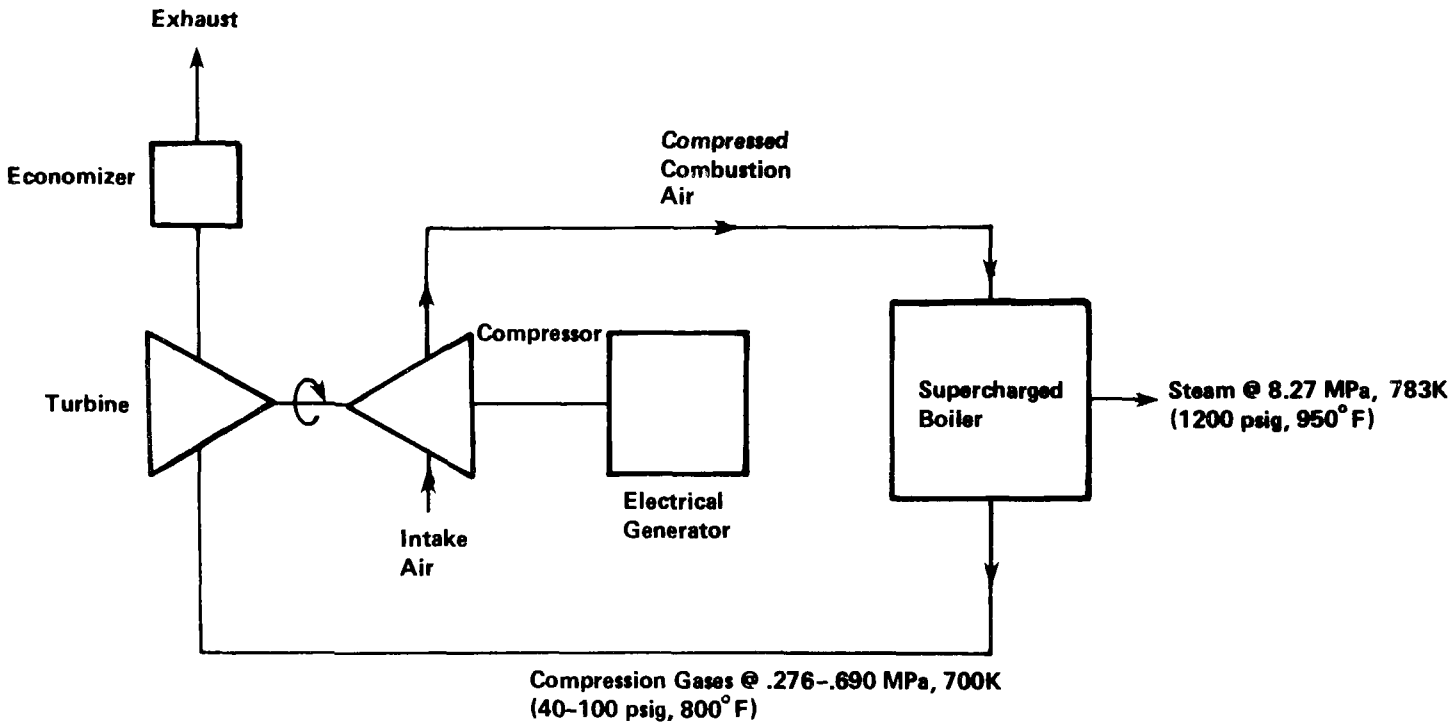

Figure 3-8. The power supercharged cycle.

At the outset, it appears that the compact heat transfer configuration of this type of boiler predisposes it to the application of catalytic combustion concepts. No requirement seems to exist for the large catalytic surface area that earlier investigators identified as a necessity for utility boiler applications. The feasibility of high pressure catalytic combustion has been demonstrated by other programs in catalytic combustion (References 3-6, 3-7).

3.3 AIR POLLUTANT EMISSION CHARACTERISTICS

Emissions data for stationary fuel burning equipment has been the subject of several recent studies. The most recent year for which complete fuel consumption data is available is 1974. Figure 3-9 gives the distribution of anthropogenic NO_x emissions for 1974, showing that gas turbine NO_x emissions

TABLE 3-4. SUPERCHARGED BOILER FULL LOAD PERFORMANCE FIGURES (Reference 3-5)

Steam Flow	126,100 Kg/hr (278,000 lb/hr)
Superheater Outlet Pressure	8.72 M Pa (1250 psig)
Superheater Outlet Temperature	783 K (950 °F)
Total Air Flow	157,800 Kg/hr (348,000 lb/hr)
Boiler Air Flow	154,400 Kg/hr (340,480 lb/hr)
Afterburner Air Flow	3410 Kg/hr (7520 lb/hr)
Air Pressure	0.59 M Pa (86.0 psia)
Air Temperature	535 K (503 °F)
Excess Air	10%
Total Fuel Flow	9741 Kg/hr (21,476 lb/hr)
Boiler Fuel Flow	9530 Kg/hr (21,014 lb/hr)
Afterburner Fuel Flow	210 Kg/hr (462 lb/hr)
Gas Leaving Afterburner	1061 K (1450 °F)
Gas Flow to Turbine	167,557 Kg/hr (369,476 lb/hr)
Net Heat to Furnace (LHV + Air)	4.49×10^{11} J/hr (425.2×10^6 Btu/hr)
Net Heat Release Per Cu. Ft. Furnace Volume	7.23×10^8 J/hr (685,000 Btu/hr)
Net Heat Release Per Sq. Ft. Projected Furnace Envelope	1.15×10^9 J/hr (1.09×10^6 Btu/hr)
Furnace Radiant Heat Absorption Per Sq. Ft. Projected Surface	2.24×10^8 J/hr (211,900 Btu/hr)

account for 2.9 percent of the total. Table 3-5 shows emission inventory results for other pollutants as a function of equipment type. The relatively low contribution of SO_x emissions from gas turbines is indicative of the fuel types used.

Table 3-6 ranks equipment/fuel combinations by annual, nationwide NO_x emissions and lists corresponding rankings for these combinations by fuel consumption and emissions of criteria pollutants. Although over 70 equipment/fuel combinations were inventoried (Reference 3-8), the 30 most significant

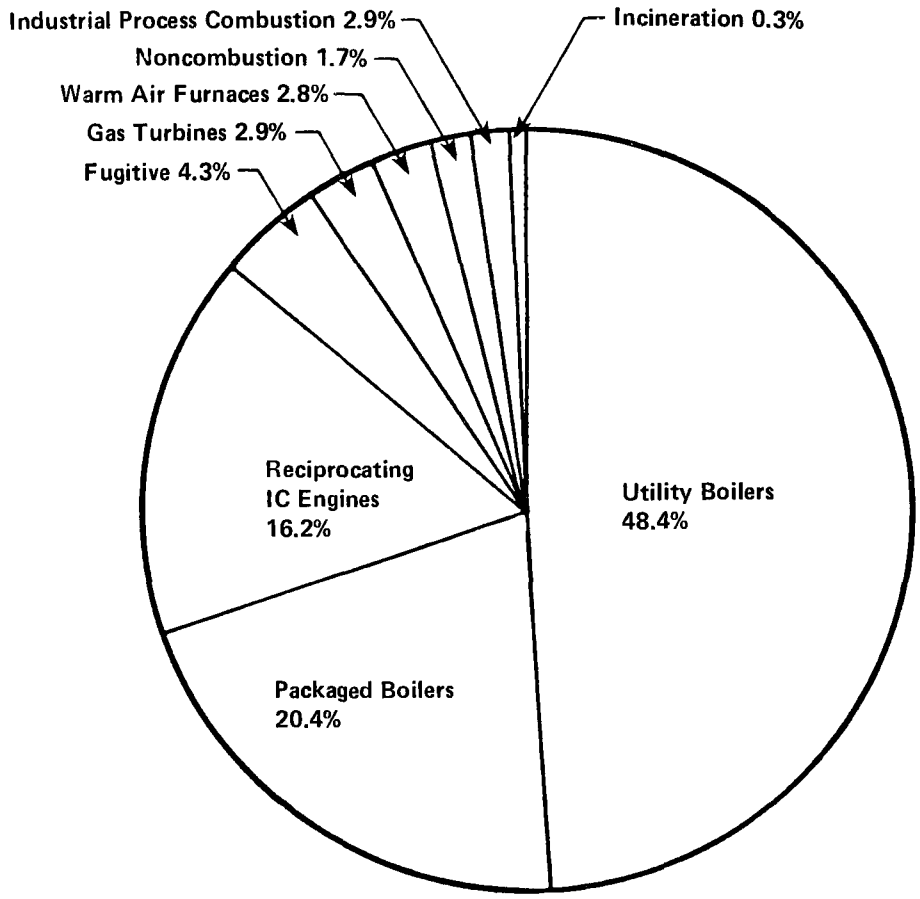

1974 Stationary Combustion Source NO_x Emissions

	1,000 Mg	1,000 Tons	Percent Total
Utility Boilers	5,553	6,116	48.4
Packaged Boilers	2,345	2,583	20.4
Warm Air Furnaces	321	353	2.8
Gas Turbines	338	372	2.9
Reciprocating IC Engines	1,857	2,045	16.2
Industrial Process Combustion	333	367	2.9
Noncombustion	193	212	1.7
Incineration	40	44	0.3
Fugitive	498	548	4.3
TOTAL	11,478	12,640	100

Figure 3-9. Distribution of stationary anthropogenic NO_x emissions for the year 1974 (stationary fuel combustion: controlled NO_x levels).

TABLE 3-5. 1974 SUMMARY OF AIR AND SOLID POLLUTANT EMISSION FROM STATIONARY FUEL BURNING EQUIPMENT (1000 Mg)

	NO_x [b]	SO_x	HC	CO	Part	Sulfates	POM	Dry Ash Removal	Sluiced Ash Removal
Utility Boilers	5,553	16,768	29.5	270	5,965	231	0.01 – 1.2	6.18	24.78
Packaged Boilers	2,345	6,420	72.1	175	5,221	146	0.2 – 67.8	4.41	1.07
Warm Air Furnaces & Misc. Comb.	321	232	29.7	132.6	39.3	6.4	0.06	--	--
Gas Turbines	338	10.5	13.7	73.4	17.3	[a]	[a]	--	--
Recip. IC Engines	1,857	19.6	578	1,824	21.5	[a]	[a]	--	--
Process Heating	333	622	166	9,079	4,861	[a]	[a]	--	--
TOTAL	10,747	24,122	889	11,554	16,125	382	69	--	--

[a] No emission factor available

[b] Controlled NO_x

[c] Based on 80 percent hopper and flyash removal by sluicing methods; 20 percent dry solid removal

TABLE 3-6. NO_x MASS EMISSION RANKING OF STATIONARY COMBUSTION EQUIPMENT AND CRITERIA POLLUTANT AND FUEL USE CROSS RANKING

	Sector	Equipment Type	Fuel	Annual NO_x Emissions (Mg)	Cumulative (Mg)	Cumulative (Percent)	Fuel Rank	SO_x Rank	CO Rank	HC Rank	Part Rank
1	Utility Boilers	Tangential	Coal	1,410,000	1,410,000	13.1	1	1	7	16	2
2	Reciprocating IC Engines	>270 MJ/hr/cyl	Gas	1,262,000	2,672,000	24.8	21	>30	4	1	>30
3	Utility Boilers	Wall Firing	Coal	946,000	3,618,000	33.5	3	2	6	23	5
4	Utility Boilers	Cyclone Furnace	Coal	863,500	4,481,500	41.5	6	3	12	9	13
5	Utility Boilers	Wall Firing	Gas	738,300	5,219,800	48.4	4	>30	13	28	>30
6	Utility Boilers	Wall Firing	Oil	481,000	5,700,800	52.8	8	9	17	27	18
7	Utility Boilers	Horizontally Opposed	Gas	378,700	6,079,500	56.3	14	>30	24	>30	>30
8	Reciprocating IC Engines	270 MJ/hr - 270 MJ/hr/cyl	Oil	325,000	6,404,500	59.4	>30	>30	3	3	26
9	Packaged Boilers	Watertube >105 GJ/hr	Gas	318,500	6,723,000	62.3	16	>30	29	19	>30
10	Packaged Boilers	Watertube Stoker >105 GJ/hr	Coal	278,170	7,001,170	64.9	7	4	11	4	1
11	Utility Boilers	Horizontally Opposed	Coal	270,800	7,271,970	67.4	23	5	>30	>30	7
12	Packaged Boilers	Watertube >105 GJ/hr	Oil	232,480	7,504,450	69.5	26	16	>30	26	22
13	Utility Boilers	Tangential	Oil	208,000	7,712,450	71.5	12	10	27	>30	19
14	Packaged Boilers	Firetube Scotch	Oil	203,990	7,916,440	73.4	11	11	>30	>30	16
15	Packaged Boilers	Watertube <105 GJ/hr	Gas	180,000	8,096,440	75.0	5	>30	>30	22	>30
16	Utility Boilers	Horizontally Opposed	Oil	177,900	8,274,340	76.7	>30	17	>30	>30	27
17	Packaged Boilers	Watertube <105 GJ/hr	Coal	164,220	8,438,560	78.2	>30	8	>30	>30	9
18	Industrial Process Comb.	Forced & Natural Draft Refinery Heaters	Oil	147,350	8,585,910	79.6	>30	29	>30	18	21
19	Utility Boilers	Tangential	Gas	146,000	8,731,910	80.9	13	>30	>30	>30	>30
20	Packaged Boilers	Firetube Firebox	Oil	139,260	8,871,170	82.2	17	13	>30	>30	20

TABLE 3-6. Concluded

Sector	Equipment Type	Fuel	Annual NO_x Emissions (Mg)	Cumulative (Mg)	Cumulative (Percent)	Fuel Rank	SO_x Rank	CO Rank	HC Rank	Part Rank
21 Packaged Boilers	Watertube Stoker	Coal	125,350	8,996,520	83.4	>30	7	28	29	8
22 Gas Turbines	13.5 - 54 GJ/hr	Oil	118,500	9,115,020	84.5	30	>30	15	14	>30
23 Packaged Boilers	Watertube <105 GJ/hr	Oil	116,430	9,231,450	85.6	27	15	>30	>30	23
24 Warm Air Furnaces	Central	Gas	106,300	9,337,750	86.5	2	>30	10	8	25
25 Packaged Boilers	Firetube Stoker <105 GJ/hr	Coal	102,040	9,439,790	87.5	29	6	>30	10	6
26 Packaged Boilers	Firetube Scotch	Gas	98,010	9,537,800	88.4	19	>30	>30	>30	>30
27 Gas Turbines	>54 GJ/hr	Oil	97,400	9,635,200	89.3	>30	>30	>30	30	>30
28 Reciprocating IC Engines	>270 MJ/hr/cyl	Oil	94,000	9,729,200	90.2	>30	>30	22	13	>30
29 Industrial Process Comb.	Forced & Natural Draft Refinery Heaters	Gas	92,608	9,821,808	91.0	15	>30	>30	7	30
30 Utility Boilers	Vertical and Stoker	Coal	90,900	9,912,708	91.9	>30	12	>20	>30	>10

combinations account for over 90 percent of the NO_x emissions. The ranking of a specific equipment/fuel type depends both on total installed capacity and emission factors. A high ranking, therefore, does not necessarily imply that a given source is a high emitter; large installed capacity may offset a low emission factor to give the high ranking. In general, coal-fired sources rank high in SO_x and particulate emissions, while IC engines rank high in emissions of CO and hydrocarbons.

Because of the extremely low population of supercharged boilers, no emissions data for this equipment class is available.

3.4 CONCLUSIONS

The characterization of residential furnaces and commercial and industrial boilers was reported in Reference 3-2. This characterization was extended to gas turbine and supercharged boilers in Section 3.2. Based upon this characterization of area sources, the principal conclusions regarding catalytic combustion redesign or retrofit are:

- The gas turbine combustor is well suited to a catalytic combustor redesign/retrofit because it operates with considerable excess air and uses clean gaseous or light distillate fuels.
- No theoretical barriers exist for a catalytic combustor redesign/retrofit on warm air residential gas- or oil-fired furnaces. These systems are ordinarily not maintained closely, but they may represent a good system for early application of catalytic combustors.
- Scotch firetube industrial boilers appear to offer some advantages to a catalytic combustor retrofit due to their unique internal, first pass furnace volume.
- Watertube boilers appear to offer very little hope for a catalytic combustor retrofit, but would be adaptable to a redesigned system using compact heat exchangers.
- The limitation of catalytic combustors to systems burning only clean, sulfur-free gases or oils may not be necessary. Further work to establish the need for fuel prevaporization is required.

REFERENCES

3-1. Roessler, W. U., et al., "Investigation of Surface Combustion Concepts for NO_x Control in Utility Boilers and Stationary Gas Turbines," Environmental Protection Technology Series Report EPA-650/2-73-014, August 1973.

3-2. Kesselring, J. P., et al., "Catalytic Oxidation of Fuels for NO_x Control From Area Sources," Environmental Protection Technology Series Report EPA-600/2-76-037, February 1976.

3-3. Daman, E. L., and Zoschak, R. J., " Supercharged Boiler Design, Development, and Application," presented at the Eighteenth Annual Meeting of the American Power Conference, March 1956.

3-4. Aquet, E., "Technical and Economic Advantages of Combined Gas Turbine and Steam Power Stations," Sulzer Bros. Technical Review No. 3/0315/ Aq. BG-MS, 1971.

3-5. Zoschak, R. J., and Gorzegno, W. P., "The Supercharged Unit -- A Projection of Experience," presented at the Pacific Coast Electrical Association Engineering and Operating Conference, Los Angeles, March 1965.

3-6. Blazowski, W. S., and Bresowar, G. E., "Preliminary Study of the Catalytic Combustor Concept as Applied to Aircraft Gas Turbines," Technical Report AFAPL-TR-74-32, Air Force Aero Propulsion Laboratory, May 1974.

3-7. De Corso, S. M., et al., "Catalysts for Gas Turbine Combustors -- Experimental Test Results," J. Eng'g for Power, vol. 99A, pp. 159-167 (1977).

3-8. "Environmental Assessment of Stationary Source NO_x Control Technologies -- First Annual Report," Aerotherm Report TR-77-58, July 1977.

SECTION 4

CATALYST MATERIALS REVIEW

This section provides a review of the characteristics and properties of currently available catalyst materials. In particular, properties of monolithic supports, washcoat substrates, and catalyst coatings are reviewed. This discussion provides the background to assess the current state of the art in catalyst materials for combustion applications.

4.1 GENERAL CONSIDERATIONS

An earlier review of catalyst materials which are suitable for the oxidation of hydrocarbon and other fuels was reported in Reference 4-1. This review included information on

- Support types, including monolithic ceramics, pellets, and ceramic fiber pads
- Substrate materials used as washcoats on monolithic ceramics
- Catalyst coatings which were known to be active in lower-temperature oxidation processes
- Temperature capability of the catalyst/substrate/support system
- Poisoning effects which were known to be deleterious to catalyst materials at lower temperatures.

To obtain maximum performance from a catalytic combustion system, the system materials should have the following properties:

- A catalyst coating capable of igniting fuel/air mixtures at the lowest possible temperature (low lightoff temperature),
- A catalyst coating of sufficient activity to maintain complete combustion conditions in the bed at the lowest possible values of combustion air preheat,

- A catalyst coating of sufficient activity to maintain complete combustion conditions in the bed at the highest possible values of mass throughput,
- A washcoat substrate capable of maintaining high surface areas (~10 m^2/g of monolith plus washcoat) under high temperature (>1370K) combustion conditions, and
- A catalyst/washcoat/support system which maintains the catalyst in a highly dispersed form under high temperature conditions, which is capable of operation at temperatures in excess of 1755K without thermal degradation or complexing of the materials, and which does not exhibit thermal shock.

The identification of a single catalyst system that is capable of the performance indicated above is probably not possible. The identification of desirable system properties which are not necessary for good performance is therefore of high priority.

For catalyst systems operating in the combustion mode (high bed temperatures and mass throughputs), the monolithic honeycomb support is superior to the pellet support in terms of both catalyst volume required and pressure drop. The fiber pad support, while used successfully for clean, prevaporized fuels as described in Section 2, is not suitable for partially vaporized fuels or pressure-drop limited systems. Therefore, the primary support material reviewed in this study is the monolithic honeycomb.

4.2 CHARACTERISTICS AND PROPERTIES OF CATALYST MATERIALS

The performance of any catalytic system depends on many factors in addition to the intrinsic catalytic properties of the active substance. In addition to the catalytic properties, the important factors include the thermal, structural, and chemical properties of catalyst, substrate, and support materials.

4.2.1 Monolithic and Cylindrical Supports

The support serves three important functions in a catalyst system:

- It increases surface area of the active metal or metal oxide by providing a matrix that stabilizes the formation of very small particles.

- It increases thermal stability of these very small particles, thus preventing agglomeration and sintering with consequent loss of active surface.
- In some cases, it provides catalytic activity due to special properties of the support.

The monolithic honeycomb is the most technologically advanced support for purposes of catalytic combustion. Monolithic supports are composed of small parallel channels, available in a variety of shapes and hydraulic diameters. These structures may be in the form of honeycombed ceramics extruded in one piece, oxidized aluminum alloys in rigid cellular configurations, or multilayered ceramic or metal corrugations. The channels in honeycomb-like structures have hydraulic diameters of 1 to 7 mm. Materials of fabrication are usually low surface area ceramics, although metal monoliths are now being made to overcome the thermal shock and material stability problems sometimes encountered in the use of ceramics (Reference 4-2). Table 4-1 lists some of the properties of high temperature ceramics.

As shown in Table 4-1, the most common high temperature ceramic family is alumina. For strengthening purposes, the alumina is alloyed with silica and/or chromium. Aluminas are relatively inexpensive, reasonably resistant to thermal shock, and can operate to high (>1756K) temperatures. Beryllia ceramics are about as strong as aluminas and have excellent thermal shock resistance but are highly toxic. This latter property makes them undesirable for many applications. Zirconia ceramics can be used at temperatures up to 2480K, the highest use temperature of all ceramics. Zirconia is extremely inert to most metals, even at high temperatures, making it attractive as a support for metal oxide catalysts.

The so-called "glass ceramics" are composed of large proportions of several metal oxides that form complex microstructures. The three common glass ceramics are:

1) Lithium-aluminum-silicate, or beta spodumene ($Li_2O \cdot Al_2O_3 \cdot 4SiO_2$)
2) Magnesium-aluminum-silicate, or cordierite ($2MgO \cdot 2Al_2O_3 \cdot 5SiO_2$)
3) Aluminum-silicate, or mullite ($3Al_2O_3 \cdot 2SiO_2$)

TABLE 4-1. CERAMIC PROPERTIES (REFERENCE 4-3)

Ceramic Family	Material Cost	Thermal Shock Resistance	Thermal Strength	Thermal Conductivity	Other
Alumina	Low	Fair	Good	Low	Most common high-temperature ceramic
Beryllia	High	Excellent	Good	High	Highly toxic
Zirconia	Moderate-High	Fair-Good	Good	Low	Can be used at temperatures above 2478 K
Lithium-Aluminum-Silicate (Beta Spodumene)	Moderate	Good	Good	Low	Not resistant to sulfur, sodium
Magnesium-Aluminum-Silicate (Cordierite)	Moderate	Good	Good	Low	More corrosion resistant than LAS
Aluminum-Silicate (Aluminous Keatite or Mullite)	Moderate	Fair-Good	Good	Low	Good corrosion resistance
Silicon Carbide	Low-High	Excellent	Excellent	Low	Does not self-bond easily
Silicon Nitride	Low-High	Excellent	Excellent	Low	Does not self-bond easily
Boron Carbide	High	Fair	Poor	Low	High hardness, low density

These three ceramics are nearly as low in cost as alumina, but have very low coefficients of thermal expansion. Lithium-aluminum-silicate (LAS) is attacked by sodium and sulfur, however. Magnesium-aluminum-silicate is more corrosion resistant and also stronger. Aluminum-silicate, prepared by leaching lithium out of LAS particles prior to forming, has both good corrosion resistance and high strength.

Silicon carbide and silicon nitride are both capable of stable high temperature operation. However, self-bonding of particles of these two materials is difficult to achieve. They are usually prepared by hot pressing, giving a dense material that is resistant to thermal shock. Boron carbide, which has high hardness and low density, has low strength at high temperatures.

Manufacturers of monolith supports include American Lava Corporation, Corning Glass Works, E. I. DuPont de Nemours & Company, General Refractories Company, W. R. Grace & Company, Johnson Matthey Corporation, Norton Company, and Kentucky Metals, Inc. A variety of materials and configurations are available, and Table 4-2 presents some of the significant characteristics of the materials.

American Lava's Thermacomb corrugated ceramics are available in six different ceramic compositions, as well as in two structure types (honeycomb and split-cell). These ceramics are prepared in corrugated layers and are very rugged. Figure 4-1 shows examples of Thermacomb corrugated ceramics.

Corning Glass Works produces Celcor, a porous cordierite ceramic, in a honeycomb structure with square or triangular cells. Examples of Celcor monoliths are shown in Figure 4-2. Celcor has been extensively used as a catalyst support for controlling automotive emissions.

In addition to cordierite, Corning has prepared higher temperature ceramics in monolith configurations. Figure 4-3 shows Corning's zirconia spinel ceramic in varying cell geometries. To help suppress thermal shock, Corning has developed a flexible rectangle geometric configuration which allows the cell walls to bend rather than crack. The flexible rectangle geometry is compared to conventional square cell geometry in Figure 4-4 for a zirconia monolith.

TABLE 4-2. MONOLITHIC SUPPORT DATA

Manufacturer	Product	Ceramic	Temperature Limit, K (°F)	Thermal Shock Resistance
American Lava Corporation (3M Company)	Thermacomb 843	Lithia-Alumina-Silica	1367 (2000)	Excellent
	Thermacomb LTE	Cordierite	1478 (2200)	Excellent
	Thermacomb 795	Cordierite	1478 (2200)	Excellent
	Thermacomb 784	Zircon-Mullite	1756 (2700)	Good
	Thermacomb MD-3	Mullite	1700 (2600)	Good
	Thermacomb 614	Dense 96% Alumina	1811 (2800)	Fair
Corning Glass Works	Celcor 9475	Cordierite	1478 (2200)	Excellent
		Mullite-Alumina-Titanate	1923 (3000)	Good
		Zirconia-Spinel	1978 (3100)	Fair
E. I. DuPont de Nemours & Company	Torvex	Alumina	1773 (2732)	Fair
		Mullite	1623 (2462)	Fair
General Refractories Company	Versagrid	Cordierite	1672 (2550)	Good
		Mullite	1922 (3000)	Fair
W. R. Grace & Company	Poramic	Cordierite	1478 (2200)	Excellent
Johnson Matthey Corporation	Fecralloy Steels	--	1573 (2371)	Excellent
Norton Company	Spectramic Honeycomb RX 387	Silicon Carbide	1922 (3000)	Good
	Spectramic Honeycomb RX 384	Silicon Nitride	1811 (2800)	Good
Kentucky Metals, Inc.	Kanthal (Metal)	--	1678 (2560)	Excellent

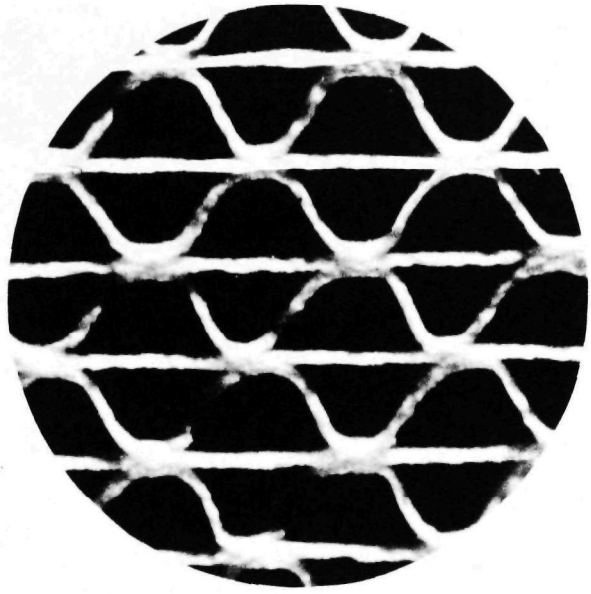

a. 8x enlargment

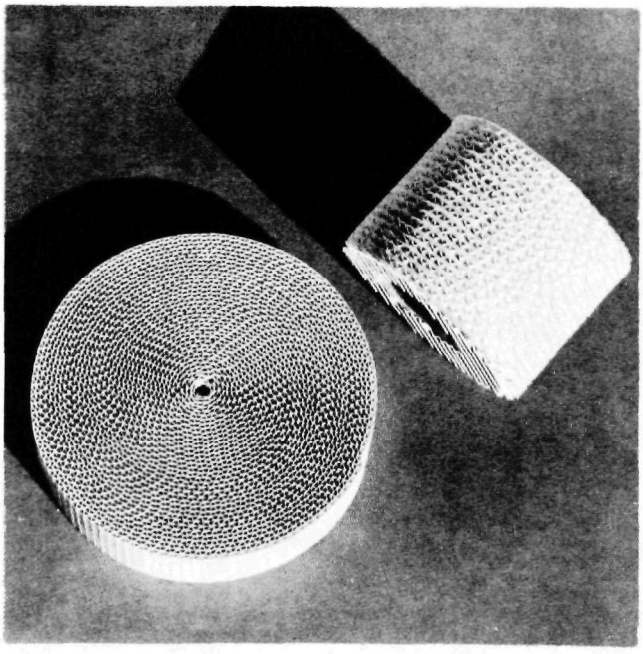

b. Rolled structures

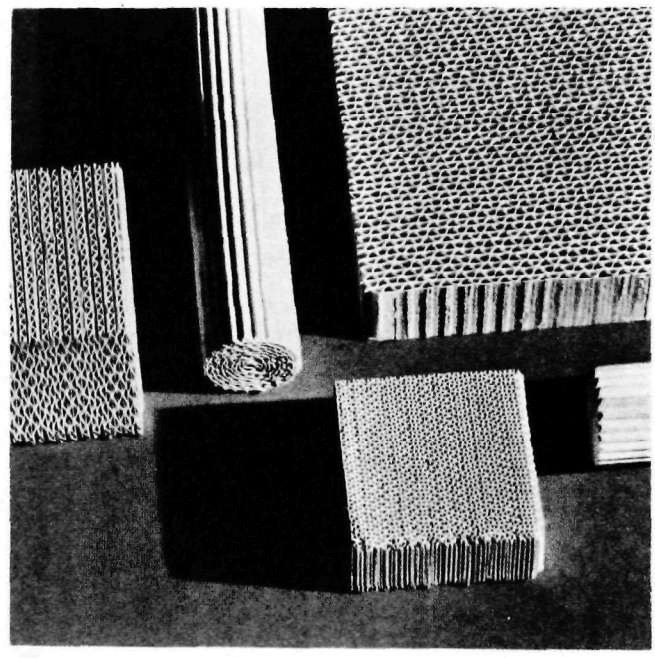

c. Rolled and stacked structures

Figure 4-1. Examples of Thermacomb corrugated ceramics, produced by American Lava Corporation.

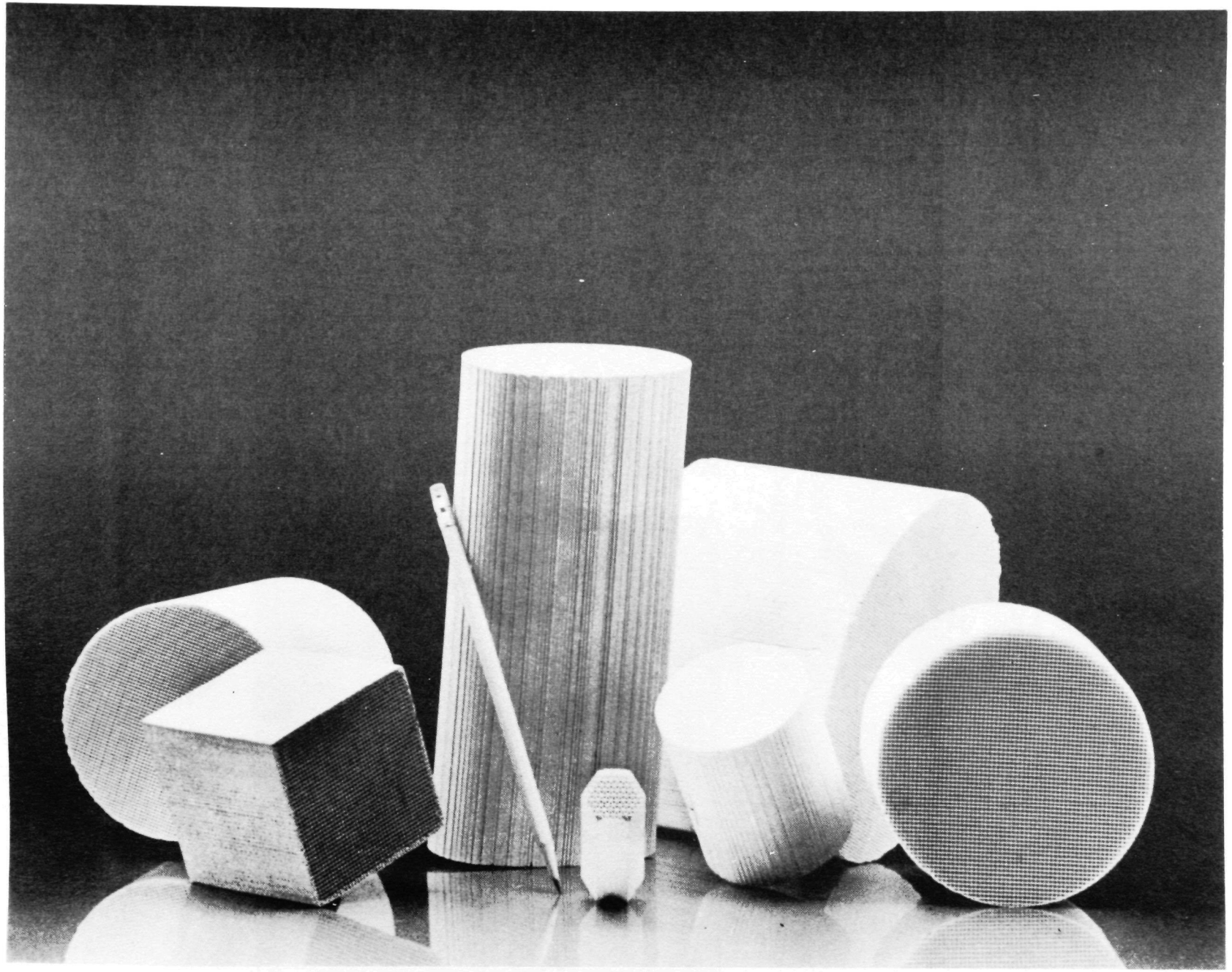

Figure 4-2. Celcor cordierite monoliths produced by Corning Glass Works.

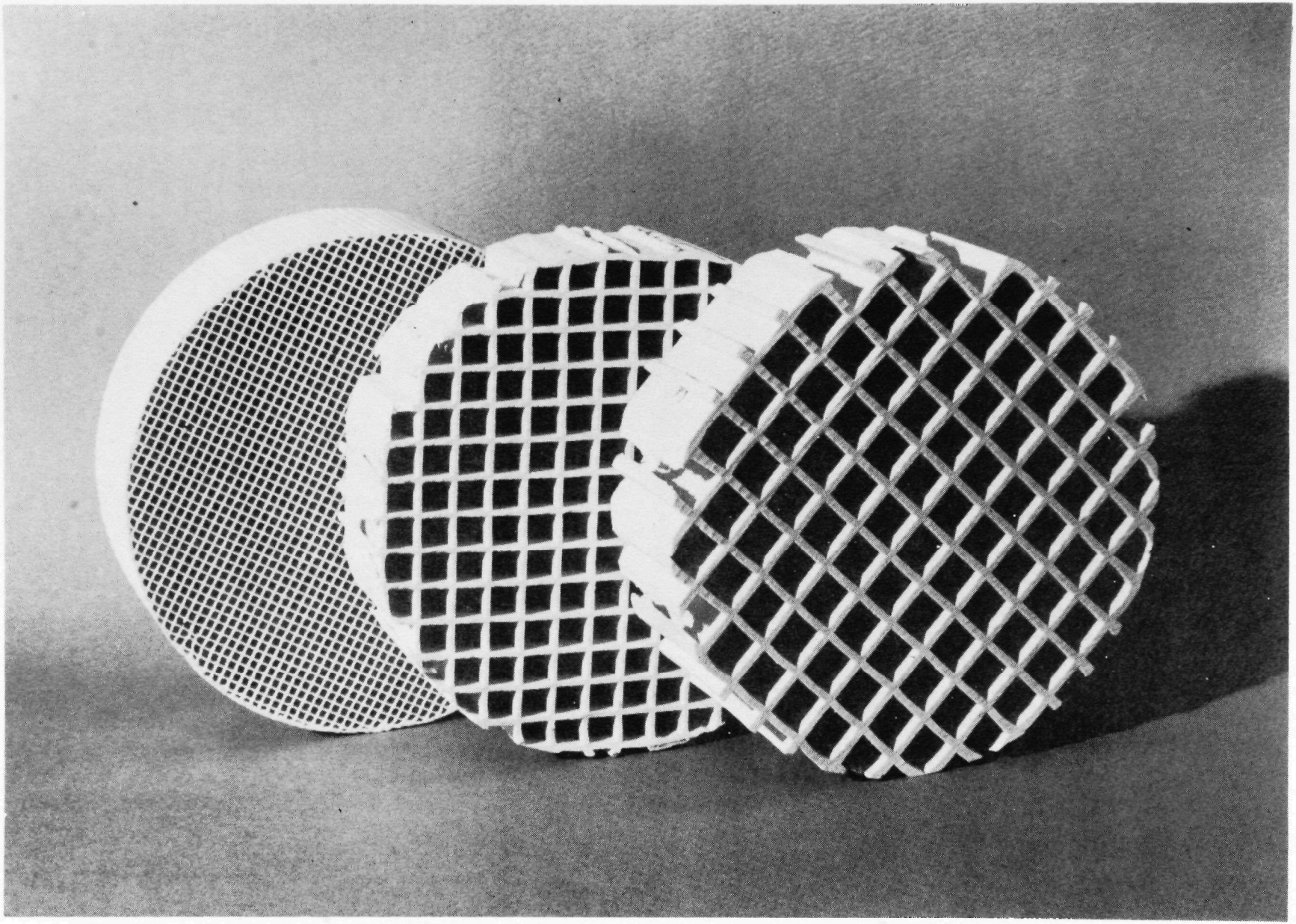

Figure 4-3. Corning high temperature graded cell ceramic.

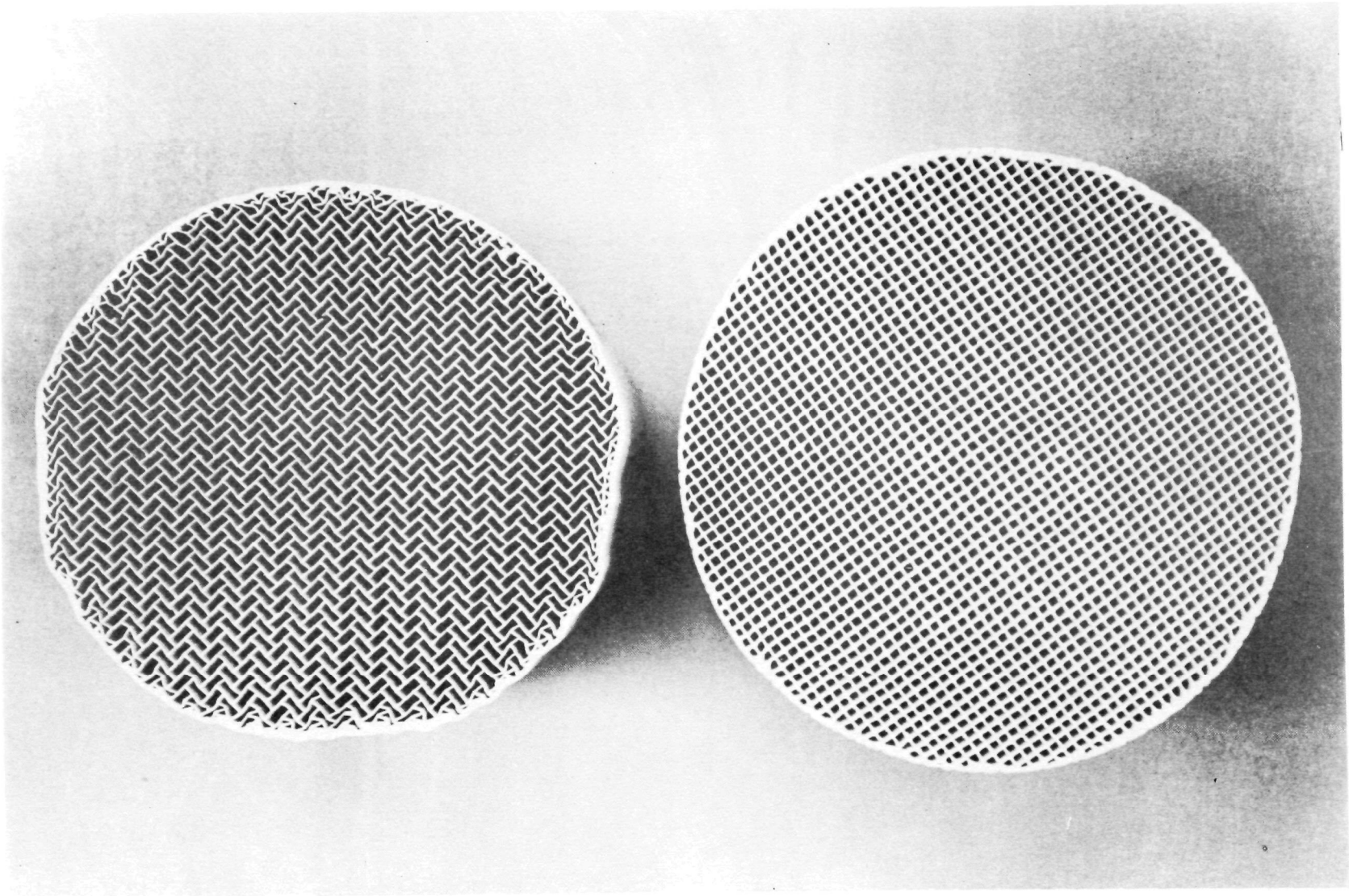

Figure 4-4. Zirconia spinel monoliths from Corning Glass Works — flexible rectangle and square cell geometries.

DuPont produces Torvex ceramic honeycomb in two compositions, alumina and mullite. Three geometric configurations (straight honeycomb, slant cell honeycomb, and cross-flow honeycomb) are available, and examples of these configurations are shown in Figure 4-5.

Versagrid ceramic honeycomb is produced by the General Refractories Company. Versagrid is available in four cell shapes (round, square, triangular, and rectangular) and two compositions (cordierite and mullite). Samples of Versagrid honeycomb are shown in Figure 4-6.

Poramic monolith structures by W. R. Grace & Company have also seen use in automotive catalytic converter systems. The ceramic components are fluxed with polyethylene and passed through rollers to form ribs on sheets of material, which are then rolled and fired as described in Reference 4-4. Examples of Poramic materials are shown in Figure 4-7.

Johnson Matthey Corporation has developed a new metal monolith for use with platinum catalysts, as described in Reference 4-2. These metal monoliths are composed of Fecralloy steels, consisting of up to 20 percent chromium, 0.5 to 12 percent aluminum, 0.1 to 3 percent yttrium, and the balance iron. They are reported to have greater resistance to thermal shock and mechanical failure than conventional ceramic monoliths.

Kentucky Metals, Inc. is also fabricating metal monolith materials, with catalyst application performed by Oxy-Catalyst, Inc. These monoliths are made from Kanthal A-1, consisting of 5.5 percent aluminum, 22 percent chromium, 0.5 percent cobalt, and the balance iron. A photograph of a catalyzed graded cell metal monolith appears in Figure 4-8.

Norton Company produces Spectramic honeycomb products in two compositions (silicon carbide and silicon nitride) and in either circular or rectangular cell shapes. The products can be supplied with the cell axis at any specified bias angle, and have high maximum use temperatures. Figure 4-9 shows Spectramic silicon carbide honeycomb.

Cylindrical supports can also be adapted to certain applications for catalytic combustion. Manufacturers of ceramic cylinders include the Coors Porcelain Company and Corning's Zircoa Products Department, as shown in Table 4-3. Coors produces mullite and alumina cylinders in sizes from

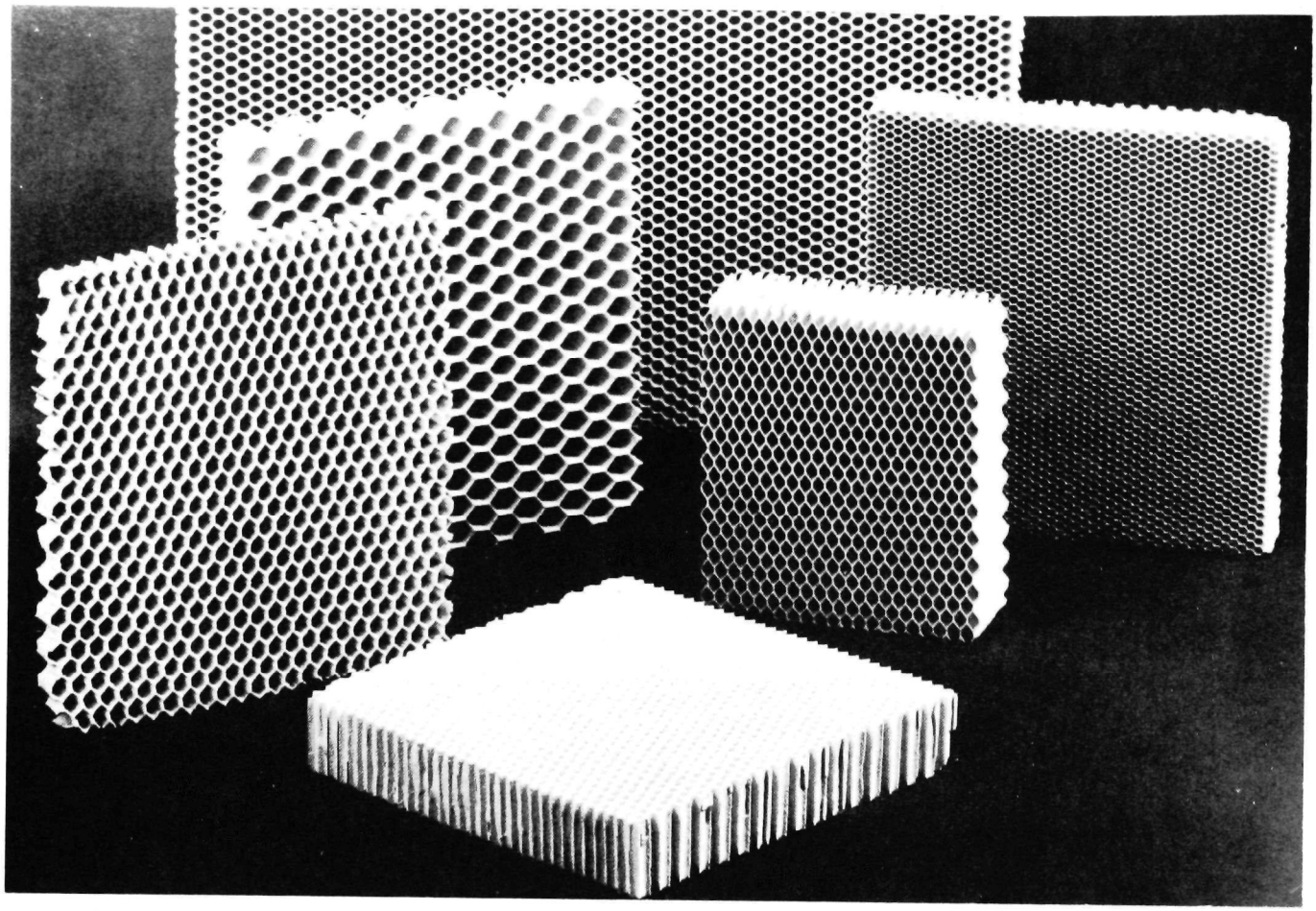

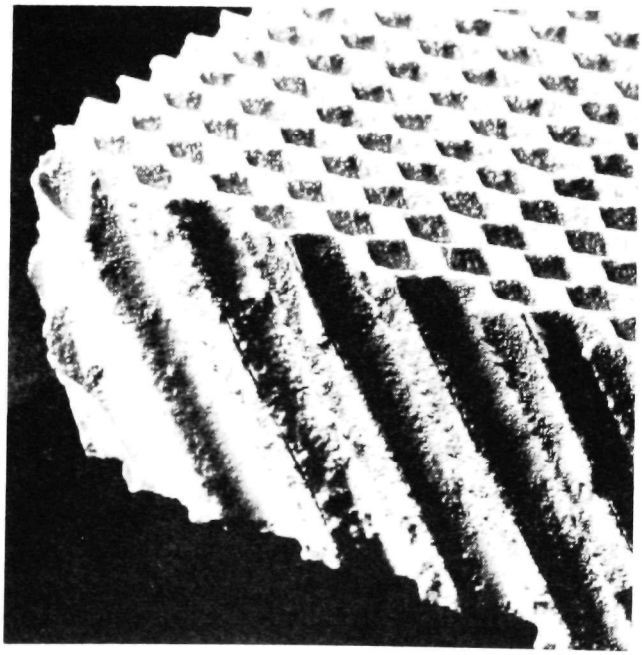

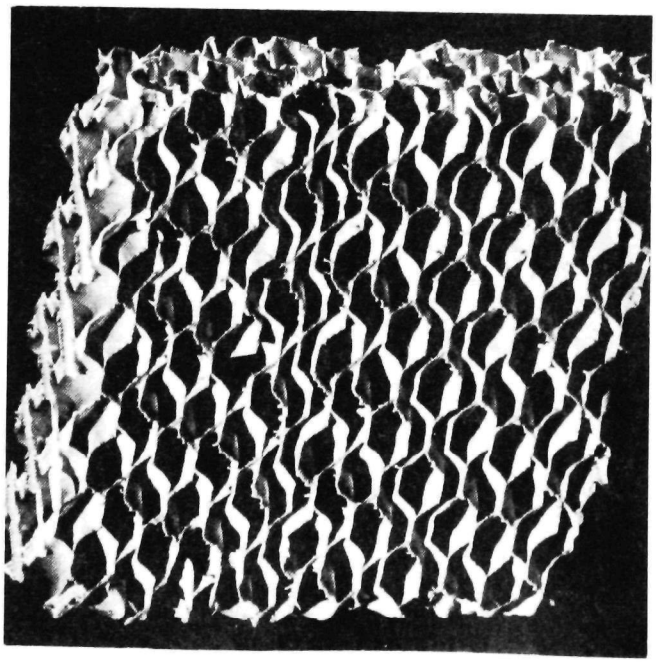

Figure 4-5. Torvex ceramic honeycomb configurations by DuPont.

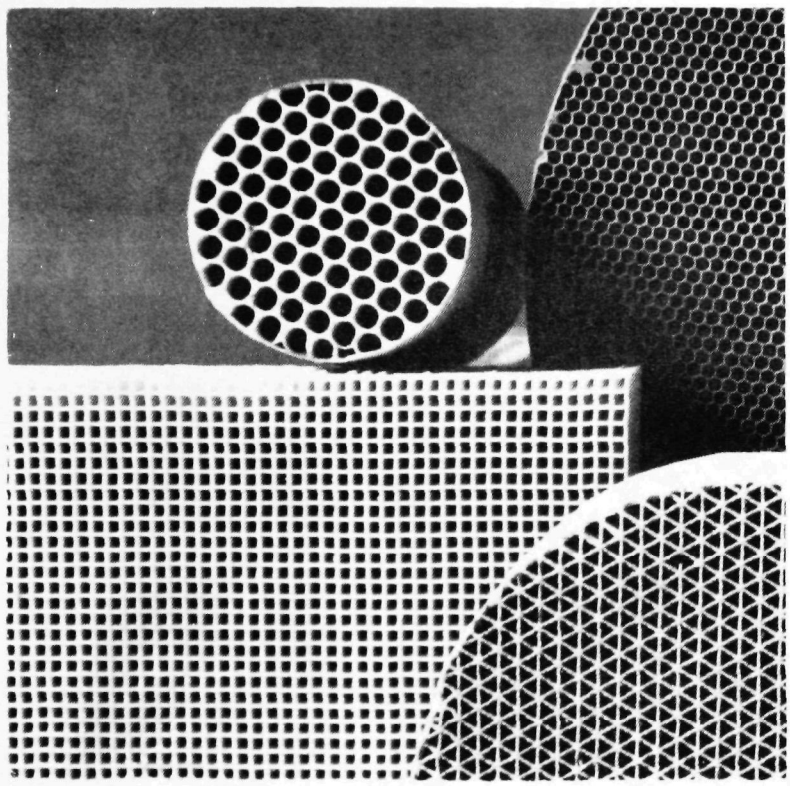

Figure 4-6. Versagrid ceramic honeycomb by General Refractories Company.

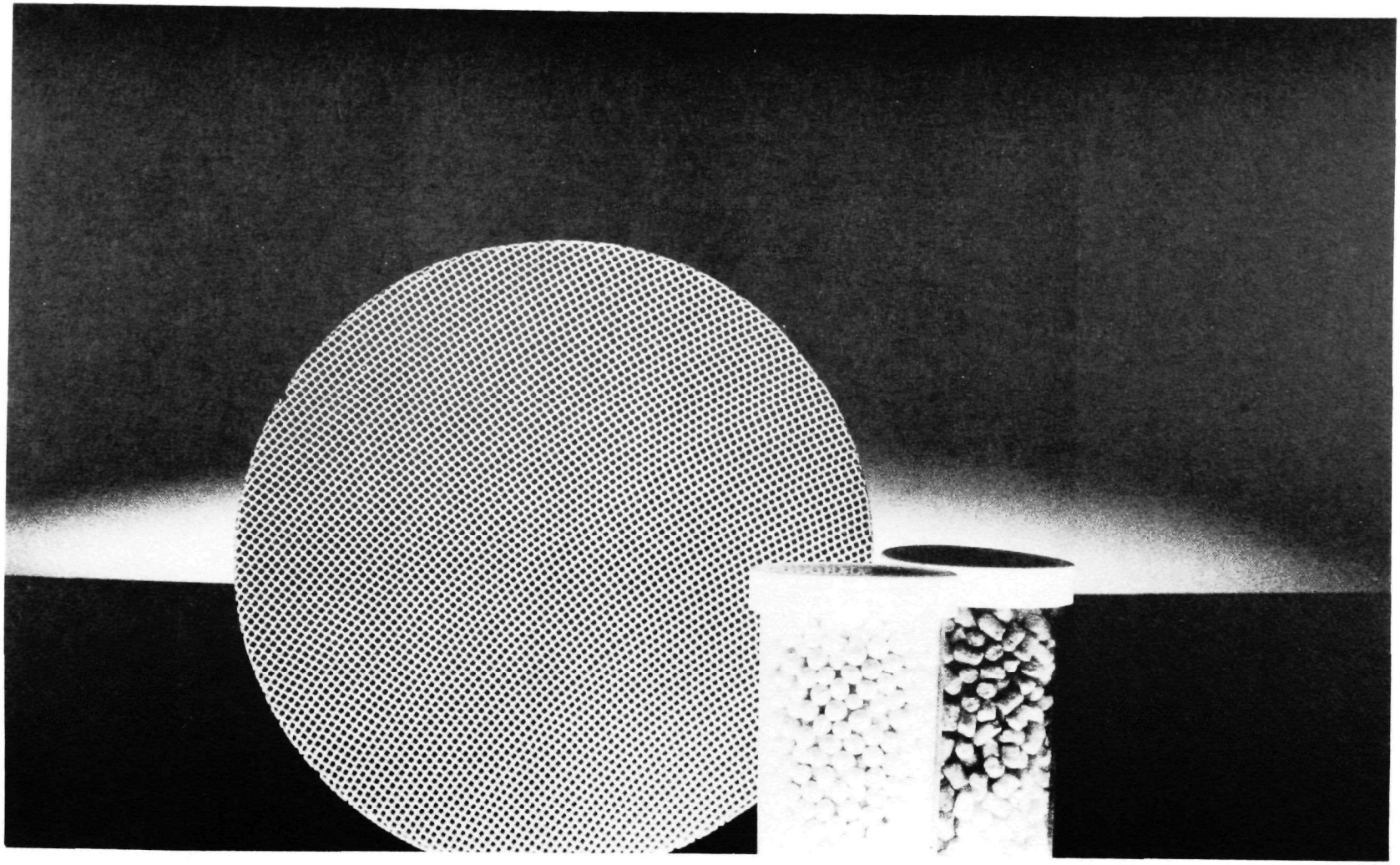

Figure 4-7. Poramic monolith structures by W. R. Grace & Co.

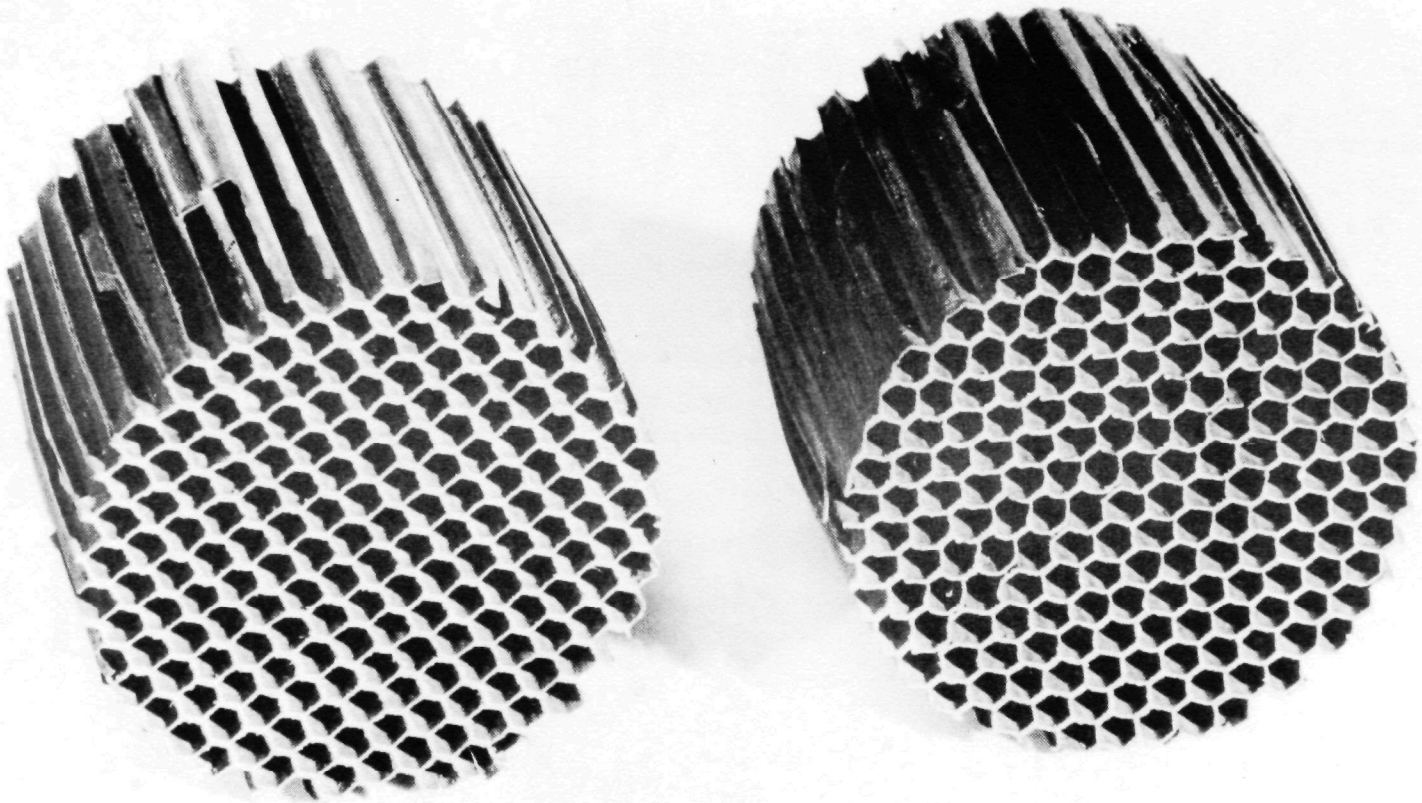

Figure 4-8. Kanthal metal monolith by Kentucky Metals, Inc.

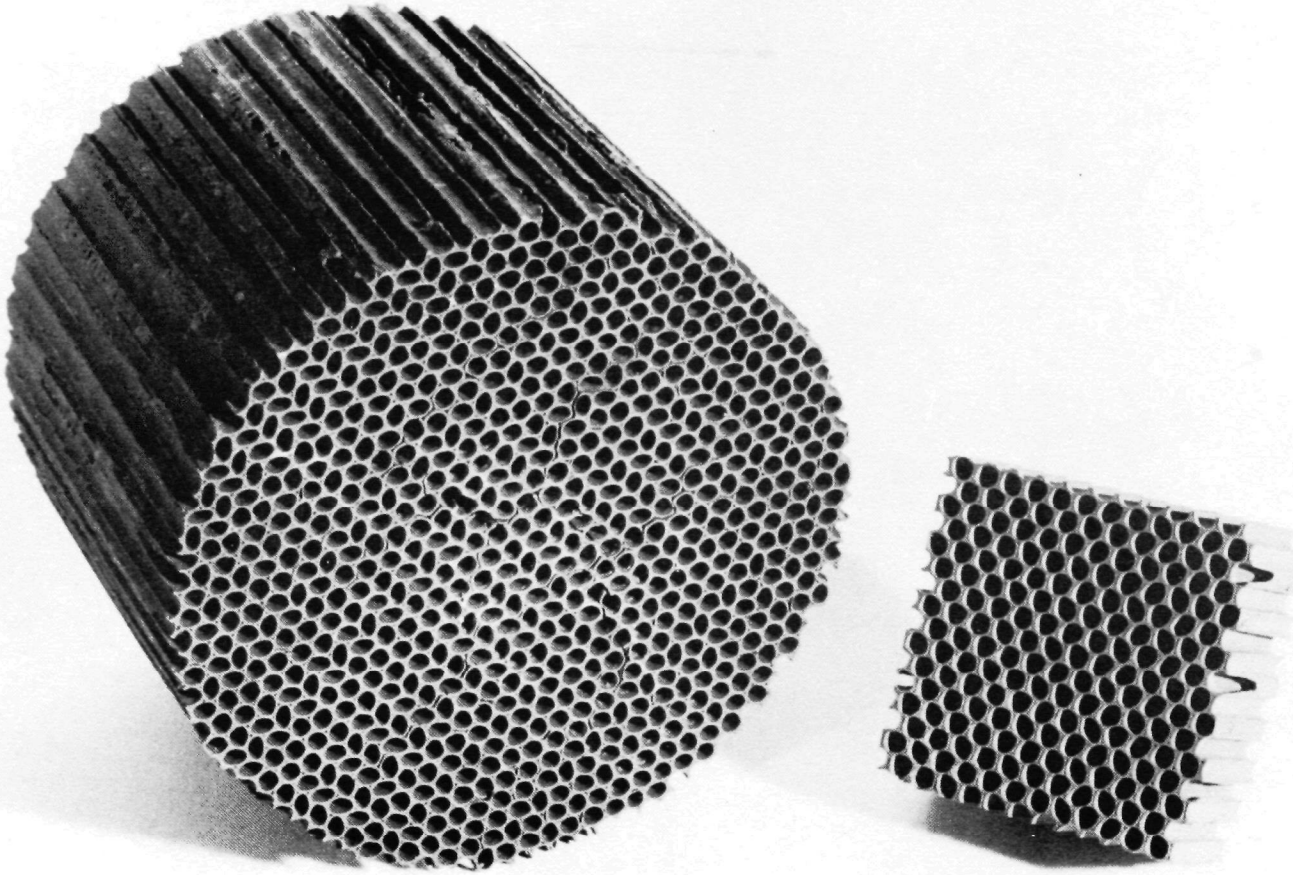

Figure 4-9. Spectramic silicon carbide honeycomb by Norton Company.

TABLE 4-3. CERAMIC CYLINDER PROPERTIES

Manufacturer	Ceramic Composition	Maximum Use Temperature, K (°F)
Coors Porcelain Company	Mullite	1973 (3100)
	Alumina	2223 (3540)
Zircoa Products Department, Corning Glass Works	Zirconia	2478 (4000)

6.35×10^{-3} m (0.25 in) to 0.178 m (7 in) outside diameter while Zircoa manufactures zirconia cylinders in a variety of sizes. These ceramics have very low porosity, but can be adapted to system configurations. The maximum use temperature of the cylinders listed in Table 4-3 are higher than for monoliths of similar materials because of trace element variations. Section 9.2 describes one suitable system using ceramic cylinders.

4.2.2 Washcoat Substrates

As mentioned earlier, the low surface area of the monolith structure can be increased by the application of a thin coat of metal oxide material, such as Al_2O_3. This washcoat strongly adheres to the ceramic support and provides a high surface area. At the same time, because the washcoat is thin (between 10×10^{-6} and 20×10^{-6} m), the catalytic material which is subsequently impregnated on it is close to the main flow of reactants. Figure 4-10 shows a schematic representation of the washcoat structure on a monolith cell wall.

The most common washcoat material is γ-Al_2O_3. At temperatures above 1172K (1650°F) the high surface area γ-Al_2O_3 undergoes a phase change to relatively low surface area α-Al_2O_3 with concomitant sintering. This phase change gives a resultant change in surface area from 300 m^2/g of washcoat to 5 m^2/g of washcoat. This sintering thus results in pore closure and a burying of active catalytic sites in the alumina washcoat. The use of presintered Al_2O_3 washcoats, Al_2O_3 washcoats stabilized with CeO_2 or Cs_2O, or more thermally resistant washcoats such as ZrO_2 and ThO_2 can also be

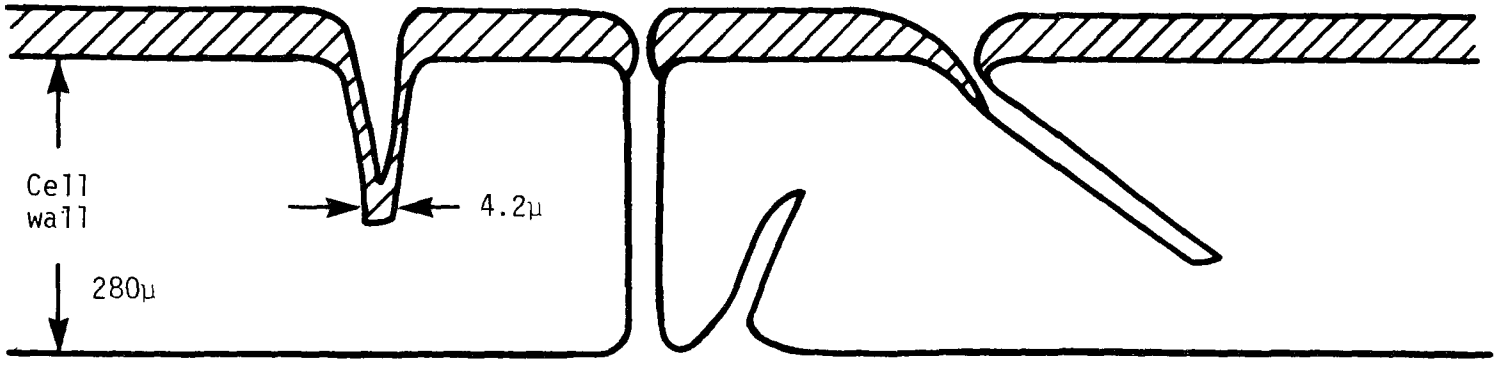

a. View of washcoat and monolith cell wall

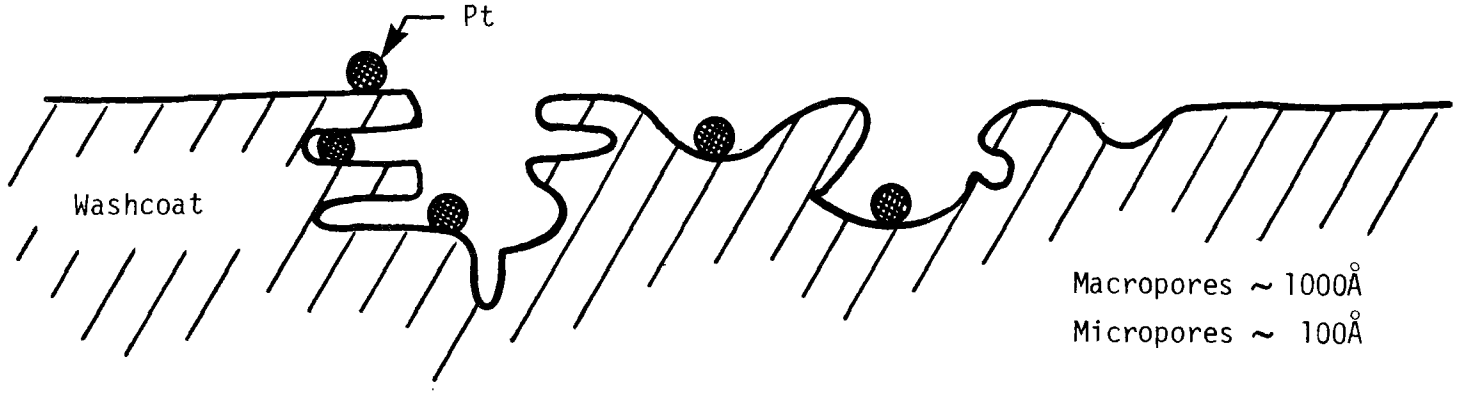

b. View of washcoat pore structure

Figure 4-10. Washcoat structure on monolith — schematic representation.

considered. Finally, the necessity of maintaining a high surface area, which is required for low temperature catalysis, may not be required for high temperature catalytic combustion systems. Thus, systems using no washcoats should also be considered.

4.2.3 Catalyst Coatings

Two broad classes of catalyst coating materials are available: metals and oxides. Much of the work on metal catalysts has been performed under the automotive emission abatement program where the catalyst operating temperature is usually around 1000K (1340°F). Metal and oxide catalysts are discussed separately in the following sections.

4.2.3.1 Metal Catalysts

The metals of catalytic interest are listed in Table 4-4. Of these metals, the only ones which have a possibility of remaining in the metallic state in a high-temperature oxidizing environment are the noble metals. The others readily form oxides and are discussed in Section 4.2.3.2. Of the noble metals, a large volume of data exists for platinum and palladium because of their use as automotive oxidation catalysts. They are among the most active catalysts for the oxidation of a number of fuels, including methane (Reference 4-5), methanol (Reference 4-6), and hydrogen (Reference 4-7). The high activity of these metals is related to their ability to activate H_2, O_2, C-H, and O-H bonds.

Problems in the operation of platinum and palladium catalysts do exist, however. Even at the low temperature (<825K) of catalytic reforming,

TABLE 4-4. METALS OF INTEREST FOR CATALYTIC COMBUSTION*

Group VIII			Group IB
Fe	Co	Ni	Cu
Ru	Rh	Pd	Ag
Os	Ir	Pt	Au

*Enclosed metals are considered noble.

a loss in platinum surface area occurs. This platinum crystallite growth can be explained by the volatility of platinum under oxidizing conditions. On the other hand, palladium tends to be converted to an inactive oxide at temperatures of 973-1073K in an oxidizing atmosphere and rapidly loses the ability to burn methane.

In spite of these problems, the development of a stable metal catalyst capable of long-term operation at temperatures of 1525 K (2285°F) appears very realizable. At 1525K a high platinum dispersion cannot be maintained, but this loss of platinum surface area may not affect low temperature light-off characteristics to a great extent. Thus, a high activity catalyst may not be required for catalytic combustion applications.

In addition, although catalyst sintering is severe at 1525K, catalyst poisoning is much less of a problem. Sulfur compounds decompose at catalytic combustor operating temperatures. Even lead is not a serious problem, since compounds such as lead oxide have an appreciable vapor pressure at combustor temperatures.

Finally, the use of traces of noble metals may greatly enhance the performance of certain base metal catalysts. One example of such behavior involves the use of platinum with mixed oxides of perovskite structure. Traces of platinum have been shown to render certain base metal perovskite catalysts insensitive to sulfur poisoning (Reference 4-8). Such catalysts can be expected to operate at a much higher temperature without loss of platinum than would be the case for a straight platinum catalyst because the platinum is chemically bound in the perovskite structure and the vapor pressure of platinum oxide is accordingly reduced. The perovskite structure is described in detail in Reference 4-9.

The use of the other noble metals listed in Table 4-4 appears limited for catalytic combustion applications. Ruthenium is known to form a volatile oxide (RuO_4) under oxidizing conditions, and this oxide is rapidly removed from conventional catalyst supports. It may be possible to anchor ruthenium to a support by forming a relatively stable perovskite structure with certain oxides such as La_2O_3 (Reference 4-10). Osmium is even more volatile than ruthenium, and the oxide is poisonous. It is also very costly and available only in a limited supply as are iridium and rhodium. Thus

the use of these metals would be restricted to small quantities in multi-metallic systems. Silver melts at low temperatures, and gold is very inactive for oxidation.

Based on these considerations, platinum and palladium show the greatest promise for use in a catalytic combustion system. They also have application to mixed metal/metal oxide systems.

4.2.3.2 Metal Oxide Catalysts

The catalytic properties of metal oxides have been studied extensively by a number of research groups for low temperature applications (Reference 4-11). Some of the simple oxides, such as Co_3O_4, have oxidation activities comparable to the very active noble metals. The primary difference between these oxides and the metals is the "lightoff" temperature, which relates the ability of a catalyst to reach a significant conversion level at low temperatures and in short periods of time. Oxides typically have lightoff temperatures significantly higher than noble metals with the same fuel. Since it is important for an oxidation catalyst to reach operating temperature quickly, doping a high-lightoff-temperature oxide with small amounts of noble metals to initiate lightoff is feasible, as is the use of a multi-bed catalyst.

Oxides of the transition metals have been shown to be the most active simple oxide catalysts. These oxides are:

Co_3O_4, MnO_2, NiO, CuO, Co_2O_3, Fe_2O_3, V_2O_5.

Inasmuch as solid state reactions can be very rapid at the high temperatures of catalytic combustor operation, the oxide catalyst and the monolithic support structure must be compatible. This means there must either be mutual insolubility (or at least limited solubility) or that the melting points of the materials used must be greater than the maximum operating temperature by a factor of at least 1.5. Recrystallization becomes appreciable at about one-half the melting point of a material. Thus alumina, with a melting point of about 2305K (3689°F) would be expected to react readily with most catalytic materials at temperatures above about 1673-1773K (2551-2731°F). Fortunately, the reaction product itself may be a suitable catalyst. Thus cobalt oxide reacts with alumina to form the less active,

though still catalytic, cobalt aluminate (Reference 4-12). It should be noted that the interaction of the catalyst and support can alter the strength and thermal shock capabilities of the support.

With the proper choice of materials, highly active stable catalysts of mixed oxides are believed possible. Also, it may be possible to fabricate honeycomb structures directly from catalytic oxide compositions. Perovskites, for example, have been proposed for catalyst supports (Reference 4-13). The high sintering temperatures required for development of structural strength will of course result in a very low surface area. However, any catalyst intended for use at combustor conditions will rapidly sinter in use, resulting in loss of the high catalyst surface area. It is far better to start with a low surface area since this should result in better retention of strength and thermal shock properties as well as catalytic activity.

There is essentially no literature specifically on catalysts (either noble metal or oxide) suitable for use under catalytic combustor conditions. Consequently, a literature review was conducted on catalyst compositions -- and materials likely to possess catalytic properties -- which could reasonably be expected to be candidates for use at temperatures as high as 1773K (2731°F). The emphasis was placed on compounds of the perovskite type since many of these compounds are known to be relatively refractory and have attracted much interest as catalytic agents. Also covered were spinels, scheelites, etc. In particular, melting point and thermal decomposition data was sought.

While materials of potential high temperature utility have been studied in the past, no studies have been reported for temperatures above 1273K (1831°F). Based on their promise for use as combustion catalysts at high temperatures, the most promising metal oxide compositions are:

1-a) $Ni_{0.5}\ MgO_{0.5}\ (Al_{0.5}\ Cr_{0.3}\ Fe_{0.2})_2\ O_4$

1-b) $Ni\ (Al_{0.3}\ Cr_{0.5}\ Fe_{0.2})_2\ O_4$ + 1%NiO

1-c) $Co\ (Al_{0.3}\ Cr_{0.5}\ Fe_{0.2})_2\ O_4$ + 5%CoO

These materials were developed for use in high temperature thermistors and were prepared by solid state sintering at 1893K (2947°F) (References 4-14 and 4-15). Materials 1-b) and 1-c) should be especially interesting since they contain free nickel oxide and cobalt oxide, respectively.

The following materials were studied as catalysts for use at conventional low temperature conditions but based on their composition can be expected to be useful at high temperatures.

2-a) $LaMnO_3$

Compound (2-a) is the base compound for a variety of analogs (Reference 4-16).

2-b) $La_{0.5}\ Sr_{0.5}\ MnO_3$

Compound (2-b) is sulfur sensitive at low temperatures. Addition of traces of platinum is said to render this composition insensitive to sulfur poisoning (Reference 4-17).

2-c) $La_{0.8}\ K_{0.2}\ Rh_{0.1}\ Mn_{0.9}\ O_3$

Compound (2-c) is an example of the almost infinite variations possible (Reference 4-18).

No catalytic data was found for the following materials, but many variations should exist which combine both catalytic activity and a reasonably high melting point.

3-a) $ZrXWO_3$

This class of zirconia-based compounds (3-a) contains candidates for high temperature operation. Stability of these materials has been studied (Reference 4-19). Compounds of this type warrant extensive investigation because many species should exhibit both catalytic activity and a very high melting point. Relatively high surface area catalysts should be possible with compounds of this type.

3-b) $LaCoFeO_3$

The catalytic and thermodynamic properties have not been determined for material (3-b) (Reference 4-20).

3-c) $LaMNiO_3$, M = Ca, Sr, or Ba

The calcium and strontium compounds should be very interesting. The barium compound would likely not be stable because of the volatility of barium oxide (Reference 4-21).

The last group is of special interest because it teaches the use of perovskite oxides as carriers or structural supports for transition metal oxide catalysts. Examples are:

4) $(Sr_{0.2} La_{0.8}) CoO_3$ or $(Sr_{0.4} La_{0.6})(Co_{0.9} Pt_{0.1}) O_3$ as catalysts on $LaAl_2O_3$ or $(Sr_{0.4} La_{0.6})(Co_{0.5} V_{0.2}) O_3$ as catalyst support (Reference 4-13).

It should be noted that all compounds containing metals with volatile oxides are unsuitable for combustor service. Therefore, the very many compounds containing barium, lead, rhenium, ruthenium, sodium, etc. have been excluded from consideration. Similarly, compounds containing halogens are not considered useful for combustor service. In addition, all compounds with known melting points below about 1873K (2911°F) have been excluded Melting points of at least 2273K (3631°F) are sought.

In summary, it appears that there are many mixed oxide catalysts likely to be operable at 1773-1873K (2731-2911°F).

$$Ni_{1+x} (Al_{0.3} Cr_{0.5} Fe_{0.2})_2 O_{4+x} \text{ and}$$

$$Co_{1+x} (Al_{0.3} Cr_{0.5} Fe_{0.2}) O_{4+x}$$

represent compounds which should be usable up to 1773K. However, it is almost certain that superior compositions exist, and a systematic study of the high temperature capabilities of the many types of mixed oxide compounds possible should be made.

4.3 CONCLUSIONS

Based upon a review of the available catalyst materials and their properties, the following conclusions have been made:

- To obtain the maximum performance from a catalytic combustion system, it is desirable to have a high temperature support material, a washcoat capable of maintaining a high surface area under high temperature operation, and a highly dispersed catalyst having a low lightoff temperature and high activity. Such a system may not exist, making performance trade-offs necessary.
- The monolithic honeycomb support is the most technologically advanced geometric configuration for catalyst carriers, minimizing both pressure drop and volume of catalyst required.
- Newly developed metal monolith materials may have advantages over ceramics in terms of thermal shock characteristics.
- It may not be necessary to maintain a high surface area in a catalytic combustor system, and hence, systems using no washcoats should be considered potentially viable.
- The most promising noble metal catalysts are platinum and palladium because of their high activity and relatively low lightoff temperature.
- Simple oxides of the transition metals should have good catalytic activity but will have higher lightoff temperatures than the noble metals.
- The most promising high temperature (>1773K) catalysts are mixed oxides containing either free nickel oxide or cobalt oxide.

REFERENCES

4-1. Kesselring, J. P., et al., "Catalytic Oxidation of Fuels for NO_x Control from Area Sources," Environmental Protection Technology Series Report EPA-600/2-76-037, February 1976.

4-2. Pratt, A. S., and Cairns, J. A., "Noble Metal Catalysts on Metallic Substrates," Platinum Metals Review, Vol. 21, No. 3, July 1977.

4-3. Bittence, J. C., "Sorting Out the Ceramics," Machine Design, Vol. 49, No. 28, December 8, 1977.

4-4. Lundsager, C. B., et al., "Thermoplastics Process for Catalyst Substrates," SAE Paper 760311.

4-5. Dixon, J. K., and Longfield, F. E., in Catalysis, edited by P. H. Emmett, Reinhold, New York, 1960, Vol. 7, p. 183.

4-6 Bond, G. C., Catalysis by Metals, Academic Press, New York, 1962, p. 464.

4-7. Kowaka, M. J., Japan Inst. Metals, Vol. 23, 1959, p. 659.

4-8. Johnson, D. W., et al., "The Nature and Effects of Platinum in Perovskite Catalysts," J. Catalysis, Vol. 48, 1977, pp. 87-97.

4-9. Evans, R. C., An Introduction to Crystal Chemistry, Cambridge University Press, London, 1952.

4-10. Shelef, M., and Gandhi, H. S., "Stabilization of Ru-Containing Nitric Oxide Reduction Catalysts," publication preprint from Scientific Research Staff of Ford Motor Company, Dearborn, Michigan.

4-11. Margolis, L. Y., Advances in Catalysis, Vol. 14, p. 429, Academic Press, New York.

4-12. Schachner, H., "Cobalt Oxides as Catalysts," Cobalt, December 1960, pp. 1-10.

4-13. McCann, E. L., "Perovskite Oxides as Carriers for Transition Metal Oxides," German Pat. Offen 2,615,352.

4-14. Matsuo, Y. and Hayakawa, S., Japan Kokai, 76-22,093.

4-15. Matsuo, Y. and Hayakawa, S., Japan Kokai, 76-22,094.

4-16. Voorhoeve, R.J.H., Remeika, J. P. and Tremble, L. E., "Defect Chemistry and Catalysis in Oxidation and Reduction over Perovskite-Type Oxides," Ann. N.Y. Acad. Sci., Vol. 272, 1976, pp. 3-21.

4-17. Johnson, D. W. Jr., Gallagher, P. K., Wertheim, G. K., and Vogel, E. M., "The Nature and Effects of Platinum in Perovskite Catalysts," J. Catalysis, Vol. 48, 1977, pp. 87-97.

4-18. Voorhoeve, R.J.H., Remeika, J. P. and Trimble, L. E., "NO and Perovskite-Type Catalysts," Cat. Chem. Nitrogen Oxides, Ed. by Klimish, R. L., and Larson, J. G., Plenum.

4-19. Ekstrom, T. and Tilley, R.J.D., "Stability of Perovskite-Type $ZrXWO_3$," J. Solid State Chem. 19, 1976, pp. 227-33.

4-20. Rao, C.N.R., Parkash, O. and Ganguly, P., "Electronic and Magnetic Properties of Perovskites," J. Solid State Chem. Vol. 15, 1975, pp. 186-92.

4-21. Obayashi, H. and Kudo, T., "Crystallographic, Electric and Thermochemical Properties of Lanthanum M Nickelate," J. Appl. Phys., Vol. 14, 1975, pp. 330-5.

SECTION 5

CATALYST PREPARATION AND CHARACTERIZATION

An essential feature of design criteria for catalytic combustion systems is information concerning the catalyst/substrate/support system in terms of catalyst type, catalyst loading, washcoat type, support type, pre- and post-test total surface area, pre- and post-test dispersion (for precious metal catalysts), and microscopic surface characteristics. Due to the proprietary nature of much of the current work in catalyst systems, it was necessary to prepare most catalysts in-house and to supplement these with commercially available systems. All systems were then subjected to pre- and post-test characterization analyses. This section provides information on the catalyst preparation and characterization techniques (Sections 5.2 and 5.3) used in this study. Also included is a description of the EPA/Acurex characterization laboratory.

5.1 GENERAL CONSIDERATIONS

A review of the available materials for use in catalytic combustion systems is presented in Section 4. While an identification of these materials is important in characterizing the catalyst system, additional information is required to fully define the system. This additional information includes:

- Catalyst loading
- Catalyst pre-treatment techniques
- Total (BET) surface area, pre- and post-test
- Precious metal dispersion, pre- and post-test
- Pore volume and pore size distribution
- SEM-EDAX analysis of catalyst surface

Measurement of these physical properties before and after combustion reaction can be correlated with catalyst performance to understand the basis for specific catalyst behavior. Combining the measurement of these physical properties with the laboratory preparation of catalyst systems provides the maximum amount of information to be gained from combustion testing.

5.2 CATALYST PREPARATION

Since a very limited number of commercially available catalysts suitable for combustion applications could be identified, most catalyst systems were prepared at Acurex. Preparation of these systems is performed with standard laboratory equipment. All catalyst systems include a monolithic honeycomb support. For those systems employing a washcoat, the washcoat is usually placed on the monolith by an outside vendor. The washcoat is either used as supplied, or pre-sintered by placing the washcoat/monolith in a muffle furnace for 8 hours at approximately 1360K. The washcoat/monolith is then dried in a muffle furnace, cooled in a desiccator, and weighed. For platinum catalysts, an aqueous solution of chloroplatinic acid (H_2PtCl_6) is then prepared to give the appropriate platinum loading. This aqueous solution is applied to large cell monoliths by brushing and to small cell monoliths by dipping.

For metal oxide catalyst systems using cobalt or nickel oxides, the monolith is dipped into a melt or an aqueous solution of the metal nitrate. Compressed air is used to gently blow out any clogged cells. The system is then dried, calcined, and weighed to determine the catalyst weight percent.

Catalyst preparation procedures are given in tabular form in Table 5-1.

5.3 CATALYST CHARACTERIZATION

Once the catalyst system has been prepared, it is further characterized in terms of total and selected surface areas. Additional characterization of the surface can be done by measurement of pore volume and pore size distribution as well as by surface microscopy.

The monolithic support is ordinarily a ceramic of low surface area ($\sim 0.01\ m^2/g$). The washcoat substrate, also a ceramic, is applied to increase the surface area. This increased surface area allows higher precious metal

TABLE 5-1. CATALYST PREPARATION PROCEDURES

Operation	Procedure	Materials Required
Monolith Wet Point Determination (for dipped catalysts)	1. Dry monolith at 673K for 3 hours. 2. Weigh monolith. 3. Cover monolith with 500 ml de-ionized water. 4. Remove monolith from water, measure water uptake.	De-Ionized Water Beakers
Washcoat Application	1. Determine monolith wet point. 2. Dip monolith in Alon 3-D (30% aqueous dispersion of alumina) or 50% $Zr(NO_3)_4$ in water. 3. For Al_2O_3 washcoat, fix Alon with NH_3; for ZrO_2 washcoat, calcine at 773 K for two hours. 4. Repeat step 3 until desired weight percent is achieved.	$Zr(NO_3)_4$ Al_2O_3 De-Ionized Water Beakers NH_3 (g)
Monolith Impregnation with Noble Metal by Dipping	1. Determine monolith wet point. 2. Prepare solution of metal salt with proper concentration to give desired weight percent of metal. 3. Dip monolith in solution until all solution is taken up. 4. For Pt catalysts, fix metal by H_2S spray while catalyst is wet. 5. Calcine at 673K for 3 hours.	Metal Salt De-Ionized Water Beakers H_2S (g)
Monolith Impregnation with Noble Metal by Brushing	1. Calculate metal salt needed to give desired loading. 2. Prepare solution of metal salt. 3. Using small brush or cotton swab, paint monolith with solution. 4. Fix Pt by H_2S spray. 5. Dry, calcine, and weigh. 6. Repeat step 3 until all solution is used.	Metal Salt De-Ionized Water Beaker Watch Glass H_2S (g) Paint Brush
Monolith Impregnation with Base Metal	1. Dry monolith at 673K for 3 hours. 2. Dip monolith in melt of appropriate nitrate, or in solution of appropriate nitrate. 3. Calcine at 673K for 3 hours. 4. Repeat step 2 until desired loading is obtained.	Base Metal Nitrate Beakers De-Ionized Water

dispersions to be achieved by reducing agglomeration of precious metal crystallites. Thus a high total surface area measurement indicates a wash-coat material of high surface area, and a high selected surface area, or dispersion, measurement indicates a precious metal that has been placed on the surface in extremely small (<50 Å) crystallite sizes.

A description of total and selected surface area, pore size and pore volume, and SEM-EDAX analyses follows.

5.3.1 Total Surface Area

The basis for surface area measurements is the Langmuir gas adsorption theory in which the surface of a solid is regarded as an array of active adsorption sites, each site with the capacity to adsorb one molecule. It is assumed that when a gas molecule strikes an active site it will remain for a period of time and then re-evaporate. Brunauer, Emmett and Teller (Reference 5-1) extended the Langmuir theory to apply to the second and higher layers of adsorbed molecules. Based on this work, the total surface area is given by

$$SA = \frac{V_m A}{W} \ (m^2/g) \qquad (5\text{-}1)$$

where W = catalyst weight in grams

A = area occupied per molecule (for argon, A = 14.6 $Å^2$)

and V_m is found from the BET equation

$$\frac{P}{V(P_o - P)} = \frac{1}{V_m C} + \frac{C - 1}{V_m C}\frac{P}{P_o} \qquad (5\text{-}2)$$

with C being a constant at a given temperature.

$$C = \exp \frac{H_1 - H_L}{RT}$$

where H_1 = heat of adsorption of first layer

H_1 = heat of liquefaction

R = universal gas constant

T = temperature

Experimentally, it is found that a plot of $P/V(P_o - P)$ versus P/P_o is linear in the range of relative pressures from 0.05 to 0.35 (see Figure 5-1). The slope is $(C - 1)/V_m C$ and the intercept is $1/V_m C$. Thus V_m = (slope +

RuCu Alloy Powder

P(cm)	P/P_o	V(cc/g)	$P/V(P_o-P)$
1.0625	.0506	4.2545	.012526
2.0408	.0972	5.1681	.020828
4.5073	.2146	6.6749	.04094

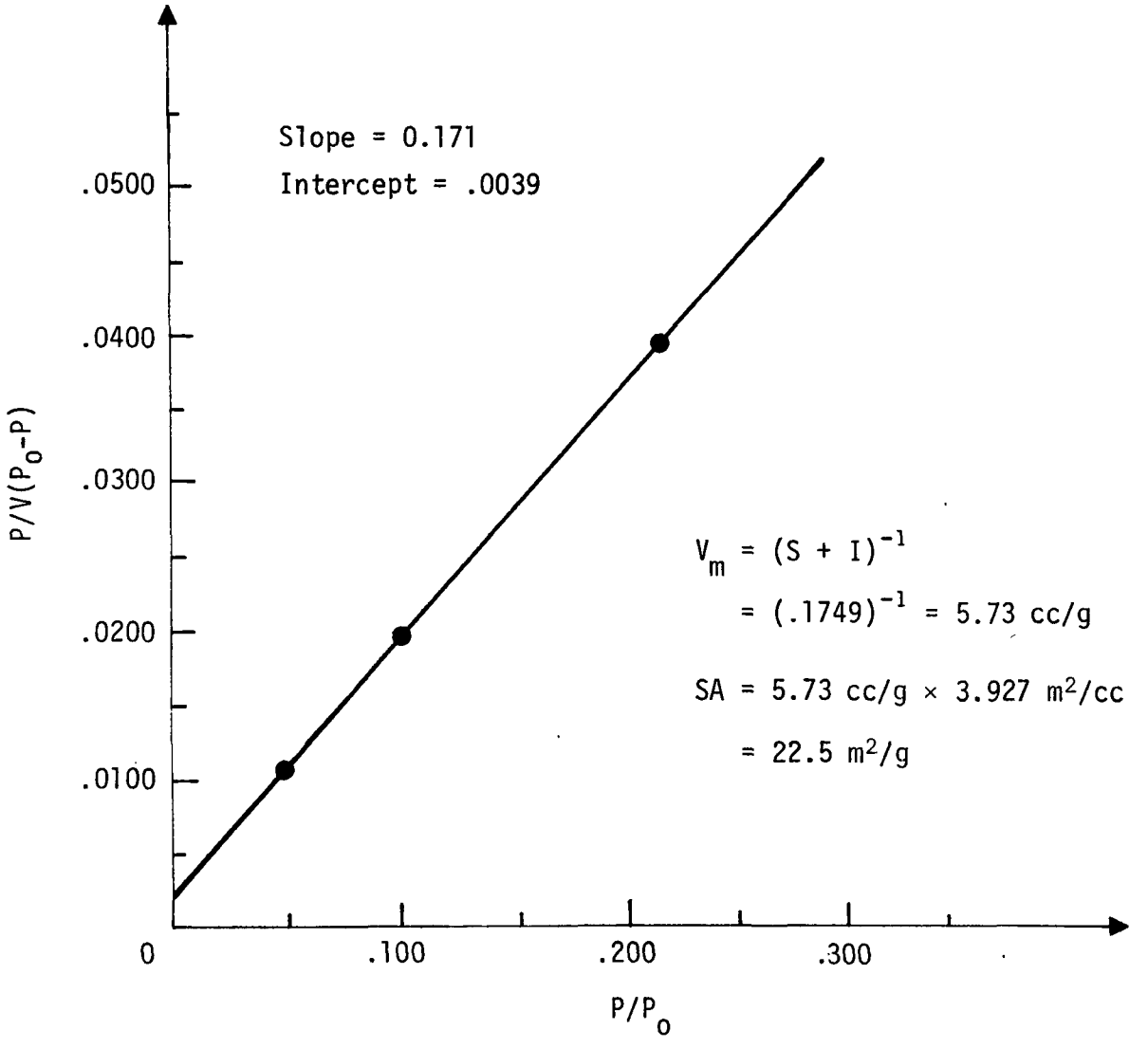

Figure 5-1. Argon BET at 77K.

intercept)$^{-1}$. An example of a total surface area calculation using the BET equation is given in Figure 5-1.

One should note that the number of molecules adsorbed on the monolayer V_m is related to the volume adsorbed by the expression

$$V_m = \frac{AN}{m_v} \tag{5-3}$$

where N = Avogadro's number (6.03×10^{23} molecules/mole)
and m_v = gram molecular volume (22,400 cc/mole)

The gas adsorbate may be nitrogen, krypton, or argon. Measurement of total surface area by physical adsorption of argon is carried out at the liquid nitrogen temperature (77K).

5.3.2 Selected Surface Area (Dispersion)

For a noble metal supported on an inactive refractory oxide, the catalytic activity should be a function of the metal surface area. The metal surface area can be determined in a number of ways, including x-ray diffraction line broadening and electron microscopy. The most convenient and accurate technique, however, is by the chemical adsorption of a gas.

The stoichiometry of selective adsorption is established on pure metal powders or on supported metal samples characterized by the techniques described above. The usual gas adsorbate is hydrogen or carbon monoxide. The two adsorption techniques described below are used in the determination of catalyst dispersion.

Hydrogen Chemisorption

After a platinum catalyst has been reduced at high temperature (673K) and the sample cell evacuated, the metal surface is measured by hydrogen chemisorption and expressed as percent dispersion. The stoichiometry is:

$$Pt(surface) + \frac{1}{2} H_2 \longrightarrow PtH(surface)$$

On very small metal crystallites the stoichiometry may change such that two atoms are adsorbed for each atom of surface Pt:

$$Pt(surface) + H_2 \longrightarrow PtH_2(surface)$$

Calculated dispersions of over 100 percent indicate well dispersed catalysts and should be rounded to 100 percent.

Hydrogen Titration

When, after reduction with hydrogen and removal of the gas, the platinum catalyst is exposed to an atmosphere of air or oxygen, a surface layer of platinum oxide forms. The stoichiometry of the reaction of hydrogen with PtO, or titration, is:

$$PtO(surface) + 3/2\ H_2 \longrightarrow PtH(surface) + H_2O$$

In the case of platinum on an alumina washcoat, the water formed is adsorbed by the alumina. The consumption of 1.5 H_2 molecules for each atom of surface Pt results in an increased sensitivity in the surface area measurement compared with chemisorption.

Dispersion is expressed as

$$\frac{n_{Pt\ active\ sites}}{n_{total\ Pt}}$$

with

$$n_{Pt\ active\ sites} = \frac{2}{3}\left(\frac{\mu\ mole\ H_2}{g}\right)$$

from the stoichiometry of the H_2 titration, and

$$n_{total\ Pt} = \frac{g\ Pt}{g\ catalyst}\ \frac{10^6}{195.09\ g\frac{Pt}{mole}} = \frac{\mu\ mole\ Pt}{g}$$

Uptake of H_2 for each expansion is

$$\Delta n = \frac{V_D \cdot 16.04}{WT}\left[P_1^i + P_2^{i-1}\left(\frac{PC-1}{PC-2} - 1\right) - P_2^i\frac{PC-1}{PC-2}\right]\frac{\mu\ mole}{g}$$

where V_D = dosing volume (cc)

W = weight of catalyst (g)

T = temperature (K)

P = initial pressure (torr)

P_2^1 = pressure after expansion (torr)

i = expansion number

$\frac{PC\text{-}1}{PC\text{-}2}$ = average ratio of initial and final pressures from dead space expansions

Extrapolation of the $\Sigma\Delta n$ vs. P_2 plot gives total uptake of H_2 at P_0; the dispersion of Pt is then calculated. A complete description of this technique is given in Reference 5-2.

5.3.3 Pore Size and Pore Volume (Reference 5-3)

A Type II Langmuir isotherm (see Figure 5-2) describes the condensation of gas molecules onto a nonporous surface. When the surface has microporosity, the relation between pressure and physical adsorption is shown by a Type IV isotherm (also shown in Figure 5-2). The differences between the two adsorption isotherms are due to the finite size of the internal pores and allow an assessment of the internal pore volume of the surface.

Type II and Type IV isotherms are nearly identical at $P/P_0 \leq 0.3$ such that the BET equation is applicable to both nonporous and porous materials. The differences arise at moderate and high relative pressures.

A Type II isotherm approaches the $P/P_0 = 1$ limit asymptotically, whereas the Type IV isotherm breaks at some finite P/P_0 value less than unity and becomes nearly horizontal at the limit. The break occurs at point G, when the pores smaller than ~1000 Å diameter (the major contributors to total surface area) are filled. Beyond this point adsorption is slight because the available surface area is relatively low.

Another feature of a Type IV isotherm is the hysteresis which occurs when the relative pressure is reduced and desorption takes place. Due to the relatively small size of the pores (assumed to be cylinders with diameter d) and the concave meniscus formed by the adsorbate liquid in the pore, the effective vapor pressure of the liquid in the pores is lower and desorption occurs at a lower pressure. The vapor pressure is a function of the meniscus curvature as given by the modified Kelvin equation

$$\ell n \frac{P}{P_0} = -\frac{2\gamma v}{rRT} \qquad (5\text{-}4)$$

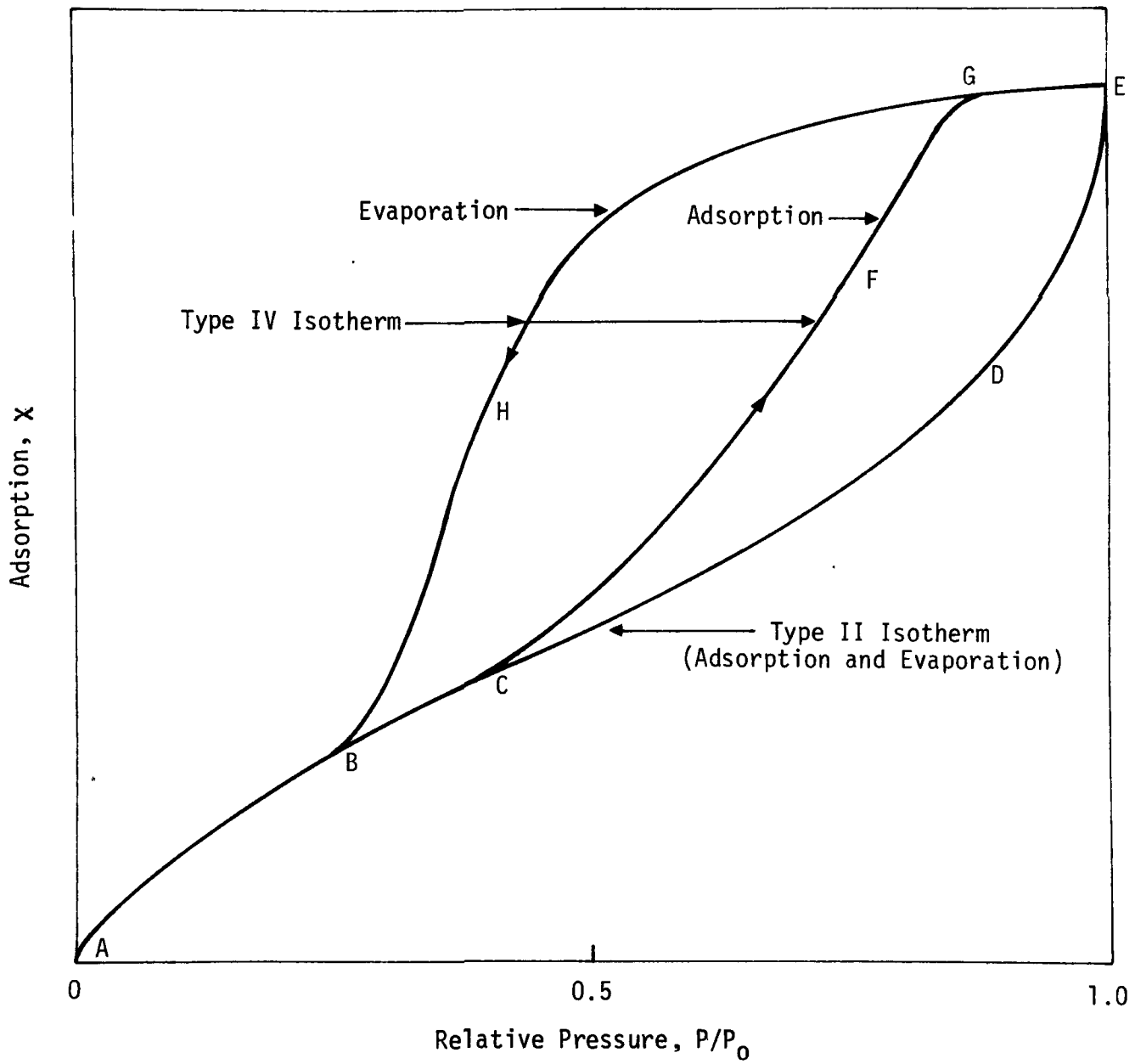

Figure 5-2. Comparison of Type II and Type IV Langmuir isotherms.

where P_o = saturation vapor pressure at temperature T (K) of the system

r = radius of pore

γ = surface tension of the adsorbate in liquid form

v = molar volume of adsorbate in liquid form

R = gas constant per mole

Thus, at any point H on the evaporation leg of a Type IV isotherm, the radius (r) of the pores (which contain saturated liquid at the relative pressure P/P_o) can be calculated. The variation of P/P_o with cylindrical pore radius varies, as shown in Table 5-2.

TABLE 5-2. VARIATION OF RELATIVE PRESSURE WITH PORE RADIUS

radius (Å)	P/P_o	
50	0.66	readily measured
500	0.96	
5000	0.996	difficult to measure

A practical upper limit for evaluation of pore volume radii is about 1000 Å.

Calculation of internal pore volume from a Type IV isotherm is done in the following manner. For idealized cylindrical pores of diameter d which are many diameters deep, total surface area SA and volume V are related by

$$\frac{V}{SA} = \frac{d}{4} \tag{5-5}$$

Extension of the isotherm to the high relative pressure break point G (Figure 5-2) allows the calculation of the radius r from Equation (5-4). Total surface area is determined as described previously; V can then be calculated.

5.3.4 SEM-EDAX Analysis

Use of the scanning electron microscope and energy dispersive x-ray analysis is helpful in determining changes in the catalyst surface structure and precious metal crystallite size. Using SEM-EDAX analysis, the surface

composition can be identified by element, and the location and size of platinum crystallites can also be determined. Examples of results from SEM-EDAX analysis are given in Sections 7 and 8.

5.4 CATALYST CHARACTERIZATION LABORATORY

5.4.1 Gas Adsorption Apparatus

The gas adsorption procedures described in Sections 5.2 and 5.3 require a finely calibrated high vacuum control volume for pretreatment and measurement of total and selected surface areas of catalyst systems. In addition, gases are delivered to and stored within the apparatus. The gas adsorption system used in this study is shown in Figure 5-3. The major components are: (1) the pumping and vacuum control system, (2) the gas delivery, storage, and cleaning system, and (3) the working volume and sample cell. These parts are described in the following sections.

5.4.1.1 Vacuum Control System

Figure 5-4 is a schematic diagram of the pumping and vacuum control system. A mechanical vacuum pump is used first to rough the unit to approximately 0.1 torr pressure, which is read on the thermal-conductivity gauge. The oil diffusion pump then is used for evacuation to 10^{-4} torr as read on the ionization gauge. A liquid nitrogen cold trap between the pumps and the working system condenses volatiles released into the unit by the pumps, mainly oil vapors.

5.4.1.2 Gas Delivery, Storage, and Cleaning System

Three gases are used routinely in adsorption measurements: helium for dead space determinations, argon for total surface area, and hydrogen for platinum dispersion. The helium and argon cylinders are connected to the adsorption apparatus by a gas line equipped with a safety pressure valve rated at 15 pounds per square inch (gauge). The inert gases also pass through a dry ice trap which condenses any water present. A second inlet port is used exclusively for hydrogen. From the cylinder, hydrogen passes first through a De-Oxo unit which removes oxygen by conversion to water, and then through a zeolite trap which dries the gas. A mercury manometer serves as a relief valve. Gases thus introduced into the apparatus are

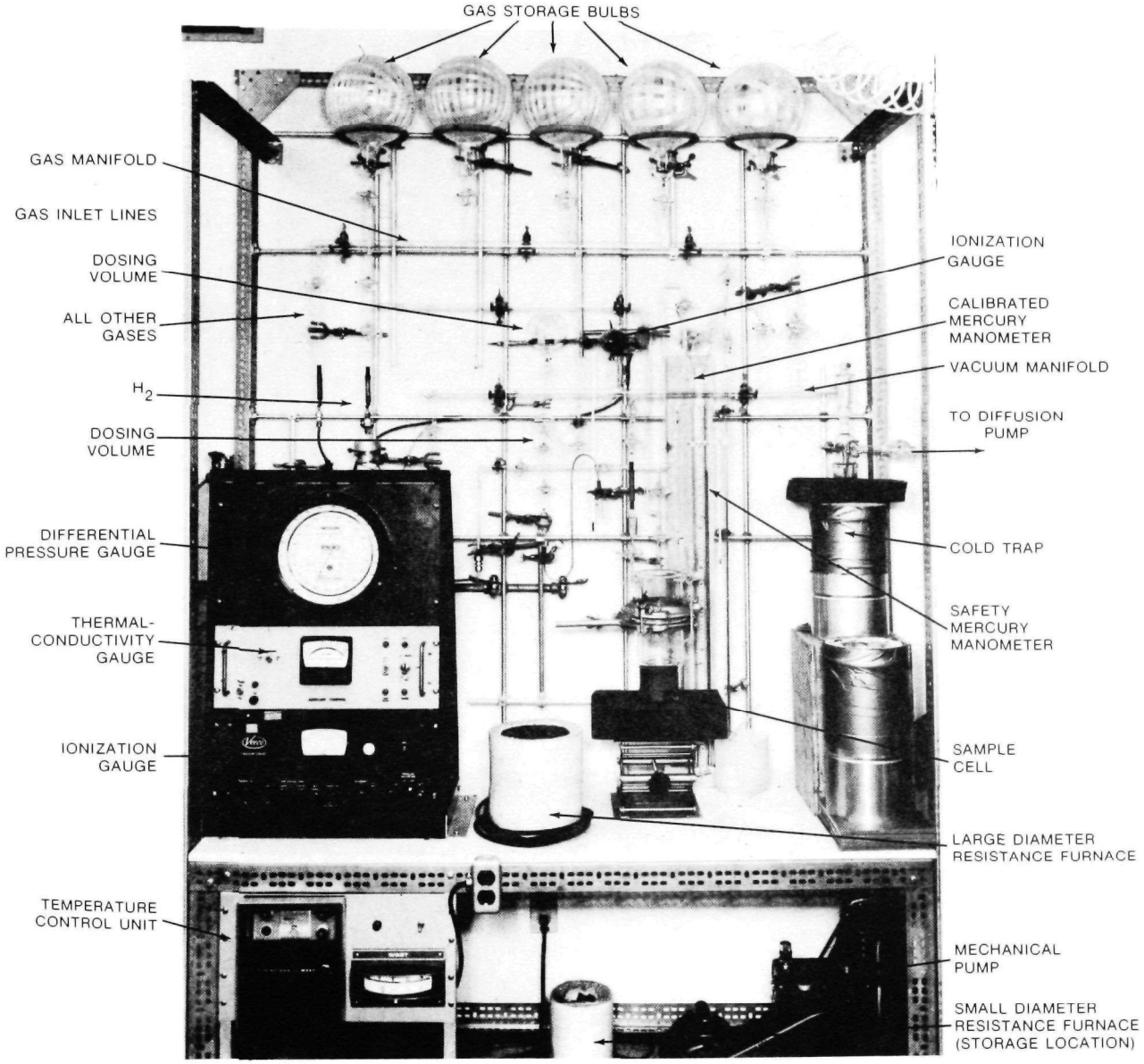

Figure 5-3. High vacuum gas adsorption apparatus.

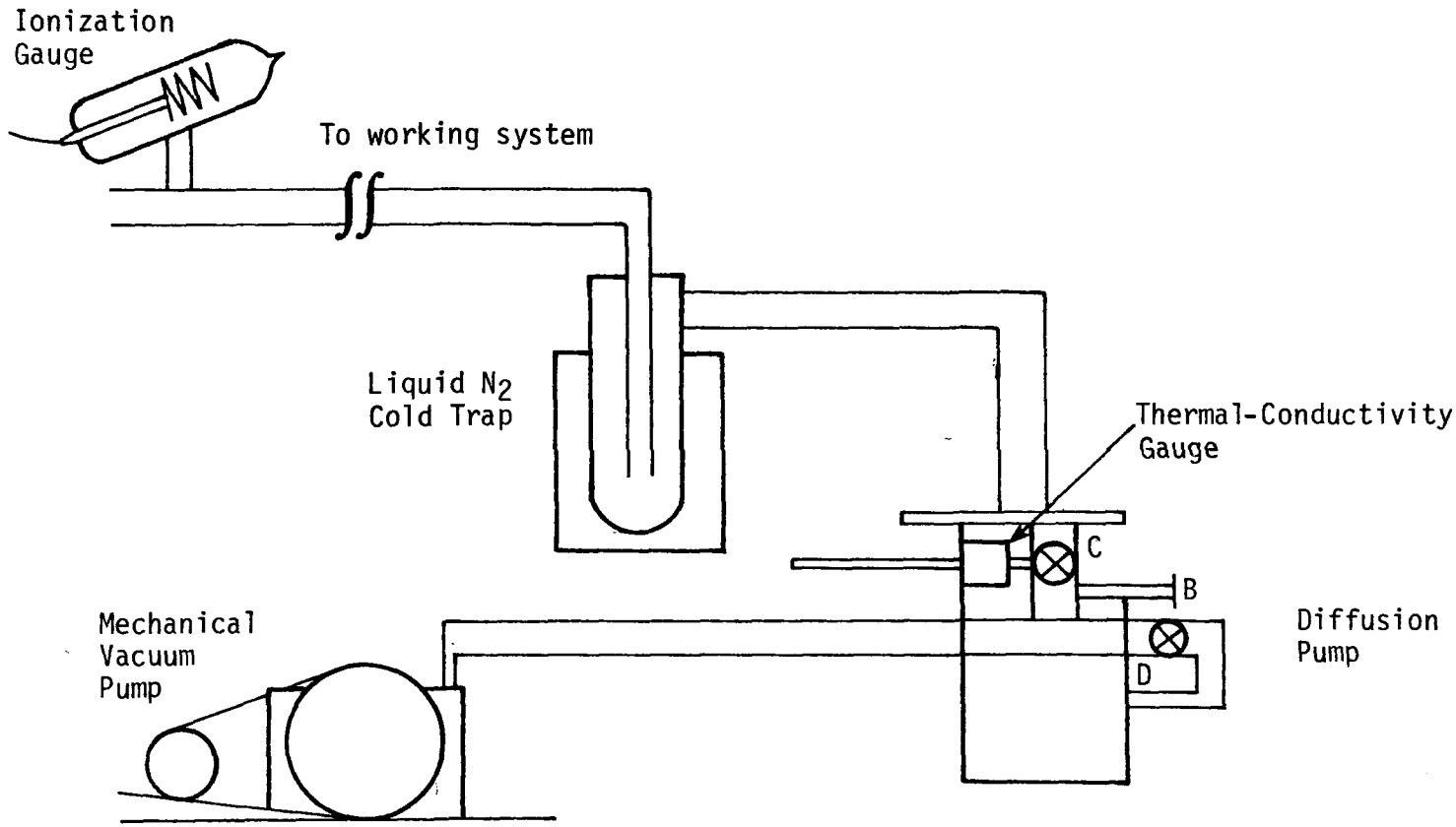

Figure 5-4. Schematic diagram of vacuum control system.

stored in 5-liter bulbs above the main manifolds. Note that a gas is introduced into a section only after the storage bulk has been evacuated or thoroughly purged with the gas.

5.4.1.3 Working Volume and Sample Cell

Figure 5-5 shows the locations of the dosing volumes (V_1 and V_4), working cross (V_2), cell connect, and pumping connection on the adsorption apparatus. The Wallace and Tiernan differential pressure gauge (shown in Figure 5-3) contains volume V_3.

The volumes used in gas adsorption measurements have been calibrated with the small dosing bulb used as a reference. Before the small bulb was sealed into place, it was weighed, filled with mercury and reweighed. The volume V_1 was calculated from the density of mercury at ambient temperature. On the basis of four measurements, the accuracy of this determination is estimated to be ±2.5 percent.

System calibrated volumes are listed in Table 5-3.

TABLE 5-3. MEASURED VOLUMES USED IN GAS ADSORPTION MEASUREMENTS

V_1 = 57.12 cc
V_2 = 3.16 cc
V_3 = 19.24 cc
V_4 = 493.40 cc

The volume extending into the Wallace and Tiernan gauge, V_3, varies slightly with pressure as the diaphragm inside the gauge shifts. The value of V_3 was established with several calibrations.

The sample cell is positioned at the pumping connection for outgassing and reduction of the catalyst system. This minimizes the time required for pretreatment since the working cross, which is made of capillary tubing, is bypassed.

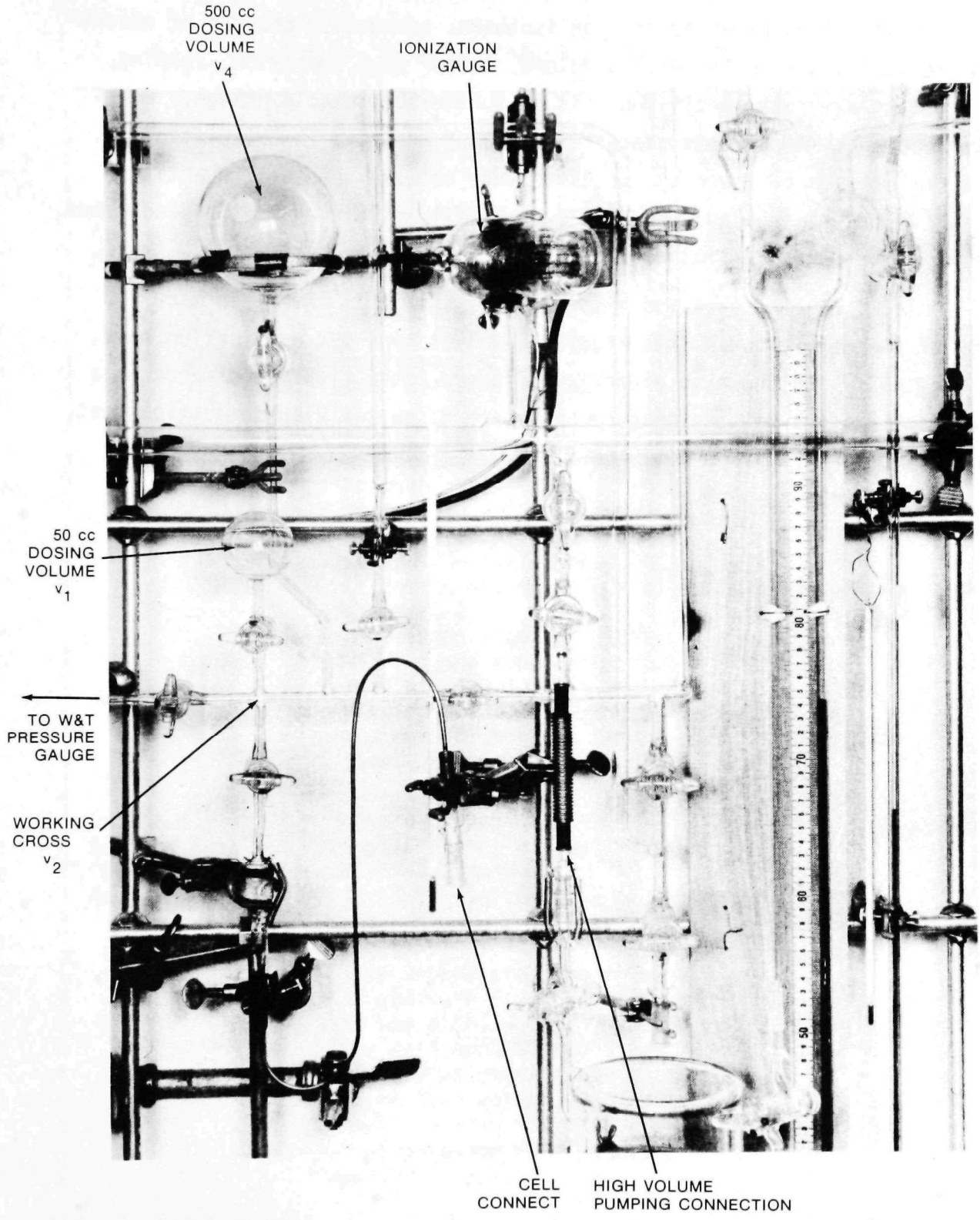

Figure 5-5. Detail of gas adsorption system showing dosing volumes.

5.4.2 Test Procedure

For the determination of BET and selected surface area by the volumetric calculation of an adsorption isotherm, successive charges of adsorbate are admitted from the dosing volume. After each admission, readings of pressure are taken until there is no further detectable change. Equilibrium is assumed at this state. The amount adsorbed is calculated for each equilibrium pressure as the difference between the total quantity of gas which has been admitted and the quantity remaining in the dead space. The catalyst characterization procedures are given in Table 5-4.

Total surface area and dispersion measurements have been made for many of the catalysts in this study. Catalyst type and application have, as a result, been shown to directly influence combustion performance in a predictable way. Catalyst measurements are discussed with combustion test data of Sections 7 through 9.

TABLE 5-4. CATALYST CHARACTERIZATION PROCEDURES

Operation	Procedure	Materials Required
Total Surface Area (BET) Measurement	1. Evacuate dosing volume, pressure gauge, and working cross; load monolith in cell. 2. Fill dosing volume with helium and measure pressure PC-1, the initial pressure in the dosing volume, and room temperature. 3. Expand helium into test cell; read pressure PC-2, the final pressure in the total volume after expansion into the test cell, at 5-minute intervals. Stop when equilibrium is reached. 4. Pump cell to vacuum and repeat steps 2-3 at different values of PC-1. 5. Steps 2-4 determine dead volume. 6. Fill dosing volume with argon and measure PC-1. 7. Expand argon into test cell; read pressure PC-2 and room temperature. 8. Repeat steps 6-7 for a minimum of five expansion points. 9. Calculate BET surface area as described in Section 5.3.1.	Nitrogen (ℓ) Helium (g) Argon (g)
Selected Surface Area (Dispersion) Measurement	1. Reduce precious metal catalyst with H_2. 2. Evacuate dosing volume, working cross, and catalyst system. 3. Fill dosing volume with hydrogen and measure pressure PC-1 and room temperature. 4. Slowly expand hydrogen into cell and read pressure PC-2. Repeat until pressure has stabilized. 5. Close test cell stopcock and repeat steps 3-4 at least three times. 6. Measure dead volume as in BET procedure. 7. Calculate dispersion as described in Section 5.3.2.	Hydrogen (g)

English

A - area
C - constant
d - diameter
i - expansion number
m_v - gram molecular volume
n - number
N - Avogadro's number
P - pressure
R - gas constant per mole
r - radius
SA - total surface area
T - temperature
V - volume
W - weight

Greek

γ - surface tension

Subscripts

o - initial or saturation condition
m - molecules
D - dosing
1 - initial condition
2 - expanded condition

Superscript

i - expansion number

REFERENCES

5-1. Brunauer, S., Emmett, P. H., and Teller, E., "Adsorption of Gases in Multimolecular Layers," Journal of the American Chemical Society, Vol. 60, p. 309, 1938.

5-2. Benson, J. E., and Boudart, M., "Hydrogen-Oxygen Titration Method for the Measurement of Supported Platinum Surface Areas," Journal of Catalysis, Vol. 4, p. 704, 1965.

5-3. Gregg, S. J., and Sing, K.S.W., Adsorption, Surface Area, and Porosity, Academic Press, New York, 1967.

SECTION 6

CATALYTIC COMBUSTOR ANALYSIS

Catalytic combustion in a honeycomb monolith is a complex process which involves the interaction of several physical and chemical phenomena. Of primary importance are (1) radial heat and mass transport between the gas and wall, (2) axial heat and mass transport in the gas, (3) axial radiative and conductive wall heat transfer, (4) heterogeneous surface and bulk gas phase chemical kinetic reactions. The interaction of these phenomena determines the maximum mass throughput and fuel conversion efficiency of the catalytic bed.

In this section, the analysis of a catalytic combustor is discussed with regard to:

- Fundamentals of operation, where a simplified version of the catalytic combustion process is described and the important system implications are introduced,
- The PROF-HET computer code, which models all of the important physical phenomena occurring within monolithic catalytic combustors and verifies some of the conclusions of the simplified model,
- Conclusions and recommendations regarding major system impacts and further analytical requirements.

The following discussion provides the information needed to understand the operation of the catalytic combustion system.

6.1 FUNDAMENTALS OF OPERATION

Catalytic combustion in a monolith bed includes the interaction of chemical reactions (surface and gas phase), diffusive heat and mass transport

(laminar or turbulent), convection, bed conduction, and radiation. These phenomena are depicted schematically in Figure 6-1. During steady operation, the catalytic combustion process can be described as follows:

- Premixed fuel and air are introduced into the combustor.
- These gases diffuse to the catalyst-coated surface of the combustor and react on the active sites at and within the surface. Near the cell entrance, where most of the gas is at low temperature, gas phase chemical reactions are unimportant.
- At the entrance, heat release is controlled by catalytic wall chemical reactions. This heat is transferred by conduction, radiation, and convection. Further down the channel, where the gas has been preheated to a high temperature, gas phase reactions become active. In this region fuel is rapidly consumed by a "flame-type" phenomenon which controls the amount of unburned hydrocarbon emissions that escape the system.
- Surface reaction products diffuse back to the main flow of gases and are carried downstream.

Under normal operating conditions, wall and gas phase reactions are active and very little unburned hydrocarbon escapes the bed for lean and stoichiometric initial mixture ratios. However, it has been experimentally observed that above a certain mass flow limit, small increases in flowrate cause an abrupt rise in unburned hydrocarbon emissions. The abruptness of the increase indicates that a "flame type" phenomenon has been extinguished. This condition, called breakthrough, represents an upper mass throughput for low unburned hydrocarbon emissions.

Increasing the mass throughput in a catalytic bed to levels much above the breakthrough point can cause the front of the bed to become cool. It has been experimentally found that small increases in mass throughput, once the front end of the bed has become cool, can cause the cool region to spread downstream. At this point, all wall reactions are extinguished and the entire bed becomes cold. This condition, called blowout, represents the maximum mass throughput for hot bed operation. It is very important to know when this blowout condition occurs for a given catalyst system.

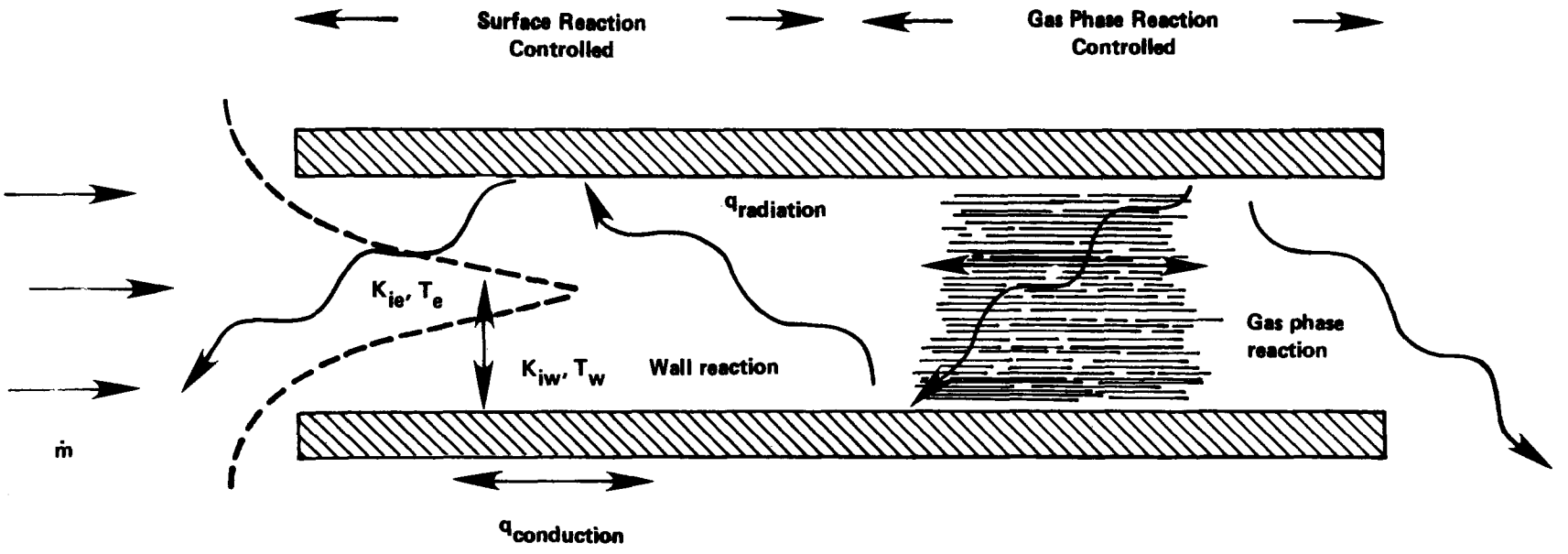

Figure 6-1. Physical events in a monolith cell.

6.1.1 Graphical Determination of Stable Surface Combustion States

For the purpose of understanding system characteristics, considerable simplification of the catalytic combustion process can be made if it is assumed that:

- No conductive or radiative heat transfer occurs
- The Lewis number is unity for all species
- The combustion reaction is a single global reaction described by an Arrhenius law equation

Based on these assumptions, the temperature at the monolith wall, T_W, can be related to the residual concentration of lean reactant at the wall, K_W, by

$$T_W = T_A - \frac{K_W}{K_E}(T_A - T_P)$$

where K_E = mass fraction of lean reactant at boundary layer edge

K_W = mass fraction of lean reactant at monolith wall

T_A = adiabatic flame temperature of fuel/oxidizer

T_P = preheat temperature of fuel/oxidizer

T_W = temperature at monolith wall

Thus, in the limit, when $K_W \to K_E$, $T_W = T_P$. When $K_W \to 0$, the surface reactions approach equilibrium conditions, and the wall temperature is equal to the adiabatic flame temperature. This relationship is shown in Figure 6-2.

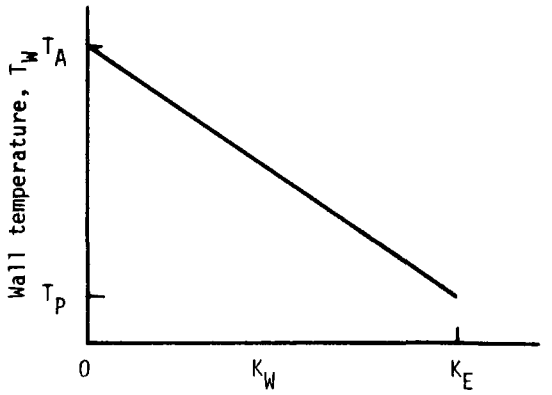

Figure 6-2. Wall temperature variation with lean reactant wall concentration.

Once the relation between T_W and K_W is established, it is possible to perform a simple mass balance on the lean reactant at the wall of the monolith bed; that is, the mass of lean reactant transported to the wall is equal to the mass of lean reactant consumed at the wall. In equation form this can be written as

$$\dot{m} = Nu \frac{\rho \mathcal{D}}{D} (K_E - K_W) = AK_W e^{-\Delta E/RT_W}$$

where $\dot{m}$ = mass of lean reactant transported to and consumed at the wall, per unit area

Nu = Nusselt number for mass transfer (Sherwood number)

ρ = gas density

$\mathcal{D}$ = diffusion coefficient

D = diameter of one channel of monolith bed

A = preexponential factor

ΔE = activation energy

R = universal gas constant

Each of these expressions for the mass flux can be shown graphically by plotting the mass flux vs. the mass fraction of lean reactant at the monolith wall (i.e., plot $\dot{m}$ vs. K_W). This is shown in Figure 6-3.

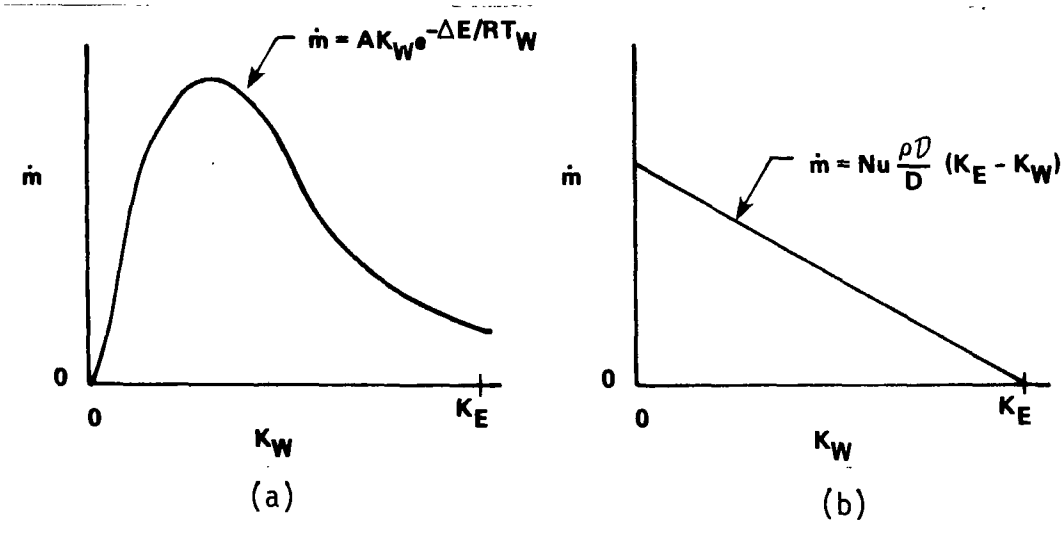

Figure 6-3. Mass flux as a function of mass fraction of lean reactant at the monolith wall.

By combining the two curves on a single graph, solutions to the simplified equation may be identified as intersections of the two curves. As shown in Figure 6-4, there are generally three solutions that can exist: a hot stable solution, an unstable solution, and a cold stable solution. Only the hot stable solution is of interest here.

For fixed preheat and inlet composition the parameters defining the rate of reactant consumption at the wall are fixed. However, the parameters defining the ordinate intercept of the reactant transport equation are functions of configuration and flowrate conditions. To study effects of these conditions on the ability to achieve hot stable solutions, it is reasonable to consider the curve of Figure 6-3(a) as fixed, and to then evaluate the cause and effect of changing the ordinate intercept of Figure 6-3(b). The solid line of Figure 6-4 represents the general case of three solutions, while the upper dashed line represents the transition to a single cold stable solution and is the blowout condition. The lower dashed line represents the transition to a single hot solution. This represents the maximum ordinate intercept to achieve self-ignition of the catalyst without an auxiliary lightoff system.

To assist self-ignition and to avoid blowout, the ordinate intercept $Nu(\rho\mathcal{D}/D)K_E$ should be minimized. For fixed entry temperature and concentration, this is achieved by

- using large diameter cells in the bed
- operating at a small value of Nusselt number

The use of large diameter cells is simply achieved, but operation at a small value of Nusselt number is more subtle. The Nusselt number at the inlet of the catalyst is of greatest importance if hot stable operation is to be achieved. In this zone, the Nusselt number increases with increasing approach velocity and decreases with the effective thickness of the cell web. Thus, blowout of the catalyst is a consequence of the increase in Nusselt number when the flowrate is increased. The benefit of using large cells should be enhanced by increasing cell web thickness at the same time.

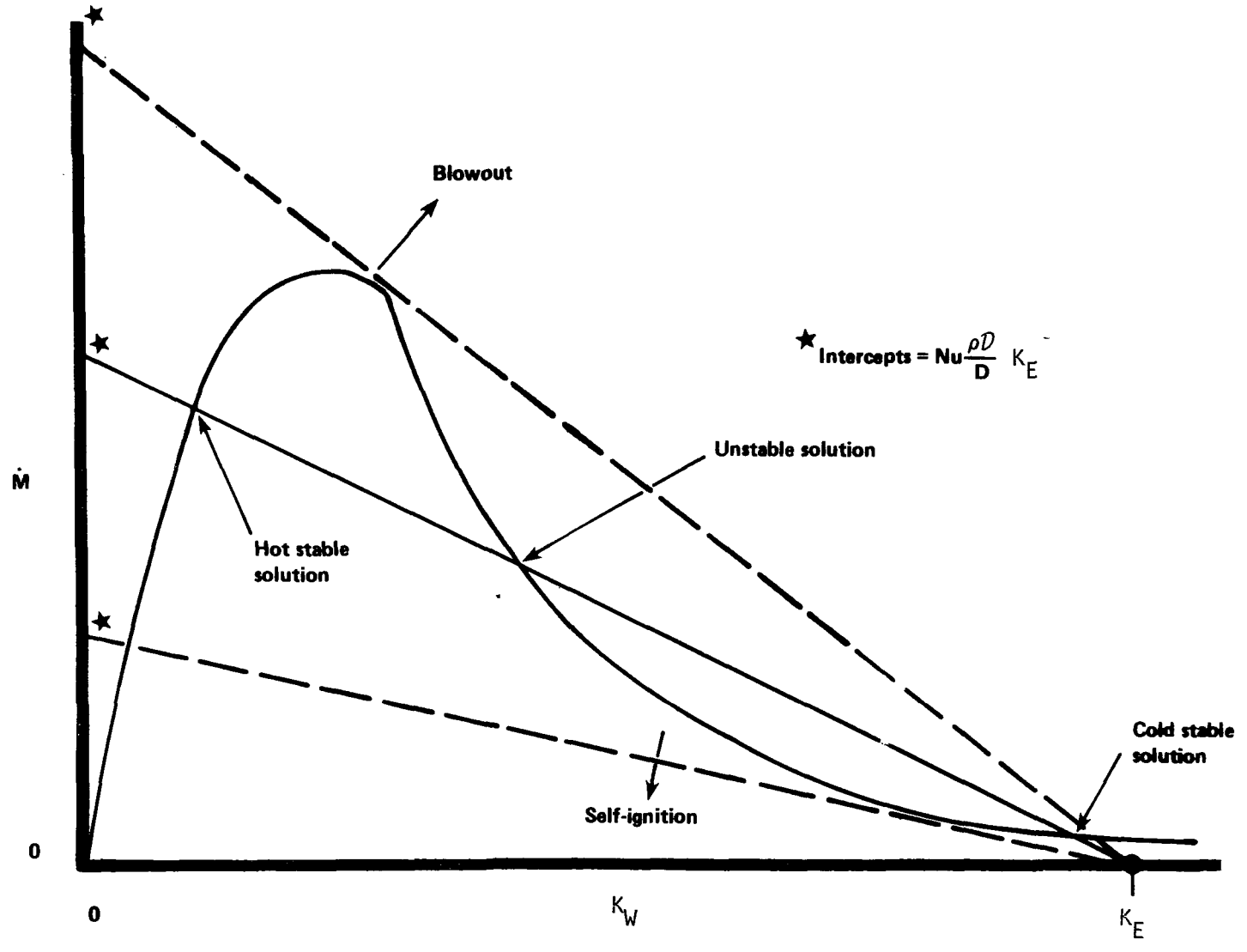

Figure 6-4. Simplified mass balance solution for catalytic combustion in a monolith bed.

Changes in the inlet concentration and temperature result in more complex effects on Figure 6-4. Of primary significance is the effect on adiabatic flame temperature, because of its exponential impact. Graphically, this causes an increase in the maximum value of the curve shown in Figure 6-3(a). To increase the adiabatic flame temperature, either preheat temperature can be raised or a concentration nearer to the stoichiometric value can be used for a given fuel/oxidizer combination.

In a practical combustion system, values of preheat temperature, composition, and flowrate are usually imposed. Thus, the most effective way to achieve stable operation is to use large diameter cells with relatively thick webs at the bed entrance. However, using large cells throughout the bed would result in poor surface conversion of combustibles to products. The amount of surface conversion is directly related to the number of transfer units in the bed, where the length of each transfer unit is equal to

$$\frac{Pr \cdot Re}{4\ Nu} \cdot D$$

where Pr = Prandtl number
Re = Reynolds number
Nu = Nusselt number
D = cell diameter

Thus, to get complete conversion on the catalyst surface, it is necessary to have many transfer units available by minimizing the length of each transfer unit. This suggests use of small diameter cells. The small cells will also accelerate gas phase reactions, which are helpful for full conversion.

6.1.2 Conclusions

As a consequence of these operational fundamentals, it appears that a catalytic monolith bed used for the purpose of combustion should use large diameter cells at the front of the bed to prevent blowout, and small diameter cells at the back of the bed to maximize the number of transfer units in a given length of bed. Therefore, for a given catalyst, it was postulated that superior performance can be obtained by using the catalyst in a graded cell

configuration, with large cells at the front end, small cells at the back end, and perhaps one or more intermediate sized cells between. A complete discussion of the model used to support these conclusions is given in Section 6.2.

6.2 THE PROF-HET COMPUTER CODE

The PROF-HET computer code models the important physical phenomena occurring within monolithic catalytic combustors. An efficient numerical technique which includes axial and radial heat and mass transport, axial radiative and conductive wall heat transfer, and heterogeneous surface and bulk gas phase chemical kinetic reactions has been developed to establish how performance varies with bed operating and design parameters. In this technique, matrix procedures are used to solve the finite difference form of the governing differential equations. The axial distribution of both wall and bulk gas properties, as well as wall temperature, are output by the code. The solution procedure is reliable and stable for the range of input parameters used to date.

6.2.1 Comparison to Existing Models

The PROF-HET model differs from previous models in that it can handle the high temperature effects of catalytic combustion, where bed radiative heat transfer and "flame type" phenomena are important. Most of the models constructed to date have focused on catalytic cleanup devices (e.g., automotive catalytic mufflers, and industrial process exhaust cleanup devices for sludge drying, PVC processing, foodstuff processing, etc.) where the temperature rise due to catalytic oxidation is small compared to that which occurs during combustion. For example, Votruba et al. (Reference 6-1) published an analytical study on the heat and mass transfer in monolithic catalysts. In their model, the heat and mass transfer normal to the channel walls was treated by a transfer coefficient approach where the detailed distribution of properties across the channels need not be known. This reduced an essentially two- or three-dimensional (for noncircular channels) problem to one dimension. Equations for the variation of wall temperature and gas conditions as a function of distance along the channel were developed. Calculations made using this model are more economical than higher dimensional

models. Illustrative predictions for catalytic monoliths where the wall temperature rise was both low and high were given. These predictions showed that monolithic structures give more stable operation and less pressure drop than packed beds. However, since radiative heat transfer and gas phase reactions were ignored and only fully developed heat transfer parameters utilized, the model cannot be accurately applied to catalytic combustors.

Cerkanowicz, et al. (Reference 6-2) presented results generated using a catalytic combustor model similar to Votruba's model, except for the inclusion of a gas phase chemical reaction. As with Votruba, only constant fully developed heat transfer coefficient values were utilized in the model. Also, the gas phase chemical reaction was assumed to be a one-step process. This approach is useful for illustrative predictions to show global effects due to gas phase reactions. However, the method is not sufficiently fundamental for exploring the types of "flame" phenomena and pollutant formation processes which occur in catalytic combustors.

Young and Finlayson (Reference 6-3) developed one-, two-, and three-dimensional models for monolithic catalytic converters. Their two- and three-dimensional models treated heat and mass transfer perpendicular to the wall by an orthogonal collocation method which determines the detailed distribution of properties across the tube. As in Votruba's model, bed radiative transfer and gas phase reactions were not included, making applications to catalytic combustors limited. Young and Finlayson's predictions showed that three-dimensional effects associated with peripheral temperature and concentration variations are not important to overall bed operation. They also showed that holding transfer coefficients constant over the bed length is not an adequate approach.

Heck (Reference 6-4), using a finite difference procedure, compared one- and two-dimensional catalytic converter model predictions. Like Finlayson, Heck concluded that one-dimensional constant heat transfer solutions were not adequate. However, he showed that if the transfer coefficients are allowed to be functions of distance and wall temperature, characteristic of developing boundary layers, predictions comparable to the two-dimensional results could be achieved at a fraction of the cost.

Following Heck, this study employs a one-dimensional model with transfer coefficients given as functions of distance, wall temperature, initial gas temperature, and inlet flow conditions. In addition to including wall reactions and bed heat conduction, the present model also includes bed radiative heat transfer and gas phase chemical reactions and axial diffusion.

6.2.2 Model Formulation

The important bed operation characteristic of blowout is controlled by events occurring near the combustor inlet. At this location, the bulk gases are relatively cool and heat release due to gas phase chemical reactions is small. Heat release in this zone is solely due to wall surface chemical reactions. The heat produced by these reactions is carried away by radial transport of heat to the bulk gases, heat conduction towards the front of the bed, and radiative transfer towards the front of the bed and into the upstream reservoir. Because the thermal boundary layer is developing in this region, the heat transfer coefficient is large. Above a certain limiting mass flow, the heat transfer coefficient for the developing boundary layer becomes so large that the radial convective heat loss plus the radiative heat loss exceeds the heat produced by wall reactions. The wall reactions are then extinguished and the bed becomes cold. To model this blowout state, the following phenomena must be treated:

- Heterogeneous surface chemical reactions
- Radial heat and mass transport
- Axial convection
- Axial bed conductive and radiative heat transfer

Unlike blowout, breakthrough and certain emissions phenomena are controlled by processes which occur away from the front of the bed where the bulk gases are hot. Breakthrough occurs when there is insufficient preheat of the bulk gases by the wall reactions to "light off" gas phase "flame-type" phenomena. Since breakthrough is believed to be flamelike in nature, in addition to the above phenomena, the following phenomena must be observed:

- Homogeneous gas phase chemical reactions
- Axial gas phase heat and mass transport

Since the controlling regions for blowout and breakthrough are spatially separated, two separate but compatible models, optimized for their respective regions, have been developed to treat blowout and breakthrough The HET numerical model is employed to determine blowout and the PROF code is used to predict breakthrough and emissions. Both codes employ compatible thermal, transport, and chemical reaction data and formulations. They differ primarily in the amount of detail included in their respective regions of application.

6.2.2.1 HET Blowout Model

The HET code governing equations are developed by integrating the steady two-dimensional gas phase species, mass, and energy equations across a plane perpendicular to the axis of a channel. This results in a set of quasi-one-dimensional equations which can be written in terms of bulk gas properties and wall heat and mass fluxes. As previously indicated, wall fluxes are treated by a transfer coefficient approach where the fluxes are directly proportional to bulk and wall gas states. The proportionality factor varies over the bed length and is a function of channel diameter, distance down the channel, inlet gas temperature, wall temperature distribution, and flow Reynolds and Prandtl numbers. The use of transfer coefficients permits the application of efficient one-dimensional solution procedures to a two-dimensional problem. Heat transport in the bed is determined by heat conduction in the solid and radiative transfer within the channel and outside into the upstream and downstream reservoirs. The radiative transfer is modeled through a view factor approach, in which all sections of the channel are able to radiatively communicate with each other and with the upstream and downstream reservoirs.

The quasi-one-dimensional governing equations are:

Species balance in the gas phase

$$\dot{m} \frac{dY_i}{ds} = AW_i - C_w J_{w_i} \qquad (6\text{-}1)$$

Species balance at the wall

$$J_{w_i} = W_{w_i} \qquad (6\text{-}2)$$

Energy balance in the gas phase

$$\dot{m}\,\frac{dh}{ds} = -C_w q_w \tag{6-3}$$

Overall energy balance

$$\dot{m}\,\frac{dh}{ds} = A_s\,\frac{d}{ds}\left(k_s\,\frac{dT_w}{ds}\right) - C_w q_r \tag{6-4}$$

Global continuity has been incorporated into these equations, and the momentum equation has been replaced by an assignment of fixed pressure. This assignment is usually reasonable for the flow rates and channel dimensions of interest.

Applying the transfer coefficient approach, wall species flux, J_{w_i}, becomes

$$J_{w_i} = \frac{\dot{m}}{A}\,C_{m_i}\left(Y_i - Y_{w_i}\right) \tag{6-5}$$

Similarly, wall heat flux, q_w, including a term due to chemical reaction between the bulk and wall gas, becomes

$$q_w = \frac{\dot{m}}{A}\,C_H\left[(h - h_w) + \sum_i \frac{C_{m_i}}{C_H}\,h_i^{T_w}\left(Y_i - Y_{w_i}\right)\right] \tag{6-6}$$

The heat transfer coefficient formulation, taken from Kays (Reference 6-5), is applicable to circular channels with variable surface temperature, and is given by:

$$C_H = \frac{1}{RePr}\left[\frac{b - 8b\sum_n \left(\frac{G_n}{\lambda_n^2}\right)e^{-\lambda_n^2 X^+} + 8a\sum_n G_n\, e^{-\lambda_n^2 X^+}}{16b\sum_n \frac{G_n}{\lambda_n^4} - 16b\sum_n \left(\frac{G_n}{\lambda_n^4}\right)e^{-\lambda_n^2 X^+} + 16a\sum_n \left(\frac{G_n}{\lambda_n^2}\right)e^{-\lambda_n^2 X^+}}\right] \tag{6-7}$$

where

$$X^+ = \frac{2x/D}{RePr}\,,\quad b = \frac{dT_w}{dX^+}\,,\quad a = T_w - T_o$$

and G_n and λ_n are constants and eigenvalues whose magnitudes (given in Reference 6-5) depend on whether the flow is laminar or turbulent. This expression is valid for flows with fully developed velocity profiles and developing thermal profiles and is assumed to be adequate for the problem of interest. Entrance effects due to channel web thickness and developing velocity profiles are not considered in the code, except to define a limiting heat transfer coefficient at the channel entrance. The limiting value is based on stagnating flow on the channel web.

The mass transfer coefficient C_{m_i} is developed from the heat transfer coefficient by:

$$C_{m_i} = C_H \, (Le_i)^{2/3} \tag{6-8}$$

Wall reactions are given by

$$W_{w_i} = k_{w_f} \, X_{w_f}^{\ell} \, X_{w_o}^{m} \tag{6-9}$$

where $k_{w_f} = A_w e^{-E_w/RT}$ and ℓ and m are arbitrary exponents on fuel and oxidizer concentrations at the wall.

Bulk gas phase reactions are given by

$$W_i = M_i \sum_m \left(\mu_{im}^{p} - \mu_{im}^{R} \right) R_m \tag{6-10}$$

where μ_i are the stoichiometric coefficients of the reaction m, and R_m is given by

$$R_m = k_{fm} \left[e^{\sum_i \mu_{im}^{R} \ln p_i} - e^{\sum_i \mu_{im}^{p} \ln p_i - \ln Kp_m} \right] \tag{6-11}$$

and k_{f_m} has the Arrhenius form $k_{f_m} = aT^b e^{-E/RT}$

The wall radiative heat flux q_r at station j is given by:

$$q_{r_j} = \varepsilon\sigma \left[\left(1 - K_{ij} \right) T_{w_j}^4 - \sum_k K_{kj} T_{w_k}^4 - K_{jr1} T_{r1}^4 - K_{jr2} T_{r2}^4 \right] \tag{6-12}$$

where K is the channel segment view factor, k denotes all other stations except j and r1, r2 denote upstream and downstream reservoirs.

Completing the definition of the problem, the boundary conditions for Equations (6-1) through (6-4) are:

$$\begin{aligned} s = 0 \qquad & Y_i = Y_{oi},\ h = h_o,\ \left.\frac{dT_w}{ds}\right|_o = 0, T_{r1} \\ s = L \qquad & \left.\frac{dT_w}{ds}\right|_L = 0,\ T_{r2} \end{aligned} \tag{6-13}$$

Applying a straightforward linear finite differencing technique, the differential Equations 6-1 through 6-4 are reduced to algebraic form. The resulting algebraic equations are solved by a Newton-Raphson matrix procedure which includes a predictor-linearized corrector step. Very briefly:

1. Initial values are guessed for T_w at all grid points
2. By applying known upstream conditions and the initial guessed T_w's, grid point values for Y_i, T, h, Y_{w_i}, T_w, h_w, etc. are found through Newton-Raphson solution procedures
3. Using the derivatives obtained from the solutions at each grid point, the rate of change of wall temperatures with respect to initially guessed wall temperatures at each grid point is constructed
4. Assuming the system is linear, corrections to all T_w's are made by applying the derivatives from step 3
5. Using the corrected T_w's as new guesses, steps 2 through 4 are repeated until guessed T_w's equal corrected T_w's

6.2.2.2 PROF Breakthrough and Emissions Model

The PRemixed One-dimensional Flame (PROF) code has been described in detail elsewhere (Reference 6-6). Very briefly, the two-dimensional governing equations are integrated across the channel, producing a set of

quasi-one-dimensional equations similar to the HET model formulation. These equations are:

Species

$$\dot{m} \frac{dY_i}{ds} = A W_i - \frac{d}{ds} (AJ_i) - C_w J_{w_i} \tag{6-14}$$

$$\dot{m} \frac{dh}{ds} = AQ - \frac{d}{ds} \left(\sum_i AJ_i h_i + Ak \frac{dT}{ds} \right) - C_w q_w \tag{6-15}$$

They differ from the HET equations by the addition of axial gas phase diffusion, J_i, and heat conduction $\sum_i J_i h_i + k\,(dT/ds)$ terms, where J_i is given by

$$J_i = - \frac{\rho \bar{D}}{\mu_1 F_i} \left[\frac{dY_i}{ds} + \frac{Y_i}{M} \left(\frac{dM}{ds} - F_i \frac{d\mu_2}{ds} \right) \right] \tag{6-16}$$

where the binary diffusion coefficient, D_{ij}, is replaced by the bifurcation approximation (Reference 6-6)

$$D_{ij} = \frac{\bar{D}}{F_i F_j} \tag{6-17}$$

and

$$\mu_1 = \sum X_i F_i, \quad \mu_2 = M \sum Y_i / F_i$$

The development of Equation (6-16) is given in Reference 6-6.

The inclusion of the axial diffusion terms makes the PROF model a multivariable (Y_i,T) boundary value problem. A difference between the PROF and HET models is the assignment of wall state (Y_{w_i}, T_w) in the PROF model, whereas in the HET model the wall state is calculated as part of the solution. For PROF calculations, the wall state is found by running the HET code for

the same inlet flow conditions. The predicted wall state is then input as a boundary condition into the PROF code. Additional boundary conditions for PROF calculations are the initial gas composition, pressure, and temperature; and the condition of no heat and mass diffusion at the downstream boundary.

The PROF code can handle many chemical species, including those which model detailed combustion and pollutant formation mechanisms. As discussed in Reference 6-6, solving the species equations, including chemical production terms, R_m, is difficult. The PROF code has been optimized so that chemical reaction rates -- from nearly equilibrated to inactive -- can be handled reliably, accurately, and efficiently. This has been demonstrated by comparison of detailed free flame species predictions and data in Reference 6-9. Also, a favorable comparison in Reference 6-9 of PROF predictions of flame quench in small diameter tubes and data demonstrates the accuracy of the code when applied to confined flame problems such as catalytic combustors.

To reduce the PROF differential equations to algebraic form, straightforward linear finite differencing is used. The resulting system of simultaneous equations are solved by a predictor-linearized corrector solution procedure which consists of the following steps:

1. Initial values are selected for Y_i, T, h at all grid points. These may be output from a prior run or may be generated by a linear interpolation between initial and guessed final values.

2. By applying known upstream conditions and the initial guessed downstream values, grid point values for Y_i, h, T, etc., are found through matrix solution of the equation set

3. When the downstream boundary is reached, the no-diffusion boundary condition is applied.

4. Using the derivatives of Y_i obtained from chemistry solutions at all grid points, the rates of change of all Y_i's with respect to initially guessed Y_i's at each grid point are constructed

5. Assuming the system is linear, corrections to all Y_i's are made by applying the derivatives from Step 4

6. Using the corrected Y_i's as new guesses, Steps 2 through 5 are repeated until the guessed Y_i equals the corrected Y_i

6.2.3 Parametric Calculations

HET code predictions illustrating the effect of bed channel diameter, preheat gas temperature, mixture ratio, conductivity (and/or void fraction) and surface activity on the important bed operating characteristics of blowout are presented. Also, PROF code predictions which show the effect of channel diameter and preheat gas temperature on the important bed operating characteristic of breakthrough are given. These results have significant system design implications for achieving catalytic combustors with high heat release (high blowout limit) and low emissions (high breakthrough limit).

Numerical results presented in Figures 6-5 through 6-10 use a surface reaction rate based on an assumed activation energy and blowout condition found experimentally at Acurex. Methane fuel and air are assigned as initial reactants in all of the calculations. For methane fuel on a platinum catalyst, Anderson (Reference 6-7) experimentally found an activation energy of 96 kj/mole. This value of activation energy was used in all of the calculations. The pre-exponential factor was obtained by matching predicted blowout mass flowrates to experimentally found values for a bed operating on methane fuel with 0.00635 m diameter channels, initial gas preheat of 672K and 193 percent excess air. The pre-exponential factor, A_w, found using this approach is 6.5×10^6 mole/m^2/sec for ℓ and m in Equation (6-9) assumed to be one and two, respectively. This pre-exponential rate factor incorporates effects of surface area, catalyst dispersion, catalyst activity, etc., and is a global rate for the experimental support/catalyst system. All calculations presented below are for a pressure of 101.3 KPa.

6.2.3.1 Blowout

Figure 6-5 gives the HET code predicted distribution of wall and bulk gas fuel concentration and temperature through a monolith bed. Initial gas conditions and bed geometrical and material properties are listed on the figure. These results are typical of catalytic combustor operation at high mass throughput and graphically illustrate how reactants are consumed.

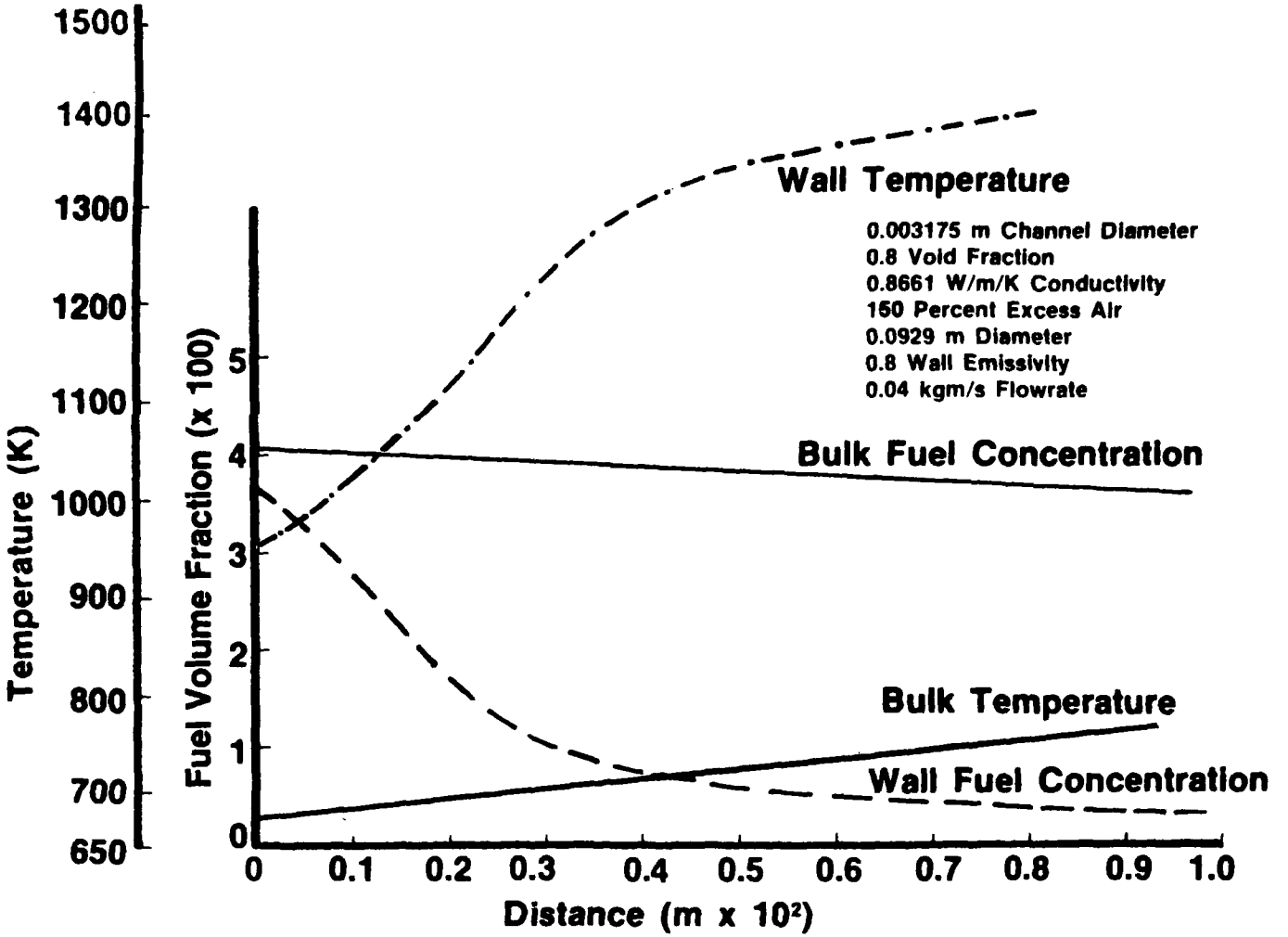

Figure 6-5. Wall and bulk gas temperature and fuel concentration through bed.

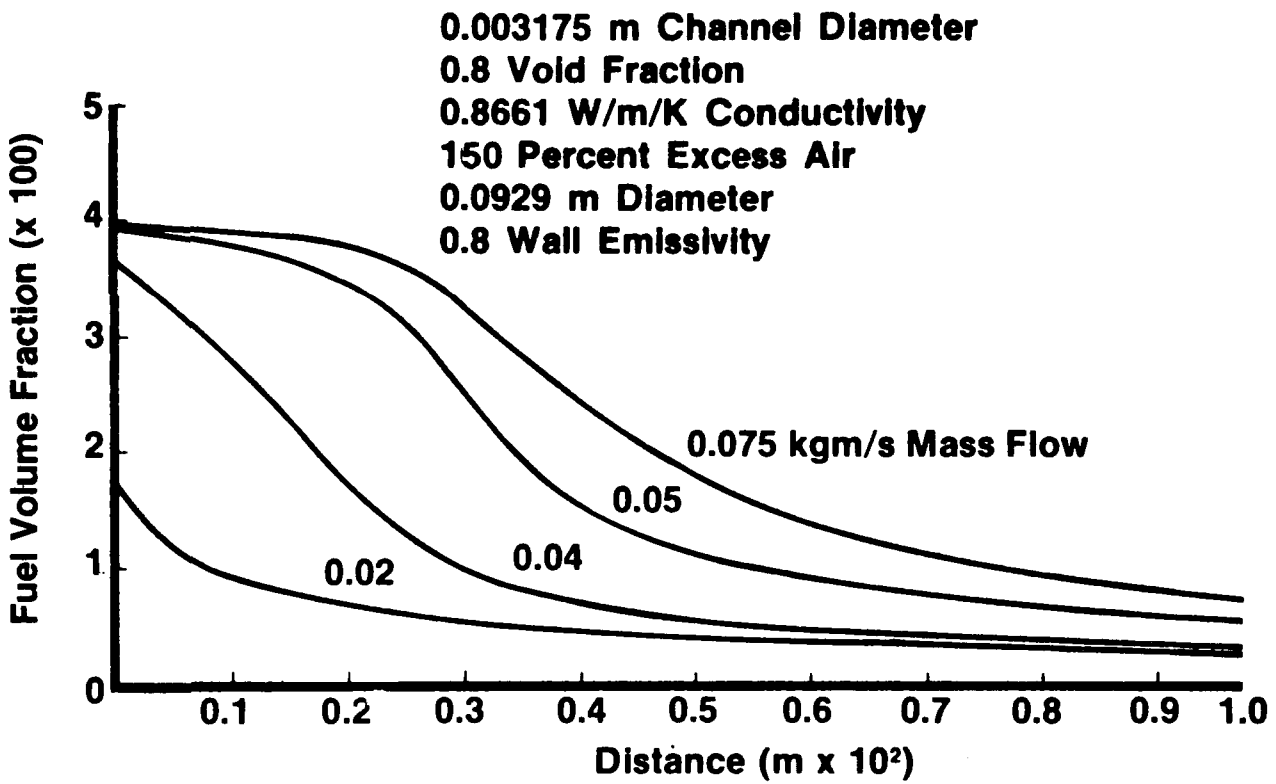

Figure 6-6. Wall fuel volume fraction distributions for several flowrates.

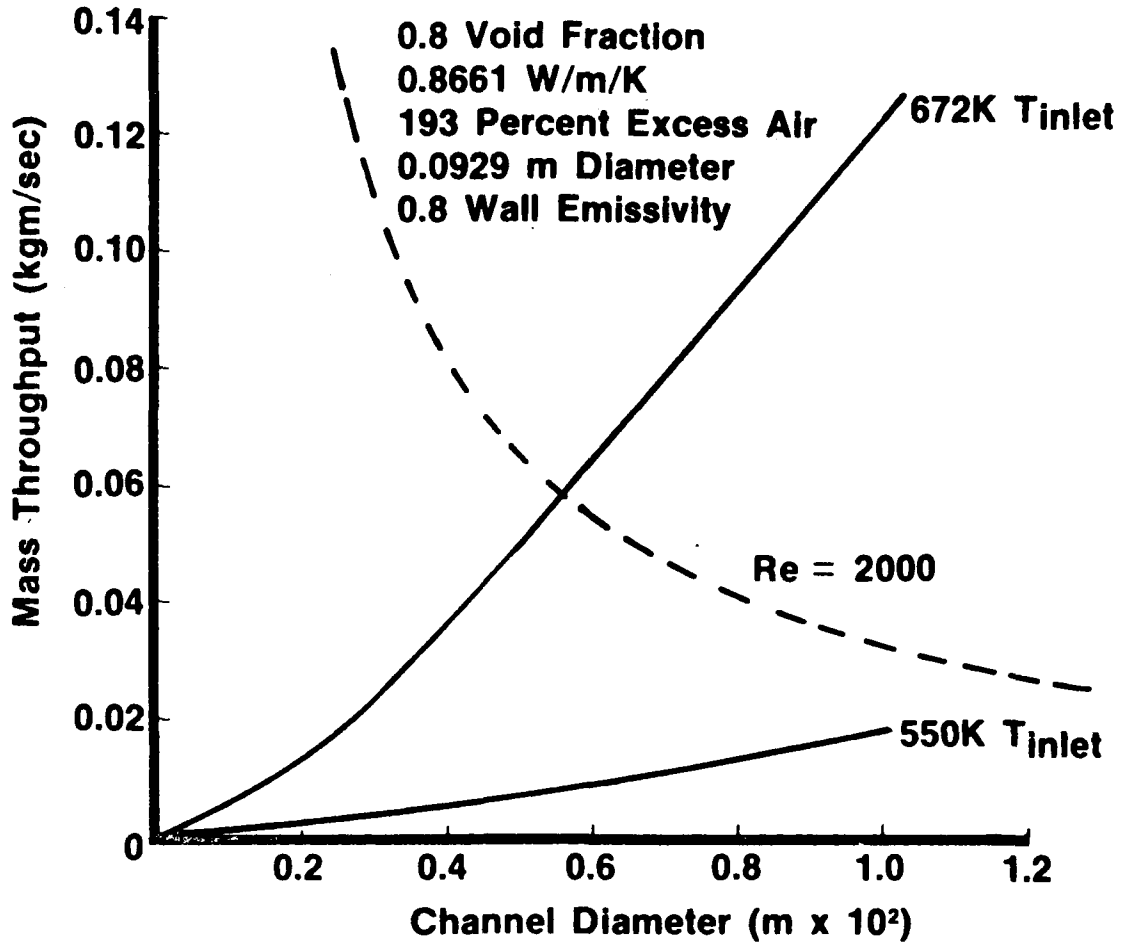

Figure 6-7. Blowout mass throughput for various channel diameters.

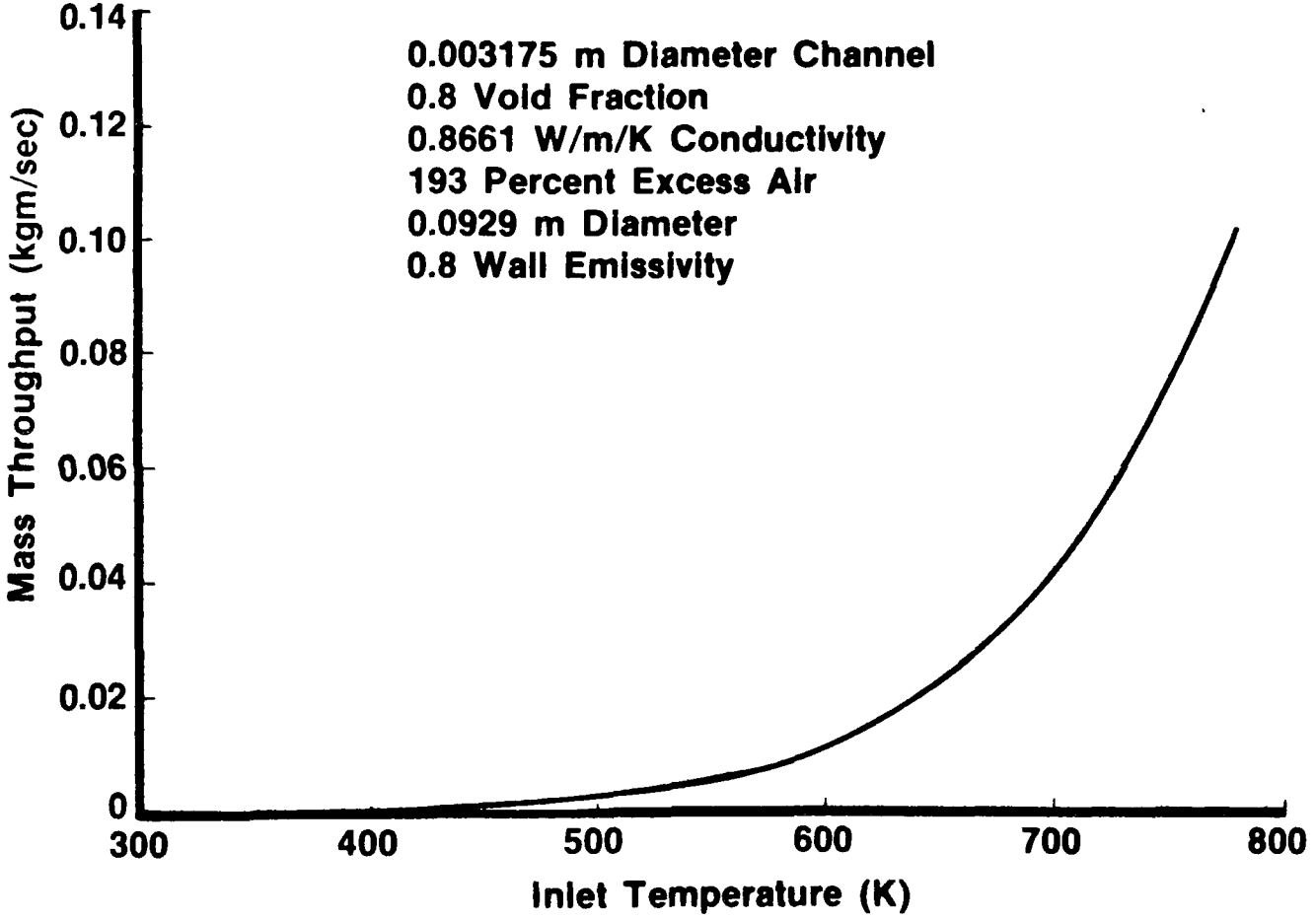

Figure 6-8. Blowout mass throughput for various gas preheats.

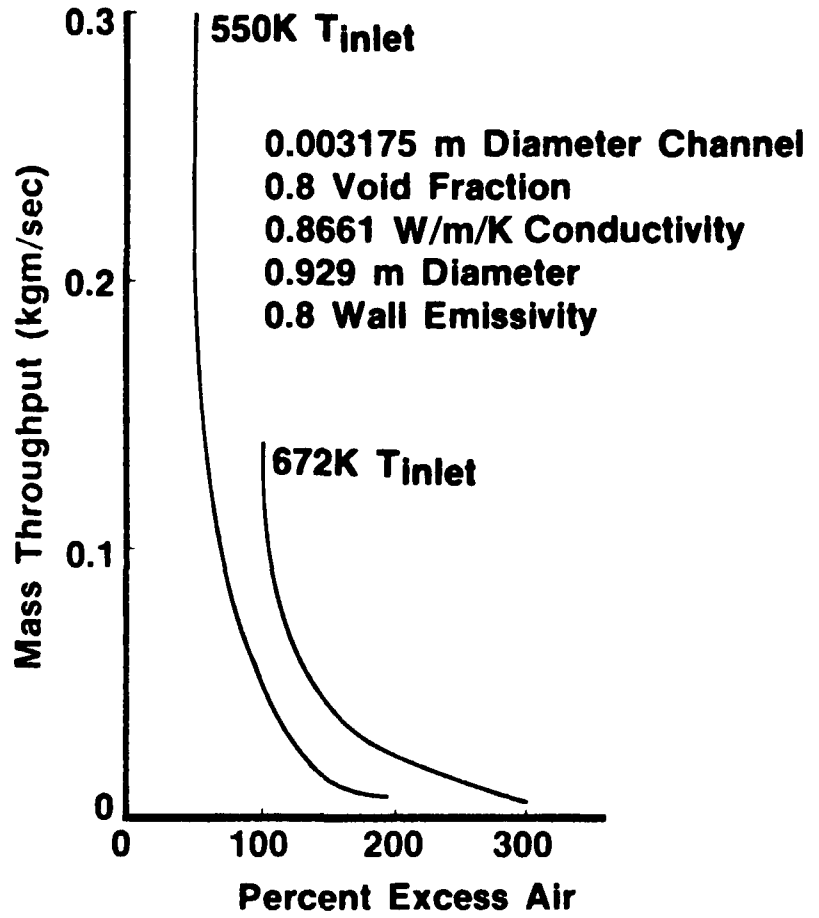

Figure 6-9. Blowout mass throughput for various excess air levels.

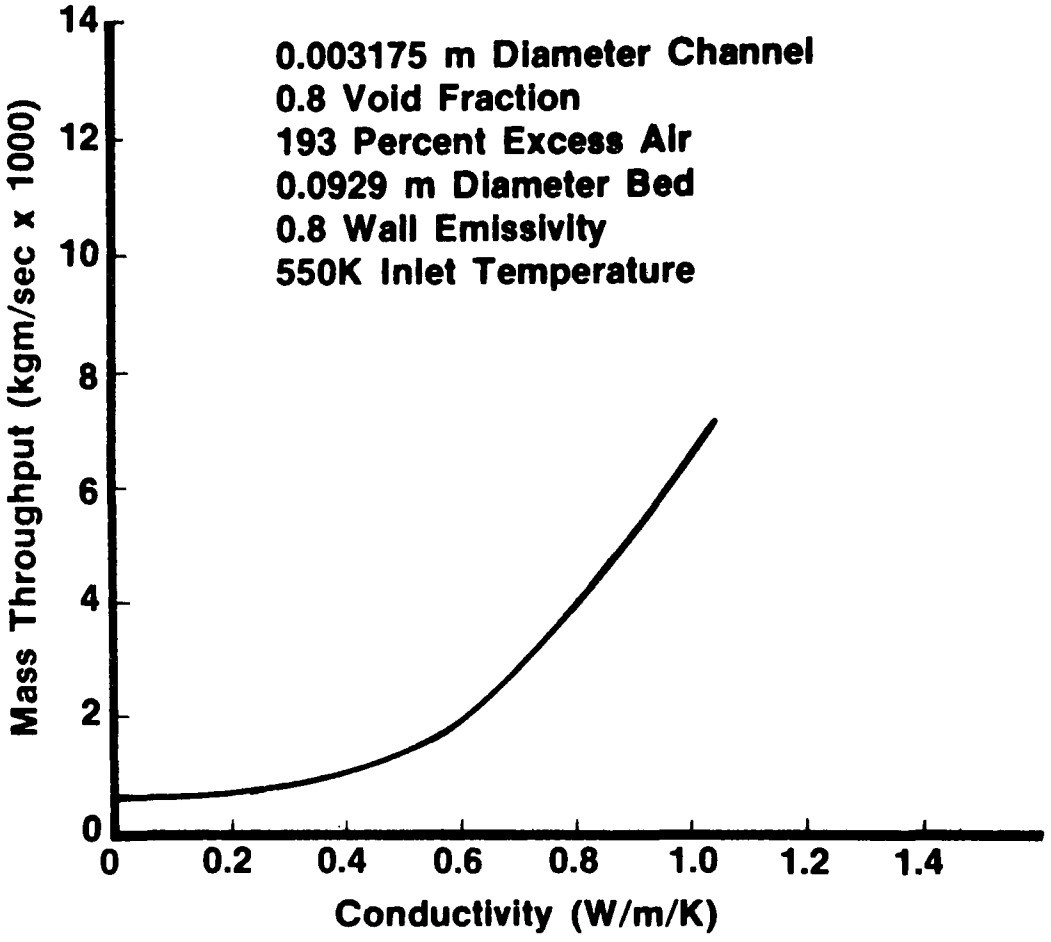

Figure 6-10. Blowout mass throughput for various bed conductivities.

Close to the channel entrance radial heat transport and radiative heat losses are large, causing the surface temperature to be much lower than the adiabatic flame temperature. At blowout, due to the low wall temperature, surface reactions become much slower than the radial transport of fuel and oxidizer to the wall, and fuel concentration at the wall is a substantial fraction of the bulk gas value. The wall reactions are controlling heat release in this case and the front of the bed is said to be kinetically controlled. Further down the channel, heat losses decrease and the wall temperature rises. This drives the wall reaction rate to much higher levels than the radial mass transport which is now controlling heat release. This region of the bed is said to be mass transfer controlled and any fuel reaching the wall is rapidly consumed giving low values of fuel concentration at the wall. As the mass flow through the channel is increased, the heat transfer coefficient and radial heat transport away from the wall is increased and a greater portion of the front of the bed becomes kinetically controlled. This is illustrated in Figure 6-6 where wall fuel concentration distributions are given for several bed mass throughputs. These results show that the kinetically controlled region spreads downstream as mass throughput increases. The wall then becomes cooler and the surface chemical reactions are extinguished.

In this study, blowout is defined as the condition where the kinetically controlled region sweeps down the bed and the wall reactions are extinguished. It should be noted that the movement of the kinetically controlled region to locations downstream where the channel flow is more hydrodynamically developed does not ease the problem of the extinguishing of wall chemical reactions. This is due to the thermal boundary layer initiation point moving concurrently with the kinetically controlled region, resulting in locally high values of heat transfer coefficient which can extinguish wall reactions.

Predictions of blowout mass throughput as a function of channel diameter are presented in Figure 6-7. The upper curve in Figure 6-7 is for a preheat temperature of 672K and the lower curve is for a preheat temperature of 550K. The parameters held constant for these calculations are

listed on the figure. These include mixture ratio, flow area, wall conductivity (or product of conductivity and wall solid cross sectional area) and surface emissivity. The dashed curve at the top of the figure is a constant Reynolds number of 2,000 line. For fully developed pipe flow, this curve represents an approximate upper limit for purely laminar flow. Between Reynolds numbers of roughly 2,000 and 10,000 is a transitional flow regime where part of the tube flow is laminar and part is turbulent. If the length-to-diameter ratio of the channel is less than 50, entrance effects and the transition of laminar to turbulent flow in the developing boundary layer must be considered.

The point of transition to turbulent flow within the channel depends on the entering freestream turbulence level, disturbances due to entrance geometry, rate of wall heating and roughness of tube wall. If the channel length is short and disturbances due to entrance effects and roughness are not severe, laminar flow can be maintained within the entire channel for values of Reynolds numbers based on channel diameter much above the fully developed 2,000 value. For the geometries and flowrates of interest, fully developed flow is never achieved in the channel and Reynolds numbers do not exceed the 2,000 limit by a large amount. Therefore, laminar flow should prevail for most of our cases of interest.

The mass throughput curves in Figure 6-7 show that blowout increases almost linearly as tube diameter increases for both the 550K and 672K preheat cases. This is primarily the result of the heat transfer coefficient, for fixed mass throughput, decreasing with increases in diameter of the cells and thickness of the web. Increasing the channel diameter permits more mass to pass through the channel before blowout occurs. However, increasing diameter also decreases the mass transfer coefficient which reduces fuel conversion efficiency. A longer bed is then required to convert all of the fuel to combustion products. Comparison of the two curves shows that preheat has a very strong influence on blowout. This is even more dramatically demonstrated in Figure 6-8 where the channel diameter is held constant at 0.003175 meters along with all the other parameters and gas preheat temperature is varied. These predictions show that preheat has a very strong influence on

blowout with higher preheat producing more than a proportionate increase in blowout mass throughput. This is due to the "activation" nature of the wall reaction rate, which is an exponential function of wall temperature. These results indicate that, for maximum heat release, beds should be operated at as high a temperature as is compatible with the degradation of the catalyst or is acceptable from an NO emissions point of view.

Figure 6-9 shows the effect of mixture ratio on blowout. The upper curve is for a preheat temperature of 672K and the lower a preheat of 550K. Numerical values of the other parameters held fixed during the calculations are listed on the figure. Both curves show a rapid rise in blowout mass flowrate as the amount of excess air is decreased. In Figure 6-9, the parameter controlling the high blowout mass throughput rates is surface temperature. For low excess air levels and no wall cooling, surface temperatures (~2200K at 0 percent excess air) are very high, exceeding present bed material operating limits. These high temperatures drive the surface chemical reaction rates to very high levels which far exceed radial (and radiative) heat losses under laminar flow conditions. Large mass flowrates are needed to produce blowout at these conditions. Once again, the strong influence of wall temperature on blowout is evident.

For the 50 percent excess air, 550K preheat case, the blowout Reynolds number based on tube diameter is in the transitional flow regime. To investigate the effect of fully turbulent flow on blowout, the HET turbulent developing boundary layer heat transfer coefficient model was activated for the 50 percent excess air case. These predictions show that the high turbulent heat transfer coefficient forces the blowout mass throughput down to very low values. At these low flowrate conditions, laminar flow would prevail and the fully turbulent flow model is not applicable. From these results, it may be conjectured that as mass throughput approaches a value such that the developing channel boundary layer transists from laminar to turbulent flow within the channel, the surface reactions in the downstream turbulent flow portion of the tube could be extinguished.

Figure 6-10 gives the effect of bed material conductivity on blowout. Since the solid cross sectional area enters the governing equations coupled

with conductivity, the variation of blowout with conductivity can also be interpreted as blowout variation with solid cross sectional area for fixed conductivity. The blowout trends in Figure 6-10 show that the blowout mass throughput varies almost linearly with conductivity. However, at low values of conductivity, the blowout limit levels off and reaches a constant value for no wall conductivity. It should be noted that radiative heat transfer is included in these calculations and, therefore, the zero conductivity calculation does not represent adiabatic conditions.

Figure 6-11 gives the effect of wall activity on blowout. Variations in wall activity model the effect of increasing surface area, catalyst loading and dispersion on blowout. Since the exponential factor in the catalyst rate expression was held fixed during these calculations, the results represent a single catalyst whose amount and distribution on a monolith bed has been varied. Results in Figure 6-11 show that the effect of surface activity on blowout is nearly linear.

The results of the parametric blowout calculations are summarized in Table 6-1. These results indicate that for maximum mass throughput, surface

TABLE 6-1. EFFECT OF PARAMETER CHANGES ON BLOWOUT

Parameter	Effect of Increase on Blowout	Comments
Channel diameter	Linear increase	
Gas inlet temperature	Exponential increase	
Initial fuel/air mixture ratio	Exponential increase in lean systems	Same type of behavior as temperature
Conductivity	Linear increase	No variation in blowout as conductivity bcomes smaller than 0.2 W/m/K.
Surface activity	Linear increase	

temperature should be as high as is compatible with the support/catalyst material combination and the channel diameter should be large. However, large

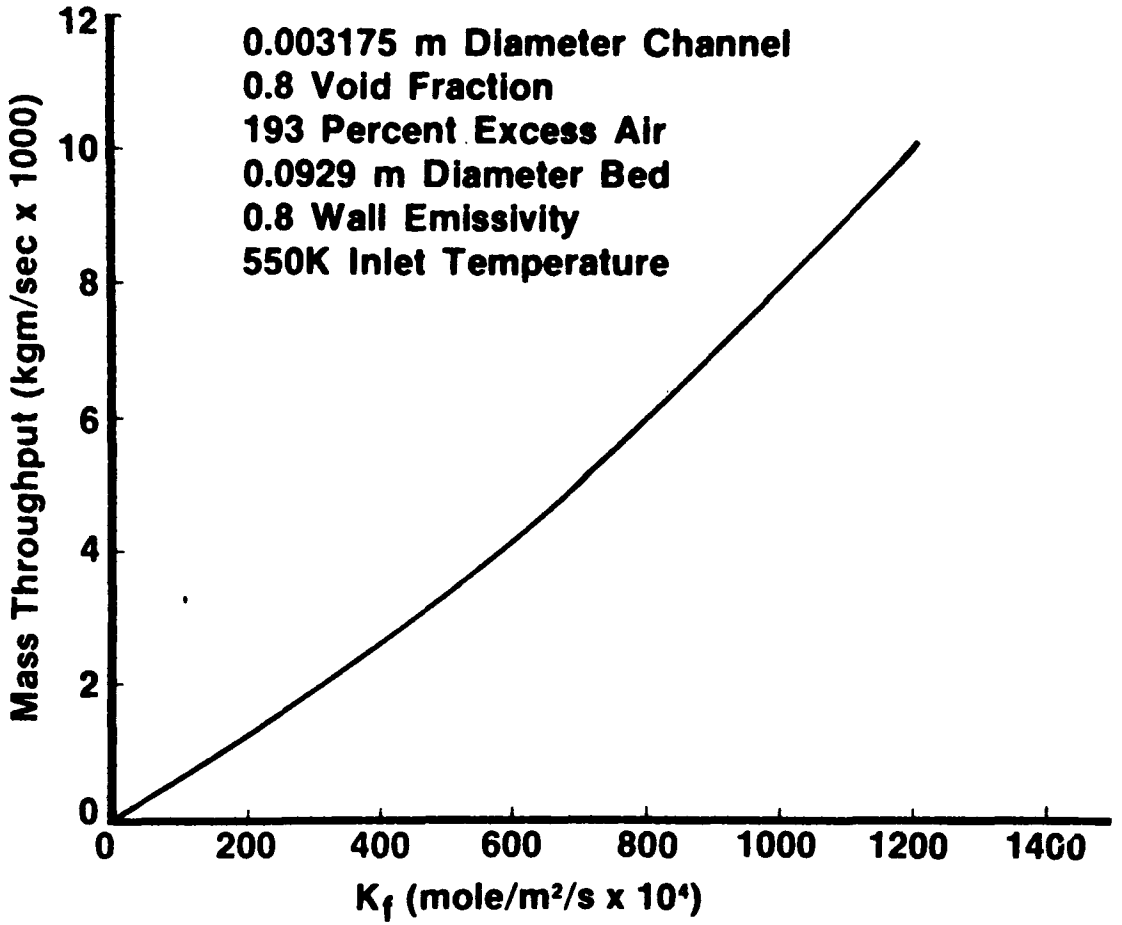

Figure 6-11. Blowout mass throughput for various surface reaction activities.

diameter channels also have poor fuel conversion performance and long beds are needed to convert all the fuel to combustion products by wall chemical reactions. This dilemma of high mass throughput but poor fuel conversion for large diameter channels can be solved by adding additional beds behind the first bed to efficiently convert the remaining fuel. Blowout should not be a severe problem for these additional beds because the entering gases are highly preheated. The next section addresses the fuel conversion or breakthrough problem.

6.2.3.2 Breakthrough

As indicated previously, large diameter channels increase blowout mass throughput but decrease fuel conversion by wall chemical reactions. Therefore, small diameter channels should be used to minimize unburned fuel emissions. However, blowout, channel mechanical forming, and pressure drop considerations limit the minimum channel diameter that can be applied. If only wall reactions are assumed to occur, complete fuel conversion in channels of practical size requires long beds. To minimize bed length, homogeneous chemical reactions must be activated to rapidly consume any fuel remaining in the bed.

As discussed previously, homogeneous gas phase reduction of fuel is postulated to be "flame-like" in nature. The PROF predictions in Figures 6-12 and 6-13 support this postulate by illustrating the importance of upstream diffusion of reactive chemical species and heat on homogeneous reactions. Boundary conditions for these calculations are listed on the figures, and Table 6-2 gives the elementary chemical kinetic reactions and associated rates applied in the calculations. The prediction represented by the dashed curve in Figure 6-12 includes both diffusion and chemical reactions. This prediction shows a rapid decay of fuel concentration, indicative of "flame-type" phenomena. In Figure 6-12, predictions represented by the solid line and circular symbols include only chemical reactions or diffusion, respectively. These predictions show the less rapid fuel decay characteristic of wall reactions only. The closeness of these results shows that axial diffusion does not significantly impact fuel concentration if homogeneous

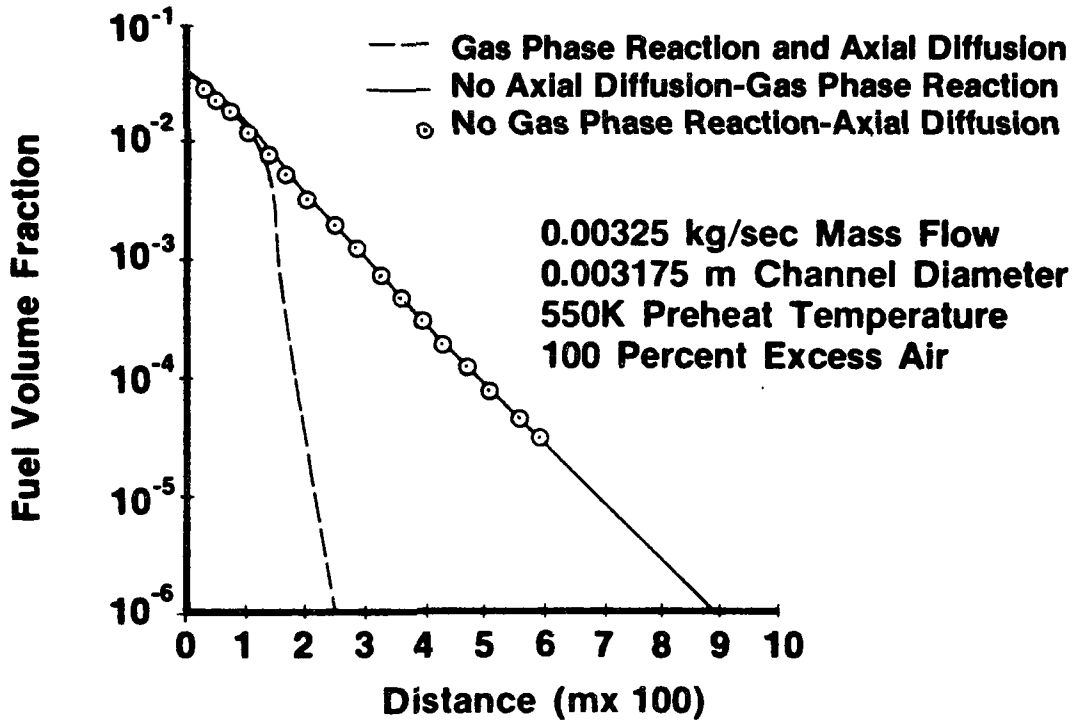

Figure 6-12. Bulk gas fuel concentration through bed.

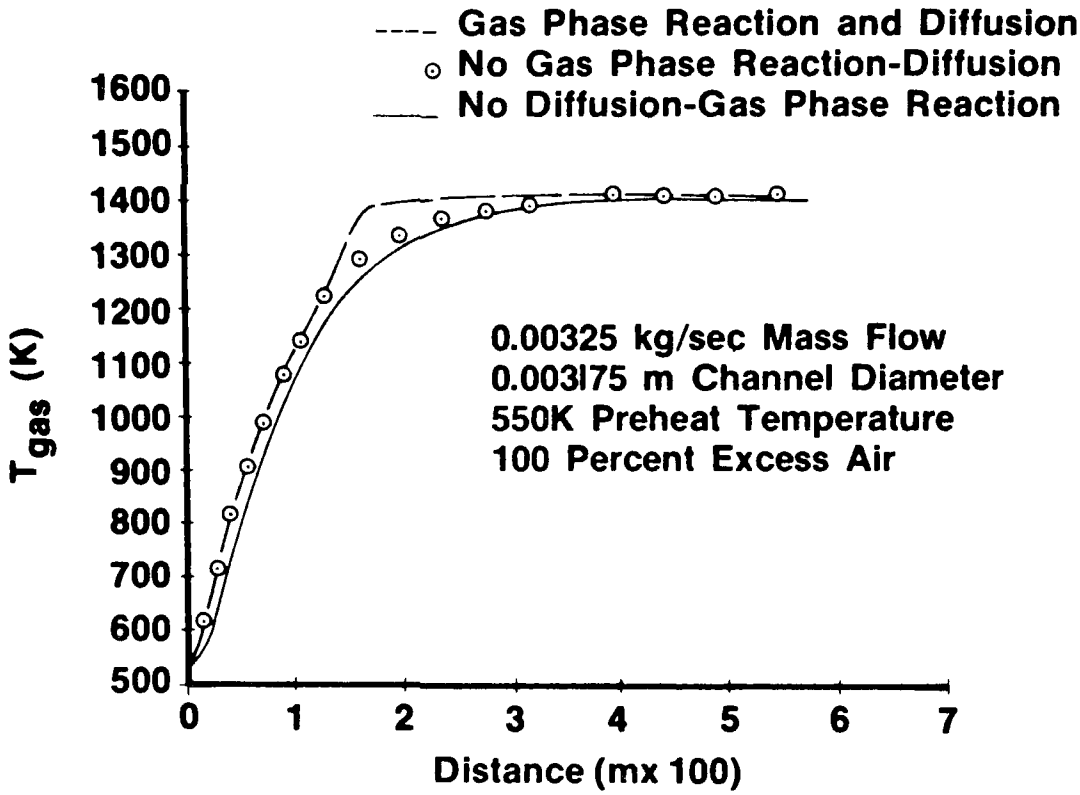

Figure 6-13. Bulk gas temperature through bed.

TABLE 6-2. CH_4 COMBUSTION CHEMICAL KINETIC REACTIONS AND RATES

KINETIC REACTION DATA

NUMBER OF REACTIONS= 28

#	REACTION		PRE EXP FACTOR	TEMP EXP	ACTIVATION ENERGY	INDIVIDUAL THIRD BODY EFFIC.	
1	CH4 +OH +	--> CH3 +H2O	.1000+14	.000	6.0000	.000	.000
2	CH4 +H +	--> CH3 +H2	.2000+15	.000	11.9000	.000	.000
3	CH4 +O +	--> CH3 +OH	.2000+14	.000	6.9000	.000	.000
4	CH3 +O +	--> CH2O+H	.3500+14	.000	3.3000	.000	.000
5	CH3 +O2 +	--> CH2O+OH	.1000+13	.000	15.0000	.000	.000
6	CH2O+ +M	--> CO +H2	.2000+17	.000	35.0000	.000	.000
7	CH2O+OH +	--> CHO +H2O	.2500+14	.000	1.0000	.000	.000
8	CH2O+O +	--> CHO +OH	.3000+14	.000	.0000	.000	.000
9	CH2O+H +	--> CHO +H2	.1700+14	.000	3.0000	.000	.000
10	CHO +O2 +	--> CO +HO2	.3000+14	.000	.0000	.000	.000
11	CHO +OH +	--> CO +H2O	.1000+15	.000	.0000	.000	.000
12	CHO +O +	--> CO +OH	.5000+12	.500	.0000	.000	.000
13	CHO + +M	--> CO +H	.2000+13	.500	28.8000	.000	.000
14	CO +OH +	--> CO2 +H	.5500+12	.000	1.0800	.000	.000
15	CO +O +M	--> CO2 +	.3600+19	-1.000	2.5000	.000	.000
16	HO2 +O +	--> O2 +OH	.2500+14	.000	.0000	.000	.000
17	HO2 +OH +	--> O2 +H2O	.2500+14	.000	.0000	.000	.000
18	HO2 +H +	--> OH +OH	.2500+15	.000	2.0000	.000	.000
19	HO2 +H +	--> O2 +H2	.2500+14	.000	.0000	.000	.000
20	H +O2 +M	--> HO2 +	.2000+16	.000	.8700	H2O 20.000	.000
21	H +O2 +	--> OH +O	.2200+15	.000	16.8000	.000	.000
22	O +H2 +	--> OH +H	.1700+14	.000	9.4600	.000	.000
23	OH +H2 +	--> H2O +H	.2200+14	.000	5.2000	.000	.000
24	OH +OH +	--> H2O +O	.6000+13	.000	.7800	.000	.000
25	H +OH +M	--> H2O +	.7000+20	-1.000	.0000	.000	.000
26	O +H +M	--> OH +	.4000+19	-1.000	.0000	.000	.000
27	H +H +M	--> H2 +	.2000+20	-1.000	.0000	.000	.000
28	O +O +M	--> O2 +	.4000+19	-1.000	.0000	.000	.000

reactions are inactive. The effect of including both diffusion and chemical reactions can also be seen in Figure 6-13. This figure shows that predictions which include both diffusion and chemical reaction have a rapid rise in temperature indicative of "flame-type" phenomena whereas other calculations show a much slower rise to the final temperature, indicative of wall reactions. The "flame-type" nature of the homogeneous fuel concentration reduction is further shown in Figure 6-14, which presents detailed species concentrations through the channel. From this figure it can be seen that the rapid decay of CH_4 is accompanied by an increase in free radicals (O atoms for example) and production of CO and H_2. The CO and H_2 are subsequently oxidized to CO_2 and H_2O. This sequence of events is very similar to those which occur in free methane/air flames, and demonstrates the "flame-type" nature of the processes occurring within the catalytic combustor. It may be concluded that, to accurately predict breakthrough, the analytical model must include the effects of axial heat and mass diffusion, as well as homogeneous chemical kinetic reactions.

PROF code predictions demonstrating the effect of channel diameter on breakthrough are given in Figure 6-15. Axial heat and mass diffusion, as well as chemical kinetic reactions, are included in these and all subsequent calculations. The boundary conditions for this case are listed on the figure and chemical kinetic reactions and rates are given in Table 6-2. Figure 6-15 shows that, as channel diameter is decreased, the rapid fuel decay region associated with "flame-type" phenomena moves towards the front of the bed. This is due to the acceleration of bulk gas heating through the increase in heat transfer coefficient which accompanies reductions in channel diameter. Examining detailed computer printout shows that for this 100-percent excess air case, the "flame-type" phenomena is initiated at a channel bulk gas temperature of approximately 1400K. These results show that wall reactions play an important role in preheating the gases to temperatures sufficiently high to light off the "flame-type" phenomenon. The importance of gas preheat is shown in Figure 6-16, where predictions of fuel concentrations for a fixed channel diameter and several inlet bulk gas mixture temperatures are presented. As can be seen, preheating the inlet gas to higher temperatures causes the "flame-type" rapid fuel decay region to

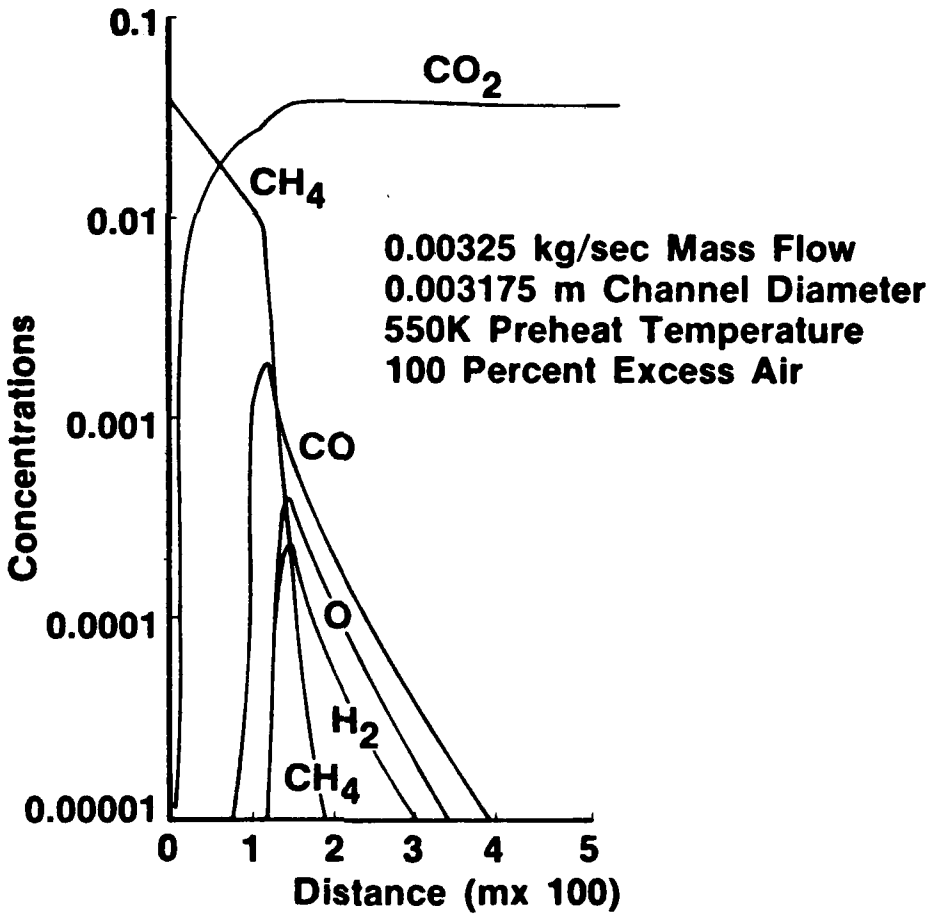

Figure 6-14. Detailed species concentrations through bed.

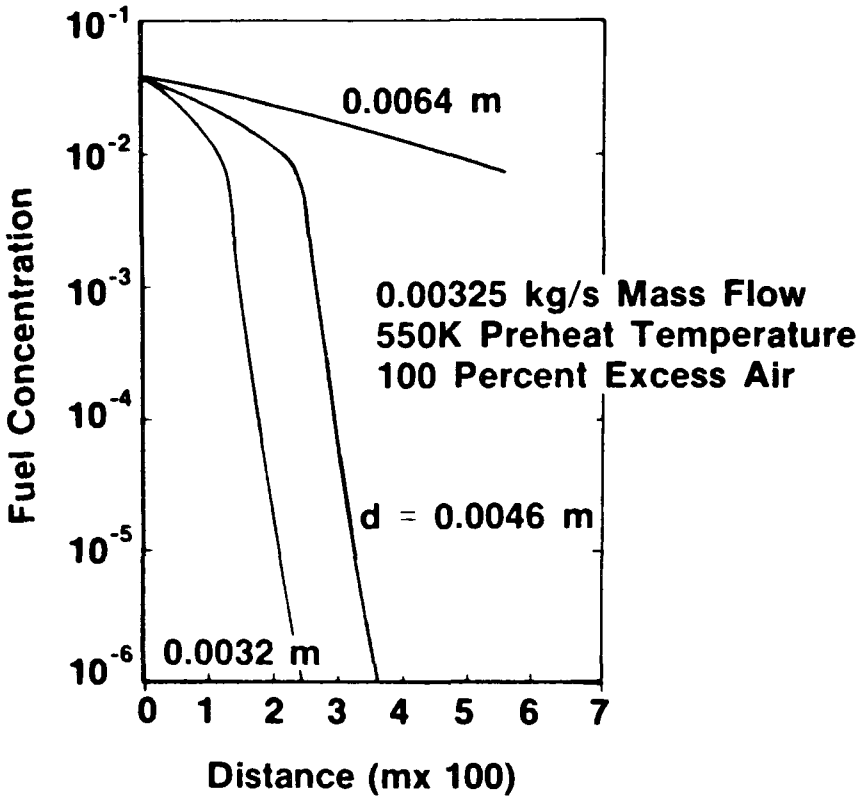

Figure 6-15. Effect of channel diameter on breakthrough.

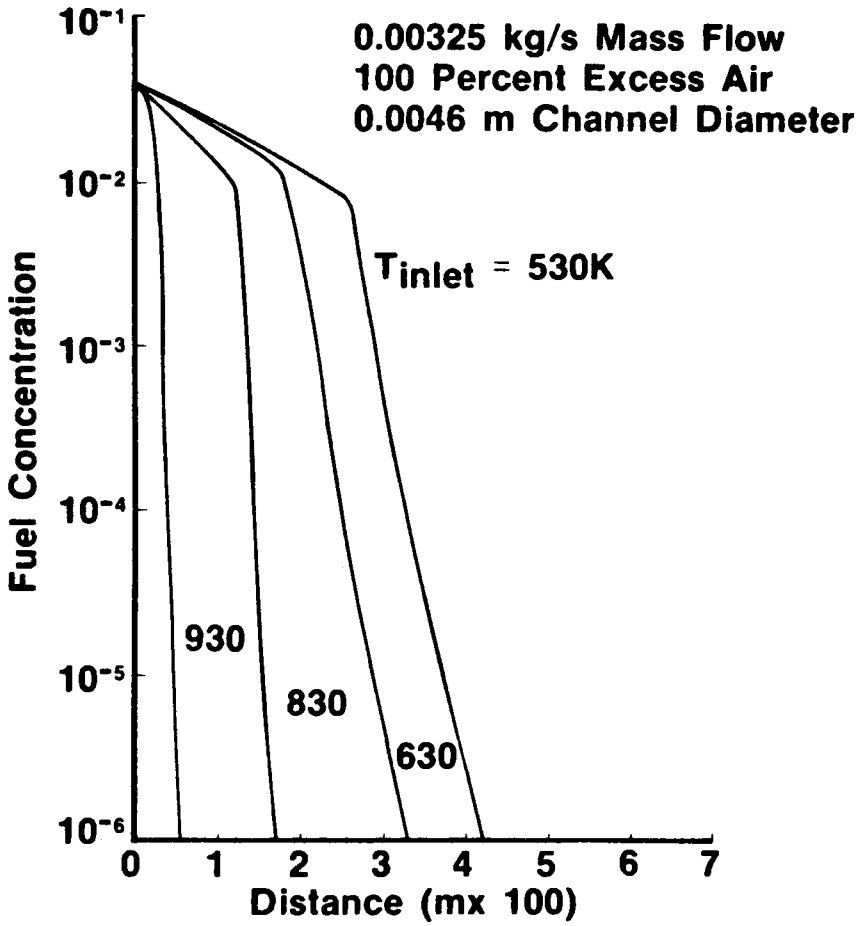

Figure 6-16. Effect of gas preheat temperature on breakthrough.

approach the front of the bed. For these cases the "flame-type" phenomenon is initiated at a bulk gas temperature of approximately 1400K.

In summary, the parametric breakthrough calculations show that initiation of "flame-type" phenomena in catalytic combustors requires high channel bulk gas temperatures. These temperatures can be achieved by a combination of wall reaction heating, which is a function of channel diameter, and/or inlet gas preheat. Once the "flame-type" phenomena are active, rapid decay of fuel and fuel fragments, characteristic of free flame behavior, is achieved. If "flame-type" phenomena are active, only short bed lengths are needed to reduce unburned fuel and fuel fragments to extremely low concentrations.

6.3 CONCLUSIONS

The PROF and HET codes have been used to characterize catalytic combustor performance. The calculations are in qualitative agreement with experimental results, but a detailed comparison at matching conditions has not been attempted. HET code predictions indicate that blowout mass throughput increases roughly linearly with increases in channel diameter, conductivity, and catalyst/support surface activity. Also, blowout increases roughly exponentially with increases in inlet mixture preheat temperature and fuel/air ratio for lean operation. Therefore, for maximum catalytic combustor mass throughput, surface temperature should be as high as is compatible with the support/catalyst material combination and channel diameter should be large. Maximum channel diameter, however, is limited by fuel conversion requirements.

PROF code predictions show that homogeneous chemical kinetic phenomena in catalytic combustors are "flame-like" in nature and proper modeling of this effect requires treatment of axial heat and mass diffusion as well as homogeneous chemical kinetic reactions. Predictions which include axial diffusion indicate that the rapid decay of fuel, associated with "flame-type" phenomena, moves towards the front of the bed as channel diameter is decreased and initial preheat temperature is increased. This occurs with the wall at an equilibrium condition and the surface at the adiabatic flame temperature, as long as the flow conditions are not near blowout.

These results show that high gas temperatures, produced by either wall reaction heating or high preheat, are needed to "light off" the "flame-type" phenomena in catalytic combustors.

Predictions suggest that a catalytic combustor system which has high mass throughput (high blowout limit) and low emissions (no breakthrough) could be constructed by joining two or more bed segments in series. The first segment would have channels large enough to prevent blowout and yet small enough to convert sufficient fuel to meet the preheat/blowout requirement of the second bed segment. The second segment would have smaller diameter channels to convert more of the fuel to products and further heat the gases. The last segment would have very small diameter channels and the entering gas preheat would be sufficient to "light off" homogeneous "flame-type" phenomena. Any fuel remaining in this segment would be rapidly consumed by homogeneous reactions. This system design, called the graded cell concept, is described in detail in Section 8. As described in Reference 6-8, tests have shown this system to have very high mass throughputs and heat release while maintaining very low unburned hydrocarbon, CO, and NO_x emissions.

6.4 RECOMMENDATIONS

The PROF-HET catalytic combustion code has been used to characterize blowout and breakthrough phenomena. Further use of the code to aid in catalytic combustor system design would be beneficial. Four recommended tasks are described below.

6.4.1 Graded Cell Catalyst Optimization Maps

The length and stability of graded cell catalytic combustors can be designed by matching the fuel conversion and preheat requirements for all combustor segments. The optimization procedure can be developed by preparing maps of fuel conversion, pressure, and bulk gas temperature as a function of combustor length for a variety of channel diameters and preheat temperatures. Blowout mass flowrate limits for these parameters should also be noted. Performing this procedure would result in a combustor design of two or more segments having optimal stability and minimal pressure drop.

6.4.2 Breakthrough Analysis

Calculations have shown that the initiation of gas phase reactions for a given mixture ratio and fuel occurs at a relatively constant bulk gas temperature, independent of channel diameter and initial preheat temperature. It is possible that the homogeneous phenomena behave as a free flame. Existing calculations should be further examined and additional calculations made to establish the nature of the initiation of gas phase reactions in a catalytic combustor. Results would be compared to free flame data, and determine if gas phase reaction initiation is similar to free flame behavior. If this is the case, it may be possible to apply free flame results to catalytic combustor gas phase phenomena, and to describe the initiation of gas phase reactions in terms of fuel type, initial mixture ratio, and bulk gas temperature alone.

6.4.3 NO_x Emission Characteristics of Catalytic Combustors

Experimental results reported in Section 8 show that the presence of a surface markedly reduces NO_x emissions. It is currently unknown how much NO_x is formed within the combustor and how much is formed downstream of the combustor in gas phase reactions. To gain insight into the potential NO_x formation mechanisms within the combustor, a NO_x formation model (Zeldovich) which has been successfully applied to free flames should be applied to catalytic combustors. Wall conditions would be varied from heat loss only to full equilibrium conditions. These calculations would then be compared qualitatively to experimental results for catalytic combustors and free flames to determine if NO_x formation processes within free flames are similar to those within catalytic combustors, and to determine how much NO_x formation takes place within the combustor.

6.4.4 Effect of Transition on Blowout

Catalytic combustors for gas turbine (and some boiler) applications will operate near the laminar/turbulent transition flowrate. The transition to turbulent flow can significantly increase the potential for blowout. Existing information on transitional flow heat and mass transfer should be included in the code to enhance its use in practical system design work.

LIST OF SYMBOLS

A	cross sectional area
C_H	Nusselt number divided by Reynolds and Prandtl numbers
C_m	dimensionless mass transfer coefficient defined by Equation (6-8)
C_p	specific heat
C_w	circumference of bounding tube
D_{ij}	binary diffusion coefficient
$\overline{D}$	diffusion constant defined by Equation (17)
E	activation energy for kinetic reaction
F_i	diffusion factor of species i
h	enthalpy
J	species flux
k	thermal conductivity
K	channel segment radiative heat transfer view factors
K_p	equilibrium constant
Le	Lewis number
$\dot{m}$	mass rate of gas
M	molecular weight
p	pressure
Pr	Prandtl number
q	heat flux
R	gas constant
Re	Reynolds number
s	distance along flame axis
T	temperature
W	chemical production rate

X	mole fraction
Y	mass fraction
ε	wall emissivity
ρ	density
σ	Stefan-Boltzmann constant

Superscripts

P	reaction products
R	reaction reactants

Subscripts

i	denotes species
m	denotes reaction
o	inlet conditions
r	radiation
r1	upstream reservoir
r2	downstream reservoir
s	solid bed material
w	wall

REFERENCES

6-1. Votruba, J., Sinkule, J., Hlavacek, V. and Skrivanek, J., "Heat and Mass Transfer in Monolithic Honeycomb Catalysts-I.", Chemical Engineering Science, 1975, Vol. 30, pp. 117-123, Pergamon Press, Great Britain.

6-2. Cerkanowicz, A. E., Cole, R. B. and Stevens, J. G. "Catalytic Combustion Modeling; Comparisons with Experimental Data," ASME paper 77-GT-85, presented at the ASME Gas Turbine Conference, Philadelphia, Pennsylvania, March 27-31, 1977.

6-3. Young, L. C., and Finlayson, B. A., "Mathematical Models of the Monolith Catalytic Convertor; Part II. Application to Automobile Exhaust," AIChE Journal, Vol. 22, No. 2, pp. 343-353, March 1976.

6-4. Heck, R. H., Wei, J., and Katzer, J. R., "Mathematical Modeling of Monolithic Catalysts," AIChE Journal, Vol. 22, No. 3, pp. 477-484.

6-5. Kays, W. M., Convective Heat and Mass Transfer, McGraw Hill, New York, 1966.

6-6. Kelly, J. T., and Kendall, R. M., "Premixed One-Dimensional Flame (PROF) Code Development and Application," Proceedings of the 2nd EPA Stationary Source Combustion Symposium, Volume IV, EPA-600/7-77-073d, July 1977.

6-7. Anderson, R. B., Stein, K. C., Feenan, J. J. and Hofer, L.J.E., "Catalytic Oxidation of Methane," Industrial and Engineering Chemistry, Vol. 53, No. 10, pp. 809-812, October 1961.

6-8. Kesselring, J. P., Krill, W. V., and Kendall, R. M., "Design Criteria for Stationary Source Catalytic Combustors," Western States Section/ The Combustion Institute Fall Meeting on Catalytic and Fluidized Bed Combustion, Paper Number 77-32, Stanford, California, 17-18 October 1977.

6-9. Kendall, R. M. and Kelly, J. T., "Premixed One-Dimensional Flame Code (PROF) — Its Formulation, Manipulation, and Evaluation," Aerotherm Report TR-75-158, July 1975.

SECTION 7

CATALYST SCREENING TESTS

7.1 GENERAL CONSIDERATIONS

A series of catalyst combustion tests were performed at the Jet Propulsion Laboratory (JPL) in Pasadena, California, to identify those catalysts which are most suitable for stationary combustion system development. A suitable combustion catalyst has the following characteristics:

- Low ignition temperature (both initially and at restart conditions)
- Low preheat requirements for sustained combustion
- Combustion uniformity throughout the catalyst bed for a variety of test conditions
- High heat release capability
- High combustion efficiency
- Low pollutant emissions
- High temperature operation capabilities (material-limited)
- Operational with a variety of fuels, both gaseous and liquid
- Long life

Catalysts were selected based on the review reported in Section 4. The JPL test series identified catalyst properties which are important for each of the above combustion characteristics. The following subsections discuss the program approach to combustion testing, the actual test data that was obtained, and conclusions and recommendations for further system

development. Pre- and post-test catalyst measurements (as described in Section 5) were used to support combustion findings.

7.2 CATALYST TEST MATRIX

Combustion screening was preceded by the development of a test matrix of catalyst models. Each model is made up of the support, washcoat, and catalyst materials which became the main variables in the matrix. More specifically, the matrix was developed to:

- Identify appropriate ceramic support materials
- Compare washcoat materials and application techniques
- Investigate catalyst types and the effects of loading
- Verify Acurex catalyst coating techniques
- Investigate the effects of catalyst bed geometry

The test matrix, therefore, provided a systematic investigation of each of these combustion-related variables.

The matrix of models tested at JPL is shown in Table 7-1. A summary of pre- and post-test surface area and dispersion measurements is presented in Table 7-2. Other tests originally existed in the matrix but were eliminated as test data was accumulated. A total of 22 models were tested in the screening program. The catalyst materials and the purpose of each test model are also listed in Table 7-1.

Test procedures were based on a review of catalyst materials and their expected performance under combustion conditions. The result was a 10-point test procedure (shown in Table 7-3) which would give primary data on ignition temperature, maximum heat release, uniformity, efficiency, and emissions as well as secondary data on temperature, fuel, and lifetime capabilities.

7.3 JPL TEST FACILITY

The JPL patio test stand (shown in Figure 7-1) includes air supply and fuel feed systems and a vertical quartz test chamber. The test stand is supported by a control console, full instrumentation and emission

TABLE 7-1. JPL TEST MODEL SUMMARY

Sample No.	T.C. Instr.	Substrate Manuf.	Substrate Type	Washcoat Manuf.	Washcoat Type	Catalyst Manuf.	Catalyst Type	Weight %	Weight Grams	Dates Tested	Pres Atm.	Fuel	Mono No.	Purpose of Test
JPL-001	30	G-R	Cord	O-C	10 Wt % G-Alumina	O-C	PT	.28	.879	11/06 - 11/14/75	1.0	M	015	GR(001)/Corning (Baseline) Comparison (Check with Baseline, 10% Difference in PT Loading)
JPL-002	9	G-R	Mull	O-C	10 Wt % G-Alumina	O-C	PT	.22	.957	10/20 - 10/29/75	1.0	M	007	Facility Checkout
JPL-003	0	G-R	Mull	O-C	10 Wt % G-Alumina	O-C	PT	.22	.957	11/03 - 11/06/75	1.0	M	036	Facility Checkout
JPL-004	30	G-R	Mull	O-C	10 Wt % G-Alumina	O-C	PT	.22	.957	12/04 - 12/12/75	1.0	M	038	Mullite/Cordierite Comparison (Check with 001 and Baseline, Note PT Loading Difference)
JPL-004X	10	G-R	Mull	O-C	10 Wt % G-Alumina	O-C	PT	.22	.957	01/22 - 01/28/76	1.0	M	037	Rerun of JPL-004
JPL-005	30	Corn	Cord	O-C	10 Wt % G-Alumina	O-C	PT	.30	.975	12/15 - 01/08/76	1.0	M	054	Baseline
JPL-005X	21	Corn	Cord	O-C	10 Wt % G-Alumina	O-C	PT	.30	.975	01/29 - 01/30/76	1.0	M	055	Rerun of JPL-005
JPL-006	21	Corn	Cord	O-C	10 Wt % G-Alumina	Acur	PT	.31	.975	01/15 - 01/21/76	1.0	M	049	Verify Acurex Coating Technique (Cordierite), Compare to Baseline
JPL-006X	21	Corn	Cord	O-C	10 Wt % G-Alumina	Acur	PT	.31	.974	02/06 - 02/09/76	1.0	M	052	Rerun of JPL-006
JPL-007	21	G-R	Mull	O-C	10 Wt % G-Alumina	Acur	PT	.22	.957	02/11 - 02/20/76	1.0	M	018	Verify Acurex Coating Technique (Mullite), Compare to JPL-004
JPL-008	21	G-R	Mull	M-B	10 Wt % G-Alumina	Acur	PT	.23	.957	02/23 - 02/27/76	1.0	M	045	Compare Washcoating Techniques (Compare 008-M-B, 007-O-C) Compare to JPL-004
JPL-009	21	DPnt	Alum	O-C	10 Wt % G-Alumina	O-C	PT	.30	.975	03/18 - 03/19/76	1.0	M	072	Effect of Increased Cell Size (1/4 in Cell), Compare to Baseline
JPL-010	21	G-R	Cord	O-C	10 Wt % G- Alumina	Acur	PT	.73	2.320	02/02 - 02/04/76	1.0	M	012	Sensitivity to Increased PT Loading, Compare to 001 Compare to Baseline

TABLE 7-1. JPL TEST MODEL SUMMARY (Concluded)

Sample No.	T.C. Instr.	Substrate Manuf.	Substrate Type	Washcoat Manuf.	Washcoat Type	Catalyst Manuf.	Catalyst Type	Weight %	Weight Grams	Dates Tested	Pres Atm.	Fuel	Mono No.	Purpose of Test
JPL-010X	12	G-R	Cord	O-C	10 Wt % G-Alumina	Acur	PT	.75	2.426	02/28 - 03/10/76	1.0	M	009	Rerun of JPL-010
JPL-010P	9	Corn	Cord	O-C	10 Wt % G-Alumina	Acur	PT	.72	2.397	04/09 - 04/23/76	1.0	M,P	103	To Establish Propane Operating Procedure
JPL-011	12	Corn	Cord	O-C	10 Wt % G-Alumina	Acur	PT	.29	.975	03/16 - 03/25/76	1.0	M,P	051	Effect of H2S Platinizing Technique, Compare to 005
JPL-012	12	Corn	Cord	O-C	10 Wt % G-Alumina	Acur	PT	.30	.975	03/11/76	1.0	M	050	Effect of Presintered Washcoat (1000 C), Compare to 006
JPL-013	12	Corn	Cord	O-C	10 Wt % G-Alumina	Acur	PT	.30	.975	03/15/76	1.0	M	048	Effect of Sintering Washcoat-Platinum, Compare to 006
JPL-016	9	Corn	Cord	O-C	10 Wt % G-Alumina CE-Stable	Acur	PT/PD 2:1	1.00	—	04/13 - 04/15/76	1.0	M	107	Multimetallics (PT/PD) Cerium Stabilized Catalyst
JPL-019	9	DPnt	Alum	DPnt	A-Alumina	Acur	PT	vars.	vars.	09/06 - 10/21/76	1.0	M,P, I,Me	vars.	Graded cell catalyst
JPL-021	8	DPnt	Alum	O-C	7 Wt % G-Alumina	Acur	PT	5.27	5.003	05/05 - 05/13/76	1.0	M	125	One Inch Long Torvex 1/4" Cells (5/13 Tests with 2 - 1" Pt/Al_2O_3 /Cordierite Segments
JPL-022	12	DPnt	Alum	DPnt	A-Alumina	DPnt	PT (Stab)	.00	.000	03/12 - 03/15/76	1.0	M	076	Single Metal (DuPont Stabilized PT)

TABLE 7-2. SUMMARY OF CATALYST CHARACTERIZATION RESULTS FOR SCREENING CATALYSTS

Model Number	Dispersion (%)		Surface Area (m^2/g)	
	Pre-Test	Post-Test	Pre-Test	Post-Test
001	--	0.6	--	0.03
002	--	--	--	--
003	--	0	--	0.70
004	--	0.5	--	0.64
004X	--	1.6	--	0.73
005	--	0.8	--	0.625
005X	40.69	0.7-1.3	10.59	0.81
006	60.33	--	8.40	0.61
006X	--	0.6	--	0.65
007	--	0	9.58	0.69
008	--	--	13.14	1.54
009	31.1	--	6.69	--
010	--	0.4	7.8	0.61
010X	94.1	0.07	7.92	0.41
010P	--	--	10.87	1.05
011	70.48	0.75	6.87	0.925
012	49.0	2.4	1.33	0.56
013	0.7	--	0.93	0.77
016	--	--	6.39	2.08
019	1.1-4.4	--	1.10-3.20	--
021	2.6	--	4.68	0.59
022	56.1	6.7	10.4	0.62

TABLE 7-3. JPL TEST PROCEDURE

a.	Start and record light-off temperature of the catalyst at 35 percent T.A.
b.	Stabilize reaction at 50 percent T.A. and record conditions.
c.	Stabilize reaction at stoichiometric and record conditions.
d.	Stabilize reaction at 150 percent T.A. and record conditions.
e.	Stabilize reaction at 200 percent T.A., if possible, and record conditions.
f.	Stabilize reaction at 250 percent T.A., if possible, and record conditions.
g.	Stabilize reaction at 300 percent T.A., if possible, and record conditions.
h.	Return to 200 percent T.A., determine maximum throughput conditions and record, if possible.
i.	Return to 50 percent T.A., and determine maximum throughput conditions and record.
j.	Determine change in light-off temperature after testing.

Throughout testing, the following conditions were set:

- Try to maintain the reaction on the front face of the catalyst or within 0.0635m thereof.
- Try to maintain a maximum reaction temperature in the catalyst within 14K (25°F) of 1367K (2000°F).
- Conduct tests at a minimum of 21.1 MJ/hr (20,000 Btu/hr) and maximum of 105.6 MJ/hr (100,000 Btu/hr) heat release.

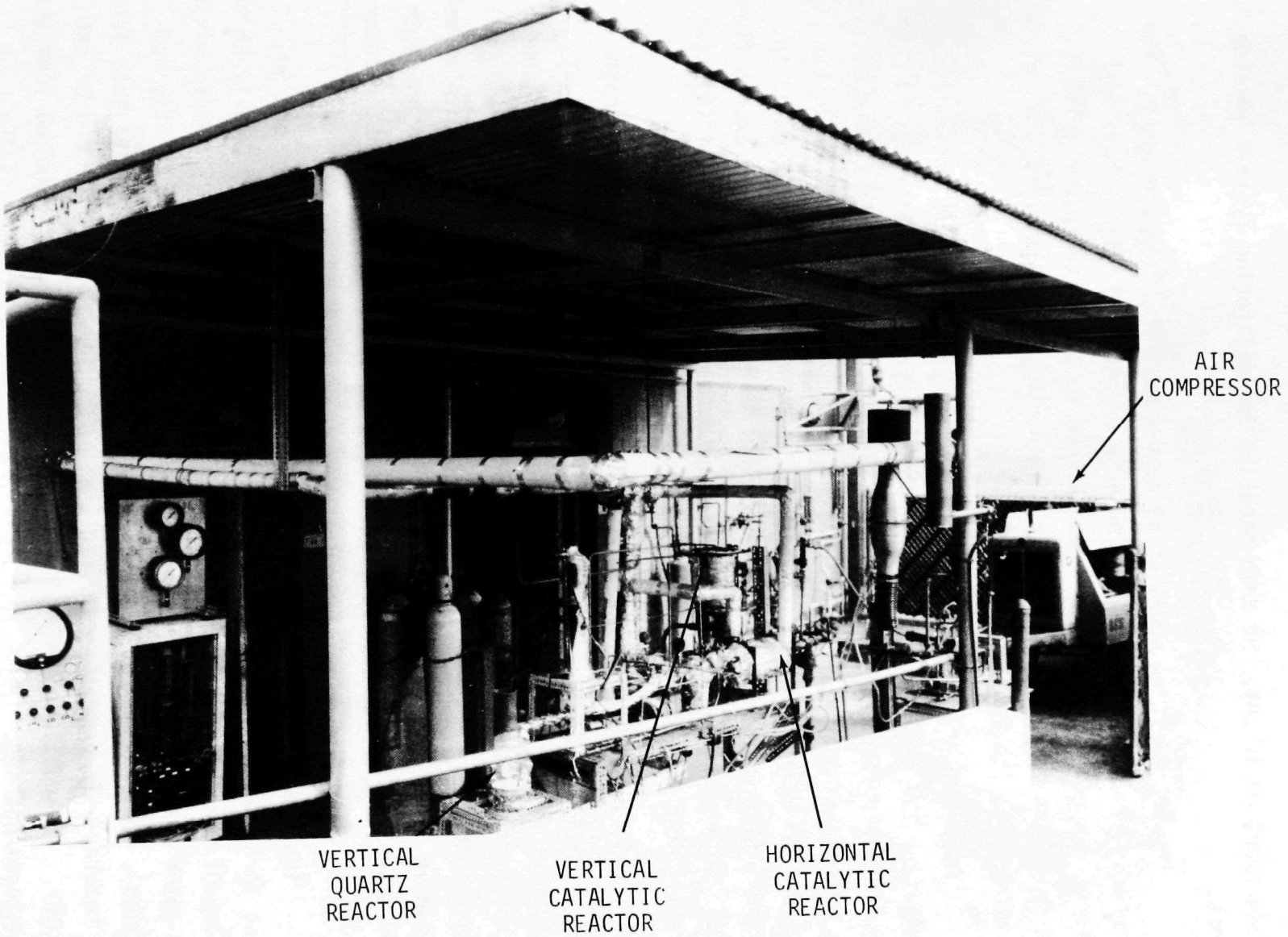

Figure 7-1. JPL patio test facility.

measurement equipment, and data handling and monitoring systems located indoors.

The JPL facility operates at near-atmospheric pressure only. The air compressor is capable of delivering 4.96 m^3/min (175 SCFM) of air and is metered (by rotameter), valved, and passed to the system preheaters. The inlet air can be heated either electrically (to 811K) or by tandem gas-fired heaters (to 922K).

Both liquid and gaseous fuels can be used in the JPL patio test facility. The gaseous fuels are supplied either as pipe line natural gas (boosted in pressure by an in-line gas compressor) or as manifolded bottles for methane or propane. Liquid fuels (distillate oil and methanol) are supplied in 55-gallon drums. The fuel is extracted from the drum by an aircraft fuel pump fitted with a return line for bypassing the excess flow-rate. Both gaseous and liquid fuels are metered, throttled, and injected directly into the heated air stream without further handling.

All catalyst beds tested at JPL were instrumented with in-depth thermocouples at Acurex. Normally, three thermocouples were placed at varying pre-determined locations within a single channel, and the channel was then sealed at both ends. The thermocouples then read the ceramic wall temperature. As indicated in Table 7-1, between 8 and 30 thermocouples were placed in each monolith. Figure 7-2 shows Test Model 001 with 30 in-depth thermocouples. The test models were placed in the vertical quartz reactor at JPL.

The quartz reactor test section with monolithic catalyst bed in place is shown in Figure 7-3. The fuel/air mixture enters vertically at the bottom of the quartz tube, passing through several screens to promote mixing. The outer surface of the reactor is insulated (to maintain adiabatic combustion), and the exit end is capped to channel the exhaust gases away from the reactor. In-bed thermocouple leads exit at the downstream end of the reactor. An additional probe for exhaust gas sampling is inserted from the downstream opening.

The JPL test stand is instrumented for temperatures, pressures, and flowrates. Orifice meters are connected directly into the data acquisition

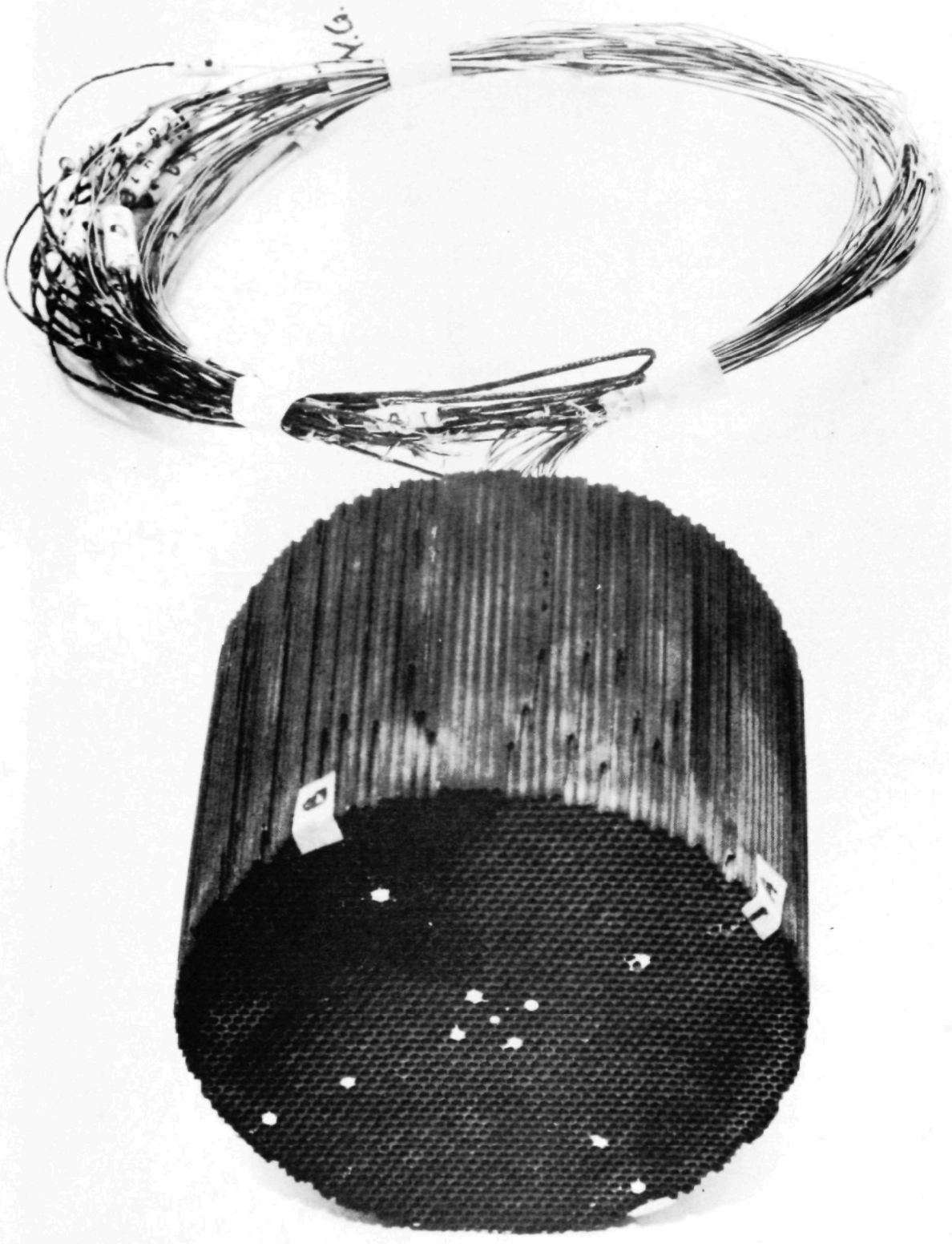

Figure 7-2. Model JPL-001, platinized cordierite with 30 thermocouples placed in monolith.

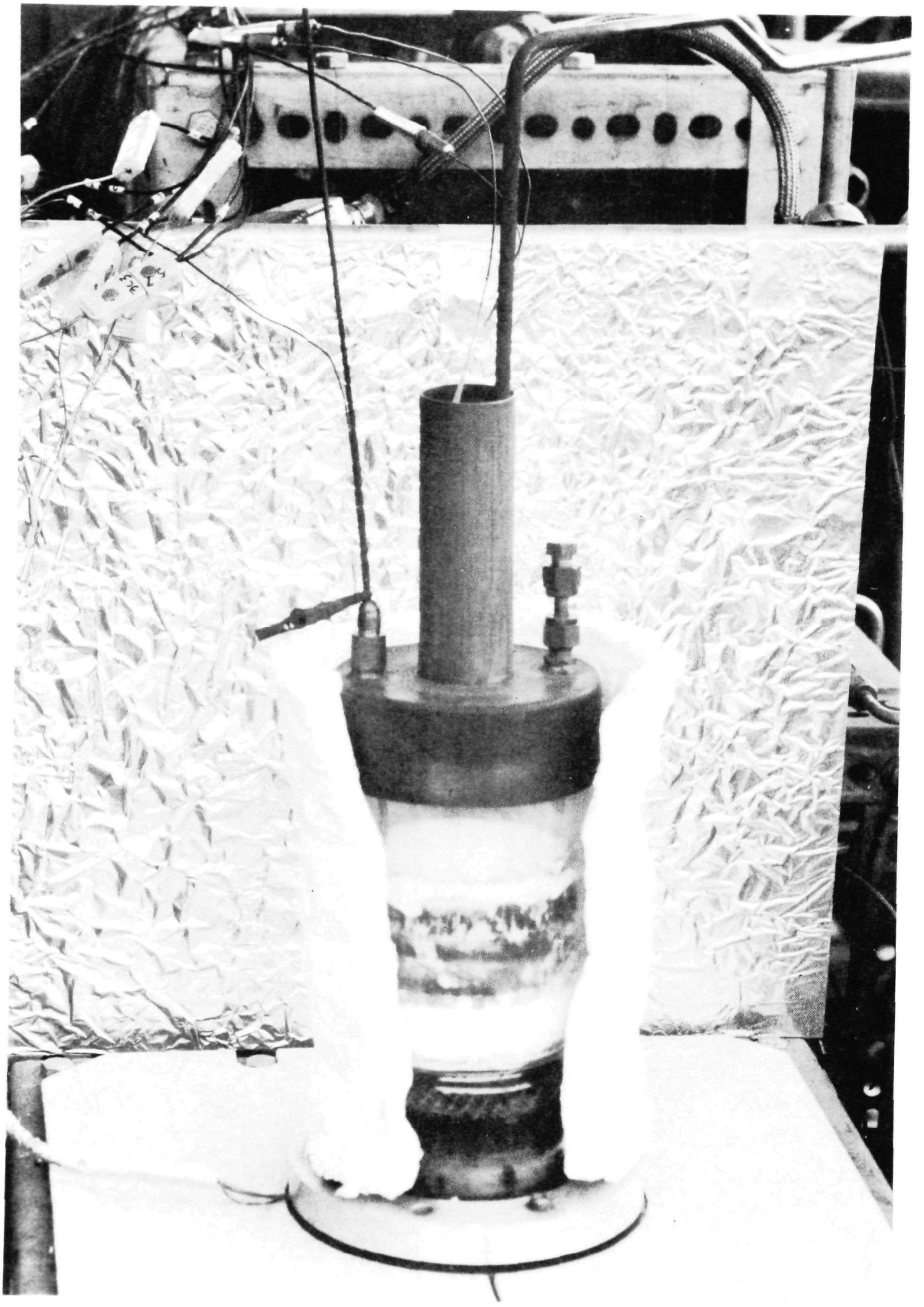

Figure 7-3. Quartz reactor with monolithic catalyst bed.

system to record the fuel and air flow rates automatically. Rotameters are used to permit local observation and flowrate control. Temperature measurements of the gas stream are made both upstream and downstream of the catalyst bed in addition to the in-bed measurements mentioned above.

Exhaust gas analysis consists of continuous analyzers for CO, CO_2, O_2, H_2, UHC, and NO_x. Heated sample lines convey all gases to the respective analyzers. Table 7-4 gives further information on the JPL emissions equipment. The combined control console and instrumentation readout equipment is shown in Figure 7-4. Data can be recorded by strip chart or magnetic tape for computer analysis.

TABLE 7-4. JPL EMISSIONS EQUIPMENT

Component	Analyzer	Range(s)	Fuel Applicability	
			Rich	Lean
Oxygen	Paramagnetic	0-25%	yes	yes
Carbon dioxide	Nondispersive infrared	0-10% 0-20%	yes	yes
	Gas chromatograph	0-10%	yes	yes
Carbon monoxide	Nondispersive infrared	0-250 ppm 0-1000 ppm	no	yes
	Gas chromatograph	0-30%	yes	no
Unburned hydrocarbon	Flame ionization	0-10 ppm 0-5000 ppm	no	yes
	Gas chromatograph	0-10%	yes	no
Nitric oxide	Chemiluminescent	0-1 ppm 0-10,000 ppm	yes	yes
Hydrogen	Gas chromatograph	0-50%	yes	no

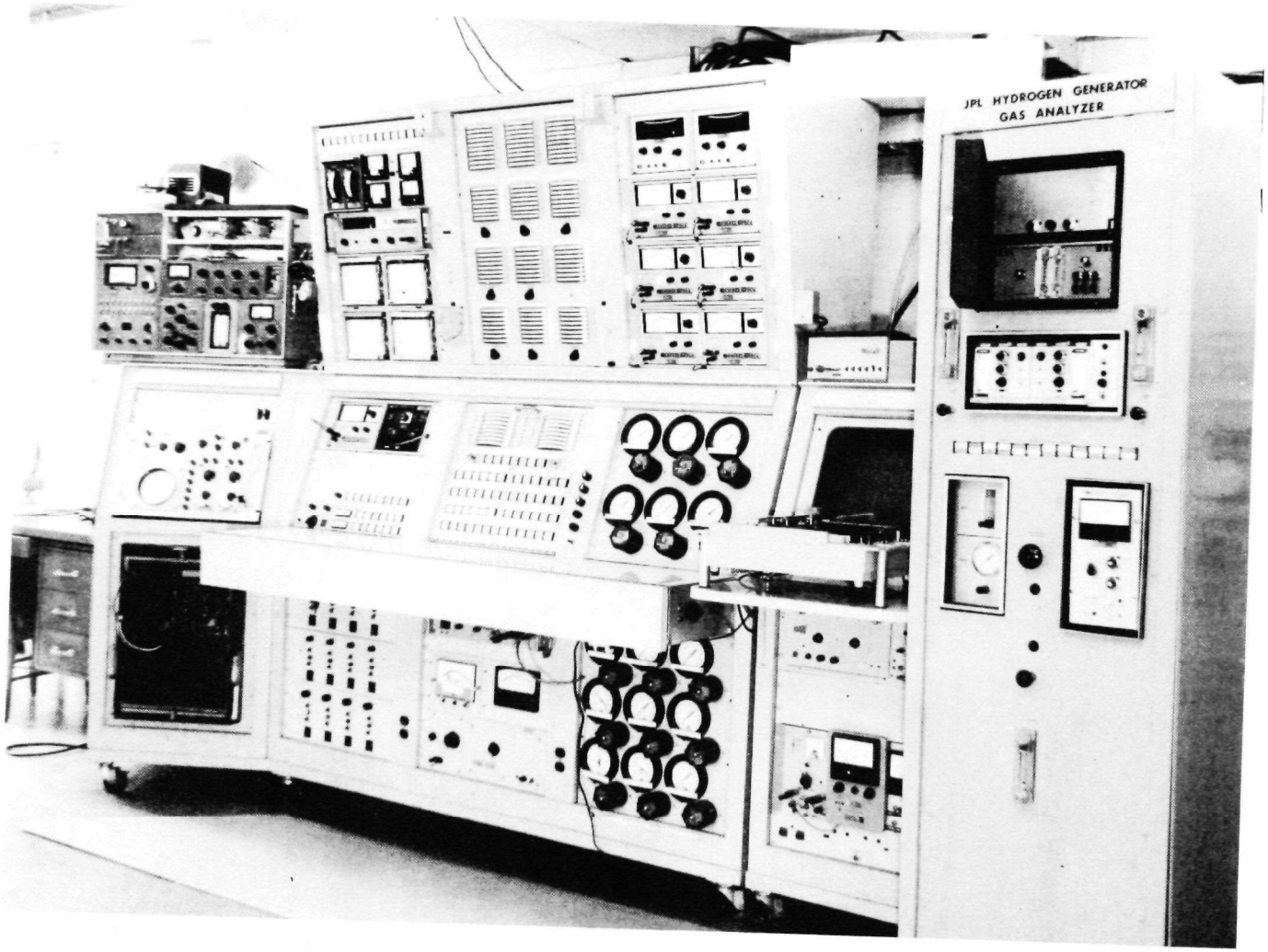

Figure 7-4. JPL patio test facility control console.

7.4 TEST DATA SUMMARY

The test data presented in this section has been prepared to facilitate comparison between test models. A table of test data points (Appendix A) and two plots are shown for each model. Data for models JPL-001, -002, -003, -004, and -005 are not included since they were used almost solely for facility checkout and test procedure verification. The two data plots show preheat requirements and space velocity (indication of maximum heat release) capabilities as a function of stoichiometry (percent theoretical air). In some instances, additional data showing bed temperature distributions, emissions, and bed degradation with time are also presented.

Test Models JPL-004X, 005X, 006, and 006X

Models 004X, 005X, 006, and 006X were tested as baseline cases for future test models and to verify Acurex catalyst application techniques. Photographs of models 005 and 006 are shown in Figures 7-5 and 7-6. Model 006X was a rerun of 006 to verify past results. Monolith 004X used a mullite support while 005X, 006, and 006X were cordierite and had a somewhat higher platinum loading than 004X. Table A-1 summarizes the test points achieved. The tests determined two catalyst characteristics. One is the maximum throughput for a given air/fuel ratio (50 percent to 200 percent theoretical air), and the other is the minimum preheat needed to maintain a uniform bed reaction for various air/fuel ratios (50 percent to 300 percent T.A.).

All test models were tested with methane fuel, and test model 006 was the first of the four to be tested. Lightoff at 35 percent T.A. was accomplished at 642K (695°F). The lightoff temperature increased to 672K to 683K (750°F to 770°F) when a second lightoff was performed following some testing, illustrating the initial degradation of a virgin catalyst.

Light-off temperatures for JPL-004X and -005X were 650K (710°F) and 661K (730°F), respectively. These correspondingly degraded to lightoff temperatures of 714K (825°F) and 706K (810°F) after finishing the first run on each. While lightoff on virgin catalysts takes place at the front face, subsequent starting may initially take place further into the catalyst. The reaction zone then normally moves back to the front face. This was observed in JPL-004X where the mid-bed temperature rose at lightoff on the

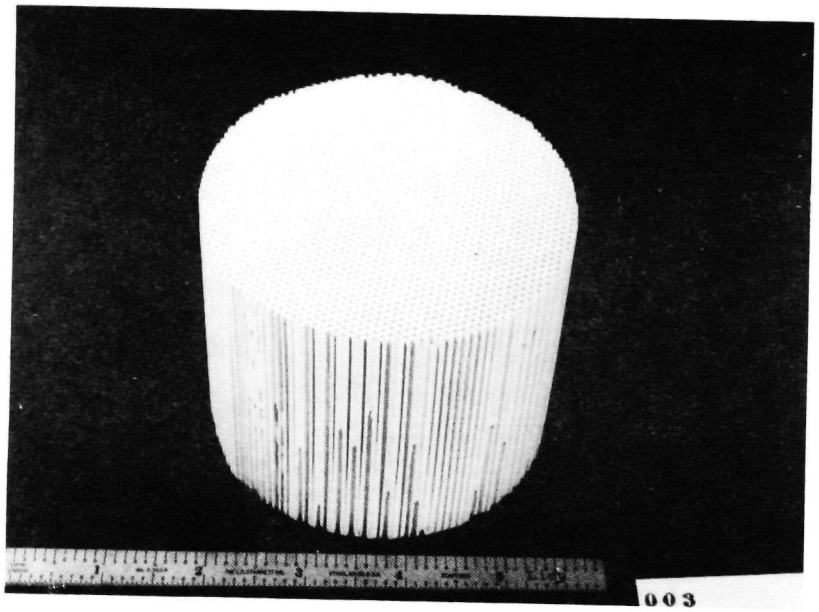

Washcoated
10 Wt % Al_2O_3

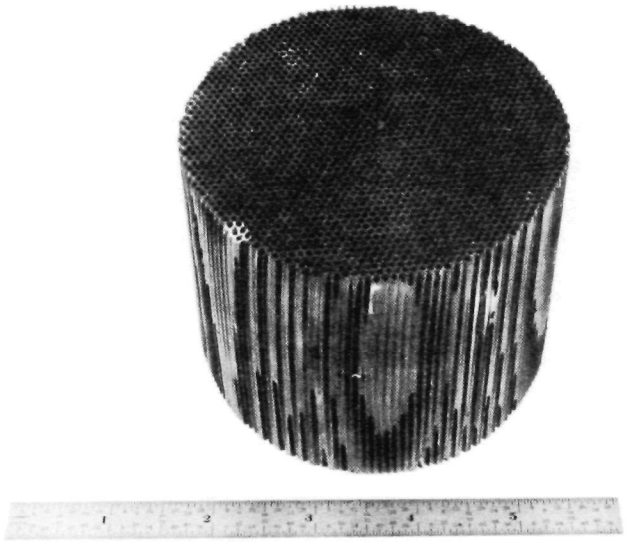

Platinized
0.22 Wt % Pt

Figure 7-5. Model 004 – mullite/alumina/platinum.

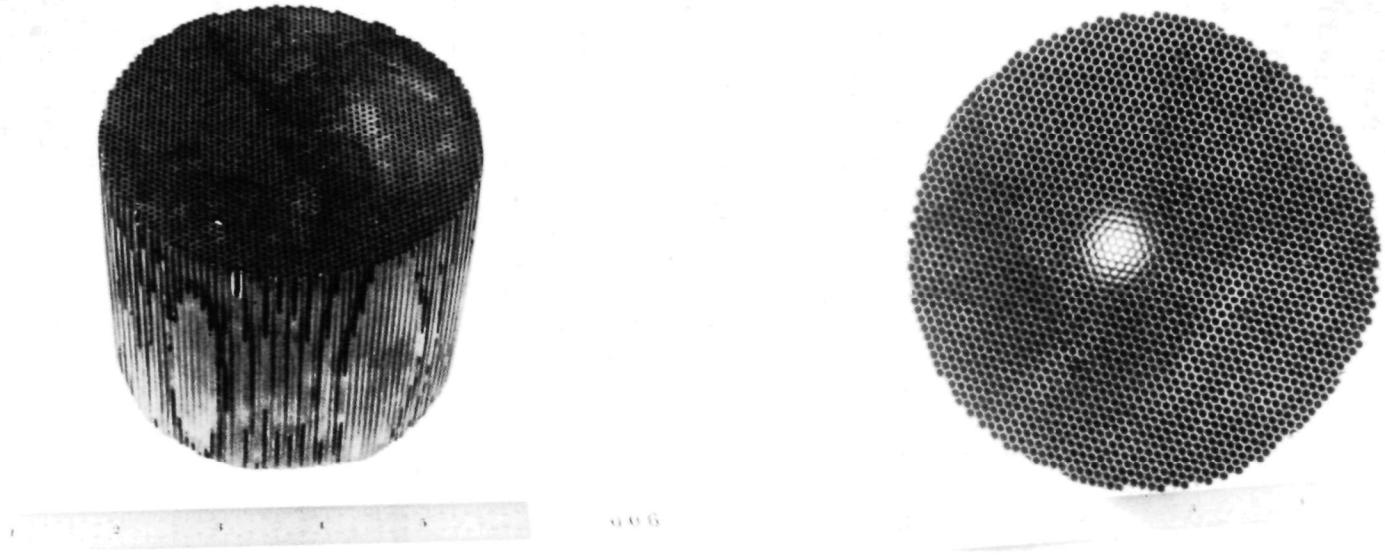

Catalyst coating @ 0.2 Wt % Pt
circular cell geometry
cell diameter (washed and coated) = 0.058 inch

Figure 7-6. Model 006 — cordierite/alumina/platinum.

second run. When the reaction left the front face of JPL-004X, two-thirds of the face darkened first, leaving a single 2 cm circular spot showing activity within that area, and the remaining one-third of the face was also still active. Breakthrough occurred off-center near one side the first time but near an adjacent side at approximately 90° when breakthrough occurred in the second run. If the temperatures are maintained near 1367K (2000°F) and breakthrough is controlled, however, the section of the bed where breakthrough first occurs will also normally be the area in which subsequent breakthrough occurs. The areas where breakthrough occurs will be in the areas where the front face loses the reaction first and have varied from near centerline to near the outside edge for this catalyst.

Minimum preheat temperatures were found throughout a range of theorectical air from 50 to 500 percent, rising from 478K (400°F) to over 811K (1000°F) as conditions went from fuel-rich to fuel-lean. Nitrogen diluent was used for operation near 100 percent theoretical air. Maximum space velocity was determined in a separate run. Figure 7-7b shows that it was initiated at a heat release rate of 21.1 MJ/hr (20,000 Btu/hr). (See Figures 7-7 through 7-10). Data points were then obtained at 27.9, 34.8, 46.5 and 58.1 MJ/hr. These were all at 50 percent theoretical air. Further data was taken at a heat release of 32.5 MJ/hr and breakthrough was found to occur at a space velocity of about 48,000 hr^{-1}.

Returning to Figure 7-7a reveals another interesting phenomenon. The data points of the second run show that a preheat temperature of 724K (844°F) was required for lightoff. This is an increase of more than 56K beyond the preheat temperature required for the first run. This indicates that a degradation of the catalyst occurred during the first run. The third run was then performed which required an additional 39K preheat (to 763K) for lightoff.

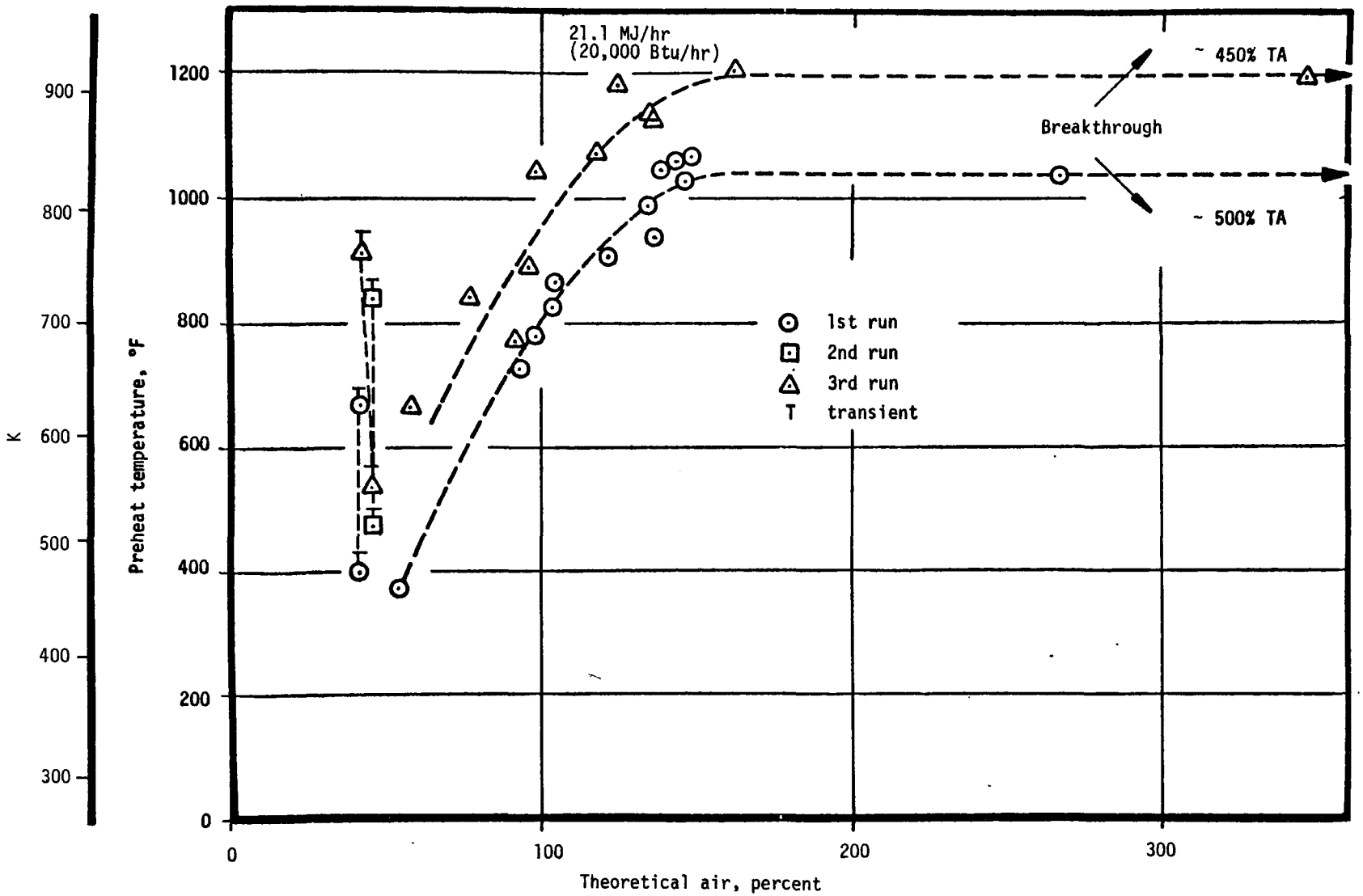

Figure 7-7a. Screening data, JPL-004X-preheat temperature (methane/air).

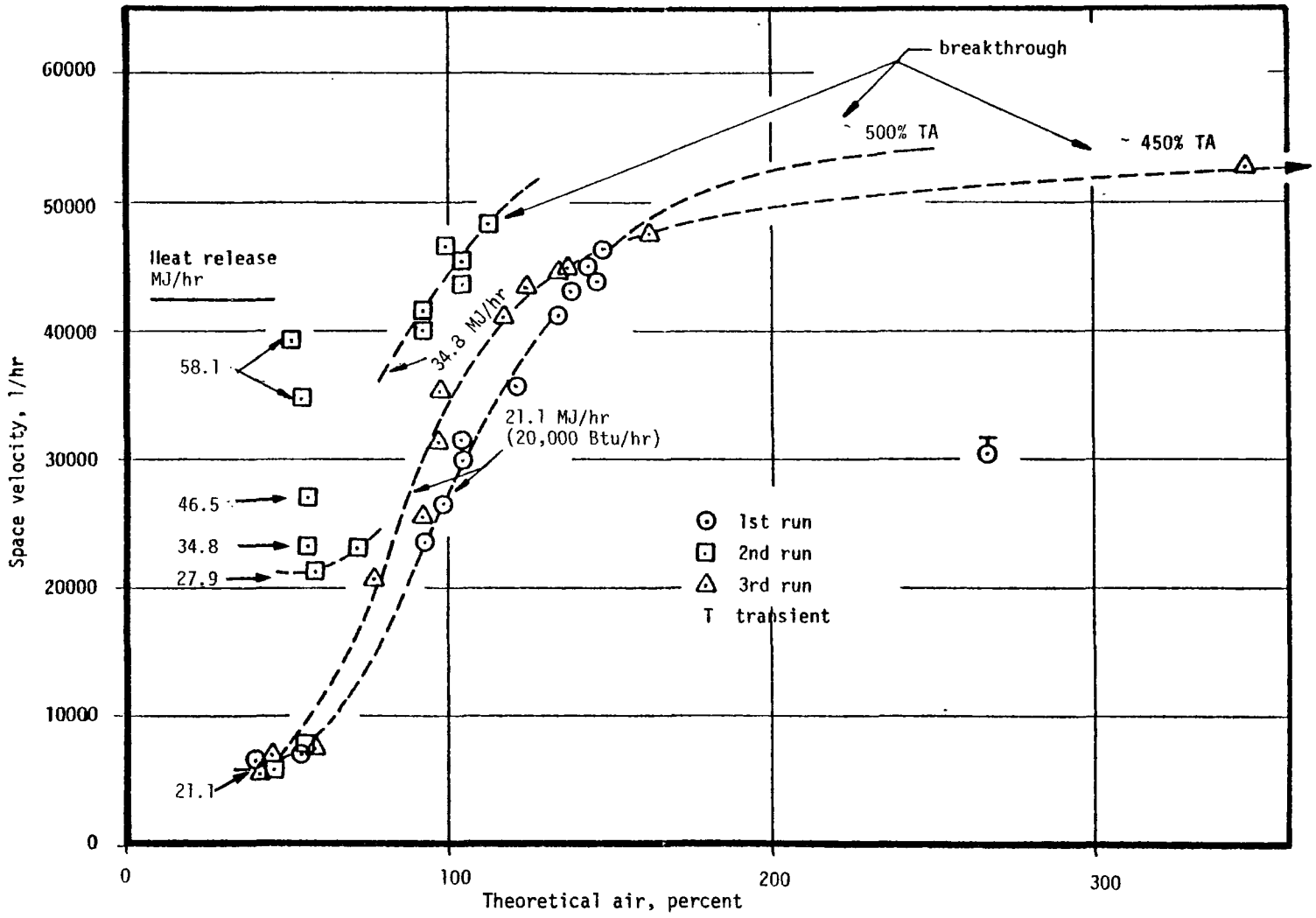

Figure 7-7b. Screening data, JPL-004X - space velocity (methane/air).

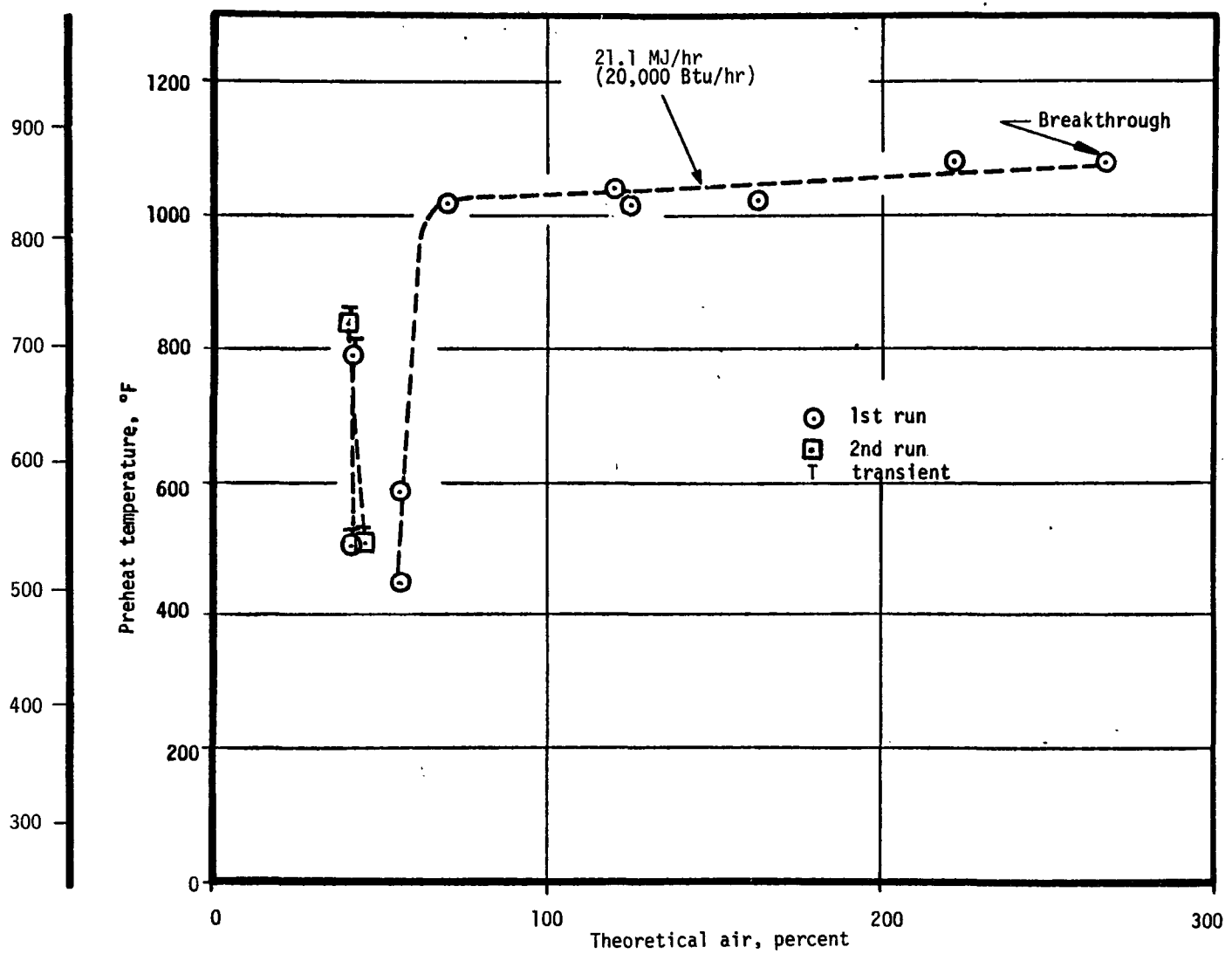

Figure 7-8a. Screening data, JPL-005X-preheat temperature (methane/air).

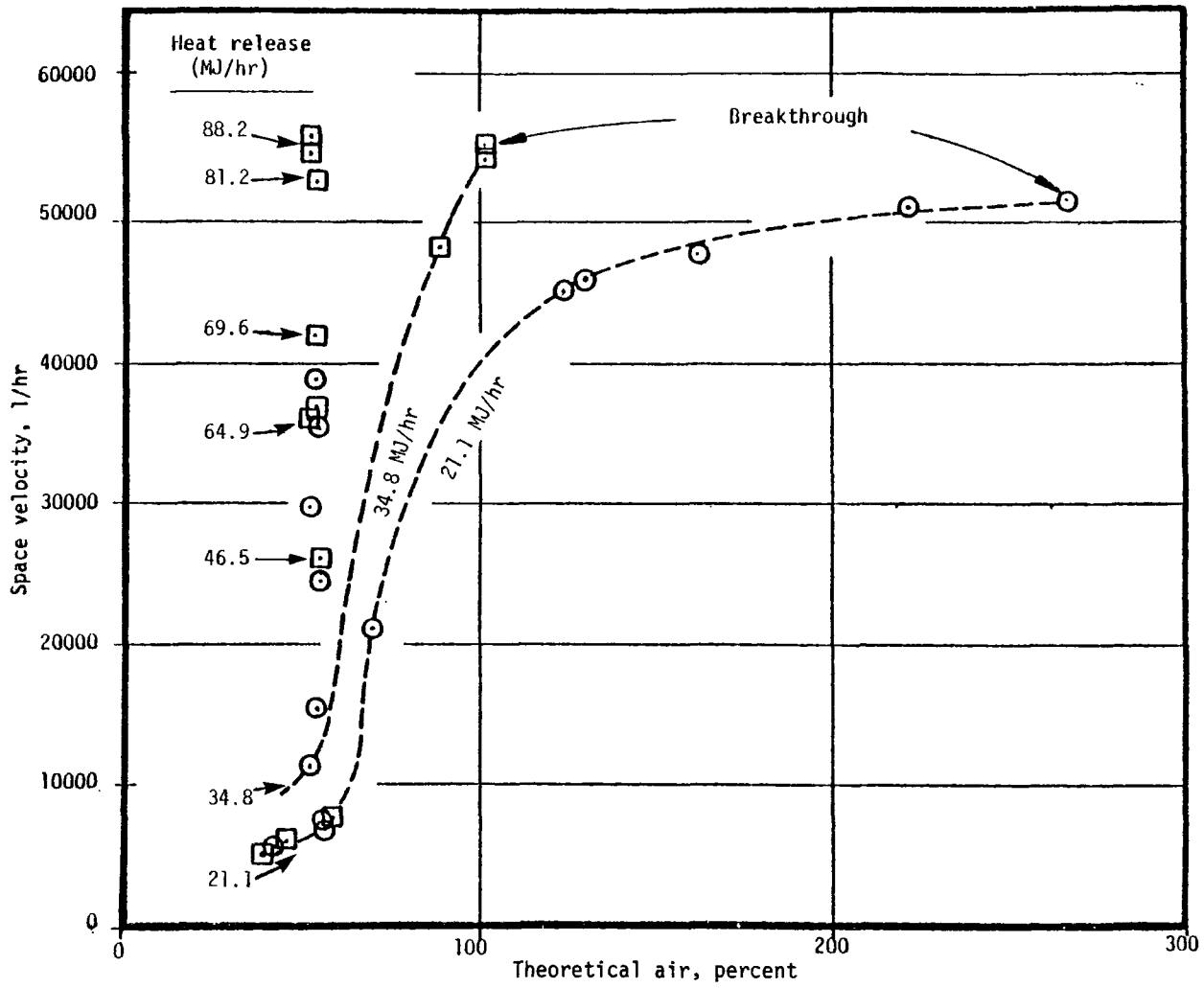

Figure 7-8b. Screening data, JPL-005X — space velocity (methane/air).

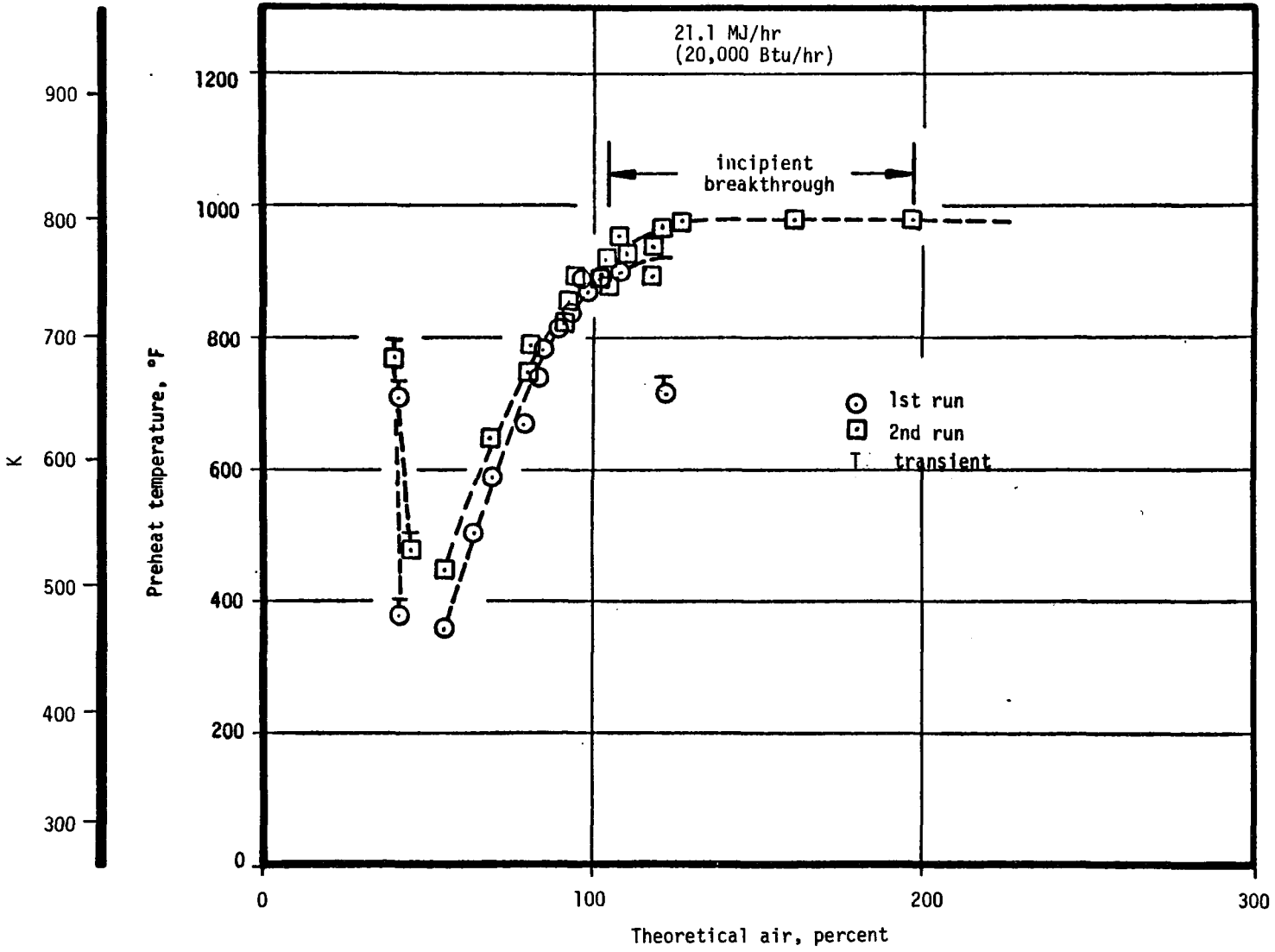

Figure 7-9a. Screening data, JPL-006-preheat temperature (methane/air).

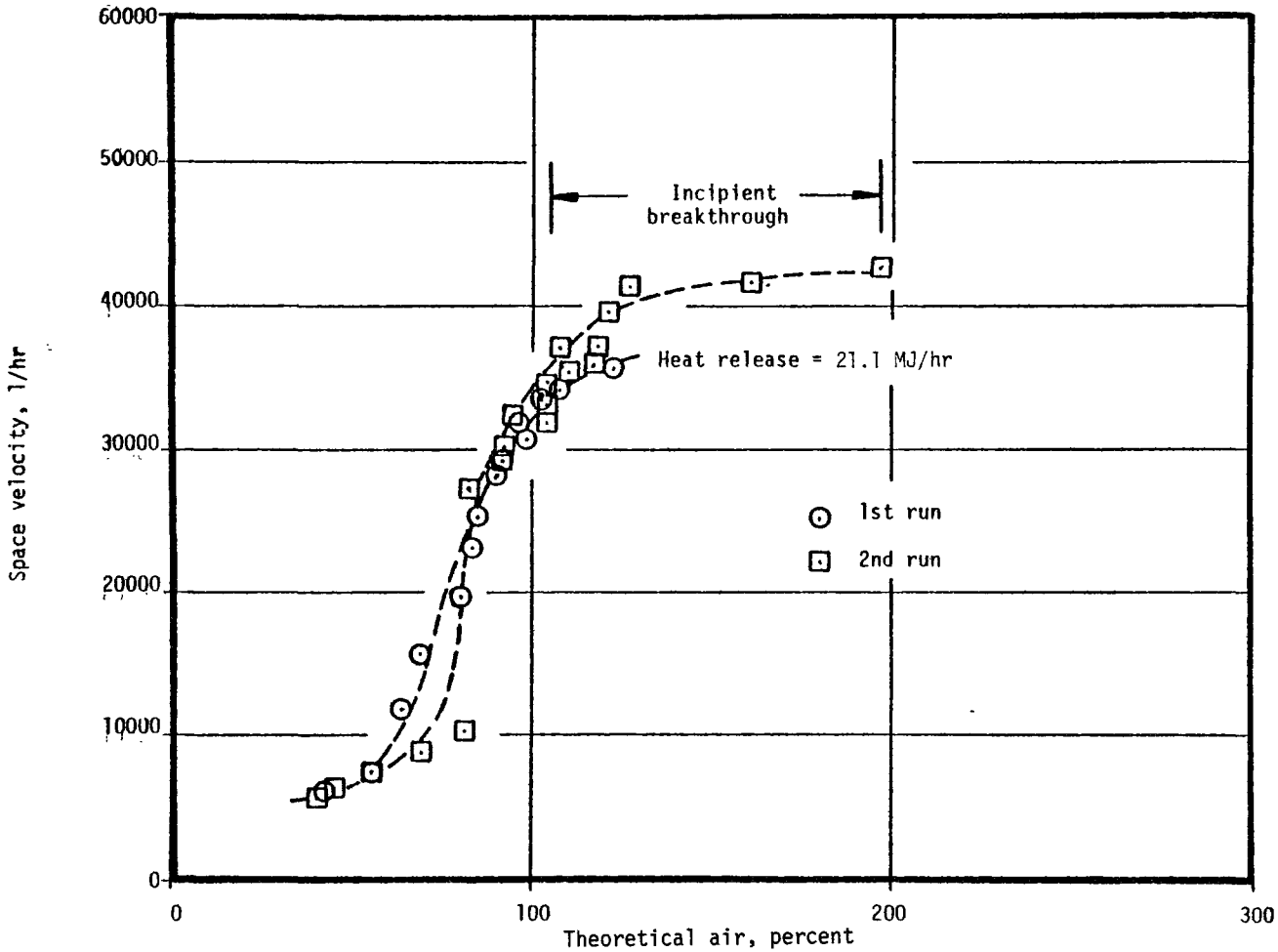

Figure 7-9b. Screening data, JPL-006 — space velocity (methane/air).

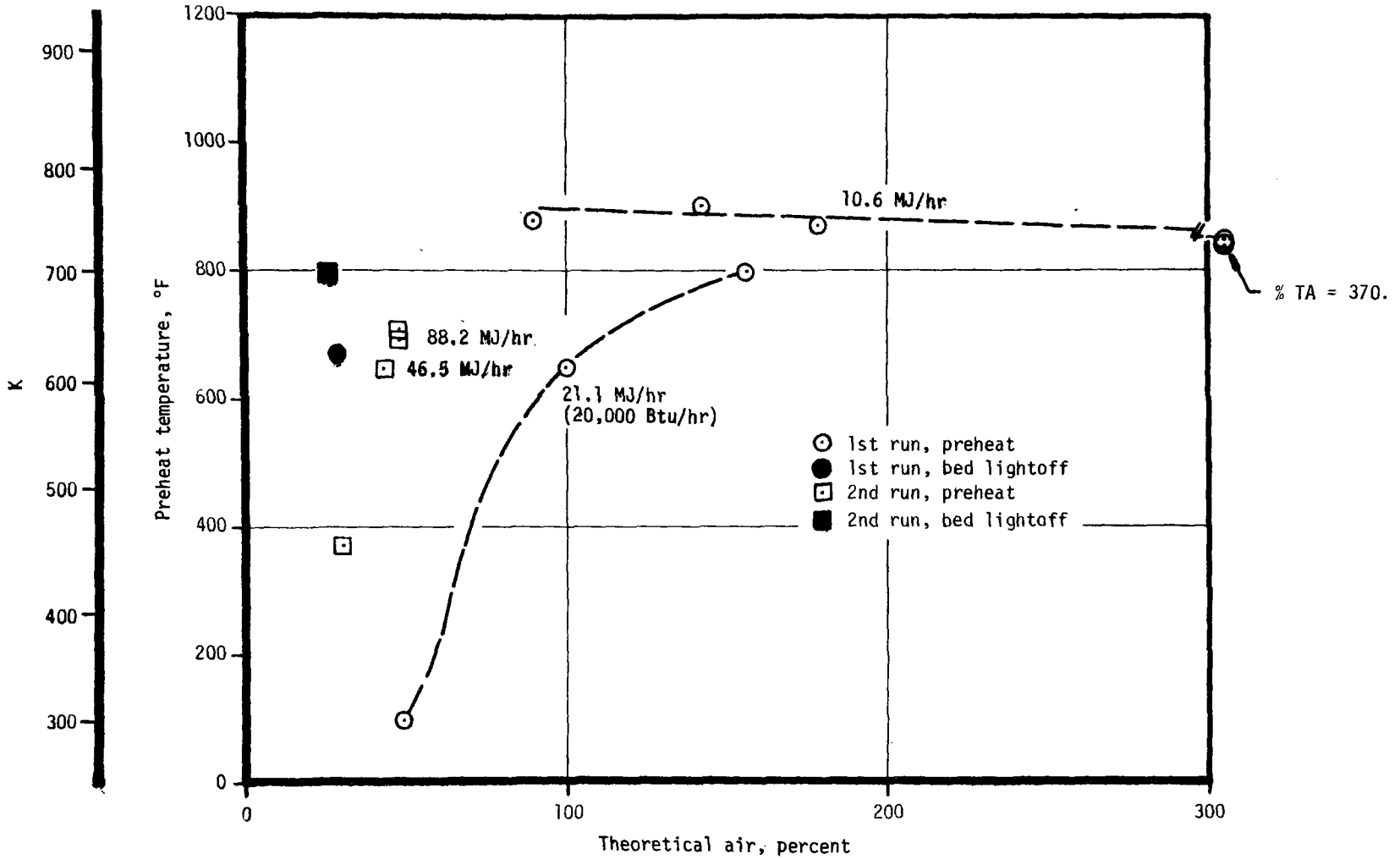

Figure 7-10a. Screening data, JPL-006X-preheat temperature (methane/air).

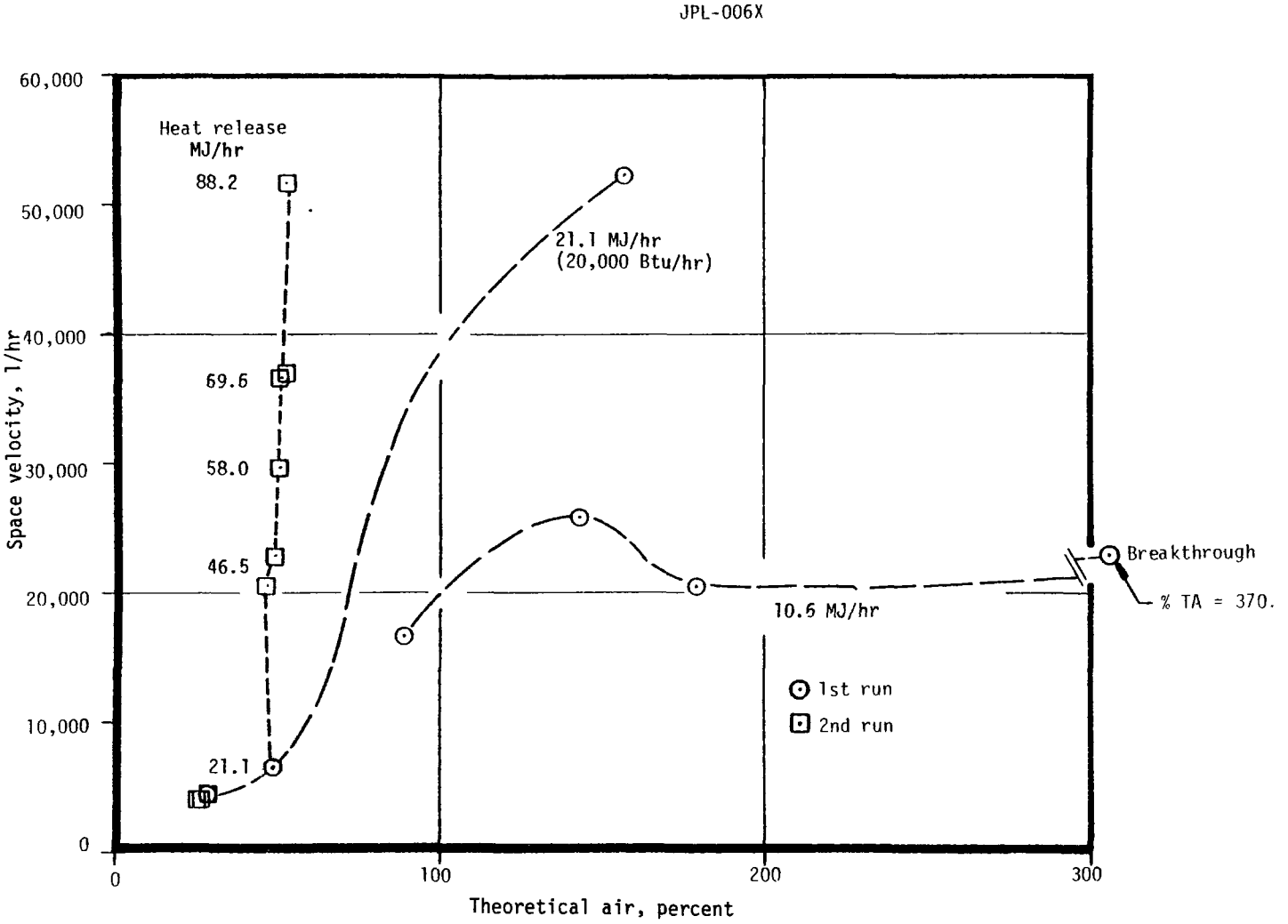

Figure 7-10b. Screening data, JPL-006X — space velocity (methane/air).

The results of testing monoliths 004X, 005X, 006, and 006X can be summarized as follows:

1. 644K to 764K (700°F to 915°F) lightoff temperatures are common for these catalysts under fuel rich conditions with methane fuel.
2. Catalyst degradation occurs rapidly with time as noted by increased lightoff temperature.
3. Both mullite and cordierite appear to be acceptable support materials at 1367K (2000°F) bed temperatures.
4. Preheat requirements increase substantially (478K to over 811K) from fuel-rich to fuel-lean stoichiometry.
5. Breakthrough occurred typically at a space velocity between 40,000 and 60,000 per hour.
6. Successive breakthoughs occur at the same bed location each time, probably at the area of minimum catalyst activity.
7. Acurex platinum application techniques were adequate.
8. The somewhat higher platinum loading of model 006 helped to promote initial lightoff at a lower temperature.

The next two catalysts to be tested, monoliths JPL-007 and -008, were to further demonstrate the effects of coating and washcoat application (see Table 7-1). The results are given below.

Test Models JPL-007 and -008

Monolith JPL-007 was tested to verify mullite coating techniques. JPL-008 compares washcoat preparation of two different manufacturers. In general, test results varied somewhat from baseline tests.

Data for JPL-007 is shown in Table A-2 and Figure 7-11. During the first run, preheats were surprisingly low in going from rich to lean conditions. Data was taken at five points between 51.8 percent theoretical air and 211 percent theoretical air, all with preheat temperatures between 317K and 497K (110°F to 435°F) (most previous runs required >811K preheat for operation above 100 percent T.A.). Operation beyond 211 percent T.A.

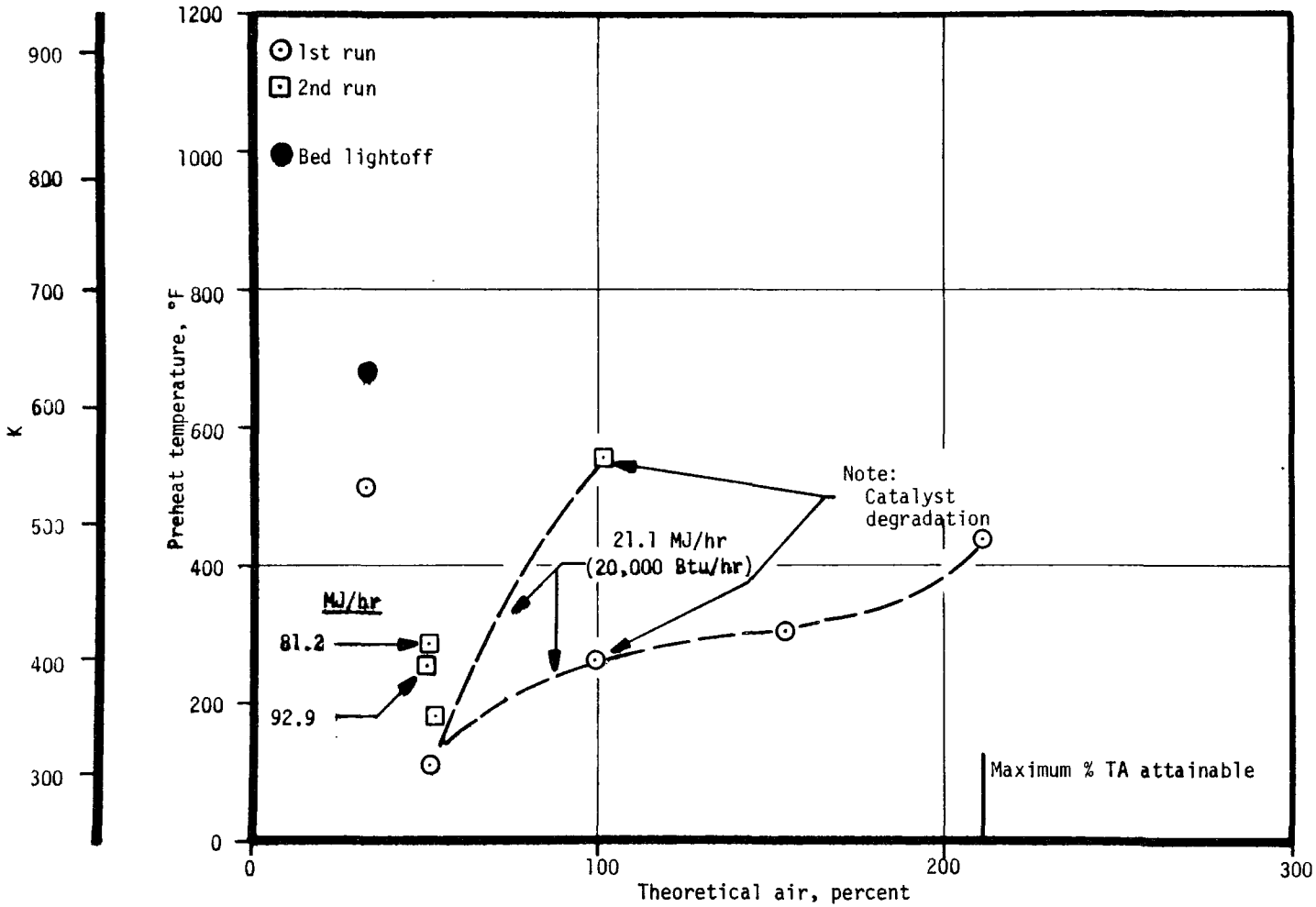

Figure 7-11a. Screening data, JPL-007-preheat temperature (methane/air).

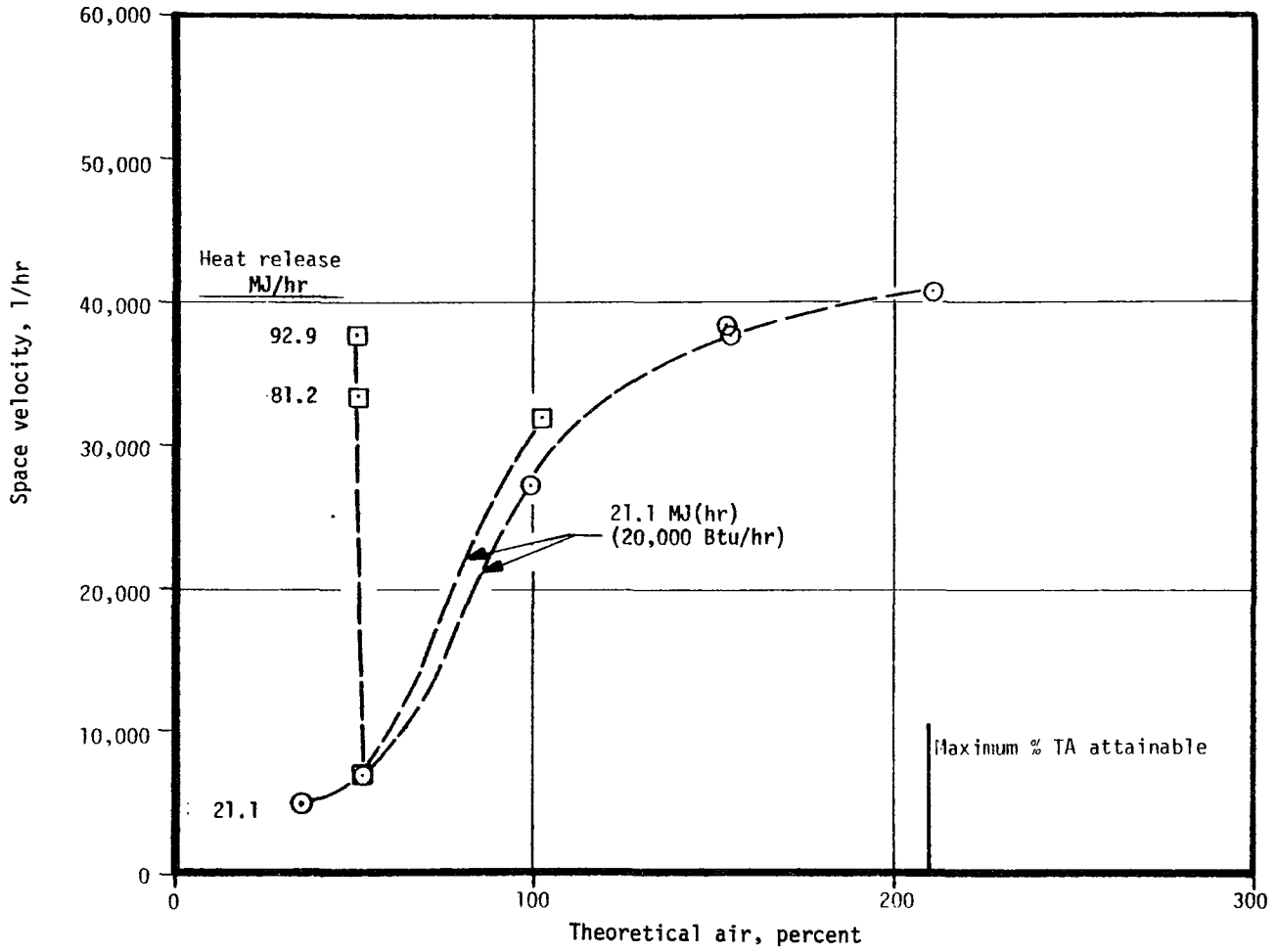

Figure 7-11b. Screening data, JPL-007 – space velocity (methane/air).

was not possible, however. The second run indicates considerable catalyst degradation. The operating point at 100 percent theoretical air indicates that a preheat of 563K (553°F) was required to sustain the reaction, where only 401K (262°F) was required for the previous run. A short maximum throughput test at 50 percent theoretical air indicated that 81.2 MJ/hr (76,900 Btu/hr) (S.V. = 37,603 hr^{-1}) could be produced at a 395K preheat.

JPL-008 (Table A-3 and Figure 7-12) performed roughly comparable to JPL-004X and -005X in that extremely lean operation was attained but at high values of preheat temperature (>680K). Maximum throughput at 50 percent theoretical air was similar to JPL-007 in that 81.2 MJ/hr (S.V. = 39,254 hr^{-1}) was attainable at a low preheat temperature (384K). Lightoff temperatures were again comparable to all other catalysts tested at 640K, 682K, and 706K for the first, second, and third runs, respectively. Another interesting point was the high pretest surface area of 13.14 m^2/g achieved by the Matthey Bishop washcoat (see Table 7-2).

It was concluded from these tests that again, platinum coating techniques on the mullite support were adequate. Other than the low preheat temperatures noted for the first run on JPL-007, no significant differences in combustion characteristics were noted in testing the different manufacturer's washcoats.

Test Model JPL-009

Model JPL-009 was a 6.35 x 10^{-3}m (0.25 inch) cell size monolith (larger than other cell sizes tested) with the baseline 0.30 weight percent platinum applied. Thus, the effects of cell size on combustion were investigated. Results appear in Table A-4 and Figure 7-13.

Testing of this catalyst revealed interesting operational characteristics. Lightoff was attained at 653K (716°F, similar to others), and data were recorded for 38.7, 51.1, and 105.5 percent theoretical air as operation on the lean side was approached. Lower preheats than all the catalysts previously discussed were needed at these points (339K - 367K). At 105.5 percent theoretical air, high levels of UHC's were recorded (1200 ppm) and further testing at lean conditions was not attempted. A maximum throughput test was also tried and a 69.6 MJ/hr (S.V. = 22,869 hr^{-1}) heat release was reached when high UHC values were evident (5360 ppm). This

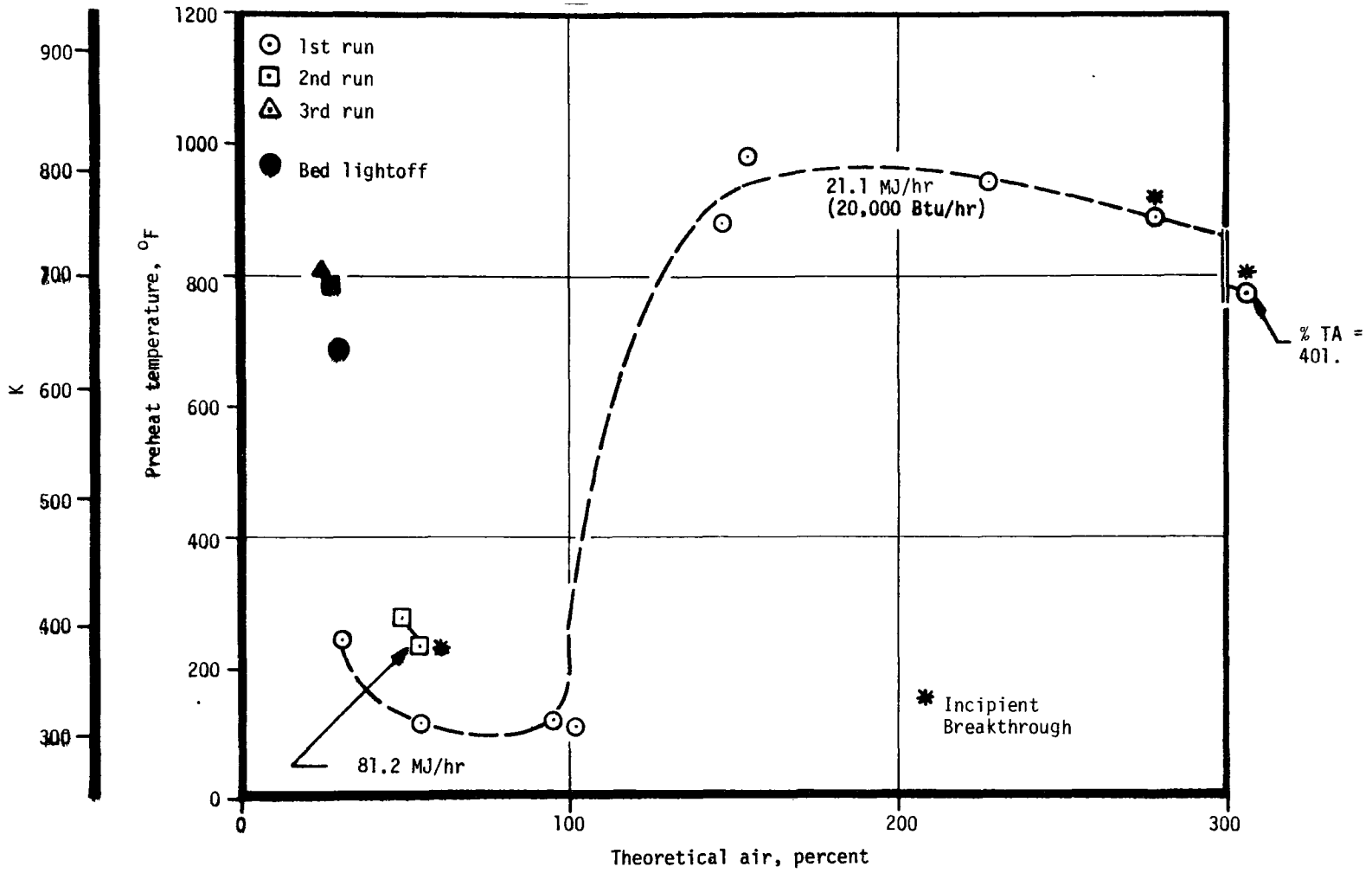

Figure 7-12a. Screening data, JPL-008-preheat temperature (methane/air).

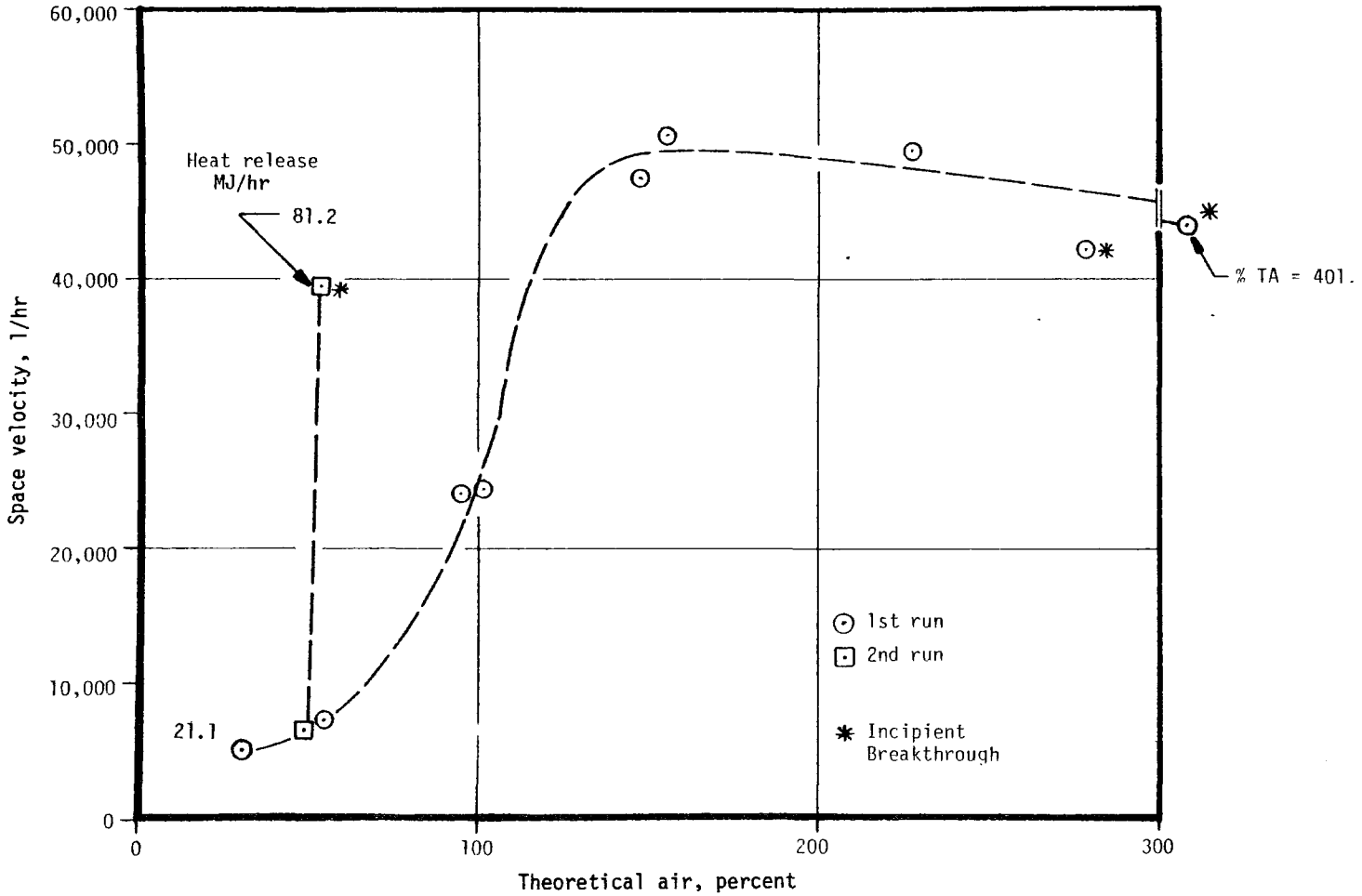

Figure 7-12b. Screening data, JPL-008 — space velocity (methane/air).

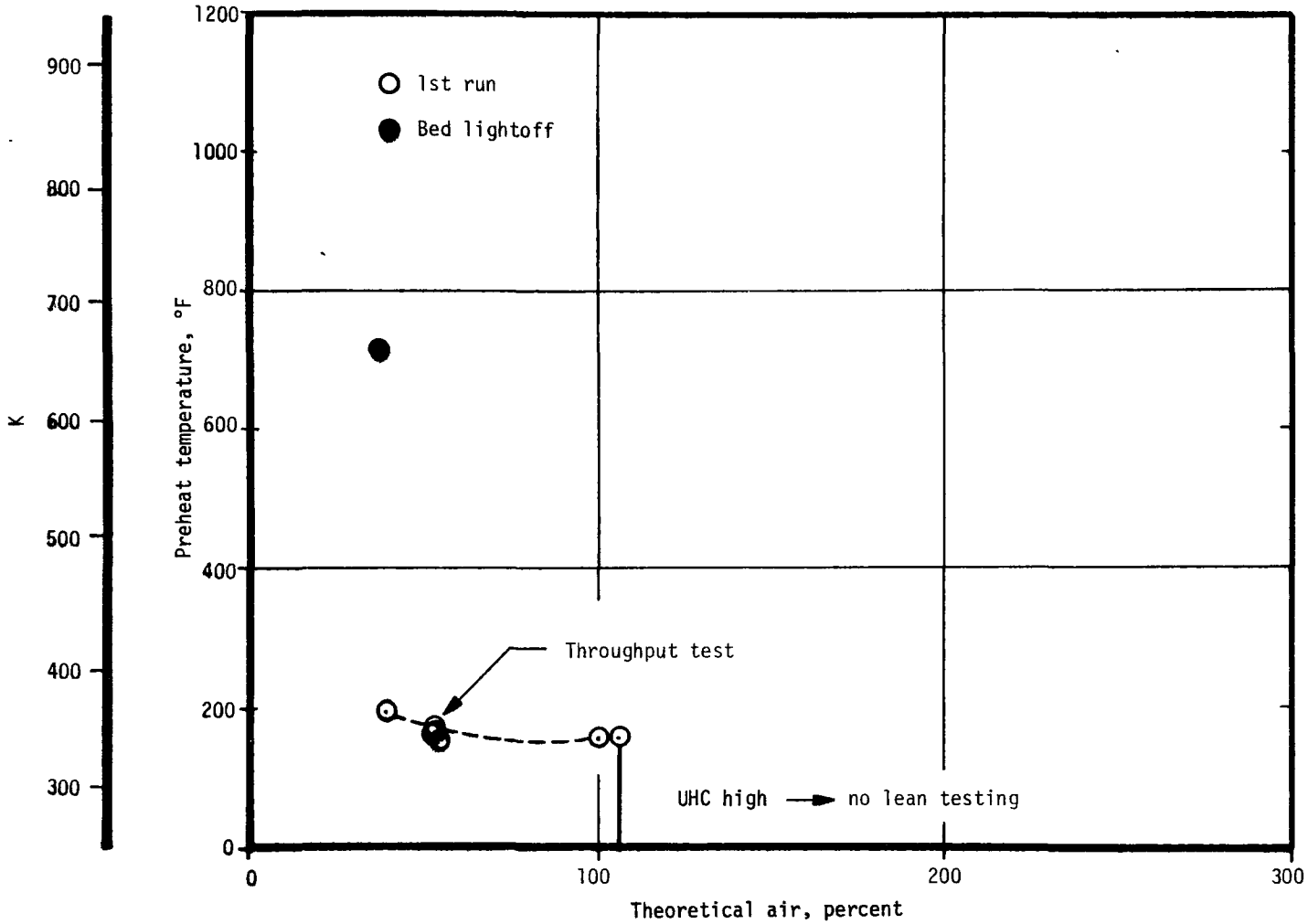

Figure 7-13a. Screening data, JPL-009-preheat temperature (methane/air).

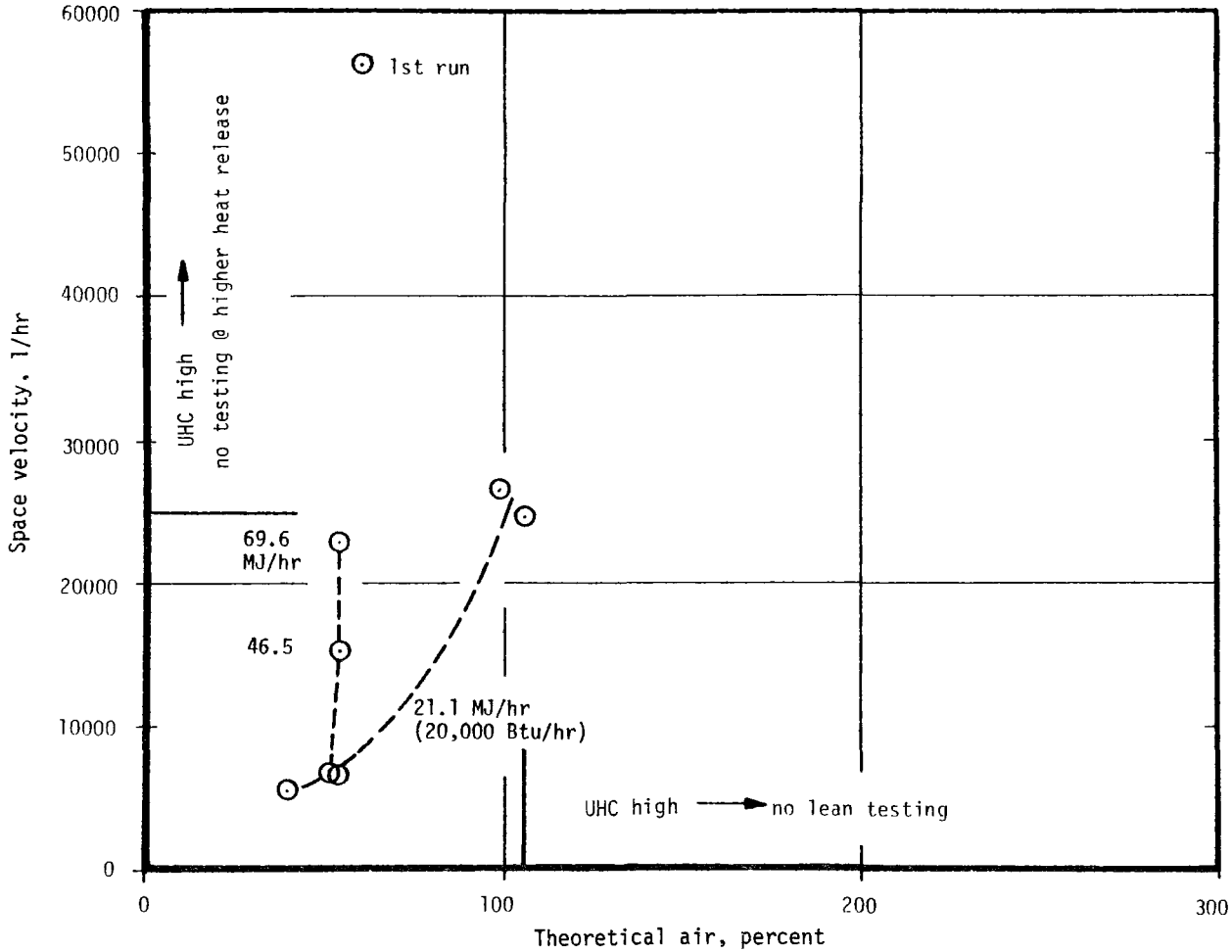

Figure 7-13b. Screening data, JPL-009 — space velocity (methane/air).

catalyst showed promise for use with others in a series arrangement. Using this catalyst upstream of others (others possibly being non-noble metal and needing high preheat to operate) it appeared that it could be used to sustain a reaction at low preheat conditions but with poor conversion. The downstream catalysts could then be used for cleanup of the UHC.

Test Models JPL-010, -010X, and -010P

This series of three catalysts was tested to evaluate the effects of high platinum loading and the properties of propane fuel. JPL-010 was tested for lightoff and one steady operating point, at which time the front face was over-temperatured. The data for both 010 and 010X are shown in Tables A-5 and A-6 and Figure 7-14.

JPL-010X was a duplicate of JPL-010 as the lightoff temperatures indicate (608K as compared to 596K). This was slightly lower than the other catalysts discussed previously. The most important feature of this catalyst was indicated by the preheat temperatures required to go from 27.5 percent theoretical air to 280 percent theoretical air. They were all less than 350K (170°F), something none of the other catalysts could approach. This indicates that the higher platinum loading had a marked effect in increasing catalyst performance. This was the first significant improvement in catalyst performance to date.

During the first run, a breakthrough test was performed at 219 percent theoretical air. A heat release of 31.7 MJ/hr (30,000 Btu/hr) (S.V. = 70,846 hr^{-1}) was achieved at a preheat of 638K. This had been the highest space velocity recorded to date in the JPL test series. The third run on this catalyst illustrates catalyst degradation. The operating point at 150 percent theoretical air was repeated after about 8 hours of testing. The preheat needed was 685K (773°F) as compared to 343K (157°F) for the first run. The fourth run attempted to measure the maximum throughput at 50 percent theoretical air. A heat release of 139.5 MJ/hr (132,000 Btu/hr) (S.V. = 53,819 hr^{-1}) was attained without breakthrough occurring. This represents the maximum fuel flow capability for the JPL test facility. In summary, this was found to be the best catalyst tested to date, although degradation was still evident.

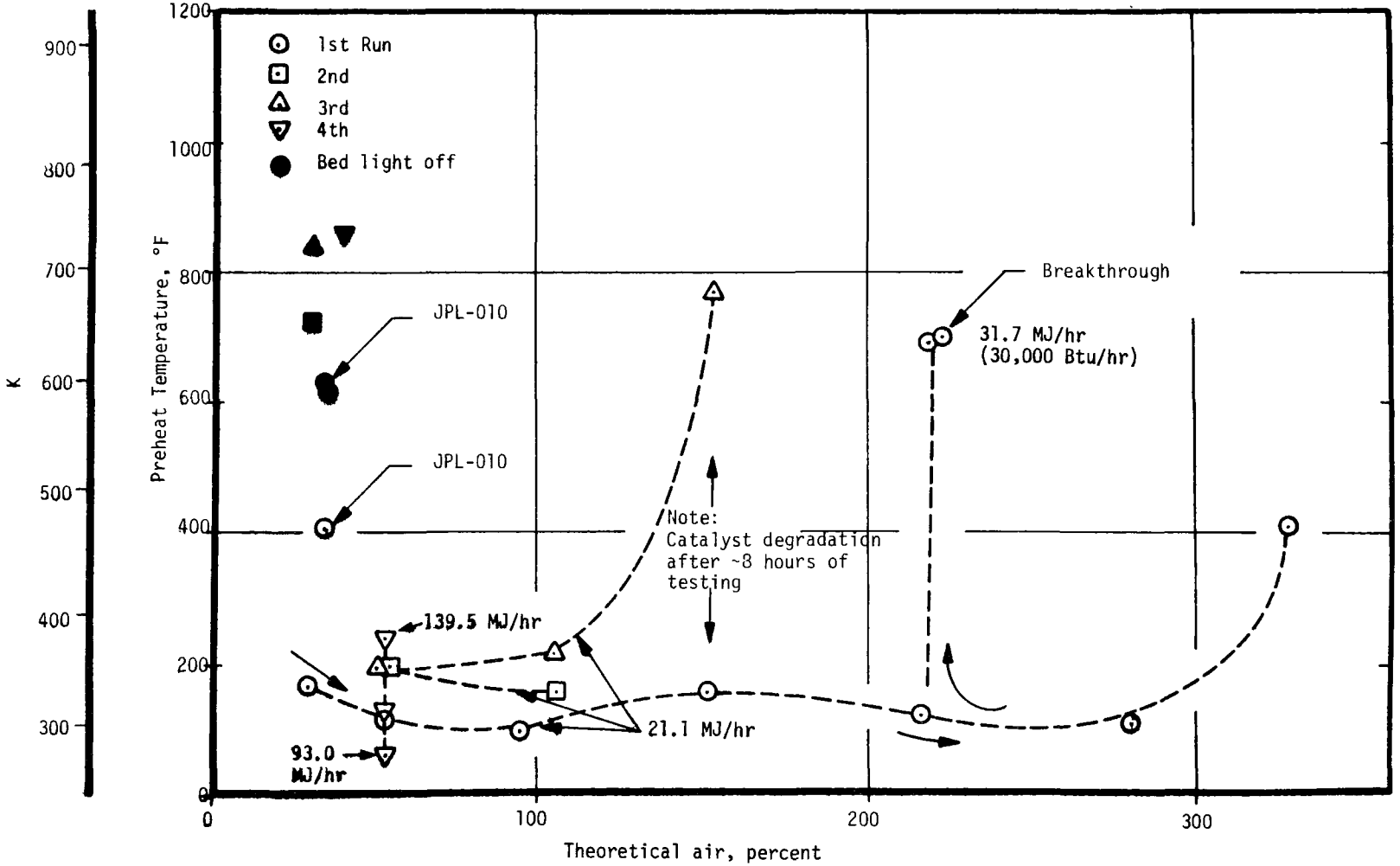

Figure 7-14a. Screening data, JPL-010 and -010X-preheat temperature (methane/air).

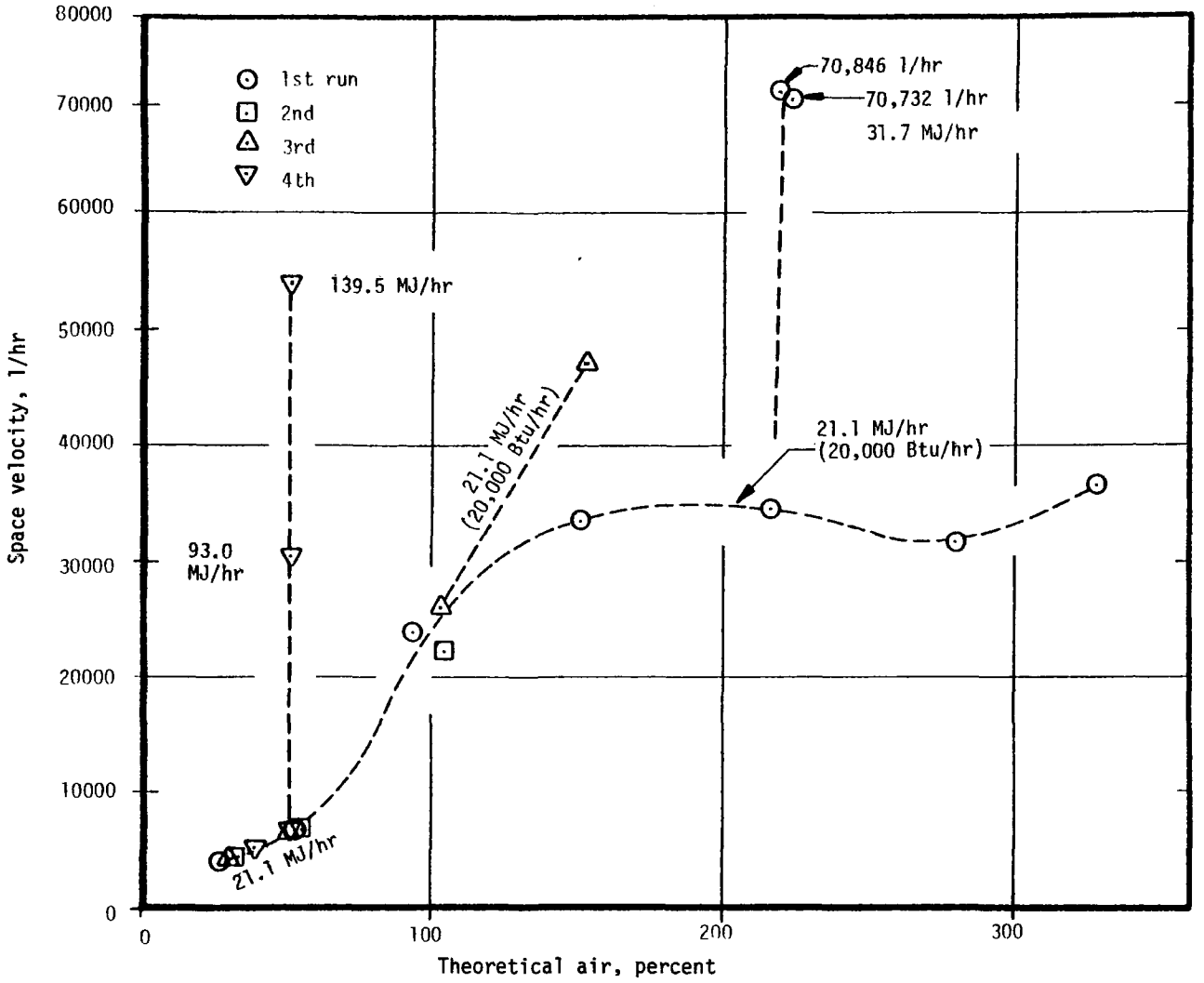

Figure 7-14b. Screening data, JPL-010 and -010X — space velocity (methane/air).

JPL-010P was tested with both methane and propane to compare combustion characteristics of the two fuels. The primary test objective was to demonstrate catalyst degradation with time. Therefore, minimum preheat data was not obtained. Rather, a constant preheat of nearly 811K (1000°F) was used, mainly under fuel-lean conditions. Data is shown in Table A-7.

Figure 7-15 shows that the catalyst lit off at a methane flow rate of 0.41 Kg/hr (0.91 lbm/hr) and attained steady-state conditions after 20 minutes. The flowrate was then dropped to 0.23 Kg/hr (0.50 lbm/hr) as the catalyst was allowed to age (from an elapsed time of 39 to 95 minutes). Fuel flow was then increased to determine the maximum throughput capability. This procedure was repeated until the maximum was found at 0.41 Kg/hr at an elapsed time of 208 minutes. After aging the catalyst at 0.23 Kg/hr for approximately 10 hours, another maximum was found at a total elapsed time of 818 minutes (13.6 hours). Here the maximum throughput capability was found to be 0.23 Kg/hr, a considerable drop from 0.41 Kg/hr.

Further testing was done at rich conditions (~50 percent T.A.) where the catalyst was able to combust as much as 2.0 Kg/hr (4.5 lbm/hr) of methane at a preheat temperature of only 301K (82°F).

Finally, the catalyst was tested with propane. Initial startup was attained at a fuel flow of 0.32 Kg/hr (0.7 lbm/hr). During the propane testing, the catalyst experienced melt down in various locations and was found to be extremely unreactive.

Figures 7-16 and 7-17 illustrate the preheat temperatures and space velocities for each test point. Most points cannot be used as a comparison to previous data since minimum preheat conditions were not sought. The exception is the fourth methane run performed at rich conditions. Lightoff occurred near 700K (800°F, see Figure 7-16a) and minimum preheats were found to fall below 375K (215°F). In comparison to previously tested catalysts, JPL-010P appeared to be very active at rich conditions after more than 13 hours of aging at lean conditions.

A number of significant conclusions were made from the tests on these three catalysts. They are:

1. High catalyst loading facilitates both low lightoff and low preheat conditions.

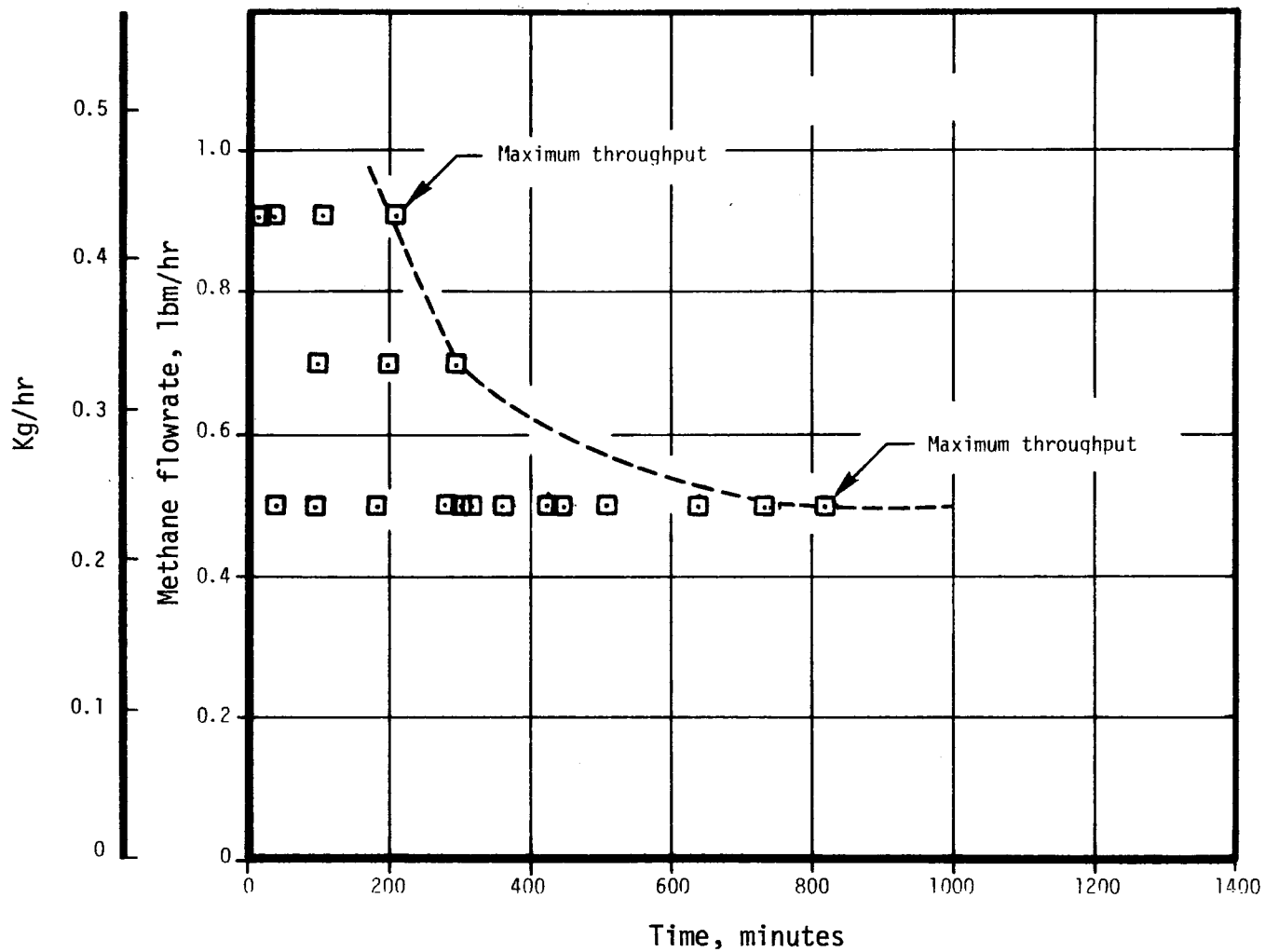

Figure 7-15. Degradation of test model JPL-010P at lean conditions (>350 percent T.A.) (methane/air)

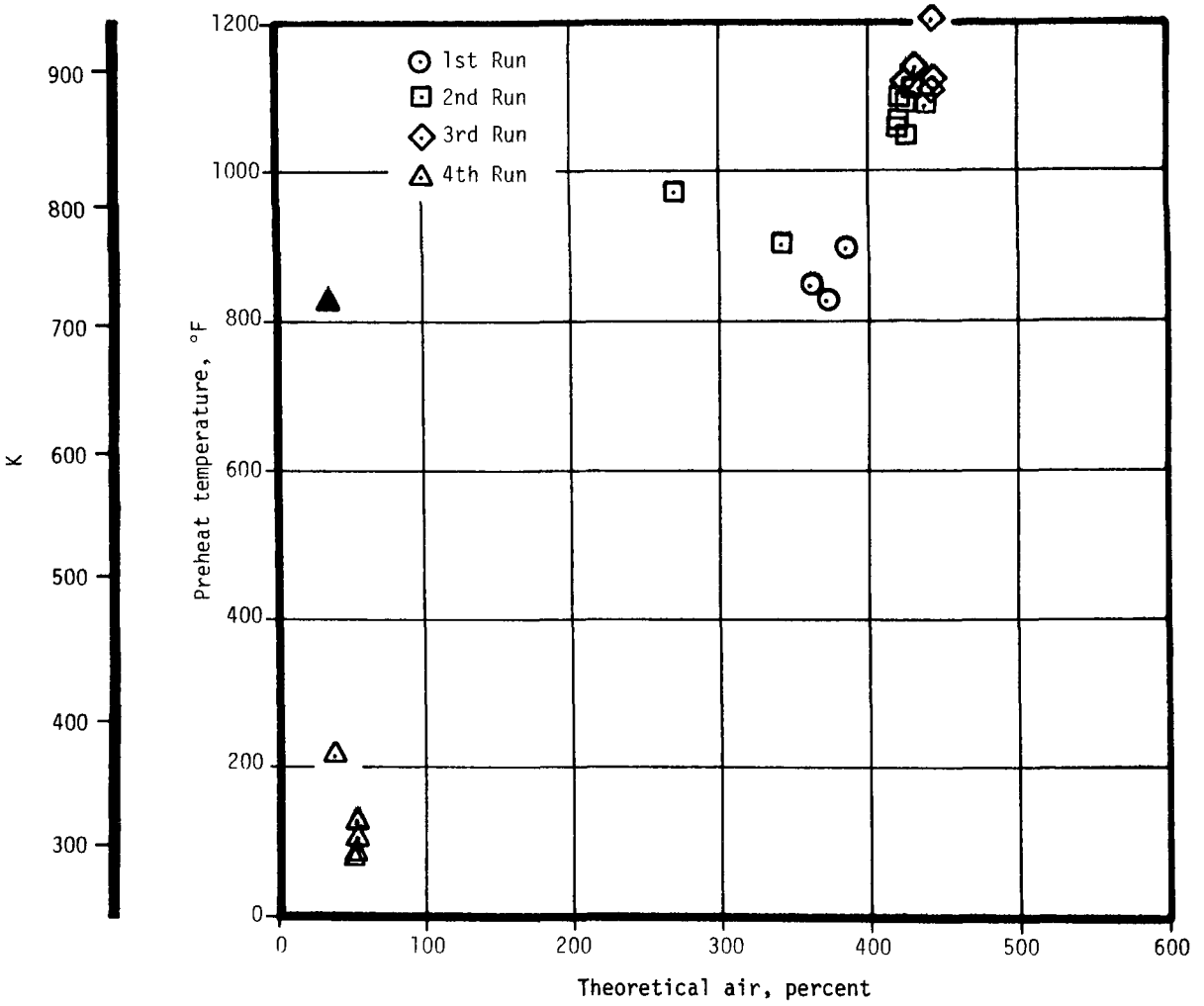

Figure 7-16a. Screening data, JPL-010P-preheat temperature (methane/air).

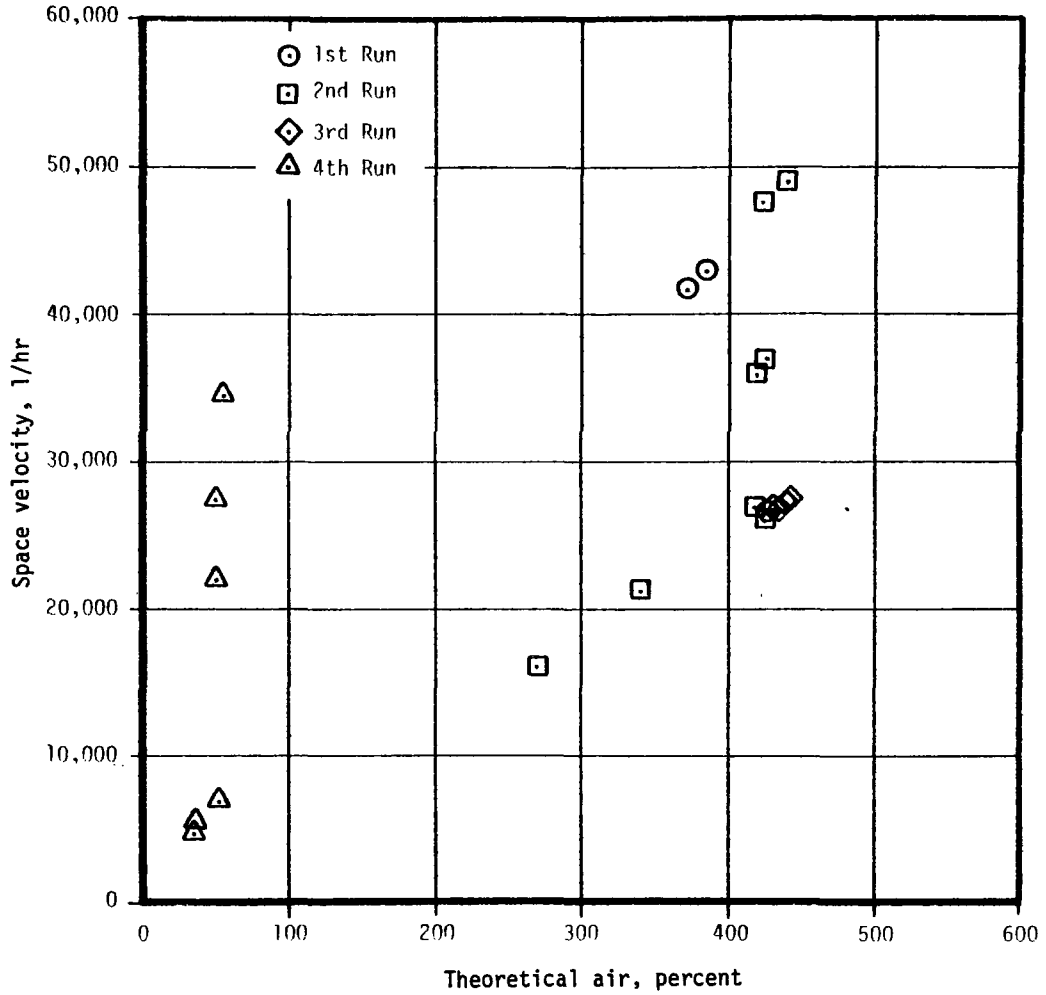

Figure 7-16b. Screening data, JPL-010P — space velocity (methane/air).

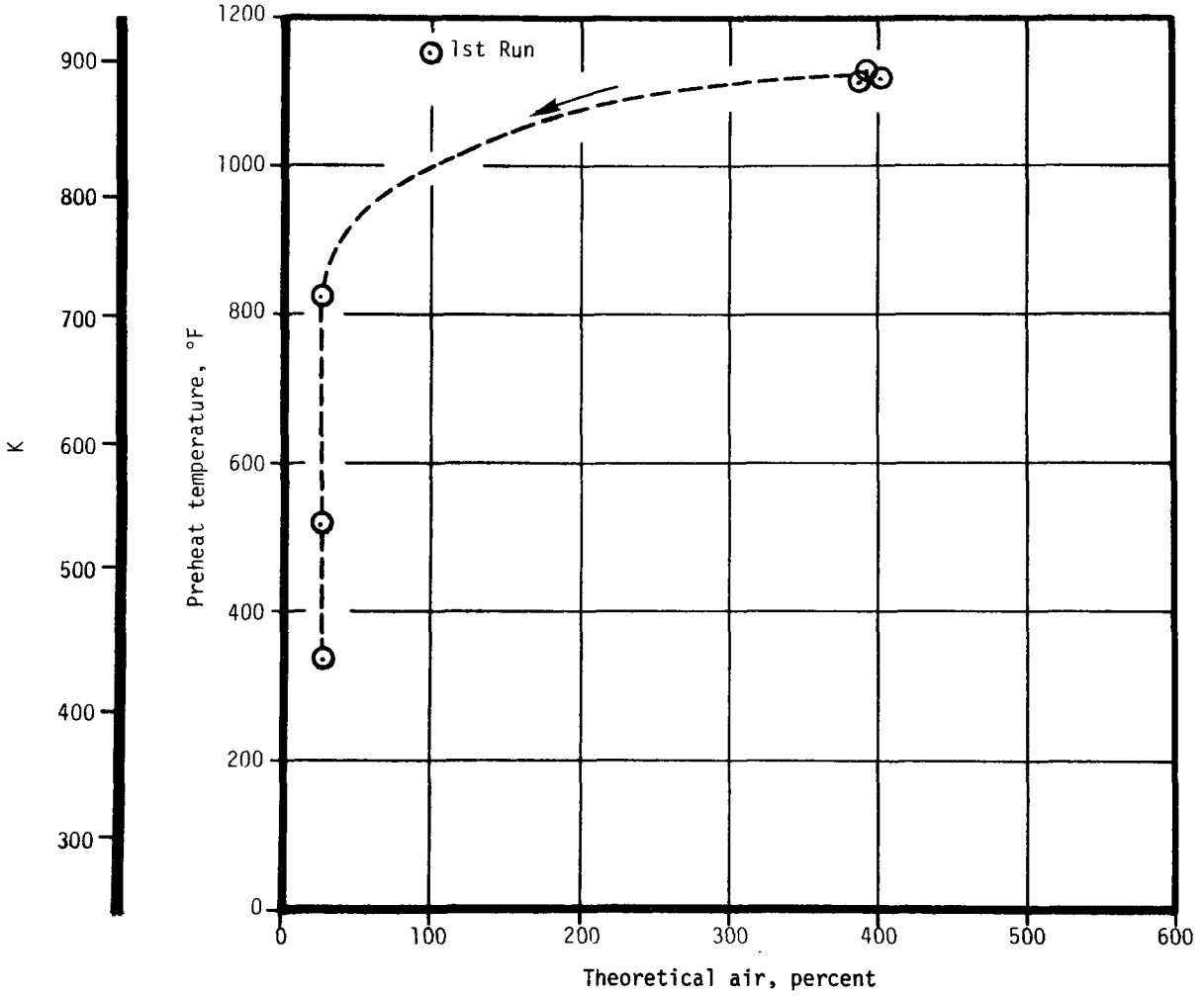

Figure 7-17a. Screening data, JPL-010P-preheat temperature (propane/air).

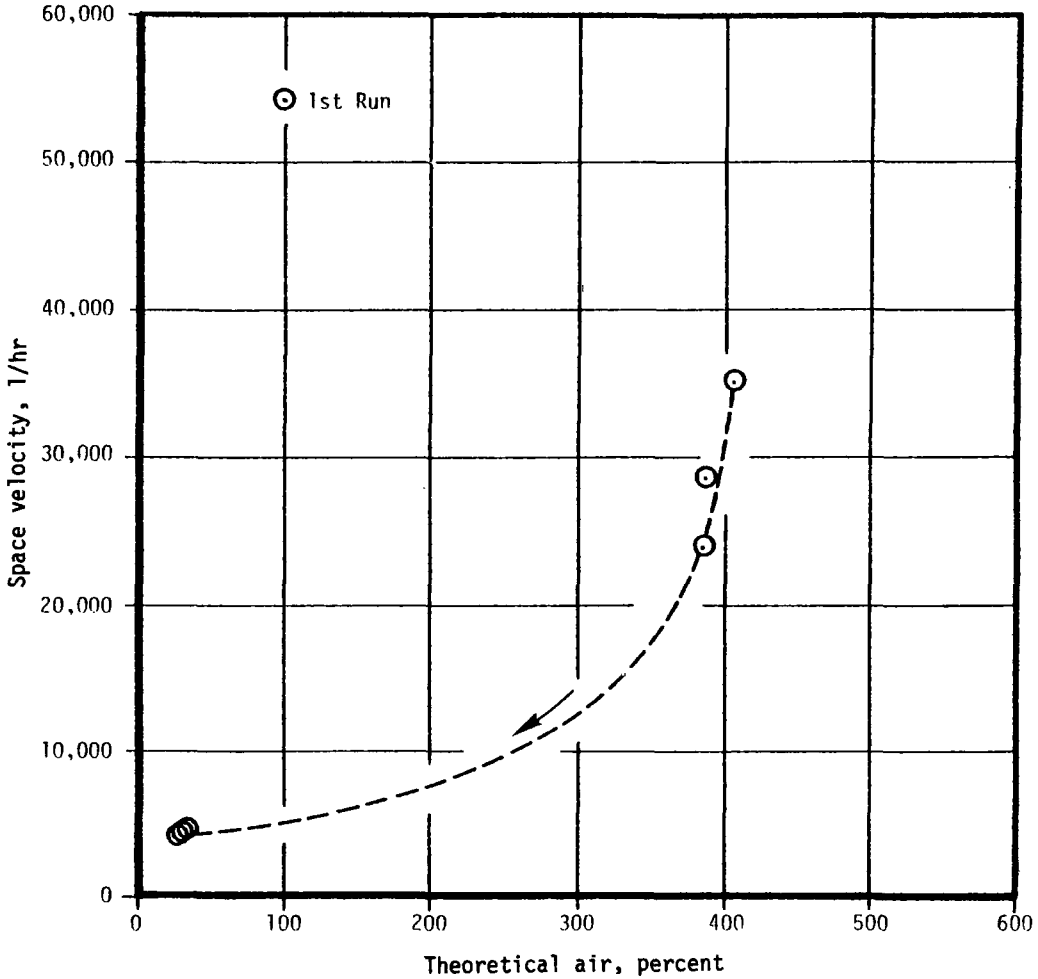

Figure 7-17b. Screening data, JPL-010P — space velocity (propane/air).

2. Catalyst degradation with time is still significant but lifetime is increased with increased catalyst loading at 1367K operating temperatures.

3. Increased catalyst loading allowed higher heat release and space velocities to be achieved.

4. Maximum throughput indicates catalyst degradation occurs in a similar manner to lightoff temperature.

Segments of test model JPL-010P were prepared and analyzed at JPL by Scanning Electron Microscopy (SEM) and energy-dispersive analysis by x-ray (EDAX). The results for the exit ends of two channels are shown in Figures 7-18 and 7-19. The micrographs show visible platinum globules in both locations, verified by the EDAX scans. Aluminum and silicon of the catalyst support and washcoat were also detected.

The detection of platinum at the catalyst surface by the JPL analyses shows that active catalyst remains at the surface (exposed to the gas flow) despite operating temperatures in excess of 1367K (2000°F). Larger platinum globules indicate that some agglomeration (loss of dispersion) has occurred. Both catalyst and washcoat structure appear similar for the two areas analyzed.

Test Models JPL-011, -012, -013, and -022

JPL-011, -012, and -013 were tested to learn more about washcoat and platinum behavior. JPL-011 was treated with H_2S gas to improve the axial Pt distribution through the monolith. JPL-012 and -013 were presintered to study the effects of the alumina washcoat phase change from gamma to alpha. Keep in mind that unlike JPL-010X these catalysts had the low platinum loading (0.22 - 0.30 weight percent).

JPL-011 was tested both with methane and propane. The results are shown in Table A-8 and Figures 7-20 and 7-21. The methane tests on this catalyst resulted in performance similar to JPL-006X and JPL-007. Lightoff was 637K (686°F) and 676K (756°F) for the first and second runs, respectively. Unlike the others a maximum throughput test was performed at 50 percent theoretical air first. Performance was excellent, requiring a low preheat ($< 340K$) to reach a heat release of 139.5 MJ/hr (132,000 Btu/hr, S.V. = 50,835 hr^{-1}) without breaking through. A subsequent walkthrough to lean

a. 20 x magnification of channels 1 and 2

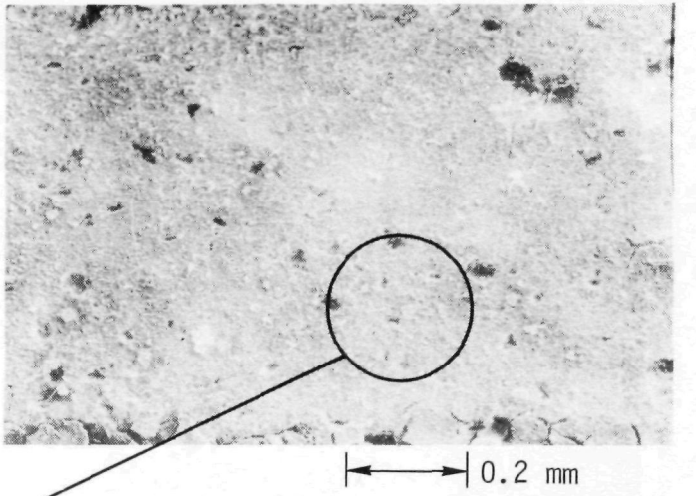

b. 100 x magnification of channel 1 bottom

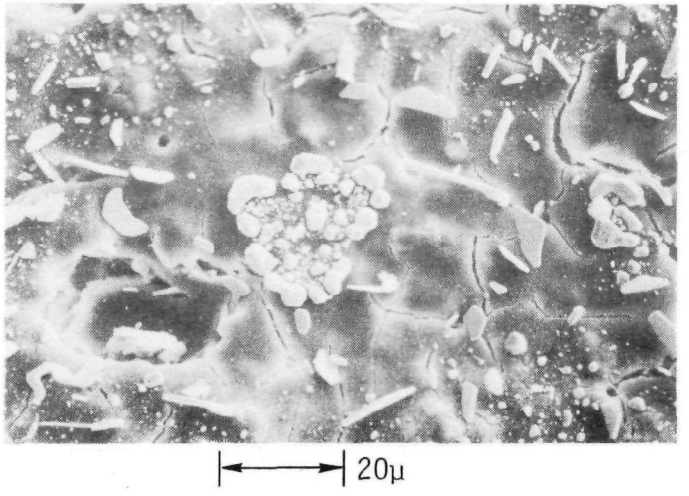

c. 1000 x magnification showing Pt crystallites

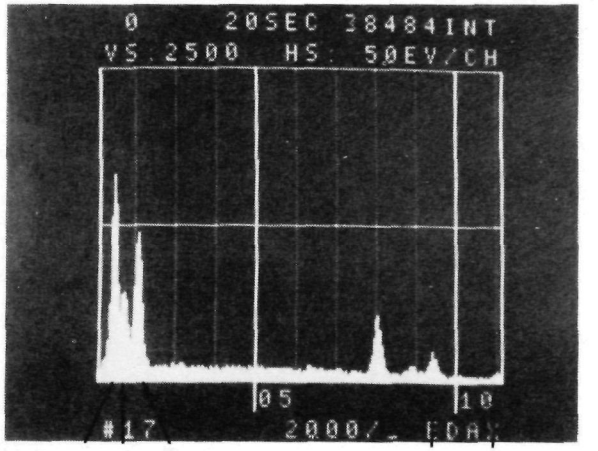

d. EDAX scan showing presence of aluminum, silicon, and platinum

Figure 7-18. Surface analysis at exit of channel 1, test model JPL-010P.

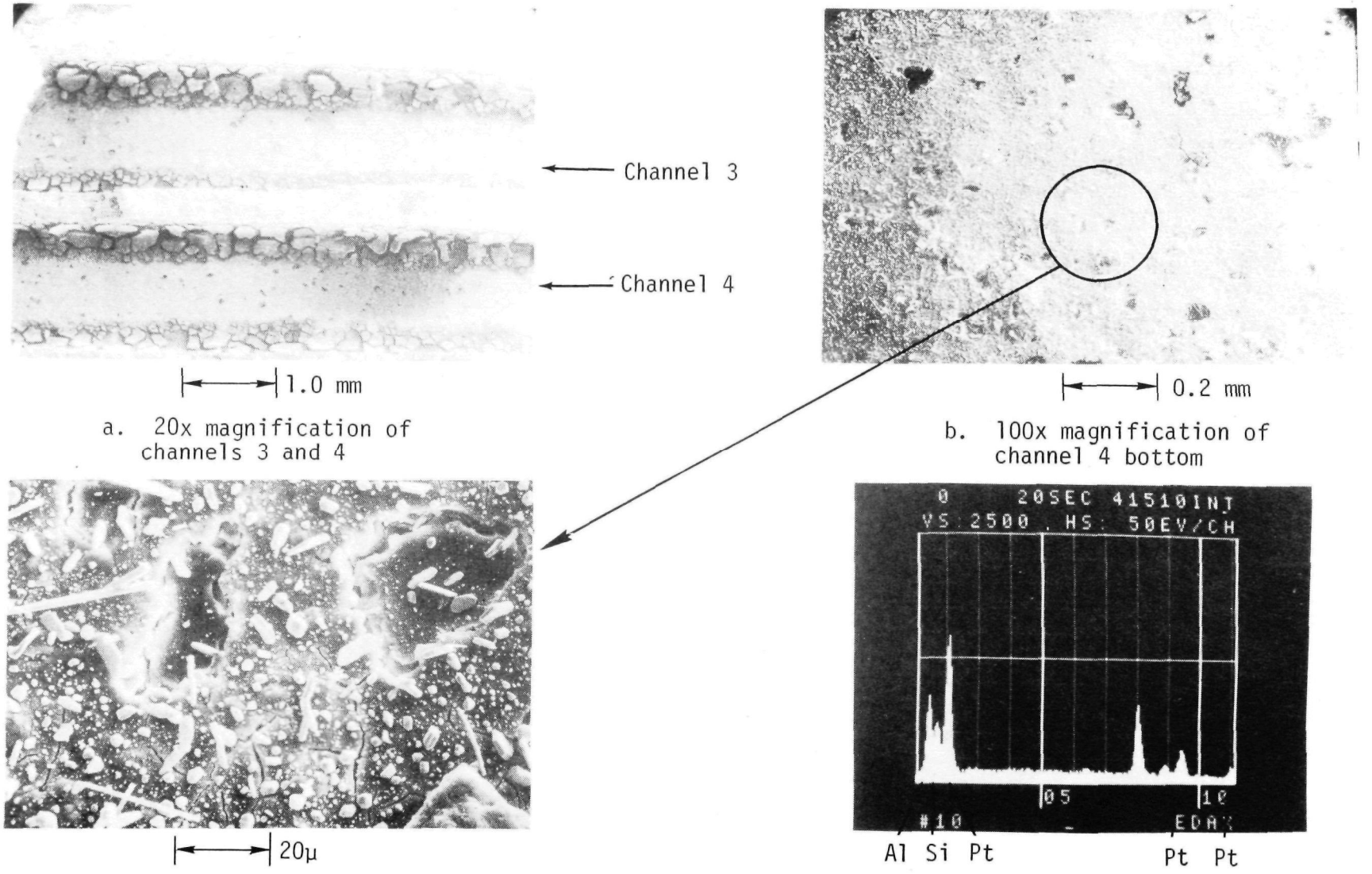

a. 20x magnification of channels 3 and 4

b. 100x magnification of channel 4 bottom

c. 1000x magnification showing Pt crystallites

d. EDAX scan showing presence of aluminum, silicon, and platinum

Figure 7-19. Surface analysis at exit of channel 4, test model JPL-010P.

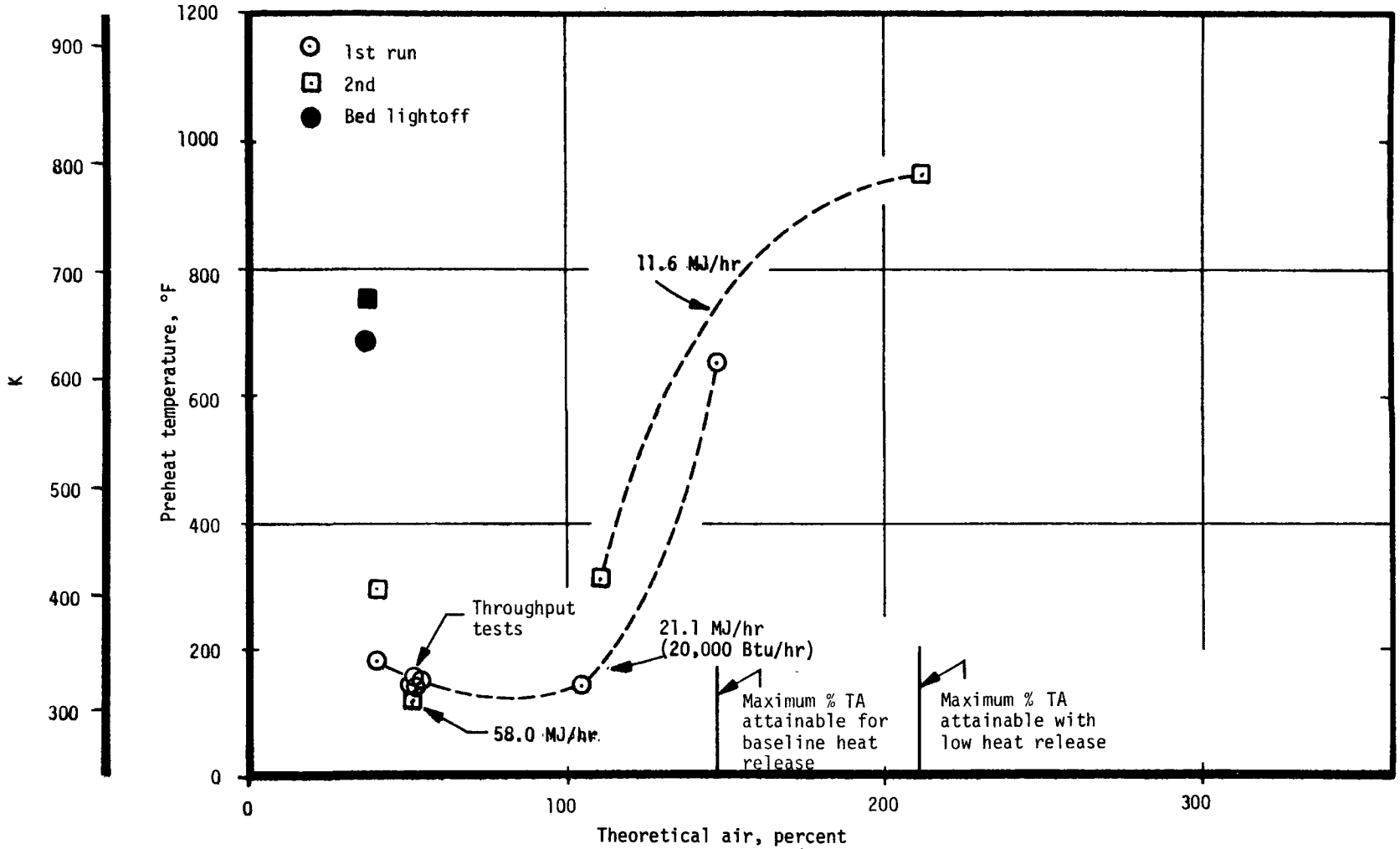

Figure 7-20a. Screening data, JPL-011-preheat temperature (methane/air).

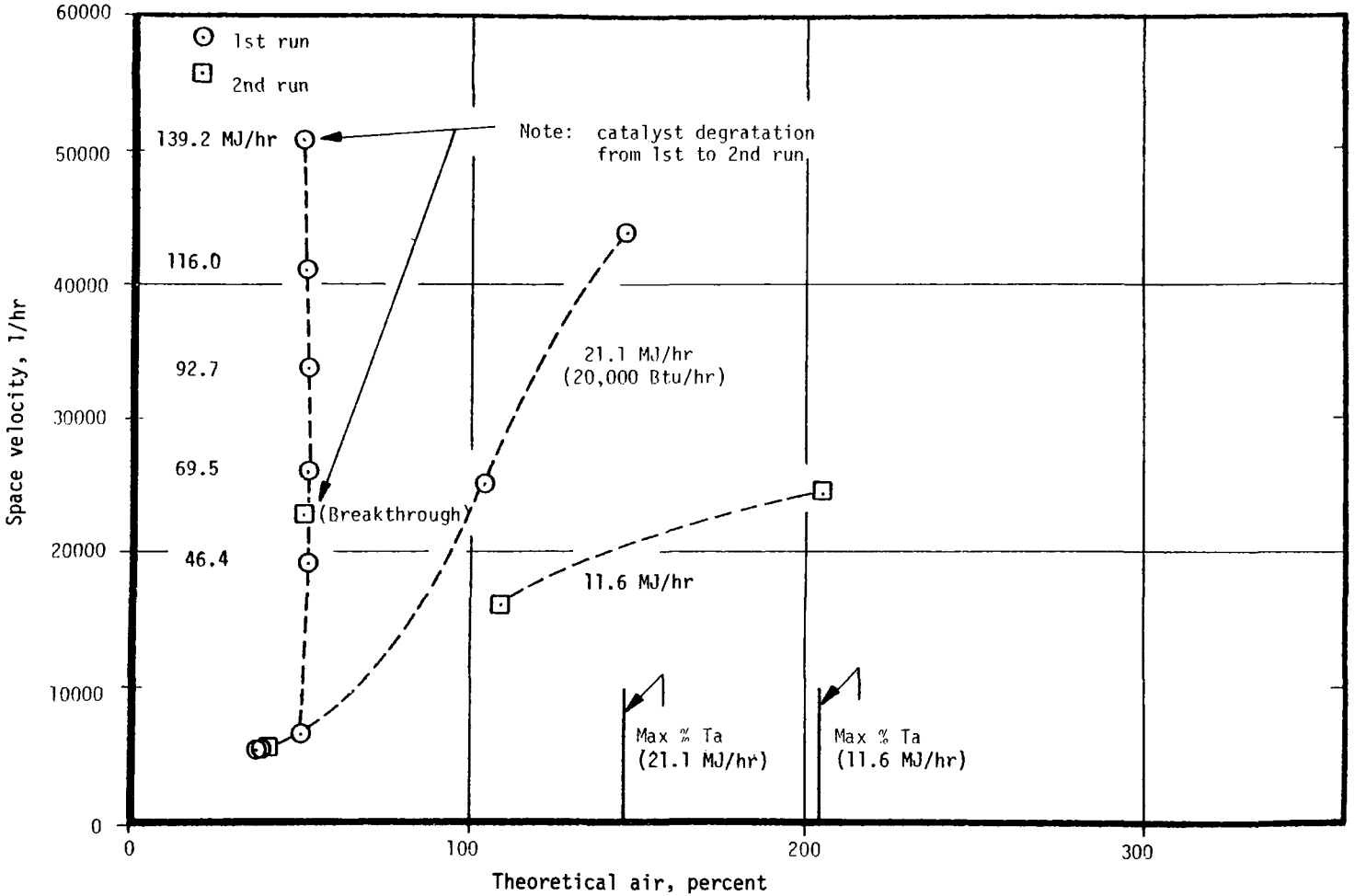

Figure 7-20b. Screening data, JPL-011 – space velocity (methane/air).

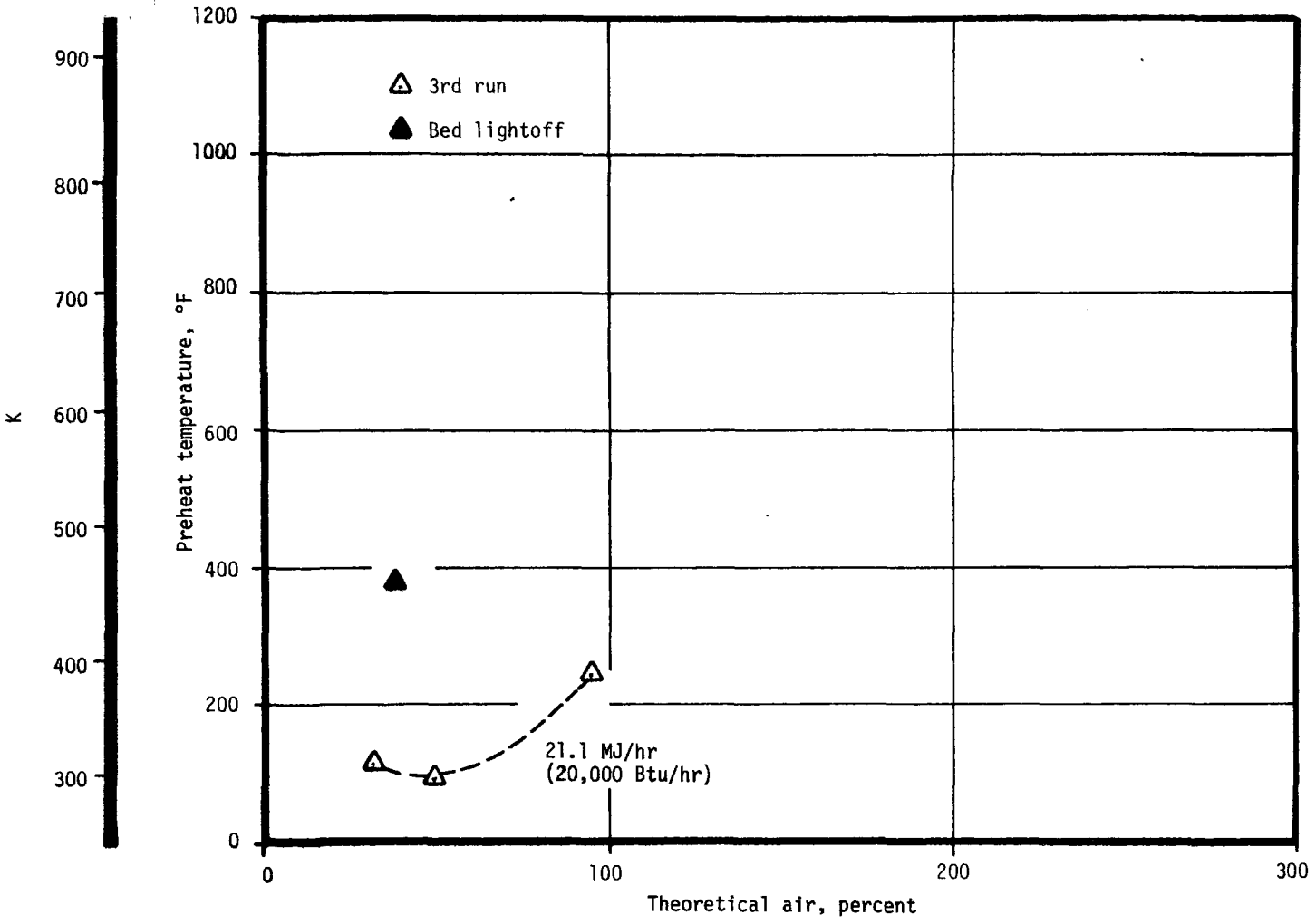

Figure 7-21a. Screening data, JPL-011-preheat temperature (propane/air).

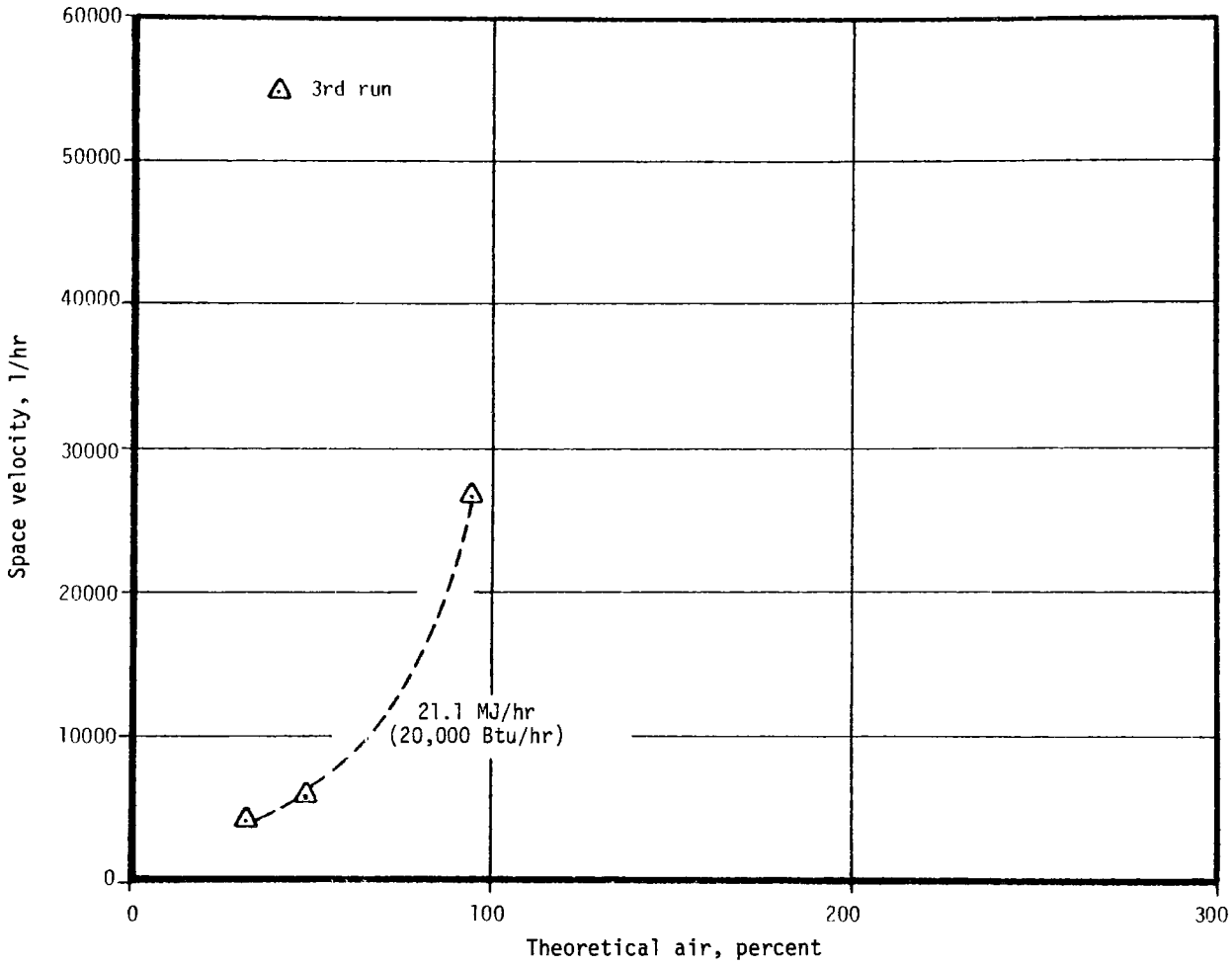

Figure 7-21b. Screening data, JPL-011 — space velocity (propane/air).

conditions was not possible beyond 147 percent theoretical air. Decreasing the heat release allowed a maximum of 211 percent theoretical air to be reached with a very high preheat (782K). To confirm that the catalyst had degraded substantially, an attempt was made to repeat the maximum throughput test at 50 percent theoretical air. Breakthrough was found to occur at a space velocity of 22,848 hr^{-1}. In the first run, no breakthrough occurred up to the maximum capability of the test rig at 50 percent theoretical air. A direct comparison of this run with JPL-006X to deduce the effect of the H_2S platinizing technique is difficult, since the tests were not carried out in the same order. JPL-006X tried a rich-to-lean walkthrough followed by a maximum throughput test at 50 percent theoretical air. JPL-011 was exposed to the reverse of that procedure. Since degradation plays such an important role, the two catalysts could not be totally compared. However, from the data obtained, it was noted that JPL-011 required a lower preheat temperature at the same values of theoretical air and heat release than JPL-006X, in spite of the early maximum throughput test. Thus, H_2S treatment of platinum appears beneficial in terms of extending platinum activity with time.

Propane testing consisted of a lightoff and three test points. The bed lightoff temperature (469K) was much lower than all catalysts tested with methane. Preheat temperatures for operation near 100 percent theoretical air were also surprisingly low (<391K) considering the long testing that the catalyst had undergone with methane.

JPL-012 was prepared by sintering the washcoat at 1273K for 48 hours before applying the platinum. Data for this test model is given in Table A-9 and Figure 7-22. The pretest surface area was 1.33 m^2/g, considerably below the unsintered values of the previous catalysts. The dispersion of platinum was measured as 49 percent. In general, this catalyst performed similar to other catalysts after they had aged for a few hours, in that operation at conditions leaner that 111 percent theoretical air was not possible. Also, maximum heat release at 50 percent theoretical air was 81.2 MJ/hr (76,900 Btu/hr), S.V. = 42,373 hr^{-1} at a relatively high preheat temperature (704K). Bed lightoff temperatures were similar to the previous catalysts reported; 614K (645°F) and 674K (754°F) for the first and second runs, respectively. In general, the performance of this catalyst was similar to JPL-006X which did not have a presintered washcoat.

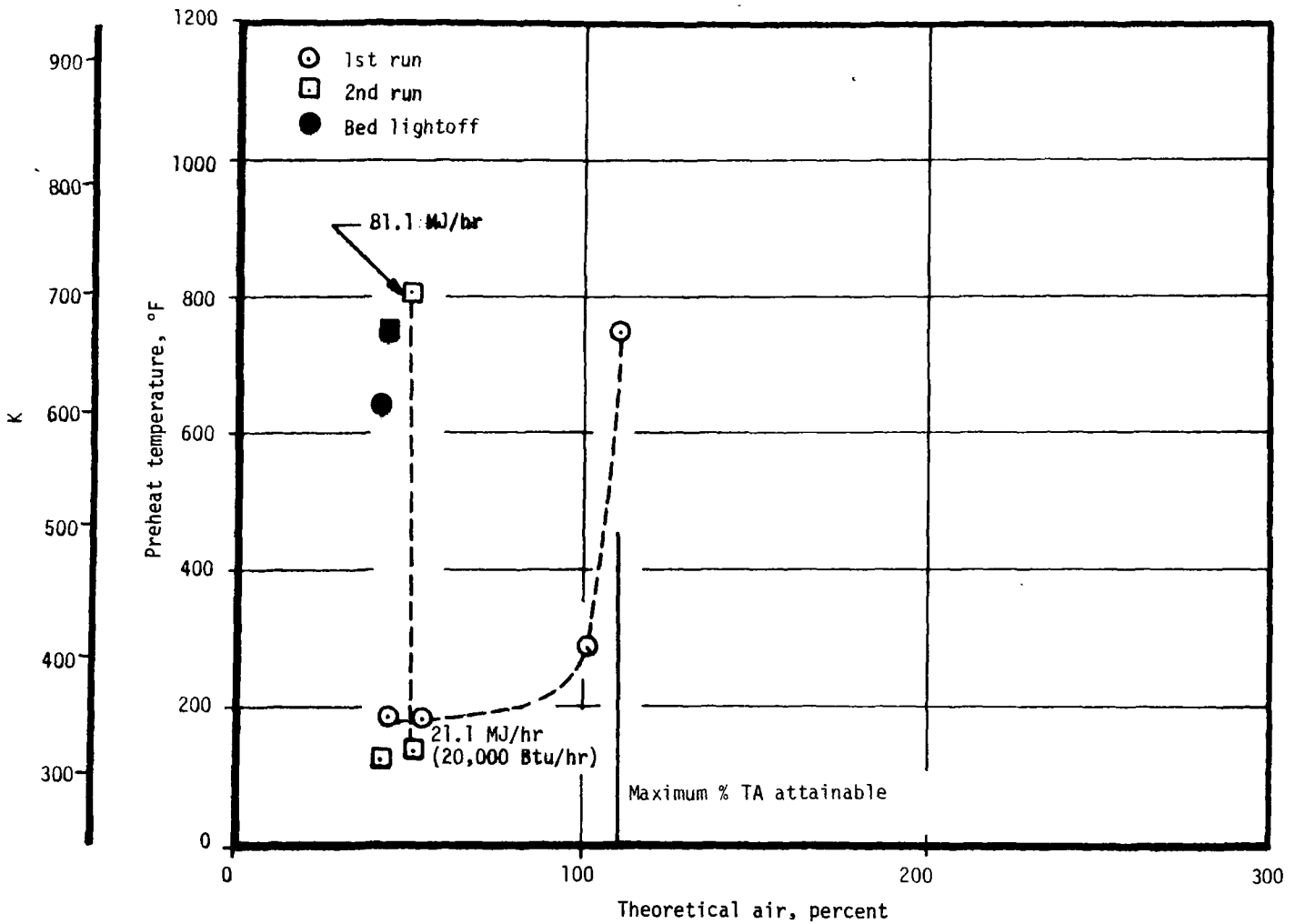

Figure 7-22a. Screening data, JPL-012-preheat temperature (methane/air).

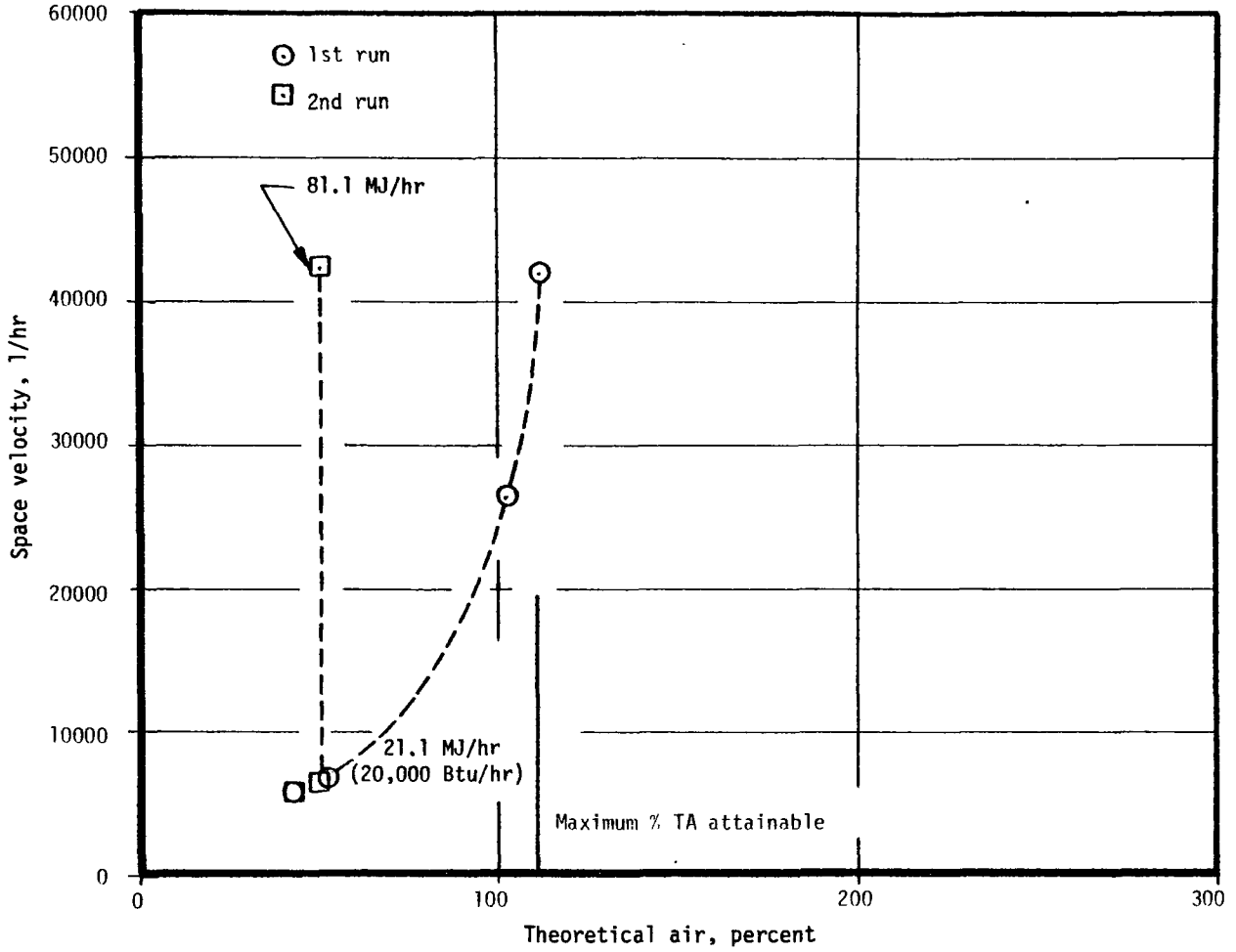

Figure 7-22b. Screening data, JPL-012 — space velocity (methane/air).

JPL-013 was prepared by sintering at 1273K for 48 hours, after the washcoat and platinum had been applied. An extremely low pretest surface area of 0.93 m^2/g and a dispersion of only 0.7 percent were measured. These are comparable to the previous post-test measurements of the other catalysts. As expected, the performance was very poor. Lightoff was high, at 734K (861°F). Breakthrough occurred at 51.1 percent theoretical air at only the baseline heat release. UHC was measured at 6300 ppm at this condition. Further testing was not attempted. Data for JPL-013 is shown in Table A-10 and Figure 7-23.

The fourth catalyst in this series, JPL-022, was prepared with a DuPont stabilized washcoat.

Performance with this catalyst was comparable to JPL-011, the Acurex prepared catalyst with H_2S treating. An initial maximum throughput test at 50 percent theoretical air showed the performance to be good. Maximum heat release of the test facility was reached (139.2 MJ/hr) at a very low preheat (306K). Upon attempting to "walk" the catalyst through to lean conditions it was found that it could not exceed 103.5 percent theoretical air. This is roughly what was found to occur for JPL-011 at 147 percent theoretical air. Note that like JPL-008 (Matthey Bishop washcoat) the pretest surface area was slightly higher than Oxy-Catalyst prepared monoliths. (See Table 7-2). Data is shown in Table A-11 and Figure 7-24.

Several important conclusions resulted from these washcoat evaluation tests.

1. Acurex-prepared catalysts performed comparably to commercial catalysts prepared by DuPont, Oxy-Catalyst, and Matthey Bishop.
2. H_2S treatment of the platinum appears effective in increasing combustion performance
3. Propane is more active with a combustion catalyst than methane.
4. Presintering the washcoat does not appear to have a deleterious effect on the performance of the baseline catalyst, implying that relatively little platinum is buried during sintering of the washcoat and that much of the initially available surface area is unused.

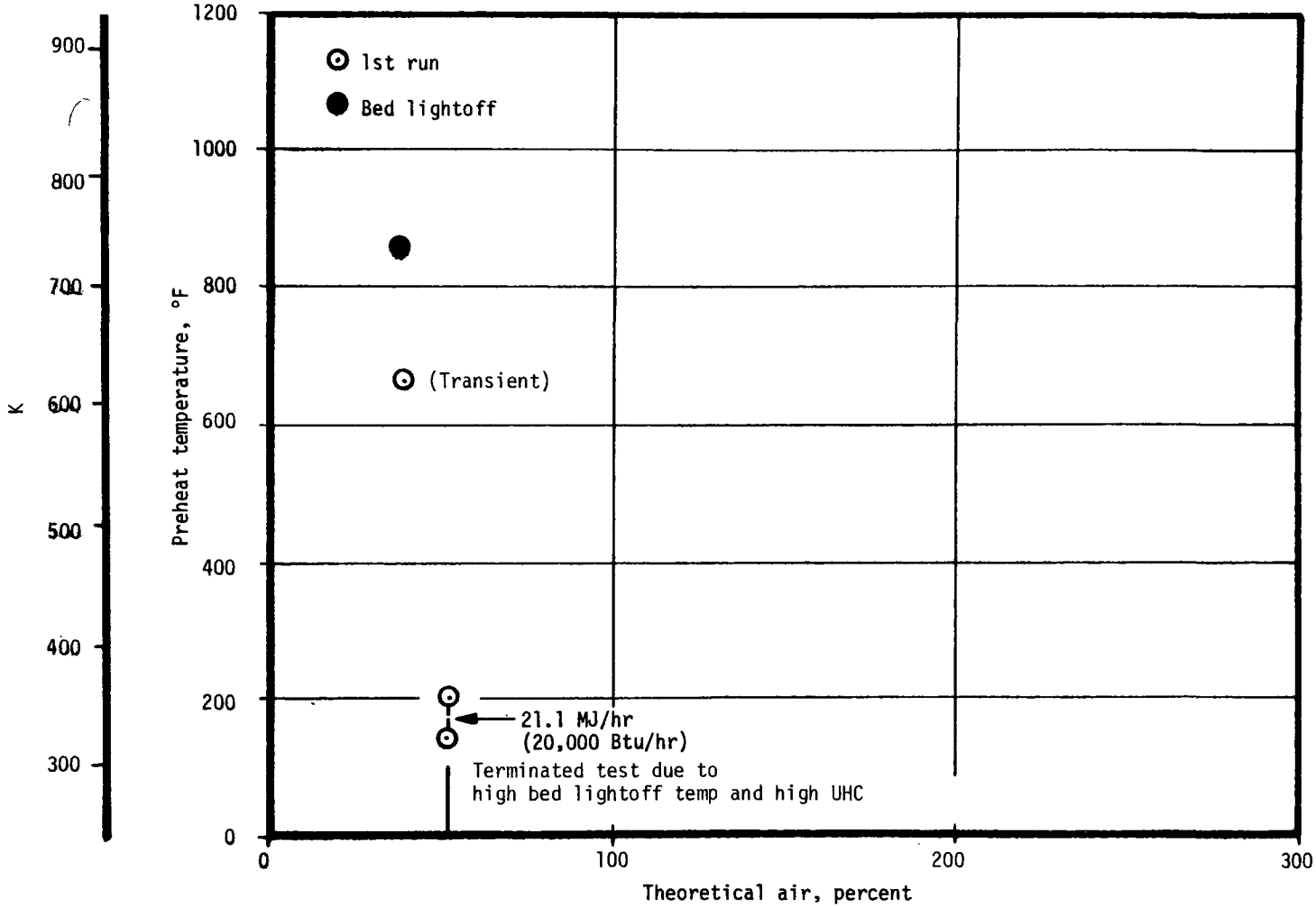

Figure 7-23a. Screening data, JPL-013-preheat temperature (methane/air).

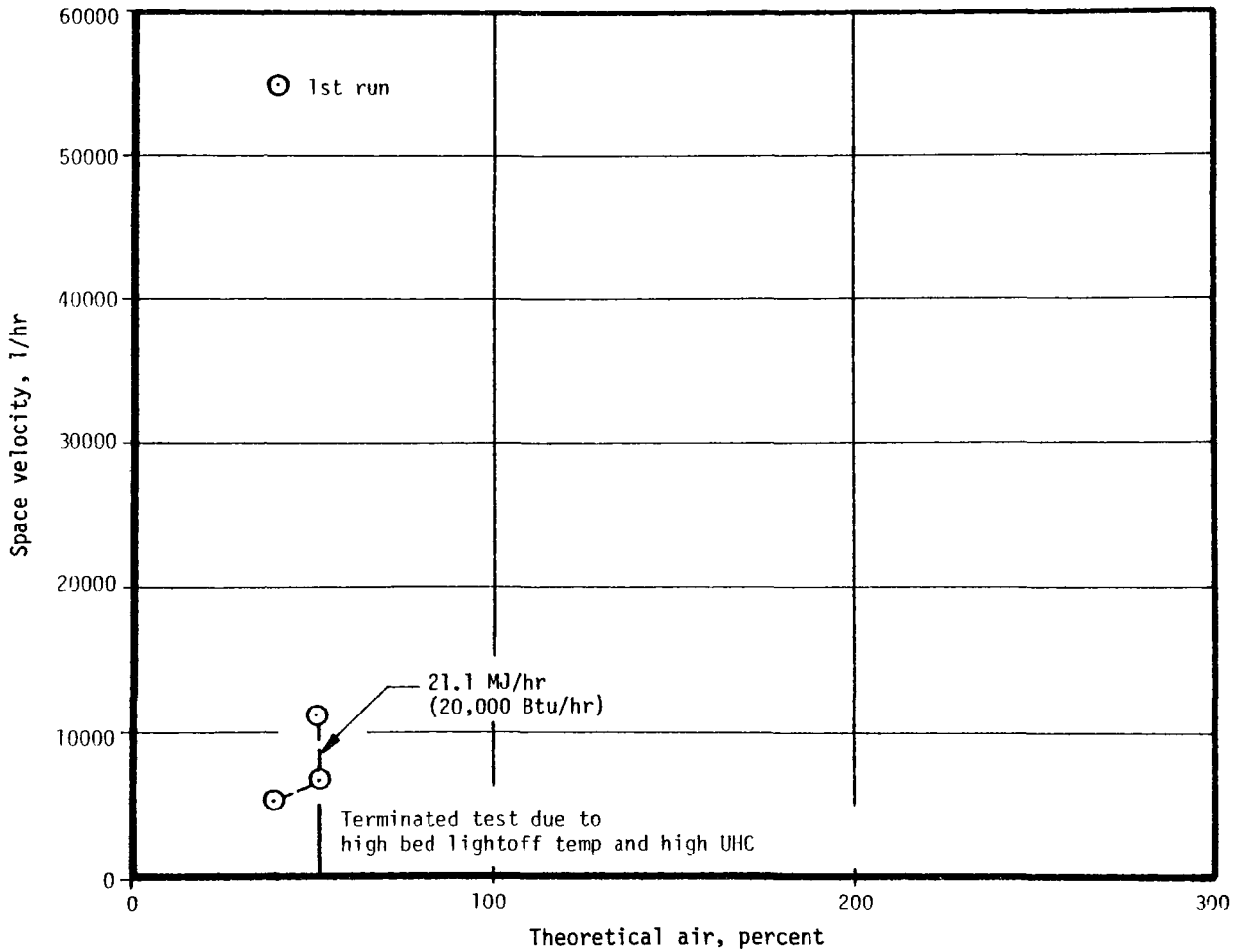

Figure 7-23b. Screening data, JPL-013 – space velocity (methane/air).

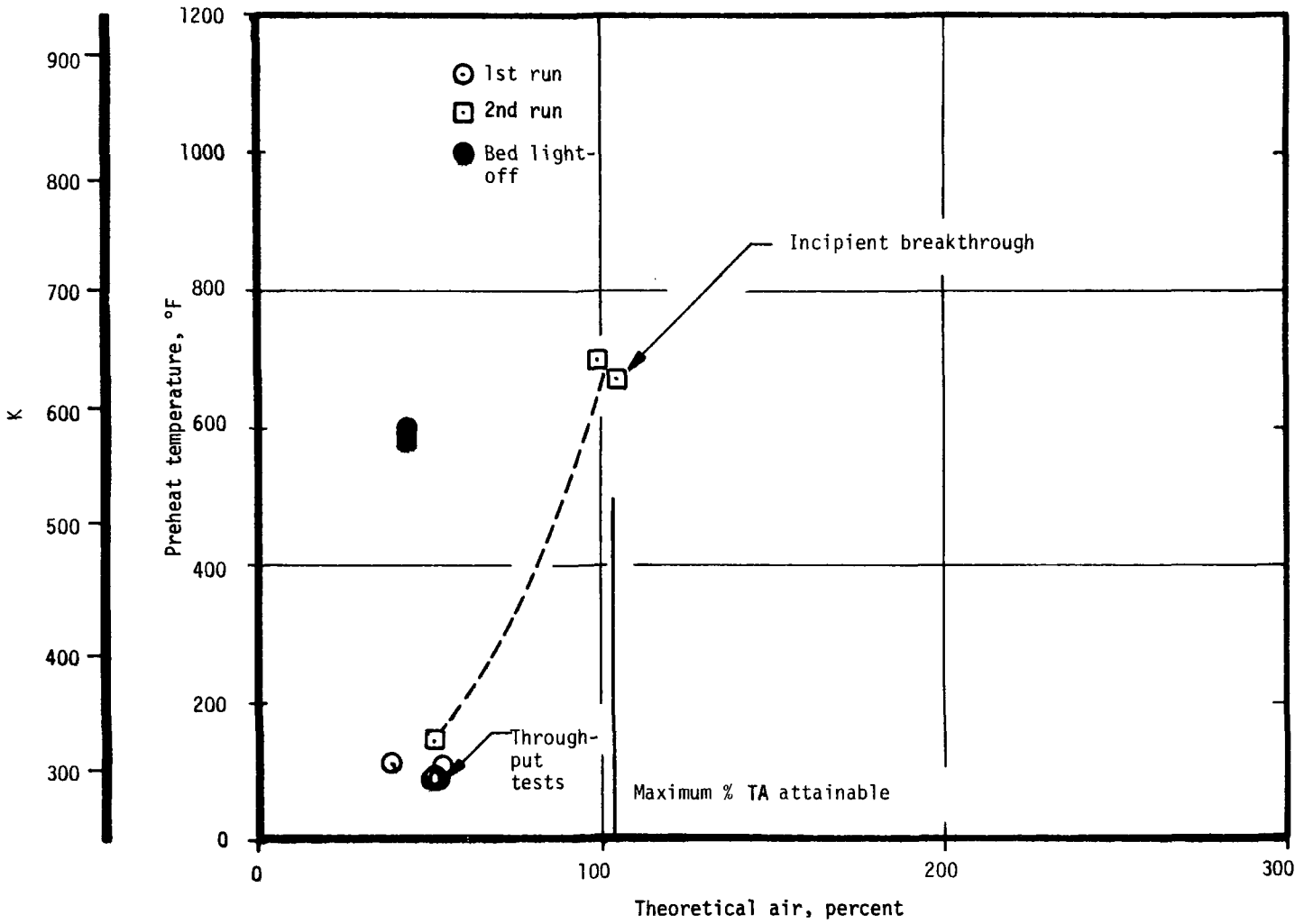

Figure 7-24a. Screening data, JPL-022-preheat temperature (methane/air).

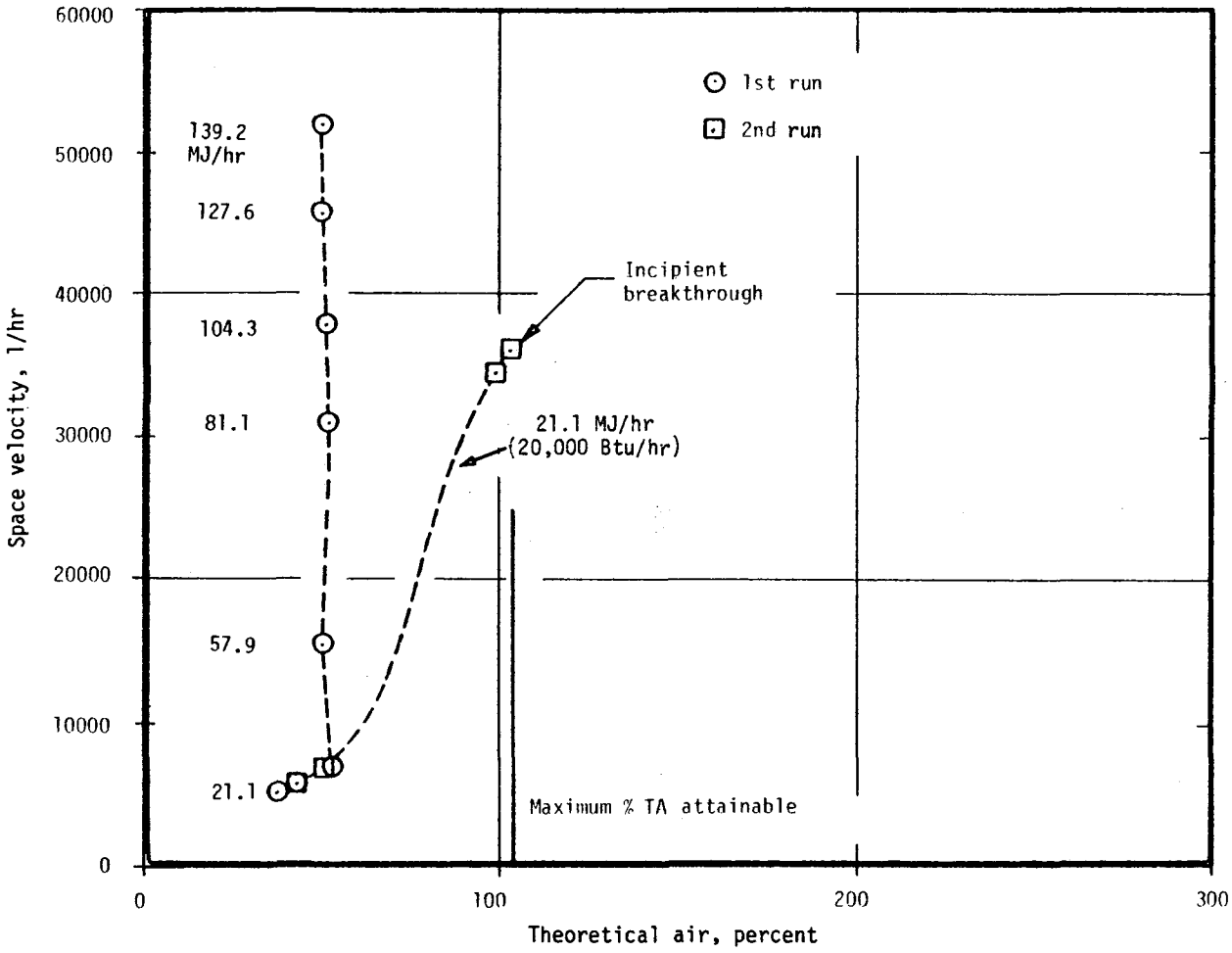

Figure 7-24b. Screening data, JPL-022 — space velocity (methane/air).

5. Presintering the platinized washcoat at 1273K for 48 hours has a marked effect on catalyst performance, reducing the catalyst activity to a very low level.

Test Model JPL-016

Stabilization techniques are available for catalyst materials as well as for washcoats. JPL-016 consisted of a Corning cordierite support with an Oxy-Catalyst 10 weight percent gamma-alumina washcoat. The washcoat was stabilized by the addition of cerium oxide and impregnated with a 2:1 molar ratio of platinum stabilized with palladium.

Table A-12 summarizes the operating points attained. These are illustrated in Figure 7-25. Initially, lightoff occurred at 608K (635°F) at 37.3 percent theoretical air. Figure 7-25a shows that preheats of less than 324K (123°F) were able to maintain activity up to 106.8 percent theoretical air. Beyond this point activity was difficult to maintain as indicated by several aborted attempts to reach theoretical airs beyond 113.4 percent. The furthest lean condition attainable is shown to be 113.4 percent theoretical air with a preheat of 357K (182°F). The catalyst was restarted and operated at rich conditions, hitting almost identical operating points as in the first run. In an attempt to reach leaner conditions, the fuel flow was then reduced to 0.23 Kg/hr (0.5 lbm/hr). A preheat of 764K (915°F) was needed at 109.7 percent T.A. to maintain activity. Maximum throughput at 50 percent T.A. was then determined by operation at 1.59 Kg/hr (3.5 lbm/hr) and then at 1.81 Kg/hr (4.0 lbm/hr). Note the low preheats required for these two conditions. The maximum throughput was even higher, attaining nearly 2.72 Kg/hr (6.0 lbm/hr). A third run was attempted which required approximately 22K more bed preheat for lightoff than the previous two runs. Operation at 90.4 percent theoretical air required 763K (914°F) of preheat, showing a large amount of degradation over the last two runs.

In summary, this catalyst appeared to be comparable to JPL-022 (prepared by DuPont). It also was unable to operate at lean conditions but performed well at rich conditions with high throughputs.

Since the post-test surface area of JPL-016 was quite high (2.08 m^2/g), as shown in Table 7-2, a further investigation into the area of washcoat

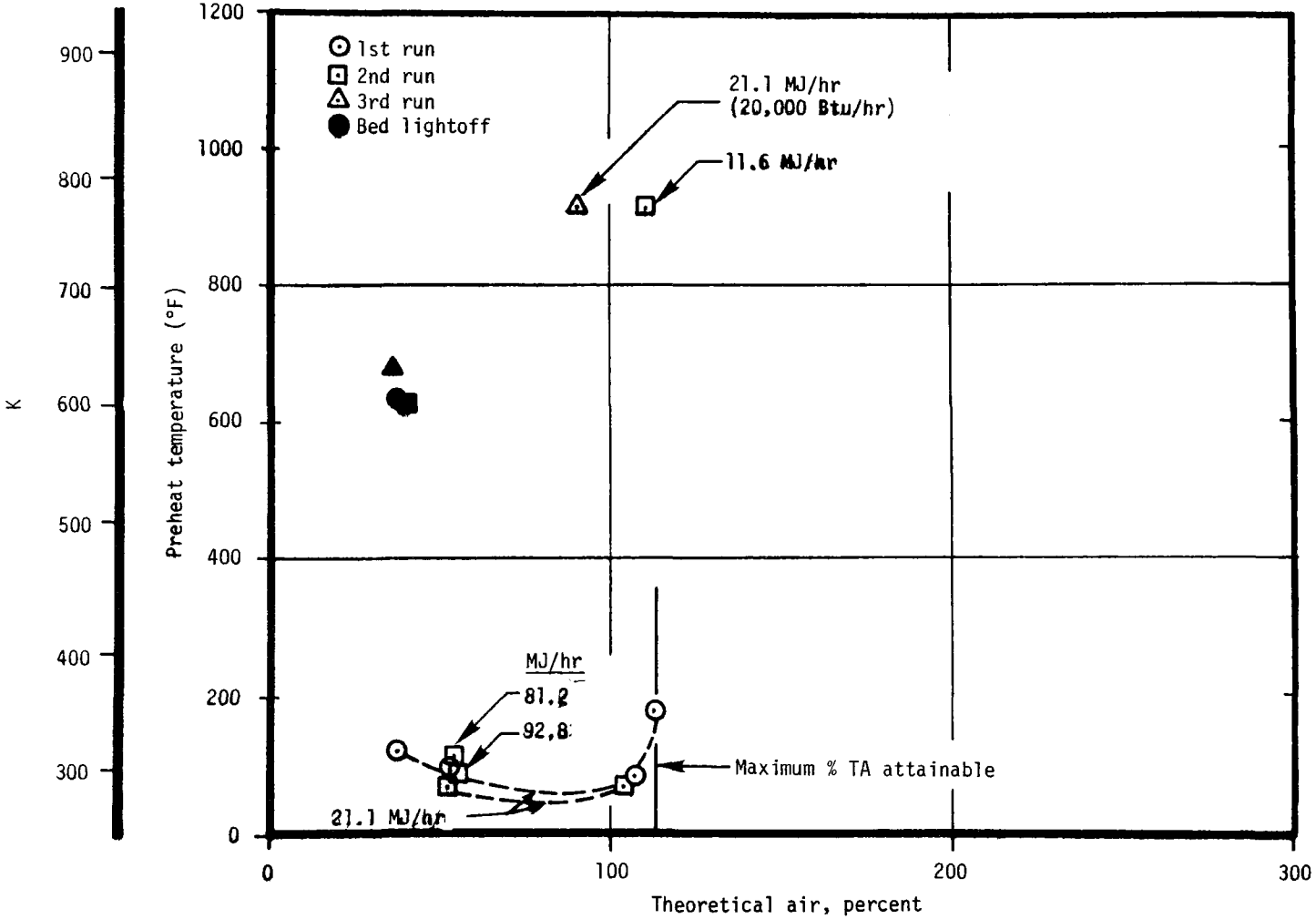

Figure 7-25a. Screening data, JPL-016-preheat temperature (methane/air).

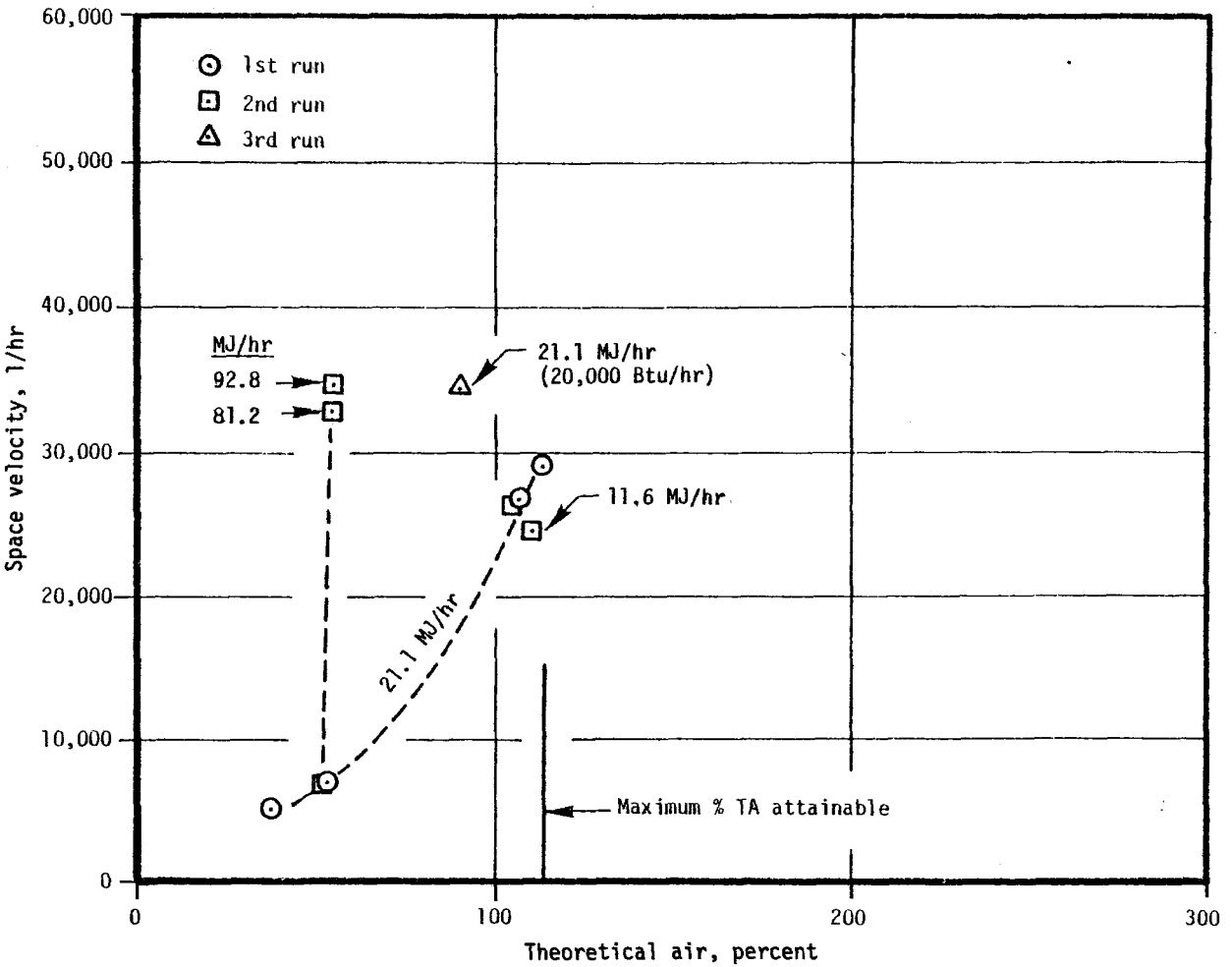

Figure 7-25b. Screening data, JPL-016 — space velocity (methane/air).

stabilization was conducted. The objective was to determine the change in surface areas of γ-alumina as a function of the amount of ceria (CeO_2) or cesium oxide (Cs_2O) deposited on the γ-alumina washcoat, when these washcoats are held at high temperatures.

To perform the study, a Corning cordierite monolith was cut in half, and then each half was cut into 12 pie-shaped wedges as shown in Figure 7-26.

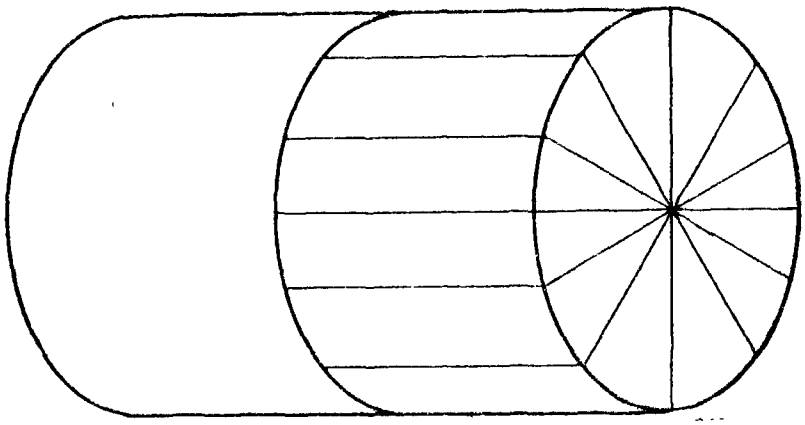

Figure 7-26. Test specimen preparation, washcoat stabilization tests.

Duplicate samples were dipped in cerium or cesium-doped solutions of alumina to give loadings of 0 percent, 0.3 percent, 1 percent, and 5 percent CeO_2 or Cs_2O. The wedges were dried at 423K. Samples were then placed in a cold oven, heated to 1273K, and held at that temperature for 16 hours. After cooling down for 8 hours, the samples were reheated to 1423K (2100°F) for 18 hours. Each sample was ground up, weighed, loaded in the BET cell, and the cell evacuated for 30 to 60 minutes at 523K. Surface area measurements were then made. Data for the analysis is presented in Table 7-5 and the results are plotted in Figure 7-27.

Based on the results of the surface area measurements, the ceria treated samples show no stabilization in surface area with up to 5 percent ceria applied. Rather a decrease in surface area to a value about 10 percent below the unstabilized samples is noted for ceria loadings of 1 percent and 5 percent. Samples treated with 0.3 weight percent cesium oxide also show no effect on surface area stabilization. However, the samples treated with 1 percent and 5 percent Cs_2O show nearly a factor of 2 increase in surface

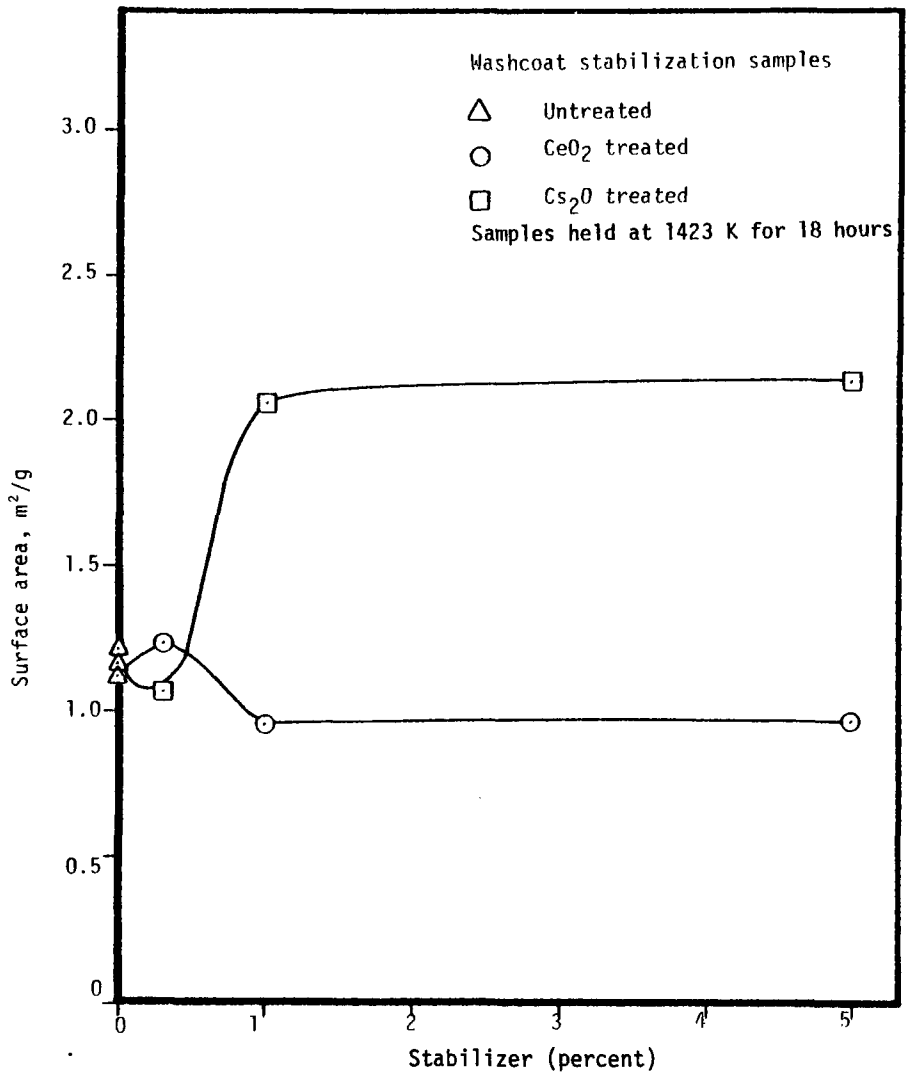

Figure 7-27. Washcoat stabilization study results.

area over presintered values for untreated washcoats. Based on these results, it appears desirable to stabilize γ-Al_2O_3 washcoats with Cs_2O.

TABLE 7-5. WASHCOAT STABILIZATION STUDY TEST RESULTS

All samples listed were heated at 1273K for 16 hours, cooled for 8 hours, and reheated to 1423K for 18 hours.			
Sample	CeO_2 loading	Cs_2O loading	Surface Area (m^2/g)
3	5%	0	0.96
5	1%	0	0.96
7	0.3%	0	1.23
10	0	5%	2.14
12	0	1%	2.06
14	0	0.3%	1.06
15	0	0.3%	1.07
16	0	0	1.12, 1.11[a]
17	0	0	1.16
18	0	0	1.20, 1.15[a]

[a]Two BET runs were made on these samples to check data. Results show excellent agreement.

Test Model JPL-021

The catalyst used for this test consisted partly of a 1-inch thick DuPont alumina support with 6.35×10^{-3}m (0.25 inch) cells and was washcoated with approximately 7 weight percent alumina. Acurex impregnated the bed with over 5 weight percent of platinum which exceeds by more than a factor of six that used in earlier tests. In previous testing JPL-009 (which also had 6.35×10^{-3}m cells) had shown much promise because of its capability of maintaining a reaction without experiencing breakthrough. The only drawback was the high amount of UHC allowed to pass through the bed due to the large cell size. This led to the system concept having a large cell catalyst upstream to maintain a reaction followed by a small cell catalyst downstream to clean up the UHC. The purpose of this test was to do more extensive testing of the large cell monolith. The latter part of testing also included downstream small cell segments to confirm system concepts.

The test procedure was similar to that performed on JPL-010P. It was intended to show the degradation of the 1-inch segment by testing at lean conditions and finding the decrease in maximum throughput with time. Table A-13 summarizes the data points taken. Note that the first 1187 minutes were all at very lean conditions with the 0.0254m (1-inch) large cell segment only. From a total elapsed time of 1187 minutes to 1370 minutes the system concept was tested at lean conditions. For the last four operating points the system concept was tested at rich conditions (50 percent theoretical air) to roughly compare it to previous tests. Figure 7-28 illustrates the fuel flow capability of the catalyst for over 20 hours of testing. Unlike the degradation tests of JPL-010, this test did not show a decreasing throughput capability of the catalyst. This is because the improved catalyst performance allowed operation at the maximum flow capability of the test facility (at ~400 percent theoretical air) throughout the test. Notice that this catalyst sustained 0.68 to 0.86 Kg/hr (1.5 to 1.9 lbm/hr) of methane for over 20 hours while JPL-010 showed a decrease in capability from 0.41 to 0.23 Kg/hr (0.91) to 0.5 lbm/hr) of methane over a 13-hour period. This demonstrated an excellent capability to maintain a reaction since it remained at or near the front face throughout the test. Like JPL-009, poor conversion was seen, as expected. Typical amounts of UHC ranged from 0.077 to 0.213 Kg/hr methane.

To reduce the amount of UHC, two segments of JPL-015 were included downstream after 1187 minutes of testing. These had 1.59×10^{-3}m (0.0625 in.) cells and were impregnated with 0.7 weight percent Pt, identical to the JPL-010 series of catalysts which were tested previously. Testing of this concept was successful in that UHC decreased substantially to less than 0.0045 kg/hr (0.01 lbm/hr) of methane. In the 3 hours of testing, the cleanup capability was seen to decrease slightly as the downstream small cell segments degraded.

Figure 7-29 illustrates the preheat temperatures and space velocities attained. Like JPL-010P, these cannot be used for a basis of comparison with other catalysts since the operating points are not at a minimum preheat condition. Exceptions are the last three data points taken at rich conditions. Figure 7-29a shows that after 25 hours of testing this catalyst still maintained 1.8 kg/hr (4.0 lbm/hr) of methane at 51.3 percent theoretical air with a very low amount of preheat (<322K). Also notice the

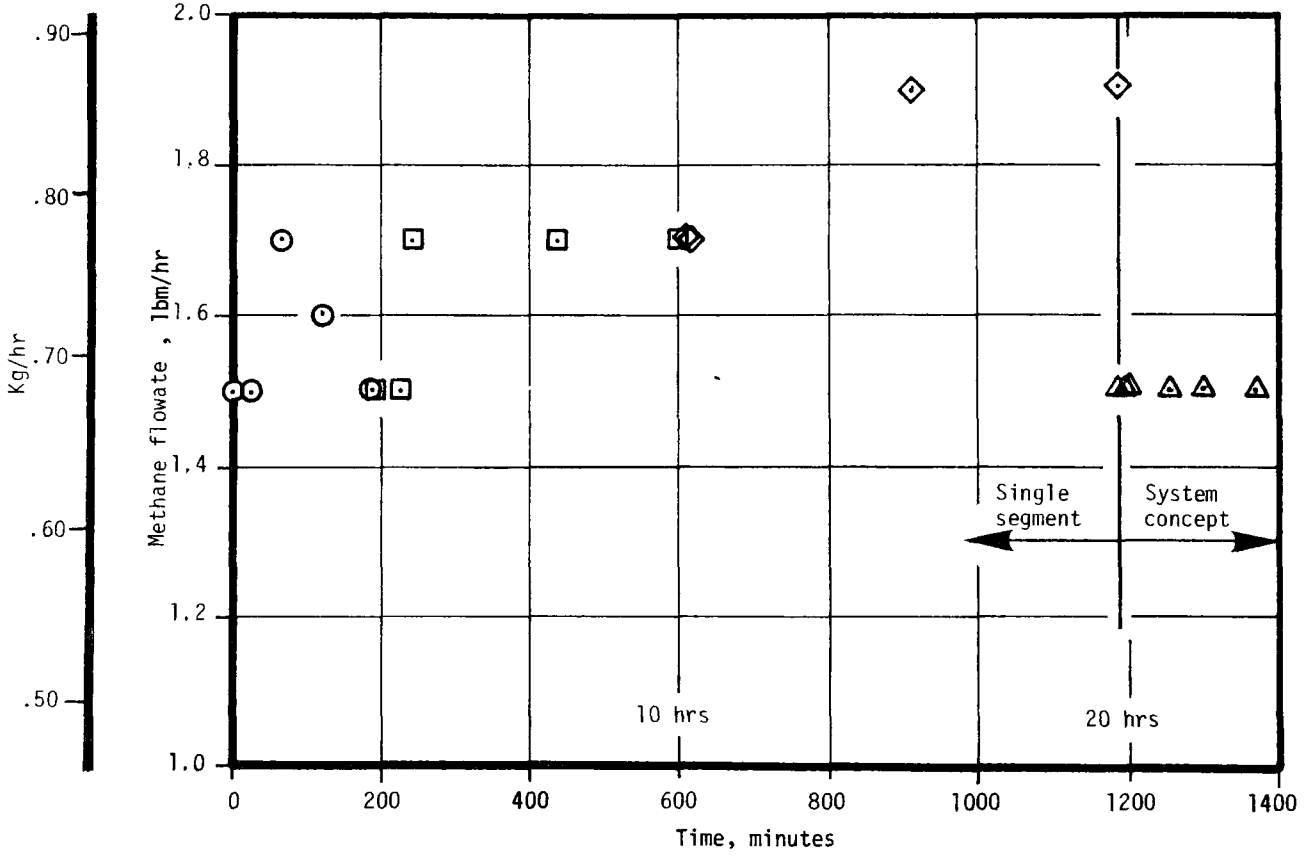

Figure 7-28. Fuel flow capability of JPL-021 catalyst at lean conditions (350% TA, methane/air).

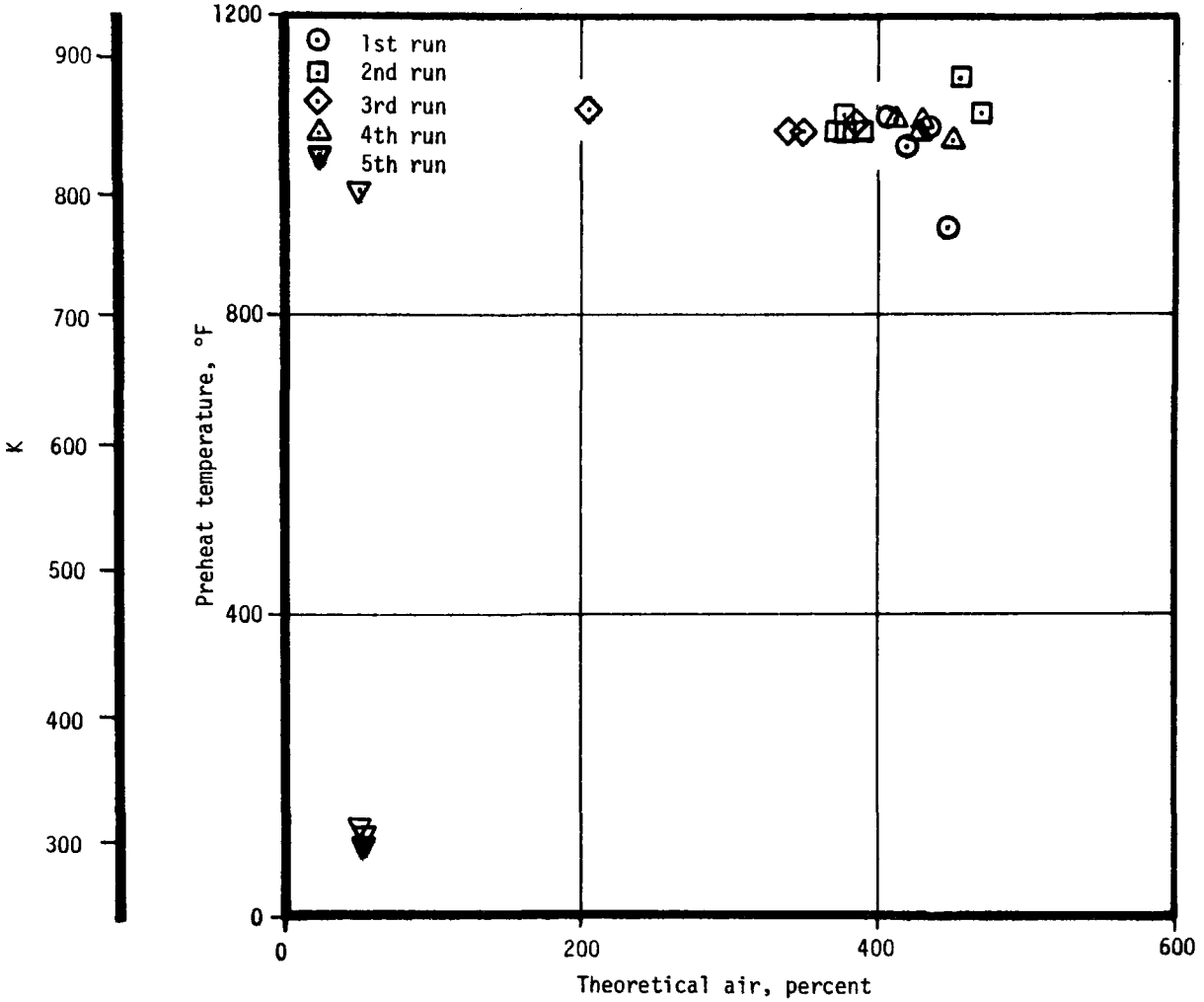

Figure 7-29a. Screening data, JPL-021-preheat temperature (methane/air).

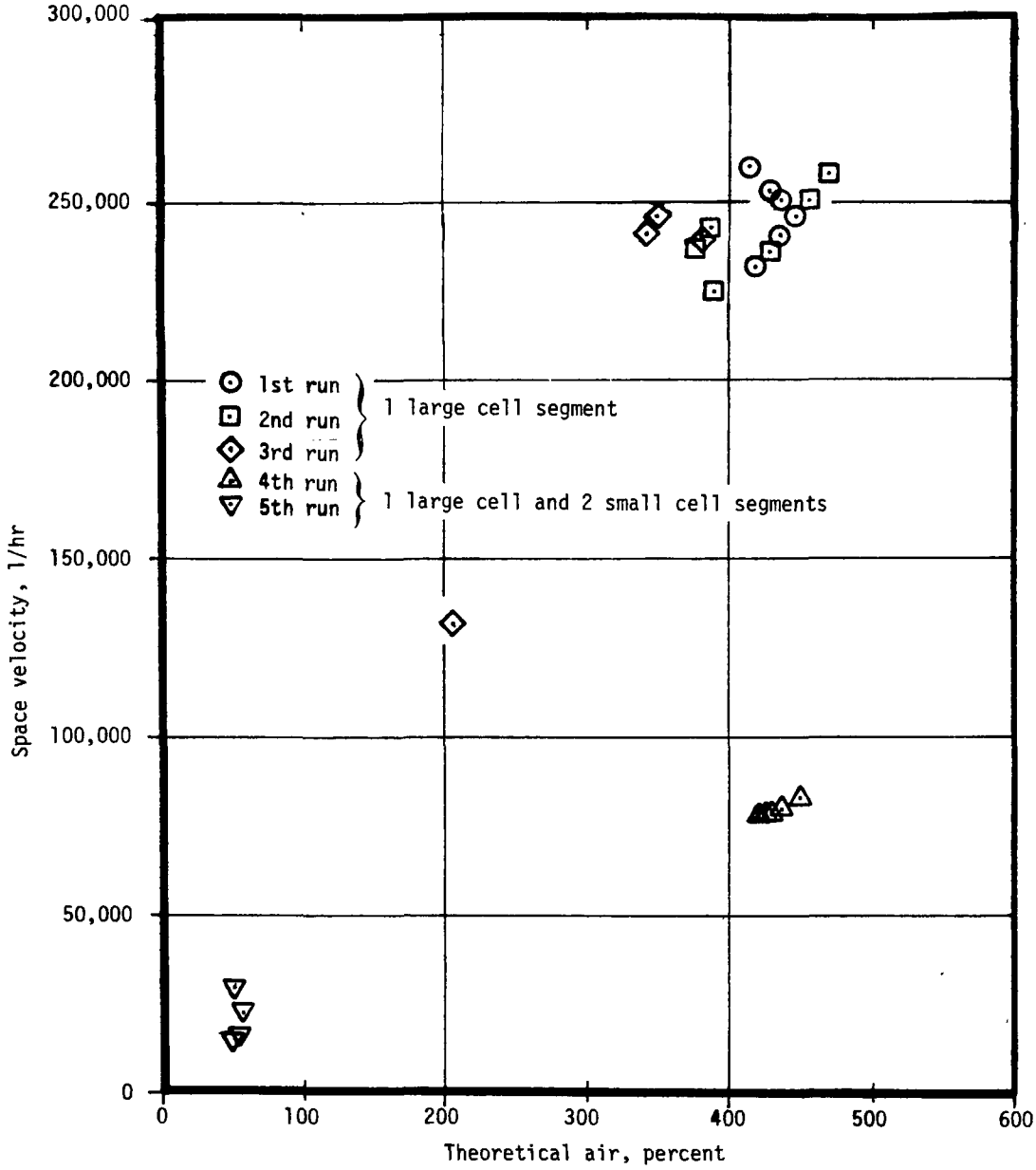

Figure 7-29b. Screening data, JPL-021 — space velocity (methane/air).

unusually high space velocities attained in Figure 7-29b. These are due primarily to the factor of three decrease in catalyst volume when testing with a 0.0254m (1-inch) thick segment rather than a 0.0762m (3-inch) thick one.

The large cell/small cell catalyst with high platinum loading showed two very promising characteristics: substantially higher throughput capabilities and increased operational lifetime. The graded cell concept was to be further tested on the last of the JPL test monoliths, JPL-019.

Test Model JPL-019

The JPL-019 monolith was termed the "graded cell catalyst." Three cell size supports (6.35, 4.76, and 3.18 cm cells) were bonded together to reduce cell size as flow passed through the catalyst bed. The catalyst was tested with four fuels at JPL (methane, propane, indolene, and methanol) in demonstrating its performance.

Test point summary, emissions, and bed temperature data are shown in Tables A-14 and 7-6 through 7-8. As can be seen from the tables, the bed was also run at temperatures up to 1672K (2550°F) with no substantial increase in pollutant emissions. The higher bed temperatures generally resulted in more uniform temperature distributions. The JPL test data shows somewhat less uniform temperatures when operating with the liquid fuels (methanol and indolene) than with the gaseous fuels. This may have resulted from incomplete fuel vaporization.

Based on the success of Test Model JPL-019, it was brought to Acurex for additional testing, including operation at pressure and at higher temperatures (to 1756K) and investigation of conversion of fuel-nitrogen species.

Atmospheric pressure tests for conversion of fuel-nitrogen were conducted first. Natural gas and propane were used as the test fuels and doped with ammonia. Tables A-15 and A-16 give the test conditions and resulting emissions. Under fuel-rich conditions, nearly all injected ammonia came through the combustor as ammonia for both test fuels. The measured NH_3 in the combustion products was higher than that measured for the incoming gases in two cases, indicating some measurement error. For fuel-lean conditions, the NH_3 was totally broken down by the catalyst. Conversion of NH_3 to NO_x was measured as approximately 20 to 26 percent for lean conditions. Bed temperature measurements for selected test points are shown in Table 7-9.

TABLE 7-6. MONOLITH 019 TEST DATA – JPL MULTI-FUEL TESTS

	Typical Emissions Data Kg/hr (lbm/hr)					
	Fuel	TA, %	CO	H_2	UHC	Run-Scan No.
1367K (2000°F) Bed Temp	Methane	320	0	0	.0227(0.05)	A41A-6
	Propane	350	0	0	0	A41C-5
	Indolene	290	0	.0045(0.01)	.0045(0.01)	A41D-5
	Methanol	326	0	.0045(0.01)	0	A41E-7
1589K (2400°F) Bed Temp	Methane	211	0	.0045(0.01)	0	A41F-4
	Propane	248	0	.0090(0.02)	0	A41F-15

NO_x measurements were not made on this series of tests; based on previous test results, no NO_x emissions were expected.

TABLE 7-7. MONOLITH 019 TEST DATA — RADIAL BED TEMPERATURE PROFILES

Methane A41A-6		Propane A41C-5		Indolene A41D-5		Methanol A41E-7		Methane A41F-4		Propane A41F-15	
TC	K (°F)	TC	K (°F)	TC	K (°F)	TC	K (°F)	TC	K (°F)	TC	K (°F)
1	1369 (2004)	1	1366 (1998)	1	1295 (1871)	1	1318 (1913)	1	1636 (2485)	1	1636 (2484)
2	1371 (2008)	2	1373 (2011)	2	1289 (1861)	2	1349 (1969)	2	1621 (2457)	2	1615 (2447)
3	1362 (1992)	3	1344 (1959)	3	1412 (2082)	3	1467 (2181)	3	1627 (2470)	3	1622 (2460)
4	1340 (1952)	4	1367 (2001)	4	1381 (2025)	4	1372 (2009)	4	1521 (2277)	4	1473 (2191)

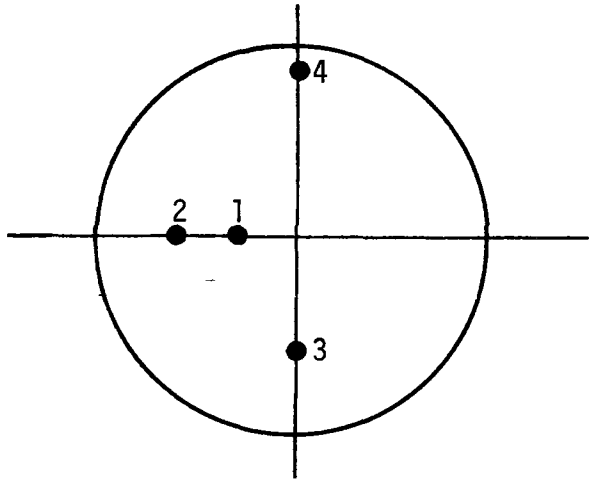

Section taken .0635 m from front face - four thermocouples in that plane.

Gaseous fuels show more uniform temperature profiles than liquid fuels.

TABLE 7-8. MONOLITH 019 TEST DATA — AXIAL BED TEMPERATURE PROFILES

Methane A41A-6		Propane A41C-5		Indolene A41D-5		Methanol A41E-7		Methane A41F-4		Propane A41F-15	
TC	K (°F)	TC	K (°F)	TC	K (°F)	TC	K (°F)	TC	K (°F)	TC	K (°F)
5	1344 (1960)	5	1359 (1986)	5	1348 (1966)	5	1379 (2022)	5	1596 (2412)	5	1594 (2409)
6	1321 (1917)	6	1208 (1714)	6	1133 (1580)	6	1324 (1923)	6	1523 (2282)	6	1513 (2263)
7	1352 (1973)	7	1261 (1810)	7	1239 (1771)	7	1402 (2063)	7	1566 (2358)	7	1614 (2446)
8	1369 (2004)	8	1366 (1998)	8	1295 (1871)	8	1318 (1913)	8	1636 (2485)	8	1636 (2484)
9	1317 (1910)	9	1351 (1971)	9	1384 (2031)	9	1412 (2082)	9	1547 (2325)	9	1541 (2313)

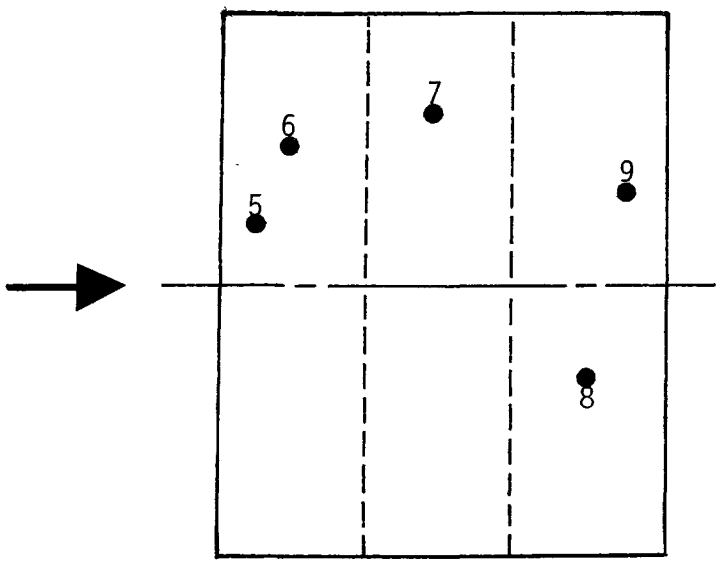

Thermocouples 5, 6, 8, and 9 lie in same plane.

Axial temperature for gaseous fuels at 1589K (2400°F) operating temperature are in excellent agreement.

Significant variations in axial temperature exist for indolene.

TABLE 7-9. MONOLITH 019 TEST DATA – AXIAL BED TEMPERATURE PROFILES

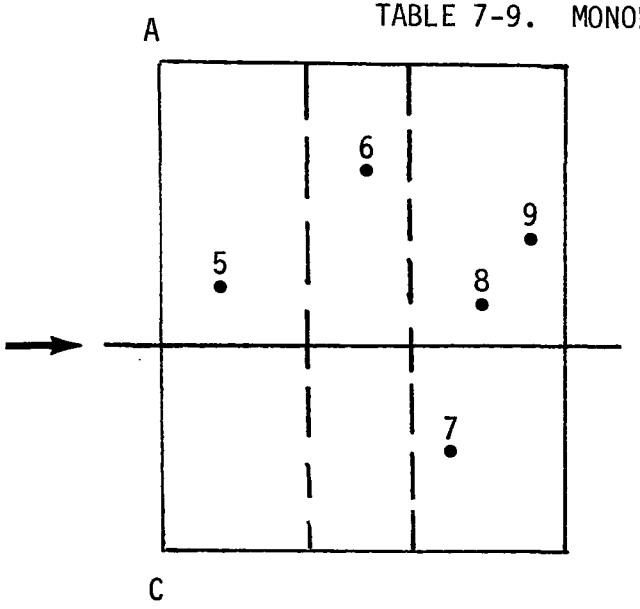

Typical test points

Thermocouples 5, 7, 8, 9 lie in same plane

FUEL RICH

FUEL LEAN

Natural Gas

Run 1122-2			Run 1124-2			Run 1201-1			Run 1201-4		
TC	K	(°F)	TC	K	(°F)	TC	K	(°F)	TC	K	(°F)
5	1273	(1831)	5	1518	(2273)	5	1144	(1600)	5	1457	(2162)
6	1303	(1886)	6	1501	(2242)	6	1432	(2118)	6	1591	(2404)
7	1342	(1956)	7	1647	(2504)	7	1486	(2214)	7	1620	(2456)
8	1359	(1986)	8	--	--	8	1434	(2121)	8	--	--
9	1333	(1940)	9	1597	(2414)	9	1441	(2134)	9	1561	(2349)

Propane

Run 1123-2		
TC	K	(°F)
5	1359	(1986)
6	1367	(2001)
7	1309	(1896)
8	1284	(1852)
9	1293	(1867)

The fuel-nitrogen conversion tests at atmospheric pressure indicated the potential of the platinum catalyst to control NO_x emissions due to fuel-bound nitrogen species under lean conditions. Further, tests on the rich side should be conducted between 40 and 100 percent theoretical air. One additional NH_3 conversion point at 0.303 MPa (3 atm) was included with subsequent pressure tests.

Data for pressure tests with methane between 0.101 and 0.606 MPa (1 and 6 atm) are given in Tables A-17 and A-18. In general, NO_x, CO, and unburned hydrocarbon levels did not vary with pressure under lean conditions. Run number 1206-6 with NH_3 dopant at 0.303 MPa showed an increase in conversion to NO_x (68 percent) over the baseline (1 atm) condition. This result suggested that catalytic control of fuel nitrogen conversion to NO_x is more effective in lower pressure combustion systems.

Table 7-10 shows bed temperature distribution with increasing pressure. No changes in relative uniformity were found.

Following fuel-nitrogen and high pressure testing, the catalyst was removed from the test fixture for surface area and platinum dispersion measurements. The results were 0.02 m^2/g and zero, respectively. Since the catalyst still retained good activity, it was re-instrumented with thermocouples and returned to the facility for testing at high temperature.

Tests were conducted with natural gas fuel at 0.101 MPa (1 atm) pressure and approximately 589K (600°F) preheat temperature. Bed temperatures of 1644 to 1700K (2,500°F to 2,600°F) were maintained for approximately one hour, with the maximum bed temperature of 1761K (2,710°F) maintained for approximately 15 minutes. Following a brief cooldown period, the catalyst was successfully relit under fuel-rich conditions at approximately 744K (880°F), virtually the same lightoff temperature as was found previously. It was then operated briefly under fuel-lean conditions to demonstrate continued successful performance and removed and sectioned for SEM and EDAX analyses.

High temperature test conditions are summarized in Table A-19 and temperature measurements are given in Table 7-11. No emissions data was obtained. Much greater bed temperature uniformity was noted as test temperature increased to the 1761K maximum obtained.

TABLE 7-10. MONOLITH 019 TEST DATA — AXIAL BED TEMPERATURE PROFILES

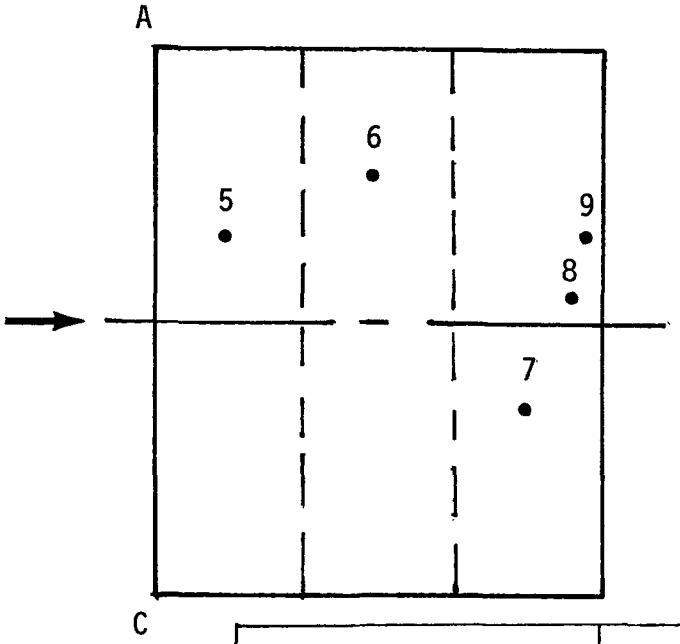

Pressure data, methane, lean conditions

Thermocouples 5, 7, 8, and 9 lie in same plane

1 ATM		3 ATM		6 ATM	
Run	1206-3	Run	1206-5	Run	1206-7
TC	K (°F)	TC	K (°F)	TC	K (°F)
5	1576 (2376)	5	1561 (2350)	5	-- (--)
6	1637 (2487)	6	1601 (2422)	6	1478 (2200)
7	1636 (2484)	7	1604 (2428)	7	1400 (2060)
8	-- (--)	8	-- (--)	8	1417 (2091)
9	1593 (2408)	9	1563 (2354)	9	1527 (2288)

TABLE 7-11. MONOLITH 019 TEST DATA – AXIAL BED TEMPERATURE PROFILES

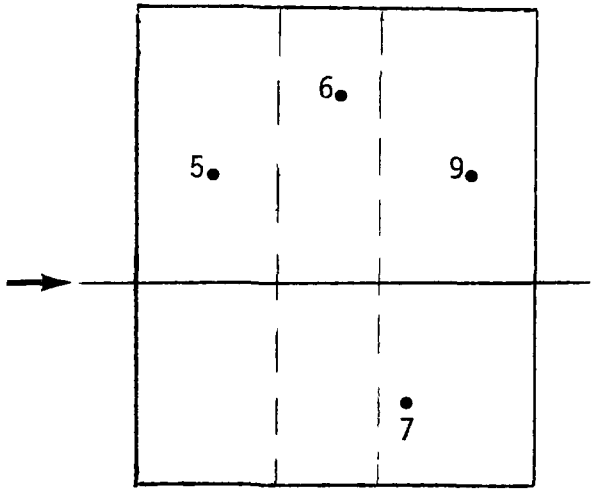

Fuel: natural gas

Thermocouples 5, 7, 9 are in the same plane

Fuel Rich

Run 1228-1			Run 1228-11		
TC	K	(°F)	TC	K	(°F)
5	958	(1264)	5	1244	(1780)
6	1365	(1997)	6	1478	(2201)
7	1533	(2299)	7	1703	(2605)
9	1209	(1716)	9	1319	(1914)

Fuel Lean

Run 1228-3			Run 1228-6			Run 1228-8			Run 1228-12		
TC	K	(°F)	TC	K	(°F)	TC	K	(°F)	TC	K	(°F)
5	1369	(2005)	5	1386	(2034)	5	1724	(2643)	5	1404	(2067)
6	1624	(2464)	6	1656	(2521)	6	1737	(2666)	6	1646	(2503)
7	1636	(2484)	7	1707	(2613)	7	1760	(2708)	7	1691	(2583)
9	1296	(1872)	9	1567	(2360)	9	1592	(2406)	9	1519	(2274)

A total test time of 74 hours was accumulated on test model JPL-019, demonstrating that the graded cell catalyst system had long life characteristics even under severe test conditions. Thus, an important program objective was met by development of a catalyst with adequate lifetime for system application.

Test model JPL-019 was sectioned for SEM/EDAX analyses at JPL. Sections from both the large and small cell segments were cut as in Figure 7-30 for mounting. Initial analyses of these segments showed little or no detectable platinum at either the inlet or exit region of either of the cell sections (Figures 7-31 to 7-34). A small platinum response on the EDAX scan of Figure 7-31 was the only evidence of catalyst at the surface. Subsequent searching of the outlet regions of both large and small cell channels revealed additional platinum but with very low dispersion and great non-uniformity from location to location. Additional platinum can be seen in the results of Figures 7-35 to 7-38. It was clearly evident that the higher operating temperatures of test model JPL-019 resulted in substantial catalyst removal from the surface.

Additional micrographs were taken to investigate washcoat structure in the small cell segment. Figure 7-39 shows that variations in surface texture were apparent which could affect catalyst adherence at the surface.

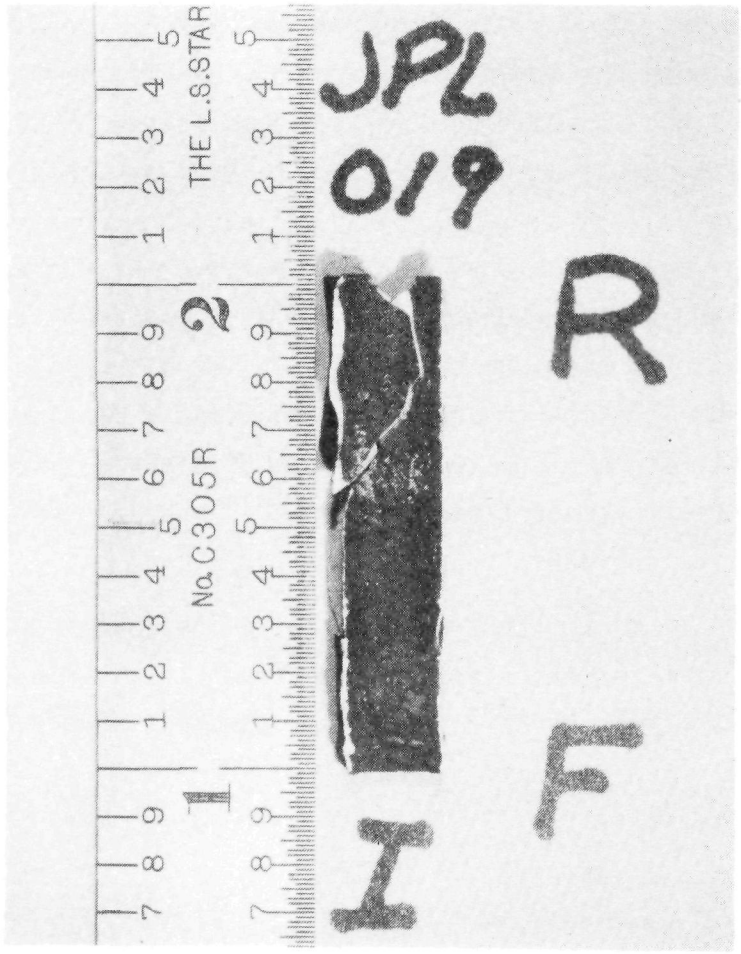

Figure 7-30. Segment from inlet (large cell) monolith, R = rear, F = front, test model JPL-019.

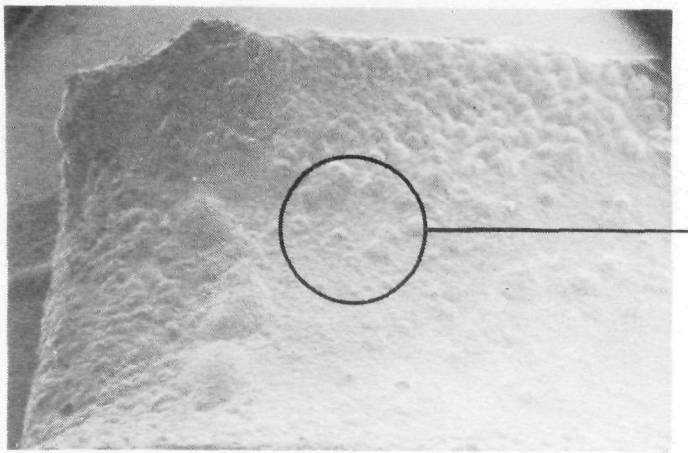

a. 16x magnification at entrance of segment

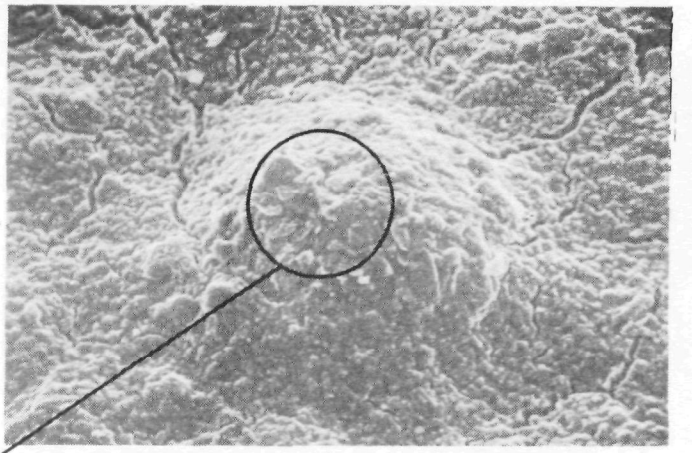

b. 400x magnification

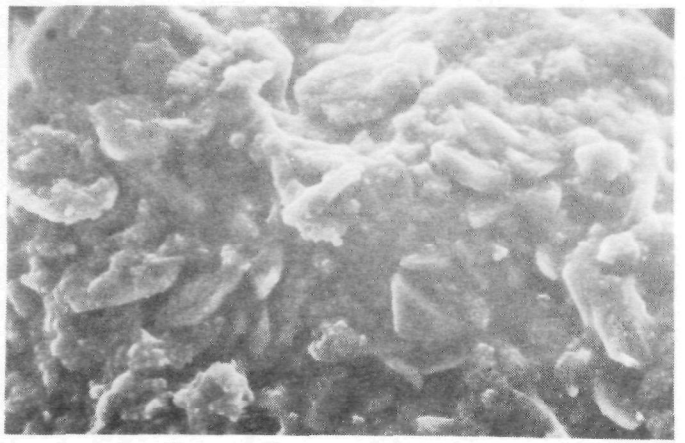

c. 1600x magnification

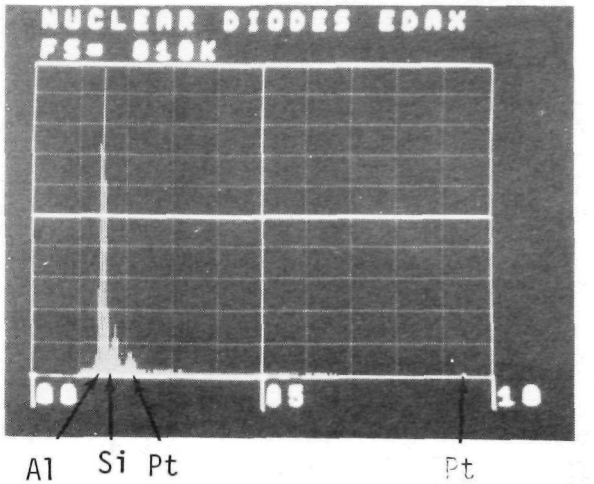

d. EDAX scan showing presence of aluminum, silicon, and platinum

Figure 7-31. Surface analysis at entrance of large cell segment, test model JPL-019.

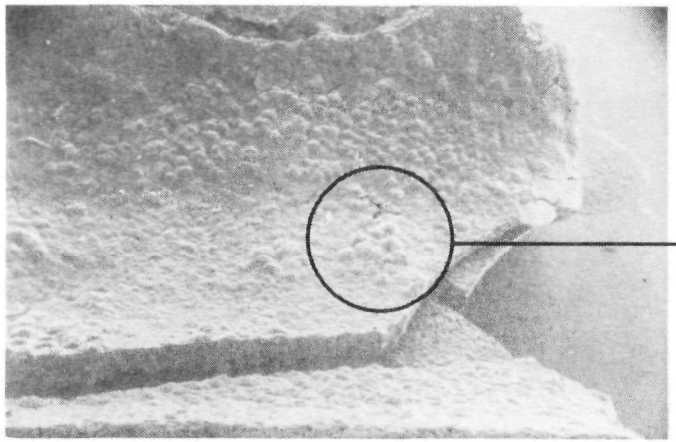

1.0 mm

a. 16x magnification at rear of segment

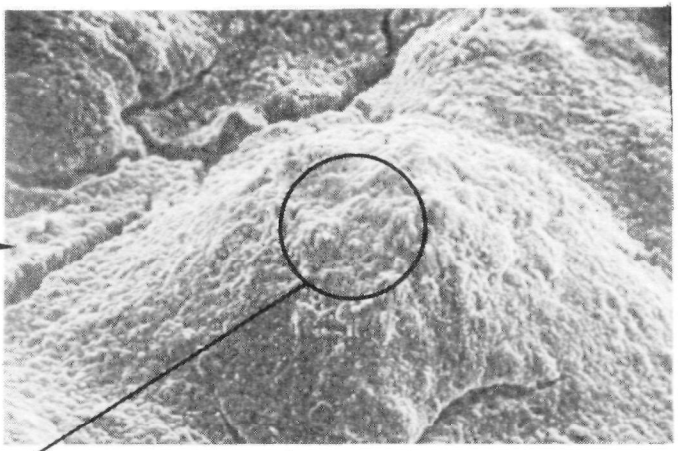

50μ

b. 400x magnification

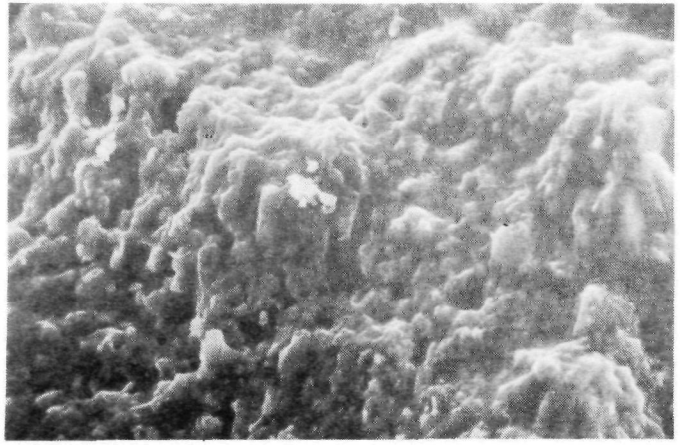

10μ

c. 1600x magnification

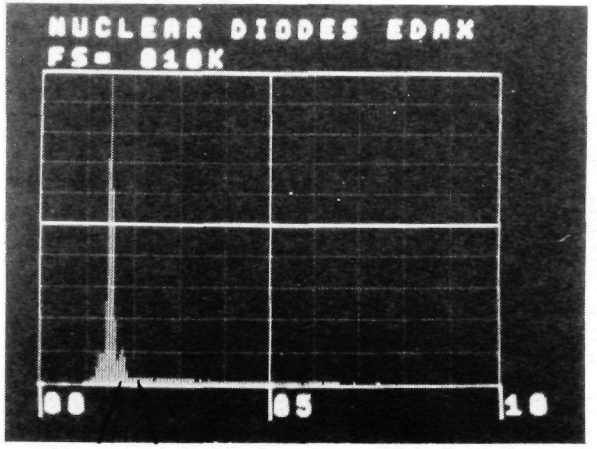

Al Si

d. EDAX scan showing presence of aluminum and silicon

Figure 7-32. Surface analysis at exit of large cell segment, test model JPL-019.

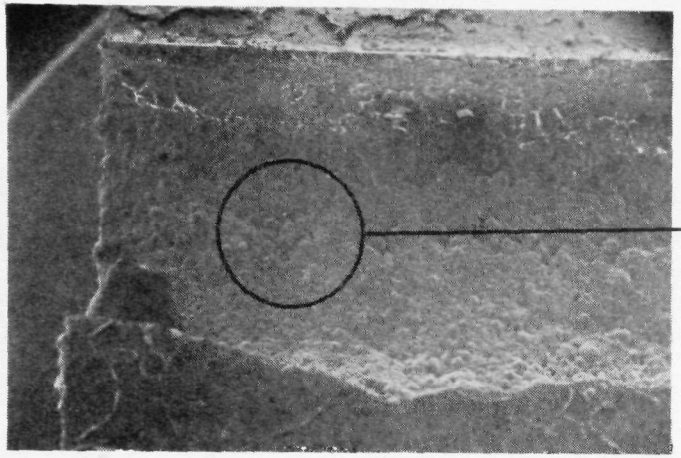

a. 18x magnification at entrance of segment

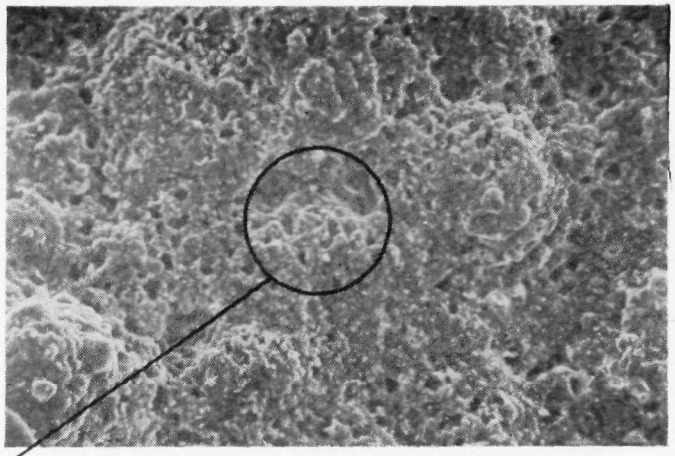

b. 450x magnification

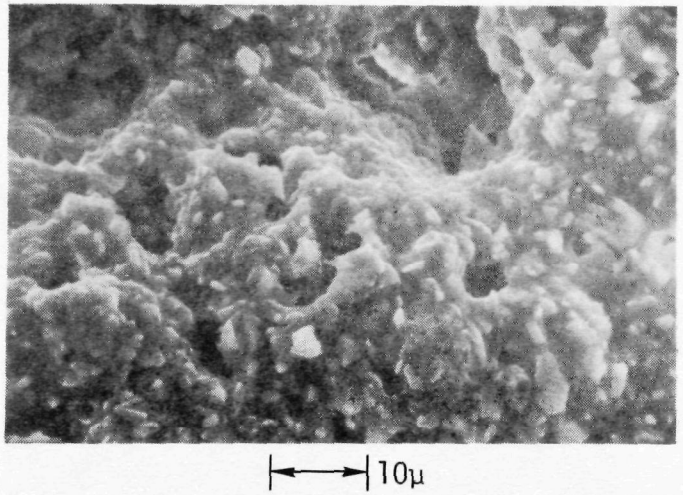

c. 1800x magnification

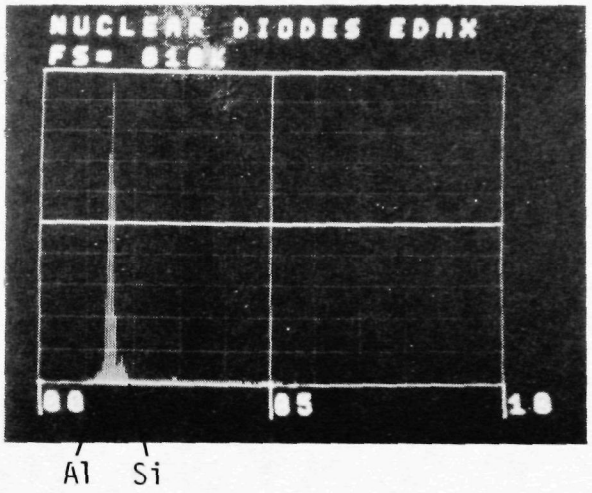

d. EDAX scan showing presence of aluminum and silicon

Figure 7-33. Surface analysis at entrance of small cell segment, test model JPL-019.

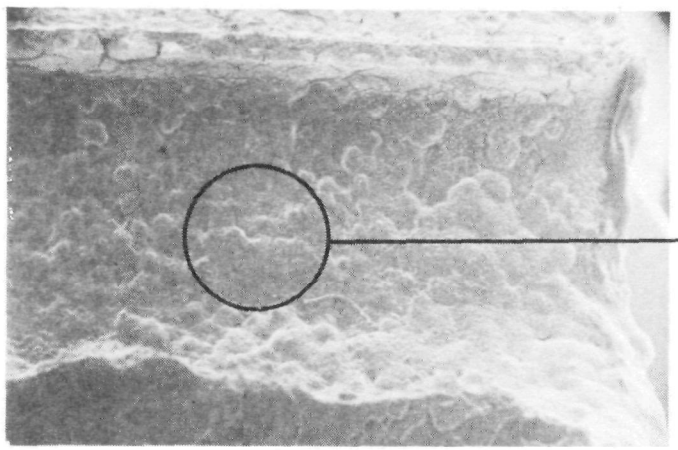

1.0 mm

a. 18x magnification at exit of segment

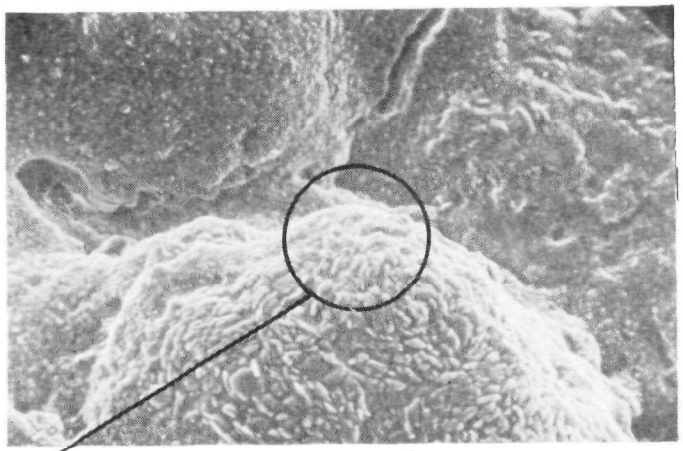

50μ

b. 450x magnification

10μ

c. 1800x magnification

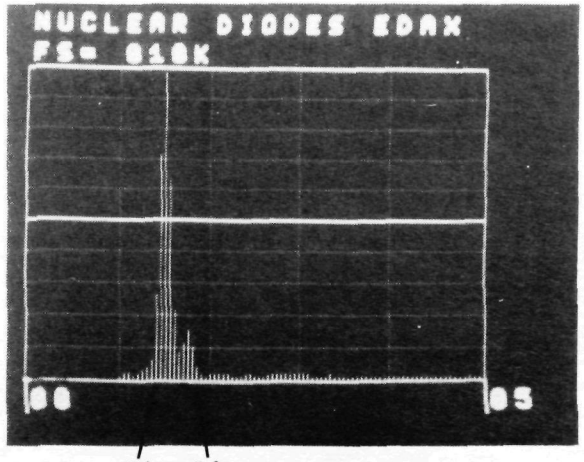

d. EDAX scan showing presence of aluminum and silicon

Figure 7-34. Surface analysis at exit of small cell segment, test model JPL-019.

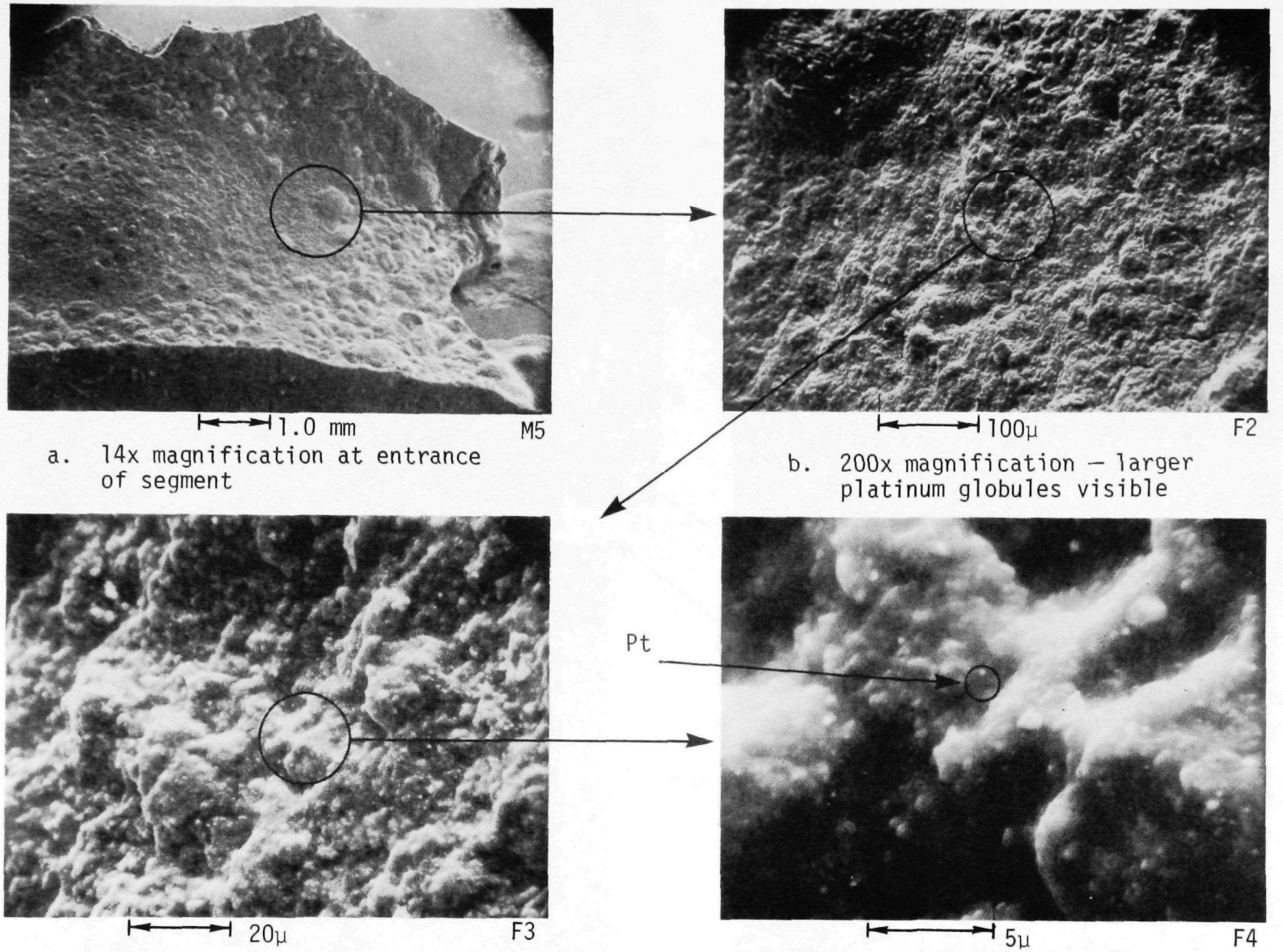

a. 14x magnification at entrance of segment

b. 200x magnification – larger platinum globules visible

c. 1000x magnification – fine globules of platinum visible

d. 5000x magnification – small globules of platinum clearly visible

Figure 7-35. Surface appearance at entrance of large cell segment, test model JPL-019.

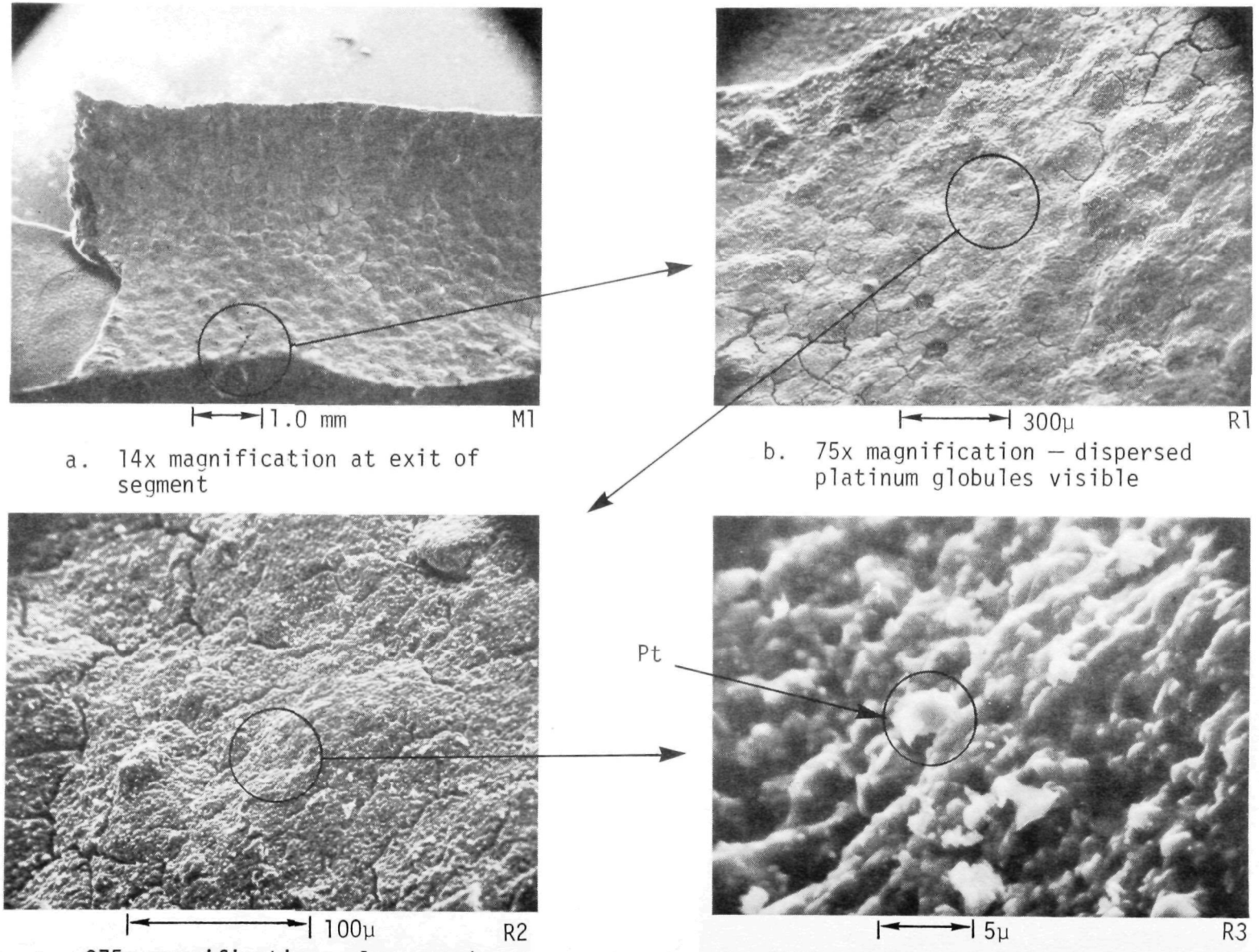

a. 14x magnification at exit of segment

b. 75x magnification — dispersed platinum globules visible

c. 375x magnification — large and small platinum globules visible

d. 3750x — platinum globules visible in center of photograph

Figure 7-36. Surface appearance at exit of large cell segment, test model JPL-019.

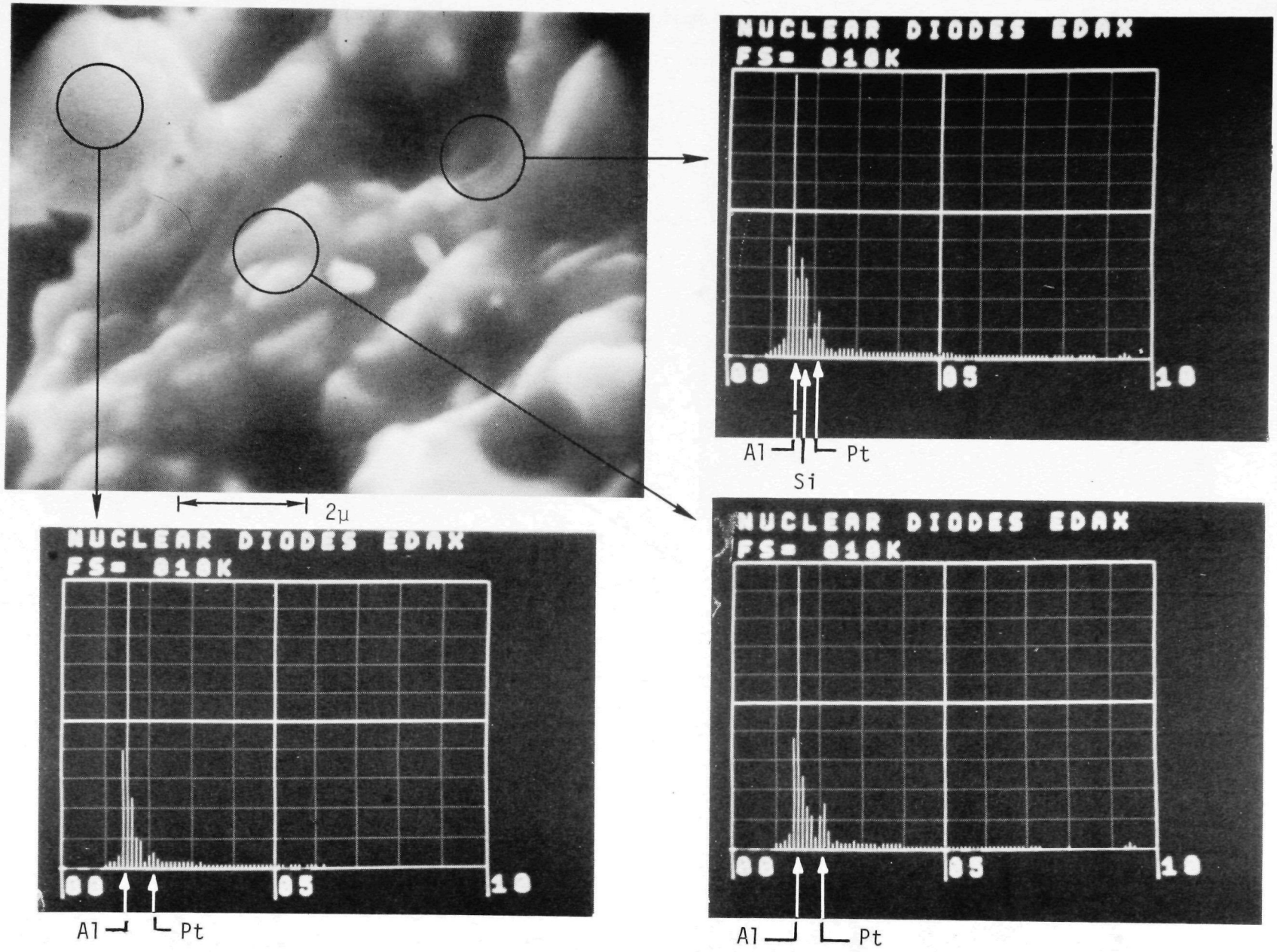

Figure 7-37. SEM/EDAX measurements on exit of large cell segment, test model JPL-019.

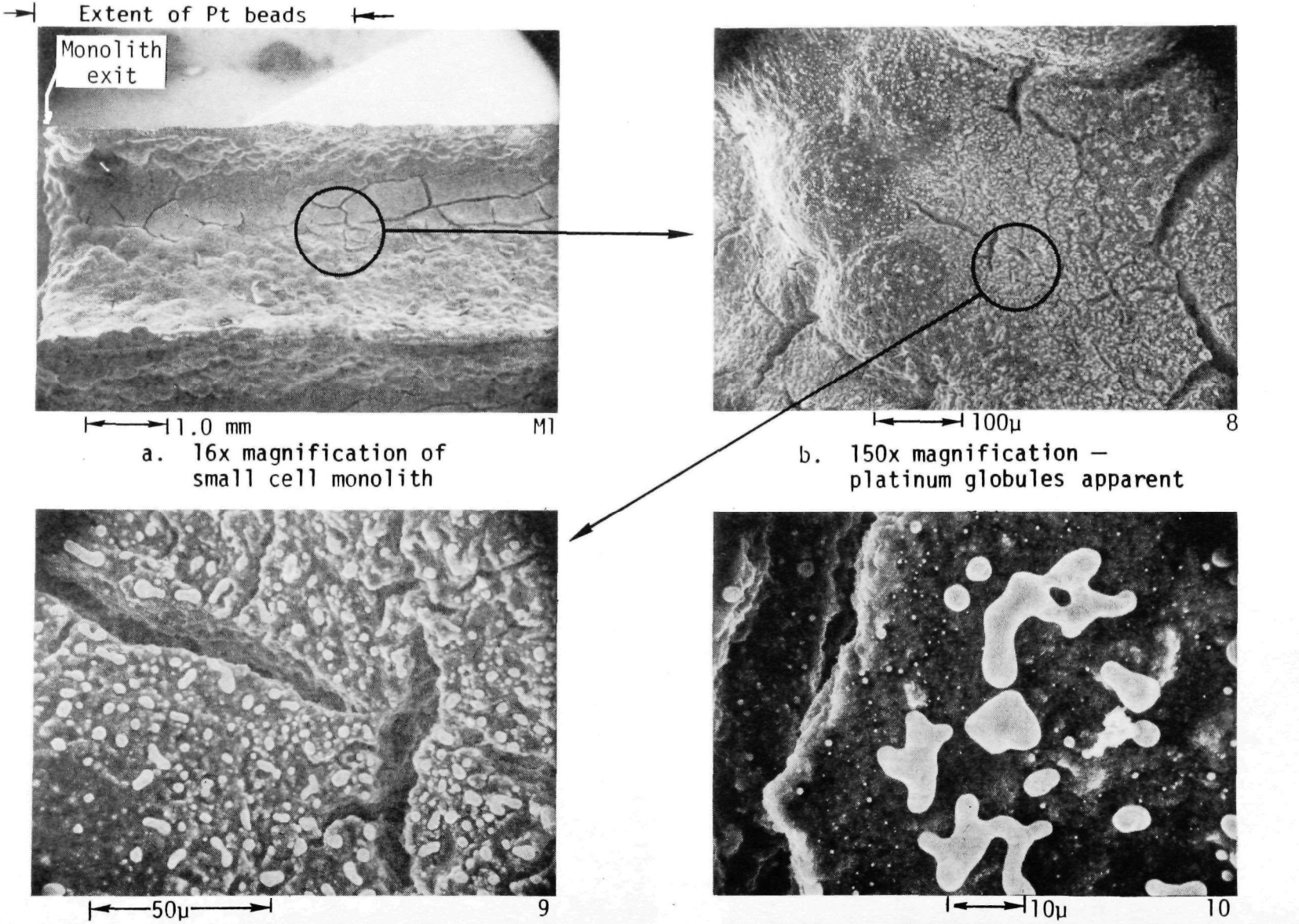

Figure 7-38. Surface appearance at exit of small cell, test model JPL-019.

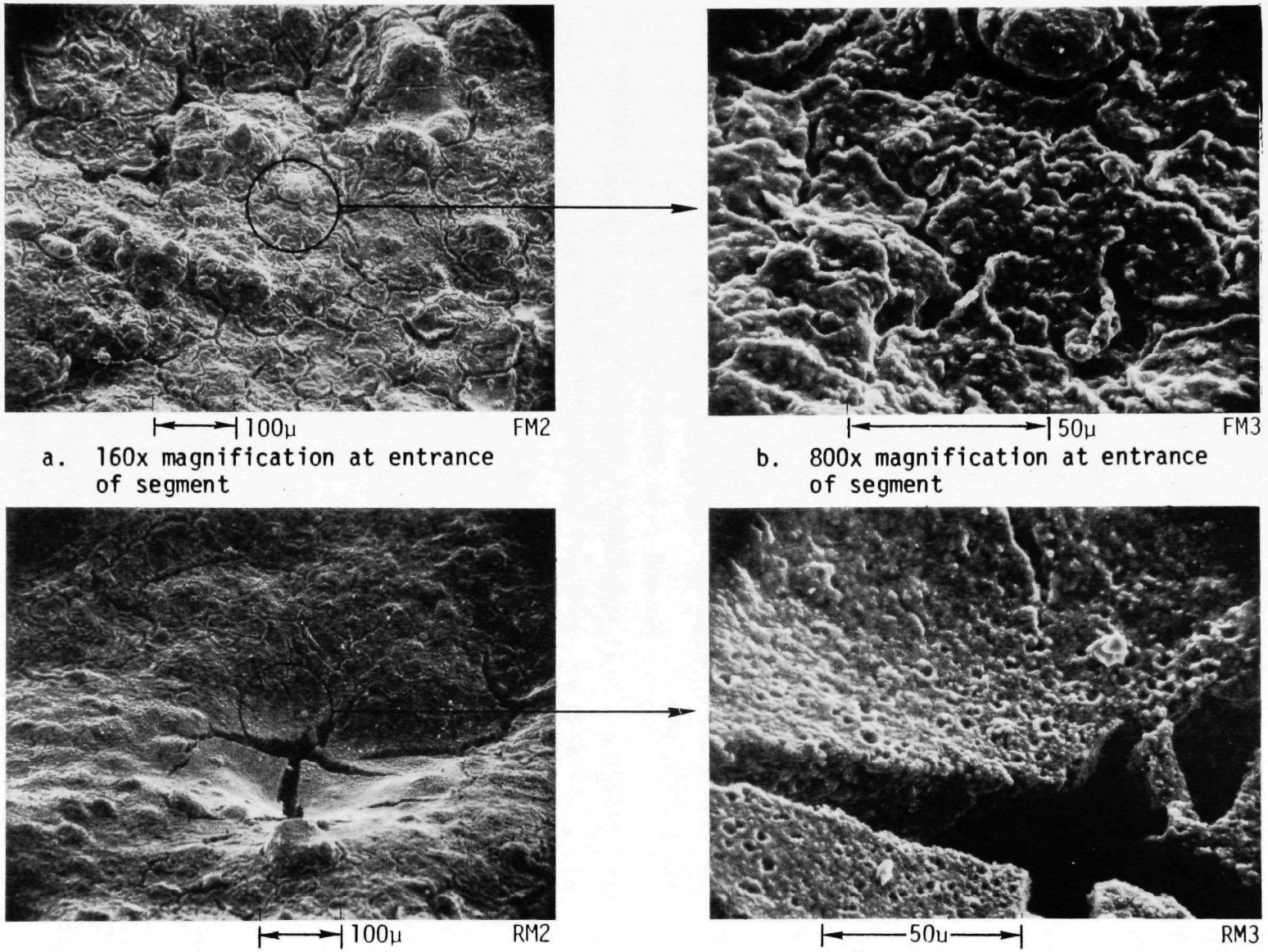

a. 160x magnification at entrance of segment

b. 800x magnification at entrance of segment

c. 160x magnification at exit of segment

d. 800x magnification at exit of segment

Figure 7-39. Washcoat comparison – small cell segment, test model JPL-019.

7.5 CONCLUSIONS

The large body of data obtained during combustion screening tests at the Jet Propulsion Laboratory and at Acurex has led to the development of catalysts that have far better combustion characteristics than those initially tested. Further, an extensive fundamental understanding of the catalytic combustion phenomenon was developed. The tests demonstrated that catalytic combustion is a high efficiency, very low emission process. More specifically, there is good promise of being able to develop catalysts with all the properties enumerated in the introduction to this section, including low ignition and preheat temperatures, high heat release, and long lifetime.

The series of catalyst screening tests showed that catalyst performance could be improved in a number of ways:

1. Increased catalyst loading resulted in lower initial lightoff temperatures, higher mass throughputs, and increased lifetime at 1367K (2000°F)

2. Increased cell size resulted in higher possible mass throughputs at the expense of increased hydrocarbon emissions.

3. Fuel-rich operation allowed lightoff at lower temperatures and increased mass throughput at a given preheat temperature than fuel-lean operation.

4. Heavier hydrocarbon fuels promote lightoff at lower ignition temperatures.

5. Hydrogen sulfide (H_2S) fixation of platinum catalysts promotes retention of platinum surface area.

6. Presintering of catalyst washcoats may reduce burying of active catalyst below the surface during combustion.

7. Stabilization of γ-Al_2O_3 washcoats with cesium oxide (Cs_2O) up to 5 weight percent increased surface area. Stabilization of alumina washcoats with ceria up to 5 weight percent had a negative effect on surface area.

8. Decreased cell size significantly reduced unburned hydrocarbon and carbon monoxide emissions.

9. Catalyst beds of combined large cell and small cell monoliths significantly increased throughput (at a given preheat temperature) and overall catalyst life with low emissions.

10. Bed temperature uniformity was increased by operation at higher temperatures.

In addition to catalyst preparation and operating conditions which were found to enhance combustion characteristics, the following information was obtained which impacts ongoing catalyst development.

1. Catalyst lightoff temperatures are fairly consistent for a given fuel and catalyst type. 672K to 783K is typical for methane on platinum catalysts.

2. Higher preheat conditions are required under fuel-lean than fuel-rich conditions for the monolithic catalysts.

3. Mullite and cordierite perform adequately at 1367K use temperatures. Alumina performs well at its maximum use temperature (1783K) but experiences mild thermal cracking.

4. Active platinum migrates and agglomerates at the surface at 1367K.

5. Washcoat presintering reduces surface area but does not have a negative effect on combustion properties.

6. Presintering of washcoat and catalyst results in reduction of active platinum available to the reactive stream and hence reduces both initial and ultimate activity.

7. Catalyst degradation results in large reductions in both active surface area and dispersion.

The graded cell platinum catalyst represents the best concept developed by the test series. It has been shown that washcoat preparation techniques are of lesser importance to combustion operation than bed geometry and catalyst loading. The graded cell catalyst also shows promise of increased activity and lifetime at high operating temperatures (1489K).

SECTION 8

GRADED CELL CATALYST TESTS

8.1 INTRODUCTION

The experimental data obtained from catalyst screening tests (Section 7) verified the high throughput, high efficiency, and low emission characteristics of the graded cell concept. The combination of large cells at the bed inlet to prevent blowout and small cells at the bed outlet for high fuel conversion provided a significant improvement in catalyst performance.

Additional catalyst screening tests were conducted at Acurex on the graded cell configuration. The objective of these tests was the identification of the best catalysts that would be appropriate for system development and testing. A wide cross-section of available combustion catalyst types was obtained by enlisting the support of catalyst manufacturers. An initial goal of 1756K (2700°F) catalyst operation and 1978K (3100°F) support use-temperature was offered as a guideline. Discussion of the catalyst matrix which follows identifies the manufacturers and catalyst types that were evaluated.

8.2 GRADED CELL CATALYST MATRIX

A summary of the sixteen graded cell catalysts prepared is given in Table 8-1. These catalyst models were used for the following test purposes:

1. Identification of a superior catalyst at small scale by screening of manufacturer-prepared catalysts
2. Identification of high temperature (to 1978K) capability catalysts and comparison to low temperature data
3. Scaleup of the best identified screening catalyst to verify scaleup criteria

TABLE 8-1. GRADED CELL CATALYST MODELS

Sample No.	No. of TC	Substrate Manu.	Substrate Type	Washcoat Manu.	Washcoat Type	Catalyst Manu.	Catalyst Type	Catalyst Loading Wt % of Segment	Catalyst Loading Gms per Segment	Dates Tested	Fuel	Test Purpose
AERO-025	9	DuPont	Alumina	Grace	Rare earth stabilized alumina 10-18 Wt. %	Grace	Pt/Ir	0.6-1.0	.47/.76/.80	4/25 – 4/29/77	Nat. Gas	Screen Grace Pt/Ir catalyst
AERO-026	6	DuPont	Alumina	UOP	Proprietary	UOP	Proprietary	–	–	6/24 – 6/29/77	Nat. Gas	Screen UOP catalyst
AERO-027	6	DuPont	Thoria impregnated alumina	None	–	W. Pfefferle	Pt/Ir/Os	0.29	.36/.24/.17	6/30 – 7/1/77	Nat. Gas	Determine effects of high melting point precious metals and catalyst without washcoat
AERO-028	–	DuPont	Zirconia impregnated alumina	None	–	W. Pfefferle	Pt/Ir/Os	0.29	.52/.08/.08	–	–	Not to be tested based on results of A-027.
AERO-029	6	Corning	Zirconia spinel	None	–	W. Pfefferle	NiO/Pt	0.29-0 Pt .29/.46/ 2.9 NiO	0.5/.31/0 .5/.8/5.0	7/10 – 7/11/77	Nat. Gas	Investigate metal oxide catalyst capabilities (no washcoat). Perform high temp. operation (3100°F).
AERO-030	*6*	*Corning*	*Zirconia* spinel	*None*	–	*Aero*	*Co_2O_3/Pt*	*2.4-0 Pt 5.4-7.8 Co_2O_3*	*4.1/0/0*	*7/14 – 7/21/77*	*Nat. Gas*	*Metal oxide comparison, extensive evaluation*
AERO-031	6	DuPont	Alumina	Matthey Bishop	Proprietary	Matthey Bishop A	Stab. Pt	.33-.76	–	8/2 – 8/10/77	Nat. Gas	Compare to A-032
AERO-032	6	DuPont	Alumina	Matthey Bishop	Proprietary	Matthey Bishop B	Stab. Pt	.86-1.09	–	7/26 – 7/29/77	Nat. Gas	Screen Matthey Bishop catalyst
AERO-033	7	Corning	Zirconia spinel	None	–	Aero	NiO/Pt-Pd	.67-0 Pt 2.2/.94/ 2.0 NiO	15/0.7/0 Pt 5.0/2.1/ 4.5 NiO	9/14 – 9/20/77	Nat. Gas	Fuel nitrogen and pressure testing } Test difficulties precluded data results
AERO-034	7	Corning	Zirconia spinel	Oxy-Catalyst	γ-Alumina 4 Wt. %	Aero	Co_2O_3/Pt	2.2-0 Pt 9.3/5.6/ 4.3 Co_2O_3	3.0/0/0 Pt 7.7/9.9/ 20.8 Co_2O_3	9/22 – 9/27/77	Nat. Gas	Comparison to A-033 } Test difficulties precluded data results
AERO-035	7	DuPont	Alumina	Matthey Bishop	Proprietary	Matthey Bishop C	Stab. Pt	1.96/1.2/ 0.9	–	10/1 – 10/6/77	Nat. Gas	Screening comparison
AERO-036	7	Corning	Zirconia spinel	Aero	Zirconia Magnesia .8-1.0 Wt.%	Aero	NiO/Pt	1.8/2.1, 2.1 NiO 1.2/0.9, 0 Pt	3.0/3.2/ 4.0 NiO 2.0/1.4/ 0 Pt	10/10 – 10/12/77	Nat. Gas	Fuel nitrogen testing
AERO-037	4	Corning	Zirconia spinel	None	–	Aero	Co_2O_3/Pt	2.7/2.8/ 3.4 Co_2O_3 4.0/0/0 Pt	4.5/4.5/ 10.1 Co_2O_3 6.7/0/0 Pt	12/5 – 12/23/77	Nat. Gas & Methane	Fuel nitrogen and pressure testing
AERO-038	5	DuPont	Alumina	None	–	W.Pfefferle	Co_2O_3	15.9/4.1/5.8	10.3/2.9/8.8	12/28 – 12/29/77	Nat. Gas	Investigate catalyst-support interactions
AERO-040	5	DuPont	Alumina	Johnson Matthey	Proprietary	Johnson Matthey	Proprietary	–	–	1/25 – 2/6/78	Nat. Gas	Screen Johnson Matthey catalyst
AERO-041	4	DuPont	Alumina	UOP	Proprietary	UOP	Proprietary	–	–	12/30/77 – 1/3/78	Nat. Gas	Catalyst scaleup, 6.06-inch diameter

4. Extensive evaluation to investigate fuel nitrogen conversion to nitrogen oxides and operational characteristics at high pressure

The tests performed are discussed separately in Sections 8.4 and 8.5.

Screening catalysts were obtained from six sources, including W. R. Grace and Company, Universal Oil Products Company, William Pfefferle (a private consultant), Matthey Bishop, Inc., Johnson Matthey, and Acurex. Support materials were either DuPont alumina or Corning zirconia spinel. Washcoats varied from proprietary preparations with high pre-test surface area to no washcoat and a subsequent low pre-test surface area. The catalyst loadings, test dates, and fuels used are listed in Table 8-1.

In support of combustion test results, catalyst physical measurements were made both pre- and post-test. These measurements included catalyst surface area and dispersion performed in the catalyst characterization laboratory described in Section 5.4. Additional scanning electron microscopy (SEM) and energy dispersive analysis by x-ray (EDAX) tests were performed at the Jet Propulsion Laboratory in Pasadena, California, as required. Table 8-2 is presented here for reference, summarizing all surface area and dispersion measurements. Specific results will be discussed with each catalyst in Sections 8.4 and 8.5.

8.3 ACUREX TEST FACILITIES

In order to conduct catalyst screening and system development tests, Acurex designed and constructed a catalytic combustion test facility. The facility provides a preheated, premixed fuel/air mixture for combustion by the catalyst and instrumentation for the monitoring of catalyst performance.

Basic facility capabilities include:

- Pressure: 1.01 to 10.1×10^5 Pa (1-10 atmospheres)
- Air capacity: 0.042 to 4.49 m^3/min (5-540 SCFM)
- Preheat: to 811K (1000°F)
- Fuel type: gaseous and liquid
- Heat release: 1055 MJ/hr (10^6 Btu/hr) maximum

TABLE 8-2. SUMMARY OF SURFACE AREA AND DISPERSION MEASUREMENTS ON GRADED CELL CATALYSTS

Sample No.	Surface Area m^2/g		Dispersion %		Catalyst	SEM/EDAX Results and Comments
	Pretest	Post-test	Pretest	Post-test		
AERO-025	1.55-2.49	0	1.5-4.9	0	Pt/Ir	No Pt or Ir found on back two segments by SEM/EDAX
AERO-026	5.94	0	–	–	Proprietary	
AERO-027	0.44	–	20.64	–	Pt/Ir/Os	
AERO-028	0.06	–	8.33	–	Pt/Ir/Os	Not combustion tested
AERO-029	0.60	0	–	–	NiO/Pt	
AERO-030	0.15	.01	–	–	Co_2O_3/Pt	
AERO-031	24.38	0	36.16	0	Stab. Pt	
AERO-032	11.99	0	9.11	0.20	Stab. Pt	
AERO-033	–	–	–	–	NiO/Pt-Pd	Invalid test data
AERO-034	–	–	–	–	Co_2O_3/Pt	Invalid test data
AERO-035	5.17	0.09	4.09	0	Stab. Pt	
AERO-036	–	–	–	–	NiO/Pt	
AERO-037	–	–	–	–	Co_2O_3/Pt	Zero surface area on each segment
AERO-038	0	–	–	–	Co_2O_3	
AERO-040	4.00	0	–	–	Proprietary	
AERO-041	6.37	0.50	–	–	Proprietary	

Additional capabilities allow a variety of system testing configurations, including inert gas dilution, staged combustion, inter- and intra-bed cooling, and fuel doping with nitrogen compounds.

A schematic of the combustion facility is shown in Figure 8-1, and photographs of the system components appear in Figures 8-2 to 8-4. A 1.01×10^6 Pa (150 psia) air compressor delivers the required air flow to a receiver tank which damps the pressure oscillations at the compressor outlet. The air is regulated in pressure and throttled at the tank outlet prior to passing through a mass flowmeter. Just prior to entering the air heater, inert gas (nitrogen) can be introduced to dilute the air supply. The electric air heater has an 811K maximum temperature capability.

Fuel and fuel dopants (when used) are injected into the preheated air stream downstream of the heater. A sufficient length of pipe (dependent on fuel injector type) allows thorough mixing before entrance to the combustor. The combustor is modular, refractory-lined, and water-cooled (as shown in Figure 8-4) to allow flexibility in test configuration. A quartz viewport allows visual observation of the catalyst bed during operation. The exhaust gases are cooled (by water spray) before passing through the backpressure valve to the stack. The backpressure valve regulates system pressure to the maximum 1.01×10^6 Pa capability.

Facility instrumentation includes pressure, temperature, and flowrate measurements. Catalyst beds are routinely instrumented with in-depth thermocouples such that bed temperature profiles and histories can be determined. Optical pyrometry is also used. Bed temperature acts as the main variable for system control. In addition, the catalyst exhaust gases are sampled and analyzed continuously for CO_2, CO, O_2, NO_x, and unburned hydrocarbons. Table 8-3 lists the on-line analyzer types and normal operating ranges. Gas chromatography (Carle 8500) is also utilized for analysis of CO_2, CO, O_2, N_2, H_2, CH_4, and other hydrocarbons.

The facility is operated from a remote control room with the power and flow controls mounted in a single console. All instrumentation is fully electronic which allows pressure, flow, and temperature measurements to be monitored from the control room. A computerized data acquisition system is employed to record test data and continuously display real-time conditions.

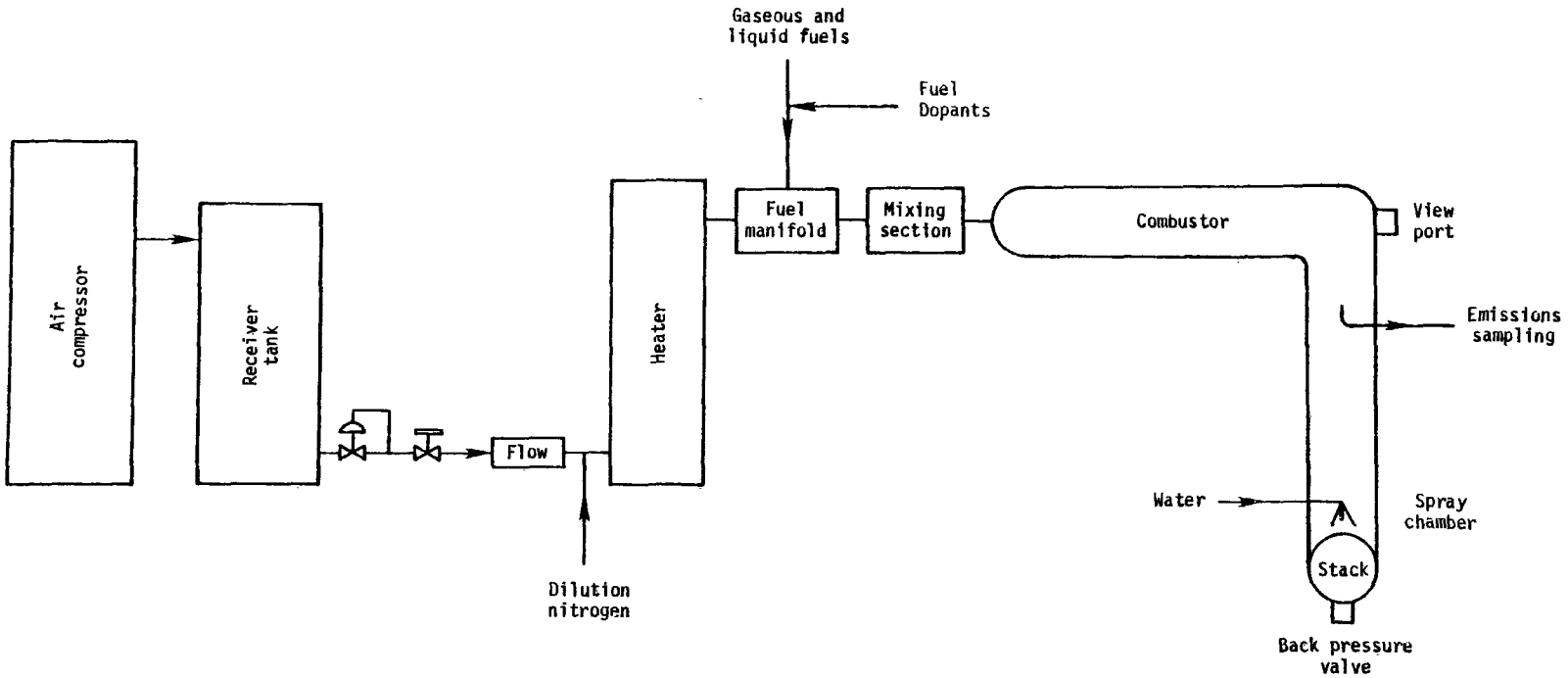

Figure 8-1. EPA/Acurex catalytic combustion test facility.

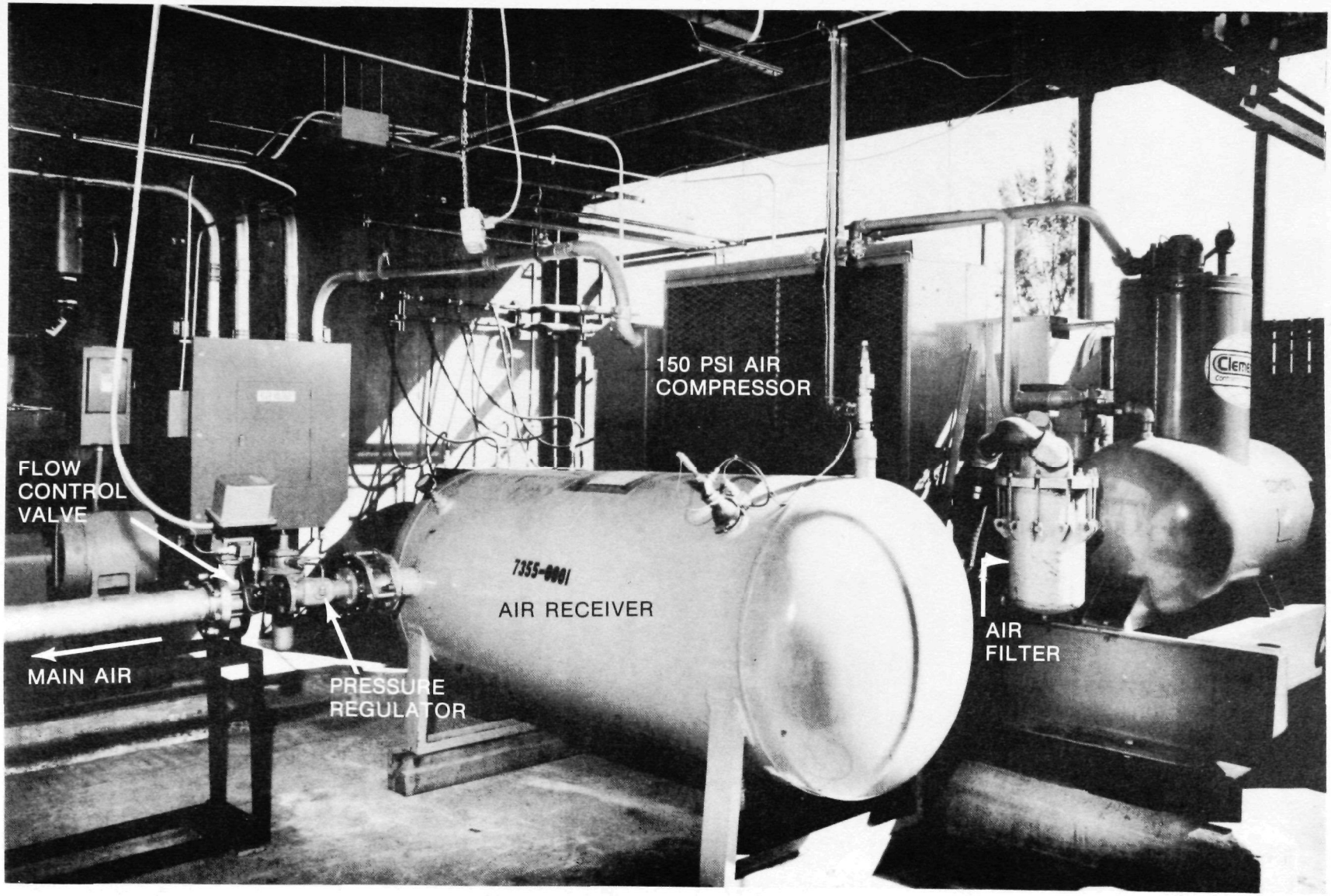

Figure 8-2. Air compressor and receiver.

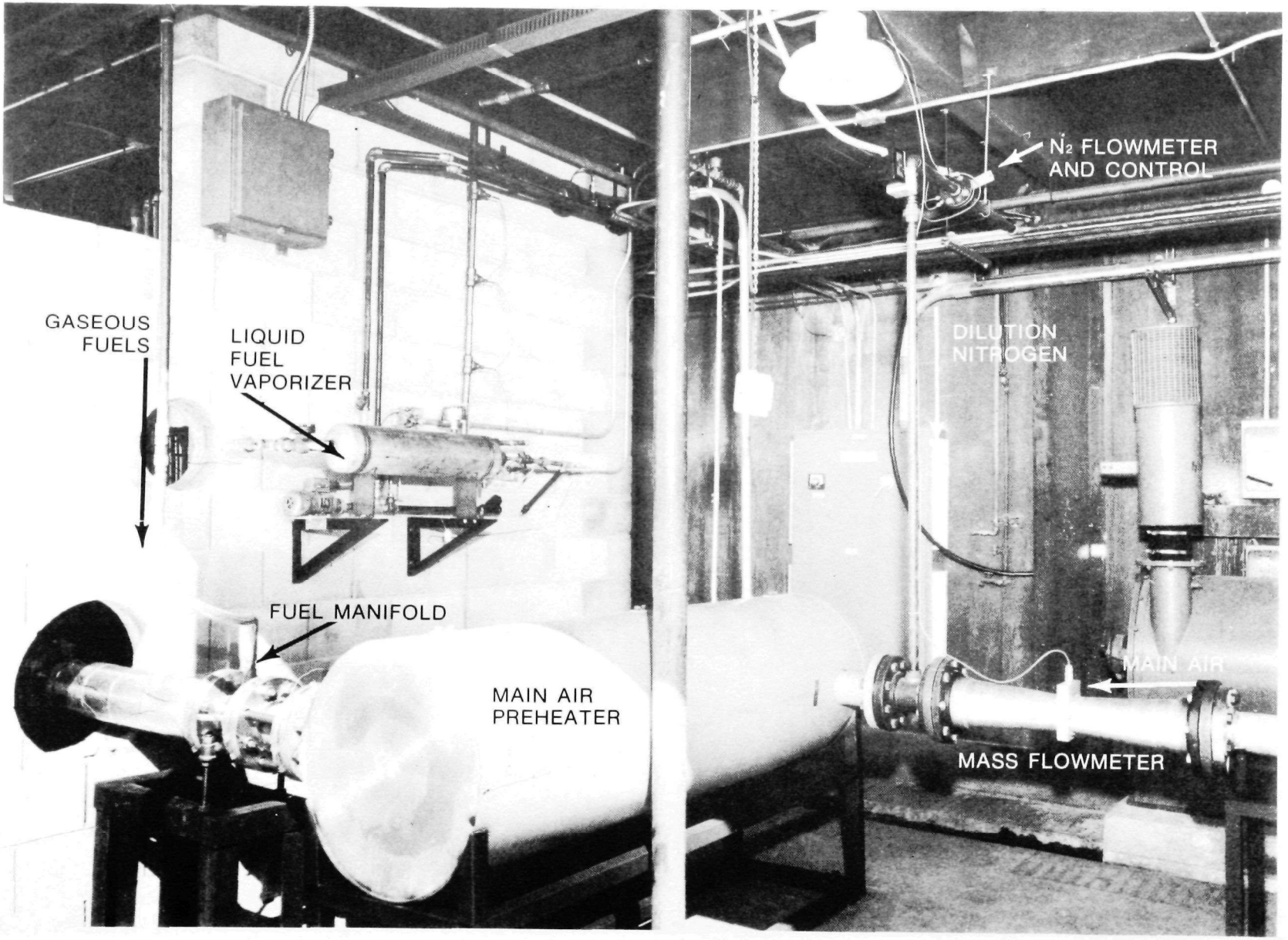

Figure 8-3. Main air preheater.

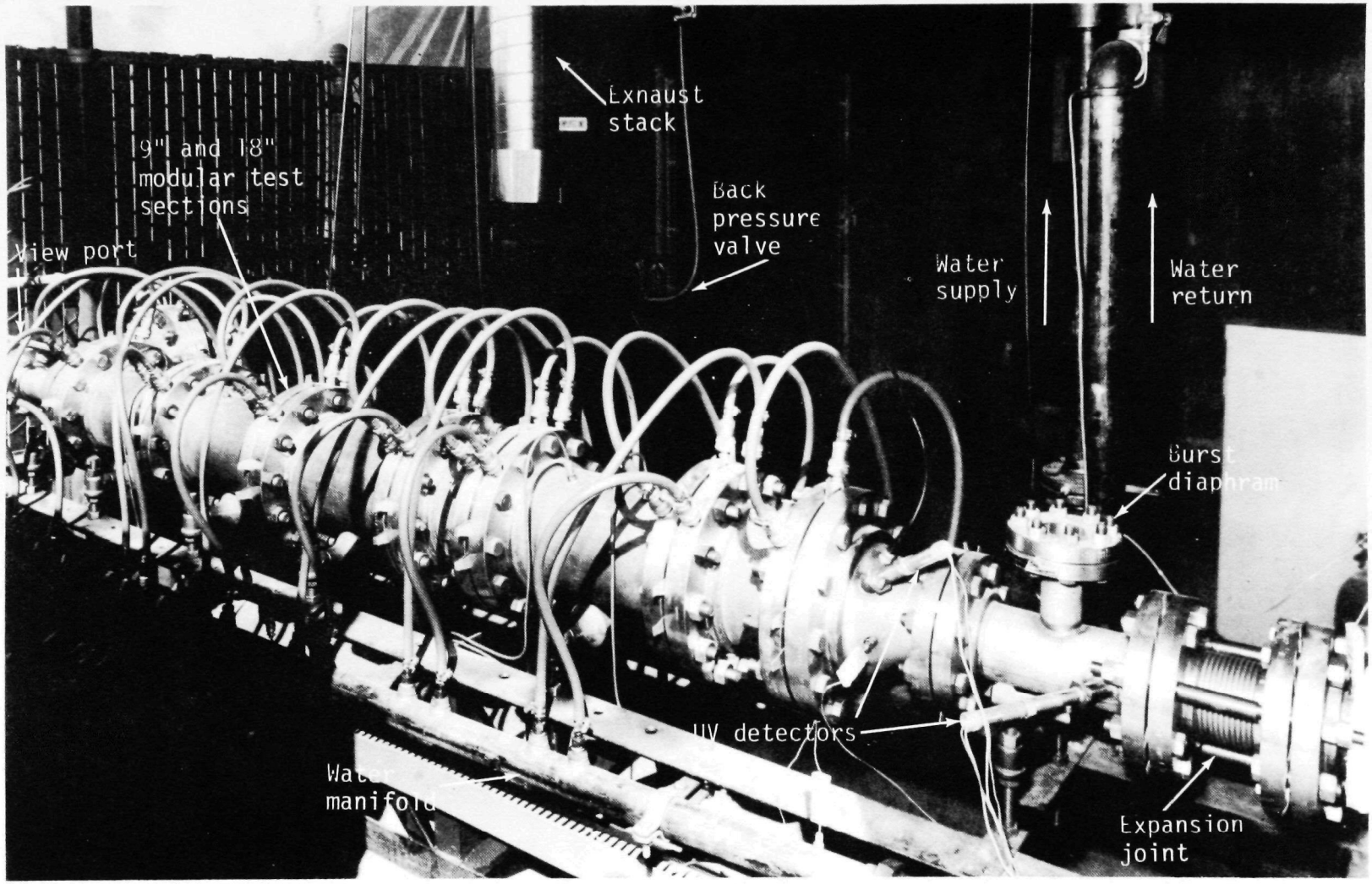

Figure 8-4. EPA/Acurex test section and exhaust systems.

TABLE 8-3. CONTINUOUS GAS ANALYSIS INSTRUMENTATION

Species	Instrument Manufacturer	Measurement Ranges
Carbon Dioxide – CO_2	Intertech 2T	0-5, 0-20 percent
Carbon Monoxide – CO	Intertech 2T	0-500, 0-2000 ppmv
Oxygen – O_2	Intertech 5T	0-5, 0-21 percent
Nitrogen Oxides – NO_x	Air Monitoring, Inc. 32C	0-10,000 ppmv

The instrumentation is linked to a central computer system which provides analog-to-digital conversion, calculations and conversions to engineering units, display capabilities, and permanent data storage. The facility operator keys in commands at a remote CRT terminal to display test variables and store operating data.

8.4 COMBUSTION SCREENING TESTS

The manufacturer-supplied graded cell catalysts were tested under a uniform test procedure. This test procedure included:

- Investigation of lightoff requirements with catalyst life, various fuels, and preheat.
- A 10-hour initial operation period to age the catalyst to a near steady state level of activity. Aging was performed at nominally 1589K (2400°F) and fuel-lean conditions at a heat release rate of 105.5 MJ/hr (10^5 Btu/hr).
- Investigation of minimum preheat requirements for both fuel-rich and lean operation.
- Maximum throughput capabilities at 1589K, fuel-lean conditions.
- Additional tests based on the initial catalyst performance, including variations of preheat temperature and throughput at higher temperatures.

Catalyst operating temperature was normally varied by varying fuel/air ratio. For operation near 100 percent theoretical air, diluent nitrogen was used.

Each of the tests performed is described in the following sections. The primary test fuel for combustion testing was natural gas. References are made to Appendix B of this report for additional test data.

8.4.1 Catalyst Comparison Tests

Catalysts were received from several manufacturers and screened by combustion testing. The best catalysts were then to be used for system development phases of the program.

8.4.1.1 W. R. Grace and Company (A-025)

As shown in Table 8-1, W. R. Grace applied a precious metal platinum/iridium catalyst on DuPont alumina support with stabilized washcoat. The three segments of the graded cell configuration are shown in Figure 8-5. The metal loadings and surface area and dispersion measurements performed on each segment at Acurex are shown in Table 8-4. The dispersion was quite low, ranging from 1.5 to 4.9 percent for the three segments. The catalyst segments were instrumented with a total of nine in-depth thermocouples and joined together prior to screening. Screening tests were performed at atmospheric pressure with natural gas.

The catalyst performed very well through the first 10 hours of aging, with some bed nonuniformities noted. Following this period, minimum preheat and maximum throughput tests were conducted. The nominal test condition of 1589K bed temperature, 672K (750°F) preheat temperature, and 105.5 MJ/hr heat release rate was repeated periodically to check catalyst degradation with time. Bed temperatures in excess of 1756K for extended periods and space velocities of 380,000 per hour were achieved. The significant test points are summarized in Table B-1 of Appendix B.

TABLE 8-4. W. R. GRACE CATALYST PRETEST CHARACTERIZATION

Segment	Noble Metal (mg)	Noble Metal (wt %)	BET Surface Area (m^2/g)	Dispersion (%)
Large cell	474	0.60	1.55	1.5
Medium cell	756	0.99	2.49	2.4
Small cell	797	0.76	1.85	4.9

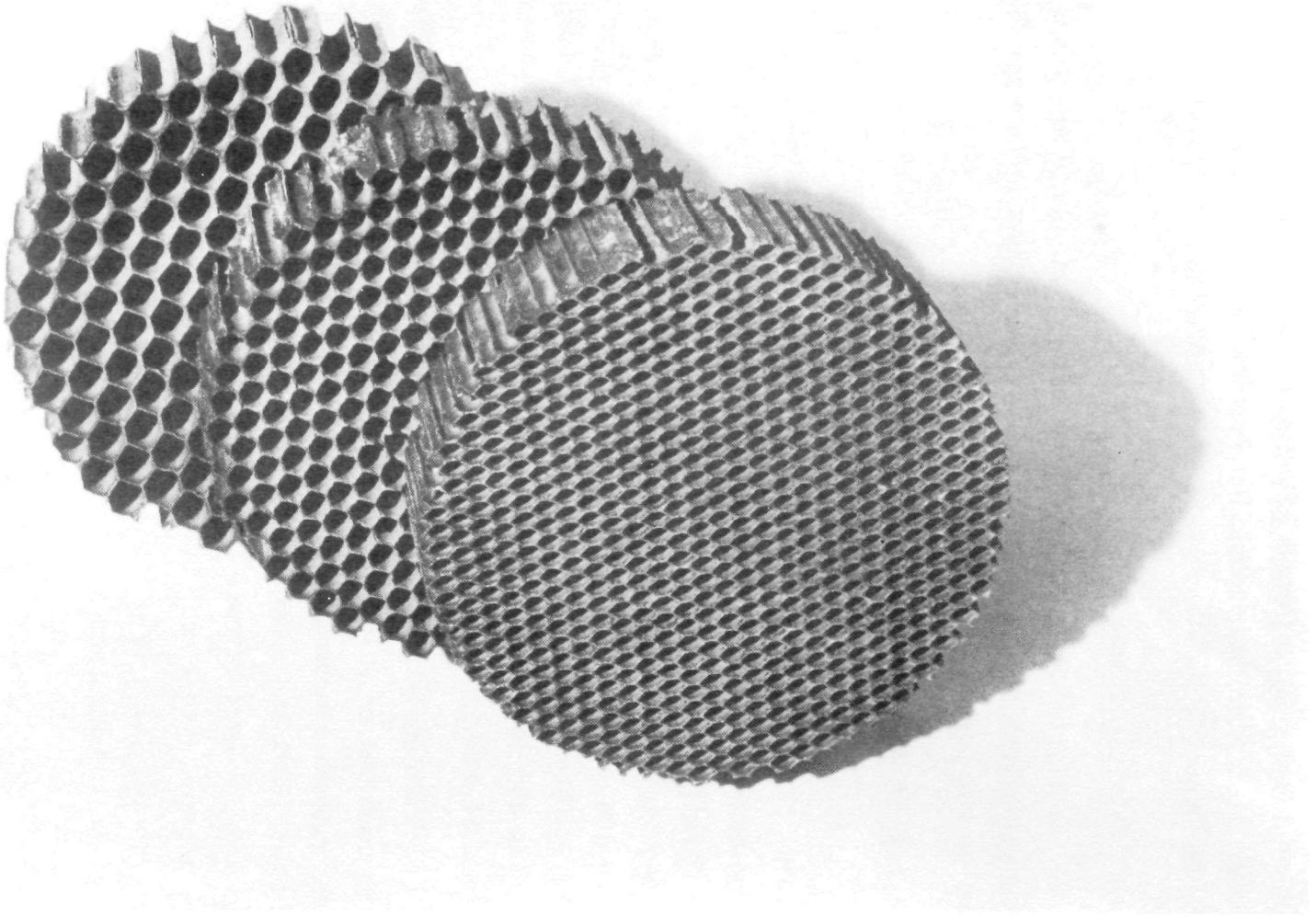

Figure 8-5. W. R. Grace graded cell Pt-Ir catalyst segments.

Measured emission levels are summarized in Table B-2 and Figure 8-6. No increase in either CO or NO_x emissions was noted over the entire 20-hour test time at the nominal 1589K test condition. Slight increases in NO_x production with increased bed temperatures were noted from the data. Increased throughput did not affect CO and NO_x emissions.

Catalyst lightoff temperature data (Table B-3) indicated degradation of catalyst activity with time. The catalyst initially lit off under lean conditions at 761K. Following only 2.5 hours of operation, lean lightoff was no longer possible. Successive rich lightoff temperatures remained essentially constant until 1756K bed temperature operation. The following lightoff attempt (fifth) resulted in a substantial increase in preheat -- 772K under rich conditions.

In general, the bed operated very nonuniformly even under steady-state conditions. Bed temperature distributions and visual observations reported in Figures B-1 to B-7 indicate the existence of relatively inactive combustion sites under various test conditions. The nonuniformity of the bed also impacted minimum preheat and maximum throughput values that could be achieved. Conclusions drawn from the data were:

- Bed temperature distributions did not change significantly during 10 hours of aging
- Operation could be maintained at reduced preheat (down to 533K), but bed nonuniformities became more pronounced
- Throughput could be increased to at least 274.3 MJ/hr (260,000 Btu/hr) at the expense of bed temperature uniformity
- Bed temperatures were more uniform at 1756K than at lower temperatures under all conditions

Although significant nonuniformities were observed throughout the test period, no substantial increases in nitrogen oxide or carbon monoxide emissions were measured. This was to be true for several additional catalysts tested at later dates. A picture of the post-test catalyst compared to an untested Grace catalyst is shown in Figure 8-7. A whitening of the catalyst is apparent. Post-test surface area and dispersion measurements both resulted in zero values, showing washcoat and precious metal sintering had occurred.

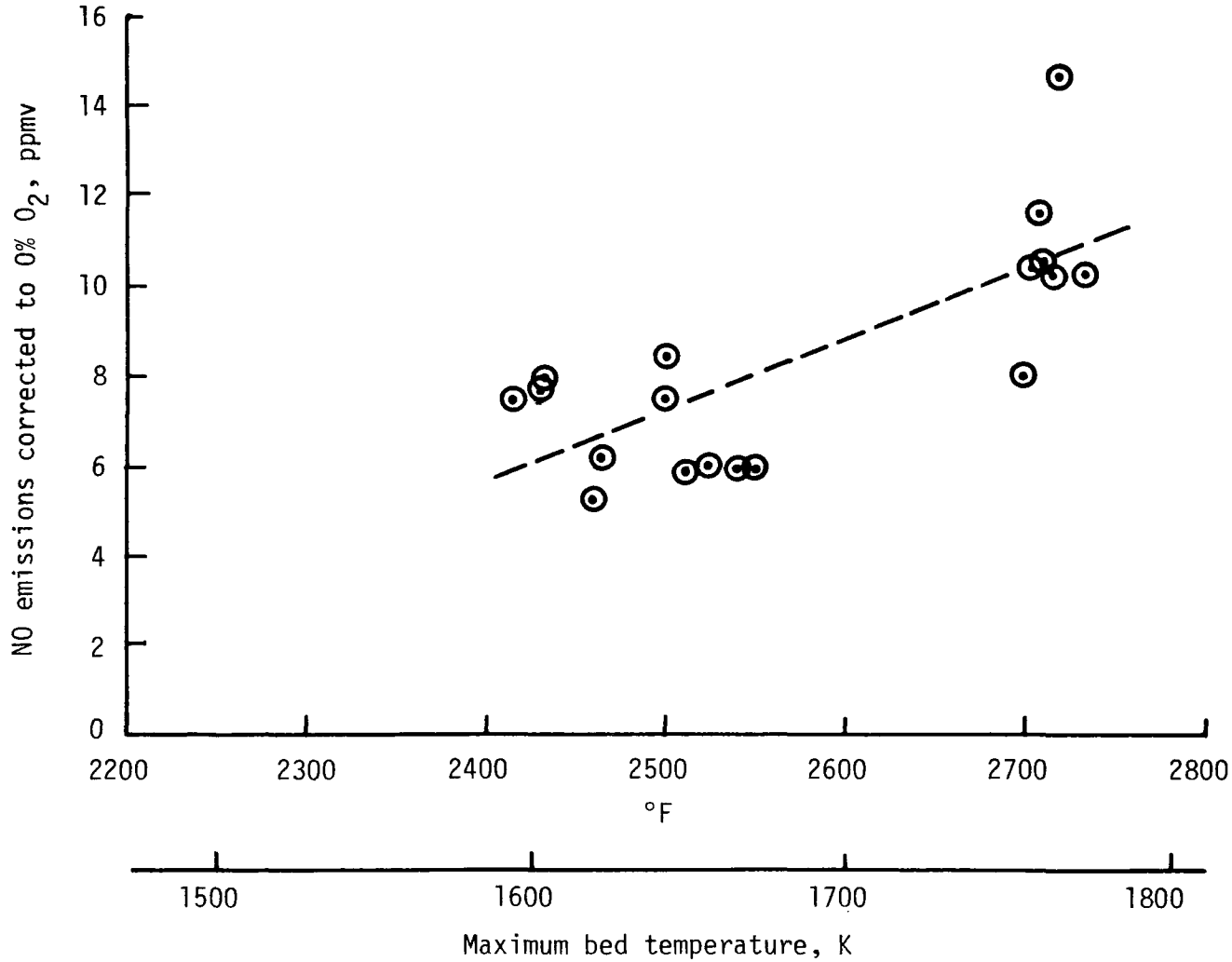

Figure 8-6. NO_x emissions corrected to 0% O_2 vs. maximum bed temperature for catalyst A-025.

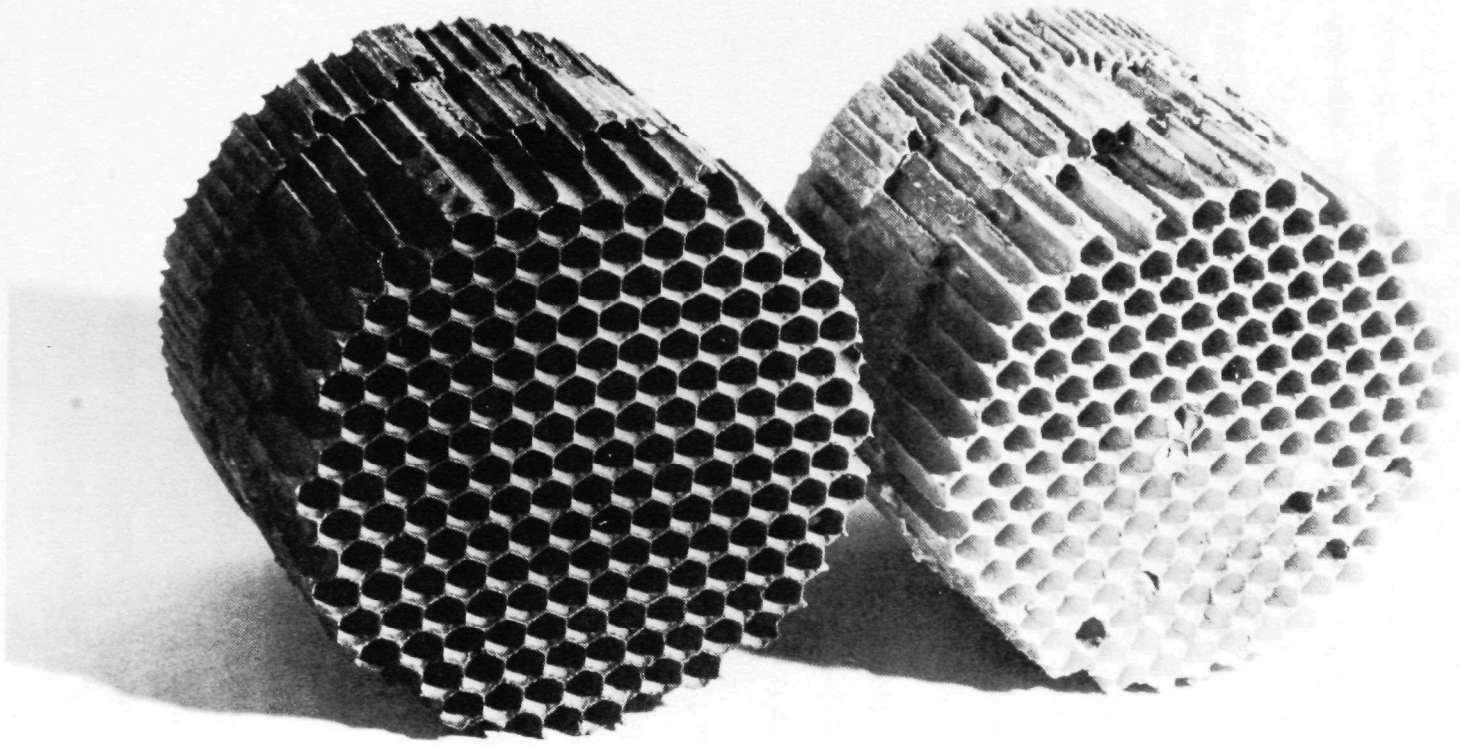

Figure 8-7. Pre- and Post-test appearance - W. R. Grace Pt/Ir catalyst.

Since significant nonuniformities in appearance were observed, segments of the catalyst from relatively active and inactive areas (observed at 1589K) were sent to the Jet Propulsion Laboratory for SEM/EDAX and chemical composition analyses. A pretest segment was also included for comparison. The samples of the post-test catalyst were taken from the middle and aft end segments of the catalyst bed.

The results of those analyses are presented in Appendix B of this report. Included are electron micrographs of the catalyst surface and X-ray diffraction spectra. The results indicated that:

1. Very little active catalyst (platinum or iridium) existed at the surface in either the active or inactive area following testing,
2. Platinum existed at 0.19 weight percent in the pretest catalyst with only trace amounts of iridium, and
3. The remaining catalyst material was well-embedded within the washcoat structure.

From these results and the results of the combustion tests, it appears that the relatively low precious metal loading and subsequent sintering resulted in zones of low catalyst activity.

8.4.1.2 Universal Oil Products Company (A-026)

Test model A-026 was obtained from Universal Oil Products (UOP). A proprietary catalyst was applied to a washcoated DuPont alumina support. Pretest surface area was measured at 5.94 m^2/g. Six thermocouples were installed for bed temperature measurements. Lightoff characteristics of the catalyst were very good (Table B-5). Initial lightoff was accomplished fuel-lean at 741K (875°F). Lightoff after 10 hours operation at 1589K, however, could only be done fuel-rich. After 23 hours of testing, rich lightoff was still possible at only 622K (660°F).

A nominal test condition of 1589K bed temperature, 644K preheat temperature, and 105.5 MJ/hr heat release rate was repeated to check catalyst degradation with time. Bed temperatures in excess of 1756K and space velocities of 420,000 per hour were achieved (see Table B-6).

Measured emission levels are summarized in Table B-7 and Figures 8-8 to 8-12. No increase in either CO or NO_x emissions was noted over the entire 23-hour test time at the nominal 1589K test condition. Variations in emissions with preheat temperature, stoichiometry, throughput, and bed temperature were noted as shown.

The UOP catalyst bed experienced some nonuniformities similar to the Grace catalyst. These nonuniformities occurred much later in the test period (at ~12 hours), however. Temperature nonuniformities became quite severe by 22 hours of testing, essentially ending testing at the 1756K temperature. Emissions were not affected significantly. Resulting bed temperature distributions are shown in Figures B-13 to B-15.

The following conclusions were drawn from the data:

- The UOP-prepared catalyst had exceptional lightoff characteristics over the entire test time,
- Operation at low preheats was possible (as low as 394K) without significant CO or NO_x emissions,
- Throughput could be increased significantly at 1589K (to 420,000 hr^{-1} space velocity). The high throughput at 1589K accelerated catalyst degradation, however, so that little testing could be done at 1756K, and
- Bed nonuniformities did not cause significant increases in emissions.

Post-test surface area for the UOP catalyst was found to be 0 m^2/g. This result, in consideration of the fact that the catalyst was still able to light off and operate at the end of the test period, suggested that a high catalyst surface area was not a significant parameter at lightoff. It further suggested that combustion catalysts could be operated under steady state conditions without high surface area.

8.4.1.3 W. Pfefferle (A-027 and A-028)

The results of the first two screening tests indicated that catalysts with low surface areas may operate well under combustion use. The services of Dr. William Pfefferle, a private consultant, were obtained to manufacture two precious metal catalysts without washcoat. These platinum/iridium/osmium

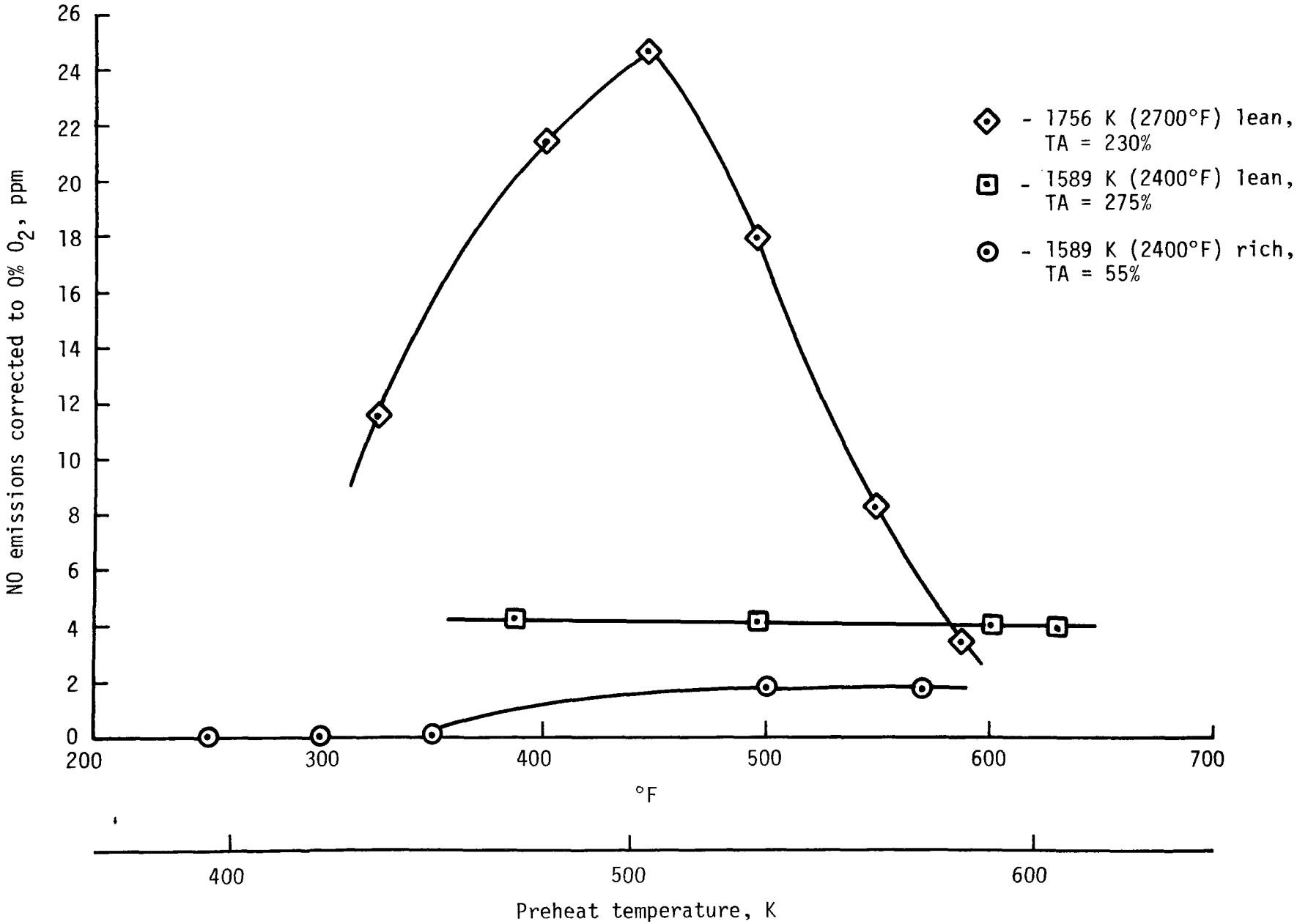

Figure 8-8. NO_x emissions corrected to 0% O_2 vs. preheat -- UOP catalyst (A-026), natural gas/air.

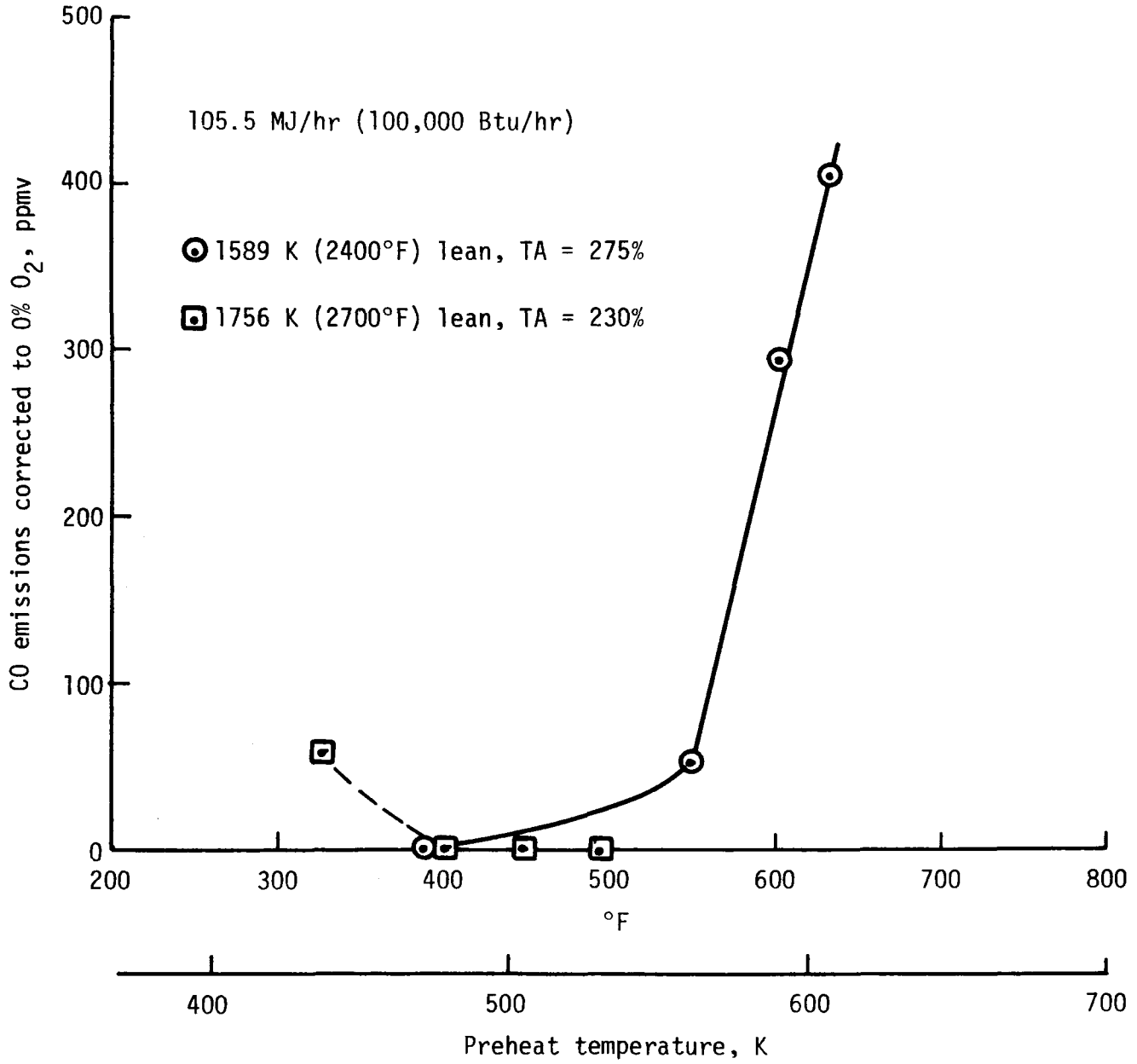

Figure 8-9. CO emissions corrected to 0% O_2 vs. preheat -- UOP catalyst (A-026), natural gas/air

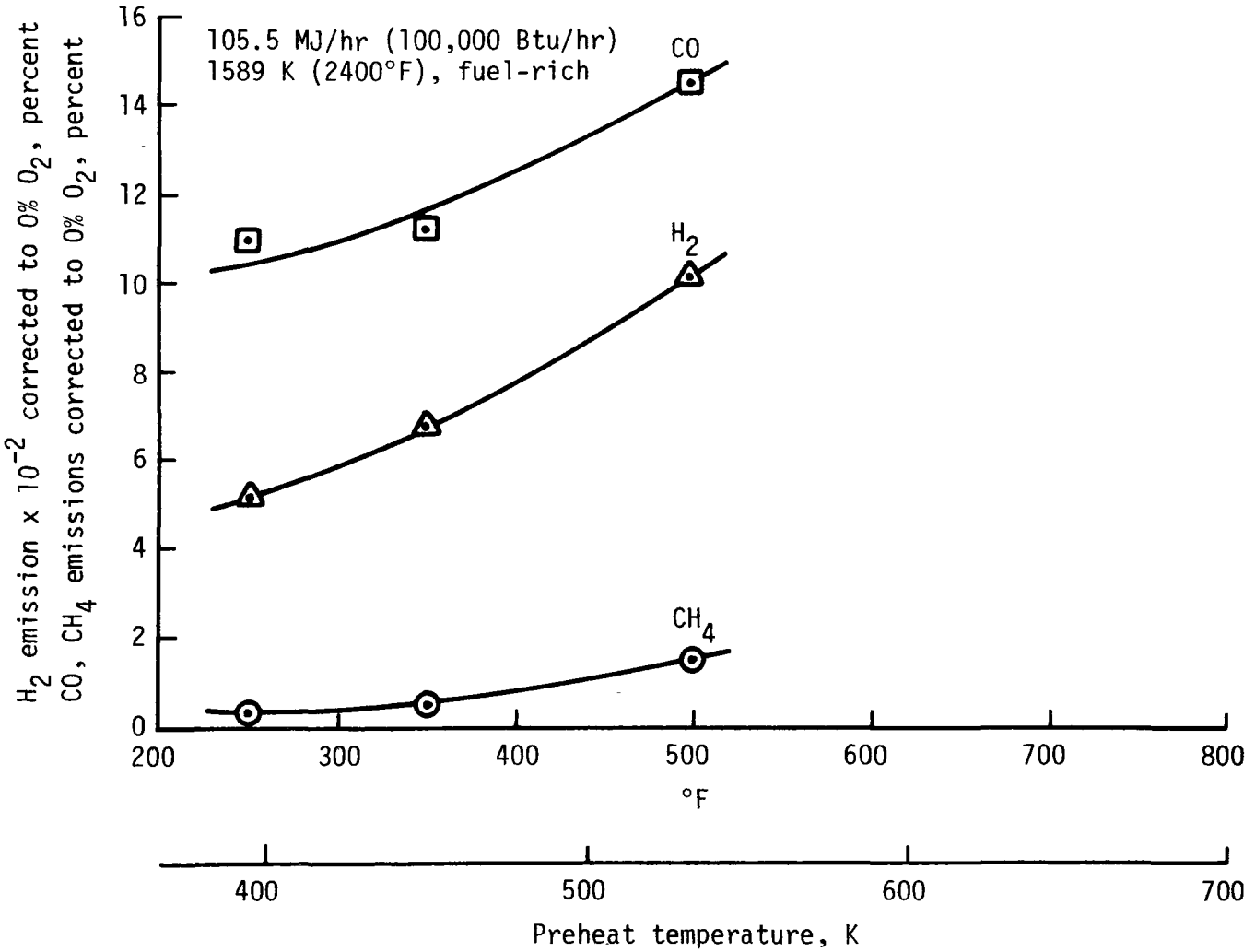

Figure 8-10. Fuel-rich emissions corrected to 0% O_2 vs. preheat -- UOP catalyst (A-026), natural gas/air.

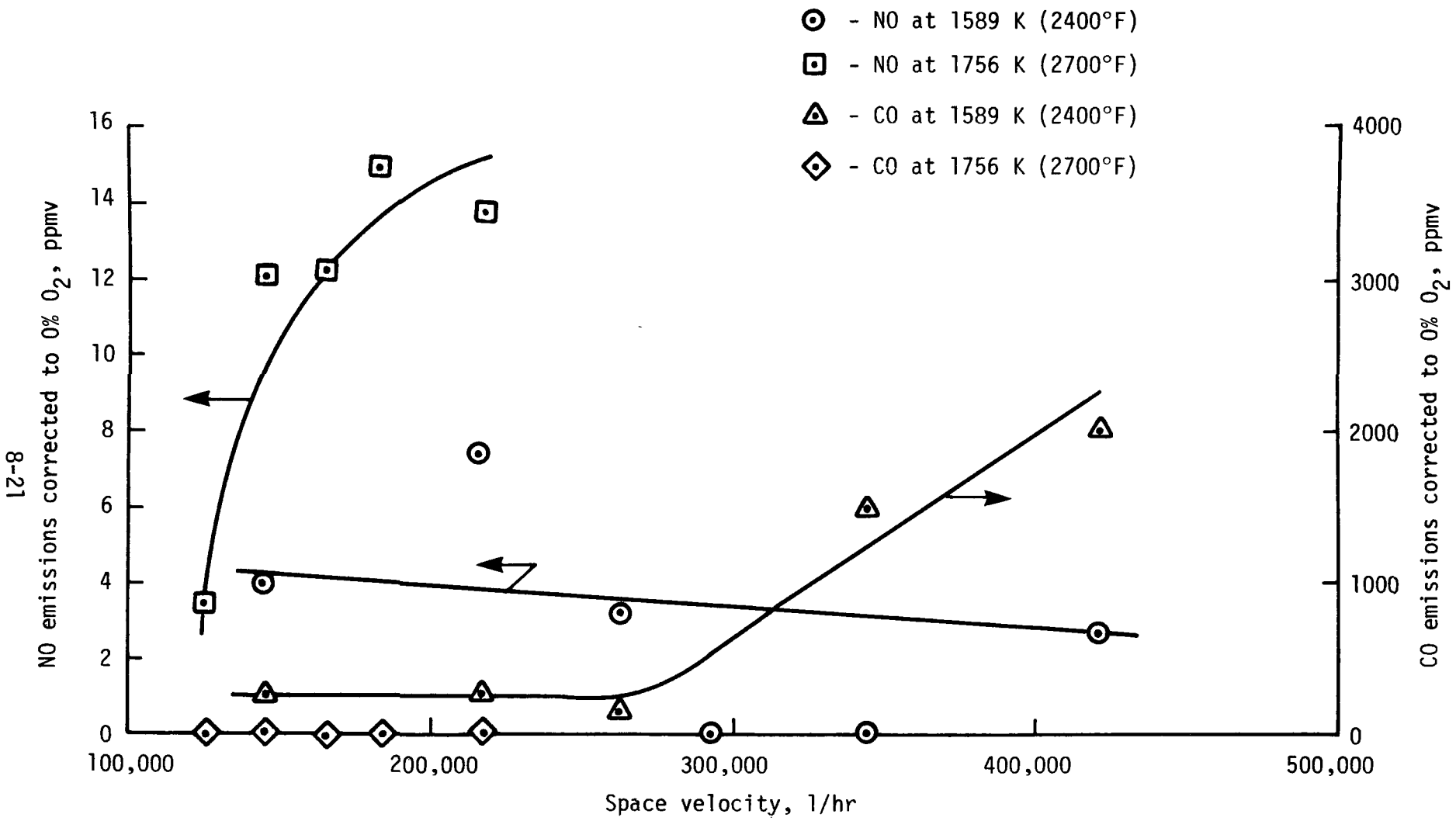

Figure 8-11. UOP catalyst (A-026) emissions as a function of throughput, natural gas/air.

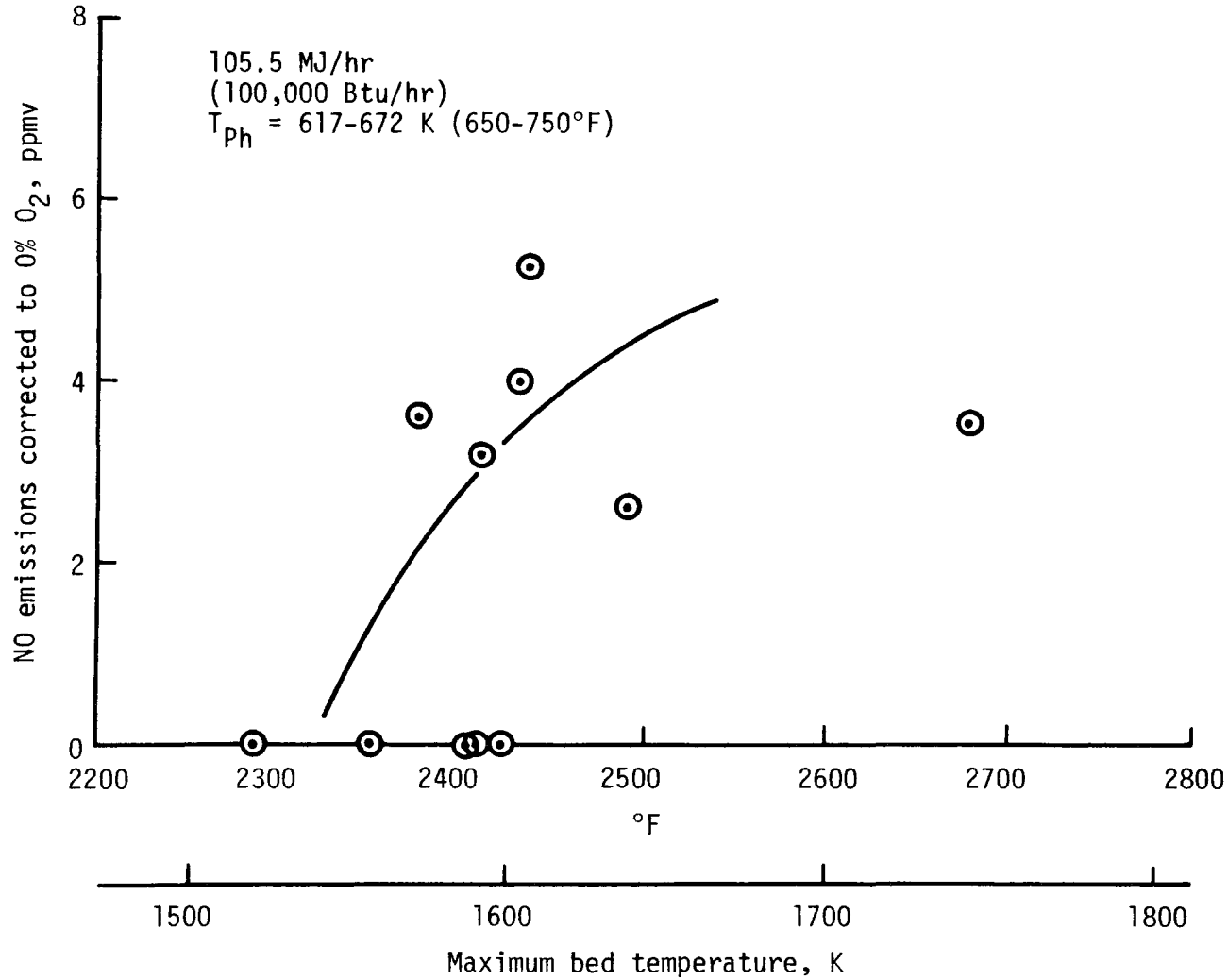

Figure 8-12. NO emissions corrected to 0% O_2 vs. bed temperature for UOP catalyst (A-026), natural gas/air.

catalysts had very low surface areas (0.44 and 0.06 m^2/g respectively) and dispersions of 20.64 and 8.33 percent.

Catalyst A-027 proved to be difficult to light off (778K, fuel-rich on the virgin catalyst) due to the low loading of precious metals. Subsequent lightoff attempts after 4.5 hours of testing were unsuccessful at 762K preheat.

The test points that were achieved are shown in Tables B-8 and B-9. Initial operation at the nominal 105.5 MJ/hr heat release rate produced temperature and visual nonuniformities. This situation was alleviated by reduction of mass throughput to a heat release of 79.1 MJ/hr.

It was concluded that the low metal/no washcoat preparation was not sufficient for complete hydrocarbon conversion. As a result, testing of catalyst A-028 was not performed. The data had not totally indicated the combustion characteristics of a no-washcoat catalyst since precious metal loadings were also significantly lower than for previous test models. Demonstration of catalysts without washcoats was left to later testing.

8.4.1.4 Matthey Bishop A, B, and C Catalysts (A-031, A-032, and A-035)

Three precious metal catalysts were obtained from Matthey Bishop for combustion screening. Test results of the three were similar and are reported below.

The Matthey Bishop B catalyst (A-032) was the first to be tested. It had a high initial surface area (12 m^2/g) with a dispersion of 9 percent. The catalyst was generally unstable during operation, however, and the decay in activity was quite rapid. After an initial 6 hours of constant lean operation at 105.5 MJ/hr and 1589 K bed temperature with natural gas, the bed lost activity and blew out. Attempts to relight the bed were unsuccessful. Although some areas of the bed showed activity, uniform combustion could not be achieved and blowout occurred rapidly at low space velocities (150,000 1/hr). The decay in bed activity is shown in the temperature profiles of Figure 8-13. A several hundred degree drop in surface temperature at the front of the bed was experienced within just 2 hours of operation. Post-test surface area was reduced to zero with 0.20 percent dispersion.

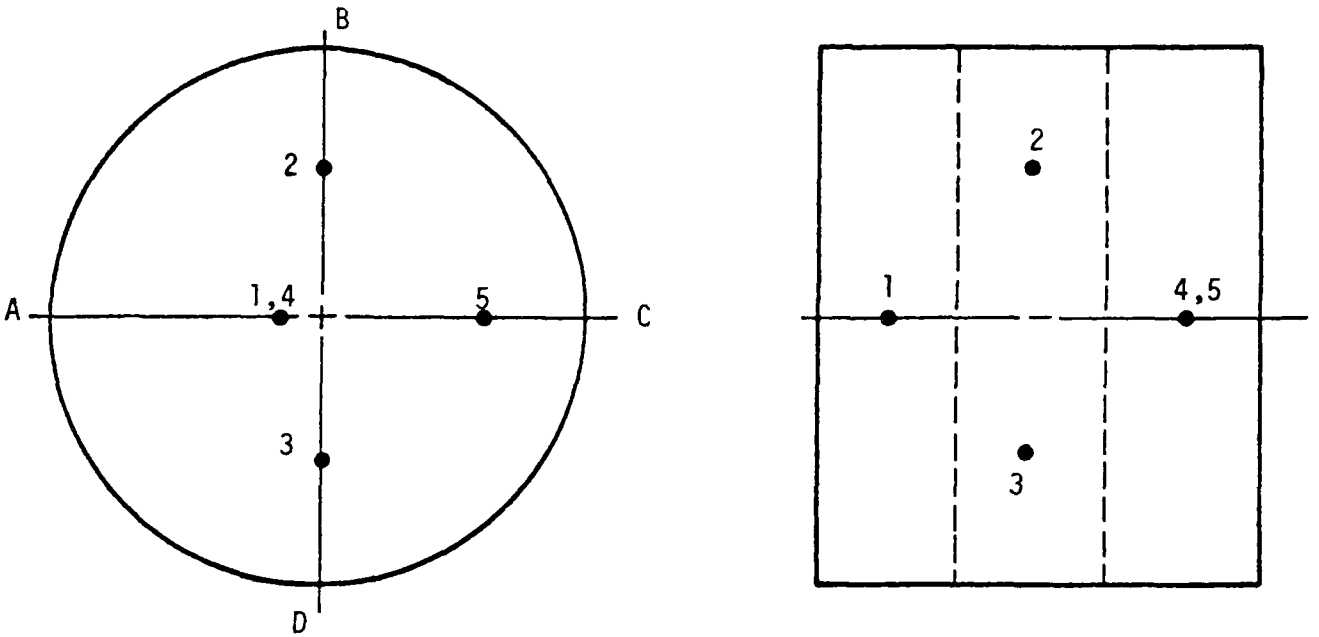

t = 3 hours 0726-4			t = 5 hours 0726-06		
TC	K	(°F)	TC	K	(°F)
1	1208	(1715)	1	1079	(1482)
2	1395	(2051)	2	1346	(1963)
3	1587	(2396)	3	1587	(2397)
4	1607	(2432)	4	1607	(2432)
5	1569	(2365)	5	1561	(2350)

Figure 8-13. Catalyst A-032 (Matthey Bishop B) bed temperature distributions during aging, natural gas/air.

The Matthey Bishop A catalyst (A-031) showed significantly higher activity than that of the B catalyst. Surface area and dispersion were very high at 24.4 m^2/g and 36.2 percent respectively.

The catalyst bed had average lightoff characteristics for a precious metal catalyst, as shown in Table B-10. After 16 hours of operation at 1589K, however, lightoff with natural gas was no longer possible. Although lightoff was difficult at this point in the test period, the bed still showed good activity in terms of throughput. The data summary in Table B-11 shows a high throughput of 6.9 Kg/hr was obtained with natural gas under lean operation.

Early in the test period (at 3.5 hours), the catalyst showed the same unstable operation at 2.1 Kg/hr of natural gas as the Matthey Bishop B catalyst had shown. Under steady operating conditions, the catalyst appeared to blow out and had to be restarted. Temperature profiles were essentially constant, however, as shown in Figure B-16. Activity remained good following that incident until 23 hours had elapsed at which time the catalyst could not be restarted.

Preheat effects on combustion uniformity were also investigated for catalyst A-031. The results are shown in Appendix B, Figure B-17 and are typical of other precious metal catalysts tested to date. Again, the post-test surface area was reduced to zero for this catalyst.

Performance of the Matthey Bishop C catalyst was similar to the A catalyst in that relatively good lightoff and steady state operating characteristics existed until approximately 20 hours of test time had elapsed. The catalyst activity had degraded significantly following 20 hours of testing.

A summary of the data points taken for catalyst aging, minimum preheat, and pressure operation is given in Table B-12. Maximum throughput test points normally included in the test matrix were not obtained due to catalyst degradation.

The generally good lightoff characteristics of the catalyst are shown in Table B-13. These results were similar to those of the Matthey Bishop A catalyst reported above with lightoff occurring consistently between 700K

and 767K. Figures B-18 and B-19 give information on bed temperature distributions.

No significant trends in emissions were found with varying preheat, pressure, or operating time. Both CO and NO emissions generally remained below 10 ppm throughout the 21-hour test period. Aging was found to promote greater bed uniformity in temperature, as did lowering the preheat temperature (at constant fuel rate) on the rich side. Lower preheat on the lean side resulted in the expected decrease in bed uniformity.

The results of the Matthey Bishop catalyst screening tests can be summarized as follows:

- The C catalyst generally performed better than the A and B catalysts
- Catalyst life was limited to 20 hours
- Lightoff temperatures, emissions, and preheat requirements were similar to other precious metal catalysts tested
- Catalyst instabilities existed for the A and B models.

8.4.1.5 W. Pfefferle Co_2O_3 Catalyst (A-038)

Dr. W. Pfefferle prepared a cobalt oxide catalyst on DuPont alumina support to investigate complexing interactions between the Co_2O_3 catalyst and support. Cobalt oxide catalyst interaction with the alumina present in support materials had been suspected from an earlier Co_2O_3 catalyst test (see Section 8.4.2.2). Four segments were prepared without washcoat, two of which included calcium oxide to act as a buffer between catalyst and support. The cobalt and calcium oxide additions are as shown in Table 8-5. All four segments were tested as a single bed, stacked in order as shown in the table.

Initially, the catalyst could not be lit off under normal preheat conditions (to 756K). A small amount of platinum was applied to the front end segment to facilitate lightoff. A total test time of 13.5 hours produced the lightoff history shown in Table B-14. The added platinum resulted in lightoff temperatures very similar to other oxide/platinum combinations tested.

TABLE 8-5. OXIDE PREPARATION OF CATALYST A-038

Channel Size	Large		Medium	Small
	LA	LB	M	S
Calcium oxide addition, g	None	3.7	5.9	None
Cobalt oxide addition, g	10.3	4.6	2.9	8.8
Percent cobalt oxide	15.9	6.7	4.1	8.5
Percent calcium oxide	-	5.4	8.4	-

Table B-15 summarizes the test data points. Emissions and bed operating characteristics were like those of other oxide catalyst tests during the 10-hour aging period. Bed temperature distributions at the beginning and end of aging are shown in Figure B-20.

At preheats below 533K under fuel-lean operation (1589K bed temperature), the front segments began to break through, producing the bed temperature distributions shown in Figure B-21. Homogeneous bed reactions could not be supported under fuel-rich combustion regardless of preheat.

Since many test points appeared to provide marginal operation at 1589 K, the bed temperature was increased to 1644K for the final maximum throughput test. An exceptionally high throughput was achieved (443,100 per hour space velocity) without experiencing blowout. This throughput represents a total heat release rate of over 464.2 MJ/hr (440,000 Btu/hr) and a volumetric heat release rate of 5.10×10^6 J/Pa-hr-m^3 (13,850,000 Btu/atm-hr-ft^3). The bed temperature distributions at the low and high throughput test conditions are shown in Figure B-22.

At maximum throughput, the catalyst came apart and was blown from the test section by the high velocity gases. Cracking had occurred as a result of catalyst/support complexing. The cobalt aluminate compound formed by the complexing of the cobalt catalyst with the alumina support at high temperatures has severe effects on support strength. No apparent differences were observable on segments where calcium was used as a buffer. The results of these tests show that further research on catalyst/support interactions is warranted.

8.4.1.6 Johnson Matthey Catalyst (A-040)

The Johnson Matthey test model (A-040) was a proprietary catalyst with a pretest surface area of 4.00 m^2/g (see Table 8-2). The catalyst operated exceptionally well under fuel-lean conditions but unstably under rich conditions. A history of catalyst lightoff is given in Table B-16 and shows continuous possibility of lean lightoffs at relatively moderate preheat temperatures. Lightoff under rich conditions generally resulted in nonuniform combustion and unstable operation.

Table B-17 summarizes the test points obtained. Lean operation at low preheats was quite good. Total mass flowrates to 367 Kg/hr were obtained (497.6 MJ/hr heat release rate) without experiencing blowout.

Emissions data showed somewhat higher NO_x values than are typical for lean-operating catalytic combustors. In some instances, readings were not repeatable at similar test conditions at later times. NO_x emissions were highest during the middle of the test period and lower during early and late testing stages.

8.4.2 High Temperature Evaluation

Two graded cell catalyst models were developed for high temperature operation (to 1978K). These high temperature catalysts required advanced support materials such as Corning zirconia spinel with use temperatures above the 1756K limit typical of alumina. In addition, catalysts which are stable above 1756K are required, with metal oxides selected as candidate catalysts. The results of the two high temperature catalyst tests (A-029 and A-030) are summarized below.

8.4.2.1 W. Pfefferle NiO/Pt (A-029)

The services of Dr. W. Pfefferle were used to develop a catalyst for high temperature applications (catalyst bed temperatures to 1978K). A base metal (nickel oxide) was selected for the catalyst since catalyst A-025 had demonstrated that very little precious metal remains after 1756K operation.

The nickel oxide catalyst was prepared on Corning zirconia spinel graded cell supports, without washcoat, as shown in Table 8-1. The zirconia spinel material, shown in Figure 8-14, has a 1978K use temperature. Platinum was added to the front two segments to enhance lightoff characteristics, with palladium and iridium added to the large cell segment as well. The pretest surface area was measured as 0.60 m^2/g as shown in Table 8-2. This low value was consistent with the no-washcoat application technique. The rear segment of the bed (small cell) had fractured during catalyst preparation but was restored for testing.

The NiO catalyst proved difficult to light off even with the added platinum. Therefore, all catalyst lightoffs were performed with propane at a bed temperature of approximately 672K. At approximately 922K, the fuel was then switched to natural gas to complete the lightoff. The first successful lightoff showed that the rear segment of the bed had refractured and fallen away from the front two segments. The test points summarized in supplement Tables B-18 and B-19 were all taken with the bed in this configuration with combustion occurring on the front two segments and downstream of the catalyst in the gas phase.

This catalyst was the first to be tested to the maximum use temperature of the Corning support. Significant NO emissions (>100 ppm) were measured above 1880K, as shown in Figure 8-15, and were somewhat higher than for the precious metal catalysts tested in the range of 1589K to 1756K. No CO emissions were measurable throughout the test period. On subsequent blowout testing, the bed further separated between segments and became disoriented to the flow direction. Testing was terminated at that time.

In general, it appeared from this test that the metal oxide performed well at the higher bed temperatures (>1700K) and could be restarted even after high temperature operation (to 1978K). The Corning zirconia spinel support did experience some thermal cracking. Since only large and medium cell segments were operational, the catalyst acted as a flameholder for downstream thermal reactions. With this geometry, fairly high levels of NO_x were observed at high temperatures. The success of high temperature catalyst operation led to the construction of a second test catalyst.

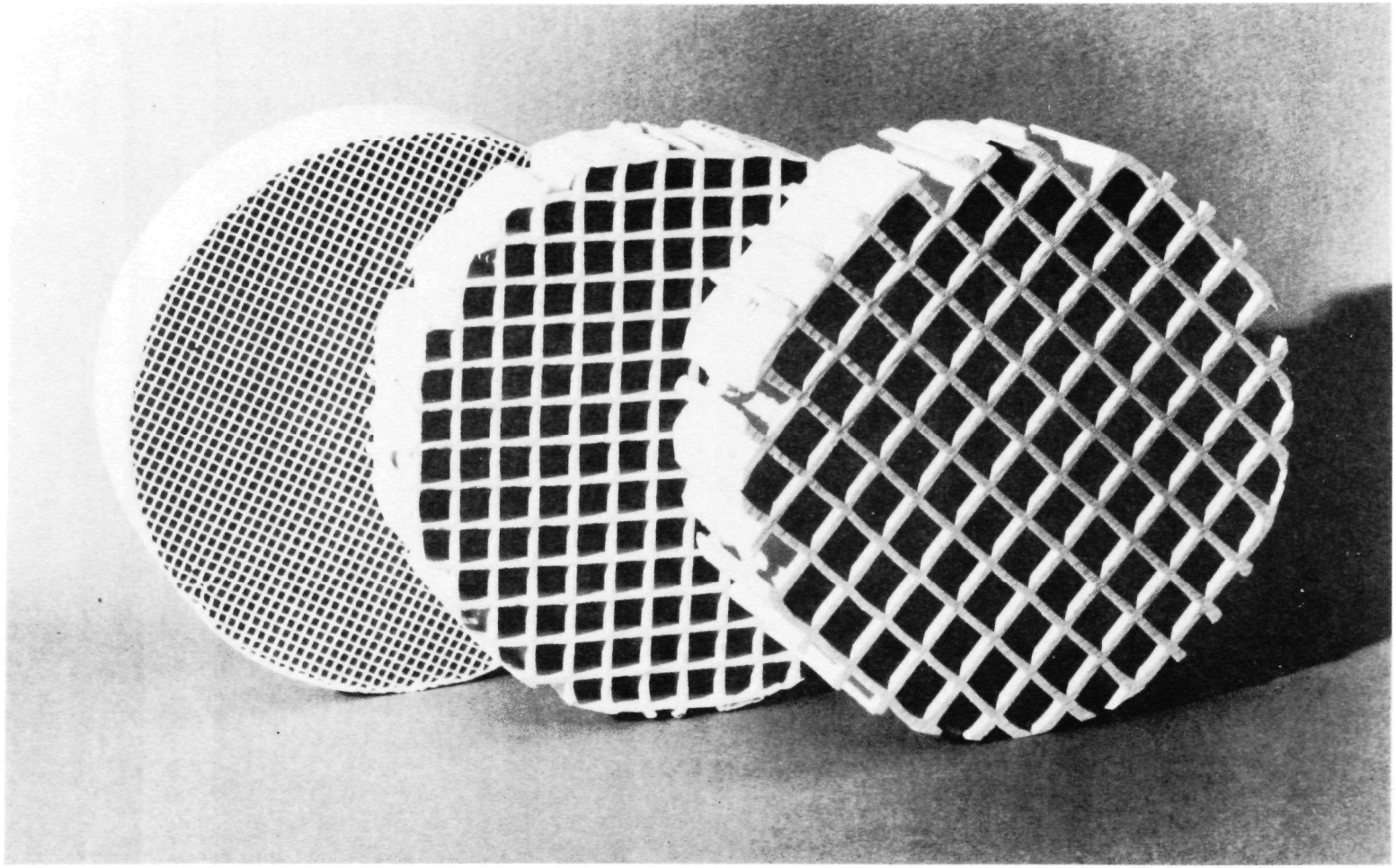

Figure 8-14. Corning square-celled extruded monolith structures.

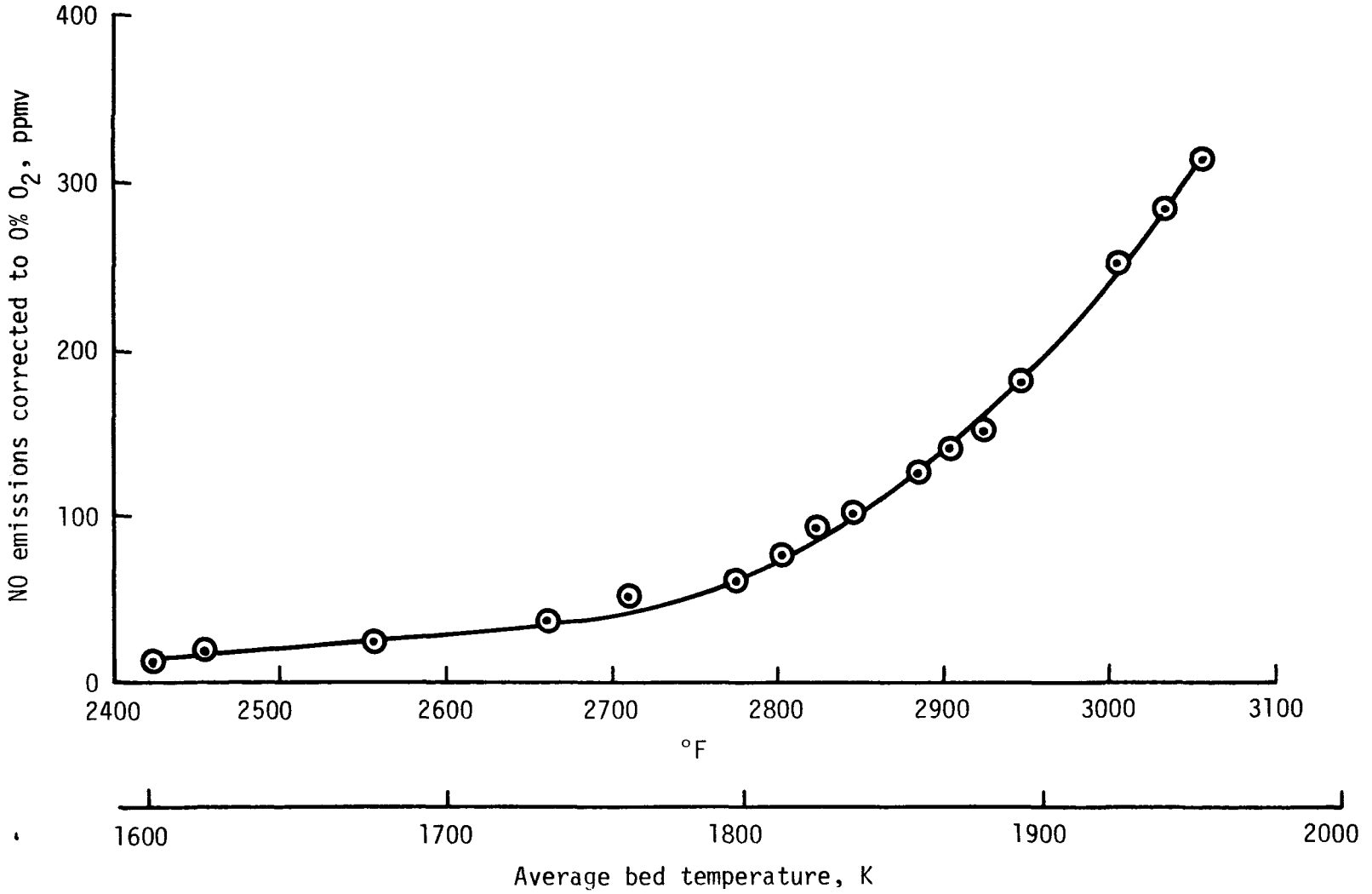

Figure 8-15. Catalyst A-029 (NiO/Pt) NO emissions corrected to 0% O_2, natural gas/air.

8.4.2.2 Acurex Co_2O_3 (A-030)

The second high temperature catalyst was cobalt oxide applied to Corning's zirconia spinel support at Acurex. Platinum was also applied to the front segment to facilitate lightoff. No washcoat was used in the preparation. Very low surface area (0.15 m^2/g) and dispersion (0.01 percent) were obtained by this technique.

The cobalt oxide catalyst was screened for a total of 24 test hours with natural gas at atmospheric pressure. Two lightoffs (one on the virgin catalyst and a second after 7 hours of testing) were accomplished fuel-rich with natural gas. Subsequent lightoffs could only be achieved with propane fuel. At ~1756K temperature operation, however, the catalyst maintained uniform conditions over the entire test time. Lightoff characteristics are summarized in Table B-20.

A summary of all test data is given in Table B-21. Bed temperatures up to 1978 K and space velocities to 490,000 per hour were achieved. Bed temperature profiles varied similar to the lower temperature precious metal catalysts under varying preheat and throughputs (see Figures B-23 and B-24). The effects of space velocity and preheat temperature on NO_x emissions under fuel-lean combustion conditions are shown graphically in Figures 8-16 and 8-17. These curves appear similar to those of precious metal catalysts tested at 1589K to 1756K.

Under high temperature operation, NO_x emissions of the Co_2O_3 catalyst were substantially lower than those of the NiO catalyst tested previously. Figure 8-18 shows this distinction in the metal oxide catalysts for reference. Since the three-segment Co_2O_3 catalyst had a much greater surface area than the two-segment NiO catalyst, it appears that maximizing the surface reactions (and thereby minimizing gas-phase reactions) minimizes NO_x formation.

The following conclusions were drawn from the test data:

- Low surface area, non-washcoated base metal catalysts have good combustion properties
- The metal oxide catalysts had good relight characteristics even after 1756K operation

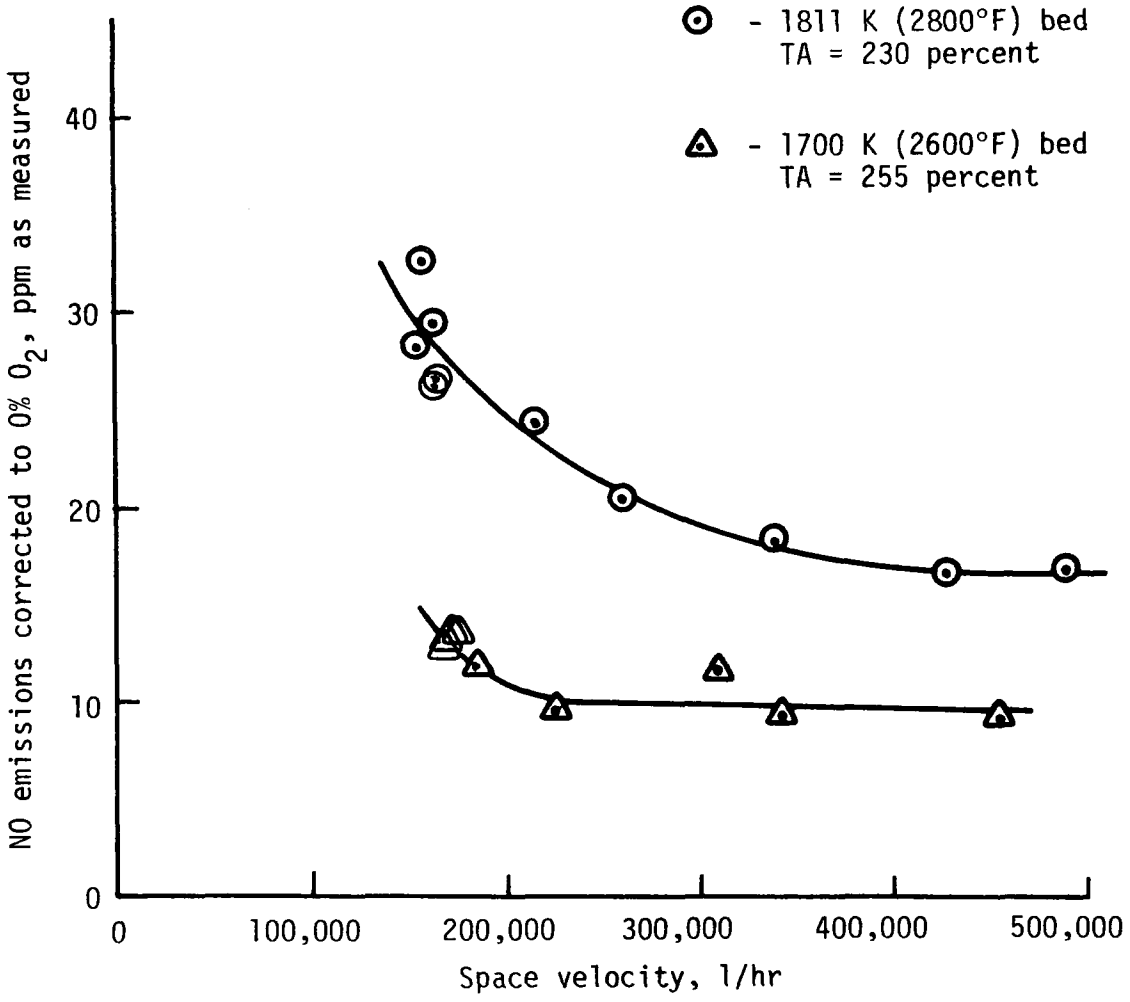

Figure 8-16. Catalyst A-030 (Co_2O_3/Pt) NO emissions corrected to 0% O_2, natural gas/air.

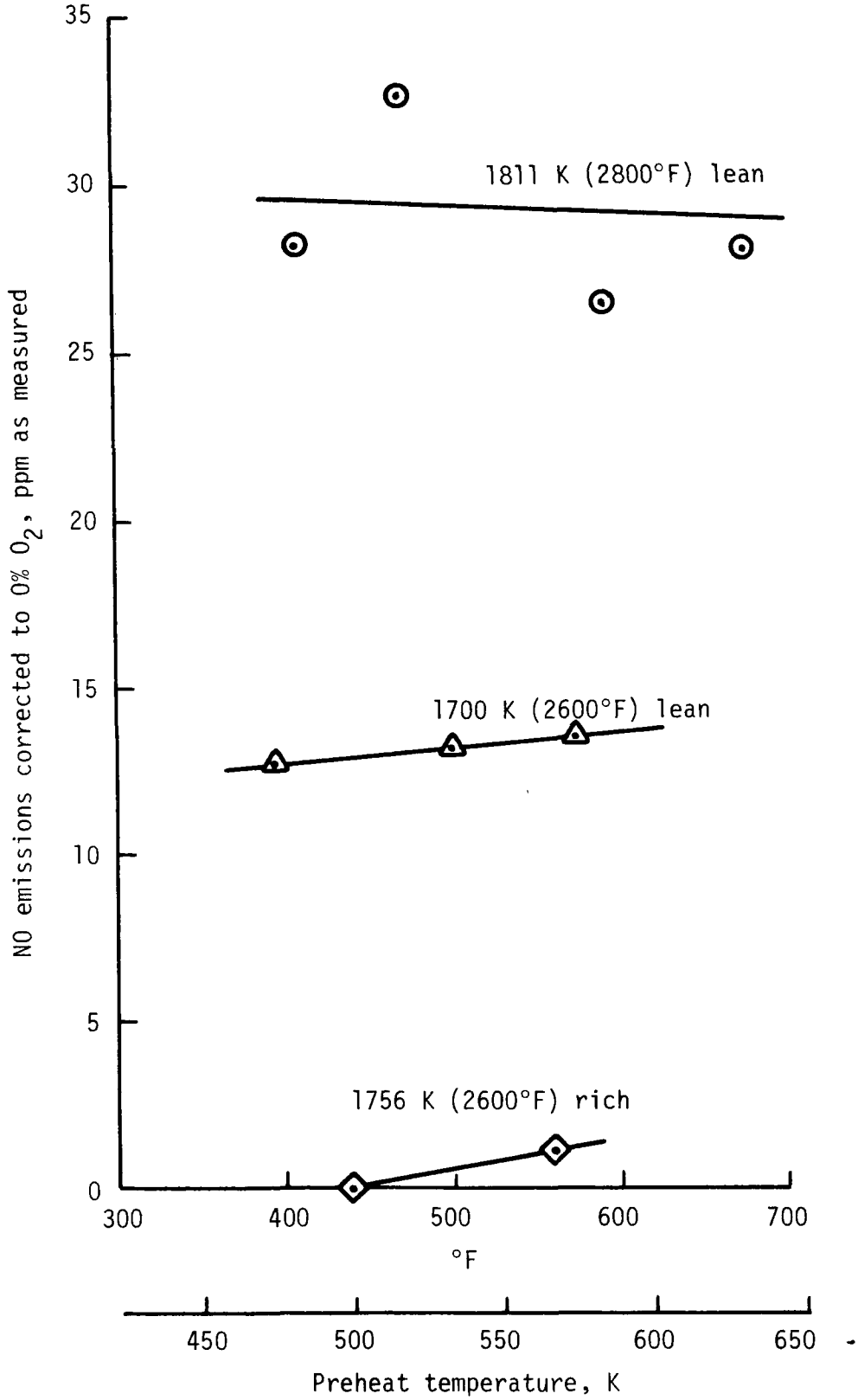

Figure 8-17. Catalyst A-030 (Co_2O_3/Pt) NO emissions corrected to 0% O_2, natural gas/air.

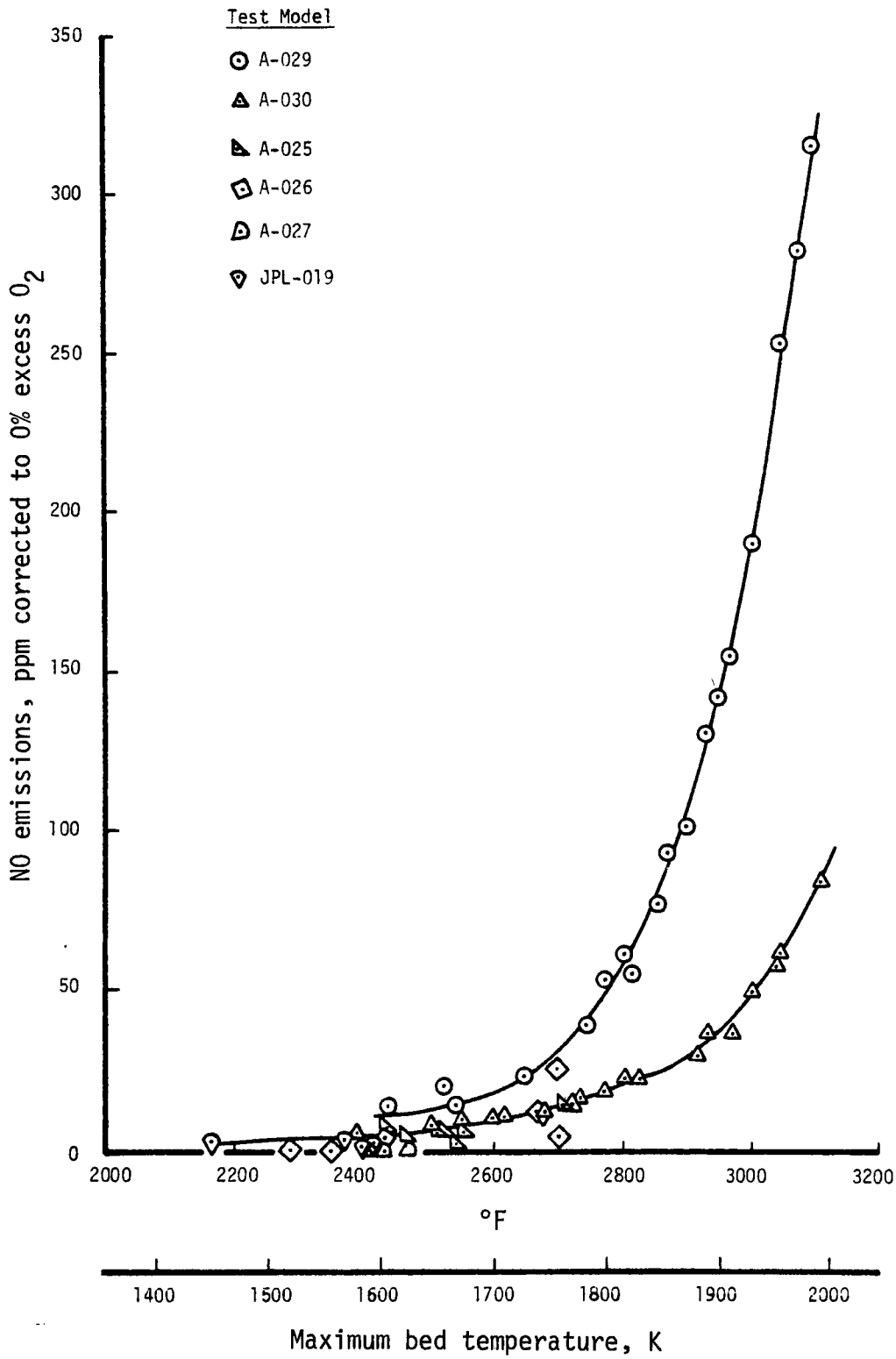

Figure 8-18. NO_x emissions comparison corrected to 0 percent excess O_2.

- Metal oxides show excellent potential for low NO_x emissions at high temperatures (to 1756K)
- High throughputs are possible with metal oxide catalysts in the graded cell configuration without experiencing blowout
- The increased surface area of the small cell catalyst segment had significant effect in reducing thermal NO_x emissions
- Significant amounts of the metal oxide remain on the support material after high temperature operation

The last conclusion resulted from a deep blue appearance of the post-test A-030 catalyst, indicating that cobalt compounds were still evenly distributed over the entire catalyst surface. It was speculated that the cobalt had complexed with the support material to form cobalt aluminate. This catalyst/support complexing may also impact the thermal shock characteristics of the ceramic support.

Post-test surface area and dispersion measurements were not made on A-030 due to the low pretest values obtained. Since catalyst activity remained good following screening, the catalyst was later used in fuel nitrogen extensive evaluation tests described in Section 8.5.

8.4.3 Catalyst Scaleup

Based on the results of all screening catalysts tested, one catalyst was selected for evaluation of scaling parameters to larger size systems. It was assumed that combustion throughput would scale proportionately to bed frontal area. Therefore, bed diameter was increased to provide a scaleup factor of 2.7 increase in frontal area over that of small scale screening catalysts, while bed length remained at 0.0762 m (3.0 inches) of graded cells.

The scaleup catalyst was prepared by Universal Oil Products Company on 0.154 m diameter DuPont alumina supports. The initial surface area was measured at Acurex at 6.37 m^2/g. This area was only slightly greater than the small scale UOP catalyst (A-026) at 5.94 m^2/g. Some variations in preparation technique were reported by UOP based on test results of model A-026.

The scaleup catalyst was tested for a total period of 27 hours to determine the catalyst scaling properties. Test sequences included:

- 10 hours aging at 1561K (2350°F) with natural gas
- fuel-lean minimum preheat operation
- fuel-rich minimum preheat operation
- blowout at 608K preheat, 1589K bed temperature, 0.101 MPa (1 atm)
- blowout at 478K preheat, 1589K bed, 0.101 MPa
- blowout at 394K preheat, 1589K bed, 0.101 MPa
- blowout at 608K preheat, 1589K bed, 0.303 MPa
- blowout at 672K preheat, 1589K bed, 0.101 MPa
- fuel-lean minimum preheat at 1055 MJ/hr (10^6 Btu/hr) heat release rate

The catalyst lightoff history shown in Table B-22 was very similar to that of test model A-026, with initial lightoff performed under fuel-lean conditions at 722K. Subsequent lightoffs could only be accomplished fuel-rich but at preheats as low as 622K.

A summary of all data points is given in Table B-23. Screening test results were similar to those of test model A-026. Maximum throughput reported for the small scale catalyst was 258.5 MJ/hr (245,000 Btu/hr) and 3.42×10^6 J/hr-Pa-m^3 (9.3×10^6 Btu/hr-atm-ft^3) volumetric heat release rate. This compares to a volumetric heat release of 4.38×10^6 J/hr-Pa-m^3 (11.9×10^6 Btu/hr-atm-ft^3) at 926.3 MJ/hr (878,000 Btu/hr) for the scaleup catalyst at 672K preheat. Emission characteristics were also similar.

A series of blowout tests were conducted to determine the operational mass throughput limit of the catalyst for varying preheat and pressure conditions. The blowout points used are shown in Table 8-6.

Data points 1 and 4 were compared to determine the effect of pressure on blowout, and a maximum fuel flowrate at 0.101 MPa was calculated for all points based on a linear variation of maximum fuel flowrate with pressure. Additional blowout curves were then calculated using the same linear variation for operation at 0.136 MPa, 0.202 MPa, and 0.303 MPa pressures. Figure

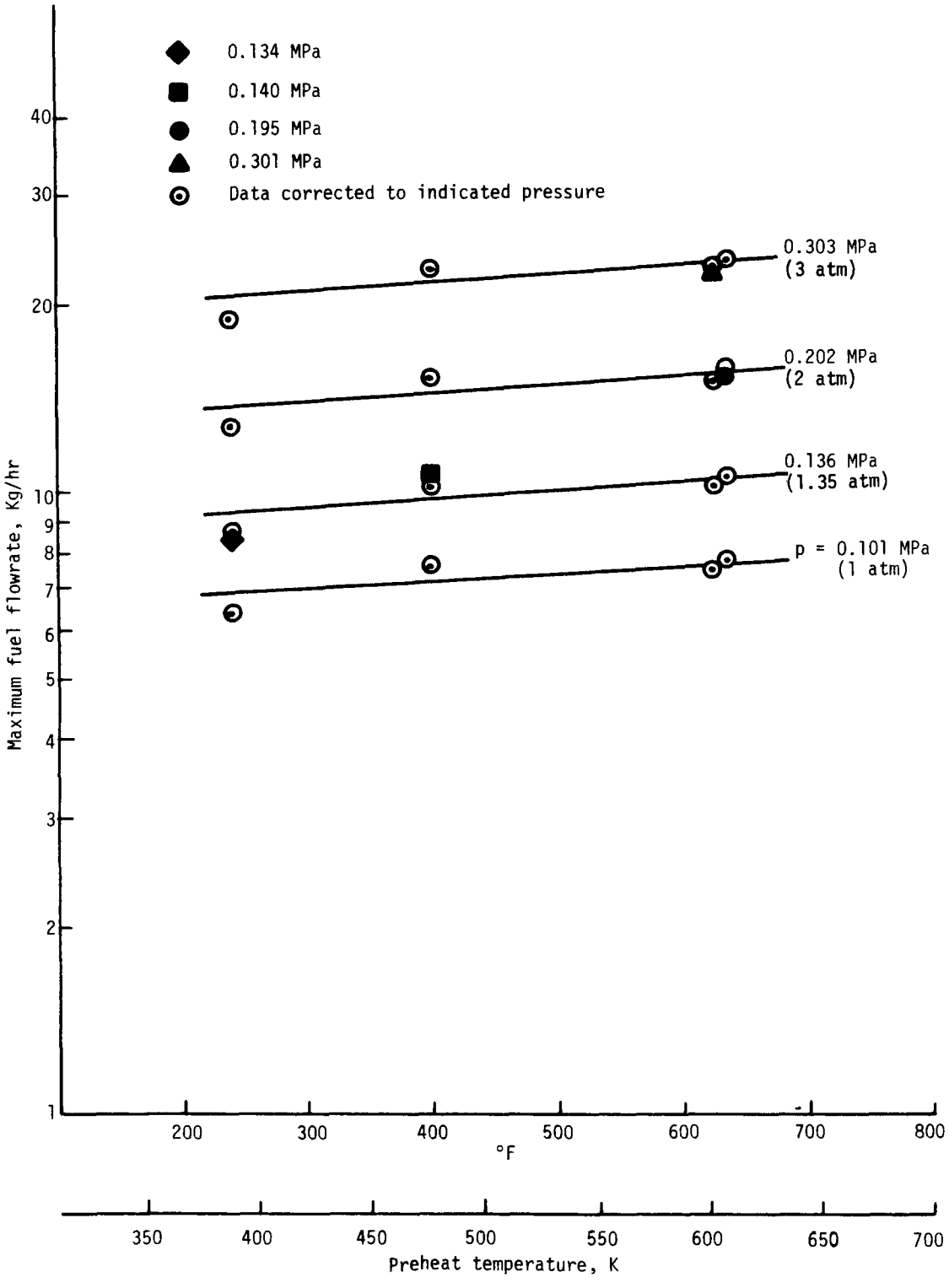

Figure 8-19. Blowout performance -- catalyst A-041, T_{BED} = 1589 K (2400°F), natural gas and methane fuels.

TABLE 8-6. BLOWOUT DATA -- CATALYST A-041

Data Point	Bed Temp, K (°F)	Preheat Temp, K (°F)	Max. Fuel Flowrate Kg/hr (lbm/hr)	Pressure MPa (atm)
1	1588 (2400)	608 (635)	15.0 (33.0)	.195 (1.93)
2	1588 (2400)	478 (400)	10.5 (23.1)	.140 (1.39)
3	1588 (2400)	389 (240)	8.4 (18.5)	.134 (1.33)
4	1588 (2400)	603 (625)	22.2 (49.0)	.301 (2.98)

8-19 shows the resultant blowout curves, and also the experimental data for each pressure. Two things are shown on Figure 8-19:

- Blowout scales linearly with pressure ($\dot{m}_{fuel}_{max} = P_{atm} \times \dot{m}_{fuel}_{max}_{1\ atm}$)
- Blowout for catalyst A-041 is approximately exponential in preheat temperature, although a relatively weak exponential factor is shown.

Operation of the catalyst was, of course, possible at any combination of preheat and fuel flowrate below the blowout curve. Figure 8-19 can be employed as a set of design curves for operation of catalyst A-041 under varying conditions.

The final minimum preheat test conducted at 1055 MJ/hr (10^6 Btu/hr) showed that it was also possible to operate outside of the blowout limit by reducing preheat temperature at a fixed heat release rate. (Previous blowout tests were conducted by increasing throughput at a fixed level of preheat.) The observed hysteresis may be of only nominal interest, however, in system applications.

The catalyst scaleup testing demonstrated that scaleup is a direct function of the bed frontal area for the graded cell configuration. Increased mass throughput capability (proportional to frontal area) and similar emission levels at all test conditions demonstrated this property.

8.5 EXTENSIVE EVALUATION TESTS

Duplicates of selected screening catalysts were constructed for extensive evaluation testing. These tests included investigation of the conversion of fuel-bound nitrogen to nitrogen oxide and the effects of high pressure operation on combustion characteristics. Both have implications in system development where fuels will contain certain quantities of bound nitrogen and higher pressure operation is required (as in turbine applications). The objectives of extensive evaluation were:

1. Demonstration of fuel nitrogen conversion characteristics for catalytic combustion systems
2. Development of operating constraints for catalytic combustors in pressurized applications

As shown in Table 8-1, test models A-036 and A-037 were constructed for additional extensive evaluation. Catalyst A-030 had previously provided some fuel-lean nitrogen conversion data, which is discussed below.

8.5.1 Fuel Nitrogen Tests

Fuel nitrogen tests were conducted with natural gas. Ammonia (NH_3) was added in known quantities to simulate fuels of varying nitrogen content. Exhaust gas analyses for nitrogen oxides (NO_x) by chemiluminescent analyzer and for ammonia (NH_3) and cyanide (HCN) by specific ion electrode were performed routinely. Ionic solutions were obtained by bubbling gas samples through the impinger train shown in Figure 8-20.

8.5.1.1 Acurex Co_2O_3 (A-030)

Following high temperature screening, fuel nitrogen extensive evaluation of the Co_2O_3 catalyst was conducted. The test points achieved were all under fuel-lean operation, with and without ammonia (NH_3) as the fuel dopant. The catalyst nitrogen conversion characteristics were investigated at the following dopant rates:

- 5000 ppm NH_3 (ppm of fuel) at nominal space velocities of 40,000, 150,000, and 250,000 per hour and 1700K, 1811K, and 1922K bed temperatures

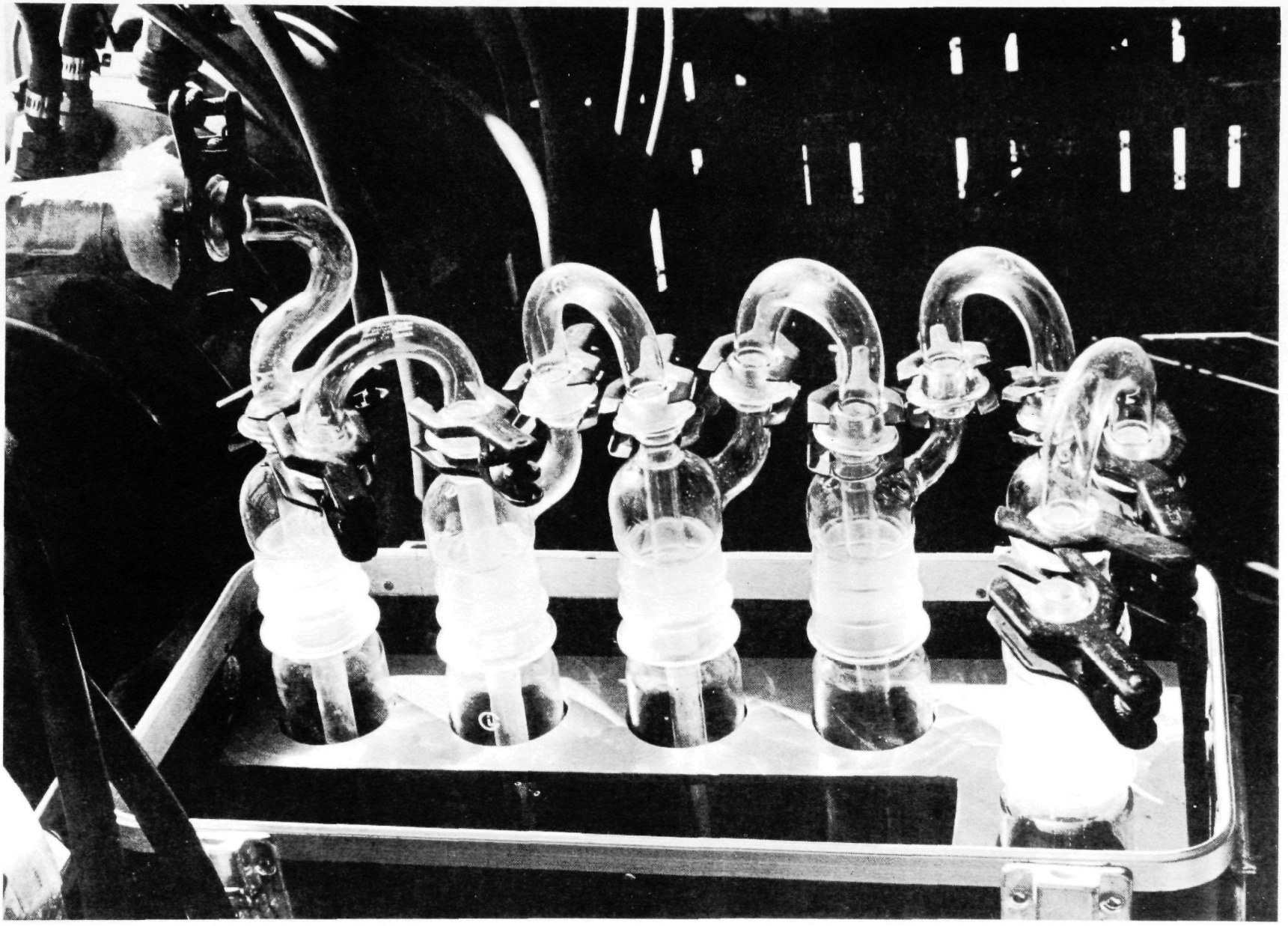

Figure 8-20. Impinger bottle gas sampling system.

- 2500 ppm NH_3 at 250,000 hr^{-1} space velocity and 1700K, 1811K, and 1922K bed temperatures

The fuel-lean test results are shown in Figures 8-21 and 8-22 as measured NO_x and percent of NH_3 converted to NO_x. The percentage of NH_3 converted to NO_x in the combustion process is shown to increase significantly with throughput (space velocity), with dopant concentration, and slightly with bed temperature. Restated, low NO_x emissions under fuel-lean combustion were favored by low throughput rates.

8.5.1.2 Acurex NiO/Pt (A-036)

A nickel oxide/platinum catalyst was prepared at Acurex and tested over a range of stoichiometries from 55 to 200 percent theoretical air. Space velocity was held constant at 100,000 per hour and bed temperature was nominally 1589K. Fuel dopant concentration ranged from 2500 to 10,000 ppmv NH_3 in the fuel.

A summary of test model A-036 data is provided in Table B-24. Several points in the data should be clarified.

1. Early thermocouple failures required optical pyrometer readings of bed temperature. The bed emissivity was assumed to be 0.6.
2. Variations in NO readings with time were noted at the baseline 5000 ppm NH_3 dopant rates in some circumstances. The variations were traced to low flowrate measurement problems. Larger dopant rates were then used to obtain steady readings.
3. Test points 1012-11 and 1012-12 were obtained when the bed was not fully active (only the front two segments were active). The NH_3 conversion data varies significantly from earlier established trends.

The data of Table B-24 is plotted in Figure 8-23 as the percentage of the incoming NH_3 converted to NH_3, HCN, and NO. The NH_3 conversion to NO increased from zero under very fuel-rich conditions to better than 90 percent on the fuel-lean side. NH_3 conversion to HCN showed the opposite trend -- high under rich conditions and decreasing to zero on the lean side.

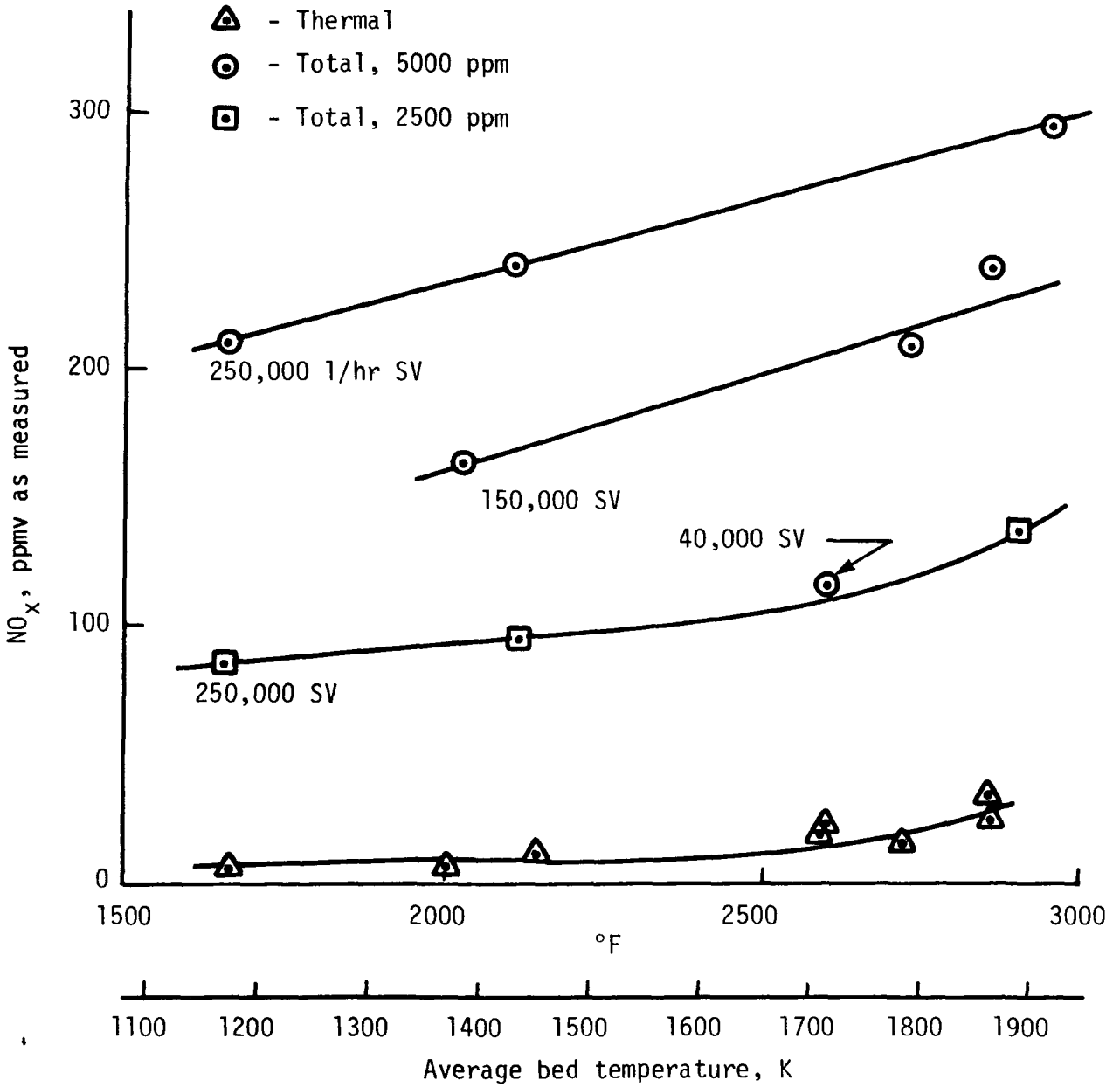

Figure 8-21. NO_x as measured, catalyst A-030, natural gas doped with ammonia.

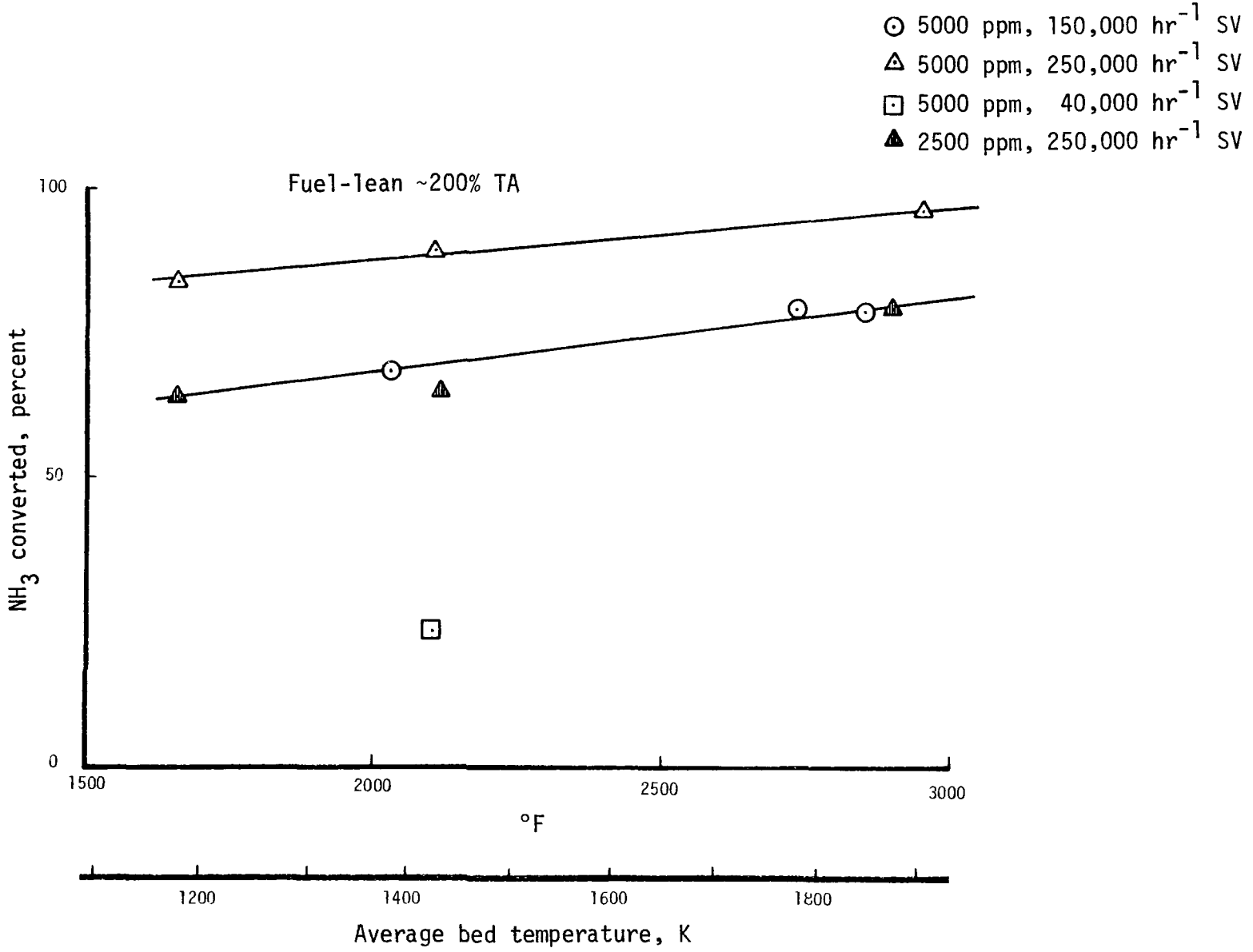

Figure 8-22. Percentage of NH_3 converted to NO_x, catalyst A-030, natural gas doped with ammonia.

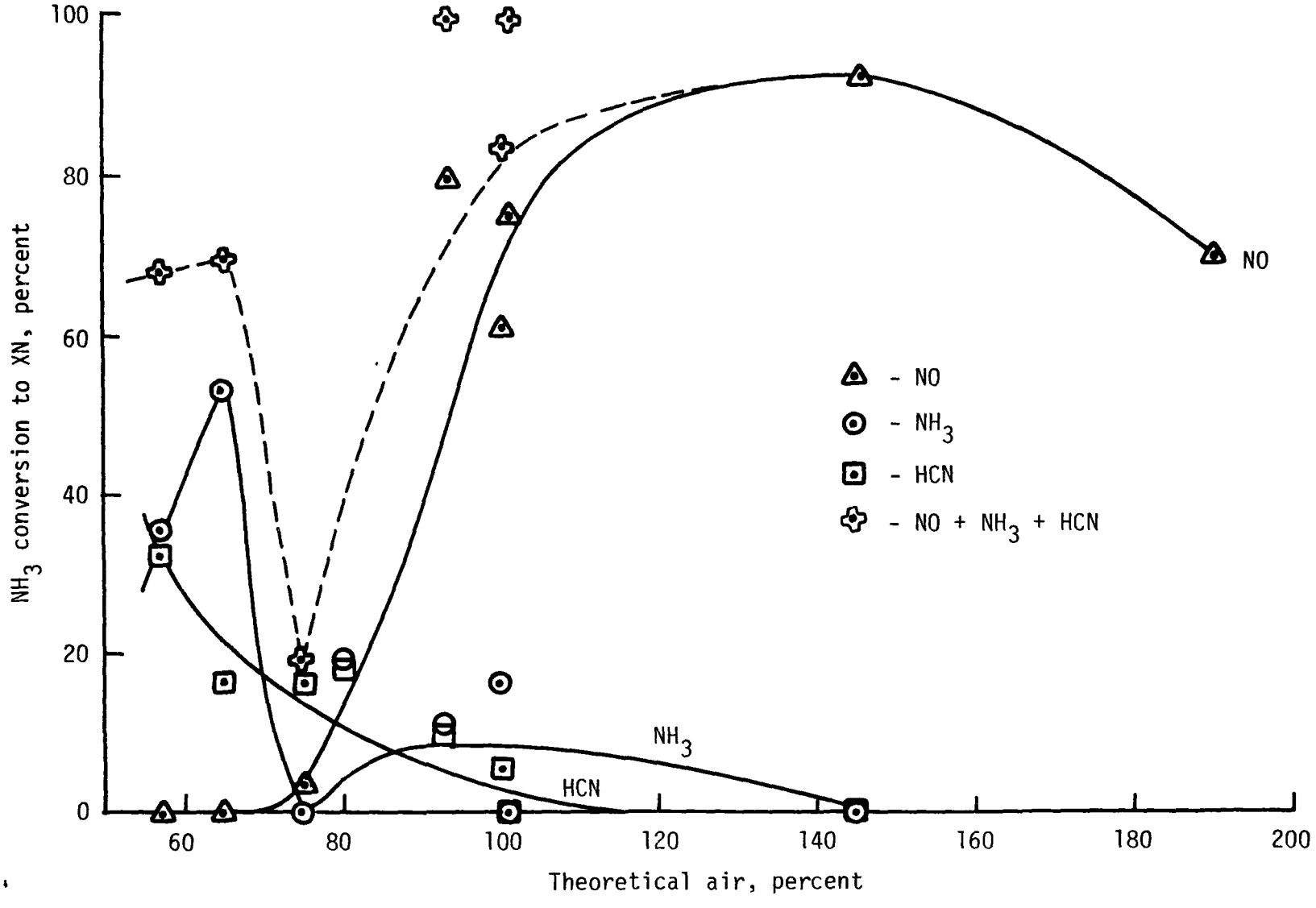

Figure 8-23. NH_3 conversion characteristics, catalyst A-036, natural gas doped with ammonia.

Unconverted ammonia was highest below 70 percent theoretical air and decreased to low levels under lean combustion.

The total of these three curves (dashed line and cross symbols) is considered to represent all NO_x precursor species for the NiO/Pt catalytic combustor. A distinct minimum occurs between 70 and 80 percent theoretical air, where only 20 percent of the fuel nitrogen is converted to NO_x precursors.

The partially active bed condition mentioned earlier is also of interest. The minimum amount of surface reactions occurring with the small cell segment not fully reactive showed a conversion of NH_3 to NO of 100 percent. It is therefore suggested that the catalytic surface reactions play a dominant role in minimizing NO_x formation under fuel-rich conditions. It should be noted that significant amounts of H_2 were measured by gas chromatography for all rich combustion conditions.

The low fuel nitrogen conversion measured at 70 to 80 percent theoretical air has important system implications. Combustors which could operate fuel-rich, possibly in a two-stage arrangement with secondary air injection, have potential for very low fuel nitrogen conversions to NO_x.

8.5.1.3 Acurex Co_2O_3/Pt (A-037)

A cobalt oxide/platinum extensive evaluation catalyst was tested for fuel nitrogen conversion and pressure operation, as shown in Table B-25. No surface area measurements were performed. Natural gas was used as the fuel and doped with 1 to 2 percent of ammonia.

The fuel nitrogen conversion data is summarized in Table B-25 and Figure 8-24. The ammonia conversion to nitric oxide provided the same curve as the previous nickel oxide/platinum catalyst (A-036). Differences in the HCN and NH_3 species measured, however, resulted in lower total NO_x precursor ($NO + NH_3 + HCN$) levels under fuel-rich conditions. The minimum occurred at a lower value of theoretical air (60 percent) than that of the previous nickel oxide catalyst (75 percent), and the conversion remained low over a much broader range of theoretical air. The cobalt oxide catalyst could thus be operated fuel-rich without dilution to achieve low conversion of fuel-bound nitrogen to nitrogen oxides.

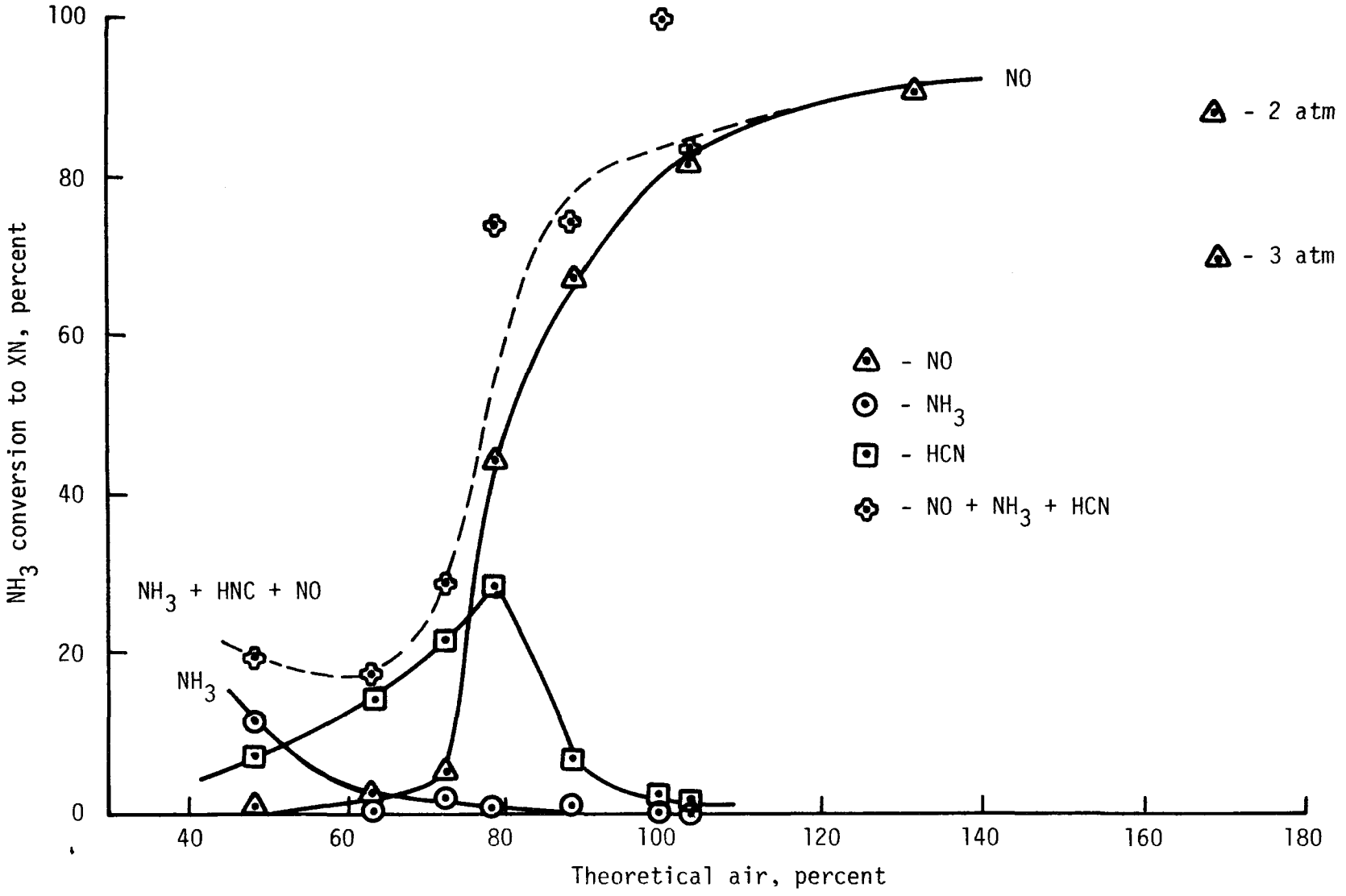

Figure 8-24. NH_3 conversion characteristics, catalyst A-037, natural gas doped with ammonia.

The testing included one partially active bed condition at 53 percent TA when the rear segment had blown out. As shown in previous test data for catalyst A-036, the loss of catalytic reactions during the blowout condition of the rear segment resulted in 100 percent conversion of fuel nitrogen to NO_x precursors.

Fuel nitrogen conversion at 0.202 MPa and 0.303 MPa (2 and 3 atmospheres) pressures is also shown in Figure 8-24 at 175 percent theoretical air. A trend to decrease nitrogen conversion with increasing pressure was found.

Attempts were made to perform blowout tests on the catalyst at both 0.101 MPa and 0.303 MPa pressures. Blowout was not reached at either pressure at the fuel flow limit of the test facility in the screening configuration. At 0.101 MPa, a heat release of 480 MJ/hr (455,000 Btu/hr) was achieved for a volumetric heat release rate of over 7.54×10^6 J/hr-Pa-m^3 (20.5 million Btu/hr-atm-ft^3). At 0.303 MPa, the results were 434.7 MJ/hr (412,000 Btu/hr) and 3.17×10^6 J/hr-Pa-m^3 (8.6 million Btu/hr-atm-ft^3).

Based on the results of the fuel nitrogen studies, a data correlation for fuel nitrogen conversion to NO_x under fuel-lean conditions was developed. The data included both Acurex test results and similar results reported in the literature. These included:

- Acurex data on a platinum catalyst (A-019). The fuel used was natural gas and methane doped with ammonia.
- Acurex data on a nickel oxide/platinum catalyst (A-036). The fuel was natural gas doped with ammonia.
- Acurex data on two cobalt oxide/platinum catalysts (A-030 and A-037). The fuel was natural gas doped with ammonia.
- NASA Lewis Research Center data (Reference 8-2), consisting of two segments of Johnson Matthey metal monolith, the first using platinum and the second palladium. The fuel was No. 2 diesel with 135 ppm by weight of nitrogen.
- Engelhard Industries data (Reference 8-3). No information was given on the catalyst type; the fuels used were ammonia-doped propane and No. 2 oil with 0.94 weight percent nitrogen as pyridine.

The data was correlated assuming that only space velocity, bed temperature, nitrogen concentration in the fuel, and pressure are significant variables. The correlation equation assumed was of the form:

$$\% \text{ conv} = A\ (SV)^B\ (T_{BED})^C\ (K_o)^D\ (p)^E\ .$$

Table B-26 lists the lean data used in the correlation procedure. Figure 8-25 shows the results of the analysis for $A = 1.152 \times 10^{-5}$, $B = 0.7$, $C = 1.5$, $D = 0.17$, and $E = 0.8$. Considerable scatter from the correlation is noted. Neither catalyst type (precious or base metal) or stoichiometry have been included in the correlation and may be important parameters in improving the correlation.

On the basis of this analysis, it appears that high conversion of fuel nitrogen to NO_x is to be expected in lean combustion unless space velocity, bed temperature, and pressure are all minimized.

8.5.2 High Pressure Tests

The results of high pressure testing of graded cell catalysts have been discussed in preceding sections. They can be summarized as:

1. Catalyst throughput capabilities scale linearly with pressure. Design criteria for mass throughput for variable pressure and preheat were developed for catalyst A-041.
2. Limited data on catalyst A-037 showed a slight decrease in fuel nitrogen conversion to NO_x with pressure increases to 0.303×10^6 Pa (3 atm).

The latter result is not consistent with the results of the lean-combustion, fuel nitrogen conversion correlation of Figure 8-25 where increased pressure was found to increase conversion. Both additional experimental data and refinement of the data correlation are required to resolve this inconsistency. Additional high pressure fuel nitrogen conversion is reported in Section 9 under system testing.

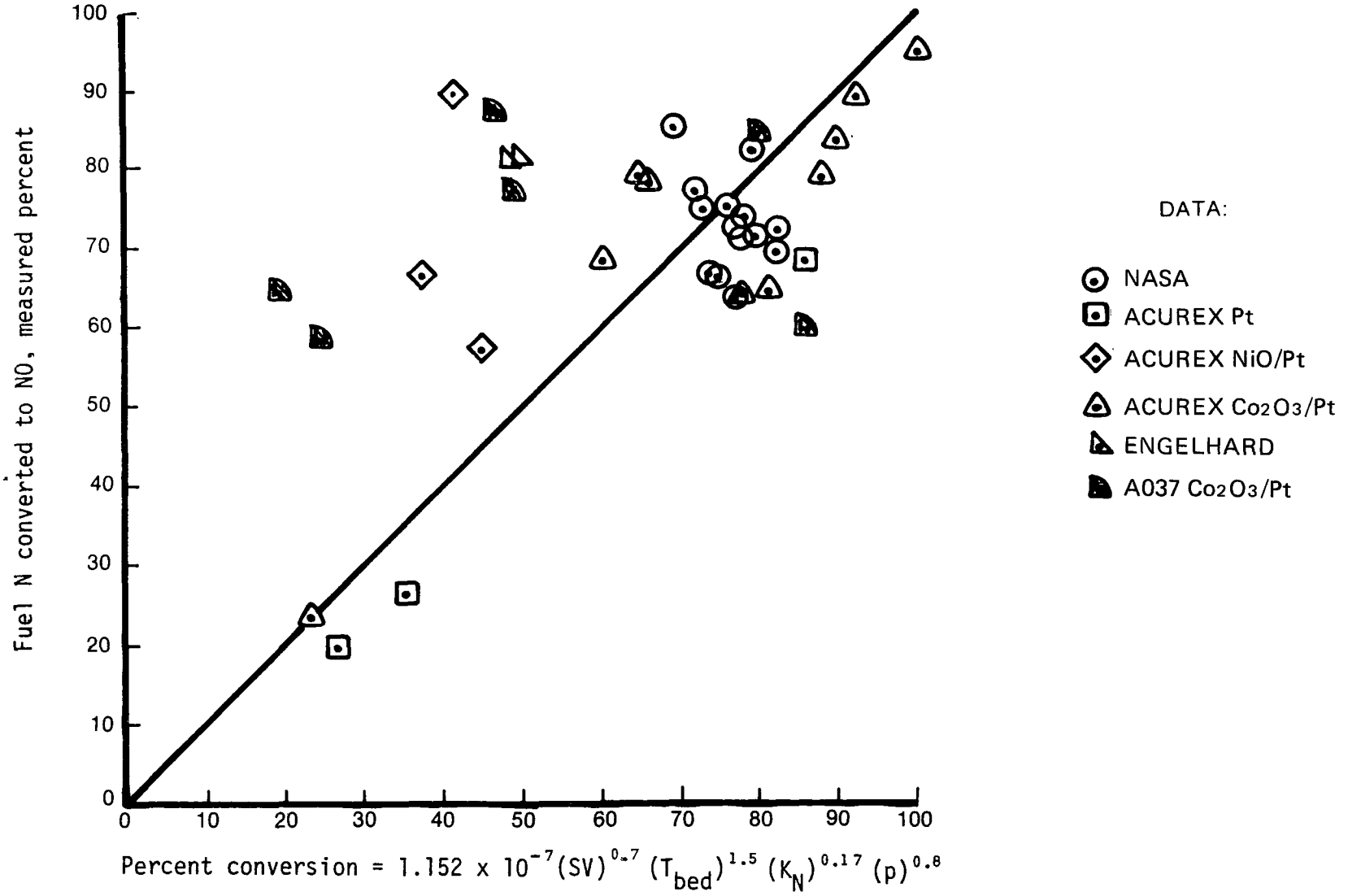

Figure 8-25. Lean data correlation: conversion of fuel nitrogen to NO_x.

8.6 CONCLUSIONS

Graded cell catalyst screening tests have identified many important performance parameters for different catalyst types in the graded cell configuration. Specifically, these parameters include mass throughput and heat release capabilities, emissions under varying operating conditions, lightoff requirements, and limited lifetime capabilities. Based on this data, it is possible to estimate catalyst size, length, temperature, and operational constraints for specific applications. Further work is required, however, to develop optimum catalyst formulation for a given application, as well as to develop long-life catalyst systems.

The maximum combustion throughput characteristics of graded cell catalyst A-040 have been shown to be directly proportional to bed frontal area and directly proportional to pressure at a given level of preheat. Further, the maximum throughput was found to increase exponentially with preheat. These results allow sizing of the catalyst bed for specific system applications. It is certain that other catalysts of different types will have different performance levels, but it is expected that the scaling of mass throughput with frontal area, pressure, and preheat will follow the same relationships. The maximum throughput levels of many catalyst types have been identified in the graded cell tests and variations with pressure, size, and preheat can be estimated.

The catalyst size for an application with given preheat, pressure, and throughput constraints can be generated. The final design is also impacted by the catalyst emissions characteristics for the given operating conditions, operational transients, and fuel properties. The graded cell tests discussed in this section have systematically identified catalyst emissions (primarily nitric oxides, carbon monoxide, and hydrocarbons) over wide ranges of throughput, preheat, pressure, bed temperature, and catalyst type. Emissions with varying quantities of fuel-bound nitrogen have also been evaluated. Clearly, catalyst specification for high efficiency, low emission systems must (as a minimum) include both catalyst sizing and emission level considerations.

The catalyst lightoff temperature has been shown to increase rapidly during early use, and then to remain fairly constant under subsequent

startups. Since catalyst lightoff temperature varies with catalyst type, catalyst surface area and dispersion, and fuel type, as well as with operational time, it remains difficult to predict. The use of non-catalytic lightoff aids in practical combustion systems should be pursued, since low temperature catalyst lightoff is not required for good high temperature steady state performance.

Optimum catalyst formulation and increased catalyst life are two additional factors requiring further work. Based on the results of the graded cell testing, it appears that noble metal catalysts on alumina supports are capable of operation at bed temperatures to 1589K (2400°F), but degrade rapidly at temperatures above 1589K. Metal oxide catalysts placed on metal oxide supports exhibit material incompatibilities, causing excessive thermal shock and subsequent support failure. No apparent degradation in metal oxide catalyst performance occurs, however. Thus, it appears that monolithic systems which include the active metal oxide in the support formulation would improve both catalyst formulation and catalyst life.

The following section (Section 9) describes system application studies for the graded cell and other catalyst configurations where graded cell data were used to predict system performance.

REFERENCES

8-1. Kelly, J. T. et al., "Development and Application of the PROF-HET Catalytic Combustor Code," presented at the 1977 Fall Meeting of the Western States Section of the Combustion Institute, Paper No. 77-33, October 1977.

8-2. Anderson, D. N., "Performance and Emissions of a Catalytic Reactor with Propane, Diesel, and Jet A Fuels," NASA TM-73786, October 1977.

8-3. Carrubba, R. V. et al., "The Proceedings of the NO_x Control Technology Seminar," EPRI SR-39, February 1976.

SECTION 9

COMBUSTION SYSTEM CONFIGURATION TESTS

9.1 GENERAL CONSIDERATIONS

The design criteria generated for graded cell catalyst configurations were used in the specification of small scale systems incorporating heat extraction techniques. Three system concepts were tested using a variety of test fuels and catalyst types. Additional system design criteria were then generated for advanced system development.

Two of the small scale system configurations utilized the graded cell catalyst directly. The third was based on a cylindrical catalyst geometry derived from catalyst preparation information obtained from the graded cell system. The three systems are:

1. The two-stage combustor, utilizing rich first-stage catalytic combustion with secondary air injection and interstage cooling
2. The gas turbine system, utilizing high excess air levels to maintain low combustor operating temperatures
3. The radiative catalyst/watertube system, utilizing intrabed heat extraction by watertubes (cylindrical catalyst support)

The design details and experimental results for the three systems are presented in the following sections. Appendix C provides supplementary data.

9.2 TWO-STAGE COMBUSTOR

The two-stage catalytic combustor appears attractive for two reasons. First, it allows control of bed temperatures to those compatible with the support material without large excess air requirements. Second, the first stage can be operated fuel-rich, which has been shown (in extensive evaluation

testing) to be advantageous for reduced conversion of fuel nitrogen to nitrogen oxides. A two-stage combustor was designed and constructed to demonstrate these concepts.

The two-stage combustor is shown schematically in Figure 9-1. A fuel-rich mixture is introduced into the primary stage which contains a graded cell catalyst bed. The fuel is partially combusted, and the energy released is removed by an interstage heat exchanger. Sufficient secondary air is then injected into the combustion products to complete combustion of the remaining fuel in the second stage. The full system combustor would also include a second heat exchanger to remove the combustion energy released in the second stage.

9.2.1 System Design and Fabrication

The combustor design had to meet several constraints in order to interface with the Acurex test facility. A design was sought that would utilize available test section hardware. Combustor operating conditions were selected as:

- Overall heat release rate -- 211 MJ/hr (200,000 Btu/hr) and
- Bed temperature limit -- 1811K (2800°F).

In order to define the temperature control requirements of the inter-bed heat exchanger, the design curve of Figure 9-2 was constructed. This curve identifies the resulting inlet temperature to the second stage catalyst for a given heat exchanger outlet temperature and secondary air injection temperature. Two regimes are identified:

1. Lightoff, where 811K to 922K (1000°F to 1200°F) temperatures are required, and
2. Steady state operation where 589K to 811K (600°F to 1000°F) preheat is desired to limit second stage flame temperatures.

In order to control the second stage inlet temperature between the two regimes, a variable heat exchanger concept was developed. The heat exchanger was constructed with two coils. The primary coil provided

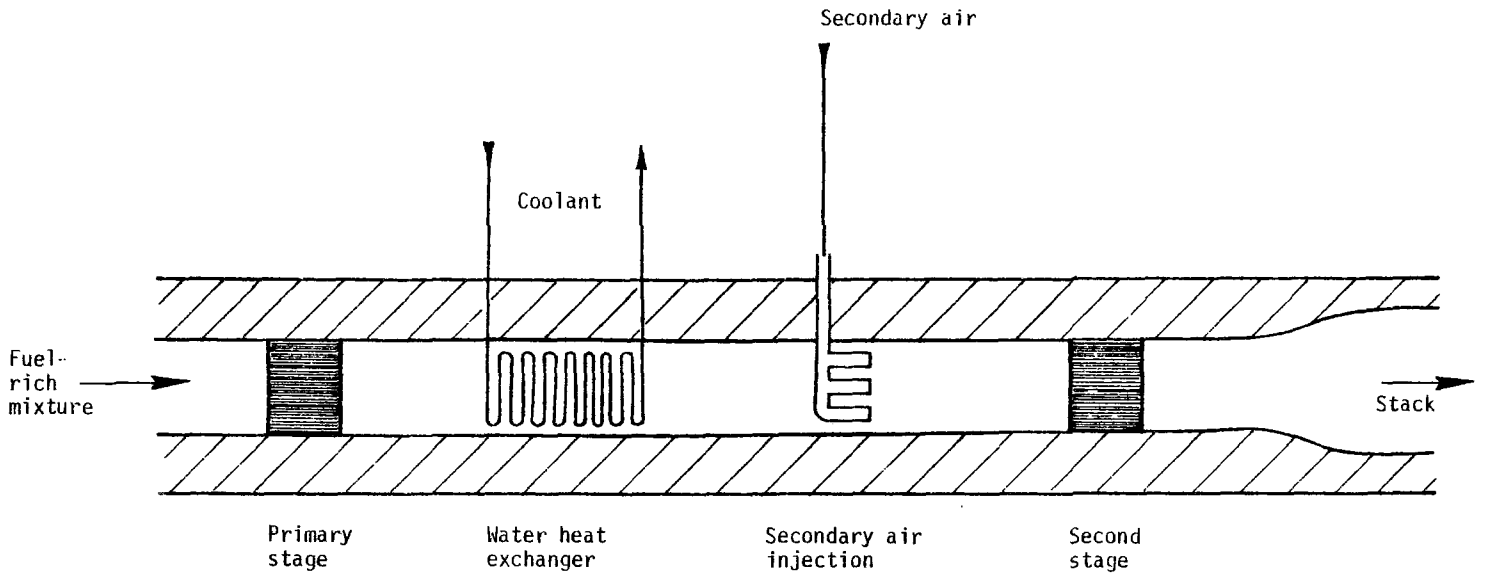

Figure 9-1. Two stage catalytic combustor concept.

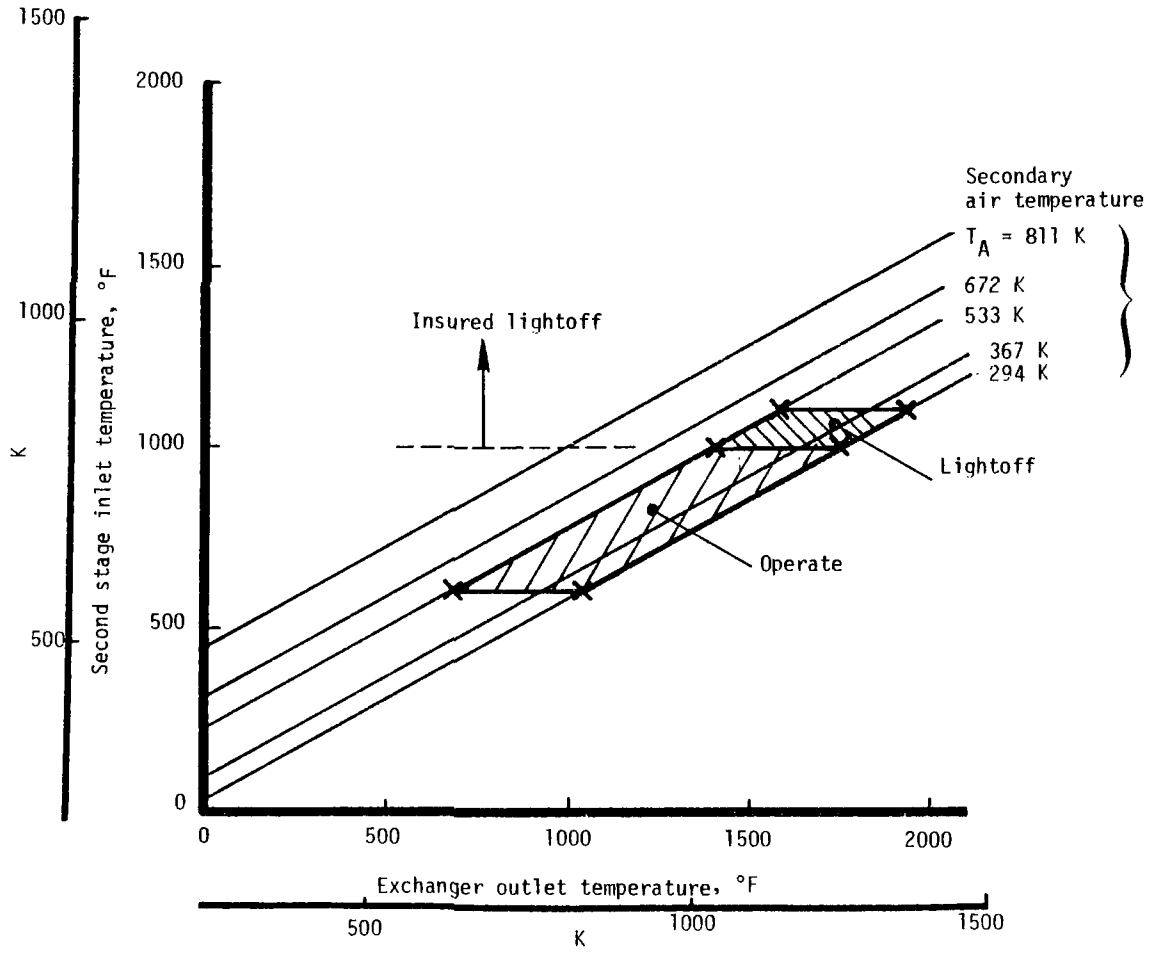

Figure 9-2. Two stage heat exchanger design envelope.

sufficient cooling to control lightoff while a secondary coil could be turned on to provide additional cooling for steady state operation. The heat exchanger would thus provide a 1033K to 1256K (1400°F to 1800°F) outlet temperature. The coils were constructed of AISI 310 stainless steel to resist corrosion in the high temperature reducing environment.

Secondary air injection involved an injector design that would provide an even distribution across the duct, promote rapid mixing, and avoid flow separation regions that could result in flame-holding. Seven conical nozzles were designed to inject air axially with the first-stage products at ambient temperature. Stainless steel (310) was again selected for the high temperature environment.

A configuration drawing of the final design is shown in Figure 9-3. Three available test section spools were utilized, resulting in an overall combustor length of 1.17 m (46 inches). All sections were refractory lined to prevent heat losses. Cooling water and secondary air were supplied from available sources. Photographs of constructed hardware are shown in Figures 9-4 and 9-5.

9.2.2 Test Results

The two-stage combustor was tested with natural gas at 0.101 MPa and 0.202 MPa pressures (1 and 2 atmospheres). Lightoff and steady state operation presented no unusual control problems. The combustor was tested at an overall stoichiometry varying from 70 to 150 percent theoretical air at a nominal fuel flow rate equivalent to 211 MJ/hr (200,000 Btu/hr) heat release rate. The first-stage stoichiometry was varied from 40 to 70 percent theoretical air. Ammonia was added to the natural gas fuel at a rate of 0.2 to 0.4 percent. The test data is summarized in Tables C-1 and C-2.

Bed temperatures ranged from 1256K to 1660K depending on theoretical air for a relatively constant preheat of 617K (650°F). The energy extracted in the interstage heat exchanger represents 50 to 60 percent of the combustion energy generated in the first stage.

The results of the fuel nitrogen conversion data are shown in Figure 9-6 as a function of overall combustor stoichiometry. When operating above

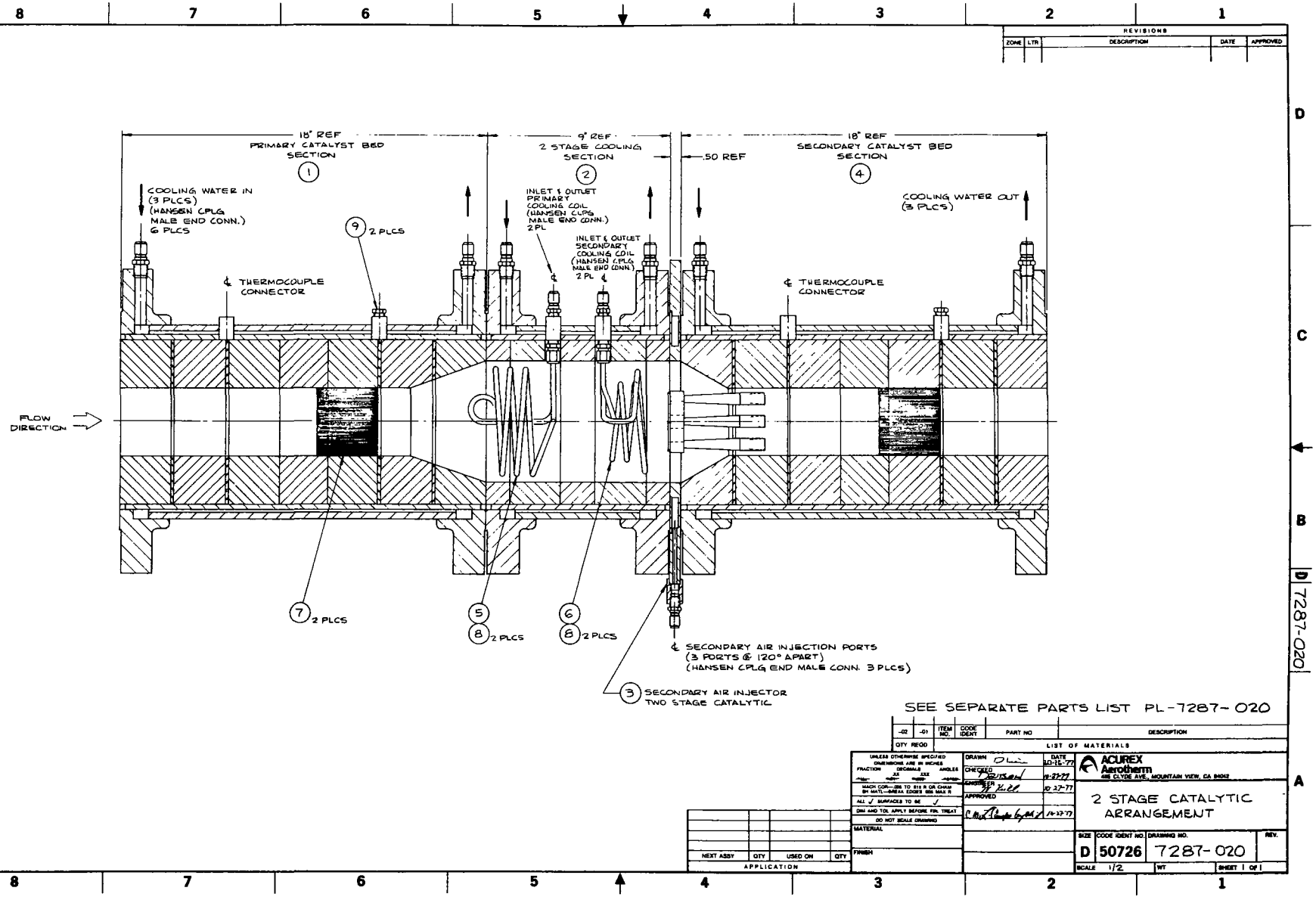

Figure 9-3. Two stage catalytic arrangement.

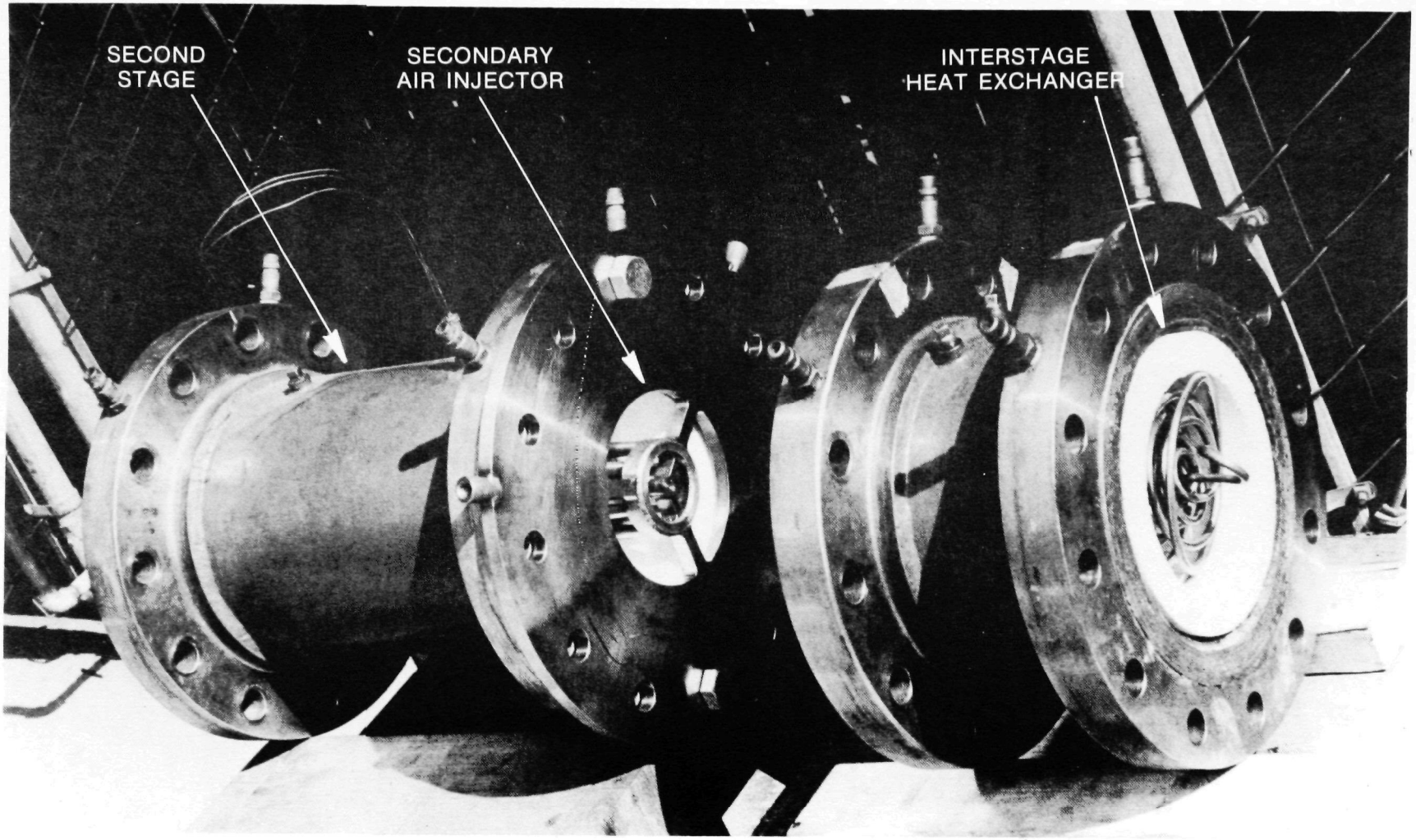

Figure 9-4. Two stage combustor assembly.

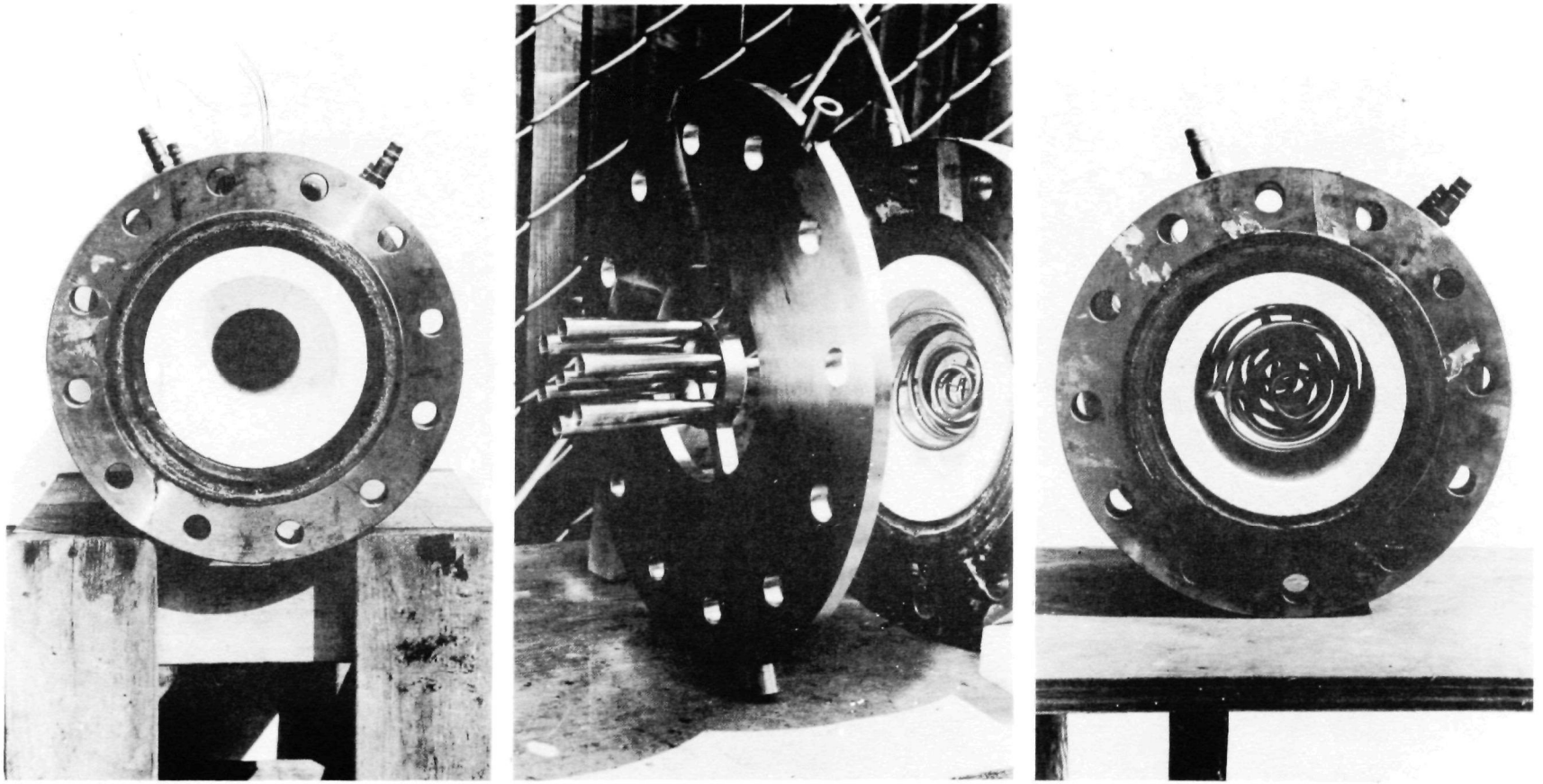

Figure 9-5. Two stage combustor details.

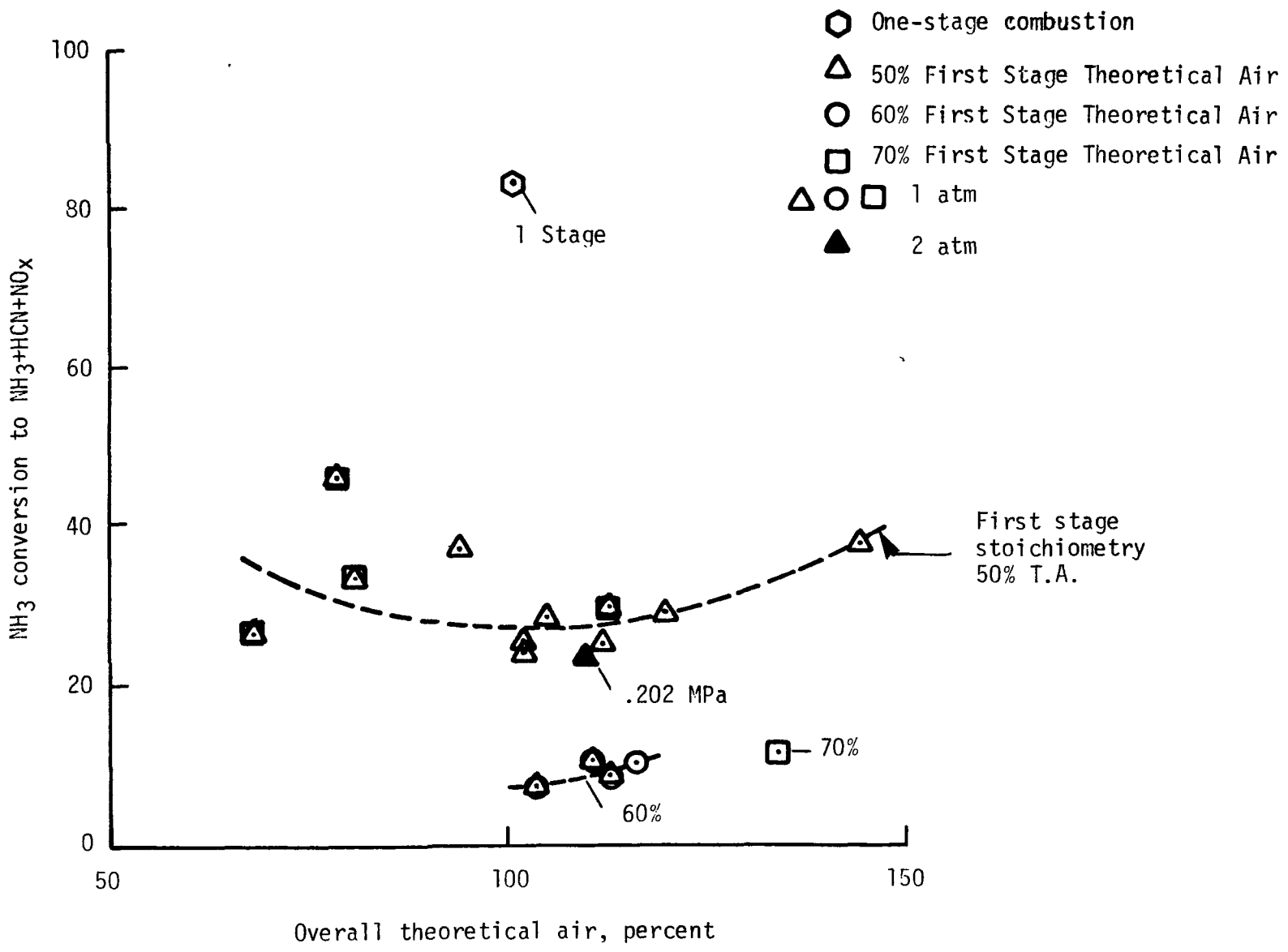

Figure 9-6. Two stage combustor fuel nitrogen conversion.

100 percent theoretical air, only nitrogen oxides are normally present. Under overall fuel-rich conditions, fractions of ammonia and cyanide were also present. These results are consistent with fuel nitrogen data obtained on the single cobalt oxide catalyst (Model A-037, Figure 8-24). The data of Figure 9-6 show a nominal 30 percent conversion rate of fuel nitrogen to NO_x precursors with a value of approximately 27 percent near overall stoichiometric conditions. A slight decrease in conversion was noted at 0.202 MPa pressures.

It appears as though the primary stage catalyst had slowly degraded with time, evidenced by the variations in bed temperatures and decreases in interstage heat extraction of Table C-2 at nearly constant stoichiometry and mass flowrate. Degradation may have resulted from either loss of catalyst activity during high temperature exposure or by the deposition of soot on the surface under fuel-rich conditions. Table C-2 also indicates decreasing emission levels of thermal NO_x with time. The decreased thermal NO_x emissions are generally accompanied by increased CO emissions, indicating that a reduction of NO_x in the presence of CO is occurring. There are three initially high values of thermal NO_x (102, 55, and 28 ppm) during operation of the system under overall rich conditions with very high CO levels which require further resolution.

The data shown in Figure 9-6 at approximately 10 percent conversion levels varied in test conditions from the other data in two respects:

1. The first stage was operated at higher values of theoretical air (60 and 70 percent) compared with 50 percent for the initial data
2. The first-stage catalyst had experienced some sooting by later test times when the data were taken, causing the catalyst to operate at lower temperatures with less complete combustion under the fuel-rich conditions.

The first-stage sooting of the cobalt catalyst proved to be a limiting factor in the test life of the system. The incomplete combustion occurring at the final test times is evident from the increasing measured carbon monoxide levels in Table C-2.

The demonstration of the two stage catalytic combustor showed a number of important results.

1. The two stage combustor is effective in controlling conversion of fuel nitrogen to nitrogen oxides under stoichiometric and fuel-lean conditions.
2. A slight decrease in nitrogen conversion was found at 0.202 MPa (2 atmospheres) pressure.
3. The variation of first stage stoichiometry may impact overall fuel nitrogen conversion.
4. First stage sooting of the cobalt oxide catalyst was a limiting factor in combustor operating life and decreased fuel conversion rate capabilities.

The identification of a catalyst suitable for first stage operation in the system is required to obtain additional data with varying first stage stoichiometry and at higher pressures.

9.3 MODEL GAS TURBINE COMBUSTOR

The gas turbine combustion system was selected for scaleup to a 1056 MJ/hr (10^6 Btu/hr) heat release rate. The graded cell catalyst was demonstrated to have the low preheat, high heat release, and pressure capabilities required for this application. A model combustor can, fuel injection system, and catalyst were prepared. Subsequent testing was performed at Acurex and Pratt and Whitney Aircraft (West Palm Beach, Florida) facilities.

9.3.1 System Design and Fabrication

The model gas turbine combustor was designed to interface with both Acurex and Pratt and Whitney test sections whose diameters are 0.22 m and 0.33 m (8 and 12 inches) respectively. The combustor can was selected as a nominal 0.14 m (5-inch) internal diameter. A fuel injection system was also required to provide both gaseous (natural gas and propane) and liquid (diesel and No. 2) fuels to the combustor. The fuel injection system had to provide a premixed, fully vaporized fuel/air mixture to the catalyst. A uniform mixture across the duct area with a minimum mixing length was also required.

Catalyst operating temperature was selected as 1367K (2000°F) with air preheat as high as 811K (1000°F), setting the material thermal requirements for the injector and can. The maximum heat release rate was to be 1056 MJ/hr at pressures up to 1.01 MPa (10 atmospheres). The combustor itself did not require pressure design since no differential would exist across its surfaces.

An assembly of the final design is shown in Figure 9-7 as interfaced with test sections for the two facilities. Both combustor and injector were constructed of stainless steel. The fabricated parts are shown in Figure 9-8 with a detail of the upstream face of the injector in Figure 9-9.

The fuel injector was a multiple conical tube type similar to a concept developed at NASA Lewis Research Center for automotive gas turbine applications. The incoming air enters the apex end of the cones at high velocity where the fuel is injected. The fuel mixes with the air stream as it expands through the cones and is injected into the combustor. Additional mixing occurs downstream of the injector exit plane. Large gaseous fuel tubes inject axially into the center of the cone inlet. Smaller fuel tubes inject the diesel fuel normal to the incoming air for vaporization and mixing. Multiple fuel ports were provided to satisfy facility interface requirements.

The graded cell catalyst used in the system is shown in Figure 9-8. Six segments of 0.0254 m (1.0 inch) length DuPont AA washcoated alumina Torvex were coated with platinum catalyst at Acurex. The six segments were two pieces of each of the standard 6.84, 5.13, and 3.42 cm cell sizes. The catalyst was instrumented with six type K thermocouples (chromel-alumel) and bonded together prior to testing. A backup catalyst was similarly constructed by Universal Oil Products Company.

9.3.2 Test Results

The model gas turbine combustor was first tested at Acurex with propane between 0.117 MPa and 0.345 MPa (1.16 to 3.42 atm) pressures. Additional testing was conducted at Pratt and Whitney Aircraft in West Palm Beach, Florida at pressures ranging from 0.299 MPa (2.96 atm) to 1.014 MPa (10.04 atm) with propane, No. 2 oil, and No. 2 oil doped with 0.5 weight percent nitrogen as pyridine (C_5H_5N).

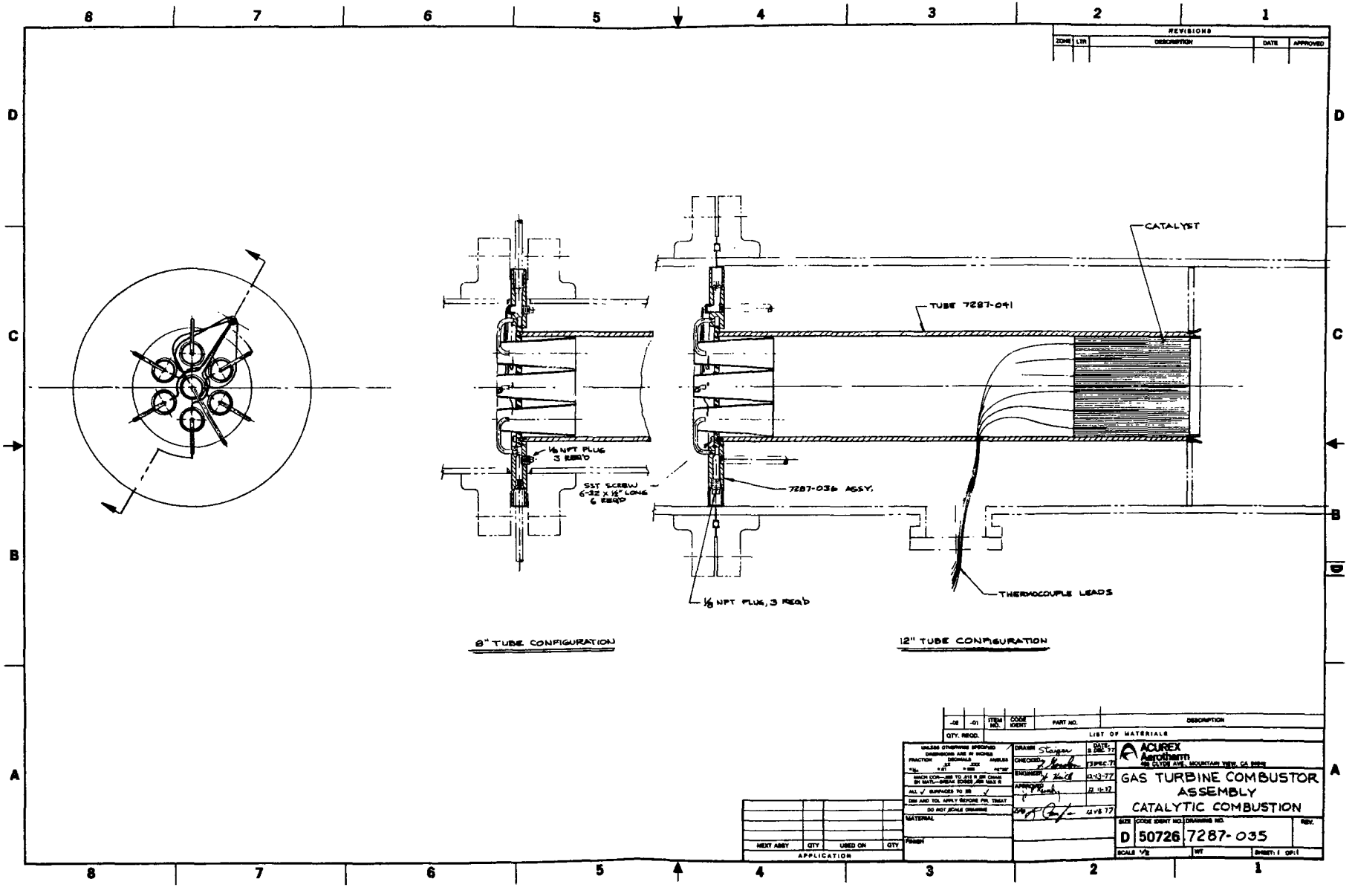

Figure 9-7. Gas turbine combustor assembly, catalytic combustion.

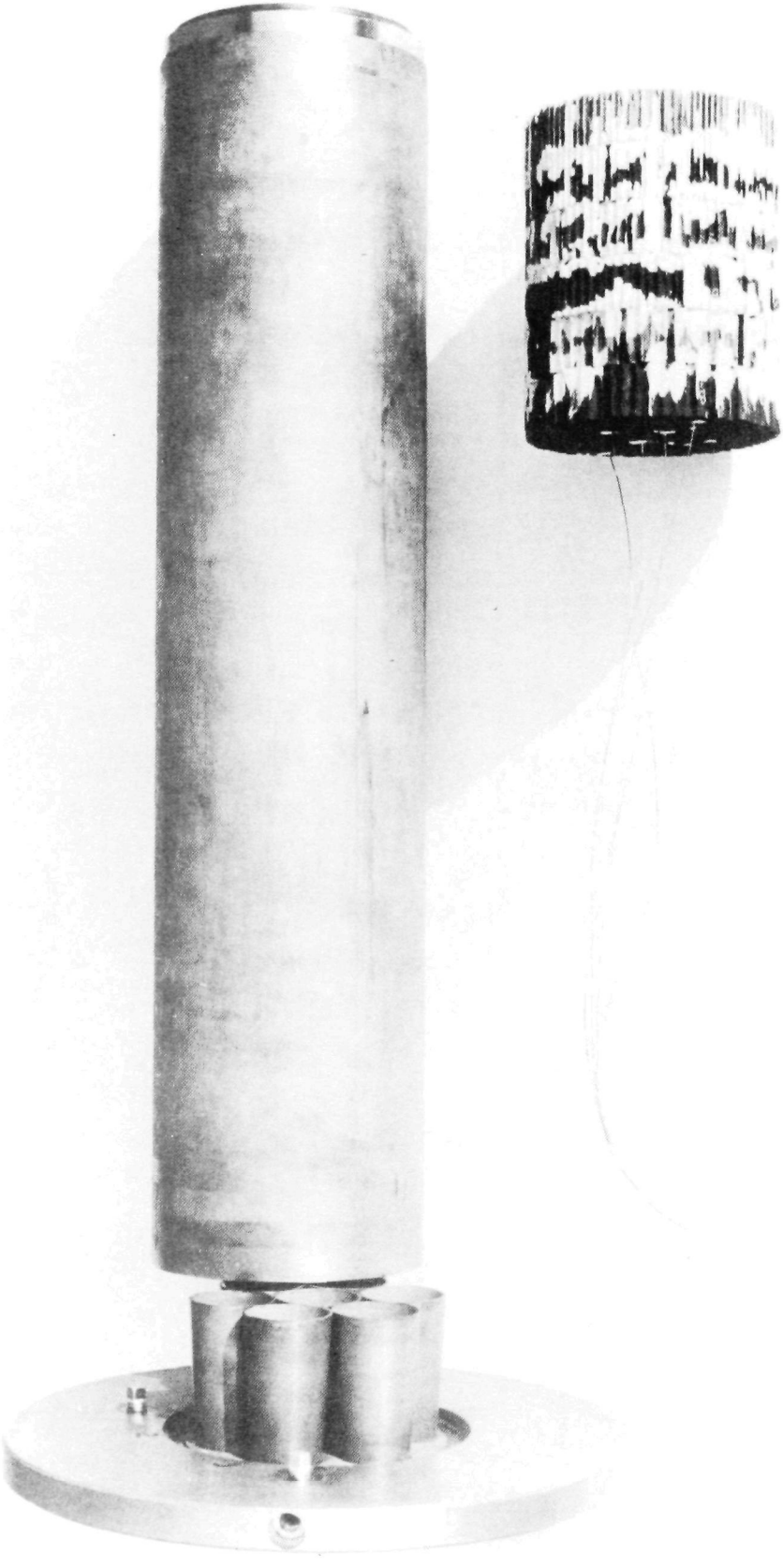

Figure 9-8. Model gas turbine combustor.

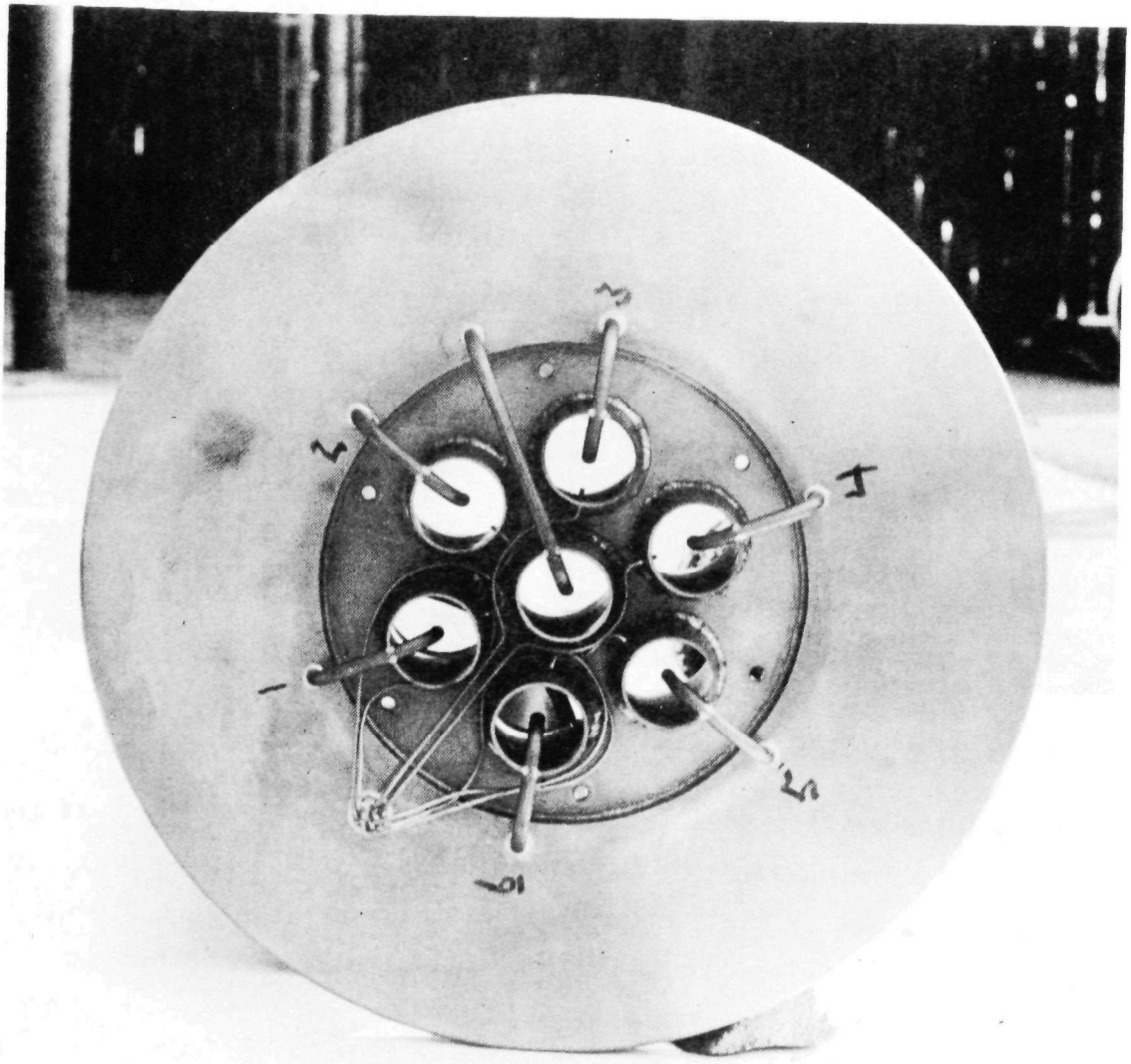

Figure 9-9. Gas turbine fuel injector assembly.

Lightoff with propane under fuel-lean conditions was found to occur repeatedly at a preheat of approximately 644K (700°F). The Acurex test points with propane are shown in Table C-3 for varying pressures. Heat release rates to 263.8 MJ/hr (250,000 Btu/hr) at approximately 1478K (2200°F) bed temperature were run as the nominal test conditions. No significant emissions of either carbon monoxide or oxides of nitrogen were obtained. The fuel injection system and catalyst performed well at the listed conditions.

The test data obtained at Pratt and Whitney Aircraft with propane, No. 2 oil, and No. 2 oil with 0.5 weight percent nitrogen are shown in Table C-3. Early propane test points were obtained with an Acurex catalyst. Later propane and all oil tests were conducted with the UOP catalyst. Heat release rates to 844 MJ/hr (800,000 Btu/hr) were achieved with low NO_x emissions for both propane and No. 2 oil. Some difficulty was encountered with flashback and flameholding on the fuel nozzles when running No. 2 oil. High CO and unburned hydrocarbon emissions resulted from operating at low bed temperatures (near the breakthrough limit) required to avoid flashback.

Tests run with pyridine-doped No. 2 fuel oil increased the NO_x emission levels to the values shown in Table C-3. These emission levels represent percentage conversions of fuel nitrogen to NO_x of 100, 61, and 55 percent for test pressures of 0.303, 0.505, and 0.707 MPa, respectively.

The results of the model gas turbine testing exhibited catalyst temperature and pressure operating conditions similar to those of current turbine combustors at steady state operation. High mass rates were achieved in a relatively small volume combustor. Overall pressure drop for the combustor and fuel injector were measured at less than one percent at 0.303 MPa (3 atmospheres) test pressure.

Close examination of the fuel injector hardware following testing indicated fabrication errors, resulting in nonuniform introduction of the diesel fuel at low inlet velocities relative to the air stream. This low liquid fuel velocity was responsible for the flashback and flameholding that occurred. The velocity mismatch was rectified prior to the next test series, although total uniformity in fuel distribution among the seven cones could not be achieved.

9.3.3 Advanced Graded Cell Concept Demonstration

A modification in the geometry of the graded cell catalyst was conceptualized, based on obtaining an equal number of transfer units in each segment of the catalyst bed. The result was a three-segment bed with 6.35×10^{-3}, 4.73×10^{-3}, and 1.80×10^{-3} m (0.250, 0.188, and 0.071 inch) cell sizes in 0.76, 0.038, and 0.019 m (3.0, 1.5 and 0.75 inch) lengths, respectively. A proprietary catalyst was applied to Corning zirconia spinel support by Universal Oil Products Company.

The advanced graded cell concept was developed for gas turbine applications (see Section 10.3). As shown in Figure 10-6, the concept included an initial large cell catalytic lightoff segment isolated from other elements by radiation shields. The concept as tested included only the graded cell catalyst and the upstream metal radiation shield. The catalyst was instrumented with six thermocouples and mounted in the model gas turbine can for testing. Figure 9-10 shows the catalyst, radiation screen, fuel injector, and combustor can of the turbine assembly.

Based on initial test results of the model turbine at Acurex and Pratt and Whitney Aircraft, design of the fuel injector was modified to increase local air and fuel velocities. Both gaseous and liquid fuel injection capabilities were retained.

The advanced graded cell catalyst was operated with natural gas at pressures between 0.117 and 0.824 MPa (1.16 to 8.16 atm) and with diesel fuel at 0.145 to 0.545 MPa (1.44 to 4.95 atm). All test points were taken under fuel-lean conditions. Ammonia was added to the natural gas at selected test points to determine fuel nitrogen conversion to NO_x characteristics with varying pressure.

A summary of the test data is shown in Table C-4. The first series of test points (0412-02 to -19) was conducted at a nominal 1422K (2100°F) bed temperature with ammonia added to the natural gas fuel in various concentrations. A decrease in ammonia converted to NO_x with pressure was observed. The results are shown graphically in Figure 9-11. These results are consistent with those obtained at Pratt and Whitney with pyridine-doped No. 2 oil between 0.101 and 0.707 MPa pressure. An increase in conversion

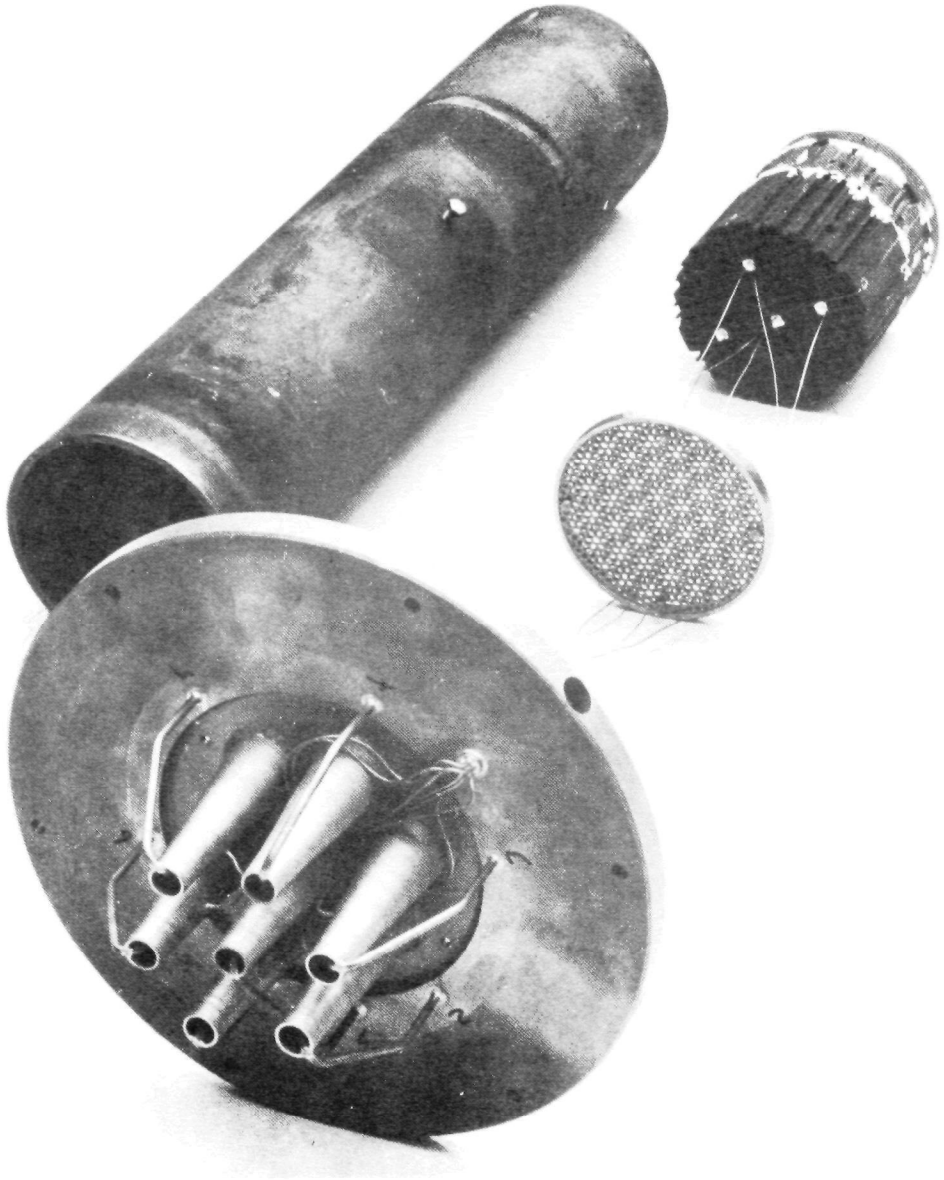

Figure 9-10. Advanced graded cell/model gas turbine combustor assembly.

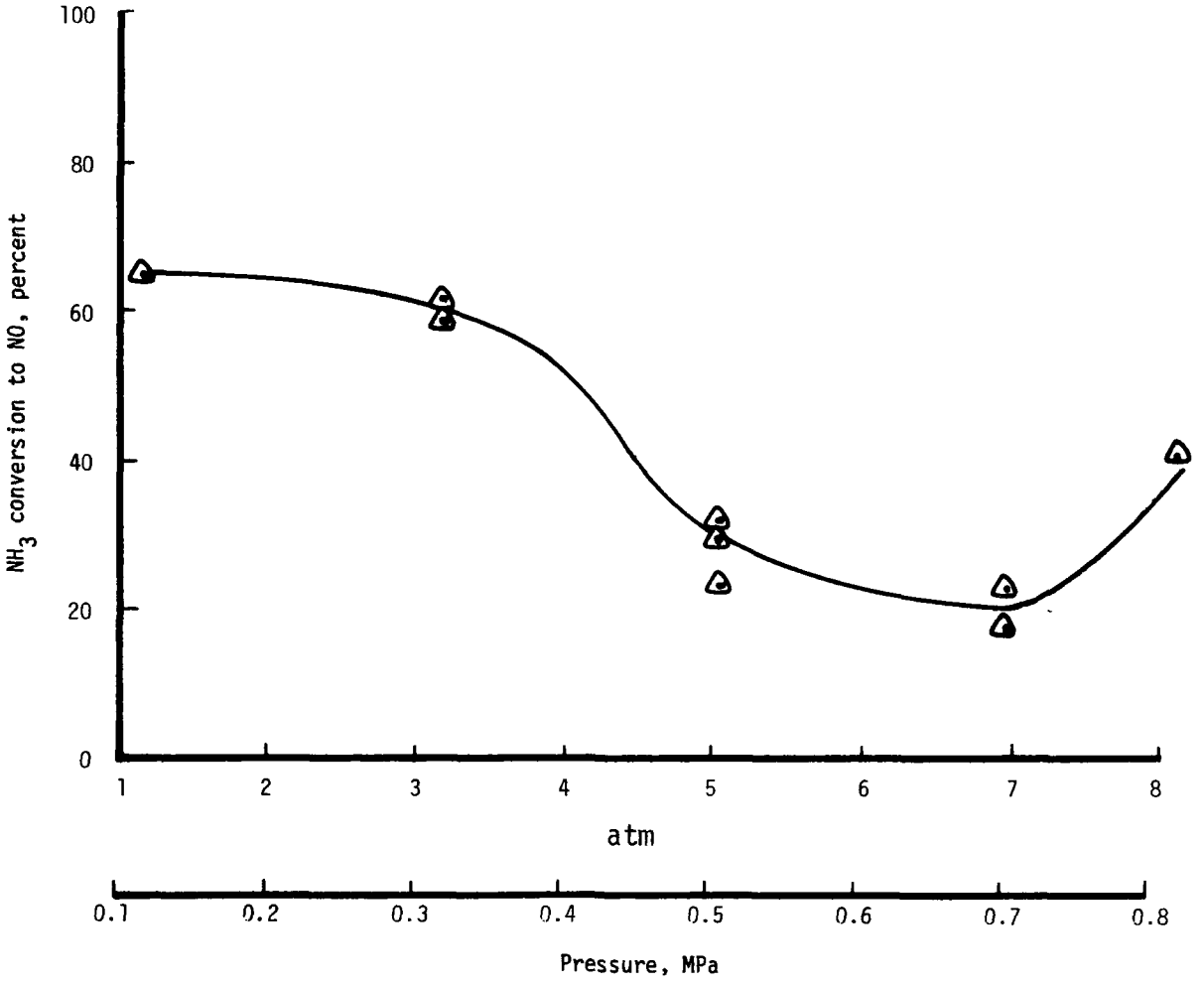

Figure 9-11. Advanced graded cell fuel nitrogen conversion.

at 0.824 MPa pressure was obtained. Additional data at these elevated pressures is required to explain the trend noted. Changes in fuel nitrogen concentration produced only small changes in nitrogen conversion at elevated pressures.

The second series of test points (0413-02 to -10) was conducted to investigate maximum catalyst throughput at 0.303 MPa pressure, 1422K bed temperature, and 561K (550°F) preheat temperature. At space velocities near 200,000 per hour, the catalyst began to break through with increasing CO and unburned hydrocarbon emissions. Nitrogen oxide emissions remained at near zero levels throughout the test. Full blowout was not achieved as control of catalyst temperature during breakthrough produced difficulties in system control. The maximum heat release obtained was 615 MJ/hr (583,000 Btu/hr).

Final tests were conducted with diesel fuel for comparison of emissions to those of natural gas. An increased bed temperature was maintained for the oil tests in order to maintain uniform bed conditions and suppression of soot formation. The NO_x levels reported in Table C-4 are somewhat higher than for natural gas (15 ppm compared to 3 ppm) due primarily to the small amount of nitrogen in diesel fuel.

It appears that the shorter small cell segment of the bed (0.019 m length rather than 0.051 m) decreased catalytic reactions and allowed a significantly higher amount of gas phase reactions to occur. Essentially complete burnout of CO and hydrocarbons was observed, however. Increased combustion pressure appeared to aid in CO burnout but had no noticeable effect on NO_x emissions.

The advanced graded cell catalyst performed similarly to other geometries tested with only minor variations in lightoff, preheat, and throughput characteristics. Measured emissions indicate that the 0.019 m length small-cell segment may be marginal in providing sufficient catalytic activity to minimize NO_x, CO, and hydrocarbon emissions. The test results did not conclusively indicate that an equal number of transfer units in each bed segment is advantageous, and additional catalyst geometry testing is required to determine optimum catalyst configurations. Further development of fuel injection for distillate oils is also needed.

9.4 RADIATIVE CATALYST/WATERTUBE SYSTEM

The objective of the radiative catalyst/watertube system was the demonstration of stoichiometric catalytic combustion with controlled catalyst temperatures. High combustion efficiency and low pollutant emissions have been demonstrated for off-stoichiometric catalytic combustion and were incorporated into the system design. The system was also designed to demonstrate the applicability of catalytic combustion to existing systems, i.e., watertube boilers.

The concept is shown schematically in Figure 9-12. A stoichiometric fuel/air mixture is fed to the radiative section which contains a close-packed array of catalyst elements and watertubes. The mixture is partially combusted by the catalyst which is kept at a low surface temperature by radiation heat loss to the watertubes. The combustion products and remaining unburned fuel and air are then passed to a dowstream catalytic adiabatic combustor to complete combustion reactions. A final convective section is utilized to extract energy from the fully combusted gases. Both catalyst sections operate well below the maximum use temperature of the catalyst supports -- the radiative section by radiative cooling and the adiabatic section by dilution of the fuel/air mixture with exhaust products from the radiative section.

9.4.1 System Design and Fabrication

Design calculations for the radiative section were performed for one specific operating condition. The section was then built and tested to define its performance for comparison to analytical predictions. Integration of the radiative section with the adiabatic combustor and downstream heat exchanger was not performed.

System requirements are:

- Overall heat release rate of 211 MJ/hr (2×10^5 Btu/hr) -- consistent with volumetric heat release rates established by catalyst screening tests
- Operating pressure of 0.101 MPa (1 atmosphere)

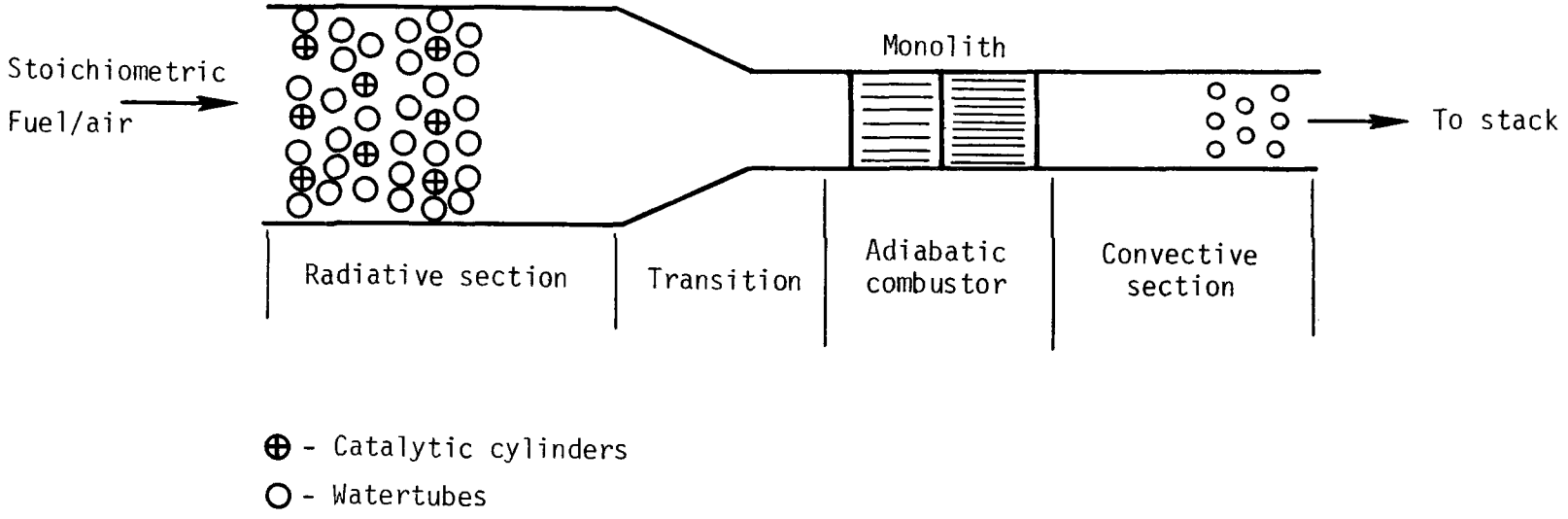

Figure 9-12. Radiative catalyst/watertube combustion system concept.

- Interface with the existing test facility -- appropriate sectional area and physical interfaces
- Ease of fabrication and low cost

Additional requirements for the radiative section include:

- Catalyst elements that can be removed when required
- Refractory-lined test sections to minimize energy losses.

The radiative stage geometric configuration was selected based on its calculated ability to achieve 50 percent combustion efficiency. The arrangement is shown schematically in Figure 9-13. A square-packed array was selected to minimize the number of watertubes required per catalytic cylinder. Large circular watertubes were selected for ease in fabrication. A cylinder length of 0.133 m (5.25 inches) was exposed to the incoming flow.

Heat transfer performance predictions of the configuration in Figure 9-13 were used to finalize the design. Critical design parameters included:

- Steady state catalyst cylinder surface temperature of 1367K at a stoichiometric fuel/air ratio and 211 MJ/hr heat release rate
- Watertube heat removal rates -- both radiative and convective
- Test section refractory thickness to maintain exterior steel surfaces at safe temperatures.

The catalyst cylinder steady state wall temperature can be determined by equating the convective energy gain to the radiative losses (Figure 9-14). The convective gain, Q_C, is given by the difference between the freestream fuel/air mixture adiabatic flame temperature and the actual surface temperature of the cylinder multiplied by the convective transfer coefficient of the cylinder in crossflow. The radiative transfer, Q_R, is dictated by the cylinder wall temperature, surrounding watertube wall temperatures, and respective emissivities and absorptivities, since the view factor is essentially unity. This analysis yielded a 1317K (1910°F) catalytic wall temperature at stoichiometric mixture ratios and 211 MJ/hr heat release conditions. This result verified that radiation transfer was an acceptable bed heat removal technique. It was then necessary only to define the heat load to the cooling tubes (combined radiation and convection) and to size the

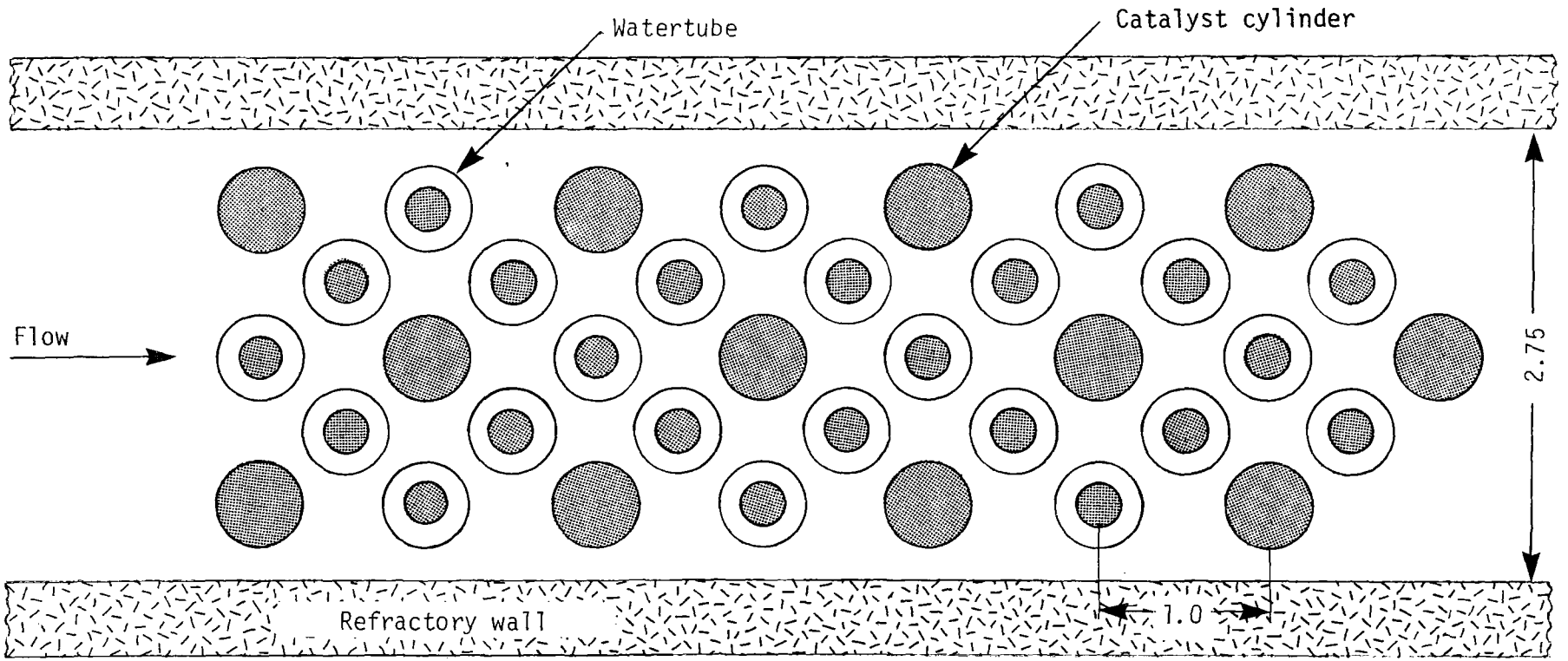

Figure 9-13. Radiative catalyst/watertube arrangement.

test section refractory to complete the design calculations. Watertube heat transfer was calculated to be half radiative and half convective with a total value of 693 MJ/hr-m^2 (61,000 Btu/hr-ft^2) of tube surface. The refractory was sized at 5.08 x 10^{-2} m thick sidewalls and 2.54 x 10^{-2} m thick top and bottom walls for the firebrick material selected.

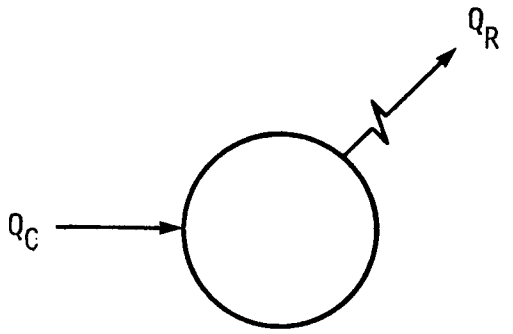

Figure 9-14. Catalyst cylinder heat transfer model.

The final radiative section configuration is shown in Figure 9-15. The catalyst cylinders (1.27 x 10^{-2} m OD) are supported by the top and bottom refractory and can be removed by screw access in the top plate. The stainless steel watertubes (also 1.27 x 10^{-2} m OD) are fitted at both ends with smaller tubes to minimize the hole size penetrating through the refractory. All tube manifolding is flexible hose on the exterior of the section. The tubes were manifolded in series to provide two complete flow paths. During operation, the water flowrate and inlet and outlet temperatures were measured in order to determine experimental heat flux to the tubes. A picture of the radiative section installed in the test facility is shown in Figure 9-16. Thermocouple wires from the catalyst cylinder surfaces can be seen at the side of the section.

Thirteen cylinders of Coors alumina were coated with an alumina washcoat by Oxy-Catalyst, Inc., and with platinum catalyst by Acurex. A summary of the catalyst loading for each cylinder is given in Table 9-1. A nominal loading of five weight percent was achieved. Cylinder number 237 was used for pretest surface area and dispersion measurements, both of which were essentially zero.

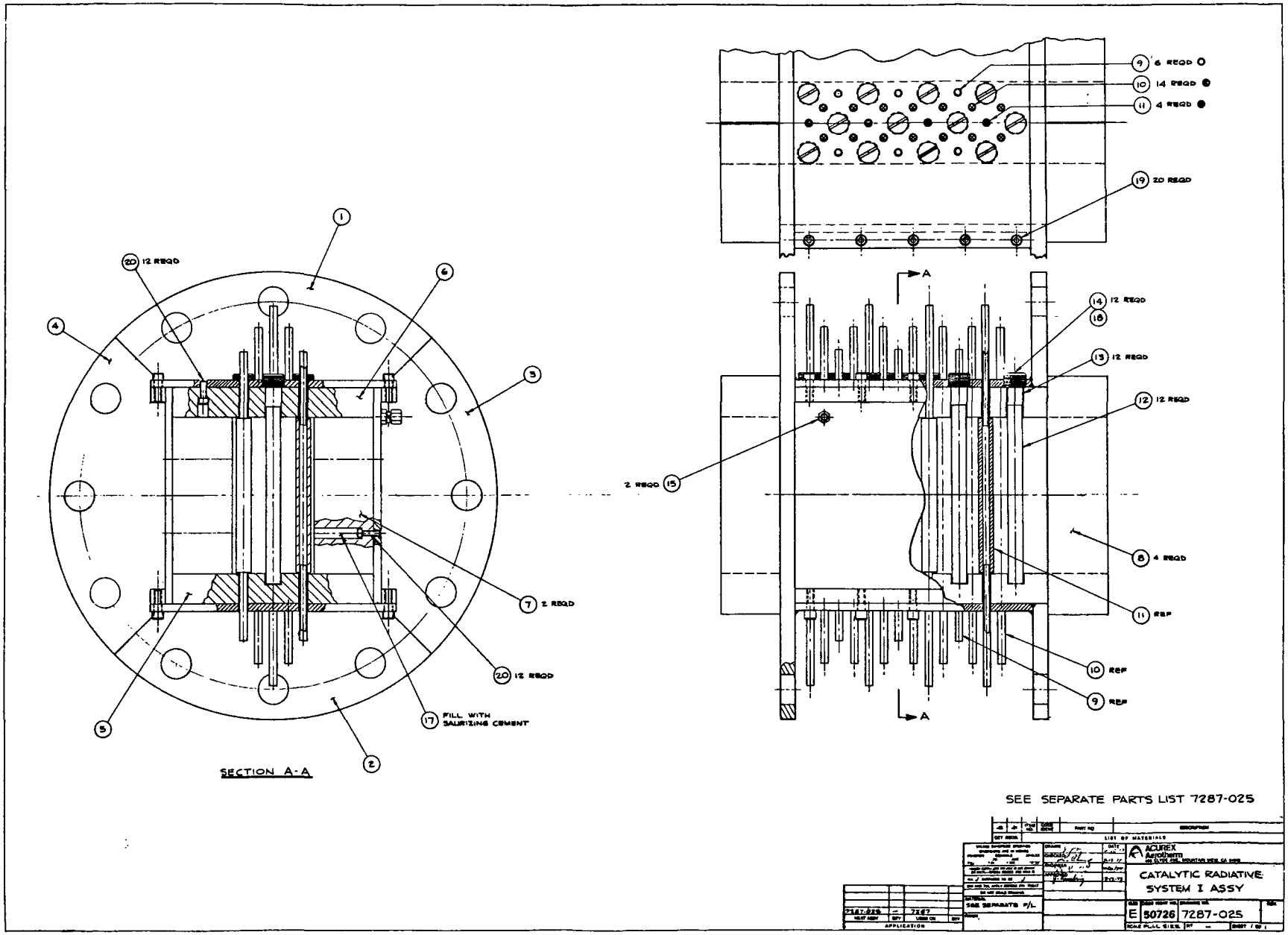

Figure 9-15. Catalytic radiative System I assembly.

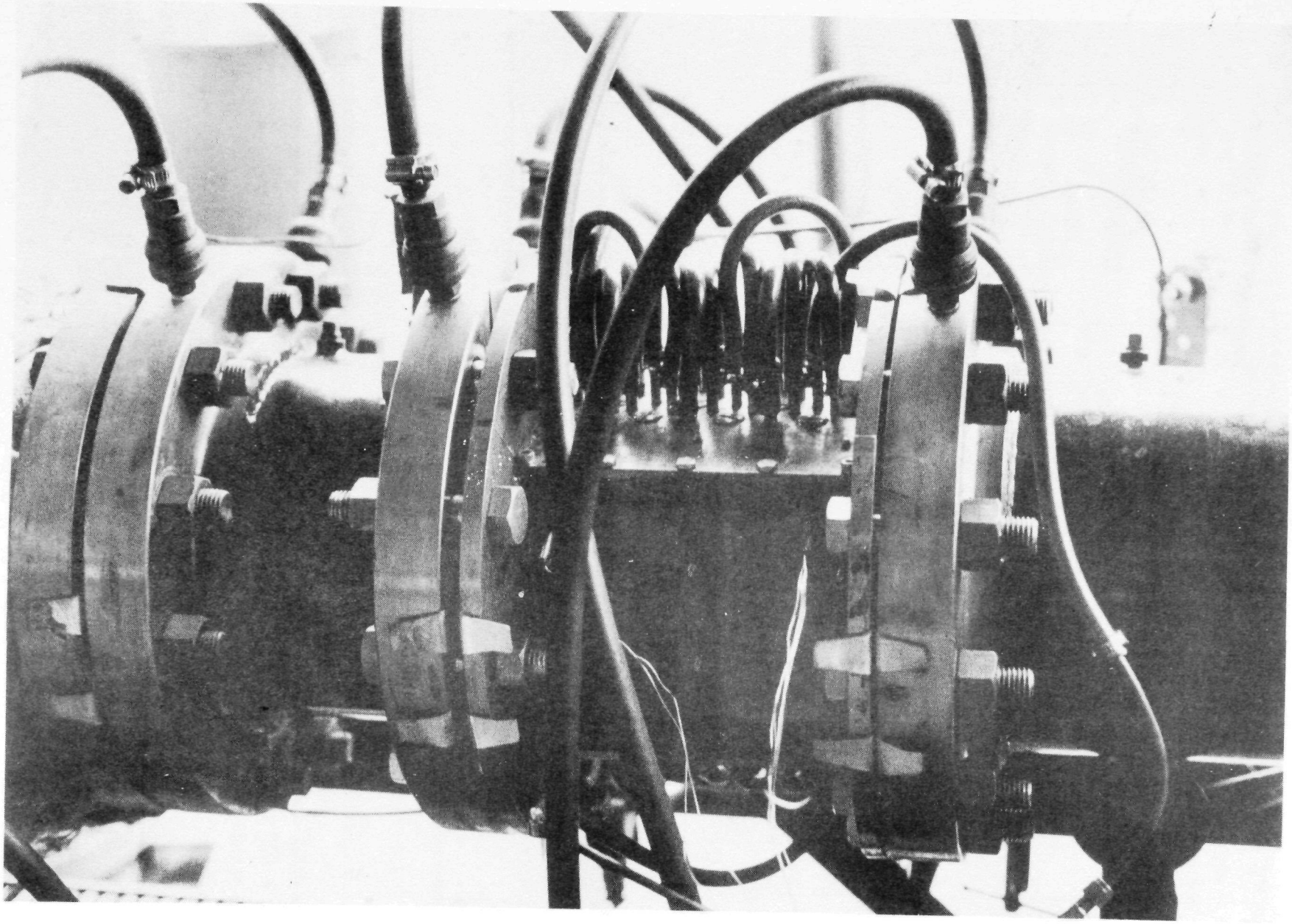

Figure 9-16. Radiative catalyst/watertube test section installation.

TABLE 9-1. PLATINUM ON ALUMINA CATALYST CYLINDERS

Cylinder Number	Original Weight (Kg x 10^3)	Final Weight (Kg x 10^3)	Platinum Loading (wt %)
226	32.05978	33.60413	4.82
227	33.23824	34.87402	4.92
228	33.46360	34.96856	4.50
229	30.52612	32.17465	5.40
230	32.21470	33.74632	4.75
231	33.68275	35.41054	5.13
232	31.78670	33.41083	5.11
233	30.82062	32.34902	4.96
234	31.97873	33.47561	4.68
235	31.99540	33.53665	4.82
236	32.65464	34.17952	4.67
237[1]	33.20850	34.60557	4.21
238	32.80017	34.54772	5.32

[1]Used for pretest BET surface area and dispersion measurements.

9.4.2 Test Results

The objectives of the radiative system tests were to:

- Identify the feasible stoichiometric operating range
- Identify mass throughput and combustion efficiency characteristics
- Determine lightoff and preheat requirements
- Evaluate the heat extraction technique

The test matrix of Table C-5 was formulated to satisfy these objectives by varying stoichiometry, fuel flowrate, and preheat.

Lightoff temperatures for the radiative system were typical of other platinum catalysts tested. After 20 hours of testing, the lightoff temperature under fuel-rich conditions (40 to 50 percent theoretical air) remained between 700 and 728K (800-850°F).

Significant test data is summarized in Tables C-6 and C-7. A range of stoichiometries from 50 to 219 percent theoretical air was run by variation of combustion air at a constant fuel flowrate. Fuel mass flowrate was later varied from 2.13 to 6.70 Kg/hr (4.7 to 14.8 lbm/hr) of natural gas to investigate the effects of mass throughput at stoichiometric conditions. Finally, operation at reduced values of preheat was investigated. Figure 9-17 shows the energy extracted by the cooling tubes out of the total available energy at the bed inlet as a function of stoichiometric ratio. The total available energy includes the fuel heating value (22,000 Btu/lbm) and the sensible preheat energy. Thermal input to the catalyst cylinders is primarily controlled by the adiabatic flame temperature of the fuel/air mixture. This temperature peaks near unit stoichiometry, and as a consequence the tube temperatures have a corresponding maximum As theoretical air percentage increases above 100 percent, catalyst surface temperature begins to decrease, decreasing the radiant exchange to the watertubes. The higher total mass throughput, however, also increases convective heating of the watertubes such that at fixed fuel flowrate the energy exchange does not fall off rapidly.

Measured CO and CH_4 emissions versus percent theoretical air are shown in Figure 9-18. CO levels increase rapidly at approximately 100 percent theoretical air going towards fuel-rich combustion. Measured methane (CH_4) increased only slightly on the fuel-rich side. No oxides of nitrogen were measured for any of the test conditions of Table C-6.

The methane measurements of Figure 9-18 were made by gas chromatography (GC). Data was taken at several test points to supplement routine continuous gas analysis for CO, CO_2, O_2, and NO_x. The species normally detected by the gas chromatograph include CO, CO_2, O_2, H_2, N_2, CH_4, and other trace hydrocarbons. A summary of the GC data is given in Table C-8.

The effects of mass throughput on the radiative system are shown in Figures 9-19 and 9-20 for stoichiometric conditions. The energy absorbed by the cooling tubes increases with mass throughput due to both increased radiation (increased bed temperature) and convection. At the 4.1 Kg/hr

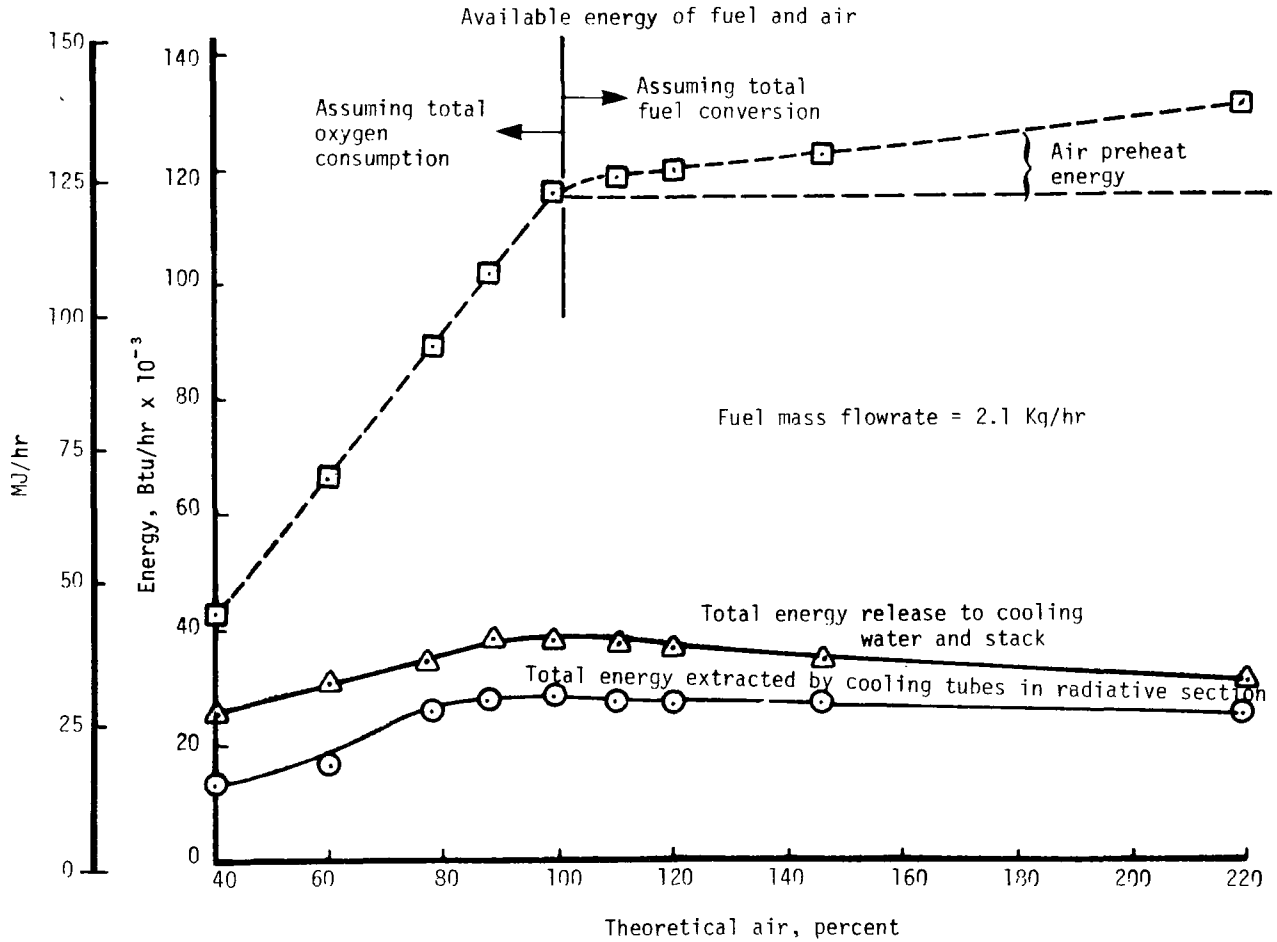

Figure 9-17. Radiative catalyst/watertube system energy release vs. theoretical air.

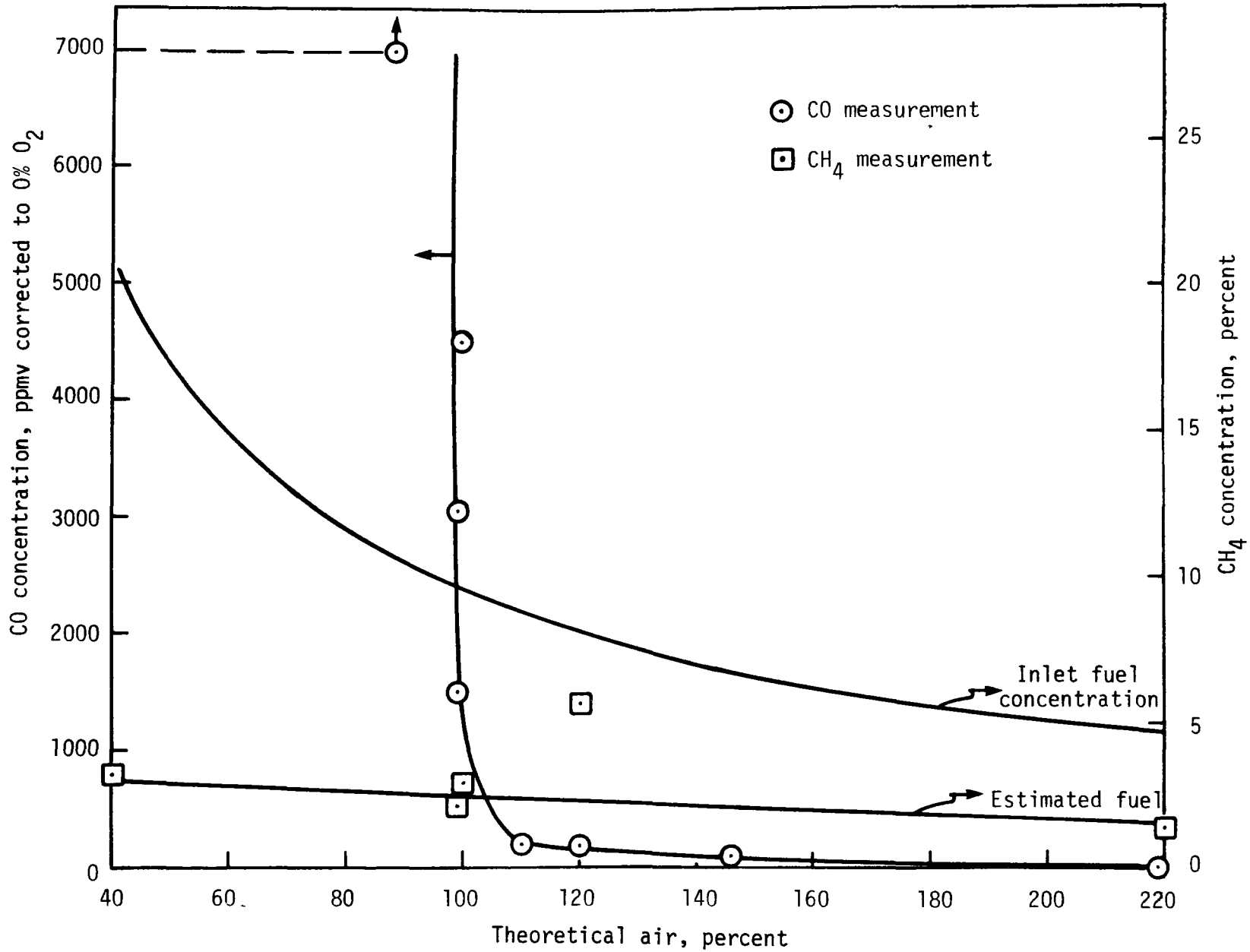

Figure 9-18. Radiative catalyst/watertube system emissions vs. percent theoretical air.

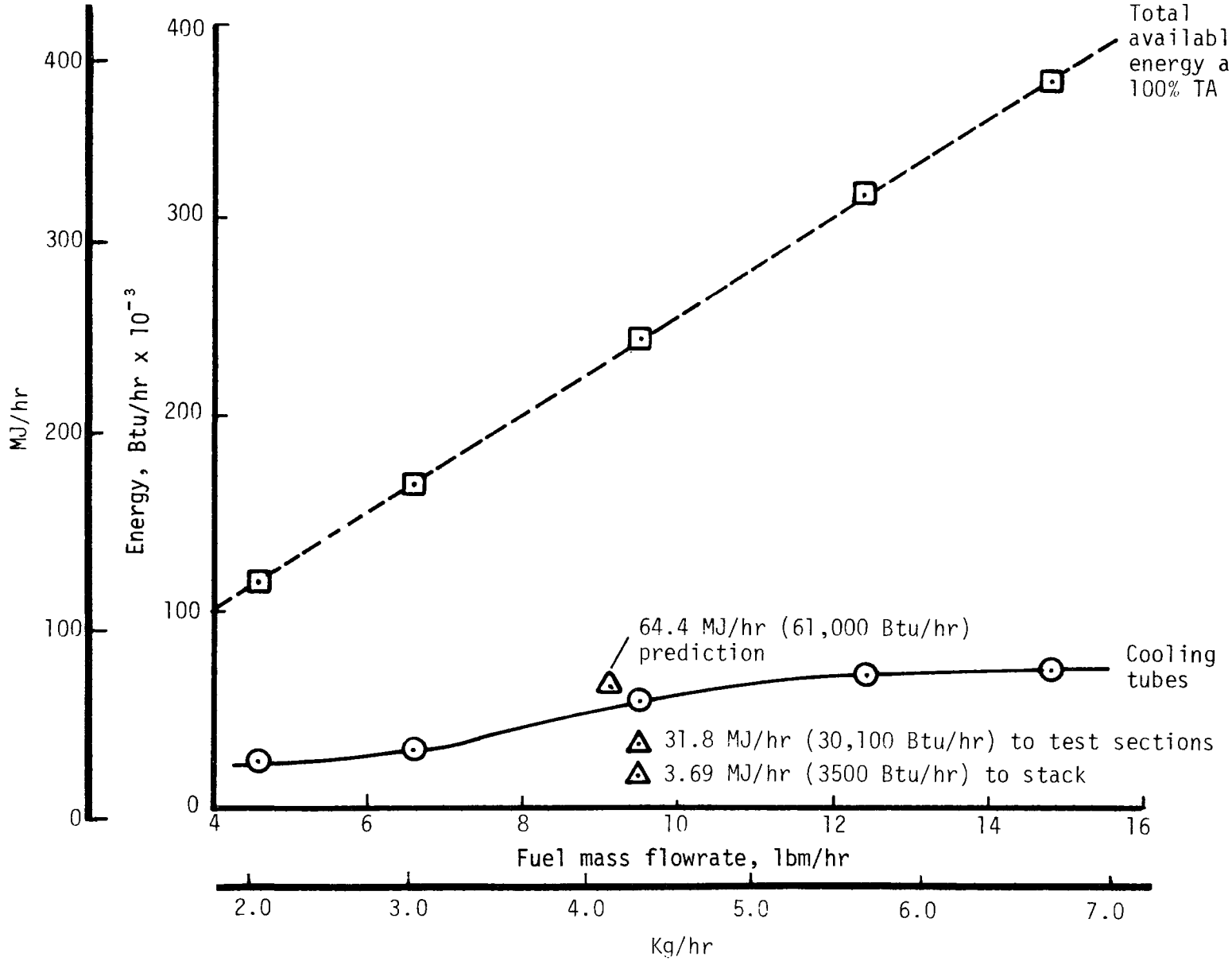

Figure 9-19. Radiative catalyst/watertube energy release vs. throughput at 100 percent theoretical air.

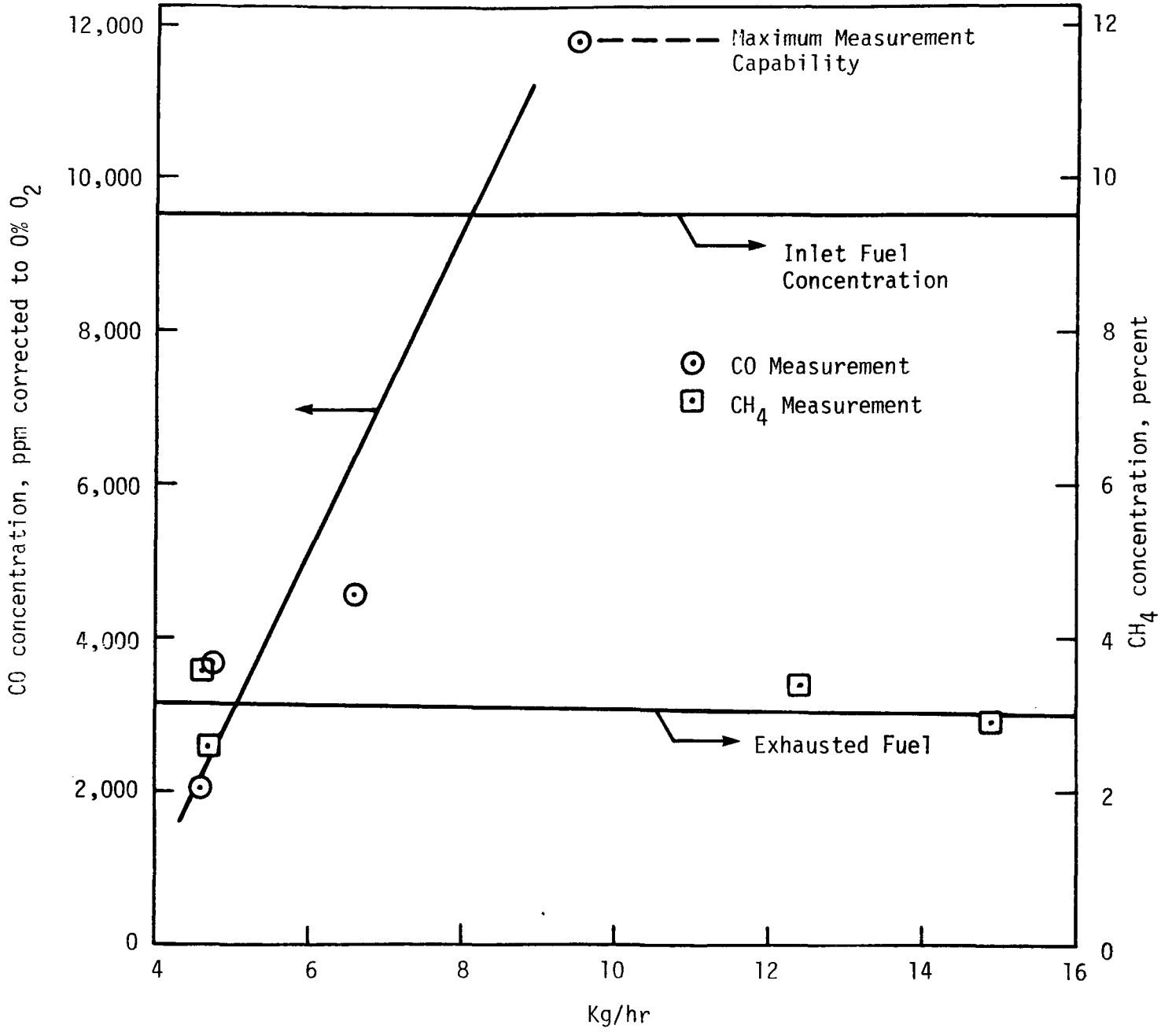

Figure 9-20. Emissions vs. throughput at 100 percent theoretical air.

design point, the actual cooling of 57.0 MJ/hr (54,000 Btu/hr) extracted by the watertubes is slightly below the predicted value of 64.4 MJ/hr (61,000 Btu/hr). At the 4.3 Kg/hr test point, an additional 31.8 MJ/hr was extracted by a separate cooling system for the surrounding test sections, and 3.69 MJ/hr was exhausted at the stack. Therefore, the combustion efficiency at the design point can be calculated as approximately 37 percent. The emission levels of Figure 9-20 show a fairly even level of unburned hydrocarbons with carbon monoxide increasing significantly above 2.7 Kg/hr of natural gas. This trend is consistent with the reduced efficiency at higher mass throughputs shown in Figure 9-19.

Typical bed temperature profiles are shown in Figure 9-21. Note the increase in catalyst surface temperature with throughput due to increased convection to the catalyst cylinders. The temperature observed near the front of the bed at the nominal 4.3 Kg/hr design point matches the predicted temperature of 1317K (1910°F) quite well. Preheat temperatures as low as 394K (250°F) were achieved with no effect on combustion stability.

A second test series was conducted with the radiative catalyst/watertube system with a base metal oxide (cobalt oxide) catalyst. Cobalt oxide was applied to Coors alumina cylinders at Acurex. Three cylinders at the entrance region of the bed had platinum added to facilitate system lightoff. The configuration was tested at atmospheric pressure with natural gas and propane.

Attempts to light off the system with natural gas at 694K (790°F) were unsuccessful. Lightoff with propane at 672K (750°F) showed initial catalyst activity as the bed temperature on the upstream cylinders increased to 950K (1250°F). Full lightoff could not be achieved, however, even at stoichiometric conditions.

The results of these tests and test data obtained for cobalt oxide catalysts in the graded cell configuration confirm that near-adiabatic surface conditions or higher ignition temperatures are required for lightoff of base metal oxide catalysts. The required heat retention at the surface was not available in the radiant system, making lightoff very difficult to achieve. It had also been observed that operation of cobalt oxide graded

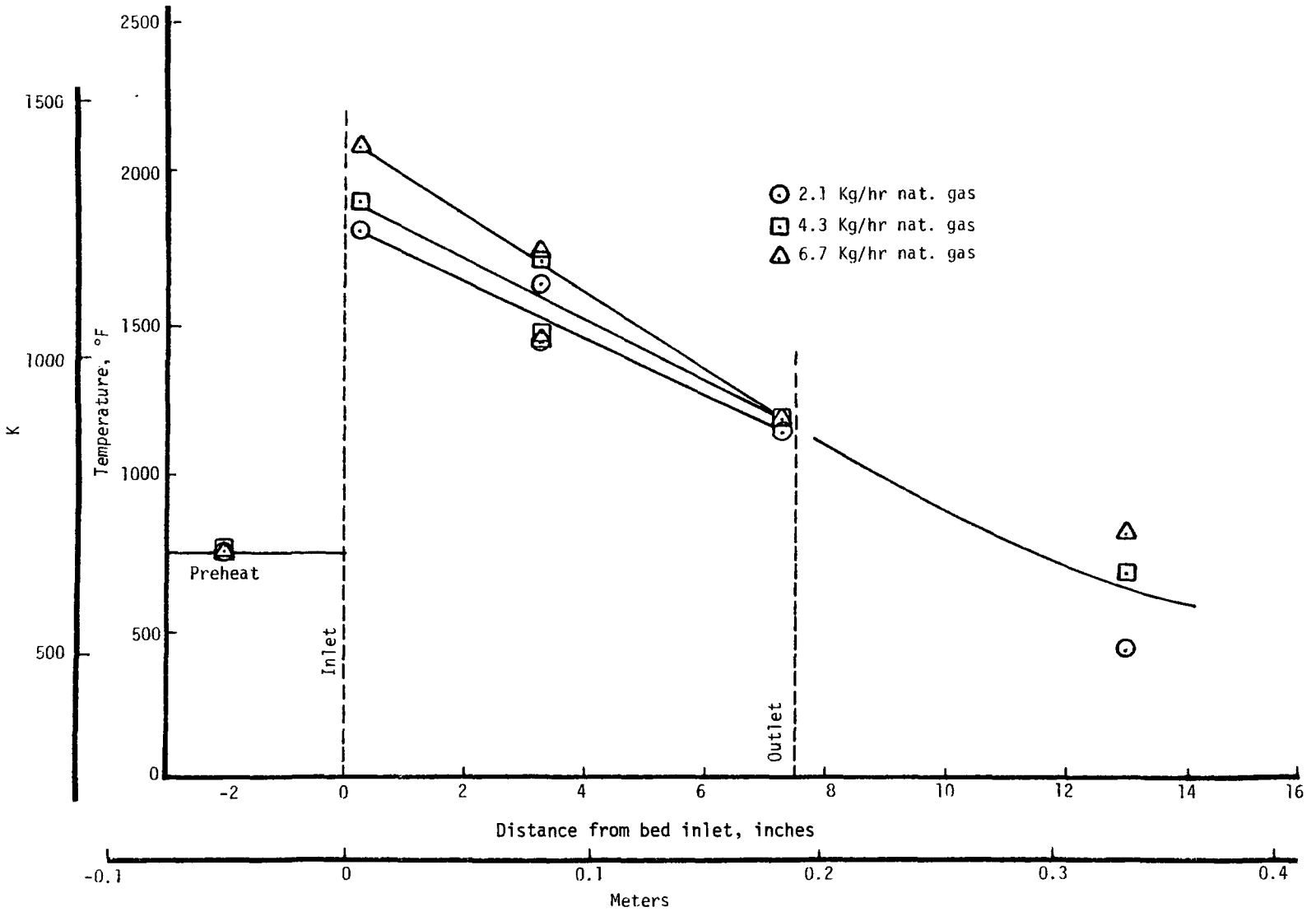

Figure 9-21. Bed temperature profiles at 100 percent theoretical air.

cell catalysts (model A-038) was less stable at the low surface temperatures of the radiant system (1367K) than at higher temperatures. This low activity of the cobalt catalyst at low temperatures explains the lightoff difficulties experienced in the non-adiabatic watertube system.

A third test sequence was conducted with the original platinum on alumina cylinders used for initial system testing. Test objectives were to evaluate fuel nitrogen conversion characteristics of the system over a range of stoichiometries for comparison to the graded cell configuration. Stoichiometry was varied from 52 to 120 percent theoretical air. Natural gas and propane were used as test fuels.

The nitrogen conversion test data is summarized in Tables C-9 and C-10 and in Figure 9-22. The test points were run in the order shown in Table C-9. Following natural gas operation at 75 percent theoretical air, catalyst degradation was apparent. Operation below 75 percent or above 120 percent theoretical air with natural gas was no longer possible. Operation with propane fuel allowed additional test points below 75 percent theoretical air, but some cylinders were observed to be inactive. Higher thermal NO_x values (Table C-10) over those of the original test series resulted due to the loss in surface activity and increased nitrogen oxidation in the gas phase. The poorer fuel conversion obtained (Table C-9 shows a maximum conversion of 22.7 percent compared to an initial 37 percent) also indicates the loss in catalyst activity with time.

Figure 9-22 shows the fuel nitrogen conversion characteristics of the radiative system for natural gas doped with 2000 ppm of ammonia. Low NO_x and high NH_3 values above 100 percent theoretical air are consistent with the incomplete combustion characteristics of the radiative system. The low point in the total NO_x precursor curve (NH_3 + HCN + NO_x) at 60 percent theoretical air is similar to those obtained for metal oxide graded cell catalysts (see Section 8.5.1). Although operating under fuel-rich conditions, excess oxygen is still present in the exhaust from the radiative system due to incomplete conversion of the fuel/air mixture. The low conversion of the fuel nitrogen to NO_x precursors even in the presence

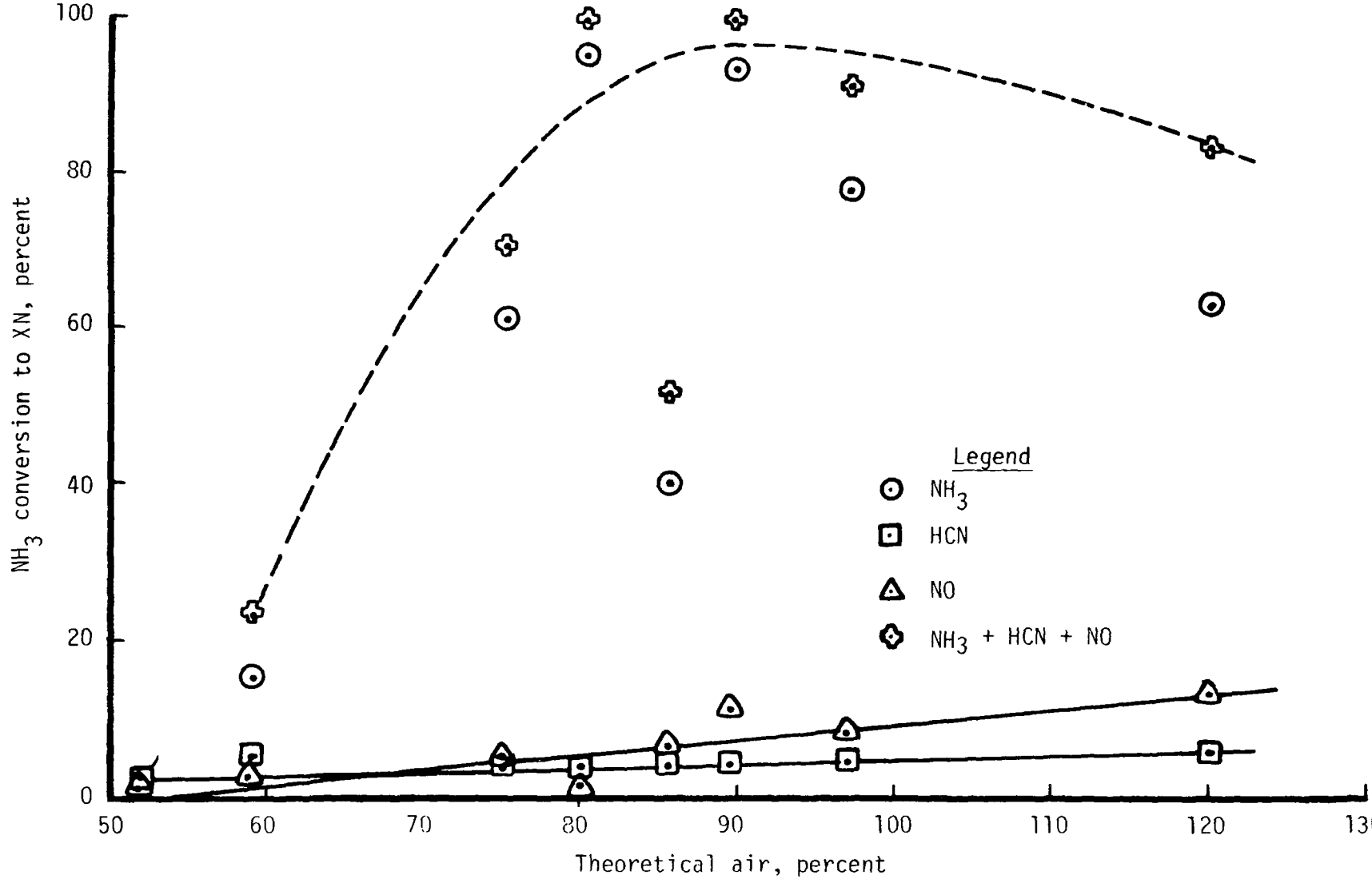

Figure 9-22. Radiative catalyst/watertube system, ammonia-doped natural gas, fuel nitrogen conversion.

of oxygen suggests the action of a NO_x reduction mechanism by the CO and unburned hydrocarbons in the exhaust stream. The data scatter in the 80 to 100 percent theoretical air range should be resolved with additional testing.

Since the actual measured heat release of the radiative catalyst/watertube system was not as high as that predicted at the nominal 4.3 Kg/hr (9.5 lbm/hr) of methane design condition (see Figure 9-19), the radiant section as tested is not fully suited for complete system development. The addition of the downstream adiabatic catalytic combustor would result in too high a temperature in that region at stoichiometric conditions since combustion efficiency in the first stage is not as high as expected. The excellent performance of the radiative catalyst/watertube section at stoichiometric conditions with very low levels of NO_x makes it attractive for further optimization to increase efficiency and compatibility with the adiabatic section. The system also appears attractive for fuels with high nitrogen content. The extremely stable operation of this first radiative system under all test conditions makes it an ideal candidate for life test considerations.

9.5 CONCLUSIONS

The combustion system data obtained from tests of the radiative catalyst/watertube, two-stage, and gas turbine systems established three potential applications of the catalytic combustor. The control of nitrogen oxide emissions from both thermal fixation and conversion of fuel-bound nitrogen was also shown. The emission characteristics of nitrogen oxides, carbon monoxide, and unburned hydrocarbons were evaluated over a range of operating conditions. The results thus provide design criteria for system combustors and their operation.

The radiative catalyst/watertube system exhibited stoichiometric catalyst operation by direct bed cooling with potential for both low thermal and fuel NO_x emissions. It is apparent that the thermal NO_x emissions obtained are sensitive to the activity of the catalyst surface. Thermal NO_x increased significantly during later test times when deactivation of

the surface was observed -- allowing greater oxidation of atmospheric nitrogen by gas phase reaction. The conversion rate of fuel nitrogen to NO_x appears to be influenced by the presence of CO and UHC species which reduces the NO_x to N_2. Therefore, the partial combustion characteristic of the radiative section may be very attractive for the control of fuel NO_x. Coupled with the downstream adiabatic combustor, full fuel conversion can be achieved. Advanced designs are required to achieve greater first stage efficiency and operation of the complete system concept. System stability during operation makes it suitable for constant operation steam raising applications.

The two stage combustor combined the advantages of low fuel nitrogen conversion under fuel-rich conditions with high overall system efficiency achieved at stoichiometric conditions. Seventy percent control of fuel NO conversion was achieved by the two stage combustor tested. It appears that even higher levels of control can be achieved by optimization of first stage stoichiometry and by operation at higher pressures. Production of thermal NO_x by the system appears to be dependent on both catalyst activity and emission levels of CO. Reduction of NO_x formed during combustion by CO appears probable under overall lean combustion but ineffective for overall fuel-rich operation. These combined properties make two stage combustion attractive to a number of applications (see Section 10). Advancements in first stage catalyst application are currently required to achieve long life in that stage without the effects of sooting. Consideration of mixed catalytic and conventional burners in two stage arrangements should also be investigated.

The model gas turbine system shows the direct application of the graded cell concept to turbine systems. Exhaust temperature control by high excess air levels was demonstrated at high volumetric heat release rates for both gaseous and liquid fuels. Low thermal NO_x emissions at up to 1.01 MPa (10 atmospheres) and decreasing conversion of fuel nitrogen with increasing pressure were observed. Advancements in fuel injection system design, graded cell design, catalyst support, and flashback control contributed to the success of the model turbine system.

Advanced design and testing of each of the three systems is required to obtain complete design data for prototype development. Advanced development data would lead directly to laboratory installation of prototype systems for long-term demonstration and finally to field process applications. Projected field applications for catalytic combustors based on the results of the system tests of this study are presented in Section 10.

SECTION 10

PROTOTYPE SYSTEM DESIGN CONCEPTS

10.1 INTRODUCTION

The characterization of stationary combustion systems to which catalytic combustor retrofit and/or redesign may be applicable (Section 3) and the catalyst performance test data generated under this program (Sections 7 to 9) have provided information for conceptualization of catalytic combustion systems. Those systems which appear most promising for future application include industrial and commercial firetube and watertube boilers, and gas turbines. Other applications, including utility boilers and mobile gas turbines, as well as rangetop burners and home furnaces (which are less frequently maintained), also appear feasible for catalytic combustors but would require more extensive development. Prototype catalytic concepts for commercial and industrial boilers are discussed in Section 10.2, for stationary gas turbines in Section 10.3, and for other systems in Section 10.4.

10.2 INDUSTRIAL AND COMMERCIAL BOILERS

Both firetube and watertube boilers appear to be attractive applications for catalytic combustion. The concepts that are developed below apply equally well to both industrial and commercial sized units.

10.2.1 Firetube Boilers

The firetube boiler utilizes radiative and convective heating by combustion products on the inside of tubes immersed in water. A thorough discussion of firetube boiler types is given in Reference 10-1. A typical scotch firetube boiler is shown in Figure 10-1. A relatively large combustion chamber exists at the center of the unit and is fed directly by the

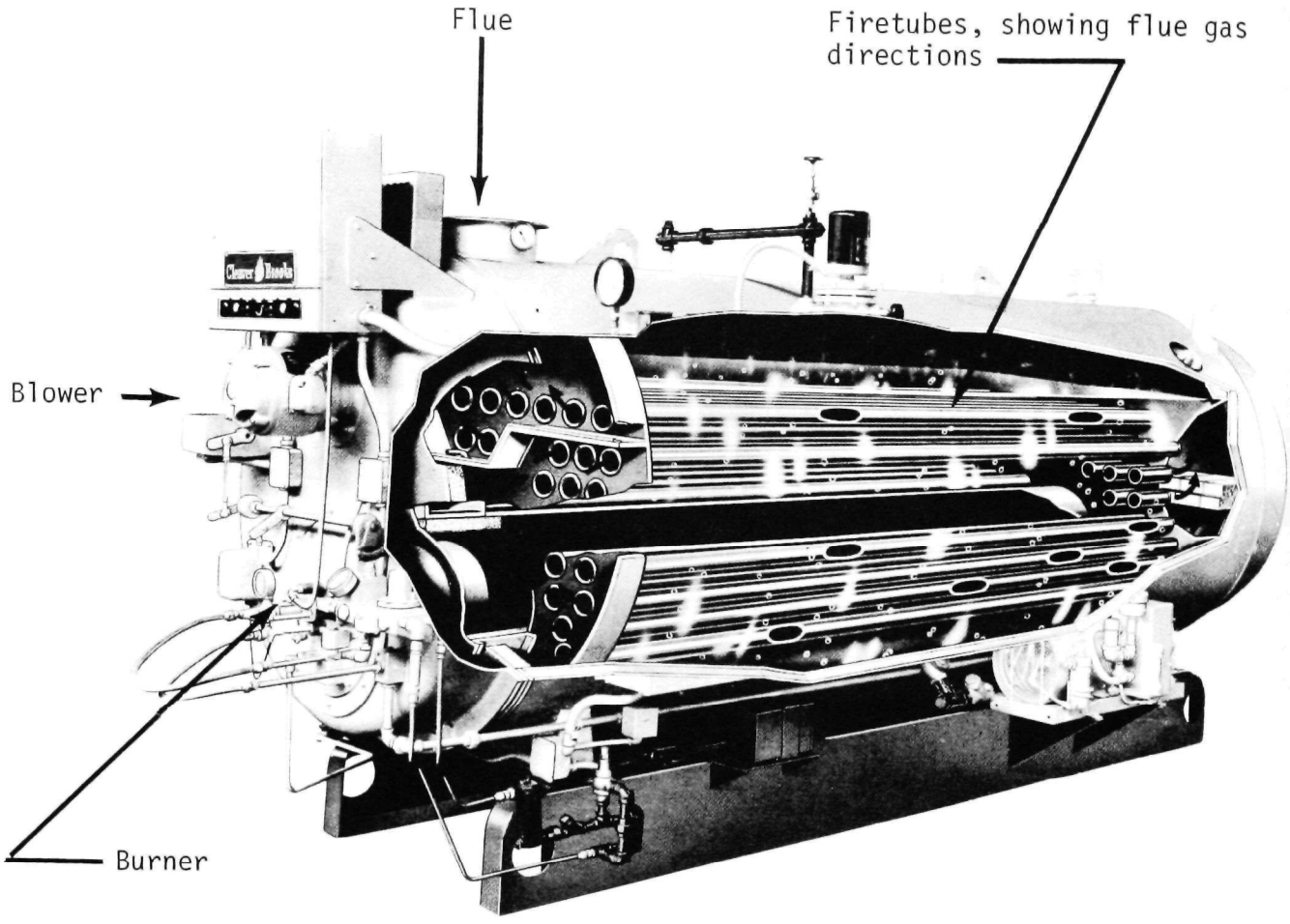

Figure 10-1. Four-pass scotch firetube boiler (courtesy of the Cleaver Brooks Company).

burner. The conventional burner could be simply replaced by a redesigned catalytic burner with no additional system modification necessary.

Two firetube boiler conceptual design concepts were completed. The first utilizes a graded cell catalyst which has been shown by screening tests to possess appropriate throughput, preheat, and emissions characteristics. The boiler burner would be replaced with the graded cell burner as shown in Figure 10-2. The graded cell burner has a preheat section in which air and/or fuel is passed through the inside of a set of cylindrical spines to provide the necessary preheat. This preheated air and fuel is then mixed and passed over the catalytically treated exterior cylindrical surfaces where combustion is initiated, thus providing the preheat energy. Following this initial section is a region in which heat transfer occurs between the partially combusted products and the furnace chamber. A graded cell catalyst then accepts the cooled, partially burned mixture and completes combustion. The products of combustion are then passed down the remaining central furnace chamber. The heat transfer rate to this water-cooled furnace is controlled by the center ceramic flow restrictor. Proper sizing of this cylindrical support (flow restrictor) would control the exhaust product velocity and, hence, the heat transfer rate.

This design is attractive in that it utilizes the extensive test experience and property knowledge of the graded cell configuration and would be a simple retrofit. The actual geometry of the catalyst would require further optimization for operation at the appropriate stoichiometry and for full fuel conversion in a minimum volume.

The second firetube boiler concept utilizes a felt-like matrix material as the catalyst element. This material has been shown to operate effectively in residential furnace application (Reference 10-2) and should be directly applicable to boiler systems. In this concept (Figure 10-3), a gaseous fuel/air mixture is passed down a metering manifold located in the center of the cylindrical felt-like matrix shell. The fuel/air mixture passes radially outward and diffuses through the matrix material. Combustion occurs on the outer matrix surface. This surface then radiates its energy to the water-cooled furnace wall. The concept again utilizes a proven catalyst type (felt-matrix) and would be a simple burner retrofit.

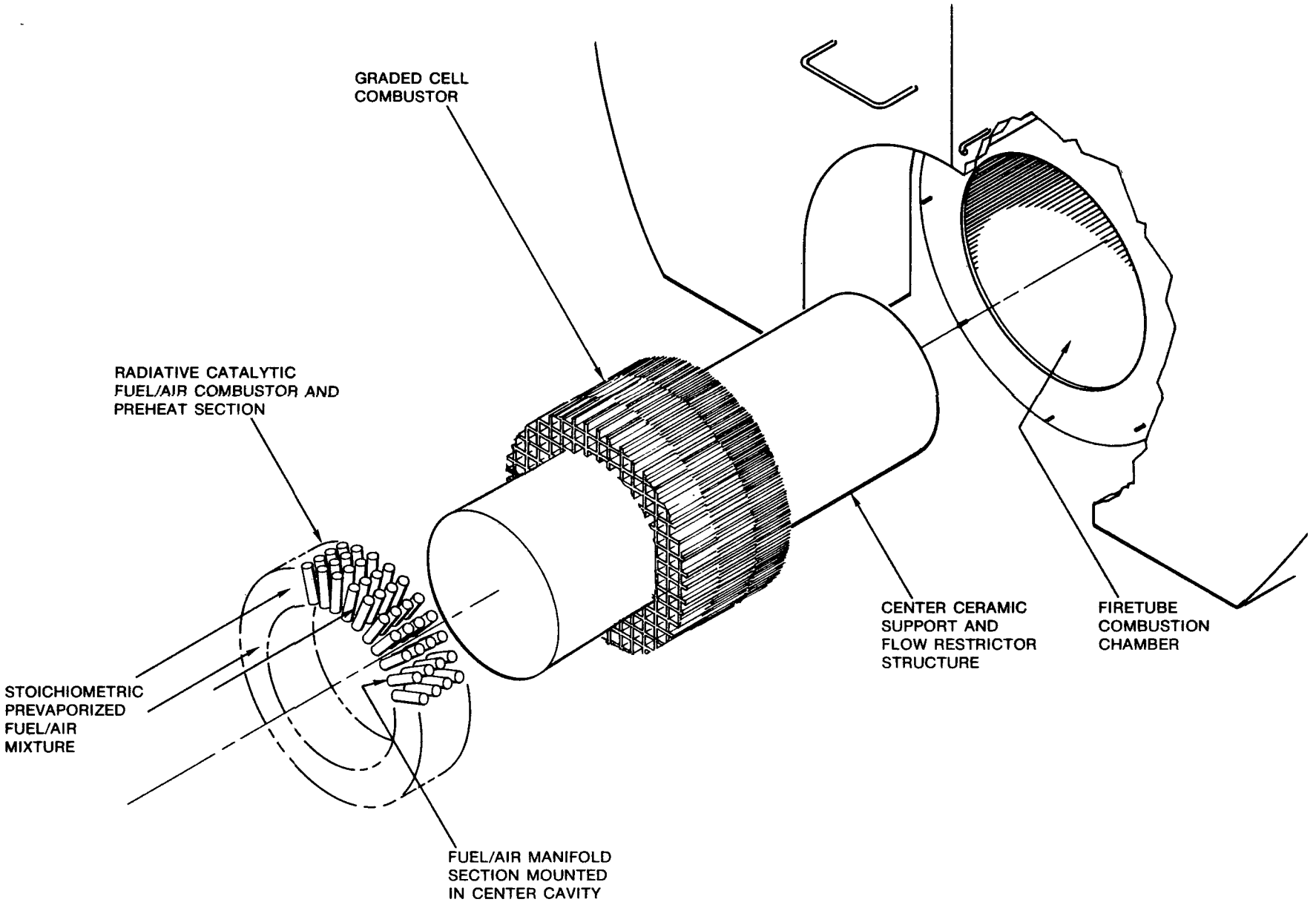

Figure 10-2. Graded cell firetube boiler concept.

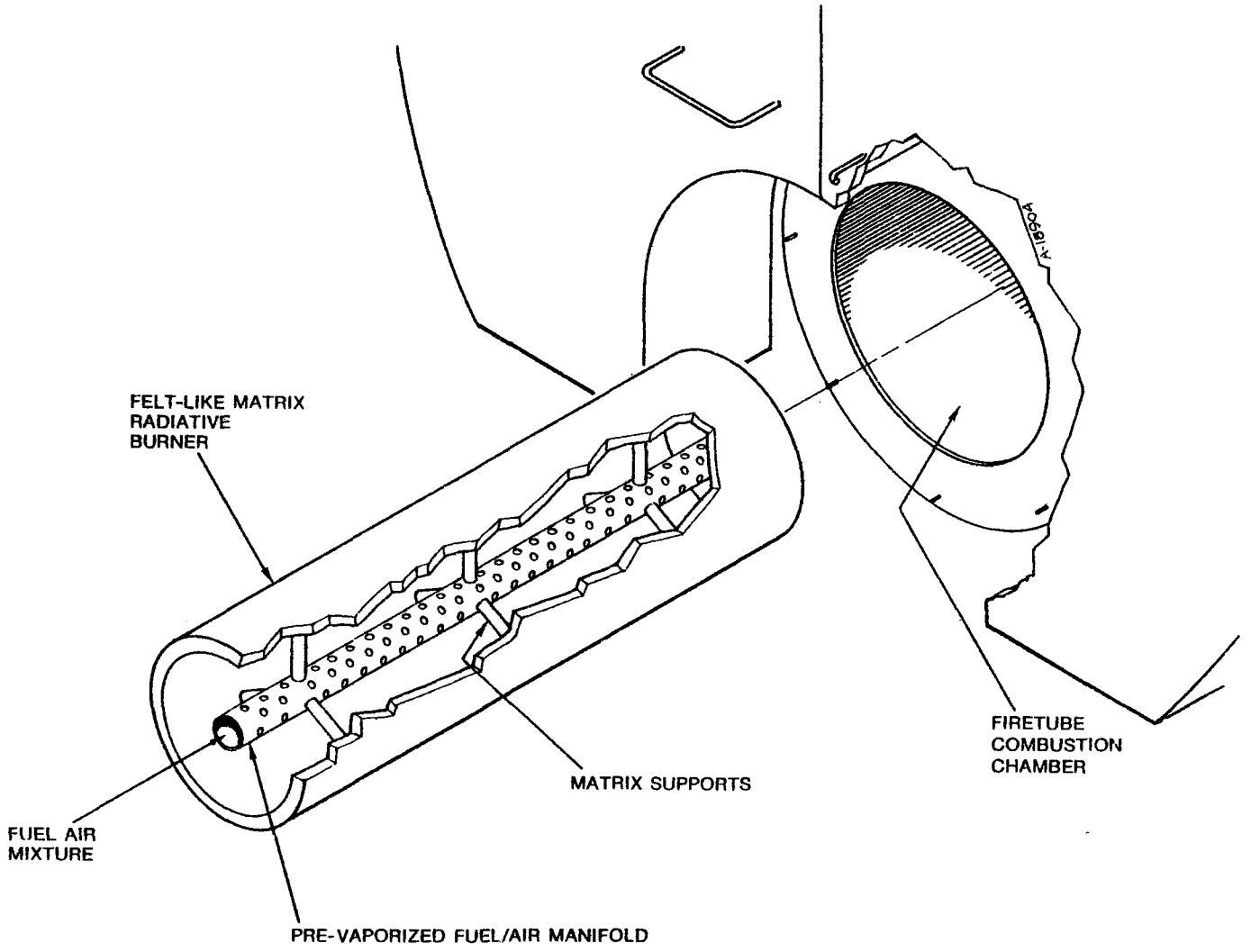

Figure 10-3. Felt pad firetube boiler concept.

10.2.2 Watertube Boilers

In the watertube boiler, hot combustion products contact the boiler outer tube surfaces and water is heated within the tubes. The radiative/watertube catalytic combustor concept discussed in Section 9 utilizes radiative and convective heat transfer within the bed to heat water-carrying tubes

As described in Section 9, the radiative/watertube system achieves partial combustion of the fuel at stoichiometric conditions. Some geometric optimization is possible to increase the amount of combustion occurring within the radiative/watertube system, but it is expected that, for a short system length, a secondary graded cell stage will be necessary to combust remaining hydrocarbons following first stage heat release.

Two concepts are presented here for the watertube boiler. The first, Figure 10-4, assumes that efficient combustion can be achieved in a single radiative combustor, A. Heat transfer to watertubes occurs both within the bed (to keep bed temperatures at acceptable levels during stoichiometric combustion) and in a downstream convective section, C, consisting of additional watertubes to extract the remaining combustion energy. Considerable extension of existing bed heat transfer experience would be required to fully implement the concept and achieve efficient single stage combustion. Simple retrofit of existing horizontal straight or bent tube boiler units would not be possible, and new designs would be required.

The second watertube boiler concept would add a graded cell catalyst stage B to the system, Figure 10-4. This second stage would be capable of converting all unburned hydrocarbons passed by the radiative/watertube stage. The final convective watertube section would be downstream of the second stage to extract remaining heat from the combustion products. The concept has the advantage of less stringent requirements on the radiative/watertube stage performance and hence less development time for that stage. Again, as with the single-stage concept, full boiler redesign would be required.

10.2.3 Two Stage Catalytic Systems

Graded cell catalyst extensive evaluation tests (Section 8) and subsequent two stage combustor system tests (Section 9) demonstrated that two

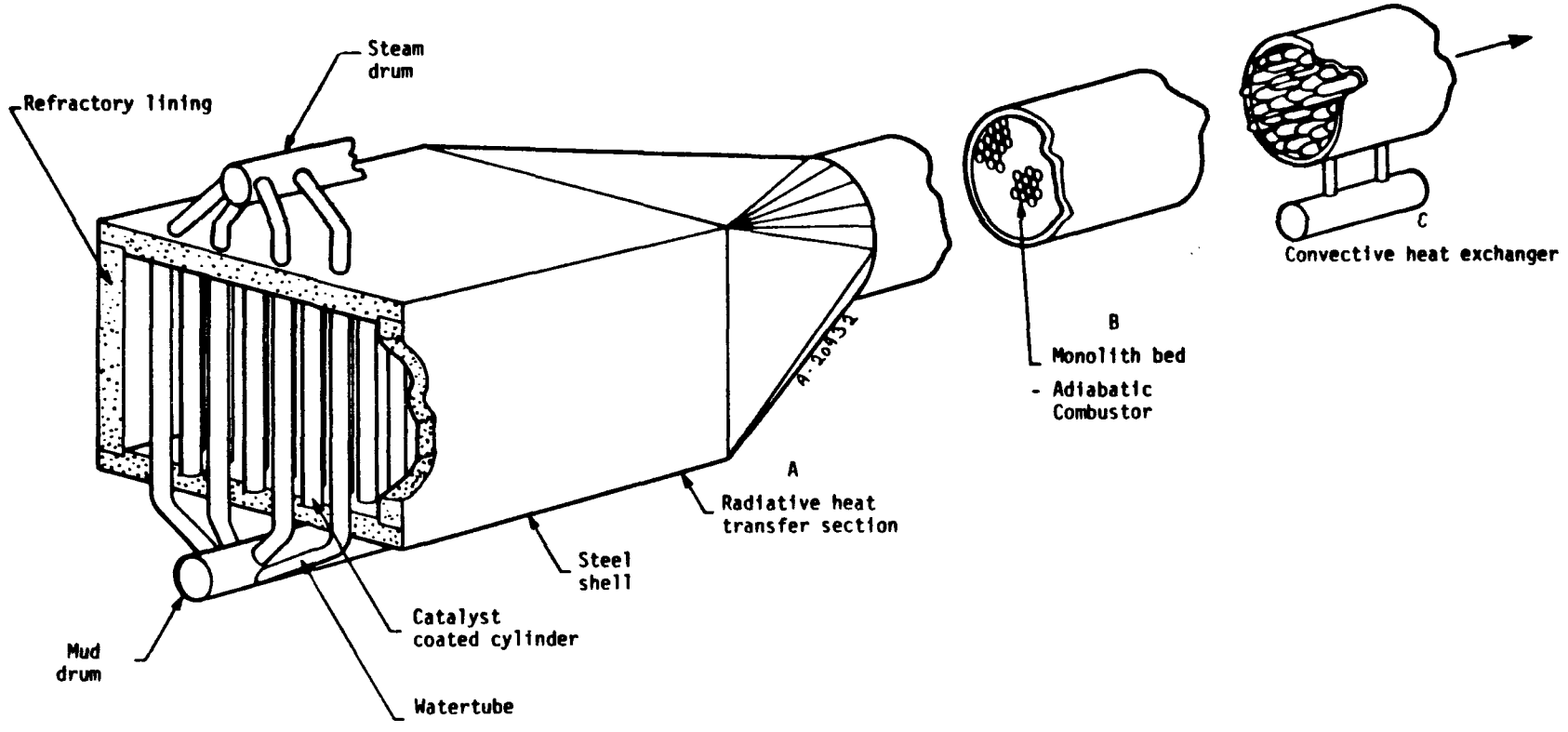

Figure 10-4. Radiant catalyst/watertube combustion system.

stage combustors operating fuel-rich in the primary stage show promise for reduced conversion of fuel-bound nitrogen to nitrogen oxides. Two stage catalytic combustors can be conceptualized that would be applicable to both firetube and watertube boilers. The only difference for the two applications is the geometrical constraint involving energy extraction following the first and second stage beds.

The two stage combustor with graded cell catalyst tested in this program (see Figure 9-3) is applicable to the watertube boiler since inter-stage heat removal occurs by watertubes. A second convective heat recovery exchanger downstream of the second stage would also be required for added energy extraction and increased boiler efficiency. Secondary air injection complicates application of the concept to the boiler system. A two-stage combustor could also be built for watertube boilers by use of the radiative catalyst/watertube system where the radiative zone operates under fuel-rich conditions and secondary air is added prior to the adiabatic combustor. Special fuel delivery and injection systems would need to be developed for high nitrogen fuel oils for this application.

The two stage combustor could also be built within the long combustion chamber of the firetube boiler with the hot gases contained within the boiler tubes. Again, secondary air injection poses a difficult design problem which would probably rule out burner retrofit of existing units.

10.3 GAS TURBINES

The stationary gas turbine has long been considered the natural application for the catalytic combustor since large excess air levels can be utilized to maintain appropriate catalyst bed temperatures and control turbine inlet temperature levels. In general, the graded cell catalyst could be applied directly to the gas turbine combustor provided sufficient air preheat is available. The graded cell system has been demonstrated to be operable over a wide range of temperature, mass throughput, and varying preheat conditions. Demonstrated high volumetric heat release rates also show that a relatively compact combustor can be achieved.

A concept for a canannular gas turbine combustor where the conventional burner is replaced by a catalytic one is shown in Figure 10-5. Stationary gas turbines are predominantly of the canannular type. Only the internal

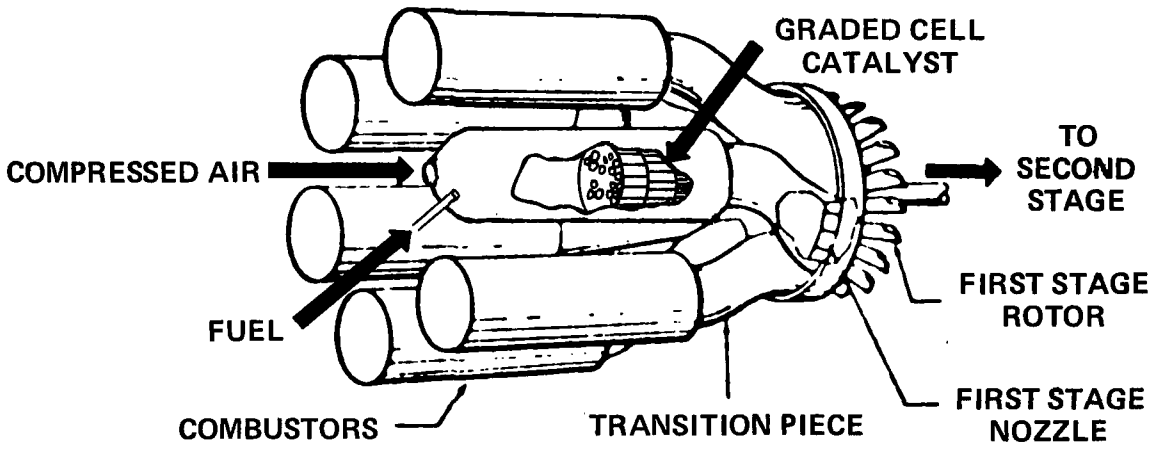

Figure 10-5. Catalytic gas turbine concept.

details and the fuel injection for the combustion can are modified. A special fuel injector to provide even fuel/air distribution without swirl would be required. The fuel would be premixed with all combustion air rather than adding additional secondary air as in present turbine systems. The manifold and turbine nozzles would not require modification.

The above concept appears feasible based upon experimental data obtained on the model turbine combustor tested under this program (Section 9). A graded cell monolith in a single can configuration was tested from 0.101 MPa to 1.01 MPa pressure with propane and from 0.303 MPa to 0.707 MPa with diesel fuel. Heat release rates as high as 844.8 MJ/hr (800,000 Btu/hr) were achieved. Simple modifications to the combustor and fuel injection system could be made for stationary gas turbine applications.

The graded cell catalyst design used in the model turbine could also be improved to achieve maximum conversion efficiency in a small combustor volume with a reasonable factor of safety. One possible concept for a more optimum gas turbine graded cell catalyst is shown in Figure 10-6. This system includes a large cell section for system lightoff and preheat. Forward of this preheat section a high emittance radiation shield is located which will absorb the radiant energy for this section and provide both preheat to the reactants and flameholding of possible flashbacks. Aft of the large cell preheater is a high reflectance metallic radiation shield which reduces radiant energy transfer from the primary bed to the preheat section, thereby minimizing the initiation of gas phase reactions in this region. The primary combustion section consists of a three-segment graded cell catalyst bed. All dimensions would be analyzed to provide the most efficient combustor.

Concepts for the larger cell preheat section are shown in Figure 10-7. Concept A is a large cell (0.0127 m) opening with 0.00318 m blunt edges to provide for lightoff with low transfer coefficients. Concept B would utilize smaller cells with larger diameter openings. The smaller cells would not support surface reactions, whereas the larger diameter openings would supply the preheat combustion. The third concept is a staggered tube arrangement, similar to the radiatively-cooled combustor described in Section 10.2.2.

Further development of the graded cell system for gas turbine application could be aided by PROF-HET code predictions of catalyst performance for

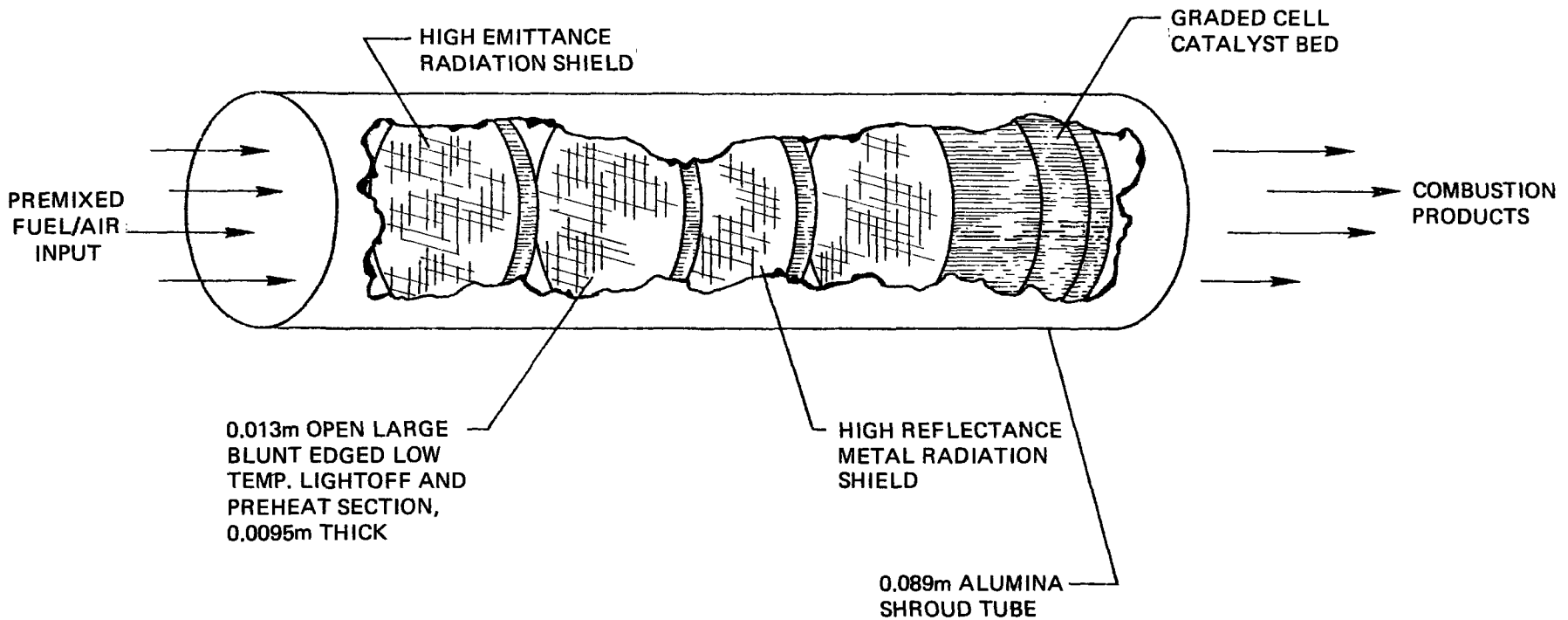

Figure 10-6. Stationary gas turbine graded cell catalytic combustor.

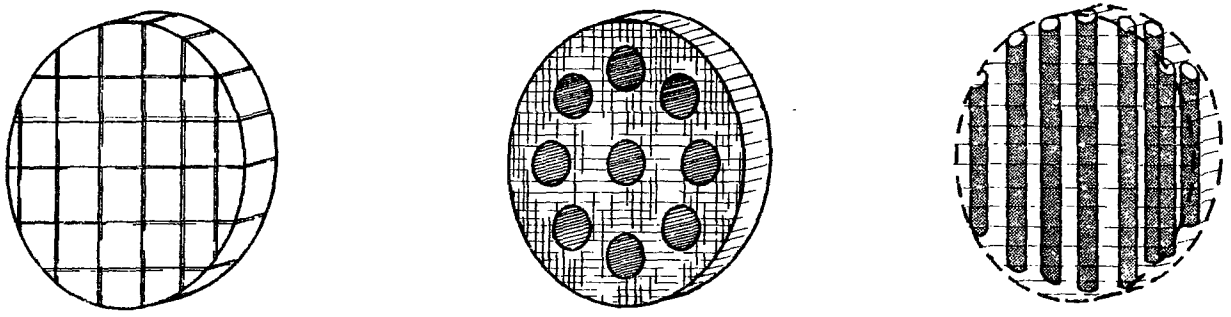

Figure 10-7. Low temperature lightoff/preheat section.

various geometries. Experimental development would further prove the validity of various design parameters. System lightoff and temperature control techniques also require further definition.

The two stage combustor could also be applied to the gas turbine. A catalytic fuel-rich first stage would be utilized for control of thermal nitrogen fixation and fuel nitrogen conversion, followed by a second stage which could be either catalytic or conventional combustion. No interstage heat removal would be required since the second stage would be operated lean (to control turbine inlet temperature) by addition of large amounts of excess air. Current advanced stationary turbine technology involves the investigation of two stage thermal combustion for NO_x control. A catalytic combustor in one or both stages may be a natural advancement.

10.4 OTHER SYSTEMS

A number of other combustion systems have been considered for catalytic applications. These include residential and industrial furnaces, rangetop burners, mobile turbines, and utility boilers. Although they are considered to be less probable applications, they are briefly mentioned here.

The residential furnace is the one system application that is currently marketed. The Bratko furnace has been described in Section 2 and in Reference 10-2. Additional schemes for both retrofit and redesigned residential furnaces are presented in Reference 10-1. Industrial combustion furnaces pose additional application possibilities but have not been investigated by this study.

Home rangetop burners pose applications problems that are similar to residential furnaces. Relatively small heat release rates and simple control systems are required. Only limited interest in the application currently exists due to their relatively small impact on the NO_x emissions inventory.

Mobile gas turbines, either automotive or aircraft, may be a natural extension of stationary turbine combustor development. Catalyst size and weight are not expected to be critical elements in the development of these systems. A high degree of system reliability is required, however, and poses the most serious current development problem.

Catalytic combustion application to utility boilers poses a large development problem due to extremely large heat release rate requirements. Demonstrated high combustion efficiency and simultaneous low emissions may warrant projected development costs. The use of lean catalytic combustors in overfire air ports may be the first generation of utility boiler applications.

10.5 CONCLUSIONS

Firetube boiler and stationary gas turbine applications appear promising for first generation catalytic combustor retrofit. The concepts of catalytic combustion have also been demonstrated for watertube boilers, home heaters, and mobile turbines, but radical system redesigns will probably be required for these applications.

The success of the two stage combustor in this program in controlling conversion of fuel-bound nitrogen to nitrogen oxides makes it appear promising in all applications. System redesign would necessarily occur in all two-stage applications since secondary air injection and/or interstage cooling systems are required. Additional work is also required to determine the applicability of mixed catalytic and conventional burner systems in two-stage combustors for the control of NO_x.

Further, all catalytic applications require additional development of fuel and air injection, premixing, and pre-vaporizing systems. Combustor control by bed temperature or stoichiometry and ignition systems also require further consideration.

The demonstration of catalytic combustor concepts in this program by the radiative/watertube, two stage, and gas turbine systems has shown that catalytic combustion is a viable technique and only awaits further development to accomplish these promising applications.

REFERENCES

10-1. Kesselring, J. P. et. al., "Catalytic Oxidation of Fuels for NO_x Control from Area Sources," EPA-600/2-76-037, February 1976.

10-2. Martin, G. B., "Evaluation of a Prototype Surface Combustion Furnace," EPA-600-7-77-073c, July 1977.

SECTION 11

CONCLUSIONS AND RECOMMENDATIONS

As a result of the extensive research and development program described in this report, significant progress has been made toward the development of a practical catalytic combustion system. Before the step to demonstration can be taken, however, additional work relating to the integration of the catalytic combustor into the total combustion system must be performed. This section briefly presents the conclusions reached under this program and makes recommendations for further work.

11.1 CONCLUSIONS

Based upon the analysis and test results of this program, the design, fabrication, and operation of catalytic combustors with high volumetric heat release rates and low emissions have been shown. Both precious metal and oxide catalysts have been tested over a wide operating temperature range. The precious metal catalysts should be limited to temperatures below 1589K (2400°F) for catalyst life considerations while oxide catalysts can be operated for long periods at temperatures above 1644K (2500°F). Catalyst performance has been greatly enhanced through the use of graded cell monoliths and higher catalyst loadings.

Catalytic combustors have been shown to be effective in controlling both thermal and fuel NO_x emissions. The thermal NO_x control appears to result from maximizing surface reactions in the combustor, while fuel NO_x can be minimized by operating at a rich fuel/air ratio which minimizes the formation of NH_3, HCN, and NO, with complete combustion of CO and HC at a later time. High pressure operation appears to give higher conversions of fuel nitrogen to NO_x if space velocity, bed temperature, and nitrogen concentration in the fuel are held constant. This implies that gas turbine

systems will have higher NO_x emissions if only one stage lean combustors are used with nitrogen containing fuels.

The maximum throughput of a catalytic combustor is a linear function of pressure and an exponential function of preheat. Thus, for a given preheat, the catalyst is face velocity limited in throughput ability. Hysteresis is also exhibited by the combustor in terms of preheat required, with less preheat required when the combustor has been operating than during the early combustor startup period.

Small scale catalytic combustion system configurations have been tested and indicate the feasibility of direct radiative removal of bed heat for temperature control, two stage catalytic combustion for temperature and fuel NO_x control, simulated exhaust gas recirculation through the use of nitrogen diluent for temperature control, and high excess air operation. The combustion system concepts that have been operated show that it is possible to operate stoichiometric conditions with less than 10 ppm NO_x and CO in a natural gas-fired catalytic combustor. While this program has provided much information on system applicability, further work with catalytic combustors in actual systems is required.

11.2 RECOMMENDATIONS

A number of areas in catalytic combustion need to be addressed to capitalize on the progress to date. Further oxide catalyst development work is required to minimize catalyst/support interactions and subsequent loss of thermostructural ability. Additional testing of simple and mixed oxide catalysts for combustion and fuel nitrogen conversion abilities is needed, along with life testing of selected catalysts to 1000 hours at various pressures.

Exploratory work with heavy fuel oils (#4, 5, 6) and pulverized coal should be conducted to determine system feasibility and fuel preparation problems. The potential of catalytic combustion in controlling NO_x emissions from the combustion of these fuels is great and needs early experimental verification.

Development of auxiliary systems required to interface with the catalytic combustor is also needed. This includes lightoff systems, temperature

control systems, and fuel and air introduction systems. In addition, further testing of the radiative catalyst/watertube, two stage combustor, and gas turbine combustor systems is needed to more thoroughly define operating ranges with a variety of fuels.

Finally, the design, fabrication, and operation of a demonstration unit should be undertaken when the above work is completed. The demonstration unit would be operated as a laboratory device for several months prior to the initiation of field demonstration tests.

APPENDIX A

SECTION 7 DATA SUPPLEMENT -- CATALYST SCREENING TESTS

TABLE A-1. SCREENING TEST DATA SUMMARY

a. JPL-004X

Fuel (lb/hr)	Air (lb/hr)	N_2 (lb/hr)	Preheat Temp. (°F)	% TA	Space Velocity (1/hr)	Approximate Bed Temperature (°F) T_{front}	$T_{ave.}$	T_{back}	Comments
.91	6.3	–	670	41.	5655.		730.		Start
	6.2	–	581		5655.	710.		790.	Transient
	6.3	–	504		5655.	1110.		900.	"
	6.2	–	400		5655.	1180.		1150.	
	8.3	–	373	54.	7084.	1500.		1470.	
	14.2	16.1	731	93.	23495.		1990.		
	14.9	19.4	781	98.	26495.		2000.		
	15.9	22.8	826	104.	29484.		2000.		
	15.8	25.3	865	104.	31606.		2000.		
	18.4	28.1	910	121.	35585.		2010.		
	20.8	–	939	136.	–		2000.		
	20.4	33.4	990	134.	41029.		2020.		
	22.3	35.3	1028	146.	43826.		2020.		
	21.0	35.7	1047	138.	43200.		2020.		
	21.8	37.2	1059	143.	49908.		2010.		
	22.6	38.4	1065	148.	46388.		2030.		
	40.8	–	1040	267.	30314.		2060.		
	61.1	–	1042	400.	44823.	2040.		2080.	
	76.4	–	1041	500.	55759.	2040.		2100.	
	76.7	–	1046	500.	55973.	1980.		2070.	
	73.4	–	1039	481.	53615.	1050.		2070.	Break-through
.91	6.9	–	844	45.	6083.		830.		Restart
.91	6.9	–	645	45.	6083.	930.		1000.	Transient
.91	6.9	–	592	45.	6083.	1450.		1100.	"
.91	6.8	–	476	45.	6012.	1720.		1550.	
.97	9.0	–	377	55.	7660.		1870.		
1.2	14.4	14.7	617	72.	22945.		1850.		
1.2	11.7	14.7	527	58.	21015.		1970.		
1.5	14.1	14.7	482	56.	23110.		1900.		
2.0	18.8	14.7	498	56.	27102.		1990.		
2.5	22.7	20.2	777	54.	34688.		1950.		
2.5	21.2	27.8	893	51.	39372.		1920.		
1.4	21.5	30.0	948	92.	39860.		1920.		
1.4	21.7	32.0	983	92.	41518.		1980.		
1.4	22.8	33.3	1005	104.	43289.		1990.		
1.4	24.3	34.6	1018	104.	45346.		1980.		
1.4	26.2	36.6	1034	112.	48218.		1990.		
1.4	23.2	37.0	1041	99.	46449.	1300		1900.	Break-through
.91	6.4	–	914	42.	5726.		880.		Restart
	6.4	–	775	42.	5726.		860.		Transient
	6.8	–	694	45.	6012.		850.		"
	6.9	–	650	45.	6083.	720.		1300.	"
	6.8	–	534	45.	6012.	1760.		1650.	
	8.8	–	665	58.	7442.		1980.		
	11.7	14.8	837	77.	20723.		1990.		
	14.0	19.0	772	92.	25548.		1970.		
	14.6	26.0	890	96.	31279.		1970.		
	15.0	30.8	1045	98.	35200.		1590.		
	17.9	36.0	1075	117.	41211.		2020.		
	20.8	38.0	1128	136.	44799.	1150.		1780.	Break-through
	20.5	38.0	1133	134.	44584.	1170.		2040.	Break-through
	18.9	38.0	1185	124.	43441.		1960.		
	24.7	38.0	1204	162.	47586.		2110.		
	52.9	18.0	1192	347.	52595.		2080.		
	69.9	–	1198	458.	51113.	1700.		2180.	
	66.8	–	1073	438.	48897.	1300.		2330.	Break-through

TABLE A-1. Continued

b. JPL-005X

Fuel (lb/hr)	Air (lb/hr)	N_2 (lb/hr)	Preheat Temp. (°F)	% TA	Space Velocity (l/hr)	Approximate Bed Temperature (°F) T_{front}	$T_{ave.}$	T_{back}	Comments
.91	6.4	—	793	42.	5726.		720.		Start
	6.4	—	648	42.	5726.		860.		Transient
	6.4	—	504	42.	5726.		1250.		
	8.5	—	590	56.	7227.		1930.		
	10.7	16.	1023	70.	20918.		1930.		
	18.5	40.	1043	121.	44670.		1960.		
	19.1	40.	1018	125.	45099.		1960.		
	24.9	38.	1055	163.	47729.		2020.		
	33.9	34.	1083	222.	51133.		2010.		
	40.7	28.	1082	267.	51449.	1200.		2000.	Break-through
.91	8.6	—	443	56.	6870.		1840.		
1.5	13.1	—	551	52.	11262.		1870.		
2.0	18.0	—	320	53.7	15397.		1930.		
2.5	23.0	6.7	522	54.9	24678.		1910.		
2.75	24.0	12.	741	52.0	29723.		1910.		
2.75	24.8	19.	778	53.8	35596.		1910.		
3.01	26.8	21.	754	53.1	38870.		1890.		End
.91	6.1	—	837	40.	5512.		810.		Restart
.91	6.2	—	748	41.	5583.	1150.		840.	Transient
.91	6.9	—	507	45.	6083.	1720.		1500.	
.91	8.9	—	460	58.	7513.		1840.		
2.0	18.6	13.5	801	55.5	26050.		1790.		
2.8	25.0	20.	845	53.2	36560.		1890.		
2.8	24.7	20.	790	52.6	36346.		1790.		
3.0	27.	26.	847	53.7	42787.		1880.		
3.5	31.7	34.	925	54.0	52838.		1900.		
3.8	33.1	35.	967	51.9	54976.		1820.		
3.8	33.1	36.5	973	51.9	56112.		1920.		
1.5	22.5	40.	1087	89.4	48275.		1960.		
1.5	25.8	45.3	1092	102.6	54648.		2000.		
1.5	25.5	46.5	1067	101.4	55343.	1150.		1900.	Break-through

TABLE A-1. Continued

c. JPL-006

Fuel (lb/hr)	Air (lb/hr)	N_2 (lb/hr)	Preheat Temp. (°F)	% TA	Space Velocity (1/hr)	Approximate Bed Temperature (°F) T_{front}	$T_{ave.}$	T_{back}	Comments
.91	6.2	–	707	41.	5583.		710.		Start Transient
	6.4	–	597	42.	5726.		770.		
	6.3	–	381	41.	5655.		1210.		
	8.4	–	357	55.	7156.		1890.		
	9.7	4.5	506	64.	11493.		1920.		
	10.6	8.5	588	69.	15166.		1930.		
	12.1	12.8	672	79	19495.		1960.		
	12.6	17.0	742	83.	23033.		1960.		
	13.0	19.5	784	85.	25212.		1960.		
	13.7	22.5	814	90.	27985.		1970.		
	14.1	23.5	836	92.	29028.		1970.		
	14.9	25.0	871	98.	30736.		1970.		
	14.7	26.5	885	96.	31729.		1970.		
	15.5	27.5	888	102.	33058.		1970.		
	15.7	27.5	902	103.	33201.		1970.		
	16.5	28.0	903	108.	34152.		1980.		
	18.6	28.0	715	122.	35653		1970.		
	15.8	28.0	899	104.	33651.		1980		End
	6.1	–	772	40.	5512.		800.		Restart
	6.8	–	477	45.	6012.	1630.		1370.	
	8.4	–	447	55.	7156.		1870.		
	10.5	–	644	69.	8657.		1860.		
	12.4	–	747	81.	10015.		1960.		
	12.5	22.4	784	82.	27051.		1950.		
	13.9	24.	819	91.	29264.		1980.		
	14.0	25.	853	92.	30093.		1990.		
	15.9	26.7	880	104.	32738.		2000.		
	14.3	27.5	893	94.	32201.		1990.		
	15.9	29.2	920	104.	34632.	1680.		2010.	Incipient break-through
	16.8	29.2	925	110.	35275.	1690.		2030.	
	18.0	30.3	939	118.	36966.	1210.		2030.	
	16.3	31.8	956	107.	36887.	1200.		1990.	
	18.5	33.0	969	121.	39368.	1180.		2000.	
	19.4	34.4	979	127.	41072.	1100.		2010.	
	24.5	30.1	981	161.	41460.	1050.		2060.	
	30.1	26.1	981	197.	42433.	1000.		2000.	
	15.8	25.6	886	104.	31834.		1970.		
	17.8	29.1	895	117.	35914.	1530.		1940.	Incipient break-through

TABLE A-1. Concluded

d. JPL-006X

Fuel (lb/hr)	Air (lb/hr)	N_2 (lb/hr)	Preheat Temp (°F)	% TA	Space Velocity (1/hr)	Approximate Bed Temperature (°F)			Emissions (ppm)			Comments
						T_{front}	T_{ave}	T_{back}	CO	UHC	NO	
.91	4.4	–	783.	28.8	4,295	683	–	662				Start
↓	↓	–	633.	↓	4,295	661	–	689				Transient
		–	571.		4,295	850	–	935				
		–	511.		4,295	1243	–	1210				
		–	477.		4,295	1264	–	1224				
	7.5	–	95.	49.1	6,509	1959	–	1792		20.	<1.	
	15.4	35.	653.	101.	38,642	2003	–	1955	11,500.	<5.	↓	
	22.	40.	607.	144.	47,141	1264	–	1980	<10.	↓		Unstable Point
	24.	45.	800.	157.	52,353	–	2008	–	<10.			
	14.	37.	852.	92.	39,156	1934	–	1891	13,800.			Not Minimum
	14.	48.	901.	92.	47,481	2007	–	1960	15,200.			Not Minimum *
	23.	54.	922.	151.	58,451	1974	–	1980	10.			Not Minimum
.50	7.5	14.	876.	89.4	16,586	2000	–	1911	9,500.			
↓	12.	22.	901.	143.	25,855	1966	–	1910	<10.			
	15.	12.	869.	179.	20,430	1766	–	1930	↓			
	31.	–	847.	370.	22,776	1522	–	1975				Incipient Breakthrough
	31.	–	841.	370.	22,776	1475	–	1970				Incipient Breakthrough
.91	3.9	–	879.	25.6	3,937	791	–	748				Restart
↓	4.0	–	764.	26.2	4,009	813	–	763				Transient
	4.5	–	370.	29.5	4,366	1717	–	1492				
2.0	15.6	9.	637.	46.5	20,486	1955	–	1848		28.	<1.	
2.0	16.6	11.	684.	49.5	22,714	1988	–	1887		15.	↓	
2.5	21.1	15.	690.	50.3	29,589	2004	–	1905		<5.		
3.0	26.3	19.	690.	52.3	36,963	1976	–	1836		↓		
3.0	25.8	19.	698.	51.3	36,606	2005	–	1875				
3.8	33.8	30.	698.	53.0	51,658	2002	–	1861				End (Breakthrough Not Reached)

*Trying to get to 200 percent TA.

TABLE A-2. TEST DATA – JPL-007

Fuel (lb/hr)	Air (lb/hr)	N_2 (lb/hr)	Preheat Temp (°F)	% TA	Space Velocity (1/hr)	Approximate Bed Temperature (°F)			Emissions (ppm)			Comments
						T_{front}	T_{ave}	T_{back}	CO	UHC	NO	
.91	4.9	–	836.	32.1	4,652	697	–	670				Start
↓	5.0	–	733.	32.8	4,723	746	–	683				Transient
	5.3	–	521.	34.7	4,937	1346	–	1304				Transient
	5.1	–	512.	33.4	4,795	1291	–	1254				
	7.9	–	110.	51.8	6,795	1949	–	1785		17.	<1.	
	15.1	20.	262.	99.0	27,075	1979	–	1909	16,300.	2.	↓	
	23.6	26.	307.	155.	37,688	1975	–	1929	<10.	2.		
	23.5	27.	302.	154.	38,373	1967	–	1927	↓	2.		
	32.2	22.	435.	211.	40,803	–	1984	–		5.	↓	End (No Breakthrough)
	5.1	–	871.	33.4	4,795	843	–	830				Restart
	4.8	–	708.	31.5	4,580	1119	–	861				Transient
	7.9	–	117.	51.8	6,795	1940	–	1765		3.	<1.	
	15.5	26.	553.	102.	31,902	1907	–	1897	19,400.	44.	↓	
↓	8.0	–	180.	52.4	6,866	1802	–	1667		6.		
3.5	30.0	10.	282.	51.1	33,427	1562	–	1788		582.		Incipient Breakthrough
4.0	33.9	11.	251.	50.5	37,603	1565	–	1774		383.	↓	Incipient Breakthrough

TABLE A-3. TEST DATA — JPL-008

Fuel (lb/hr)	Air (lb/hr)	N_2 (lb/hr)	Preheat Temp (°F)	% TA	Space Velocity (1/hr)	Approximate Bed Temperature (°F)			Emissions (ppm)			Comments
						T_{front}	T_{ave}	T_{back}	CO	UHC	NO	
.91	4.5	—	707.	29.5	4,366	—	692	—				Start
↓	4.4	—	572.	28.8	4,295	846	—	750				Transient
↓	4.7	—	243.	30.8	4,509	—	1201	—				
↓	8.3	—	112.	54.4	7,080	1882	—	1740		37.	<1.	
↓	14.5	16.5	117.	95.0	23,997	1980	—	1928	19,400.	<5.	↓	
↓	61.2	—	765.	401.	44,867	1432	—	1891	<10.	↓	↓	Incipient Breakthrough
↓	15.6	16.	107.	102.	24,405	1965	—	1898	18,200.	8.	↓	
↓	15.8	23.	460.	104.	29,845	1959	—	1913	13,900.	23.	↓	Not Minimum
↓	22.5	40.	880.	147.	47,498	1717	—	2072	<10.	<5.	↓	
↓	23.7	43.	981.	155.	50,625	1953	—	2035	↓	↓	↓	
↓	34.8	31.	941.	228.	49,472	1856	—	2081	↓	↓	↓	
↓	42.5	14.	883.	279.	42,106	1859	—	2075	↓	↓	↓	Incipient Breakthrough
↓	4.2	—	804.	27.5	4,152	—	785	—	↓	↓	↓	Restart
↓	4.2	—	669.	27.5	4,152	1170	—	865	↓	↓	↓	Transient
.91	7.4	—	277.	48.5	6,438	1835	—	1639	↓	1600.	<1.	
3.5	31.8	16.	232.	54.2	39,254	1983	—	1818	↓	2800.	<1.	Incipient Breakthrough
.91	3.8	—	828.	24.9	3,866	—	811	—	↓	↓	↓	Restart

TABLE A-4. TEST DATA – JPL-009

Fuel (LB/HR)	Air (LB/HR)	N2 (LB/HR)	Preheat Temp (°F)	% TA	Space Velocity (1/HR)	Approximate Bed Temp (°F)			Emissions PPM			Comment
						T_{Front}	T_{ave}	T_{Back}	CO	UHC	NO	
.91	5.5		689.	36.0	5,080		716					Start
↓	5.9		197.	38.7	5,366		1,366					
	7.8		164.	51.1	6,723		1,765				< 1.	High
	16.1	16.	161.	105.5	24,762		1,849			1200.	↓	High
↓	8.0		177.	52.4	6,866		1,774			84.4		
2.0	17.9		168.	53.4	15,317		1,916			1350.		
3.0	26.7		159.	53.1	22,869		1,890			5360.		High
.91	15.1	15.	161.	99.0	26,670		1,867		9630	1170.	↓	End

TABLE A-5. TEST DATA — JPL-010

Fuel (LB/HR)	Air (LB/HR)	N2 (LB/HR)	Preheat Temp. (°F)	% TA	Space Velocity (1/HR)	Approximate Bed Temp (°F)			Emissions PPM			Comments
						T_{Front}	T_{ave}	T_{Back}	CO	UHC	NO	
.91	5.0	—	684.	32.8	4,723		635					Start
↓	5.0	—	574.	32.8	4,723		670					
	5.0	—	518.	32.8	4,723	1234		704				Transient
	5.0	—	405.	32.8	4,723		1198					
	7.5	—	638.	49.1	6,509					47.4	0.	
	13.5	36.0	795.	88.5	38,042		BAD		14,000.	0.3	↓	
	17.2	40.0	735.	112.7	43,712				3,440.	0.3		
	22.8	40.0	822.	149.4	47,712		DATA		.2	2.8		
↓	33.8	31.0	836.	221.5	48,758				644.	2010.	↓	End ↓ Catalyst Damaged at Front Face

TABLE A-6. TEST DATA — JPL-010X

Fuel (LB/HR)	Air (LB/HR	N2 (LB/HR)	Preheat Temp. (°F)	% TA	Space Velocity (1/HR)	Approximate Bed Temp (°F)			Emissions PPM			Comment
						T_{Front}	T_{ave}*	T_{Back}	CO	UMC	NO	
0.91	5.25	—	643.	34.4	3,865		619.					Start
↓	5.1	—	462.	33.4	4,795	494.		840.				Transient
	4.2	—	165.	27.5	4,152		1197.					
	7.9	—	117.	51.8	6,795		1727.			40.	< 1.	
	14.2	16.5	96.	93.1	23,783		1930.		3370.	< 5.	↓	
	23.0	21.0	157.	151.	33,475		1957.		< 10.	↓	↓	
	33.0	13.0	118.	216.	34,563		1946.		↓	↓	↓	
	42.7	—	107.	280.	31,653		2017.		↓	↓	↓	
	50.0	—	407.	328.	36,867		1993.		↓	↓	↓	
↓	33.3	20.0	516.	218.	40,075		1954.		↓	↓	↓	Not Minimum
1.5	56.1	38.0	698.	223.	70,732		2105.		↓	↓	↓	
1.5	55.2	39.0	688.	219.	70,846	781.		1811.	↓	↓	↓	Breakthrough
0.91	4.5	—	738.	29.5	4,366		726.					Restart
↓	8.2	—	192.	53.7	7,009		1792.		59,300	44.0	< 1.	
↓	15.9	13.0	154.	104.2	22,348		2060.		16,700	17.6	↓	End

*Thermocouples 0.1" back were not included in average.

TABLE A-6. Concluded

JPL-010X

Fuel (LB/HR)	Air (LB/HR)	N_2 (LB/HR)	Preheat Temp. (°F)	% TA	Space Velocity (1/HR)	Approximate Bed Temp (°F)			Emissions (PPM)			Comments
						T_{Front}	T_{ave}*	T_{back}	CO	UMC	NO	
0.91	4.5	—	786.	29.5	4,366		839.					Restart
↓	4.5	—	708.	29.5	4,366	1632.		847.				Transient
	7.6	—	195.	49.8	6,580		1786.			30	< 1.	
	15.7	18	214.	103	25,990		1944.		22,200	< 5	↓	
	15.7	27	644.	103	32,801		1978.		2,600	↓		Not Minimum
	23.3	39	773.	153	47,312		1970.		< 10.			End**
	5.9	—	784.	38.7	5,366		858.					Restart
	7.8	—	125.	51.1	6,723		1785.			52.2	< 1.	
4.0	35.	—	62.	52.2	30,063		1889.		59,700	4.8	↓	
6.0	52.	12	243.	51.7	53,819		1931.		53,600	227.		End

*Thermocouples 0.1" back were not included in average.
**Approximately 8 hours of testing has occurred by this point.

TABLE A-7. DATA SUMMARY — JPL-010P

Fuel (lb/hr)	Air (lb/hr)	N_2 (lb/hr)	Preheat Temperature (°F)	Percent TA	Space Velocity (1/hr)	Comments	Time (min)
0.91	54.9		908	359.7	40367	Methane start	0
	55.5		880	363.7	40796	Transient	
	54.1		880	354.5	39796		
	54.8		882	359.1	40296		
	58.6		894	384.0	43010	Stable	20
	56.8		829	372.2	41724		39
0.5	22.7		971	270.7	16848	Restart	39
0.5	28.8		902	343.5	21205		39
0.5	35.3		1059	421.0	25848		95
0.7	49.3		1067	420.0	36101		100
0.91	65.0		1050	426.0	47582		105
0.5	35.8		1090	427.0	26205		185
0.7	49.2		1105	419.1	36030		198
0.91	67.1		1091	439.7	49082		208
0.5	36.1		1121	430.6	26419		283
0.7	50.4		1112	429.4	36887	End	293
0.5	36.1		1141	430.6	26419	Restart	295
0.5	37.2		1220	443.7	27205		308
0.5	37.2		1120	443.7	27205		362
0.5	36.8		1119	438.9	26919		428
0.5	36.6		1097	436.5	26777		444
0.5	36.3		1126	432.9	26705		512
0.5	35.7		1121	425.8	26134		639
0.5	36.3		1120	432.9	26705		741
0.5	36.2		1118	431.7	26491	End	818
0.91	5.4		825	35.9	5009	Restart	830
	5.7		215	37.4	5223		853
	8.2		107	53.7	7009		873
3.0	25.7		82	51.1	22154		890
3.8	31.9		78	50.1	27595		899
4.5	40.5		124	53.7	34624		926
4.5	40.6		82	53.8	34696	End	1003
0.7*	48.0		1119	408.9	35173	Propane restart	1063
0.6*	39.0		1126	387.6	28617		1113
0.5*	32.4		1121	386.4	23776	End	1128
1.0*	4.55		827	27.1	4516	Restart	1138
1.0*	4.5		521	26.8	4480	Restart	1138
1.0*	4.7		339	28.0	4623	End	1141

*Propane

TABLE A-8. TEST DATA — JPL-011

Fuel (LB/HR)	Air (LB/HR)	N2 (LB/HR)	Preheat Temp. (°F)	% TA	Space Velocity (1/HR)	Approximate Bed Temp (°F)			Emissions PPM			Comments
						T_{Front}	T_{ave}*	T_{Back}	CO	UHC	NO	
.91	5.7		642.	37.4	5,223		686					Start
↓	5.9		183.	38.7	5,366		1,358					
↓	7.7		158.	50.5	6,652		1,792			26.2	< 1.	
2.0	17.4	5.5	143.	51.9	19,123		1,662			6.9	↓	
3.0	26.4	4.5	149.	52.5	26,060		1,766			< 5.		
4.0	35.3	4.5	151.	52.6	33,683		1,927			↓		
5.0	42.9	5.5	152.	51.2	41,134		1,934					
6.0	51.0	9.0	146.	50.7	50,835		1,951					
.91	15.9	17.	141.	104.2	25,376		1,896		14,800.			
↓	22.4	36.	655.	146.8	44,399		2,005		< 10.	↓	↓	End - (Could not get to 200% TA)
↓	5.7		804.	37.4	5,223		756					Restart
↓	6.1		299.	40.0	5,509		1,515					
0.5	9.2	12	312.	109.7	16,287		1,916		< 10.	< 5.	< 1.	
↓	17.7	15	947.	211.1	24,629		1,952		↓	↓	↓	

*Thermocouples 0.1" back were not included in average.

TABLE A-8. Concluded

JPL-011

Fuel (LB/HR)	Air (LB/HR)	N2 (LB/HR)	Preheat Temp. (°F)	% TA	Space Velocity (1/HR)	Approximate Bed Temp (°F)			Emissions PPM			Comments
						T_{Front}	T_{Ave}*	T_{Back}	CO	UHC	NO	
2.5	21.2	6	118.	50.6	22,848		1,894			1,000.	< 1.	Break-through (High UHC)
(PROPANE)												
1.0	5.9	—	400.	37.7	4,694		384					Restart
	5.1	—	115.	32.6	4,122		1,725					
	7.7	—	95.	49.2	5,980		1,769					
	14.8	21	244.	94.6	26,945		1,911		5120.	< 5.	< 1.	End

*Thermocouples 0.1" back were not included in average.

TABLE A-9. TEST DATA — JPL-012

Fuel (LB/HR)	Air (LB/HR)	N2 (LB/HR)	Preheat Temp. (°F)	% TA	Space Velocity (1/HR)	Approximate Bed Temp (°F)			Emissions PPM			Comments
						T_{Front}	T_{ave}*	T_{Back}	CO	UHC	NO	
0.91	6.2		567.	40.6	5,580		645					Start
↓	6.6		188.	43.3	5,866		1,523			< 5.	< 1.	
	8.0		186.	52.4	6,866		1,832			35.5	↓	
	15.5	19.	290.	102.	26,604		1,904		10,100.	< 5.		
	17.0	38.	751.	111.	42,055	967		1,974	6,750.	153.		END**
	6.6		707.	43.3	5,866		754					Restart
	6.2		127.	40.6	5,580		1,518					
↓	7.7		138.	50.4	6,652		1,757			40.6	< 1.	
3.5	29.1	27.	808.	49.6	42,373		1,979			417.	↓	END***

*Thermocouples 0.1" back not included in ave.

**Could not go to leaner conditions (150% TA)

***Maximum throughput at 50% TA

TABLE A-10. TEST DATA — JPL-013

Fuel (LB/HR)	Air (LB/HR)	N2 (LB/HR)	Preheat Temp. (°F)	% TA	Space Velocity (1/HR)	Approximate Bed Temp (°F)			Emissions PPM			Comments
						T_{Front}	T_{ave}*	T_{Back}	CO	UHC	NO	
.91	5.8		757.	38.0	5,295		861 *					Start
↓	5.9		666.	38.7	5,366	1,824		892				Transient
	7.9		141.	51.8	6,795	2,079		1,803		600.	< 1.	
↓	7.8	6.	201.	51.1	11,264		1,718 *			6,300.	↓	Break-through (High UHC)

*Thermocouples 0.1" back were not included in average.

TABLE A-11. TEST DATA — JPL-022

Fuel (LB/HR)	Air (LB/HR)	N2 (LB/HR)	Preheat Temp. (°F)	% TA	Space Velocity (1/HR)	Approximate Bed Temp (°F)			Emissions PPM			Comments
						T_{Front}	T_{ave}*	T_{Back}	CO	UHC	NO	
.91	6.6		594.	43.2	5,866		606					Start
↓	5.8		114.	38.0	5,295		1,320					
↓	8.1		109.	53.1	6,938		1,782			23.7	< 1.	
2.5	21.0		86.	50.1	15,317		1,821			5.7	↓	
3.5	30.8	6.0	87.	52.5	30,971		1,864			< 5.		
4.5	38.8	6.0	97.	51.4	37,951		1,844			↓		
5.5	46.2	8.0	93.	50.1	46,016		1,824					
6.0	50.6	11.0	90.	50.3	52,063		1,845			↓	↓	END
.91	6.5		542.	42.6	5,795		597					Restart
↓	7.8		148.	51.1	6,723		1,860			15.4	< 1.	
↓	15.1	30.	705.	99.0	34,643		1,959		12,700.	< 5.	↓	
↓	15.8	31.	679.	103.5	35,900	1,285		1,977	10,800.	↓	↓	Incipient Break-through

TABLE A-12. TEST DATA – JPL-016

Fuel (lb/hr)	Air (lb/hr)	N_2 (lb/hr)	Preheat Temp (°F)	% TA	Space Velocity (1/hr)	Approximate Bed Temp (°F) T_{ave}	Comments
0.91	5.7	0	650	37.3	5223	687	Start
		0	498			895	Transient
		0	123			1403	
	8.1	0	93	53.1	6938	1859	
	16.3	18.4	85	106.8	26720	1931	
	17.3	20.5	182	113.4	29025	1971	
	16.6	35.9	798	108.8	40180	1950	Not minimum
	17.1	28.8	589	112.1	35164	1958	Not minimum
	6.1	0	625	40.0	5509	752	Restart
	7.9	0	66	51.8	6795	1859	
	16.0	17.9	68	104.8	26128	1931	
0.5	9.2	22.7	915	109.7	24385	1935	
3.5	31.6	7.5	112	53.8	32678	1820	
4.0	36.0	5.0	91	53.7	34562	1934	
0.91	5.6	0	665	36.7	5152	1139	Restart
0.91	13.8	31.0	914	90.4	34472	1954	

TABLE A-13. TEST DATA — JPL-021

Fuel (lb/hr)	Air (lb/hr)	N_2 (lb/hr)	Preheat Temp (°F)	% TA	Space Velocity (1/hr)	Comments	Time (min)
1.5	105.6	0		419.8	231,990	Start	0
1.5	109.7		1029	436.1	240.774		23
1.7	118.2		1060	414.6	259,749		65
1.6	115.4		1059	430.1	253,368		122
1.5	109.8		1054	436.5	240,990		183
	112.4		917	446.9	246,561		190
	114.8		1114	456.4	251,703	Restart	190
	118.1		1069	469.5	258,774		192
	107.7		1053	428.2	236,490		223
1.7	111.4		1046	390.8	245,178		239
	107.5		1046	377.1	236,820		434
	110.3		1051	386.9	242,820		599
	58.4		1072	204.9	131,601	Restart	606
	108.8		1052	381.6	239,604		617
1.9	109.0		1047	342.1	240,792		908
1.9	111.2		1043	349.0	245,508		1187
1.5	106.2		1059	422.2	77,758	Restart*	1187
	113.1		1029	449.6	82,687		1187
	108.1		1044	429.8	79,115		1192
	109.7		1055	436.1	80,258		1201
	108.0		1053	429.4	79,044		1253
	108.0		1050	429.4	79,044		1298
	107.5		1047	427.4	78,687		1370
2.0	16.8		967	50.1	14,531	Restart*	1370
2.0	17.1		117	51.0	14,746		1446
3.0	26.9		101	53.5	23,012		1487
4.0	34.4		98	51.3	29,634		1503

*Two 1-inch segments of JPL-015 included downstream.

TABLE A-14. MONOLITH 019 TEST DATA — JPL TESTS

1 atm Pressure							
Fuel	TA, %	SV, hr^{-1}	$\dot{m}_{fuel}$, lbm/hr	$\dot{m}_{air}$, lbm/hr	T_{PH}, °F	T_{BED}, °F	Run-Scan No.
Methane	320	87,800	2.2	118.1	852	1980	A41A-6
Methane	320	88,200	2.2	118.7	957	2040	A41A-17
Propane	350	78,800	1.9	106.1	864	1980	A41C-5
Indolene	290	80,800	2.5	108.2	855	1950	A41D-5
Methanol	326	64,400	4.0	84.2	689	2000	A41E-7
Methanol	241	72,500	6.0	93.4	293	1930	A41E-15
Methane	211	66,300	2.5	88.4	854	2400	A41F-4
Methane	200	74,500	3.0	99.1	843	2550	A41F-8
Propane	248	72,700	2.5	97.1	862	2400	A41F-15
Propane	261	61,000	2.0	81.6	752	2340	A41F-19

TABLE A-15. MONOLITH 019 TEST DATA — ACUREX TESTS

1 ATM PRESSURE

FUEL	TA, %	SV, hr^{-1}	$\dot{m}_{fuel}$, lbm/hr	$\dot{m}_{air}$, lbm/hr	T_{ph}, °F	$\bar{T}_{bed}$, °F	RUN #
Natural Gas	28	21,100	4.4	20.9	660	1,950	1122-2
Natural Gas	28	21,400	4.4	21.5	460	1,940	1122-3
Natural Gas	42	29,300	4.4	32.1	520	2,240	1122-4
Natural Gas	42	29,200	4.4	32.1	524	2,250	1122-5
Natural Gas	42	28,400	4.4	31.1	527	2,230	1122-7
Propane	38	40,000	5.3	50.6	417	2,010	1123-1
Propane	37	39,100	5.0	49.5	421	1,970	1123-2
Natural Gas	40	37,800	5.8	39.8	634	2,400	1124-2
Natural Gas	227	105,000	3.5	135.9	721	2,120	1201-1
Natural Gas	217	97,600	3.4	127.4	738	2,350	1201-2
Natural Gas	205	92,700	3.4	120.3	740	2,340	1201-3
Natural Gas	196	92,500	3.6	120.0	730	2,360	1201-4

TABLE A-16. MONOLITH 019 TEST DATA — ACUREX TESTS, EMISSIONS DATA FOR SIMULATED FUEL NITROGEN TESTS

FUEL	TA, %	$\bar{T}_{bed}$, °F	NH_3 fuel conc, ppm	NH_3 comb gases, ppm	CO, ppm	UHC, ppm	NO_x ppm	HCN, ppm	NH_3, ppm
Natural Gas	27	1,950	—	—	> 2,000	> 300	2	—	—
Natural Gas	28	1,940	1,000	270			4	2.3	173
Natural Gas	42	2,240	—	—			3	—	—
Natural Gas	42	2,250	1,000	200			4	35	223
Natural Gas	42	2,230	6,000	1,212			25	NG	964
Propane	38	2,010	—	—			13	—	—
Propane	37	1,970	1,000	62			NG	NG	77
Natural Gas	40	2,400	—	0			<1	NG	0
Natural Gas	227	2,120	—	—	15	NG	2	—	—
Natural Gas	217	2,350	—	—	17	10	2	—	—
Natural Gas	205	2,340	6,000	292	13	2	78	5	3.4
Natural Gas	196	2,360	1,000	51	16	1	10	6	0

TABLE A-17. MONOLITH 019 TEST DATA — ACUREX TESTS, HIGH PRESSURE OPERATION

FUEL	P, Atm	TA,%	SV, hr^{-1}	$\dot{m}_{fuel}$, lbm/hr	$\dot{m}_{air}$, lbm/hr	T_{ph}, °F	$\overline{T}_{bed}$, °F	RUN #
Methane	1	33	21,700	4.0	22.8	520	1980	1206-2
	1	212	98,200	3.6	130.5	688	2430	1206-3
	2	197	88,000	3.4	114.9	697	2350	1206-4
	3	187	84,000	3.3	106.6	702	2400	1206-5
	3	210	89,300	3.3	120.3	710	2400	1206-6
	6	232	123,300	4.1	161.5	762	2170	1206-7

Total bed operating time: >74 hours

TABLE A-18. MONOLITH 019 TEST DATA – ACUREX TESTS, EMISSIONS DATA FOR FUEL NITROGEN SIMULATION TESTS AT PRESSURE

FUEL	TA, %	P, atm	$\overline{T}_{bed}$, %	NH_3 fuel, ppm	NH_3 comb, gas, ppm	CO, ppm	UHC, ppm	NO_x, ppm	HCN, ppm	NH_3, ppm
Methane	32	1	1930	---	---	>2000	>300	1	---	---
Methane	212	1	2430	---	---	30	2	2	---	---
Methane	197	2	2350	---	---	23	4	6	---	---
Methane	187	3	2400	---	---	24	2	5	---	---
Methane	210	3	2400	6,000	286	22	1	195	0	0
Methane	232	6	2170	---	---	--	--	---	---	---

TABLE A-19. MONOLITH 019 TEST DATA — NATURAL GAS, HIGH TEMPERATURE OPERATION

TEST PT.	TA, (%)	SV,[a] (hr^{-1})	$\dot{m}_{fuel}$, (lbm/hr)	$\dot{m}_{air}$, (lbm/hr)	T_{ph}, (°F)	$\bar{T}_{bed}$, (°F)	$T_{max,bed}$, °F
1228-1	42	30,300	4.6	34.0	532	1820	2300
1228-3	238	141,200	4.5	184.1	678	2210	2485
1228-4	250	142,200	4.3	185.9	625	2070	2530
1228-6	225	126,400	4.3	164.4	594	2382	2615
1228-7	211	120,200	4.3	155.9	581	2500	2660
1228-8	195	111,900	4.3	144.5	582	2610	2710
			— Shutdown and Relight —				
1228-11	48	32,000	4.4	35.6	642	2110	2600
1228-12	236	136,800	4.4	178.4	720	2360	2580

[a]Space velocity based on standard conditions

SECTION B

SECTION 8 DATA SUPPLEMENT -- GRADED CELL CATALYST TESTS

SECTION B-1

W. R. GRACE CATALYST
TEST MODEL A-025

TABLE B-1. TEST DATA SUMMARY — CATALYST A-025

Run #	TA%	SV, hr^{-1}	$\dot{m}_{fuel}$, lbm/hr	$\dot{m}_{air}$, lbm/hr	T_{ph}, °F	$\overline{T}_{BED}$, °F	$T_{BED_{max}}$, °F
0425-01	269	146,700	4.2	193.3	761	2027	2231
0426-10	233	135,700	4.4	177.8	676	2251	2431
0427-03	250	143,000	4.4	187.8	697	2263	2432
0427-05	264	150,100	4.4	197.6	602	2092	2461
0427-07	253	146,600	4.4	192.7	500	1967	2414
0427-08	272	157,500	4.4	207.6	755	2265	2500
0428-04	306	186,500	4.7	246.8	758	2129	2551
0428-07	308	248,700	6.2	329.2	778	1780	2466
0428-10	302	327,400	8.3	433.2	797	1806	2511
0428-12	321	193,300	4.6	256.4	785	2144	2523
0428-14	291	175,900	4.6	232.5	778	2455	2711
0428-18	297	176,900	4.6	234.0	600	2365	2721
0428-20	272	163,500	4.6	215.6	501	2406	2709
0429-01	251	156,400	4.8	205.6	759	2024	2542
0429-02	232	143,100	4.7	187.5	752	2437	2717
0429-05	234	204,900	6.7	268.5	769	2203	2705
0429-07	223	273,800	9.3	358.0	785	2096	2699
0429-09	252	383,300	11.6	503.8	800	2145	2735
0429-11	287	182,300	4.9	240.8	788	2092	2511

Total test time = 20 hrs

at Q = 100,000 Btu/hr nominal heat release rate

TABLE B-2. EMISSIONS DATA[c] — CATALYST A-025

Run No.	Test Time, hrs	TA %	$\dot{m}_{fuel}$, lbm/hr	CO, ppm	NO, ppm[d]	
0425-06	2.0	269	4.2	0	0	Emissions time history and throughput effects at the nominal condition $T_{bed} \simeq 2400°F$ $T_{ph} \simeq 750°F$
0426-10	10.0	233	4.4	0	3	
0427-03	11.7	250	4.4	0	3	
0427-08	12.5	272	4.4	0	3	
0428-04	15.0	306	4.7[a]	0	2	
0428-07	15.5	308	6.2[a]	0	2	
0428-10	16.0	302	8.3[a]	48[b]	2	
0428-12	16.5	321	4.6	437[b]	2	
0429-01	17.7	251	4.8	0	2	
0429-11	20.0	287	4.9	0	2	
0429-02	18.2	232	4.7	0	4	Emissions vs throughput at $T_{bed} \simeq 2700°F$
0429-07	18.7	223	9.3	0	3	
0429-09	19.6	252	11.6	0	4	

[a] Increased mass throughput to demonstrate the effects on emissions.

[b] May not be steady operating values. Wide variations (0 to 1200 ppm) in CO emissions were noted as test conditions were changed.

[c] No emissions changes with reduced preheat were noted.

[d] All NO_x measured was present as NO.

TABLE B-3. LIGHTOFF TEMPERATURE HISTORY — CATALYST A-025

Cumulative Test Time (hrs)	Lightoff Stoichiometry	Lightoff Temperature (°F)	Comments
0	Fuel lean	910	Uneven bed temperature distribution immediately apparent
2.5	Fuel rich	900	Unsuccessful lean lightoff at 990°F. May not have been minimum rich lightoff temperature. Very sooty combustion.
10.0	Fuel rich	830	Soot not apparent
13.0	Fuel rich	830	Combustion on one side of bed only
17.5	Fuel rich	930	

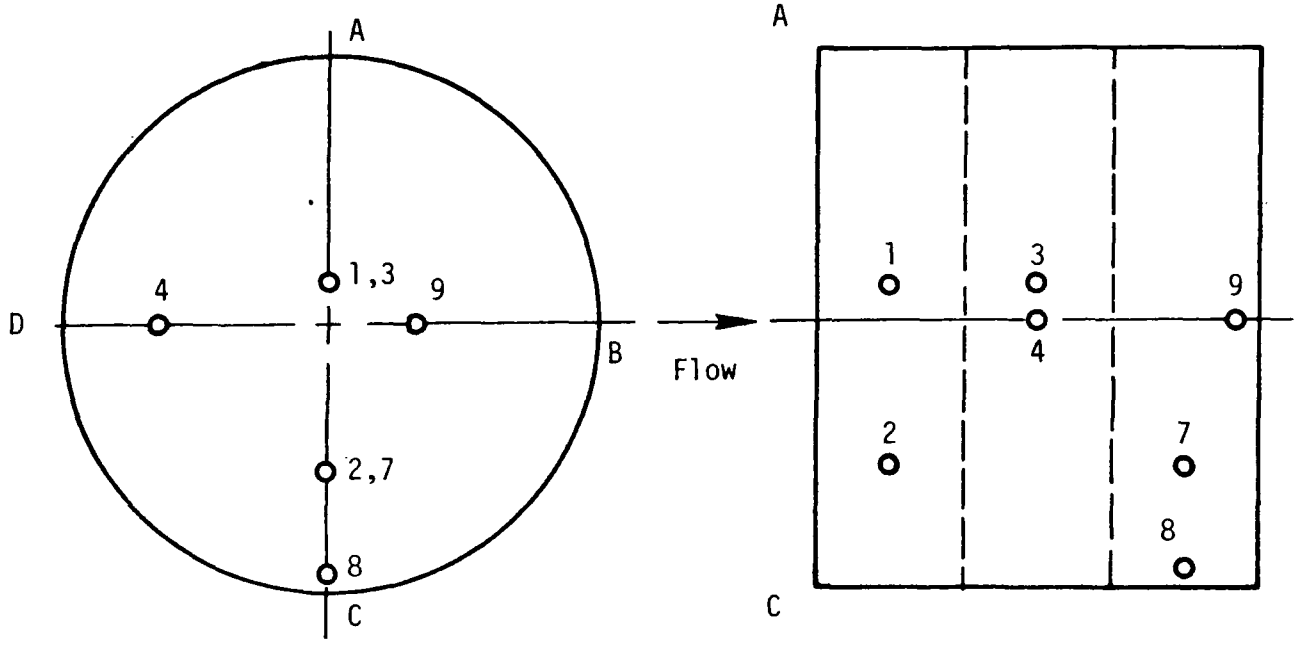

BEGINNING OF AGING

t = 1 hr

Run 0425-01

TC	°F
1	2032
2	1947
3	2205
4	1457
7	2222
8	2093
9	2231

END OF AGING

t = 10 hrs

Run 0426-10

TC	°F
1	2306
2	2314
3	2375
4	1657
7	2431
8	2358
9	2314

Figure B-1. Catalyst A-025 bed temperature distribution, effects of aging.

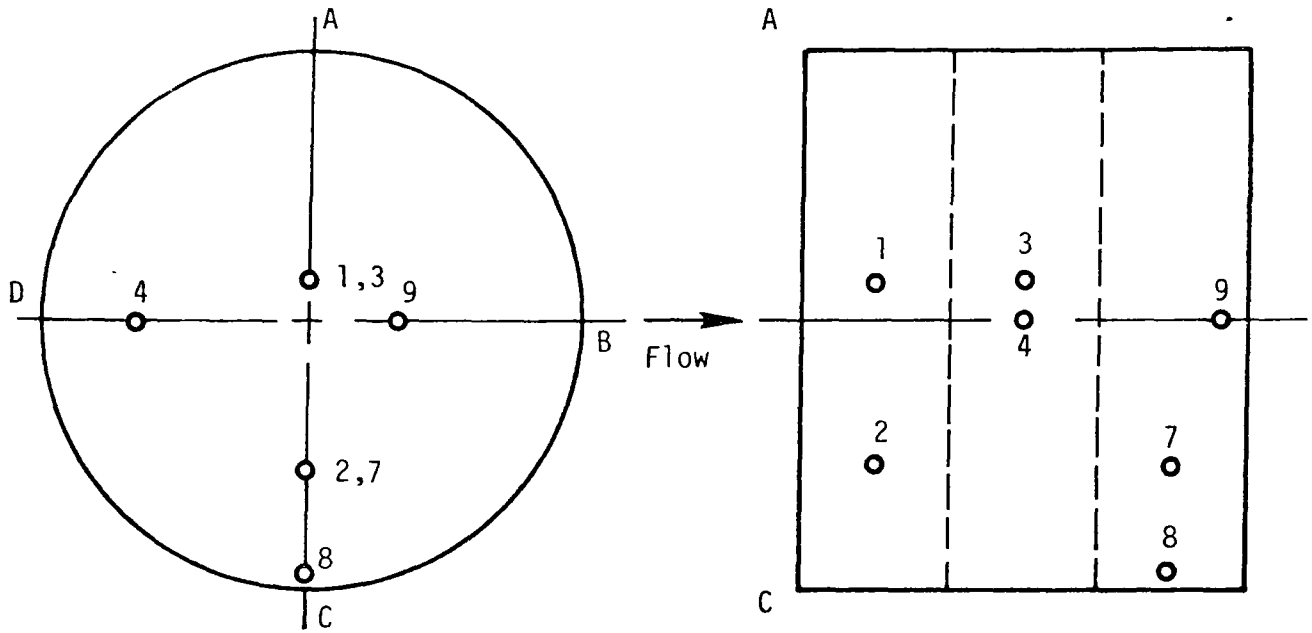

2400°F BED

T_{PH} = 697°F		T_{PH} = 500 °F	
Run 0427-03		Run 0427-07	
TC	°F	TC	°F
1	2277	1	1754
2	2110	2	2015
3	2432	3	2109
4	1964	4	969
7	2390	7	2414
8	2341	8	2334
9	2324	9	2173

2700°F BED

T_{PH} = 778°F		T_{PH} = 501°F	
Run 0428-14		Run 0428-20	
TC	°F	TC	°F
1	2461	1	2342
2	2203	2	2551
3	2577	3	2588
4	2415	4	1454
7	2464	7	2649
8	2391	8	2546
9	2711	9	2709

Figure B-2. Catalyst A-025 bed temperature distribution, effects of preheat.

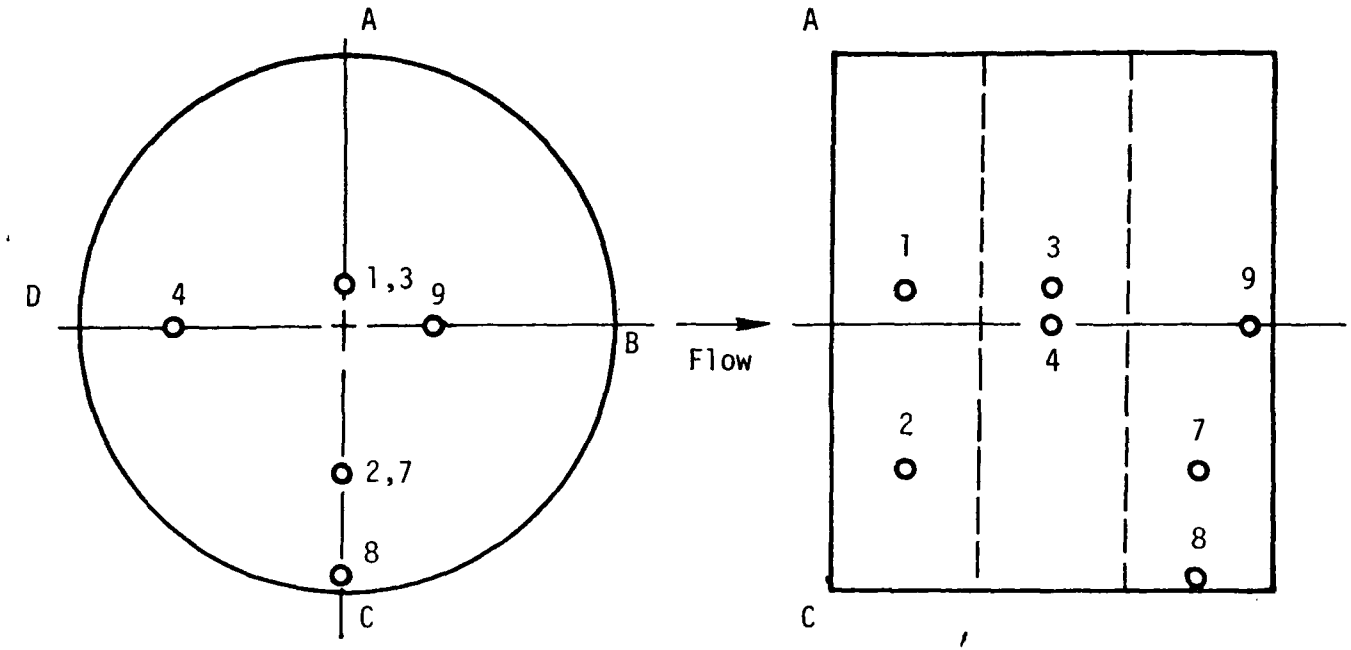

2400°F BED

$\dot{m}_f$ = 4.7 lbm/hr $\dot{m}_f$ = 8.3 lbm/hr

Run 0428-04		Run 0428-10	
TC	°F	TC	°F
1	1899	1	1365
2	1725	2	1625
3	2218	3	1641
4	2270	4	1742
7	2246	7	2297
8	1997	8	1458
9	2551	9	2511

2700°F BED

$\dot{m}_f$ = 4.7 lbm/hr $\dot{m}_f$ = 11.6 lbm/hr

Run 0429-02		Run 0429-09	
TC	°F	TC	°F
1	2428	1	2287
2	2245	2	1716
3	2587	3	1835
4	2407	4	2403
7	2496	7	2489
8	2419	8	1551
9	2717	9	2735

Figure B-3. Catalyst A-025 bed temperature distribution, effects of throughput.

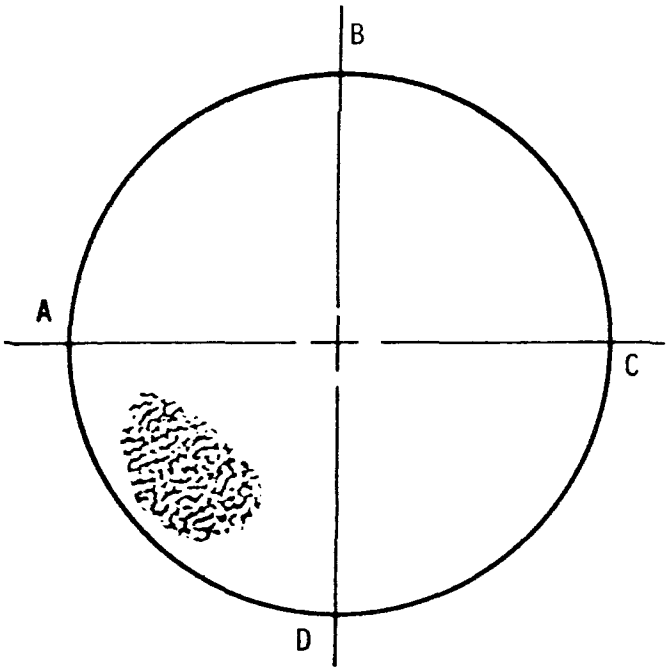

Nominal test condition
TA ≃ 200 %

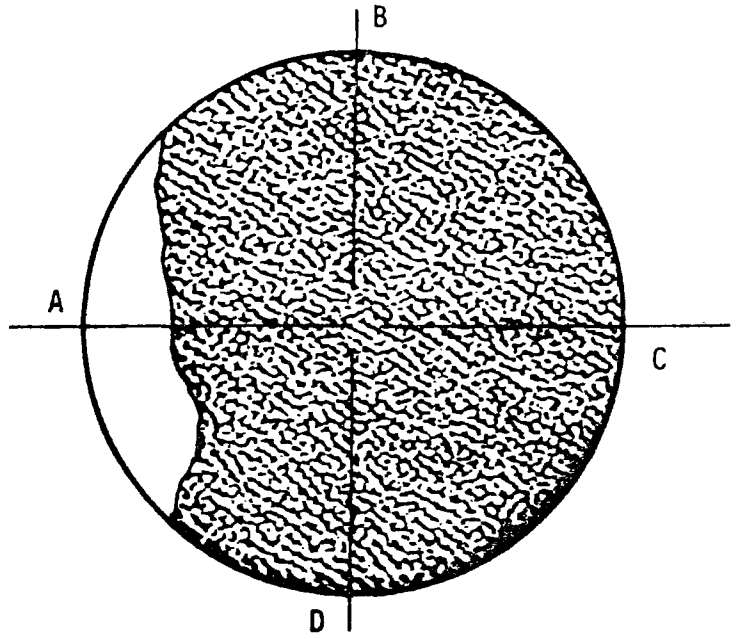

TA ≃ 50%

Q = 100,000 Btu/hr

T_{PH} ≃ 750°F

T_{BED} ≃ 2400°F

Figure B-4. Catalyst A-025 bed appearance rear view, varying stoichiometry.

Varying bed temperature*

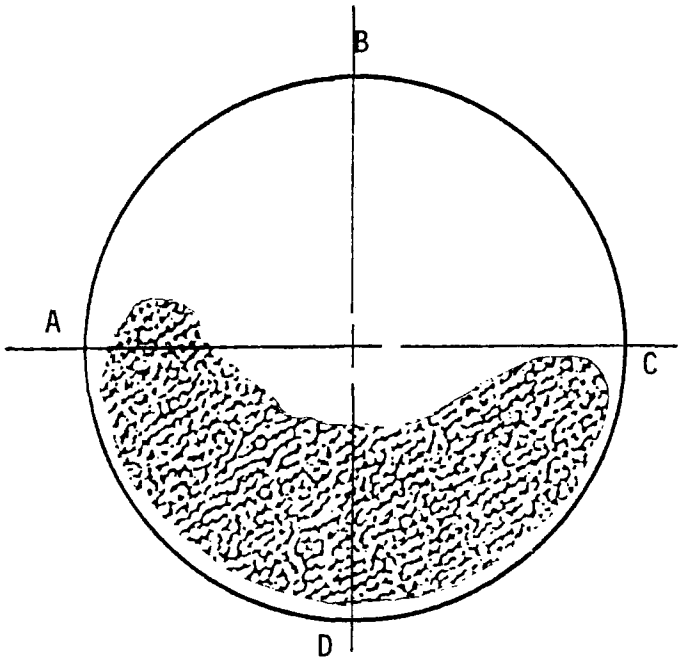

T_{BED} = 2200°F

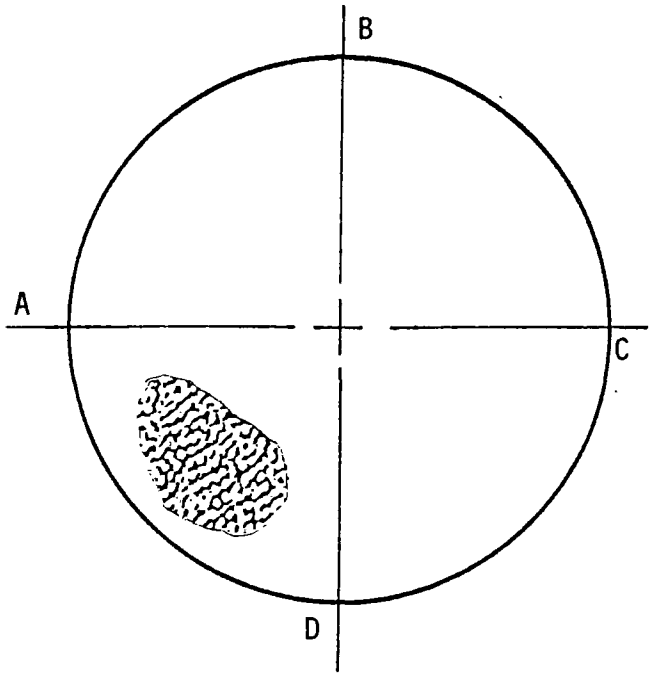

T_{BED} = 2400°F

Q = 100,000 Btu/hr

T_{PH} ≃ 750°F

LEAN

*At T_{BED} ≃ 2700°F, combustion appeared uniform from the rear face until approximately 15 hours of test time was accumulated. The appearance then began to approach that of T_{BED} ≃ 2400°F.

Figure B-5. Catalyst A-025 bed appearance rear view, varying bed temperature.

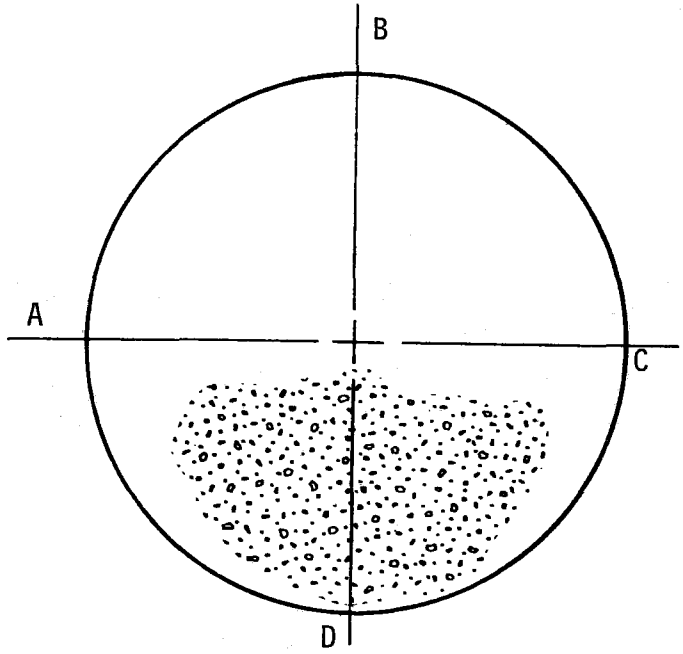

T_{BED} = 2400°F

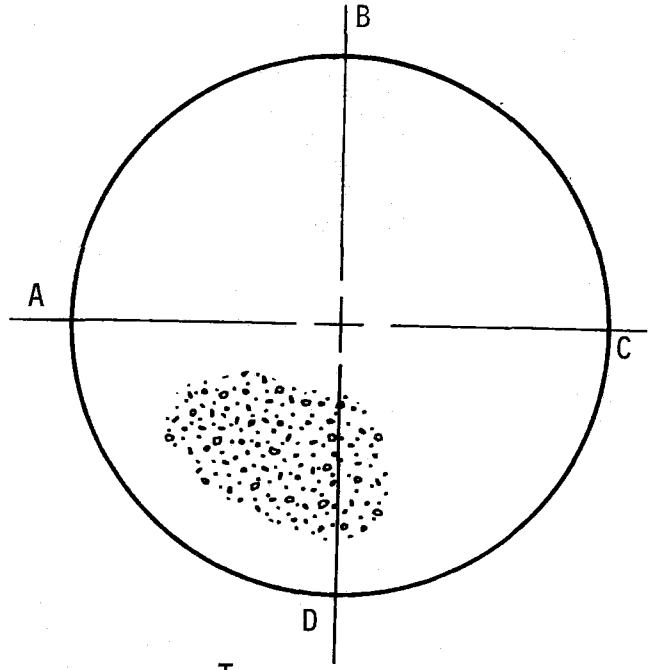

T_{BED} = 2700°F

T_{PH} = 500°F
Q = 100,000 Btu/hr
TA ≃ 200%

Figure B-6. Catalyst A-025 bed appearance rear view, minimum preheat.

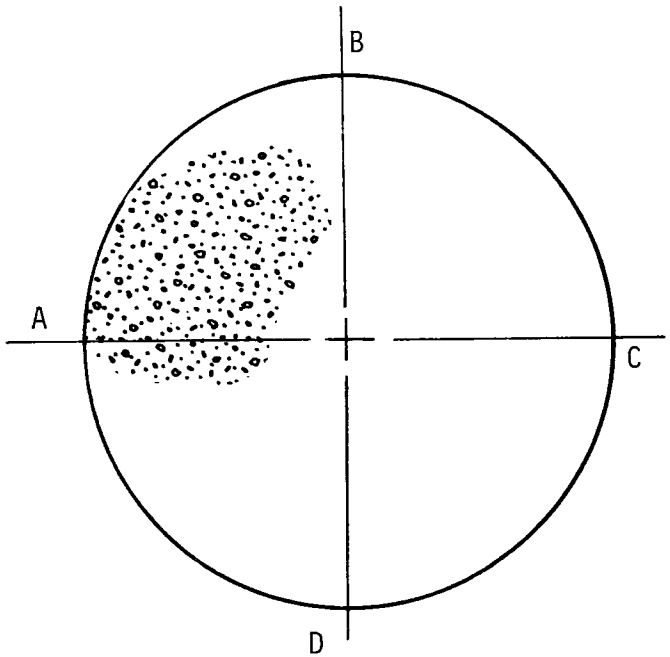

$\dot{m}_{fuel}$ = 8.3 lbm/hr

T_{BED} = 2400°F

TA ≃ 200%

T_{PH} ≃ 750°F

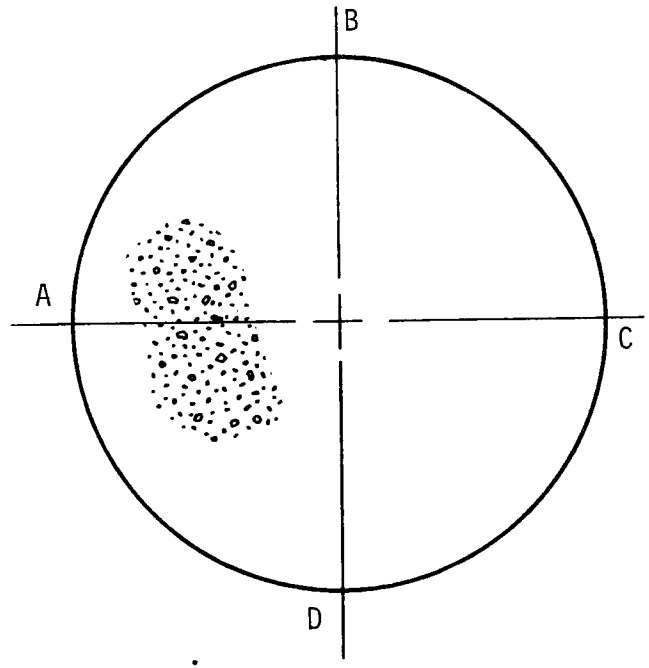

$\dot{m}_{fuel}$ = 11.6 lbm/hr

T_{BED} = 2700°F

Figure B-7. Catalyst A-025 bed appearance rear view, maximum throughput.

SEM/EDAX Analyses of Catalyst A-025

Small Cell Segment (Aft-End) Results

An extensive visual and X-ray evaluation of sections from the downstream end of the catalyst bed showed no variations in either appearance or chemical composition of the observed active and inactive catalyst sites. Figure B-8 shows a representative series of photomicrographs from the flow inlet region of the small cell segment and a high resolution EDAX count result for the area depicted. No platinum or iridium was detectable at the specimen surface. An EDAX result of Figure B-8c (Figure B-8d) shows the aluminum (line at 1.5), silicon (line at 1.7), and cerium (line at 4.8) composition of the catalyst washcoat.

A significant difference in surface appearance was noted, however, between the flow entrance and exit regions of the small cell segment. This difference can be seen by comparing the micrographs of Figure B-9 to those of Figure B-8. In general, the surface at the outlet site (Figure B-9) appears to have a much larger surface area than that of the inlet region. The characteristic surface cracking seen at low magnifications is predominant in all areas analyzed. Again, no platinum or iridium was detectable for the outlet area sample, indicating at least that active catalyst sites are not available at the surface within the detectable limits of the EDAX equipment (1 percent). The aluminum/silicon/cerium washcoat composition is again apparent in Figure B-9d (analysis of the area in B-9c), although in varying ratios as is typical over the catalyst surface. Additional trace quantities of iron were also detected in some areas.

Medium Cell Segment (Mid-Bed) Results)

The appearance of the medium cell segment is similar to that of the rear, small cell segment. Micrographs of two different areas and their

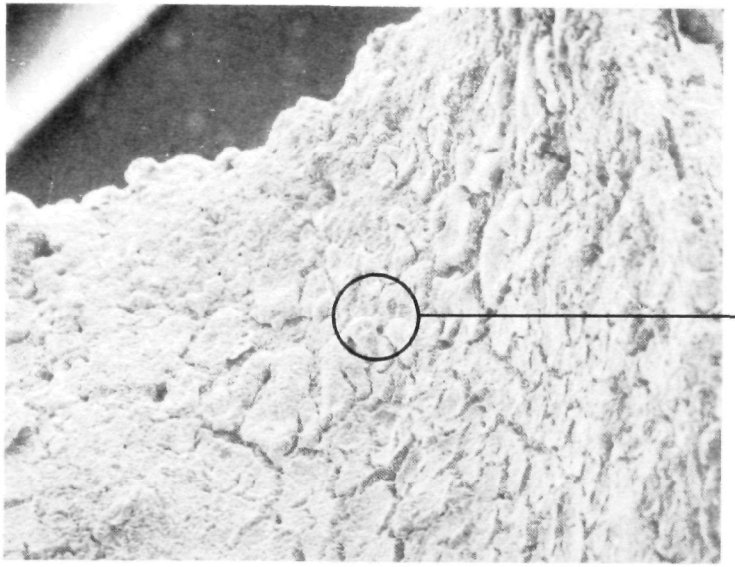

a. 35 x magnification at segment inlet

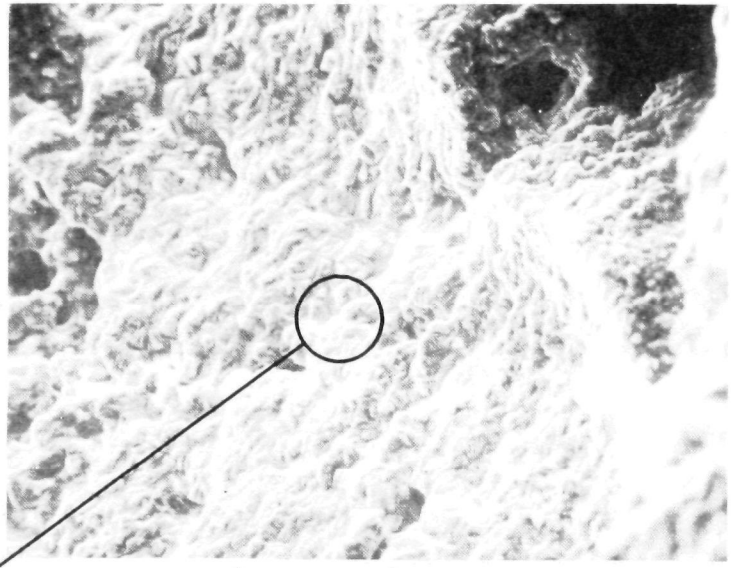

b. 500 x magnification

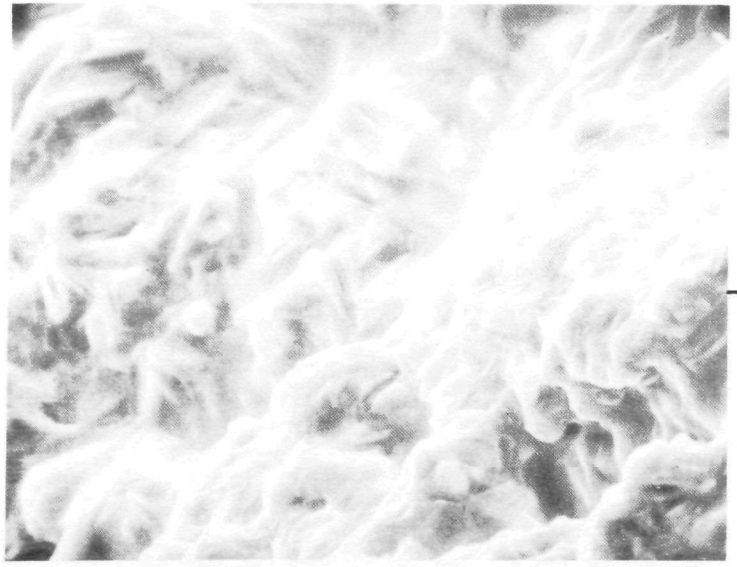

c. 2000 x magnification

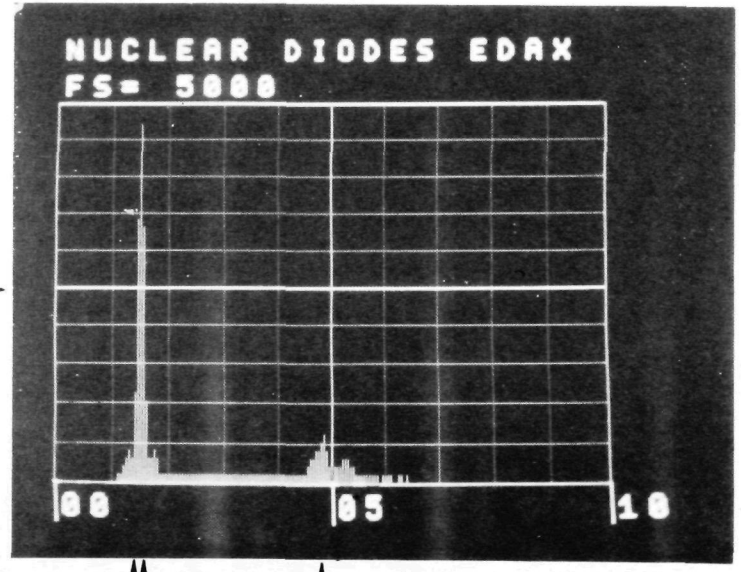

d. EDAX analysis of area c

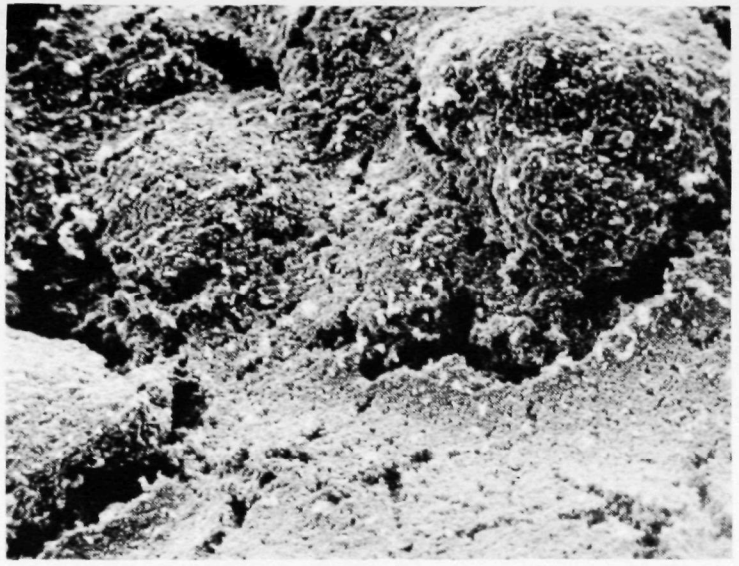

a. 200 x magnification at segment outlet

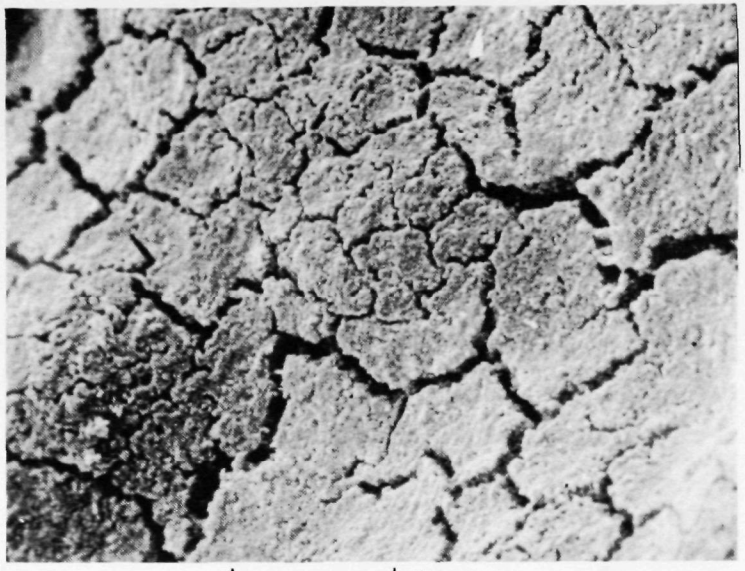

b. 260 x magnification of a similar area

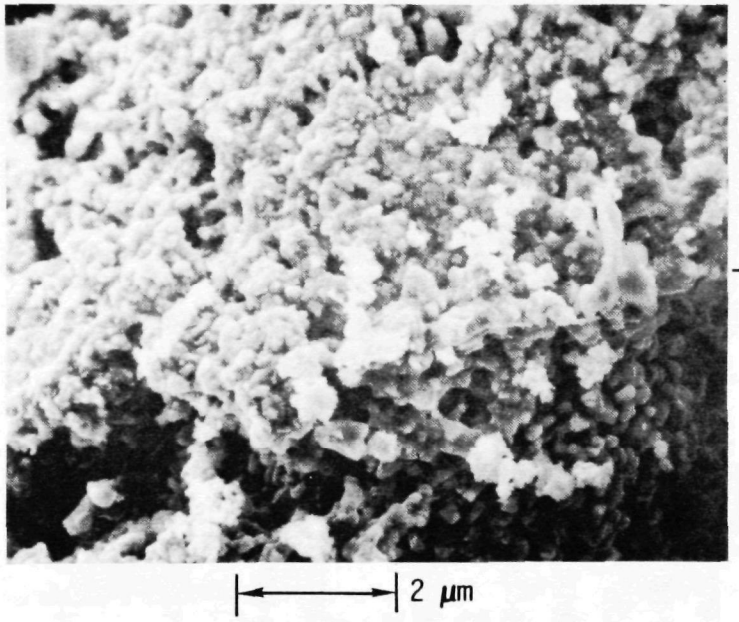

c. 2000 x magnification

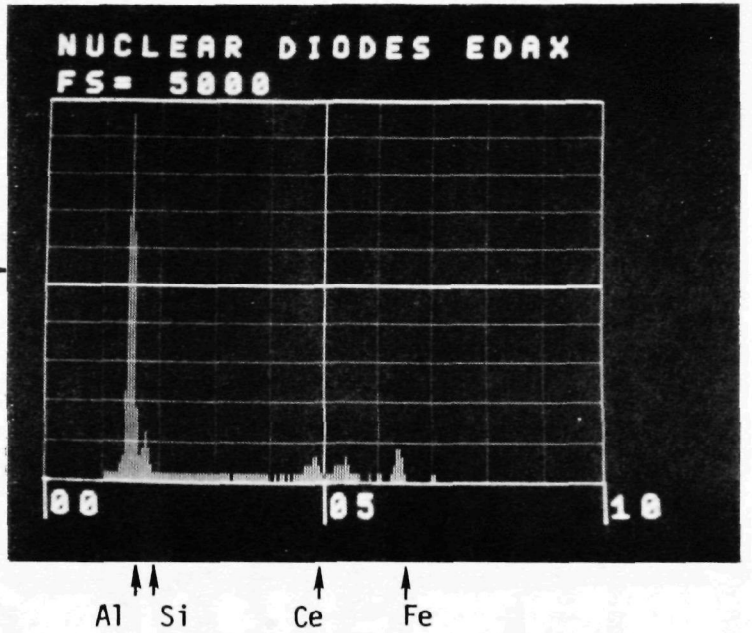

d. EDAX analysis of area c

Figure B-9. Surface appearance and EDAX analysis of small cell segment outlet area, W. R. Grace and Co. catalyst.

respective EDAX results are shown in Figure B-10. Variations in appearance along the cell length were not significant.

Extensive EDAX data was taken at specific surface sites -- with broad area scans, at specific grain sites and into cracked areas. Again, no active precious metal was detectable. Wide variations in the washcoat composition are apparent in Figures B-10b and B-10d.

It was concluded from the above results that for the catalyst to remain active at the end of the 20-hour test period, the precious metal must be embedded well below the surface or finely dispersed such that local concentrations were below the 1-percent detectability of the EDAX analyzer. A series of data was therefore generated on an untested catalyst segment prepared at the same time as the tested segments.

Untested Catalyst Segment Results

Photomicrographs of the untested segment are shown in Figure B-11. Note the change in washcoat surface structure following testing (Figures B-8 and B-9). Figure B-11a shows the washcoat edge with a relatively smooth surface (foreground) covering the more granular structure below the surface. Figures B-11b through B-11d show these edge details at greater magnification. The EDAX analysis for Figures B-11c and B-11d are shown in Figures B-12a and B-12b respectively. Extensive searching of the surface composition revealed platinum in some areas (B-12b) but not in others (B-12a). No iridium was detected at any location.

Chemical Analysis of a Post-test Segment

Since very little catalyst material (platinum or iridium) could be detected by the EDAX analyses on the post-test catalyst, a chemical analysis was performed. This technique would verify the relative quantities of catalyst within the complex structure that might not be detectable by the surface measurements of the EDAX.

The results of the semiquantitative analysis are listed below in Table B-4.

a. 285 x magnification at segment outlet

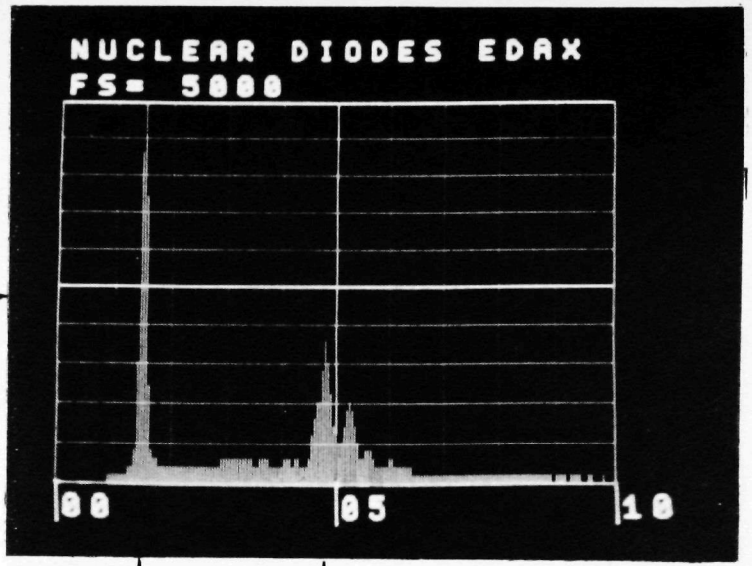

b. EDAX analysis of area a.

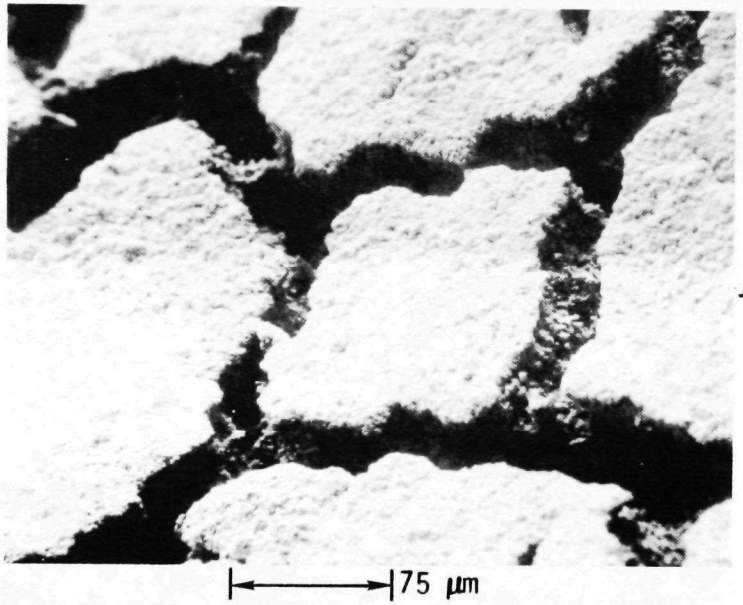

c. 265 x magnification of a similar area

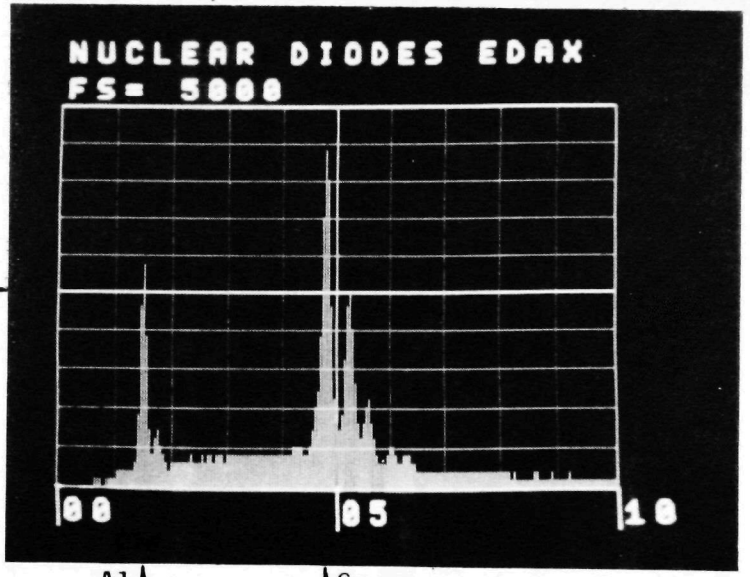

d. EDAX analysis of area c.

Figure B-10. Surface appearance and EDAX analyses of medium cell segment, W. R. Grace and Co. catalyst.

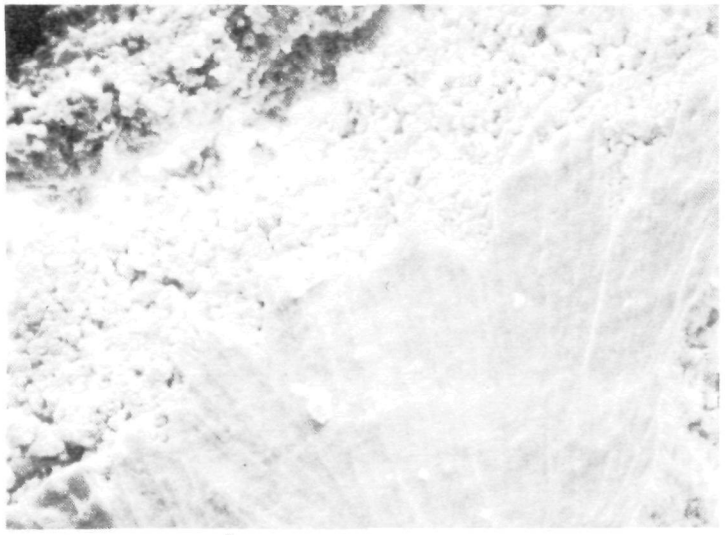

a. 700 x magnification of washcoat edge

b. 1500 x magnification of typical washcoat surface

c. 1400 x magnification of unusual washcoat crystalline growth

d. 3500 x magnification of washcoat edge

Figure B-11. Surface appearance of pretest catalyst surface, W. R. Grace and Co. catalyst.

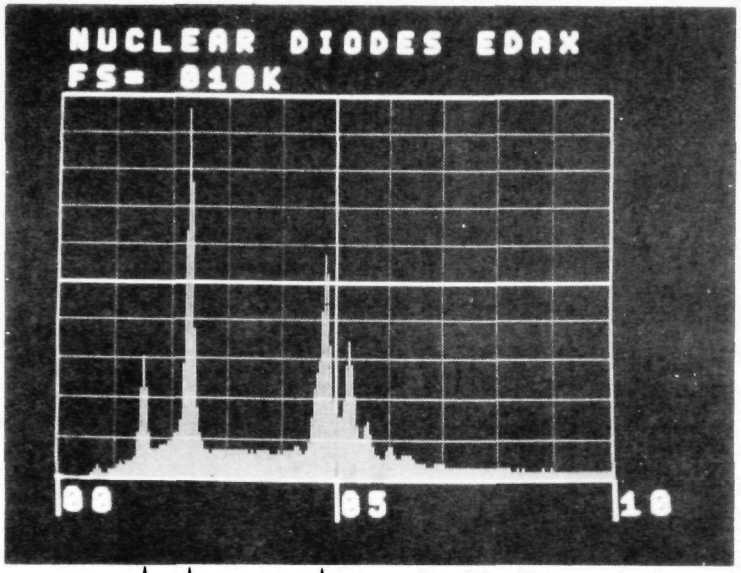

a. EDAX analysis of area c.

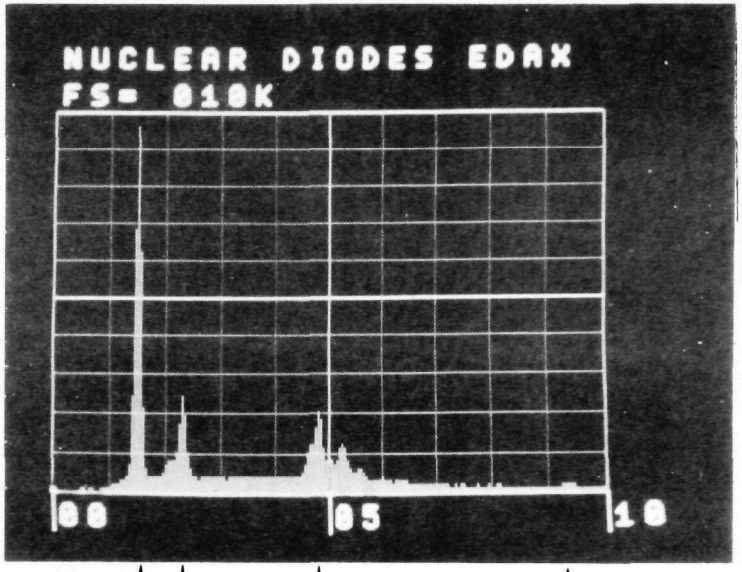

b. EDAX analysis of area d.

Figure B-12. EDAX analysis of untested catalyst surface.

TABLE B-4. RESULTS OF SEMIQUANTITATIVE ANALYSIS

Al-	44.%
Si-	4.8
Mg-	0.52
Mn-	0.015
Fe-	0.081
La-	0.89
Ce-	0.79
Ca-	0.026
Pt-	0.19
Ni-	0.0013
Ag-	0.0012
Ti-	0.0081
Na-	0.26
Cu-	0.00022
Cr-	0.066
Pb-	TR < 0.01
Ga-	0.0080
Sm-	TR < 0.03
Ir-	ND < 0.07
Other elements	nil

The measurements indicate that platinum was present in the sample at 0.19 percent by mass, and iridium was not detectable at the 0.07 percent sensitivity limit.

The presence of platinum (not detected by EDAX) indicates that platinum is not present at the surface at the minimum detectable limit of 1 percent. Because EDAX measurements were made extensively at varying magnifications, it does not appear that the catalyst materials have accumulated at the surface of the tested catalyst. Similarly, the relative difficulty of detecting platinum on the untested segment indicates that the metal is probably dispersed within the washcoat during preparation rather than applied at the surface. Finally, the relative activity of the catalyst after 20 hours of testing indicates that although the catalyst may not exist primarily at the washcoat surface, adequate contact between it and the reactants is provided to sustain combustion.

SECTION B-2

UNIVERSAL OIL PRODUCTS CATALYST TEST MODEL A-026

TABLE B-5. UOP LIGHTOFF TEMPERATURE CHARACTERISTICS — CATALYST A-026

Cumulative Test Time (Hrs)	Lightoff Condition	Lightoff Temperature (°F)	Comments
0	Fuel Lean	875	May not be minimum lightoff temp. nonuniform temp. profiles
10	Rich	900	Not a minimum. Unsuccessful lean lightoff at 940°F more uniform temp. profiles
14	Rich	780	
17	Rich	765	Not minimum lightoff temps.
21	Rich	750	
23	Rich	660	Subsequent lightoff at 635°F was unsuccessful

TABLE B-6. TEST DATA SUMMARY — CATALYST A-026

Test Pt.	TA%	SV, hr^{-1}	$\dot{m}_{fuel}$, lbm/hr	$\dot{m}_{air}$, lbm/hr	T_{ph}, °F	$T_{BED_{max}}$, °F	Test Objective
0624-02	292	173,400	4.5	229.1	667	2350	10-hr aging
0624-05	270	161,100	4.6	212.3	651	2409	
0624-09	267	160,300	4.6	211.1	647	2421	
0624-13	274	162,500	4.5	214.3	646	2438	
0624-17	288	165,400	4.4	218.6	645	2432	
0624-21	265	153,100	4.4	201.6	718	2376	
0627-02	50	33,100	4.4	37.5	570	2410	Minimum preheat fuel-rich 2400°F
0627-03	50	33,400	4.4	37.8	501	2419	
0627-04	55	36,200	4.4	41.6	350	2409	
0627-05	56	37,300	4.4	43.1	300	2435	
0627-06	58	37,700	4.4	43.8	251	2431	
0627-07	269	153,200	4.4	201.9	633	2405	Minimum preheat fuel-lean 2400°F
0627-08	268	151,500	4.3	199.6	602	2460	
0627-09	289	165,500	4.4	218.7	549	2430	
0628-16	253	147,000	4.4	193.3	388	2535	
0628-07	253	144,100	4.4	189.5	597	2702	
0628-08	247	146,900	4.5	193.0	550	2702	Minimum preheat fuel-lean 2700°F
0628-09	224	135,800	4.6	177.6	496	2713	
0628-10	228	139,700	4.7	182.8	448	2698	
0628-11	234	142,500	4.6	187.6	401	2707	
0628-14	227	134,000	4.5	175.4	326	2680	

TABLE B-6. Concluded

Test Pt.	TA%	SV, hr^{-1}	$\dot{m}_{fuel}$, lbm/hr	$\dot{m}_{air}$, lbm/hr	T_{ph}, °F	$T_{BED_{max}}$, °F	Test Objective
0627-11	256	145,600	4.4	191.5	603	2425	Maximum thruput fuel lean 2400°F
0627-16	305	216,900	5.4	287.1	732	2504	
0627-12	321	262,300	6.5	347.5	719	2419	
0627-15	253	292,300	8.8	384.3	740	2285	
0627013	275	343,900	9.6	453.5	725	2406	
0627-14	290	420,700	11.1	556.0	751	2492	
0629-03	213	126,100	4.5	164.5	642	2680	Maximum thruput fuel lean 2700°F
0629-04	206	144,700	5.3	188.5	587	2713	
0629-05	219	165,800	5.7	216.6	601	2669	
0629-06	197	183.500	7.0	238.5	606	2716	
0629-07	186	217,500	8.8	281.8	611	~2650	

TABLE B-7. EMISSIONS DATA — CATALYST A-026

Test Pt.	Test Time, hrs	TA%	$\dot{m}_{fuel}$, lbm/hr	CO, ppm	NO, ppm	UHC, %	H_2, %
0624-02	0.7	292	4.5	0	0	0	0
0624-05	2.7	270	4.6		0		
0624-09	4.2	267	4.6		0		
0624-13	6.2	274	4.5		1		
0624-17	8.2	288	4.4		1		
0624-21	10.0	265	4.4	0	1	0	0
0627-02	10.3	50	4.4		1	—	
0627-03	11.6	50	4.4		1	0.72	0.04
0627-04	12.1	55	4.4		0	0.32	0.04
0627-05	12.3	56	4.4		0		
0627-06	13.5	58	4.4		0	0.22	0.03
0627-07	14.0	269	4.4	105	1		
0627-08	14.3	268	4.3	76	1	0	
0627-09	14.5	289	4.4	13	2		
0628-16	20.6	253	4.4	0	1		
0628-09	19.0	224	4.6		5		
0628-10	19.3	228	4.7		7		
0628-11	19.7	234	4.6	0	6		
0628-14	20.2	227	4.5	15	3		

TABLE B-7. Concluded

Test Pt.	Test Time, hrs	TA%	$\dot{m}_{fuel}$, lbm/hr	CO, ppm	NO, ppm	UHC, %
0627-07	14.0	269	4.4	105	1	
0627-08	14.3	268	4.3	76	1	0
0627-09	14.5	289	4.4	63	1	
0628-16	20.6	253	4.4	13	2	
0628-07	17.3	253	4.4	0	1	
0628-08	17.6	247	4.5	↕	2	
0628-09	19.0	224	4.6	↕	5	
0628-10	19.3	228	4.7	↕	7	
0628-11	19.7	234	4.6	0	6	
0628-14	20.2	227	4.5	15	3	
0627-11	15.2	256	4.4	52	1	
0627-16	16.5	305	5.4	75	2	
0627-12	15.4	312	6.5	48	1	
0627-15	16.2	275	9.6	1393	0	
0627-13	15.5	253	8.8	565	0	
0627-14	16.1	290	11.1	771	1	
0629-03	21.2	213	4.5	0	1	
0629-04	21.8	206	5.3	↕	3	
0629-05	22.2	219	5.7	↕	3	
0629-06	22.5	197	7.0	↕	4	
0629-07	22.6	186	8.3	0	4	

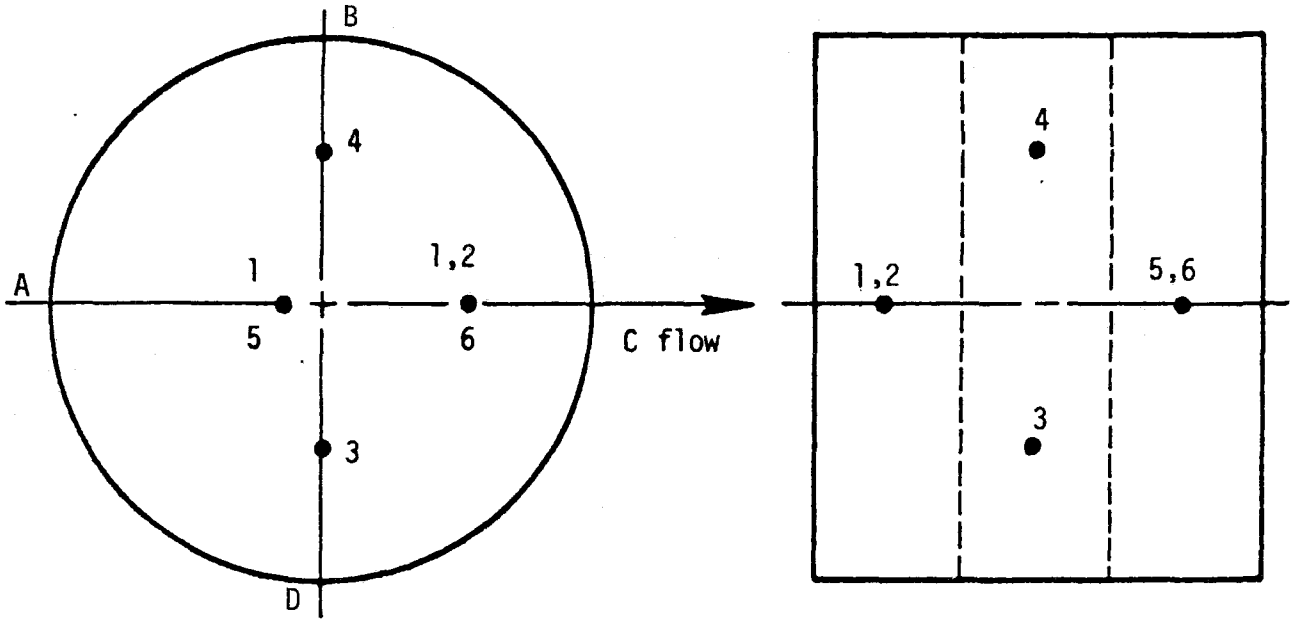

2400°F Bed

0627-07		0628-16	
TC	°F	TC	°F
1	2221	1	2305
2	2048	2	2299
3	2212	3	1571
4	2435	4	2535
6	1803	6	2352

2700°F Bed

0628-07		0628-14	
TC	°F	TC	°F
1	2017	1	2500
2	2248	2	2680
3	1951	3	2501
4	2702	4	2519
6	2532	6	2677

Figure B-13. Catalyst A-026 bed temperature distribution -- effects of preheat, fuel lean.

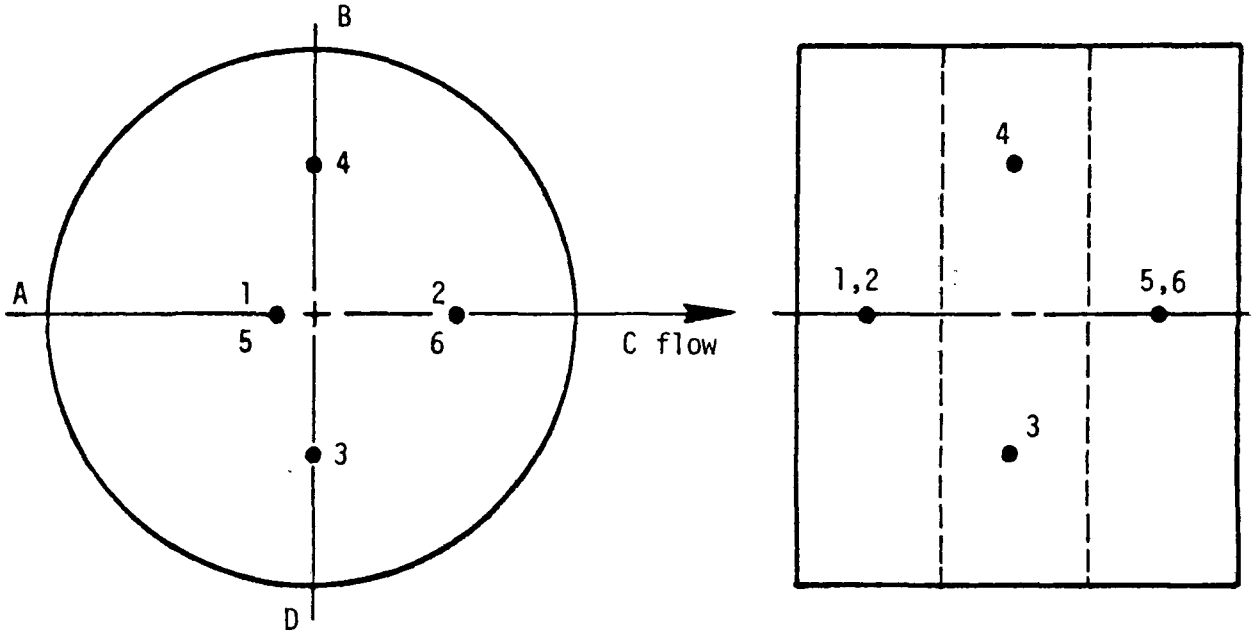

T_{ph} = 570°F

0627-02

TC	°F
1	2202
2	2214
3	2411
4	2313
6	2411

T_{ph} = 251°F

0627-06

TC	°F
1	2212
2	2175
3	2407
4	2253
6	2426

Figure B-14. Catalyst A-026 bed temperature distribution -- effects of preheat, fuel rich 1598K (2400°F) bed.

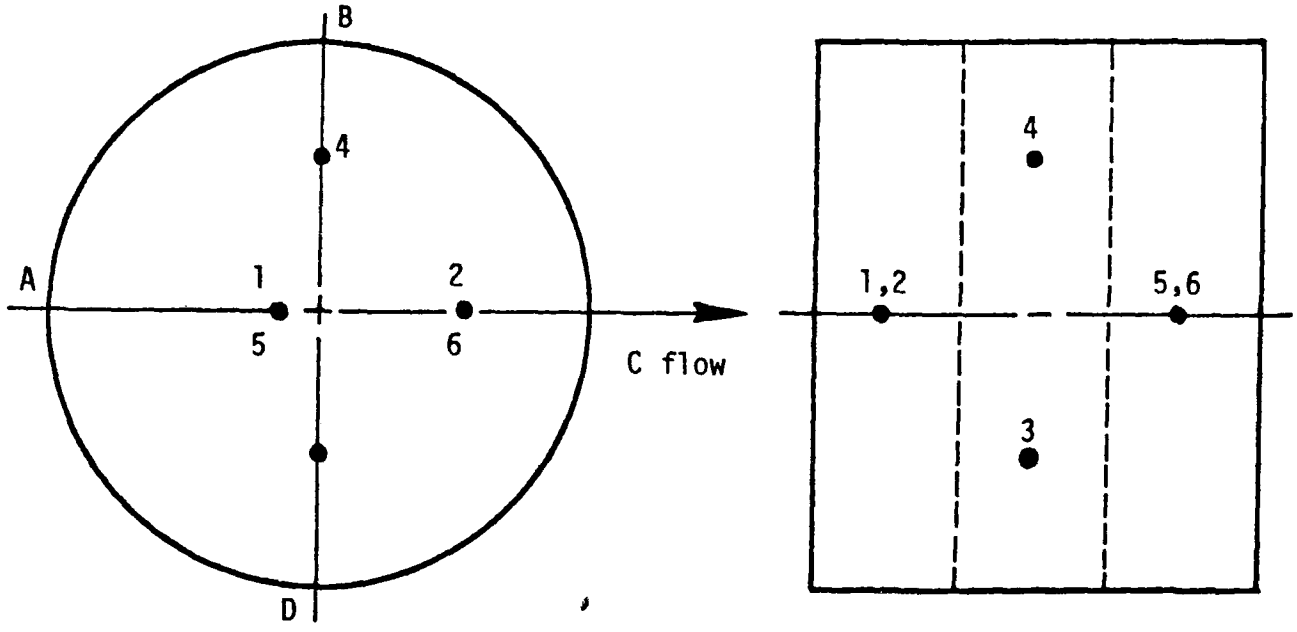

2400°F Bed

$\dot{m}_f$ = 4.4 lbm/hr

0627-11

TC	°F
1	2287
2	2307
3	2214
4	2425
6	2380

$\dot{m}_f$ = 11.1

0627-14

TC	°F
1	2212
2	2005
3	1753
4	2492
6	1351

2700°F Bed*

$\dot{m}_f$ = 4.5

0629-03

TC	°F
1	2211
2	678
3	1868
4	2680
6	670

$\dot{m}_f$ = 8.8

0629-07

TC	°F
1	699
2	635
3	707
4	2650
6	642

* Bed showed significant degredation at 21 hours of testing

Figure B-15. Catalyst A-026 bed temperature distribution -- effects of throughput.

SECTION B-3

W. PFEFFERLE PRECIOUS METAL CATALYST TEST MODEL A-027

TABLE B-8. TEST DATA SUMMARY — CATALYST A-027

Test Pt.	Test Time, Hrs.	TA%	SV, hr^{-1}	$\dot{m}_{fuel}$, lbm/hr	$\dot{m}_{air}$, lbm/hr	T_{ph}, °F	$T_{BED_{max}}$, °F
0630-02	0.2	35	25,500	4.5	26.8	677	2358
0630-04	0.4	296	172.300	4.5	227.8	724	2467
0630-05	0.8	297	155,800	4.0	206.1	707	2444
0630-07	1.0	299	127,500	3.3	168.7	675	2408
0630-11	3.0	302	125,400	3.2	165.9	688	2450
0630-14	4.5	280	118.500	3.2	156.4	504	2432

Initial Lightoff: Fuel rich at 935°F
Subsequent Lightoff: Unsuccessful at 965°F

TABLE B-9. EMISSIONS DATA — CATALYST A-027

Test Pt.	TA%	$\dot{m}_{fuel}$, lbm/hr	CO, ppm	NO, ppm
0630-02	35	4.5	—	—
0630-04	296	4.5	240	0
0630-05	297	4.0	231	0
0630-07	299	3.3	70	0
0630-11	302	3.2	0	0
0630-14	280	3.2	21	0

SECTION B-4

MATTHEY BISHOP CATALYSTS
TEST MODELS A-031 AND A-035

TABLE B-10. MATTHEY BISHOP A LIGHTOFF CHARACTERISTICS – CATALYST A-031

Cumulative Test Time (Hrs)	Lightoff Condition	Lightoff Temperature (°F)	Comments
0	Fuel Lean	790	
10	Lean	840	Very slow lightoff (6 to 8 min); unstable combustion until 2200°F temperature was reached
14	Rich	950	Unsuccessful lean lightoff at 930°F
16	Rich (Propane)	735	Unsuccessful rich lightoff with natural gas
23	Rich	870	Would lightoff with natural gas but would not sustain combustion – testing terminated

TABLE B-11. DATA SUMMARY — CATALYST A-031

Test Pt.	TA (%)	SV (1/hr)	$\dot{m}_{fuel}$ (lbm/hr)	$\dot{m}_{air}$ (lbm/hr)	T_{PH} (°F)	$\bar{T}_{Bed}$ (°F)	$T_{Bed\ max}$ (°F)	CO (ppm)	NO (ppm)	Test Type
0802-03	232	140,600	4.6	184.1	578	2154	2406	—	—	Aging
0802-13	258	146,400	4.3	192.6	635	2118	2406	0	0	
0804-02	245	146,100	4.6	191.8	596	2073	2489	0	—	Minimum
0804-03	231	137,800	4.5	180.5	508	2182	2620	0	1	preheat
0804-04	250	148,800	4.6	195.5	443	1754	2473	0	1	fuel lean
0804-05	241	142,100	4.5	186.5	352	1679	2440	3	1	2400°F
0804-07	245	143,000	4.5	187.6	296	1738	2434	1	1	
0804-12	242	143.800	4.5	188.7	255	1509	2300	1	—	
0808-01	31	24,400	4.7	24.9	632	2050	2394	—	—	Minimum
0808-14	34	27,000	4.8	28.3	493	2067	2444	1141	0	preheat
0808-12	34	27,100	4.8	28.4	452	2062	2431	1139	0	fuel rich
0808-11	34	27,100	4.8	28.4	409	2027	2384	1141	0	2400°F
0808-10	36	28,300	4.8	30.1	358	2035	2442	1137	0	
0808-02	37	28,100	4.8	29.9	324	2012	2394	>2000	1	
0808-03	39	29,500	4.8	31.8	276	2031	2440	>2000	1	
0808-05	39	29,700	4.8	32.0	198	1996	2411	1134	0	
0808-09	40	30,700	4.9	33.2	173	2021	2445	1129	0	
0808-16	210	136,900	4.9	78.5	626		2446	—	13	Maximum
0808-17	207	143,600	5.2	187.2	591		2431	—	10	Throughput
0808-18	175	154,600	6.6	199.6	592		2455	0	6	
0808-20		.	7.3	250.0[a]	602		2467	0	12	
0808-22	173	203,000	8.8	262.0	609		2450	0	10	
0808-25			12.2	419.0[a]	628		2545	0	19	
0808-24			13.1	450.0[a]	622		2489	0	20	
0808-23			15.1	519.0[a]	615		2442	30	—	

[a]Airflow values estimated from temperature data.

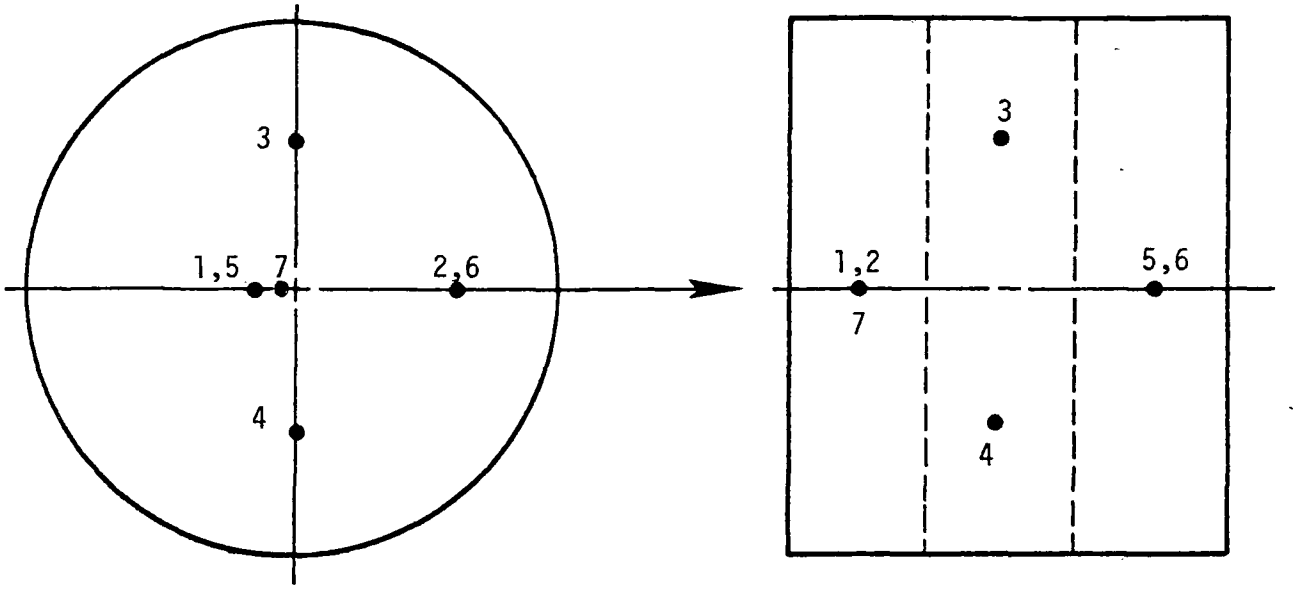

t = 0.5 hours 0802-03		t = 5.5 hours 0802-13	
TC	°F	TC	°F
1	1990	1	1970
4	2026	4	2060
5	2335	5	2077
6	2406	6	2406
7	2013	7	2076

Figure B-16. Catalyst A-031 Matthey Bishop A bed temperature distributions during aging.

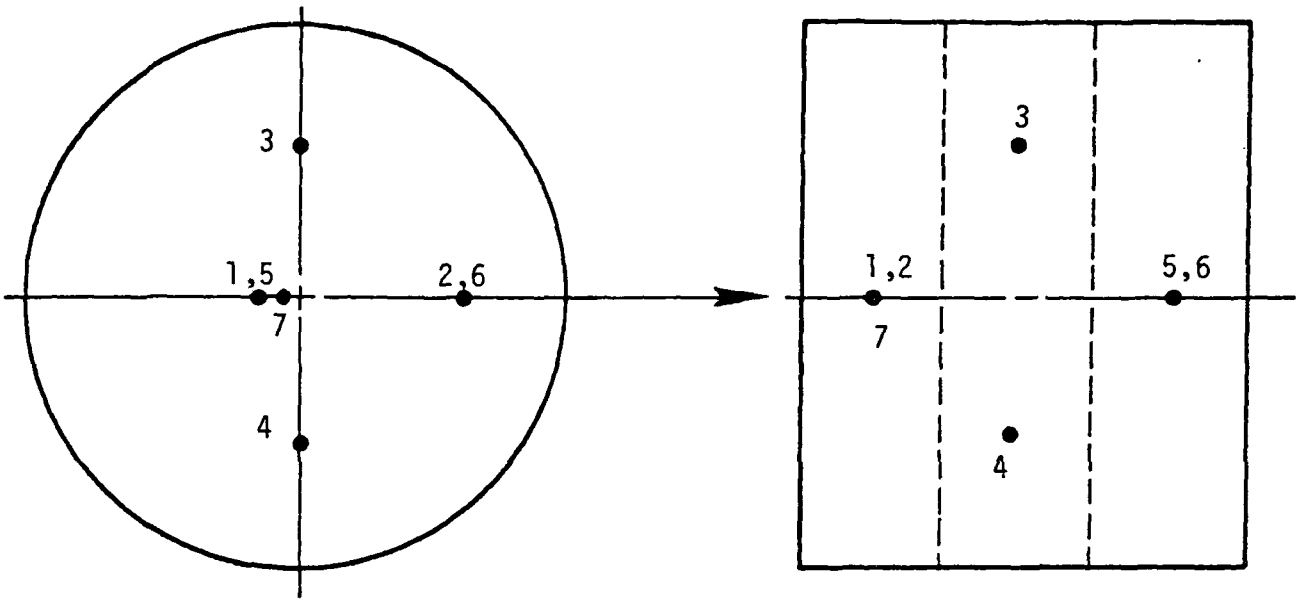

Fuel Rich

T_{PH} = 632°F
0808-01

TC	°F
1	2273
4	2394
5	2084
6	1923
7	1575

T_{PH} = 173°F
0808-09

TC	°F
1	2198
4	2445
5	2018
6	2292
7	1151

Fuel Lean

T_{PH} = 596°F
0804-02

TC	°F
1	2111
4	2024
5	2325
6	2489
7	1417

T_{PH} = 255°F
0804-12

TC	°F
1	1070
4	2160
5	1057
6	2299
7	959

Figure B-17. Catalyst A-031 Matthey Bishop A bed temperature distributions, effects of preheat.

TABLE B-12. DATA SUMMARY — CATALYST A-035

1	2	3	4	5	6	7	8	9	10	11	12	13	14
Test Pt.	TA (%)	SV (1/hr)	$\dot{m}_{fuel}$ (lbm/hr)	$\dot{m}_{air}$ (lbm/hr)	T_{PH} (°F)	$\bar{T}_{BED}$ (°F)	$T_{BED,MAX}$ (°F)		CO (ppm)	NO (ppm)			Test Type
1001-03	255	155,700	4.7	204.8	560	2031	2417		—	—			
1003-02	196	120,600	4.6	156.7	510	2290	2429		0	6			Aging
1003-10	175	104,700	4.5	135.2	535	2368	2489		5	11			
1004-02	188	109,700	4.4	142.2	790	2046	2486		49	2			
1004-08	199	120,000	4.5	156.0	600	2307	2432		0	4			
1004-09	196	116,900	4.5	151.9	600	2301	2425		0	4			Minimum preheat, fuel lean 2400°F
1004-10	186	112,100	4.5	145.3	550	2288	2407		0	5			
1004-12	188	114,000	4.6	147.8	500	2270	2426		0	5			
1004-14	179	108,700	4.6	140.6	470	2209	2440		0	4			
1004-16	184	113,100	4.6	146.5	435	2178	2432		0	5			
1004-17	177	109,200	4.6	141.1	400	2106	2454		0	4			
1004-20	181	111,100	4.6	143.8	365	2080	2427		5	3			
1004-23	178	108,100	4.5	139.8	310	2075	2379		9	4			
1004-26	172	101,600	4.4	131.1	260	2095	2374		0	5			
1005-02	41	28,500	4.4	31.0	580	2207	2429		>2000	1			Minimum preheat, rich 2400°F
1005-03	41	30,100	4.6	32.9	350	2290	2432		>2000	1			
1005-06	226	125,100	4.2	163.7	610	1213	2514		4	3			Pressure comparison 2 Atm

TOTAL TEST TIME = 21 HOURS

TABLE B-13. MATTHEY BISHOP C LIGHTOFF CHARACTERISTICS — CATALYST A-035

Cumulative Test Time (Hrs)	Lightoff* Condition	Lightoff Temperature (^{o}F)	Comments
0	Fuel Rich	920	Lean lightoff at 950^{o}F was unsuccessful
1	Rich	820	Rich lightoff at 750^{o}F was unsuccessful
7	Rich	850	
14	Rich	890	
18.5	Rich	920	Probably not a minimum lightoff temperature

*All lightoffs performed with natural gas.

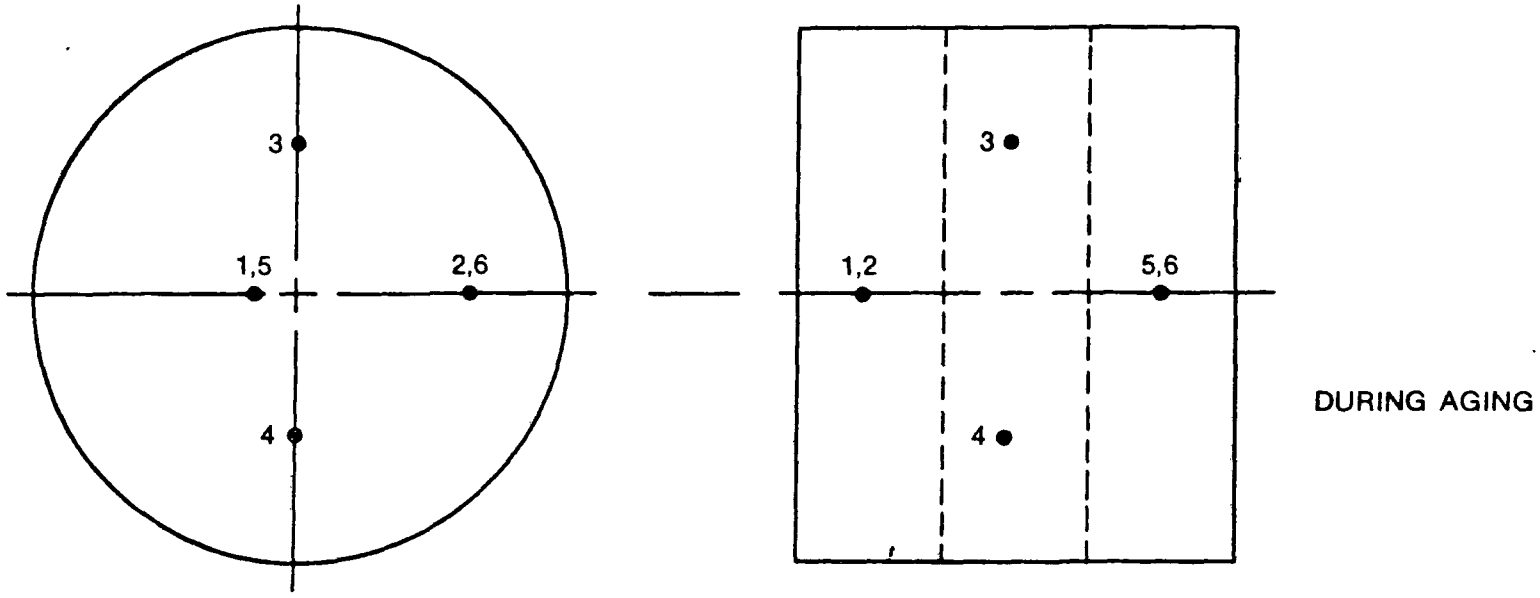

t = 1.0 hr

1001-03

TC	°F
1	1676
2	2182
3	1847
4	2417

t = 10.0 hrs

1004-08

TC	°F
1	2212
2	2432
3	2199
4	2385

Figure B-18. Catalyst A-035 bed temperature distributions.

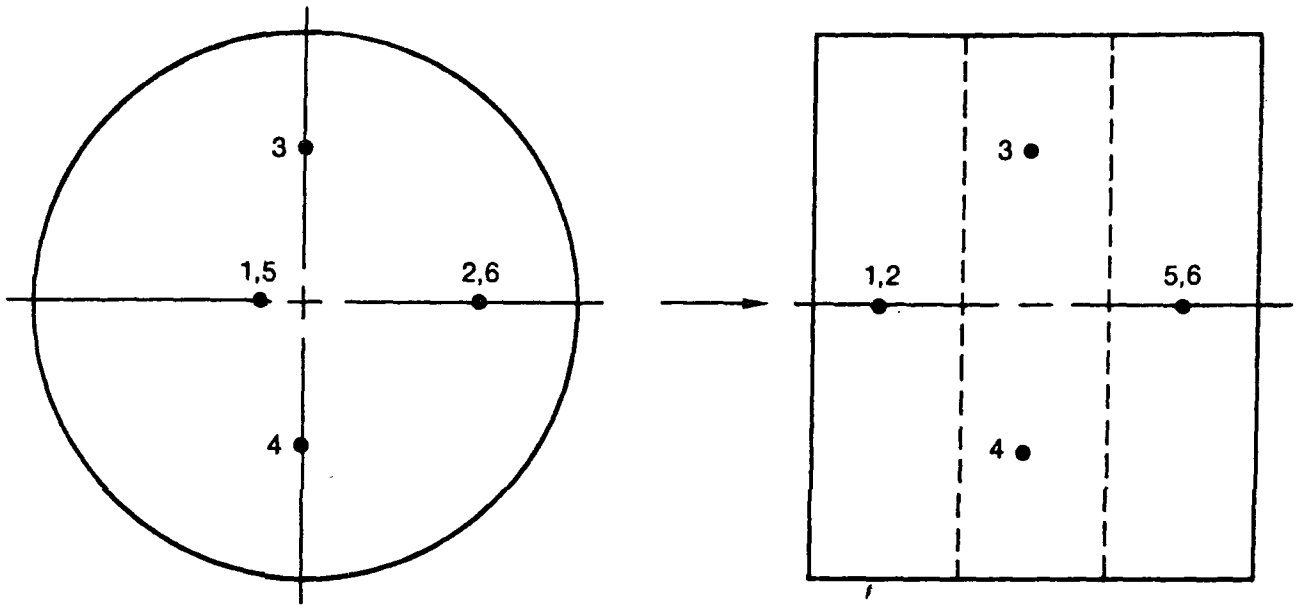

EFFECTS OF PREHEAT

FUEL LEAN, 2400°F

1004-09, T_{PH} = 600

TC	°F
1	2212
2	2425
3	2193
4	2375

1004-20, T_{PH} = 365

TC	°F
1	2202
2	2108
3	1582
4	2427

FUEL RICH, 2400°F

1005-02, T_{PH} = 580

TC	°F
1	2122
2	2056
3	2220
4	2429

1005-03, T_{PH} = 350

TC	°F
1	2220
2	2140
3	2403
4	2432

Figure B-19. Catalyst A-035 bed temperature distributions.

SECTION B-5

W. PFEFFERLE METAL OXIDE CATALYST TEST MODEL A-038

TABLE B-14. PFEFFERLE LIGHTOFF CHARACTERISTICS – CATALYST A-038 (Co_2O_3)

CUMULATIVE TEST TIME (HRS)	LIGHT OFF CONDITION	LIGHT OFF* TEMPERATURE (°F)	COMMENTS
0	FUEL-RICH	890	PLATINUM ADDED TO CATALYST TO PROMOTE LIGHT OFF WITH NATURAL GAS
10.8	RICH	890	
11.0	RICH	850	
11.5	RICH	850	

TABLE B-15. DATA SUMMARY – CATALYST A-038

1	2	3	4	5	6	7	8	9	10	11	12	13	14
Test Point	TA (%)	SV (1/hr)	$\dot{m}_{fuel}$ (lbm/hr)	$\dot{m}_{air}$ (lbm/hr)	T_{ph} (°F)	$\overline{T}_{BED}$ (°F)	$T_{BED, MAX}$ (°F)		CO (ppm)	NO (ppm)			TEST TYPE
1228-03	172	80,400	4.4	130.9	732	2392	2423		9	5			
05	157	82,100	4.9	132.7	605	2474	2492		0	17			aging at
07	162	78,300	4.5	126.6	614	2219	2459		0	9			2400°F
10	160	73,700	4.3	118.5	607	2348	2474		0	10			
11	167	77,000	4.3	124.1	615	2369	2474		0	8			
1228-12	159	74,500	4.4	120.0	613	2376	2465		0	9			
13	164	77,100	4.4	124.6	574	2298	2455		0	9			fuel lean
14	157	76,600	4.6	123.5	548	2209	2449		0	11			minimum
15	149	76,800	4.8	123.5	524	2261	2467		0	15			preheat
16	150	73,200	4.6	117.4	498	2201	2469		0	14			2400°F
1229-05	174	135,100	7.5	224.8	696	2481	2517		0	7			
06	168	130,600	7.5	216.5	692	2476	2512		0	7			
07	170	151,700	8.6	253.2	668	2464	2503		0	6			
08	177	183,100	10.1	308.0	656	2476	2498		0	5			
09	189	214,400	11.2	363.0	645	2474	2503		0	5			maximum
10	177	223,200	12.4	377.0	642	2510	2530		0	5			through-
11	184	257,200	13.8	436.5	637	2517	2539		0	5			put
12	190	284,600	14.9	484.6	632	2515	2530		0	4			at
13	192	316,400	16.4	539.7	628	2521	2542		0	4			2500°F
14	188	328,200	17.3	559.7	625	2534	2550		0	4			
15	216	425,900	19.8	733.5	622	2347	2445		0	7			
16	221	443,100	20.1	764.3	628	2426	2479		3	4			

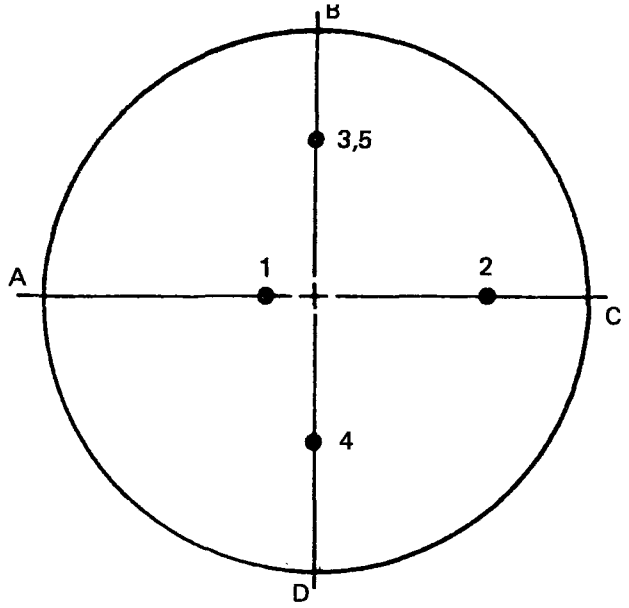

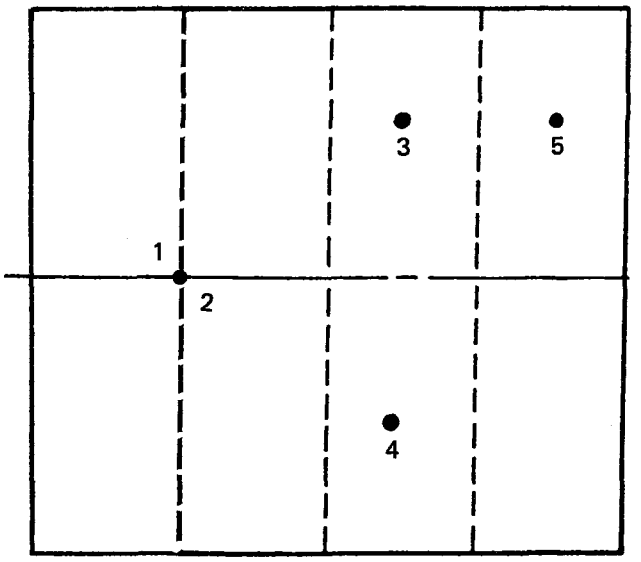

DURING AGING

1228-03	
TC	°F
1	2423
2	2342
3	2386
4	2415
5	2374

1228-11	
TC	°F
1	2216
2	2331
3	2474
4	2456
5	2442

Figure B-20. Catalyst A-038 bed temperature distributions.

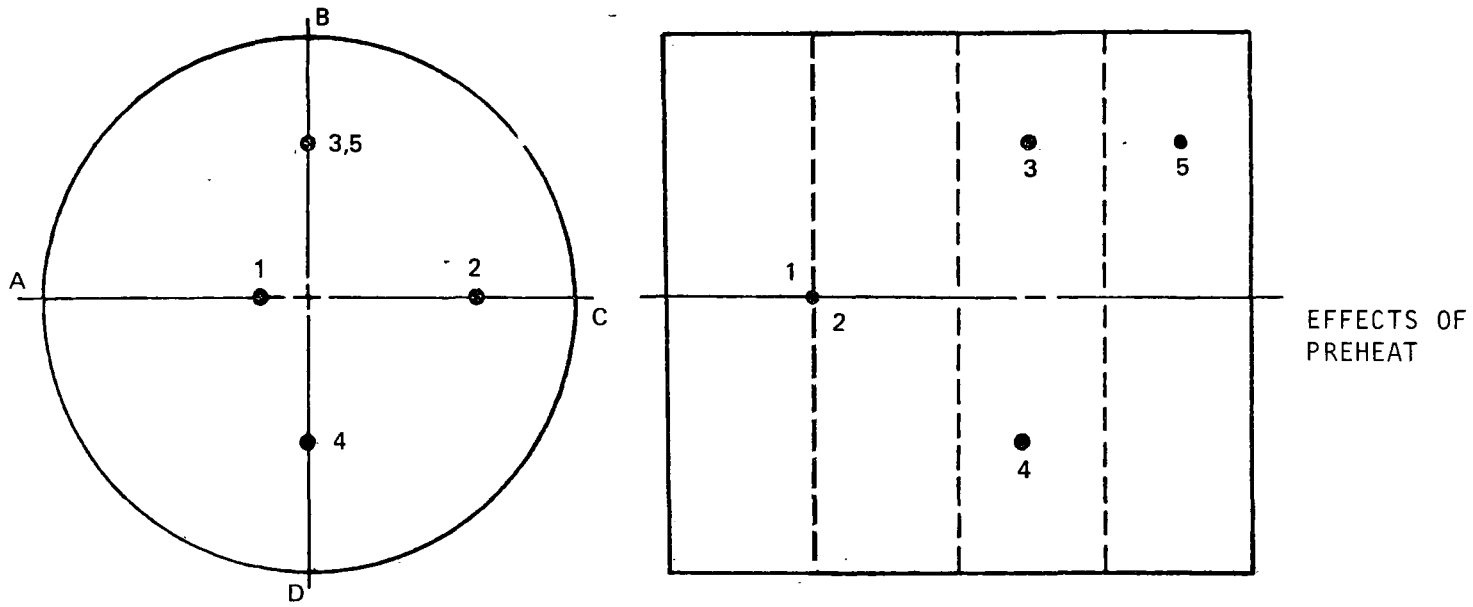

FUEL LEAN, 2400°F

1228-12, T_{PH} = 613 °F		1228-16, T_{PH} = 498 °F	
TC	°F	TC	°F
1	2251	1	1760
2	2328	2	2109
3	2459	3	2469
4	2465	4	2467
5	2462	5	2467

Figure B-21. Catalyst A-038 bed temperature distributions.

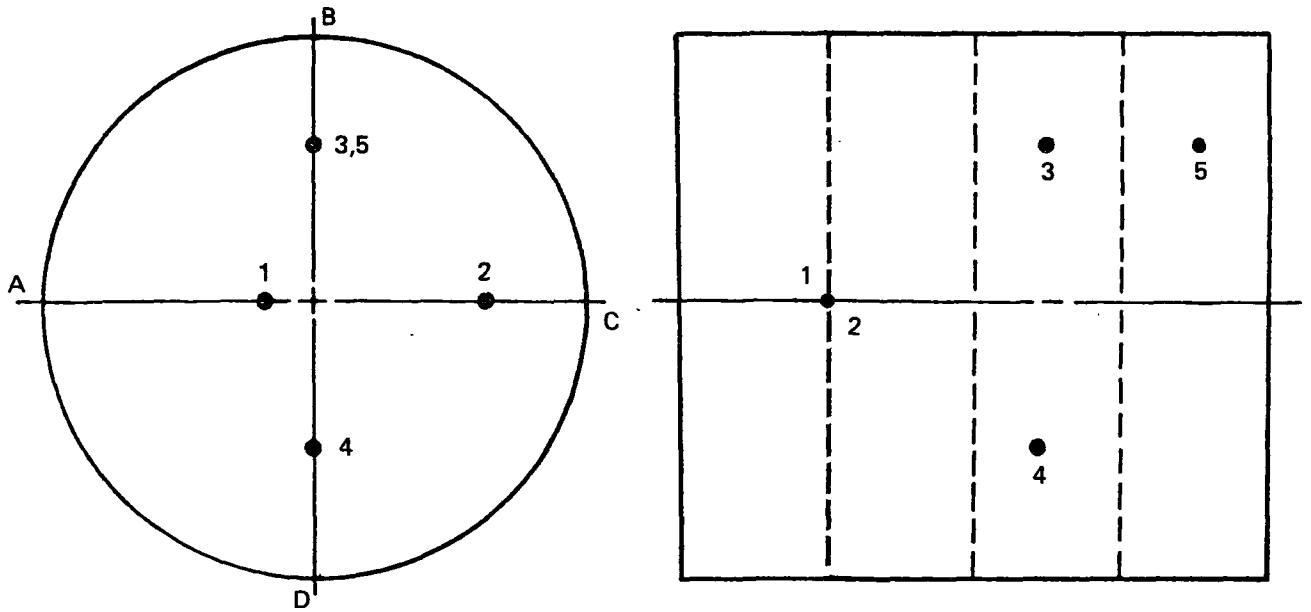

FUEL LEAN, 2400°F

1229-05, T_{PH} = 696 °F

TC	°F
1	2467
2	2517
3	2494
4	2447
5	2561

1229-15, T_{PH} = 622 °F

TC	°F
1	2445
2	2195
3	2389
4	2357
5	2463

Figure B-22. Catalyst A-038 bed temperature distributions.

SECTION B-6

JOHNSON MATTHEY CATALYST
TEST MODEL A-040

TABLE B-16. LIGHTOFF CHARACTERISTICS – CATALYST A-040

Cumulative Test Time (Hrs.)	Lightoff Condition	Lightoff Temperature (°F)	Comments
0	Fuel Lean	760	
0.2	Lean	790	
7.8	Lean	800	
14.5	Lean	850	Rich lightoffs were unsuccessful
17.3	Rich	800	Apparent poor conversion
18.3	Rich	850	Nonuniform combustion

TABLE B-17. DATA SUMMARY — CATALYST A-040

Test Pt.	TA. (%)	SV (1/hr)	ṁ fuel[a] (lbm/hr)	ṁ air (lbm/hr)	Tph (°F)	$\bar{T}$bed (°F)	Tbed max (°F)	CO (ppm)	NO_x (ppm)	Test Type
0126-02	240	149,700	4.77	196.9	793	2303	2484	22	6	Aging
0126-03	244	144,100	4.52	189.7	700	2301	2353	13	8	
0126-04	240	143,100	4.56	188.3	692	2306	2371	5	9	
0126-06	240	130,600	4.16	171.8	714	2308	2377	1	11	
0126-07	240	131,300	4.19	172.7	701	2316	2373	0	9	
0126-08	246	133,100	4.15	175.3	698	2316	2366	26	6	
0126-09	250	132,700	4.07	174.9	699	2302	2353	1	11	
0127-02	234	120,000	3.94	158.6	665	2341	2389	-	-	
0127-03	232	121,900	4.01	160.1	665	2341	2393	-	-	
0127-04	236	116,800	3.78	153.5	678	2359	2414	5	-	
0127-05	246	137,500	4.28	181.1	688	2283	2327	42	26	Lean Minimum Preheat
0127-07	230	124,200	4.13	163.1	622	2320	2386	0	20	
0127-09	236	161,600	5.24	212.4	528	2333	2377	0	19	
0127-10	216	165,000	5.82	216.1	499	2324	2371	0	19	
0127-12	206	135,500	5.00	177.1	327	2341	2388	7	45	
0127-14	203	142,800	5.34	186.5	304	2342	2385	27	39	
0127-15	201	138,900	5.25	181.3	277	2324	2360	28	0	
0130-01	258	127,200	3.78	167.8	852	2341	2401	19	-	Maximum throughput
0130-02	250	158,900	4.87	209.4	707	2343	2406	17	18	
0130-04	230	233,600	7.76	306.8	689	2358	2452	15	8	
0130-06	236	287,300	9.31	377.7	591	2349	2403	18	5	
0130-07	231	383,000	12.68	503.6	643	2369	2403	15	3	
0130-09	230	438,900	14.58	576.4	637	2369	2407	14	2	
0130-12	214	602,500	21.44	788.7	568	2340	2402	12	1	

TABLE B-17. Concluded

Test Pt.	TA (%)	SV (1/hr)	$\dot{m}$ fuel[a] (lbm/hr)	$\dot{m}$ air (lbm/hr)	Tph (°F)	$\bar{T}$bed (°F)	Tbed max (°F)	CO (ppm)	NO_x (ppm)	Test Type
0130-13	224	585,800	19.96	768.4	523	2310	2376	12	1	High throughput Lean Minimum preheat
0130-14	212	552,500	19.84	722.9	466	2280	2346	12	1	
0130-16	218	527,200	18.43	690.7	396	2303	2352	14	3	
0130-18	200	502,200	19.06	655.3	347	2367	2408	8	5	
0130-20	198	480,000	18.39	625.9	299	2360	2401	7	5	
0130-22	194	479,300	17.86	595.6	250	2356	2403	5	5	
0130-24	192	478,600	18.88	623.1	199	2362	2397	5	5	
0130-25	189	482,900	19.34	628.3	175	2352	2397	5	6	
0130-26	56	34,900	4.18	40.4	633	-	-	-	10	Rich Operation
0130-27	57	35,700	4.25	41.4	720	-	-	-	19	

[a]Fuel flow rates and stoichiometry are approximated based on bed temperature due to fuel flow meter calibration errors.

SECTION B-7

HIGH TEMPERATURE CATALYSTS
TEST MODELS A-029 AND A-030

TABLE B-18. TEST DATA SUMMARY — CATALYST A-029 (NiO/Pt)

Test Pt.	TA%	SV, hr^{-1}	$\dot{m}_{fuel}$, lbm/hr	$\dot{m}_{air}$, lbm/hr	TpH, °F	T_{bed} Avg, °F	T_{bed} max, °F
0710-03	231	93,400	2.6	104.0	638	2423	2437
0710-04	219	148,200	4.4	164.6	644	2454	2543
0710-05	210	141,200	4.3	156.6	645	2557	2648
0710-06	207	142,400	4.4	157.8	643	2669	2745
0710-08	189	129,600	4.4	143.0	642	2776	2805
0710-09	189	129,300	4.4	142.6	641	2803	2856
0710-11	186	126,600	4.4	139.6	643	2845	2902
0710-13	177	121,900	4.4	133.9	644	2905	2952
0710-15	171	119,400	4.5	130.9	644	2947	3005
0710-16	171	120,200	4.5	131.8	644	3004	3049
0710-18	161	113,400	4.5	124.0	642	3056	3100

TABLE B-19. EMISSIONS DATA – CATALYST A-029 (NiO/Pt)

Test Pt.	TA%	$\dot{m}_{fuel}$, lbm/hr	CO, ppm	NO, ppm
0710-03	231	2.6	0	6
0710-04	219	4.4		9
0710-05	210	4.3		11
0710-06	207	4.4		20
0710-08	189	4.4		33
0710-09	189	4.4		43
0710-11	186	4.4		58
0710-13	177	4.4		86
0710-15	171	4.5		119
0710-16	171	4.5		166
0710-18	161	4.5	0	213

TABLE B-20. LIGHTOFF CHARACTERISTICS – CATALYST A-030 (Co_2O_3/Pt)

Cumulative Test Time (Hrs)	Lightoff Condition	Lightoff Temperature (°F)	Comments
0	Fuel Rich	960	Lean lightoff at 860°F unsuccessful Natural gas
7	Rich	950	Lean lightoff at 950°F unsuccessful Natural gas
14	Rich	800	Propane lightoff, switch to natural gas
21.5	Rich	750	Propane lightoff

TABLE B-21. SCREENING DATA SUMMARY — CATALYST A-030 (Co_2O_3/Pt)

Test Pt.	TA%	SV, hr^{-1}	$\dot{m}_{fuel}$, lbm/hr	$\dot{m}_{air}$, lbm/hr	T_{ph}, °F	T_{BED}, °F	T_{BED}, Max	Test	CO, ppm	NO, ppm
0714-04	249	170400	4.4	190.4	652	2084	2597	Aging	0	5
0714-10	253	174000	4.5	194.5	597	2054	2756			8
0715-04	252	177100	4.6	197.9	675	2181	2710	Min.		13
0715-07	250	173200	4.5	193.5	576	2020	2665	preheat		6
0715-08	243	169500	4.5	189.1	502	1970	2647	2600°F		6
0715-11	243	169800	4.5	189.5	394	2214	2657	lean		6
0715-05	256	160500	4.6	178.6	649	2561	2856	Min.		14
0715-06	232	164000	4.6	182.7	591	2490	2839	preheat		13
0715-09	224	156900	4.5	174.5	471	2459	2835	2800°F		17
0715-10	221	154400	4.5	171.6	409	2432	2845	lean	0	15
0715-13	274	185000	4.4	207.4	786	2235	2683	Max.	18	5
0715-14	265	225700	5.6	252.8	747	2091	2647	thruput	0	4
0715-15	255	309900	7.9	346.5	683	2211	2666	2600°F		5
0715-16	256	342700	8.7	383.2	676	1869	2618	lean		4
0715-17	279	455500	10.7	511.1	683	1764	2657			4
0715-18	260	175900	4.4	196.9	662	1999	2664			6
0715-19	239	163500	4.4	182.4	652	2670	2863	Max.		13
0715-20	232	215000	6.0	239.4	653	2233	2872	thruput		12
0715-21	226	260700	7.5	290.1	658	2233	2842	2800°F		10
0715-22	229	337400	9.5	375.6	661	2052	2869	lean		9
0715-23	241	427900	11.5	477.4	670	1965	2875			8
0715-24	251	489700	12.5	547.7	676	1935	2846			8
0715-25	237	163800	4.5	182.6	649	2747	2876			15
0719-03	~200			186.7	652	1914	2553	3100°F		3
0719-04	-250%			176.3	648	1968	2598	emissions		4
0719-06	TA			188.4	644	2151	2719	lean		6
0719-08			~4.4[a]	194.2	644	2365	2830			10
0719-10			lbm/hr	216.6	643	2741	2913			14
0719-12				202.8	640	2862	2997			25
0719-14				184.6	633	2950	3111		0	46
0719-21	~50%			39.4	559	2734	2773	Min.	>2000	1
0719-22	TA			37.5	439	2679	2741	preheat 2700°F rich	>2000	0

[a]Inaccuracies in fuel flow measurements make exact values unknown.

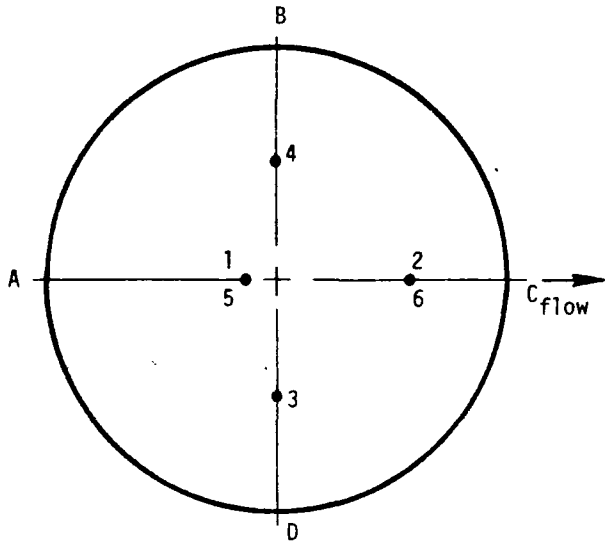

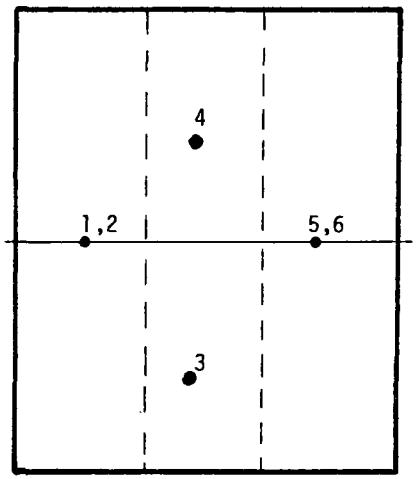

Bed temperature distributions effects of preheat

2600°F Bed

T_{PH} = 787

0715-14

TC	°F
1	2532
2	1936
4	2344
5	2690
6	1648

T_{PH} = 394

0715-11

TC	°F
1	2316
2	1708
4	2663
5	2608
6	1742

2800°F Bed

T_{PH} = 650

0715-05

TC	°F
1	2665
2	2542
4	2719
5	2856
6	2141

T_{PH} = 410

0715-10

TC	°F
1	2664
2	2605
4	2845
5	2791
6	2563

Figure B-23. Catalyst A-030 (Acurex Co_2O_3/Pt) bed temperature distributions.

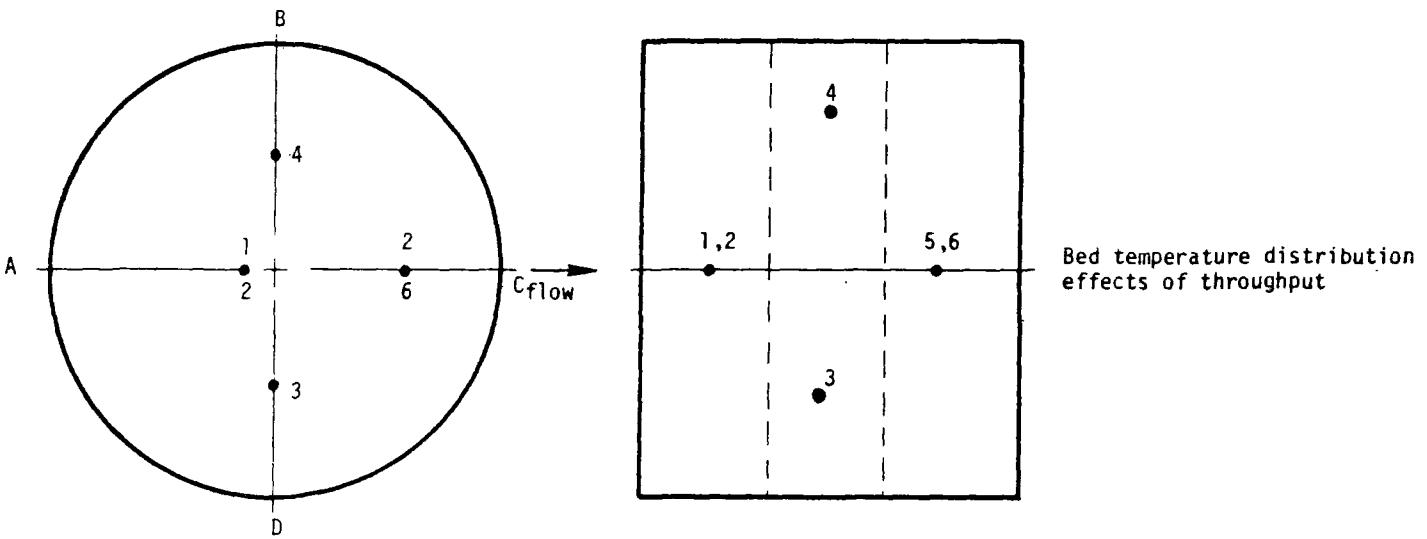

Bed temperature distribution effects of throughput

2600°F Bed

$\dot{m}_{fuel}$ = 4.4

0715-13

TC	°F
1	2564
2	1925
4	2341
5	2683
6	1661

$\dot{m}_{fuel}$ = 10.7

0715-17

TC	°F
1	1023
2	1140
4	1807
5	2657
6	1126

2800°F Bed

m_{fuel} = 4.5

0715-19

TC	°F
1	2672
2	2629
4	2723
5	2854
6	2461

m_{fuel} = 12.5

0715-24

TC	°F
1	1851
2	1143
4	2604
5	2831
6	1176

Figure B-24. Catalyst A-030 (Acurex Co_2O_3/Pt) bed temperature distributions.

SECTION B-7

CATALYST SCALEUP
TEST MODEL A-041

TABLE B-22. UOP SCALEUP CATALYST LIGHTOFF CHARACTERISTICS — CATALYST A-041

Cumulative Test Time (Hrs)	Lightoff Condition	Lightoff Temperature (°F)	Comments
0	FUEL LEAN	840	NATURAL GAS
6	RICH	750	
12.5	RICH	770	
18.0	RICH	660	
19.5	RICH	700	
22.0	RICH	860	
24.0	RICH	860	

TABLE B-23. DATA SUMMARY — CATALYST A-041

1	2	3	4	5	6	7	8	9	10	11	12	13	14
Test Point	TA (%)	SV (1/hr)	$\dot{m}_{fuel}$ (lbm/hr)	$\dot{m}_{air}$ (lbm/hr)	T_{pH} (°F)	T_{BED} (°F)	$T_{BED, MAX}$ (°F)		CO (ppm)	NO (ppm)			TEST TYPE
1230-02	248	127,800	10.4	442.4	662	2349	2351		0	3			
05	259	133,200	10.4	462.2	636	2354	2354		0	4			Aging
07	244	124,800	10.3	431.7	639	2344	2347		0	3			
10	255	129,600	10.3	449.8	607	2332	2334		0	3			
0102-02	230	120,100	10.7	422.8	630	2354	2356		0	3			
05	220	107,500	10.0	377.4	642	2353	2355		0	3			
0102-06	231	115,800	10.3	407.6	640	2401	2402		0	5			
07	221	112,200	10.4	394.0	599	2400	2405		0	5			
09	212	108,400	10.4	379.9	549	2389	2396		0	5			lean fuel
11	210	107,700	10.4	377.3	500	2389	2402		0	5			minimum
13	215	109,600	10.4	384.5	451	2380	2394		0	5			preheat
15	200	106,200	10.3	371.3	349	2398	2402		0	5			2350°F
16	188	102,800	11.1	358.1	299	2395	2397		0	7			
17	189	104,700	11.3	364.8	250	2397	2401		0	8			
18	186	108,000	11.8	376.0	201	2408	2411		0	10			
19	176	106,300	12.2	369.1	177	2393	2396		0	17			
0103-02	55	30,500	10.0	94.1	501	2373	2406		>2000	1			
03	54	30,700	10.2	94.4	449	2352	2376		>2000	1			
04	55	31,200	10.2	96.2	448	2352	2375		>2000	1			
05	54	31,300	10.3	96.4	400	2364	2388		>2000	1			rich fuel
06	56	31,900	10.2	98.7	349	2379	2407		>2000	1			minimum
07	56	32,500	10.4	100.7	299	2375	2400		>2000	1			preheat
08	54	33,400	11.1	102.8	250	2383	2406		>2000	1			2400°F
09	57	34,100	10.8	105.8	225	2376	2397		>2000	1			
10	58	35,200	11.0	109.6	200	2384	2404		>2000	2			

TABLE B-23. Continued

1	2	3	4	5	6	7	8	9	10	11	12	13	14
Test Point	TA (%)	SV (1/hr)	$\dot{m}_{fuel}$ (lbm/hr)	$\dot{m}_{air}$ (lbm/hr)	T_{PH} (°F)	$\bar{T}_{BED}$ (°F)	$T_{BED, MAX}$ (°F)		CO (ppm)	NO (ppm)			TEST TYPE
0103-13	221	137,800	12.8	483.9	616	2339	2354		44	3			maximum
14													through-
15	240	173,600	14.9	612.0	644	2348	2363		20	2			put
16	235	199,500	17.4	702.8	637	2372	2388		21	2			2400°F
17	240	233,900	20.0	824.7	634	2372	2391		31	2			
18	256	281,200	22.6	994.0	636	2351	2371		0	1			
19	258	310,100	24.7	1096.3	634	2384	2394		2	1			
20	252	338,600	27.6	1195.9	634	2373	2397		42	1			
21	266	386,850	30.0	1369.4	635	2334	2349		149	1			
22	274	433,700	32.6	1537.2	637	981	1249		52	1			
0104-03	202	108,000	10.9	377.9	399	2371	2377		15	6			blowout
04	189	117,000	12.5	408.9	379	2363	2378		11	9			@400°F PH
05	198	137,600	14.1	480.8	382	2359	2371		6	7			2400°Fbed
06	230	209,700	18.6	738.9	395	2355	2368		7	7			
08	229	253,700	22.6	892.7	407	1413	1868		0	3			
0104-09	174	97,900	11.3	339.6	251	2367	2385		1	10			blowout
10	180	105,700	11.8	367.6	248	2370	2379		0	10			@2500°F PH
11	200	125,700	12.8	439.3	241	2342	2375		0	7			2400°F bed
12	203	143,800	14.4	503.1	238	2331	2354		0	6			
13	215	174,700	16.6	613.0	242	2326	2375		19	12			
14	232	207,100	18.3	728.9	239	2015	2183		10	6			
0105-03	175	96,600	11.1	335.3	615	2386	2390		1	5			blowout
04	221	151,400	14.0	531.8	604	2381	2386		0	2			@635°F PH
05	221	213,200	19.7	749.0	613	2389	2398		0	2			2400°Fbed
06	234	297,300	26.0	1047.1	628	2374	2377		14	2			

TABLE B-23. Continued

1	2	3	4	5	6	7	8	9	10	11	12	13	14
Test Point	TA (%)	SV (l/hr)	$\dot{m}_{fuel}$ (lbm/hr)	$\dot{m}_{air}$ (lbm/hr)	T_{PH} (°F)	$\overline{T}_{BED}$ (°F)	$T_{BED, MAX}$ (°F)		CO (ppm)	NO (ppm)			TEST TYPE
0105-08	248	385,900	32.0	1362.1	626	2347	2349		15	2			
09	242	430,000	36.4	1516.5	624	2405	2408		15	1			
10	240	512,700	43.9	1807.2	626	2408	2418		17	1			
11	238	504,400	43.5	1777.6	625	2431	2437		21	1			
12	262	601,800	47.2	2129.1	626	2324	2346		20	1			
13	248	589,500	48.7	2081.0	625	2268	2313		22	1			
14	250	588,600	48.3	2078.4	625	856	973		21	2			
0105-17	197	104,700	10.8	365.8	776	2361	2370			5			blowout@
													750°F PH
													2400°F bed
20	245	265,300	22.2	936.2	761	2405	2411		38	1			
21	249	307,400	25.4	1085.3	765	2381	2387		31	1			
22	255	314,600	25.3	1112.0	768	2388	2397		33	1			
23	263	345,300	27.0	1221.8	765	2372	2379		0	1			
24	259	410,100	32.6	1450.1	761	2369	2374		0	1			
25	257	406,100	32.5	1435.7	761	2370	2379		0	1			
26	261	429,300	33.9	1518.5	758	2390	2398		0	1			
27	252	432,800	35.2	1528.7	756	2355	2367		0	1			
28	246	433,800	36.2	1530.9	756	2344	2355		0	1			
29	237	443,000	38.3	1561.0	753	2371	2380		0	1			
30	236	453,300	39.3	1597.0	754	2361	2373		0	2			

TABLE B-23. Concluded

1	2	3	4	5	6	7	8	9	10	11	12	13	14
Test Point	TA (%)	SV (1/hr)	$\dot{m}_{fuel}$ (lbm/hr)	$\dot{m}_{air}$ (lbm/hr)	T_{PH} (°F)	$\bar{T}_{BED}$ (°F)	$T_{BED,MAX}$ (°F)			CO (ppm)	NO (ppm)		TEST TYPE
0105-31	235	457,600	39.9	1611.7	704	2329	2344		0	1			lean
32	230	454,600	40.4	1600.0	652	2360	2372		0	2			minimum
33	229	450,700	40.3	1585.6	650	2355	2367		0	1			preheat@
34	225	448,300	40.7	1575.8	595	2367	2379		0	2			10^6 Btu/hr
35	210	429,800	41.7	1506.4	506	2367	2379		0	2			2400°F
36	192	396,500	41.9	1383.4	386	2365	2380		0	2			1 Atm
37	191	389,200	41.4	1357.3	296	2379	2397		0	3			
38	183	395,500	43.7	1376.5	248	2367	2391		0	4			
39	169	383,200	45.5	1327.7	200	2382	2397		0	11			
40	164	369,900	45.4	1279.1	150	2346	2379		0	18			
41	159	367,300	46.3	1267.9	125	2362	2385		0	17			

SECTION B-8

EXTENSIVE EVALUATION
TEST MODELS A-036 AND A-037

TABLE B-24. EXTENSIVE EVALUATION SUMMARY — CATALYST A-036 (NiO/Pt)

1	2	3	4	5	6	7	8	9	10	11	12	13	14
Test Point	TA (%)	SV Hr^{-1}	ppm NH_3 Fuel	$\dot{V}_{fuel}$ SCFM	$\dot{V}_{air}$ SCFM	ppm NH_3 Gas	Bed max. Temp max.	ppm NO Thermal	ppm NO Total	ppm Fuel NO		% NH_3 Converted	
1010-03	57	113,800	0	4.44	23.60	0	2650	0					
1010-04	57	115,700	5000	4.45	24.12	779	2630		0	0		0	
1010-05	65	103,100	0	3.46	20.84	0	2685	0					
1010-06	65	103,600	5000	3.47	20.94	711	2680		0	0		0	
1010-07	75	119,800	0	2.91	19.65	0	2580[1]	0					
1010-08	75	119,600	5000	2.91	19.60	646	2580		15	15		2.32	
1010-09	93	115,700	0	1.90	16.13	0	2480[1]	45					
1010-10	93	115,300	5000	1.90	16.11	527	2480		298	253		48.0	
1010-11	100	106,200	0	1.83	16.58	0	2500[1]	47					
1010-12	100	106,900	5000	1.84	16.82	493	2500		140-[2] 360	93-313		41.2[3]	
1012-03	190	103,600	0	1.36	24.00	0	2340	9					
1012-04	190	104,000	5000	1.36	24.09	267	2340		187	178		66.7	
1012-05	145	101,100	0	1.37	19.56	0	2375	22					
1012-06	145	98,400	5000	1.36	18.85	336	2375		80-460	58-438		73.7[3]	
		98,400	2500	1.36	18.85	168			60-255	38-233		80.8[3]	
		98,400	10,000	1.36	18.85	673			625	603		89.6	
1012-07	101	108,100	0	1.48	13.55	0	2400	30					
1012-08	101	108,200	5000	1.49	13.55	495	2400		100-360	70-330		40.4[3]	
1012-09	101	109,500	10,000	1.48	13.90	991	2400		600	570		57.5	
1012-11	80	111,200	0	2.03	16.02	0	2440	26					
1012-12	80	107,500	5000	2.03	15.12	592	2440		605	579		97.8	

1. Pyrometer estimates ($\varepsilon = 0.6$)
2. Continuously varying data
3. Averaged values

TABLE B-25. FUEL NITROGEN DATA — A-037 (Co_2O_3/Pt)

1	2	3	4	5	6	7	8	9	10	11	12	13	14
Test Point	Theoretical Air (%)	Space Velocity (Hr^{-1})	Dopant Concentration (ppm)	Fuel Rate (SCFM)	Air Rate (SCFM)	Max. Bed Temp. (°F)		ppm NH_3 in gas	Thermal NO_x (ppm)	Total NO_x (ppm)	Fuel NO_x (ppm)		Conversion NO_x (%)
1222-04	53	39,000	0	1.7	8.4	2483	Rear Segt.		1				
1222-05	53	40,200	20,770	1.7	8.7	2438	blowout	3395		95	94		2.8
1222-07	48	37,000	0	1.7	7.8	2542	Raise bed		5				
1222-08	48	36,800	20,770	1.7	7.8	2538	temp.	3717		22	17		0.46
1222-09	63	45,100	0	1.7	10.0	2564			3				
1222-10	63	45,100	20,770	1.7	10.0	2549		3018		30	27		0.39
1222-11	~71	47,600	0	1.7		2552			4				
1222-12	72	57,000	15,980	1.9	12.9	2528		2051		66	62		3.0
1222-13	82	60,700	0	1.8	13.9	2573			9				
1222-14	78	60,500	15,980	1.9	13.8	2554		1934		440	431		22.3
1222-15	89	56,300	0	1.4	13.1	2545			24				
1222-16	88	56,800	22,550	1.5	13.1	2537		2317		775	751		32.4
1222-17	97	58,500	0	1.5	13.7	2534			25				
1222-18	99	59,900	22,550	1.5	14.0	2536		2182		1090	1065		48.8
1222-19	105	66,400	0	1.6	15.6	2559			25				
1222-20	103	65,400	21,760	1.6	15.4	2571		2048		1350	1325		64.7
1222-21	104	65,800	29,260	1.6	15.5	2579		2747		1635	1610		58.6

TABLE B-25. Concluded

	1	2	3	4	5	6	7	8	9	10	11	12	13	14
	Test Point	Theoretical Air (%)	Space Velocity (Hr^{-1})	Dopant Concentration (ppm)	Fuel Rate (SCFM)	Air Rate (SCFM)	Max. Bed Temp. (°F)		ppm NH_3 in gas	Thermal NO_x (ppm)	Total NO_x (ppm)	Fuel NO_x (ppm)		Conversion NO_x (%)
	1222-22	131	80,700	0	1.6	19.3	2555			55				
	1222-23	131	81,100	21,630	1.6	19.4	2568		1648		1490	1435		87.1
	1222-24	131	81,000	29,360	1.6	19.4	2569		2237		1780	1725		77.1
	1223-04	178	195,600	0	2.7	46.0	2532	2 Atm		54				
	1223-05	178	197,000	17,330	2.7	46.2	2503		985		865	831		34.4
	1223-08	176	205,200	0	2.9	48.2	2545	3 Atm		88				
	1223-09	176	207,900	20,860	2.9	48.3	2522		1170		789	701		59.9

TABLE B-26. FUEL LEAN DATA FOR FUEL NITROGEN CONVERSION

	Type	SV, 1/hr	T_{BED}, °F	Ko, % N in fuel	P, atm	Conversion Measured, %	Conversion Calculated, %
1	NASA	.2842+06	1826.	.1350-01	3.000	85.30	68.40
2		.2842+06	1880.	.1350-01	3.000	77.20	71.46
3		.2842+06	1898.	.1350-01	3.000	75.00	72.48
4		.2842+06	2006.	.1350-01	3.000	82.80	78.76
5		.2842+06	1952.	.1350-01	3.000	75.60	75.60
6		.2842+06	1988.	.1350-01	3.000	74.00	77.70
7		.2842+06	1970.	.1350-01	3.000	72.30	76.65
8		.2842+06	1979.	.1350-01	3.000	71.10	77.17
9		.2842+06	2015.	.1350-01	3.000	71.60	79.29
10		.2842+06	2060.	.1350-01	3.000	72.50	81.96
11		.2842+06	2060.	.1350-01	3.000	69.70	81.96
12		.2842+06	1916.	.1350-01	3.000	66.70	73.52
13		.2842+06	1925.	.1350-01	3.000	66.40	74.04
14		.2842+06	1961.	.1350-01	3.000	63.90	76.12
15	AERO Co_2O_3/Pt	.1583+06	2658.	.4370	1.000	68.60	59.81
16		.1489+06	2866.	.4370	1.000	79.20	64.15
17		.1406+06	2985.	.4370	1.000	78.80	65.51
18		.2739+06	2685.	.4370	1.000	84.00	89.13
19		.2685+06	2663.	.2180	1.000	64.00	77.14
20		.2525+06	2846.	.4370	1.000	89.50	91.88
21		.2503+06	2842.	.2180	1.000	64.90	80.96
22		.2407+06	3070.	.4370	1.000	96.10	99.55
23		.2407+06	3050.	.2180	1.000	79.30	87.58
24		.3960+05	2681.	.4370	1.000	23.40	22.97
25	AERO Pt	.9270+05	2340.	.5240	1.000	26.70	35.03
26		.9250+05	2400.	.8730-01	1.000	19.60	26.12
27		.8930+05	2400.	.5240	3.000	68.20	85.37
28	AERO NiO/Pt	.1040+06	2340.	.4370	1.000	66.70	36.82
29		.9840+05	2375.	.8730	1.000	89.60	40.73
30		.1095+06	2400.	.8730	1.000	57.50	44.59
31	ENGELHARD*	.1900+06	2340.	.1700	1.000	81.50	47.81
32		.1300+06	2340.	.9400	1.000	81.50	49.02
33	AERO Co_2O_3/Pt	.2176+05	2573.	.1901+01	1.000	64.7	18.2
34		.2936+05	2579.	.2566+01	1.000	58.6	23.8
35		.8110+05	2568.	.1891+01	1.000	87.1	45.6
36		.8100+05	2569.	.2566+01	1.000	77.1	48.0
37		.1970+06	2504.	.1558+01	2.000	84.4	79.1
38		.2079+06	2522.	.1823+01	3.000	59.9	85.3

*Engelhard bed temperature was assumed to be 2340°F based on reported stoichiometry.

APPENDIX C

SECTION 9 DATA SUPPLEMENT -- COMBUSTION SYSTEM CONFIGURATION TESTS

TABLE C-1. DATA SUMMARY — TWO STAGE COMBUSTOR

Test Pt.	Fuel Rate (lbm/hr)	Primary Air (lbm/hr)	Primary T_{Bed} (°F)	Primary SV (1/hr)	T_{ph} (°F)	Primary TA (%)	Interstage Energy Extracted (Btu/hr)	Secondary Air (lbm/hr)	Secondary T_{Bed} (°F)	Overall SV (1/hr)	Overall TA (%)	Pressure (Atm)
0302-03	8.76	60.9	2250	66,100	665	40	43,900	41.9	2204	50,400	68	1
0302-04	8.73	61.0	2228	66,200	649	40	46,800	41.9	2188	50,400	69	
0302-05	8.50	74.7	2230	77,600	635	51	53,300	40.0	2269	55,300	79	
0302-06	8.48	75.0	2165	77,800	635	51	54,600	40.0	2251	55,400	79	
0302-07	8.80	82.1	2232	84,400	642	54	65,600	40.0	2309	58,700	81	
0302-08	8.74	81.5	2120	83,800	642	54	68,200	40.0	2289	58,400	81	
0302-09	8.83	76.6	2314	79,700	641	50	60,500	66.4	2343	67,700	94	
0302-10	8.84	76.7	2183	79,900	643	50	66,900	66.4	2318	67,700	94	
0302-11	8.74	76.5	2319	79,500	644	51	64,900	76.5	2206	71,900	102	
0302-12	8.65	75.5	2235	78,500	644	51	66,500	76.5	2177	71,400	102	
0302-13	8.64	76.0	2507	78,900	645	51	67,400	89.6	2256	77,300	112	
0302-14	8.61	75.6	2527	78,600	646	51	66,900	89.6	2241	77,100	112	
0302-15	8.97	77.1	2393	80,400	645	50	66,000	80.8	2257	74,200	102	
0302-16	9.00	77.3	2386	80,600	645	50	65,500	80.8	2253	74,300	102	
0302-17	9.07	78.0	2466	81,300	646	50	65,300	85.5	2271	76,700	105	
0302-18	9.08	77.7	2341	81,000	647	50	65,500	85.5	2278	76,600	105	
0302-19	9.40	78.6	2197	82,400	649	49	63,300	115.2	2333	89,900	120	
0302-20	9.44	78.9	2227	82,700	650	49	62,700	115.2	2326	90,100	120	
0302-21	9.49	78.7	2275	82,500	650	48	60,900	155.7	2231	107,500	144	
0302-22	9.42	77.8	2256	81,600	651	48	62,300	155.7	2225	107,000	144	1
0302-23	9.02	77.8	2554	81,000	656	50	55,700	92.7	2338	79,700	110	2
0302-24	9.02	77.5	2430	80,800	657	50	55,300	92.7	2341	79,500	110	2

TABLE C-1. Concluded

Test Pt.	Fuel Rate (lbm/hr)	Primary Air (lbm/hr)	Primary T_{Bed} (°F)	Primary SV (1/hr)	T_{ph} (°F)	Primary TA (%)	Interstage Energy Extraction (Btu/hr)	Secondary Air (lbm/hr)	Secondary T_{Bed} (°F)	Overall SV (1/hr)	Overall TA (%)	Pressure (Atm)
0308-02	4.45	37.6	2350	46,900	642	49	25,400	49.1	2195	40,700	113	1
0308-03	4.45	37.4	2341	46,600	642	49	25,600	49.1	2212	40,600	113	↓
0308-04	4.45	38.1	2345	46,300	637	50	25,500	41.6	2104	37,700	104	
0308-05	4.45	38.6	2355	47,000	651	50	26,000	41.6	2098	37,900	104	
0308-07	4.42	52.4	2406	67,800	690	69*	38,300	49.1	1807	47,100	134	
0308-08	4.42	52.6	2476	67,800	693	69*	39,100	49.1	1805	47,100	134	
0308-09	4.47	41.1	2197	53,000	659	54*	30,900	45.0	1932	40,500	113	
0308-10	4.47	42.0	2206	53,900	662	54*	30,900	45.0	1772	40,900	113	
0308-11	4.56	42.4	2269	50,500	654	54*	30,000	45.0	1952	41,100	111	↓
0308-12	4.56	42.2	2271	50,200	654	54*	29,600	45.0	1952	41,000	111	1
0309-02	8.03	86.9	2096	87,300	662	63	37,800	72.9	2020	74,900	116	1
0309-03	7.99	86.6	2092	88,700	656	63	37,800	72.9	1952	74,700	116	1

*With nitrogen dilution

TABLE C-2. EMISSIONS DATA — TWO STAGE COMBUSTOR

Test Pt.	CO (ppmv)	NH_3 Dopant Conc. (ppm fuel)	ppm NH_3 Overall	Thermal NO_x (ppm)	Total NO_x (ppm)	Fuel NO_x (ppm)	Percent Conversion			% NH_3 + HCN + NO_x
							NH_3	HCN	NO_x	
0302-03	> 2000	0		102						
0302-04	> 2000	2080	274		125	23	0	18.6	8.4	27.0
0302-05	> 2000	0		55						
0302-06	> 2000	2080	242		90	35		31.8	14.5	46.3
0302-07	> 2000	0		28						
0302-08	> 2000	2080	237		88	60		8.9	25.3	34.1
0302-09	90	0		28						
0302-10	74	2080	207		105	77		0	37.2	37.2
0302-11	95	0		24						
0302-12	65	2100	194		72	48			24.7	24.7
0302-13	120	0		19						
0302-14	80	2110	180		65	46			25.6	25.6
0302-15	33	0		23						
0302-16	29	2040	188		70	47			25.0	25.0
0302-17	52	0		23						
0302-18	35	2030	183		76	53			29.0	29.0
0302-19	40	0		24						
0302-20	47	2140	171		75	51			29.8	29.8
0302-21	310	0		14						
0302-22	165	2140	144		69	55			38.2	38.2
0302-23	22	0		13						
0302-24	13	2040	176		55	42	0	0	23.9	23.9

TABLE C-2. Concluded

Test Pt.	CO (ppmv)	NH_3 Dopant Conc. (ppm fuel)	ppm NH_3 Overall	Thermal NO_x (ppm)	Total NO_x (ppm)	Fuel NO_x (ppm)	Percent Conversion			% NH_3 + HCN + NO_x
							NH_3	HCN	NO_x	
0308-02	230	0		8						
0308-03	170	4080	343		39	31	0	0	9.0	9.0
0308-04	> 2000	0		11						
0308-05	> 2000	4020	362		39	28	0	0	7.7	7.7
0308-07	> 2000	0		3						
0308-08	> 2000	4100	271		19	16	7.0	0	5.9	12.9
0308-09	1666	0		4						
0308-10	700	4000	322		87	83	5.6	0	25.8	31.4
0308-11	> 2000	0		5						
0308-12	1650	3920	334		40	35	0	0	10.5	10.5
0309-02	> 2000	0	276	7	7	0	10.8	0	0	10.8
0309-03	> 2000	2020								

TABLE C-3. DATA SUMMARY — MODEL GAS TURBINE

Test Pt.	TA. (%)	SV (1/hr)	$\dot{m}$ fuel (lbm/hr)	$\dot{m}$ air (lbm/hr)	Tph (^{o}F)	$\bar{T}$bed (^{o}F)	P (atm)	CO (ppm)	NO (ppm)	UHC (ppm)	Fuel
Acurex Tests											
0112-05	~250	91,500	11.3	460.3	713	2200	1.16	0	2	-	Propane
0112-06		96,600	12.5	426.7	724	2200	2.06	0	1	-	
0112-03		87,300	11.3	441.7	801	2200	3.13	0	3	-	
0112-09		92,400	11.9	465.3	806	2200	3.42	0	2	-	
Pratt and Whitney Tests											
1976	312	162,900	16.5	806.4	703	-	3.06	10	2	0.6	Propane
1977	350	165,800	15.1	823.7	722	-	4.97	9	1	0.3	
1978	283	167,100	18.6	824.4	711	-	4.97	10	2	0	
1981	397	185,000	14.87	922.0	723	-	6.77	110	1	0.3	
1982	504	428,400	27.24	2147.0	829	-	10.04	23	1	0	
1983	326	141,300	13.75	700.2	679	-	3.10	9	0	0.6	
1985	860	288,400	11.8	1475	894	1700*	2.99	1195	3	79.5	No. 2 Oil
1986	752	291,900	13.7	1493	901	1850*	3.03	710	5	34.7	
1987	829	644,000	27.5	3294	819	1850*	5.21	1592	3	23.9	
1988	819	901,100	38.5	4609	681	1600*	7.01	2202	3	222.6	
1989	1277	276,600	7.7	1415	881	1600*	2.96	1860	44	high	No. 2 oil + pyridine
1991	541	291,900	19	1493	778	-	3.06	82	145	80.1	
1992	583	564,000	34	2885	754	-	5.07	1285	74	24.8	
1993	573	699,500	43	3578	746	-	6.77	1362	68	15.6	

*Bed temperature estimates due to bed nonuniformities.

TABLE C-4. DATA SUMMARY – ADVANCED GRADED CELL/MODEL GAS TURBINE

Test Pt.	~TA (%)	SV (1/hr)	$\dot{m}$ fuel (lbm/hr)	$\dot{m}$ air (lbm/hr)	T_{PH} (°F)	T_{BED} (°F)	P (Atm)	NH_3 Added ppm fuel	NO_x (ppm)	CO (ppm)	UHC (ppm)	% NH_3 Converted	Fuel
0412-02	270	42,500	4.22	195.9	730	2,112	1.16		1	20	6		Natural
03		41,900	4.15	192.6	733	2,115	1.16	5,610	320	8	--	65.0	Gas
05		42,000	4.20	195.0	861	2,111	1.21		1	556	--		
06		43,400	4.35	202.1	864	1,953	1.21		--	556	--		
07		35,300	3.48	161.4	775	2,105	1.22		1	610	--		
08		34,200	3.36	155.9	767	2,093	3.16	5,290	120	62	--	61.2	
09		34,600	3.41	158.2	765	2,093	3.16	10,420	228	32	--	59.0	
10		33,700	3.31	153.6	766	2,080	3.14		6	536	--		
11		41,600	4.12	191.1	779	2,098	5.03		1	383	150		
12		40,700	4.02	186.6	779	2,089	5.03	5,040	60	252	8	32.1	
13		42,300	4.20	194.9	781	2,079	5.02	11,290	125	162	0	29.9	
14		41,900	4.15	192.7	780	2,076	5.02	18,960	165	151	3	23.5	
15		59,600	5.95	276.0	790	2,041	6.97		5	339	69		
16		57,500	5.71	265.0	778	2,030	6.96	5,160	44	170	40	23.0	
17		62,100	6.14	285.0	782	2,145	6.94	18,650	125	16	0	18.1	
18		89,000	8.96	416.0	787	2,101	8.16		1	249	16		
19		91,600	9.20	427.2	787	2,084	8.12	3,820	58	18	0	41.0	
0413-02	230	44,900	5.32	210.3	825	2,109	1.99		3	560	50		Natural
03		46,000	5.38	212.9	680	2,109	3.00		0	509	2		Gas
04		64,000	7.54	298.0	582	2,089	2.97		0	639	40		
05		82,800	9.78	386.8	576	2,082	2.88		0	714	75		
06		98,400	11.55	456.5	573	2,141	2.98		0	399	17		
07		133,100	15.8	623.1	562	2,130	2.82		0	870	160		
08		192,900	23.0	910.1	542	2,127	2.84		0	1,524	820		
09		200,200	23.9	946.6	542	2,106	2.79		0	459	730		
10		221,700	26.5	1,046.6	537	2,106	2.79		0	79	870		
0427-02	300	47,900	5.4	242.5	834	1,864	1.44		10	0	--		Diesel
04	220	47,100	7.2	238.3	839	2,400	1.45		15	1,800	--		Fuel
05	127	46,300	12.3	234.4	839	2,500	1.46		200	292	--		
0428-01	300	27,000	2.3	116.9	877	2,100	1.07		--	17	--		NG
02	250	85,000	9.6	410.7	745	2,350	3.15		--	18	--		NG
03	250	180,800	20.6	885.7	857	2,350	4.64		6	13	0		NG
05	245	162,500	25.3	827.9	911	2,175	4.67		66	0	0		Diesel
07	140	161,000	39.2	819.9	923	2,700	4.95		263	0	0		Fuel

TABLE C-5. RADIATIVE CATALYST/WATERTUBE SYSTEM TEST MATRIX

Test Pt.*	Stoichiometry (% TA)	Surface Temp. Heat Removal Rate	Fuel Rate kg/hr	Fuel Rate (lbm/hr)	Preheat temp. K	Preheat temp. (^{o}F)	Lightoff Characteristics
1	40		2.06	(4.55)	478-533	(400-500)	
2	80	Determine T_w	↓	↓	↓	↓	To be determined - specific test points not required
3	100	↓					
4	200						
5	150						
6	100						
7-10	100	Vary water velocity to optimize T_w	↓	↓			
11	100	Optimum cooling	4.1	(9.1)			
12		↓	8.2	(18.2)	↓	↓	
13	200		4.1	(9.1)			
14	100		2.06	(4.55)	Identify minimum		

*Full emission measurements to be taken at all test points.

TABLE C-6. TEST DATA SUMMARY — RADIATIVE CATALYST/WATERTUBE SYSTEM

Run #	TA%	SV, hr^{-1}	$\dot{m}_{fuel}$, lbm/hr	$\dot{m}_{air}$, lbm/hr	T_{ph}, °F	$T_{BED_{max}}$, °F
0610-02	40	8900	4.7	31.3	557	1513
0610-03	60	12600	4.7	47.8	617	1662
0610-04	78	15800	4.7	62.4	690	1842
0610-05	88	17500	4.7	70.6	722	1816
0610-06	99	19200	4.7	77.9	740	1788
0610-07	110	21400	4.7	88.4	742	1760
0610-08	120	23300	4.7	96.9	741	1738
0610-09	146	27800	4.7	117.6	721	1669
0610-10	219	40700	4.7	173.6	714	1540
0610-11	100	19500	4.6	79.6	742	1804
0610-12	100	27500	6.6	114.1	761	1853
0610-13	100	39800	9.5	166.3	756	1898
0610-14	97	50100	12.4	205.9	816	1960
0610-15	99	60900	14.8	246.9	756	2005
0610-16	100	26500	6.3	109.3	754	1853
0610-17	100	26300	6.3	108.1	675	1815

TABLE C-6. Concluded

Run #	TA%	SV, hr^{-1}	$\dot{m}_{fuel}$, lbm/hr	$\dot{m}_{air}$, lbm/hr	T_{ph}, °F	$T_{BED_{max}}$, °F
0613-03	102	33700	7.8	138.7	610	1824
0613-05	101	32700	7.7	135.2	500	1742
0613-07	100	35100	8.4	144.8	400	1689
0613-09	99	35000	8.4	143.8	300	1700
0613-11	100	33800	8.3	139.7	230	1667

TABLE C-7. EMISSIONS DATA[a] — RADIATIVE CATALYST/WATERTUBE SYSTEM

Run #	TA%	m_{fuel}, lbm/hr	CO, ppm	CH_4, Vol %
0610-02	40	4.7	>2000	4.0
0610-03	60		>2000	-
0610-04	78		>2000	-
0610-05	88		>2000	-
0610-06	99		577	2.6
0610-07	110		34	-
0610-08	120		23	5.6
0610-09	146		9	1.2
0610-10	219	4.7	0	1.4
0610-11	100	4.6	292	3.6
0610-12	100	6.6	792	1.5
0610-13	100	9.5	>2000	1.5
0610-14	97	12.4	>2000	3.4
0610-15	99	14.8	>2000	2.9
0610-16	100	6.3	850	-
0610-17	100	6.3	1004	-

[a]No measurable NO_x emissions (>1 ppm) at any test condition

TABLE C-8. EMISSIONS DATA — RADIATIVE CATALYST/WATERTUBE GAS CHROMATOGRAPHY

Run No.	Concentrations, Volume Percent, Dry Basis			
	H_2	O_2	N_2	CH_4
0610-02	4.6	15.6	75.4	4.0
0610-06	0	16.5	81.0	2.6
0610-08	0	14.7	79.7	5.6
0610-10	0	19.0	79.6	1.4
0610-11	0	16.9	79.5	3.6
0610-12	0	16.5	82.0	1.5
0610-14	0	15.0	81.6	3.4
0610-15	0	15.7	81.5	2.9

TABLE C-9. DATA SUMMARY — RADIATIVE CATALYST/WATERTUBE SYSTEM

Test Point	TA (%)	SV (1/hr)	$\dot{m}_{fuel}$ (lbm/hr)	$\dot{m}_{air}$ (lbm/hr)	T_{PH} (°F)	Fuel[a]	Heat Balance (Btu/hr)				Fuel Conv. (%)	CO (ppmv)	NO_x (ppmv)
							Inlet	Tubes	Test Sec.	Stack			
0221-02	59	39,500	14.9	151.7	726	1	354,500	58,810	24,610	4840		>2000	0
0221-04	59	29,400	14.9	151.5	646	2	351,200	57,310	19,950	4660	17.5	>2000	9
0223-02	97	39,400	9.6	161.0	767	1	240,300	37,910	18,500	5910		31	7
0223-03	97	39,300	9.6	160.7	760	2	240,000	37,410	25,420	5900	17.7	35	24
0223-04	90	38,200	10.1	154.9	751	1	249,700	38,820	12,680	5890		33	19
0223-05	89	38,100	10.0	154.3	752	2	247,500	38,690	12,610	5870	17.6	39	44
0223-06	85	37,300	10.3	150.4	749	1	253,300	39,680	10,810	5680		37	35
0223-07	86	37,800	10.3	152.7	748	2	253,700	39,560	13,190	5820	17 .5	42	50
0223-08	80	38,300	11.1	153.3	745	1	271,400	44,170	16,880	6040		51	18
0223-09	80	38,200	11.0	153.0	746	2	269,200	45,050	17,160	5970	18.6	53	22
0223-10	75	38,600	11.9	153.3	744	1	289,000	46,840	13,350	6240		100	41
0223-11	75	38,600	11.9	153.4	742	2	289,000	49,300	14,780	6250	18.8	106	54
0223-12	120	37,700	7.6	156.9	757	1	194,900	31,660	8,410	5010		7	0
0223-13	120	37,600	7.6	156.5	758	2	194,900	28,530	7,664	4770	17.1	9	22
0224-03	70	41,300	13.1	155.8	622	3	284,800	39,290	10,470	6270		>2000	57
0224-04	70	41,100	13.4	154.2	626	4	290,800	39,290	11,920	6196	14.7	>2000	62
0224-05	65	27,300	9.3	101.6	624	3	201,100	39,480	16,470	3770		>2000	11
0224-06	65	27,100	9.6	100.1	616	4	206,700	38,560	18,230	3720	20.1	>2000	8
0224-07	52	28,500	11.5	101.6	666	3	245,500	46,600	17,250	2880		>2000	8
0224-08	52	27,900	11.3	99.4	660	4	242,000	51,260	14,760	3720	22.7	>2000	17

[a]Fuel Code: 1 — Natural gas
2 — Natural gas + ammonia
3 — Propane
4 — Propane + ammonia

TABLE C-10. FUEL NITROGEN DATA — RADIATIVE CATALYST/WATERTUBE SYSTEM

Test Point	Dopant Conv. (ppmv)	ppm NH_3 in gas	Thermal NO_x (ppm)	Total NO_x (ppm)	Fuel NO_x (ppm)	Percent Conversion			% NH_3 + HCN + NO_x
						NH_3	HCN	NO_x	
0221-02	0		0						
0221-04	2000	302		9	9	15.3	5.20	2.98	23.5
0223-02	0		7						
0223-03	1900	191		24	17	78.0	5.24	8.90	92.1
0223-04	0		19						
0223-05	2000	212		44	25	93.4	4.72	11.79	109.9
0223-06	0		35						
0223-07	2000	216		50	15	40.3	4.63	6.94	51.9
0223-08	0		18						
0223-09	2000	229		22	4	95.2	4.37	1.75	101.3
0223-10	0		41						
0223-11	2000	243		54	13	61.3	4.12	5.35	70.8
0223-12	0		0						
0223-13	2000	160		22	22	63.1	6.25	13.75	83.1
0224-03	0		57						
0224-04	7200	401		62	5	81.6	3.49	1.25	86.3
0224-05	0		11						
0224-06	6000	347		8	0	83.6	2.88	0	86.5
0224-07	0		8						
0224-08	7000	487		17	9	42.1	2.05	1.85	46.0

TECHNICAL REPORT DATA
(Please read Instructions on the reverse before completing)

1. REPORT NO.	2.	3. RECIPIENT'S ACCESSION NO.
EPA-600/7-79-181		

4. TITLE AND SUBTITLE	5. REPORT DATE
Design Criteria for Stationary Source Catalytic Combustion Systems	August 1979
	6. PERFORMING ORGANIZATION CODE
7. AUTHOR(S)	8. PERFORMING ORGANIZATION REPORT NO.
J. P. Kesselring, W. V. Krill, H. L. Atkins, R. M. Kendall, and J. T. Kelly	78-278
9. PERFORMING ORGANIZATION NAME AND ADDRESS	10. PROGRAM ELEMENT NO.
Acurex/Energy and Environmental Division 485 Clyde Avenue Mountain View, California 94042	EHE624A
	11. CONTRACT/GRANT NO.
	68-02-2116
12. SPONSORING AGENCY NAME AND ADDRESS	13. TYPE OF REPORT AND PERIOD COVERED
EPA, Office of Research and Development Industrial Environmental Research Laboratory Research Triangle Park, NC 27711	Final; 6/75 - 8/78
	14. SPONSORING AGENCY CODE
	EPA/600/13

15. SUPPLEMENTARY NOTES IERL-RTP project officer is G. Blair Martin, Mail Drop 65, 919/541-2235.

16. ABSTRACT The report gives results of an investigation of the applicability of catalytic combustion to stationary gas turbine, boiler, and furnace systems, identifying system operating characteristics and potential for NOx emissions reduction. An experimental program was conducted to develop catalyst materials and combustor concepts with useful heat extraction. Catalyst development included: screening of over 30 single-cell reactor material combinations, development of a graded-cell reactor concept, and extensive testing of graded-cell catalysts to determine catalyst performance as a function of pressure, temperature, heat release rate, and fuel nitrogen content. Catalyst development was supported by complete surface characterization analyses and a computer model of catalytic combustion in honeycomb structures. Small scale concept testing included a lean-burning model gas turbine, a radiative catalyst/watertube configuration for watertube boiler application, and a two-stage combustor for fuel-NOx control. Tests of these concepts focused on techniques for energy extraction, obtaining high combustion efficiency, and minimizing emissions of both thermal and fuel NOx. Test results from both catalyst and system concept development were used to conceptualize prototype design for gas turbine, boiler, and other systems.

17. KEY WORDS AND DOCUMENT ANALYSIS

a. DESCRIPTORS	b. IDENTIFIERS/OPEN ENDED TERMS	c. COSATI Field/Group
Pollution Nitrogen Oxides Combustion Catalysis Gas Turbines Boilers Furnaces	Pollution Control Stationary Sources Catalytic Combustion	13B 07B 21B 07D 13G 13A

18. DISTRIBUTION STATEMENT	19. SECURITY CLASS *(This Report)*	21. NO. OF PAGES
Release to Public	Unclassified	478
	20. SECURITY CLASS *(This page)*	22. PRICE
	Unclassified	

EPA Form 2220-1 (9-73)